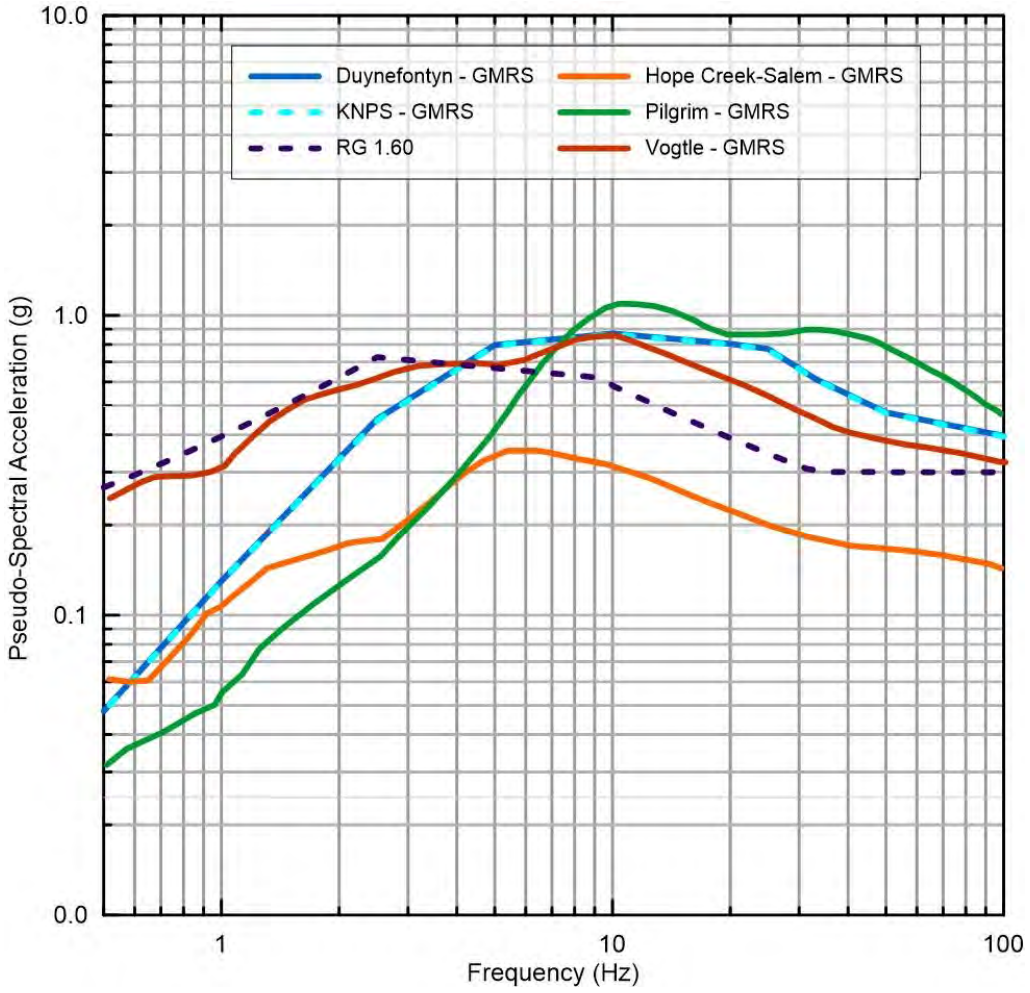

Figure 10-31. GMRS Comparison of South Africa and Eastern United States

10.3.2 Hazard sensitivities

The sensitivity analyses are presented for 100, 10, and 1 Hz representing the spread of frequencies for the new build site at Duynefontyn. Sensitivity plots for the remaining seven oscillator frequencies are presented in Appendix G. The analyses are presented in two forms: (1) sensitivity tornado plots, and (2) sensitivity hazard curves. The sensitivity tornado plots are presented in this section. The following subsections include more detailed discussions of the ground-motion variability due to each of the individual parameters summarised in the tornado plots below, as well as the associated hazard curves.

Each sensitivity analysis is done systematically by setting one branch on the respective logic tree to 1.0 and the others to 0.0. Figure 10-32 to Figure 10-34 show sensitivity tornado plots for 100, 10, and 1 Hz for annual frequency of exceedance values of 10^{-4} and 10^{-5}. Each tornado plot depicts parameters that changed the total mean ground motion at AFEs of 10^{-4} and 10^{-5} by more than 1%.

As shown in Figure 10-32 to Figure 10-34, the only logic-tree branches that contribute 1% or more to hazard sensitivities are within the GMM and the SDZ branches of the SSM. The single greatest contributor to hazard sensitivity is epistemic uncertainty in site amplification, represented by SAFs or Amp. Factors. This is consistent with the high epistemic uncertainty

in the V_S profiles and κ_0 at the site. Overall, the epistemic uncertainty in the GMM has a higher contribution to the hazard sensitivity than the SSM. The most significant contributor to hazard sensitivity in the SSM is the smoothing methodology for the SDZ and Mmax at oscillator frequencies below 1 Hz. These sensitivities are explored in more detail in the following sections.

a)

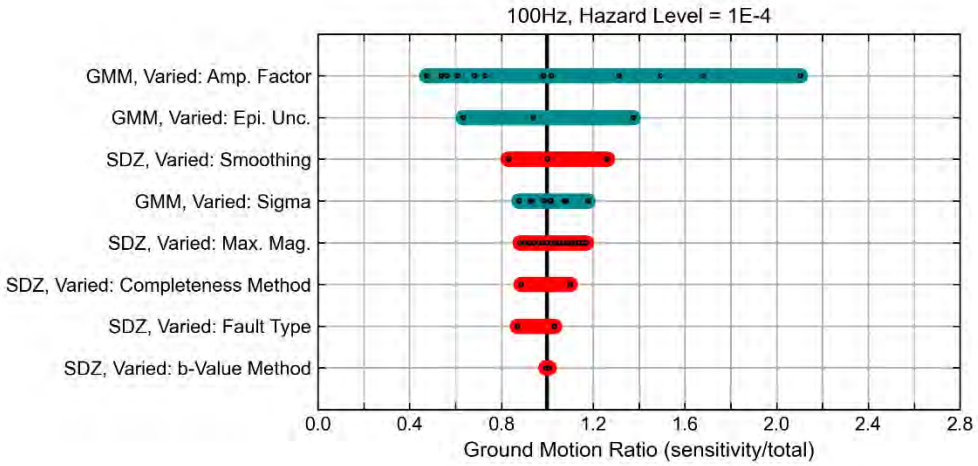

b)

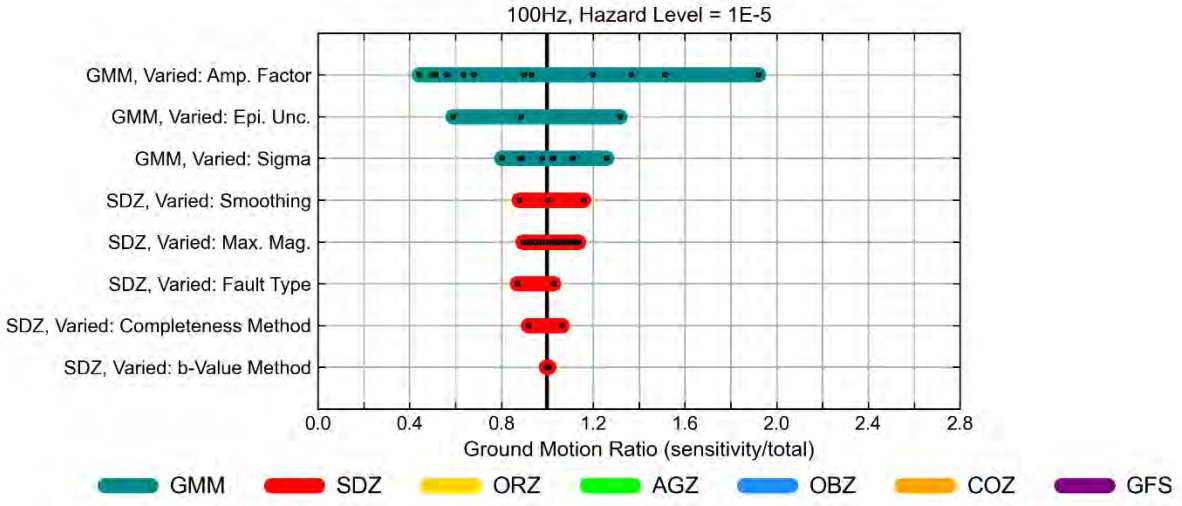

Figure 10-32. Ground motion sensitivity tornado plots for AFEs of a) 10^{-4} and b) 10^{-5} at 100 Hz for the new build site at Duynefontyn.

a)

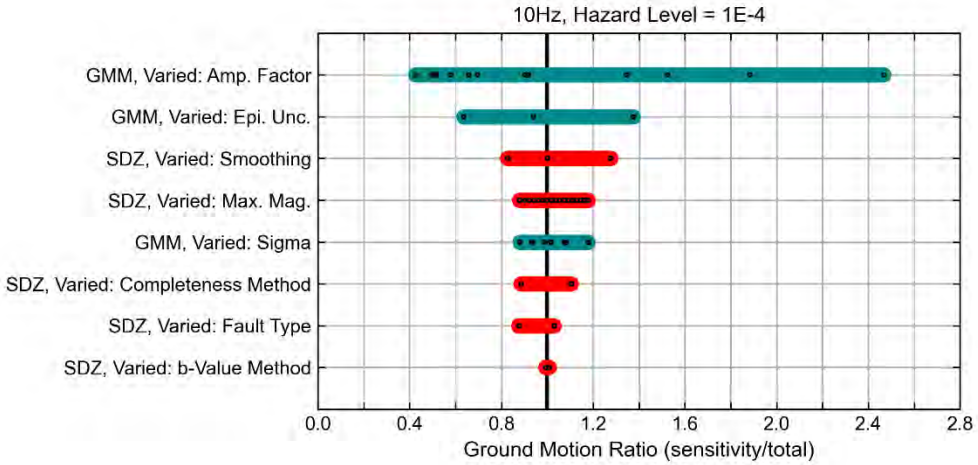

b)

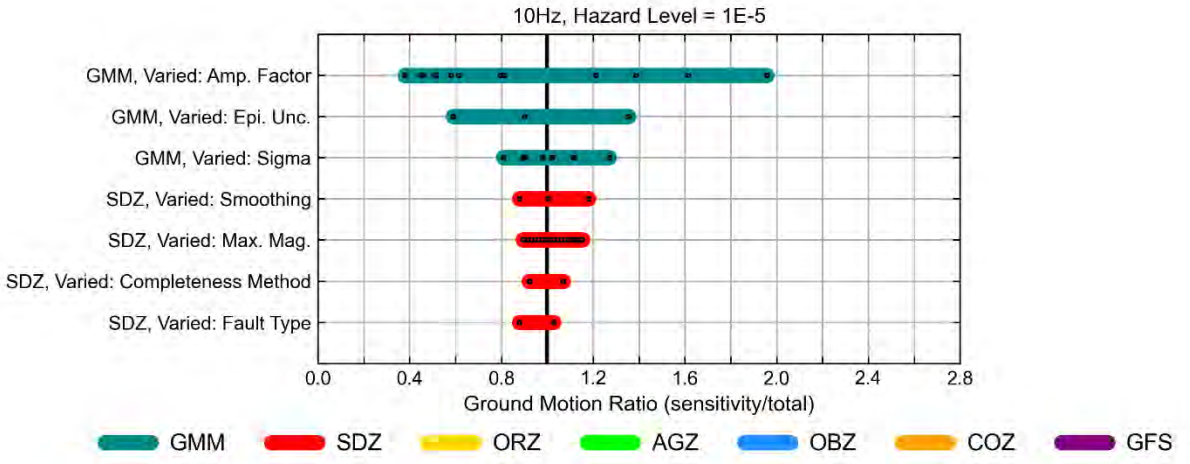

Figure 10-33. Ground motion sensitivity tornado plots for AFEs of a) 10^{-4} and b) 10^{-5} at 10 Hz for the new build site at Duynefontyn.

a)

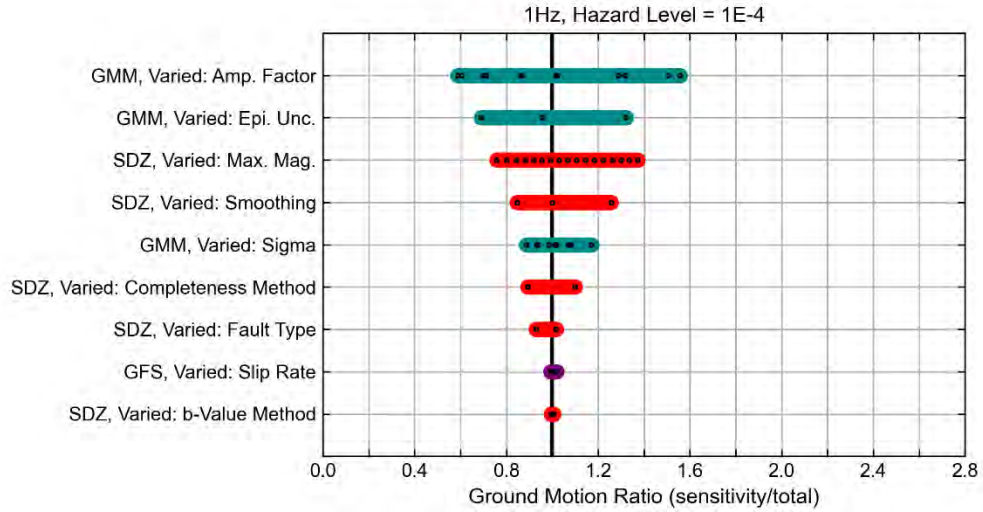

b)

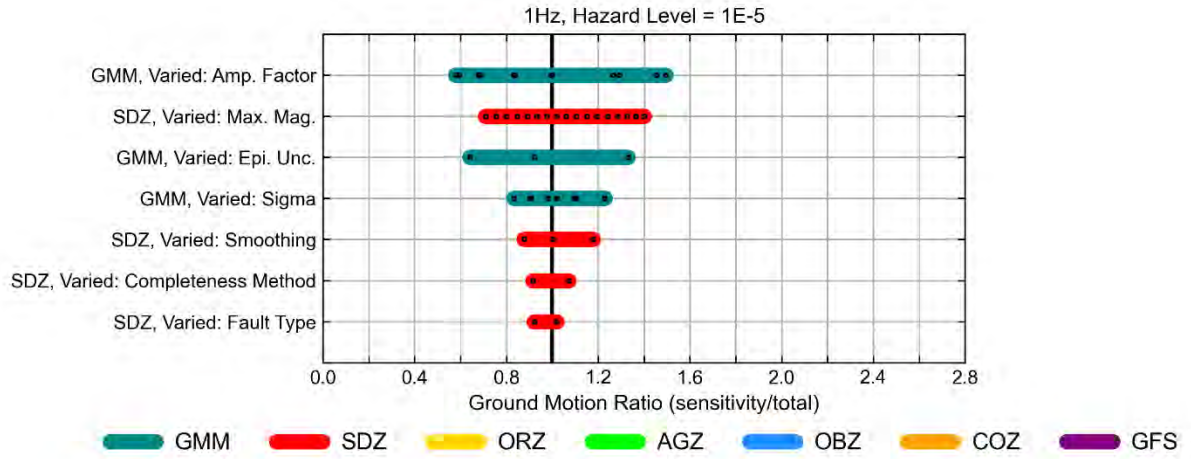

Figure 10-34. Ground motion sensitivity tornado plots for AFEs of a) 10^{-4} and b) 10^{-5} at 1 Hz for the new build site at Duynefontyn.

10.3.2.1 Sensitivity to ground-motion model

There are three main components of the GMM: the epistemic uncertainty branch, site-specific amplification branch, and aleatory variability branch. Further detail regarding the epistemic uncertainty branch and the aleatory variability branch can be found in Section 9.2.5 and 9.3, respectively. Details regarding the site-specific amplification branch are presented in Section 9.4.

10.3.2.1.1 Sensitivity to epistemic uncertainty in site adjustment factor

The first component of the GMM sensitivity and the parameter with the largest contribution to hazard sensitivity in the presented frequencies and AFEs, is the SAF. In total, there are twelve SAF values. These consist of two model groupings (denoted M1 and M2, below) of six SAF values (denoted SAF1 through SAF6, below). The two major groupings were developed to account for two methods of handling epistemic uncertainty. The six SAF values were resampled from the 408 site response branches. Details regarding the SAF values are presented in Section 9.4.

The final development of the SAFs (Section 9.4.9) shows a large range in uncertainty in SAF, particularly at high frequencies. This large uncertainty is due to the complicated geology at the site and its impact on the epistemic uncertainty of the V_S profiles and κ_0. This uncertainty leads to both large amplification and deamplification, shown in the spread of hazard curves presented in Figure 10-35 to Figure 10-37.

A comparison of the hazard curves resulting from the 12 different SAF models with the total mean hazard curve is presented in Figure 10-35, Figure 10-36, and Figure 10-37 for oscillator frequencies of 100, 10, and 1 Hz, respectively. Hazard curves showing the sensitivity to uncertainty in the SAF for the remaining seven frequencies are presented in Appendix G.

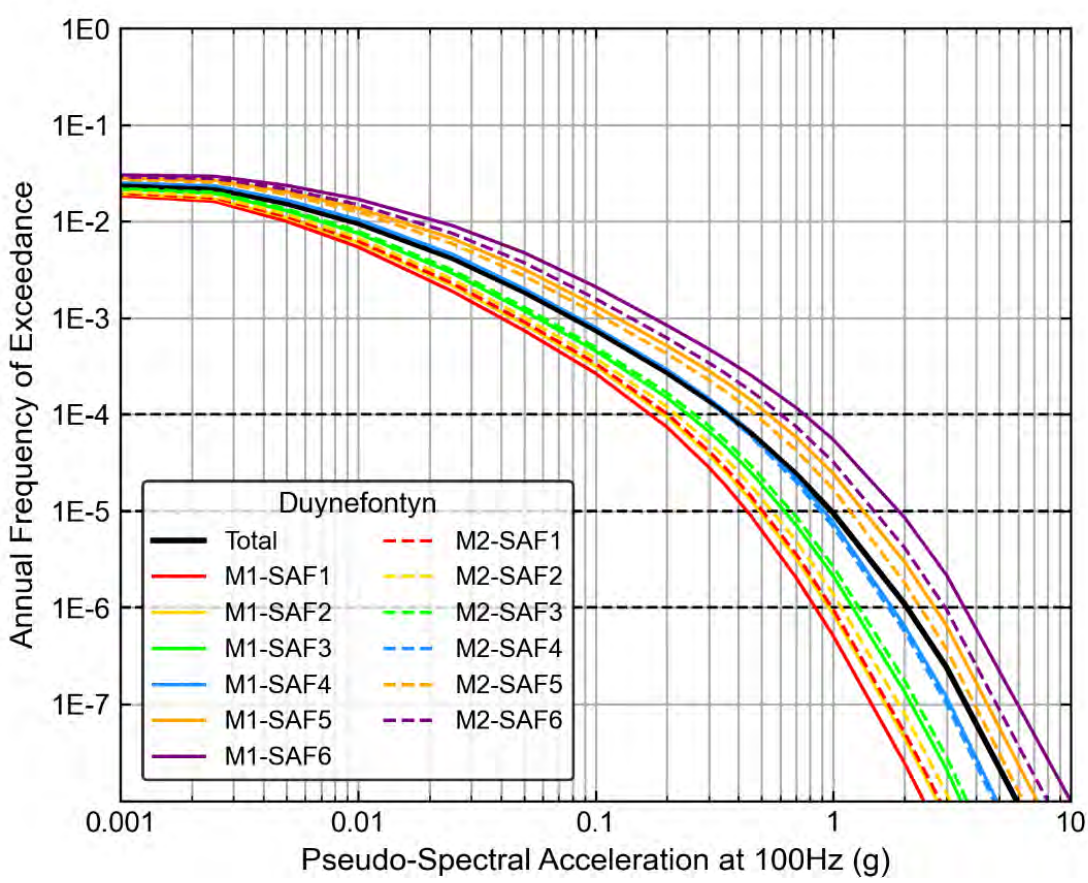

Figure 10-35. Hazard sensitivity to the site response branches for 100 Hz at the new build site at Duynefontyn.

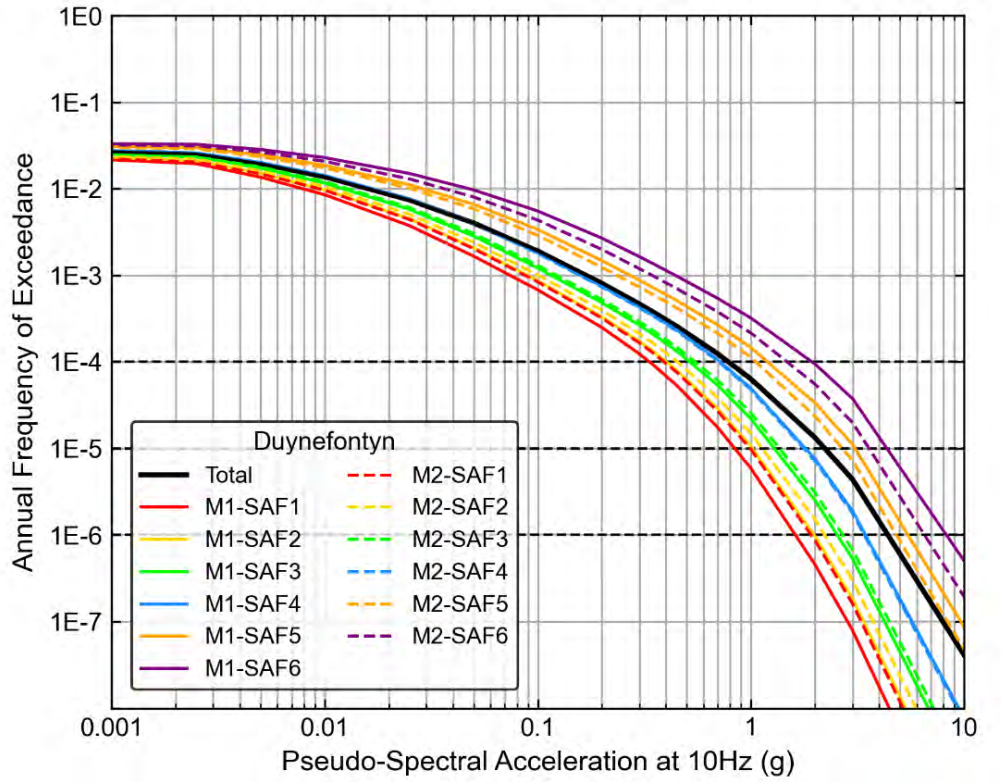

Figure 10-36. Hazard sensitivity to the site response branches for 10 Hz at the new build site at Duynefontyn.

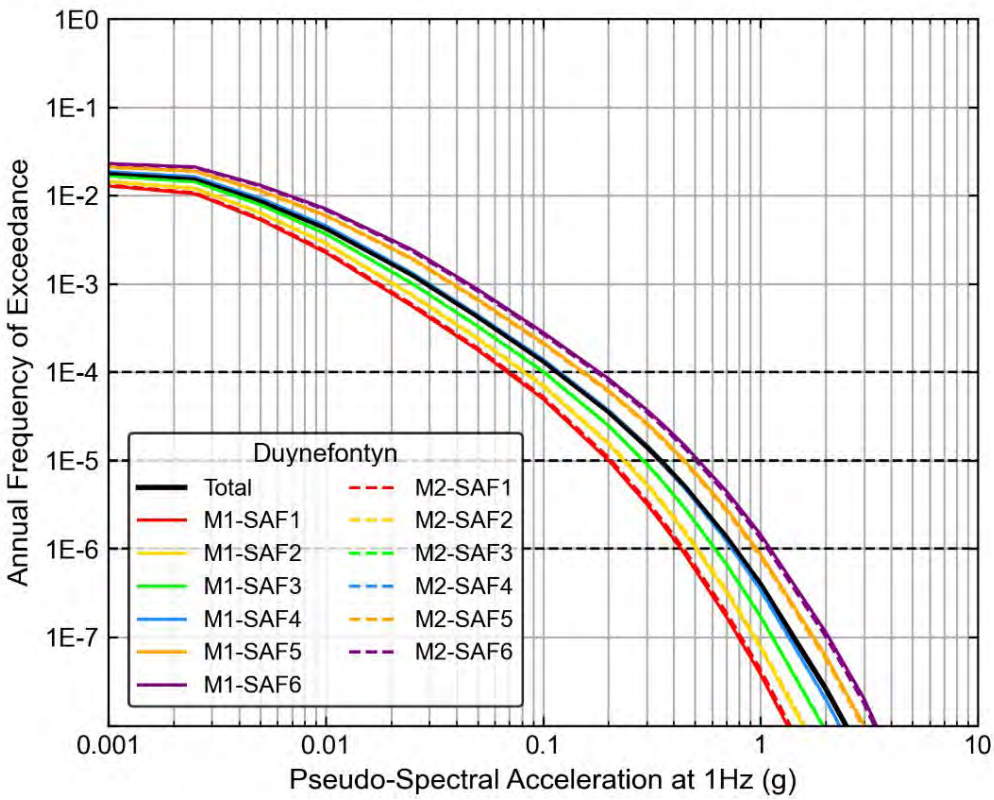

Figure 10-37. Hazard sensitivity to the site response branches for 1 Hz at the new build site at Duynefontyn.

10.3.2.1.2 Sensitivity to epistemic uncertainty in the mean GMM

Epistemic uncertainty in the mean GMM was captured in the three-branch model developed for the project by the GMM TI Team. The GMM TI Team developed this model to capture the epistemic uncertainty in the seismic properties of South Africa based on the inversion results of the GMM TI Team and the specialty contractor Ben Edwards (Edwards, 2023). This model characterises the median (mean in log-space) ground-motion for each earthquake scenario (magnitude and distance), as well as the epistemic uncertainty in the median. As described in Section 9.2.5, a median spectral acceleration value was computed for each of the seven individual models (adjustments made to the CY14 GMPE) and a weighted average was then calculated to develop the spectral acceleration for the central (middle) model. The epistemic uncertainty in the median (mean in log-space), designated as $\sigma_{\mu ln,Sa,}$ was also computed to account for: 1) model-to-model differences from the seven individual models; 2) uncertainty due to near-source saturation; and 3) additional uncertainty.

The final model includes three branches: one with the weighted average GMM (middle branch); one where 1.28 is multiplied by $\sigma_{\mu ln,Sa}$, which is then added to the weighted average (upper branch); and one where 1.28 is multiplied by $\sigma_{\mu ln,Sa}$, which is then subtracted from the weighted average (lower branch).

A comparison of the hazard curves resulting from the three branches with the total mean hazard curve is presented in Figure 10-38, Figure 10-39, and Figure 10-40- for oscillator frequencies of 100, 10, and 1 Hz, respectively. Hazard curves showing the sensitivity to uncertainty in the mean GMM for the remaining seven frequencies are presented in Appendix G.

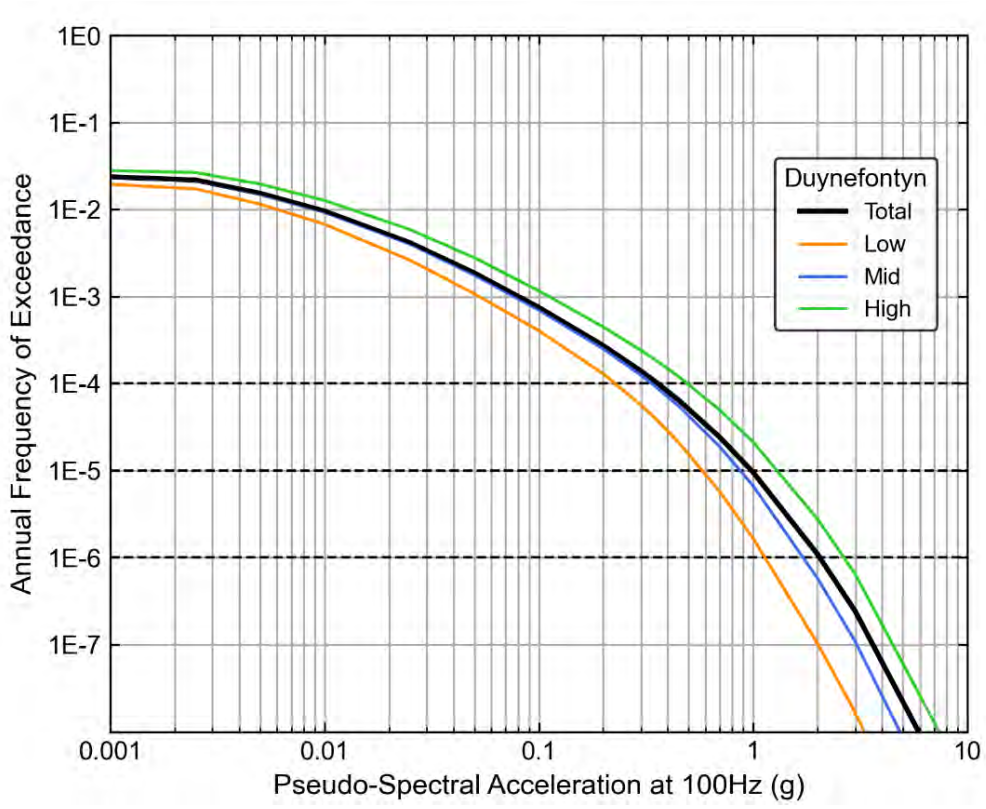

Figure 10-38. Hazard sensitivity to the epistemic uncertainty in the GMM median for 100 Hz at the new build site at Duynefontyn.

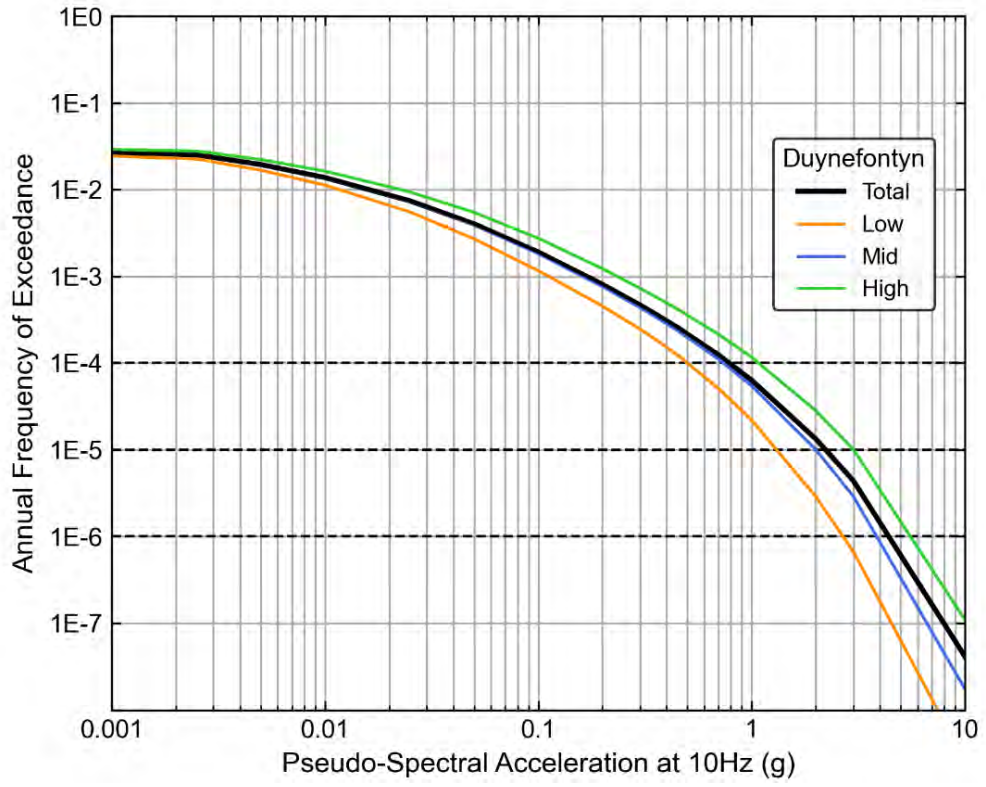

Figure 10-39. Hazard sensitivity to the epistemic uncertainty in the GMM median for 10 Hz for the new build site at Duynefontyn.

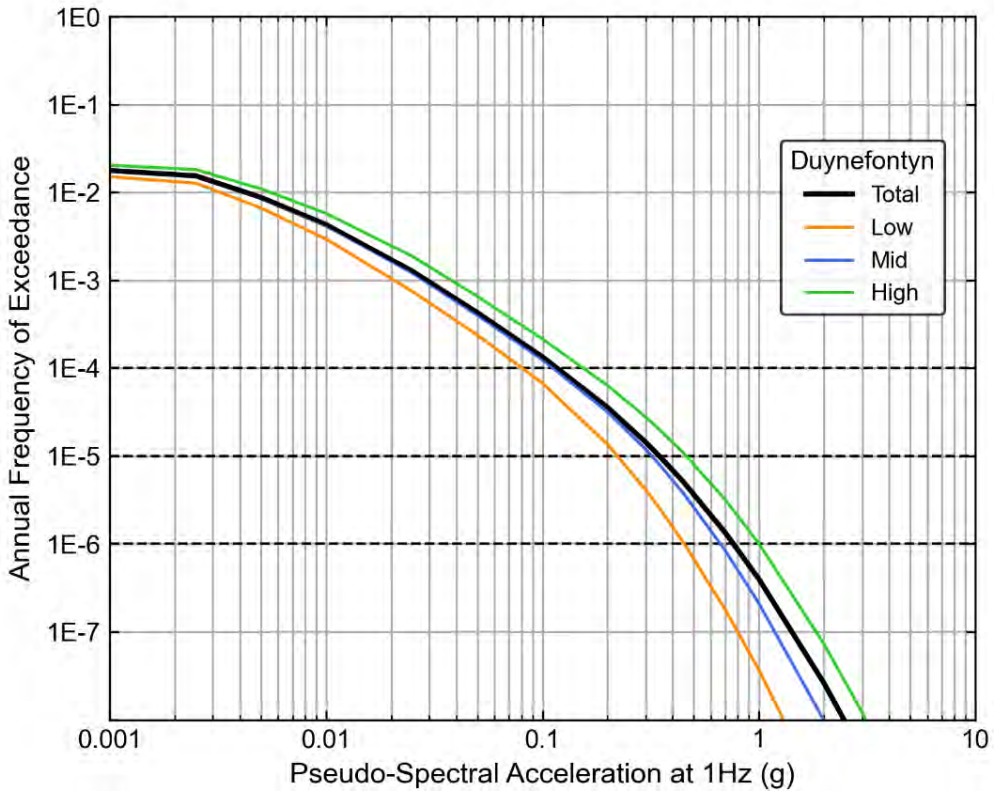

Figure 10-40. Hazard sensitivity to the epistemic uncertainty in the GMM median for 1 Hz at the new build site at Duynefontyn.

10.3.2.1.3 Sensitivity to uncertainty in the GMM aleatory variability model

The uncertainty in the GMM includes aleatory variability branches as presented by Al Atik (2015) and discussed in Section 9.3. The logic-tree branches of the aleatory variability model capture the epistemic uncertainty in applying a single-station sigma model based on world-wide data to a single location that lacks sufficient data for its own single-station sigma evaluation. There are a total of nine standard deviation (σ) values (designated as S1 through S9) computed by varying three within-event variability (ϕ_{ss}, global) terms and three between-event variability (τ, global) terms, the branch pairings are described in Table 10-8. Figure 10-41, Figure 10-42, and Figure 10-43 demonstrates the spread in the hazard results due to variation in the aleatory variability used in the analysis for oscillator frequencies of 100, 10, and 1 Hz, respectively. Hazard sensitivity to the GMM aleatory variability for the remaining seven oscillator frequencies is presented in Appendix G.

Table 10-8. The within-event and between-event logic tree pairings for each σ number.

σ No.	ϕ_{ss}	τ
S1	Low	Low
S2	Middle	Low
S3	High	Low
S4	Low	Middle
S5	Middle	Middle
S6	High	Middle
S7	Low	High
S8	Middle	High
S9	High	High

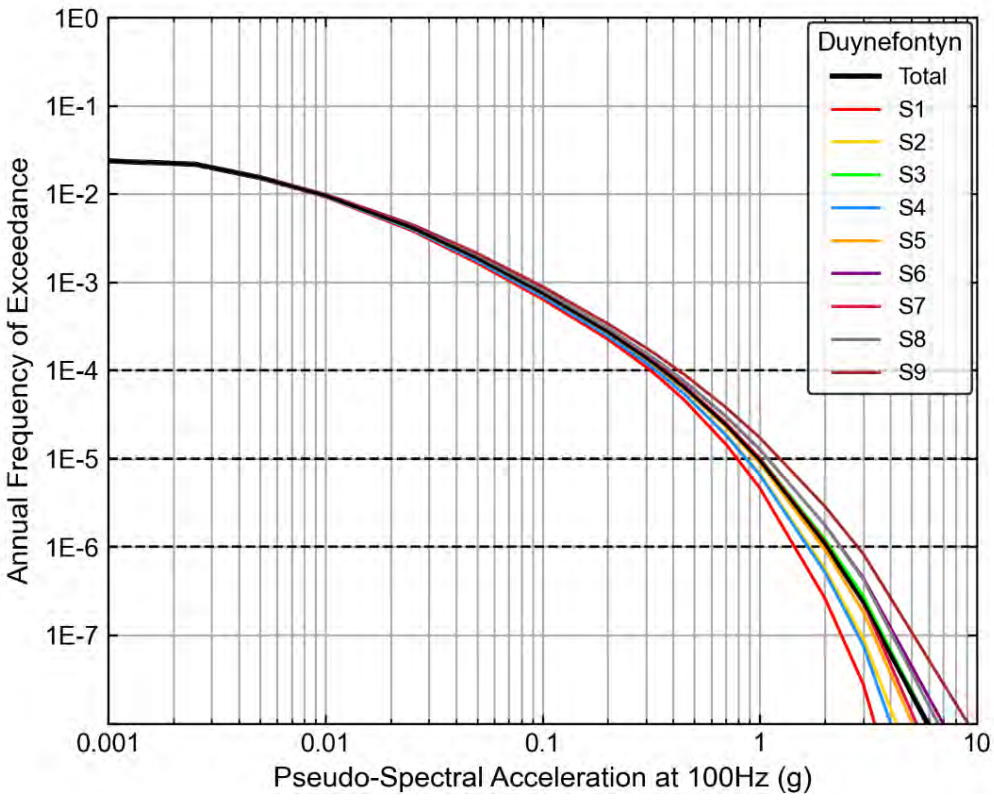

Figure 10-41. Hazard sensitivity to the aleatory variability branches for 100 Hz at the new build site at Duynefontyn.

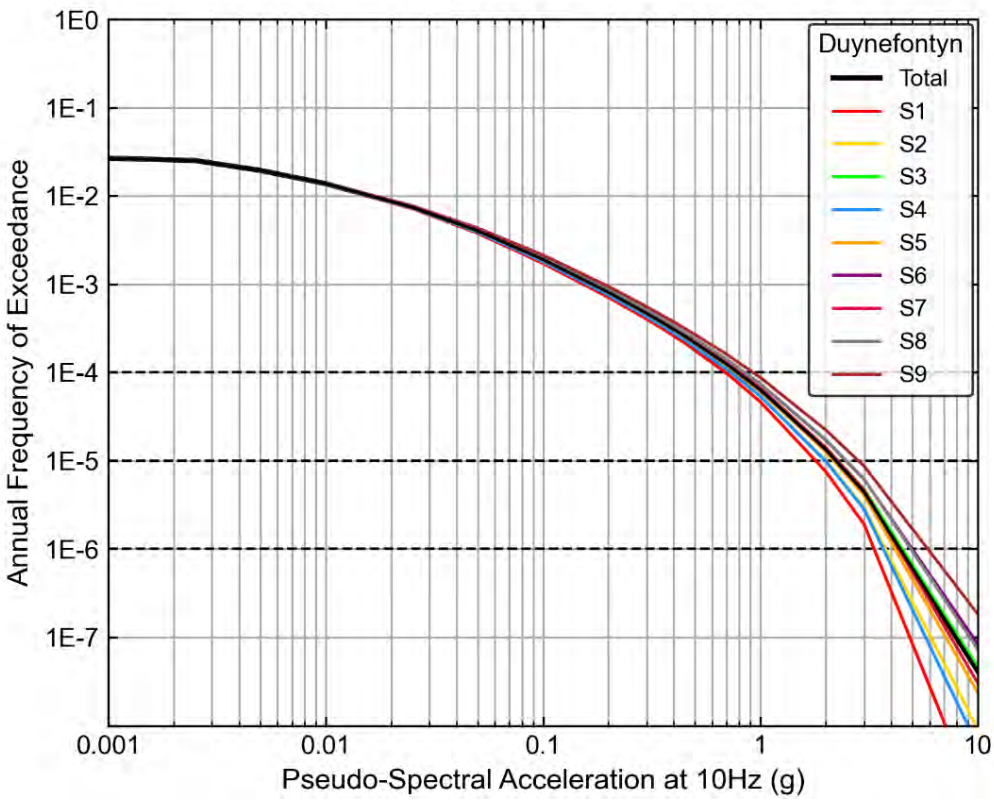

Figure 10-42. Hazard sensitivity to the aleatory variability branches for 10 Hz at the new build site at Duynefontyn.

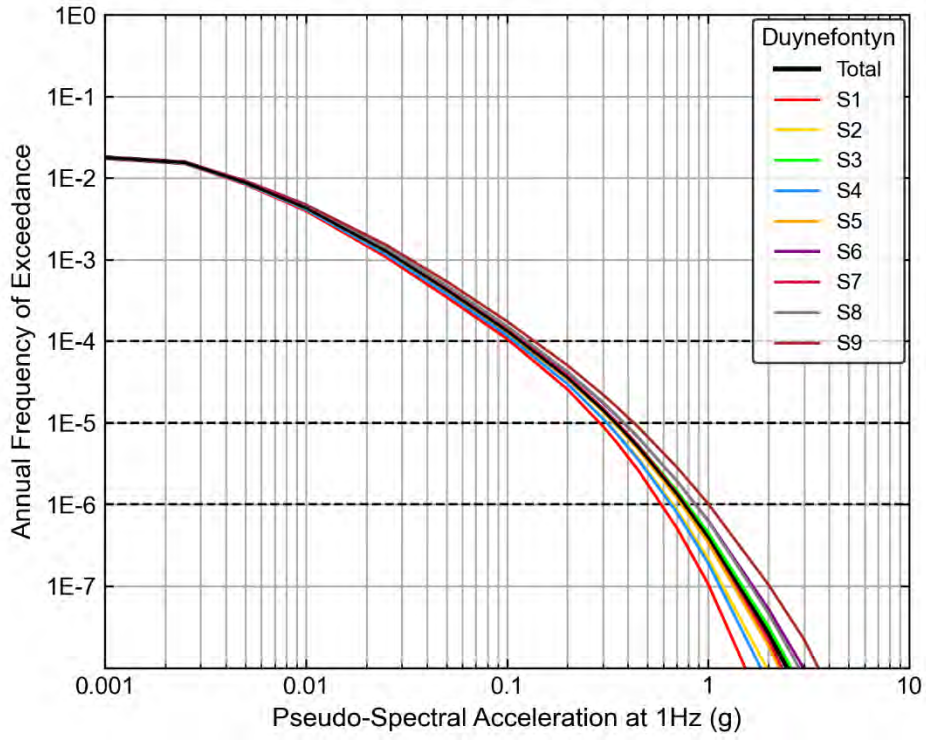

Figure 10-43. Hazard sensitivity to the aleatory variability branches for 1 Hz at the new build site at Duynefontyn.

10.3.2.2 Sensitivity to SSM

This section presents results of sensitivity calculations performed for logic-tree nodes in the SSM including: spatial smoothing, completeness method, regional *b*-value calculation method, the maximum magnitude values and fault type.

10.3.2.2.1 Sensitivity to epistemic uncertainty in spatial smoothing models

The SSM utilised three methods for spatial smoothing of past earthquakes in the source zones. The three methods are uniform smoothing, an adaptive kernel method, and fixed kernel with a 100 km radius. These three alternatives were included in the SSM because the SSM TI Team could not establish the assumption of stationarity for future earthquakes. The SSM TI Team concluded that these three alternatives capture the epistemic uncertainty in the future location of earthquakes based on the spatial distribution of past earthquakes. The hazard curves resulting from the three smoothing types in the host zone for oscillator frequencies of 100, 10, and 1 Hz are presented in Figure 10-44, Figure 10-45, and Figure 10-46, respectively. Hazard curves showing the sensitivity to spatial smoothing for the remaining seven oscillator frequencies are presented in Appendix G.

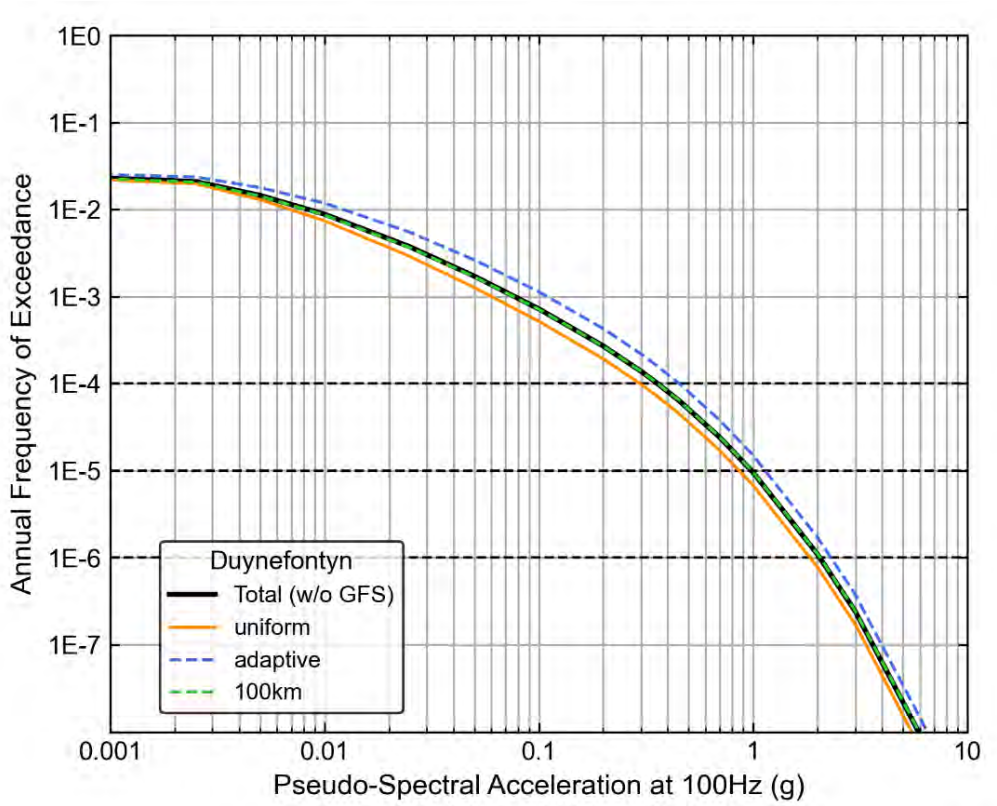

Figure 10-44. Hazard sensitivity for 100 Hz to spatial smoothing in the host zone at the new build site at Duynefontyn.

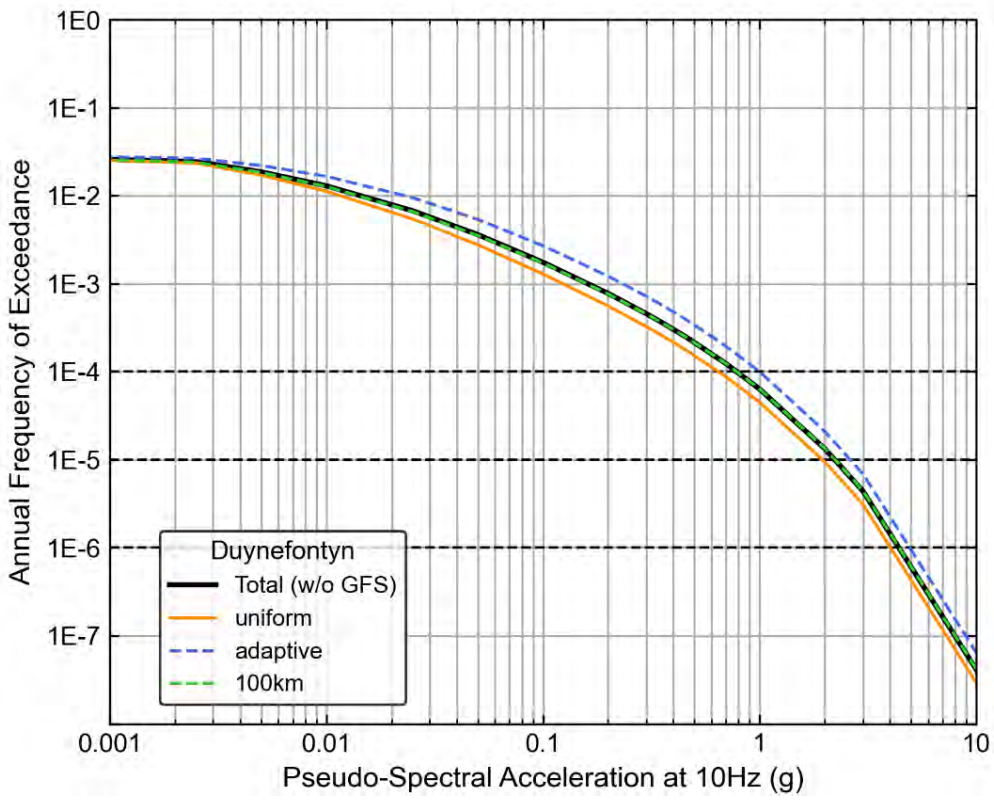

Figure 10-45. Hazard sensitivity for 10 Hz to spatial smoothing in the host zone at the new build site at Duynefontyn.

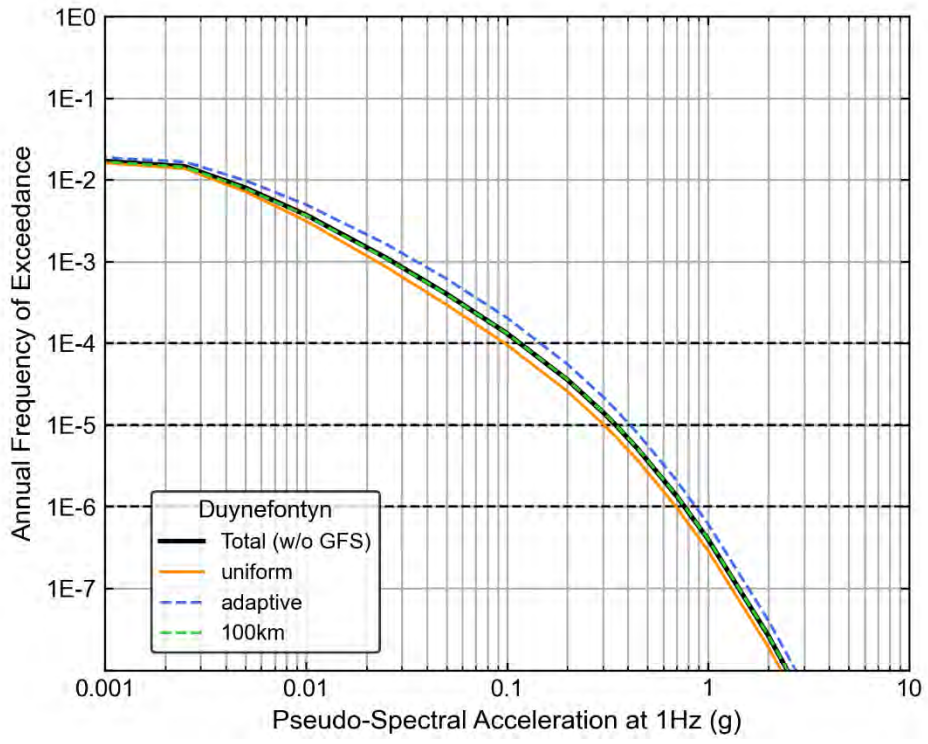

Figure 10-46. Hazard sensitivity for 1 Hz to spatial smoothing in the host zone at the new build site at Duynefontyn.

Unsurprisingly, the adaptive kernel smoothing model produced the highest hazard because it concentrated future seismicity closest to the site. To demonstrate this result virtual ruptures within SDZ for the three smoothing models are shown in Figure 10-47. Uniform smoothing distributes the virtual ruptures evenly throughout the SDZ, the fixed kernel with a 100 km radius has a relatively higher proportion of ruptures in the eastern reaches of SDZ, while the adaptive kernel has the highest concentration of future ruptures nearest the site. These observations are also evident in the CDF plots shown in Figure 10-48. The CDF plots also show the differences in the spatial distribution of virtual ruptures depending on different distance metrics (R_{rup} vs R_{hypo}).

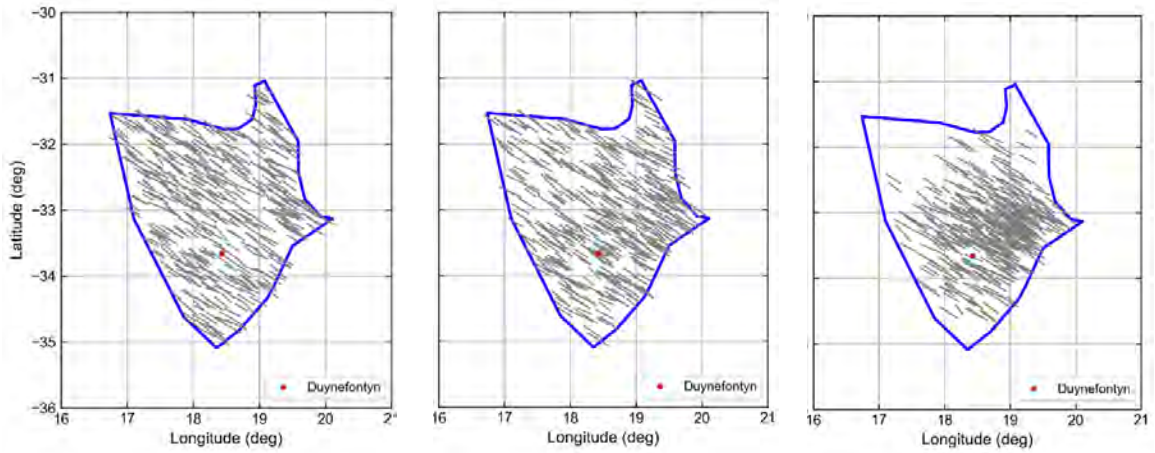

Figure 10-47. Virtual ruptures in the host zone for three smoothing models. a) Uniform, b) fixed kernel with 100 km radius, c) adaptive kernel.

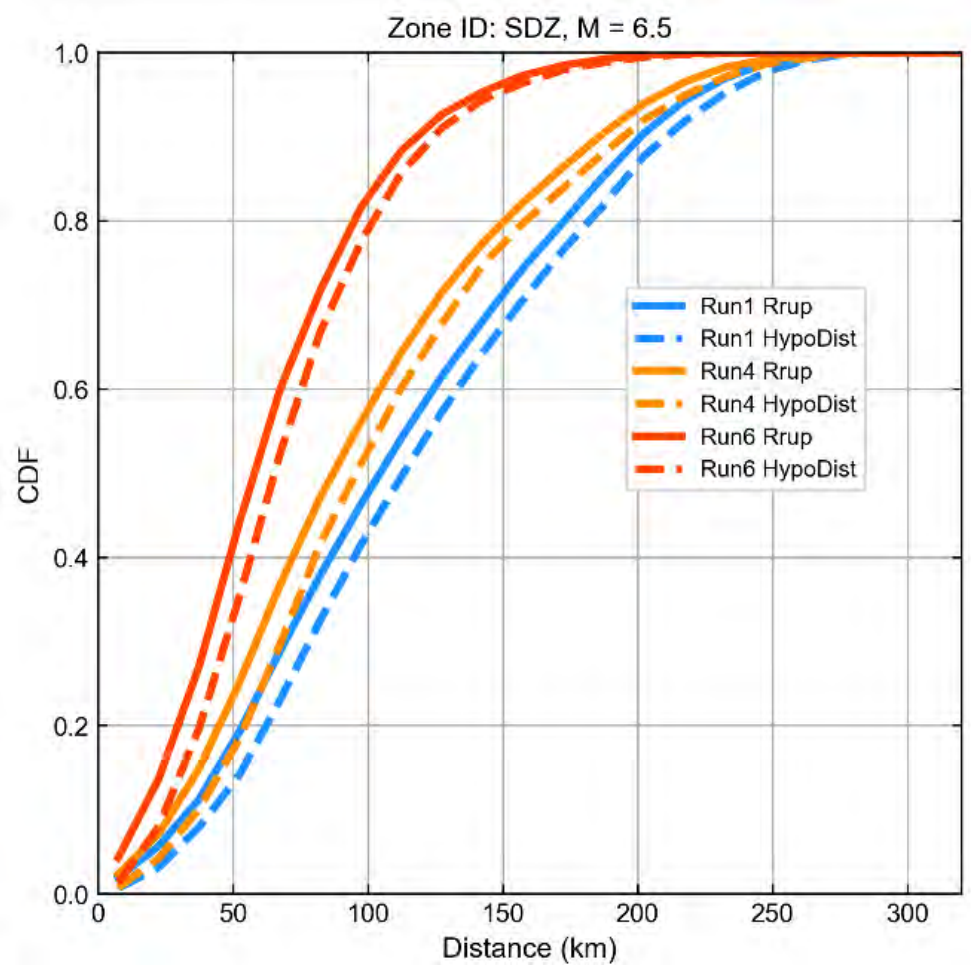

Figure 10-48. CDFs of R_{rup} and R_{hypo} in the host zone for three smoothing models. a) Uniform, b) fixed kernel with 100 km radius, c) adaptive kernel.

10.3.2.2.2 Sensitivity to epistemic uncertainty in Mmax

The SDZ parameters include 17 alternative estimates of Mmax from a fine sample of the continuous posterior Mmax distributions. Additional information about Mmax can be found in Section 8.2.9. The hazard curves resulting from the different Mmax for SDZ for oscillator frequencies of 100, 10, and 1 Hz are presented in Figure 10-49, Figure 10-50, and Figure 10-51, respectively. Hazard curves showing the sensitivity to Mmax for SDZ for the remaining seven oscillator frequencies are presented in Appendix G.

Similar to the Thyspunt PSHA (Bommer et al. 2013), the wide range of Mmax values starting at 6.2, not just the maximum, contributes to hazard sensitivity, but is relatively less important than spatial smoothing models and the epistemic uncertainty in the GMM. The larger epistemic uncertainty at low oscillator frequencies is due to the larger impact of magnitude on low oscillator frequencies as compared to high oscillator frequency, see Figures 10-49 through 10-51.

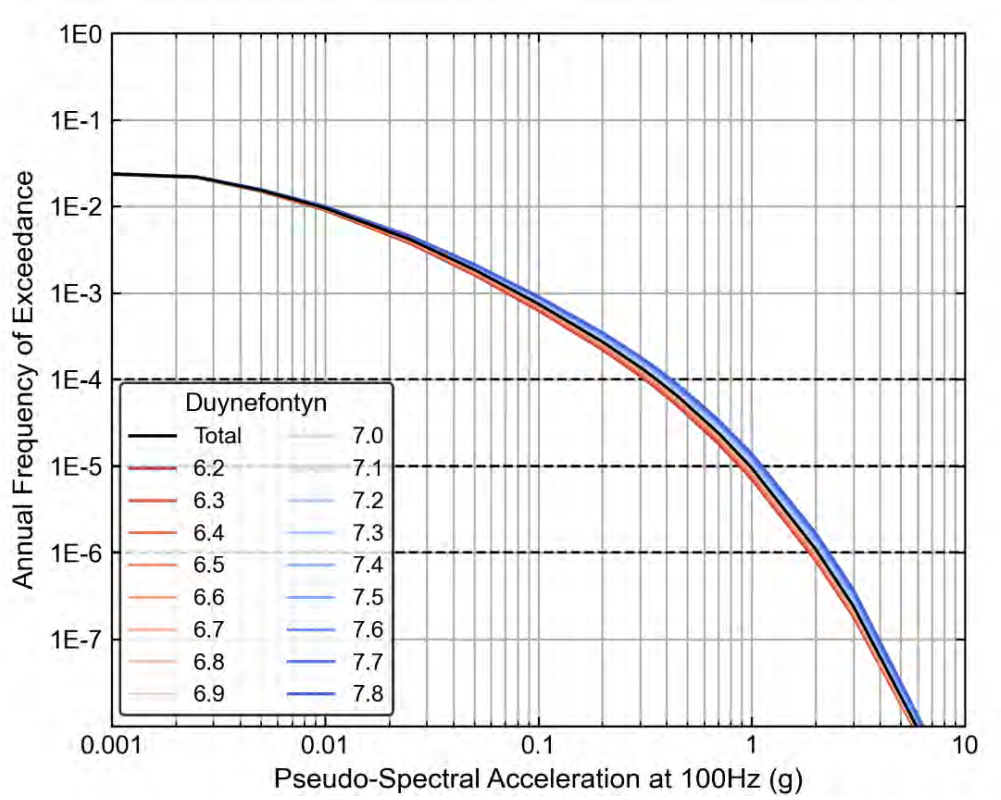

Figure 10-49. Hazard sensitivity for 100 Hz to the host zone maximum magnitude branches at the new build site at Duynefontyn.

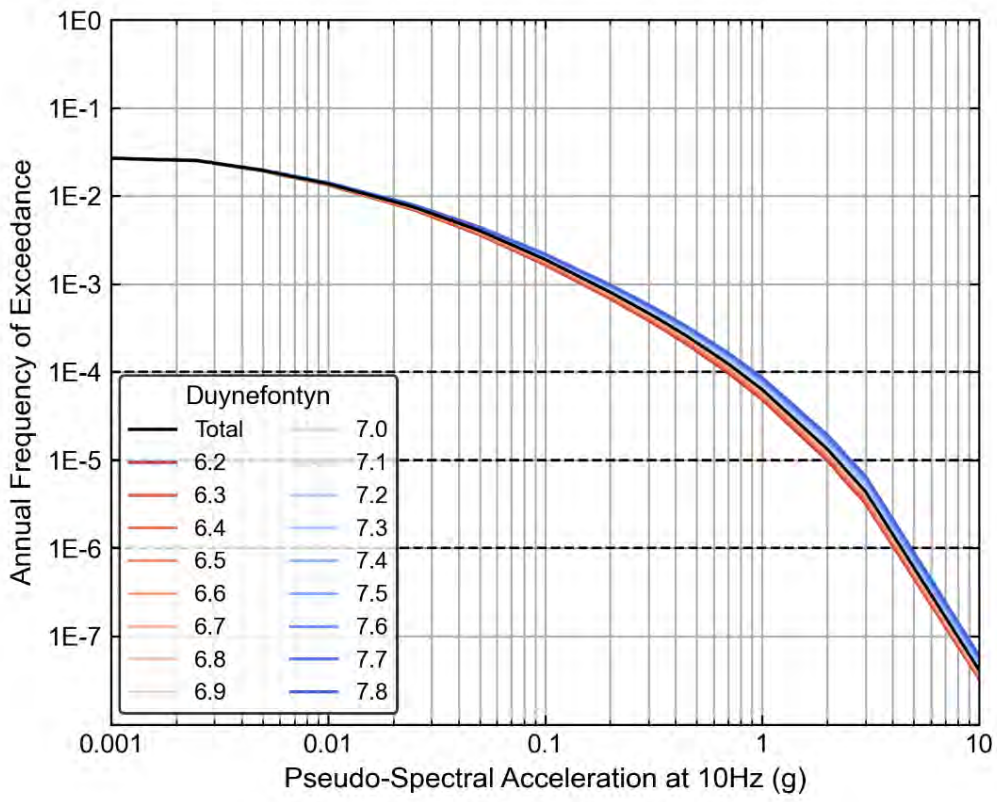

Figure 10-50. Hazard sensitivity for 10 Hz to the host zone maximum magnitude branches at the new build site at Duynefontyn.

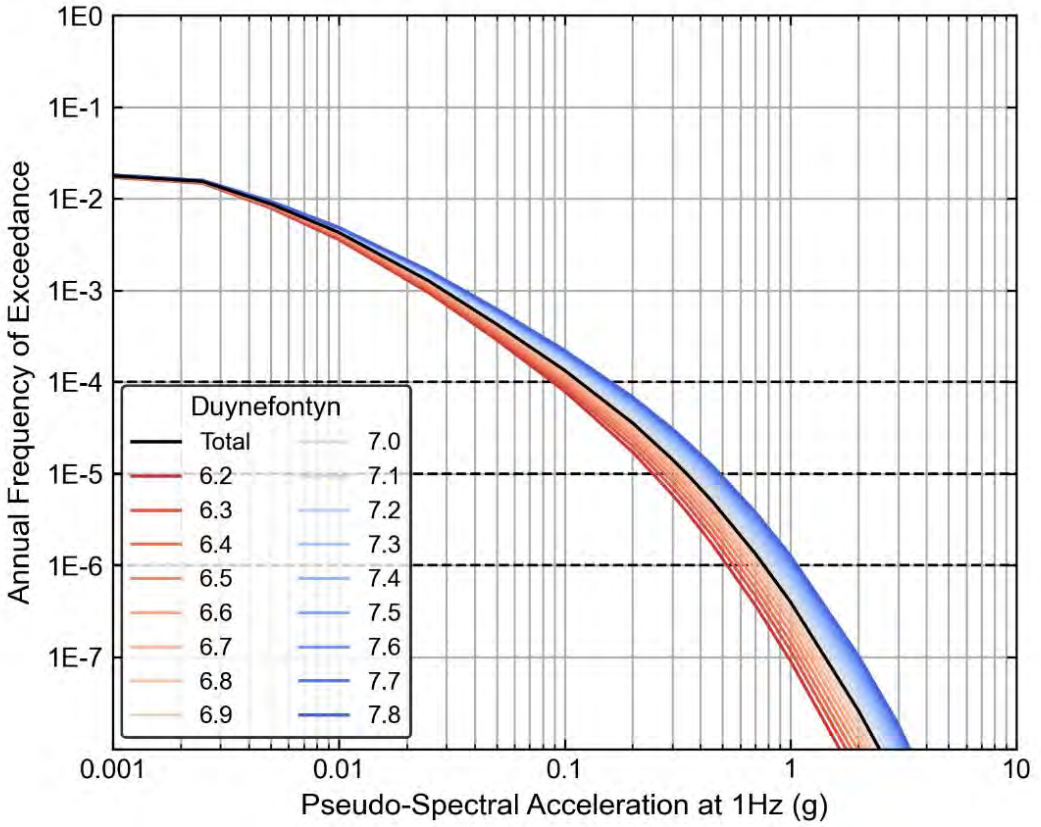

Figure 10-51. Hazard sensitivity for 1 Hz to the host zone maximum magnitude branches at the new build site at Duynefontyn.

10.3.2.2.3 Sensitivity to epistemic uncertainty in completeness method

The SSM included two different completeness methods as described in Section 8.2.4. These are the probability of detection method (PD) and Stepp plot analysis (CC). The hazard curves resulting from the different completeness methods for oscillator frequencies of 100, 10, and 1 Hz are presented in Figure 10-52, Figure 10-53, and Figure 10-54, respectively. Hazard curves showing the sensitivity to completeness method for the remaining seven oscillator frequencies are presented in Appendix G. The mean presented in these figures removes the contribution of the GFS (indicated as w/out GFS) to directly compare the impact of completeness method on hazard results from the source zones. The completeness method effects the number, and thus rate, of small earthquakes and shows some spread in the hazard curve results for AFE above 10^{-2}.

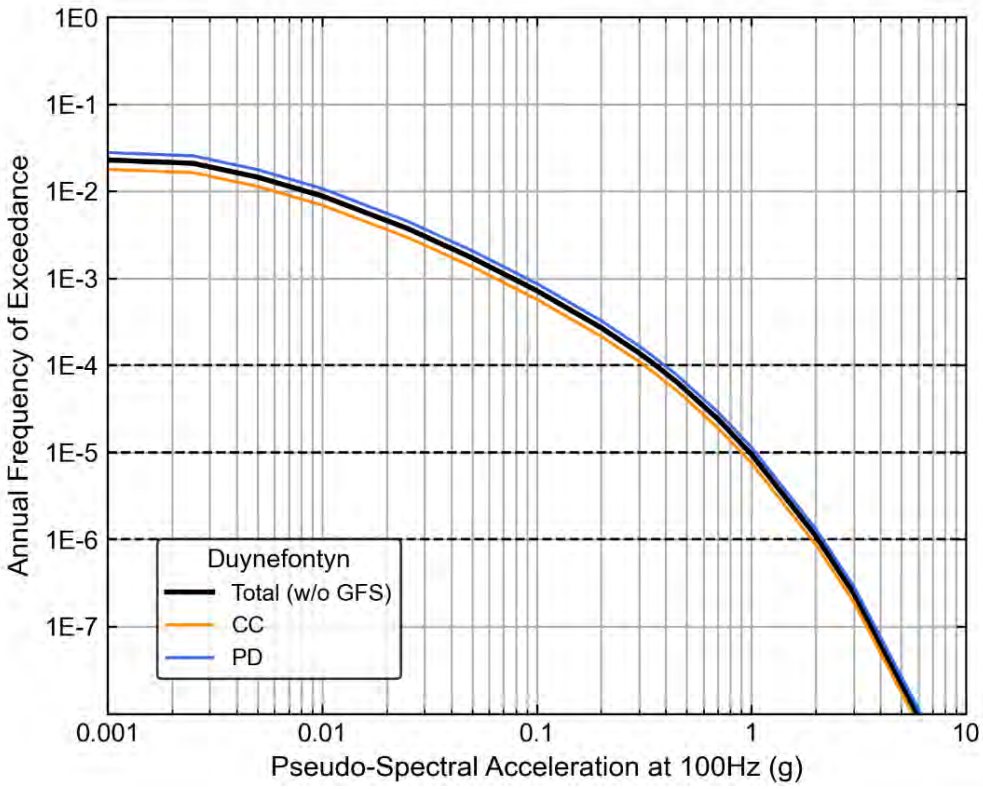

Figure 10-52. Hazard sensitivity for 100 Hz to completeness method branches at the new build site at Duynefontyn.

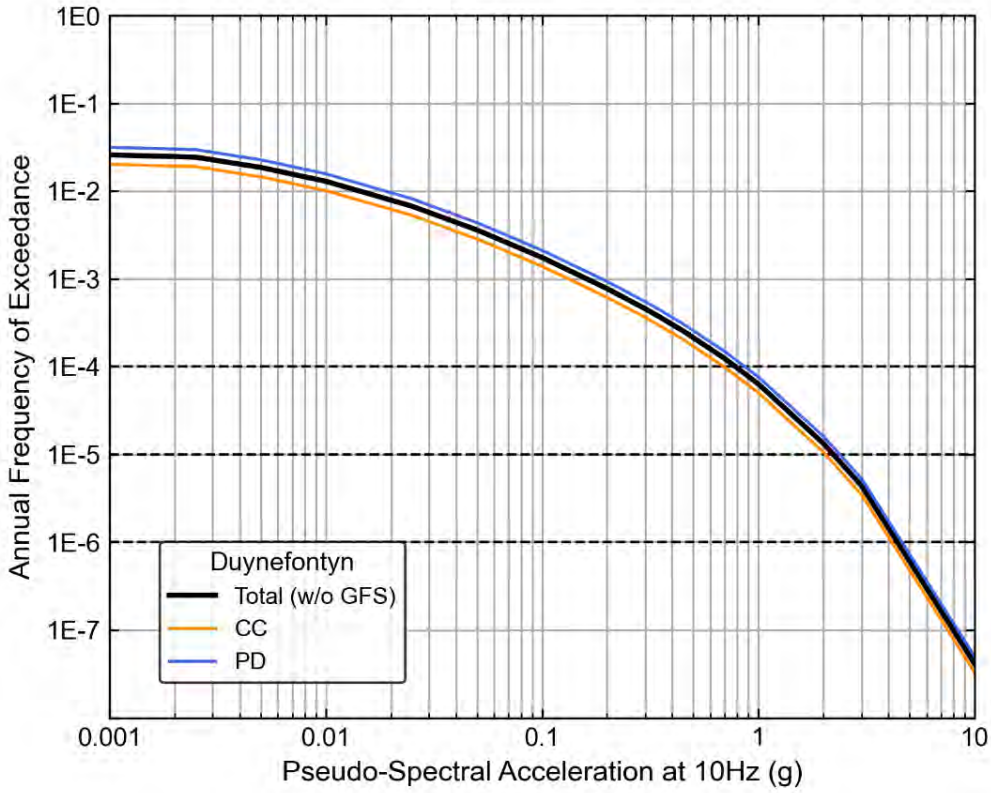

Figure 10-53. Hazard sensitivity for 10 Hz to completeness method branches at the new build site at Duynefontyn.

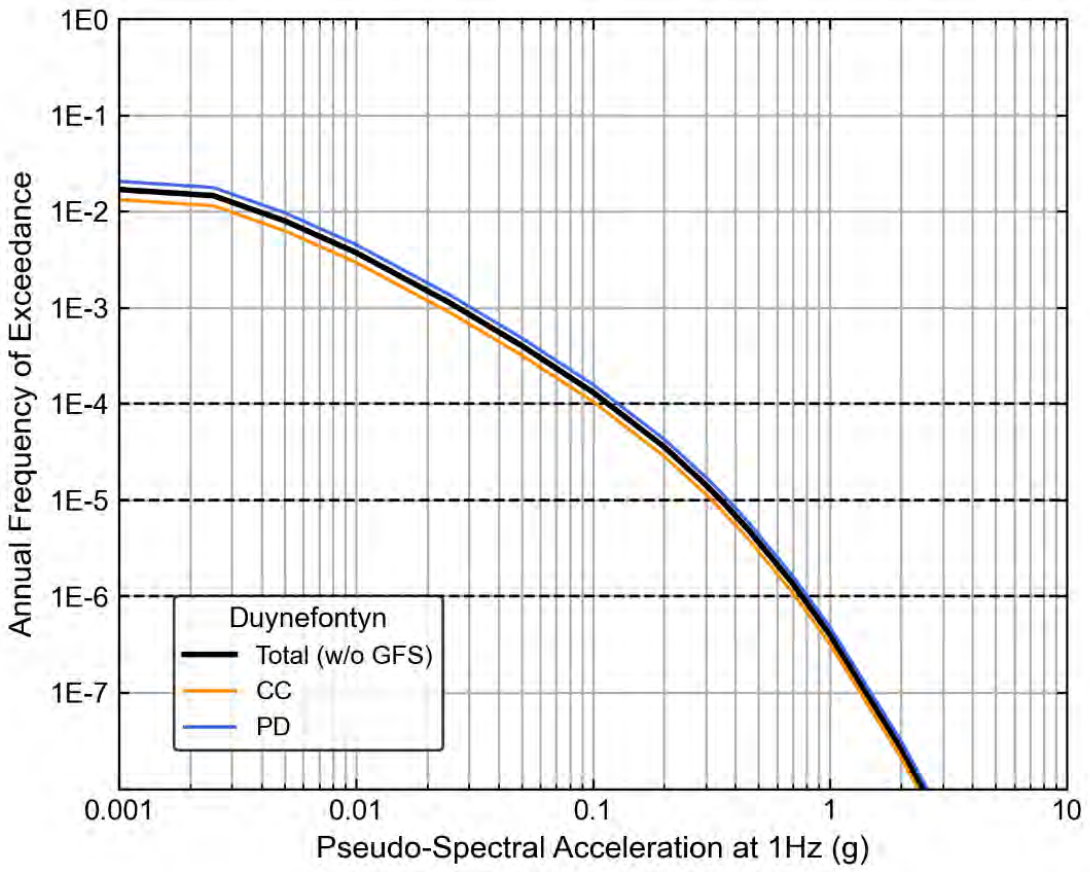

Figure 10-54. Hazard sensitivity for 1 Hz to completeness method branches at the new build site at Duynefontyn.

10.3.2.2.4 Sensitivity to aleatory variability in SDZ rupture type

Virtual ruptures in the SDZ were modelled as a combination of strike-slip (SS) and normal (NM) earthquakes. The details are discussed in Section 8.2.5. The hazard curves resulting from the two different rupture types for oscillator frequencies of 100, 10, and 1 Hz are presented in Figure 10-55, Figure 10-56, and Figure 10-57, respectively. Hazard curves showing the sensitivity to SDZ fault type for the remaining seven oscillator frequencies are presented in Appendix G. Though not an element of epistemic uncertainty, sensitivity results for this analysis show that SS ruptures produce slightly larger ground-motions than NM earthquakes. This difference reflects the difference in GMM for these two styles of earthquake ruptures.

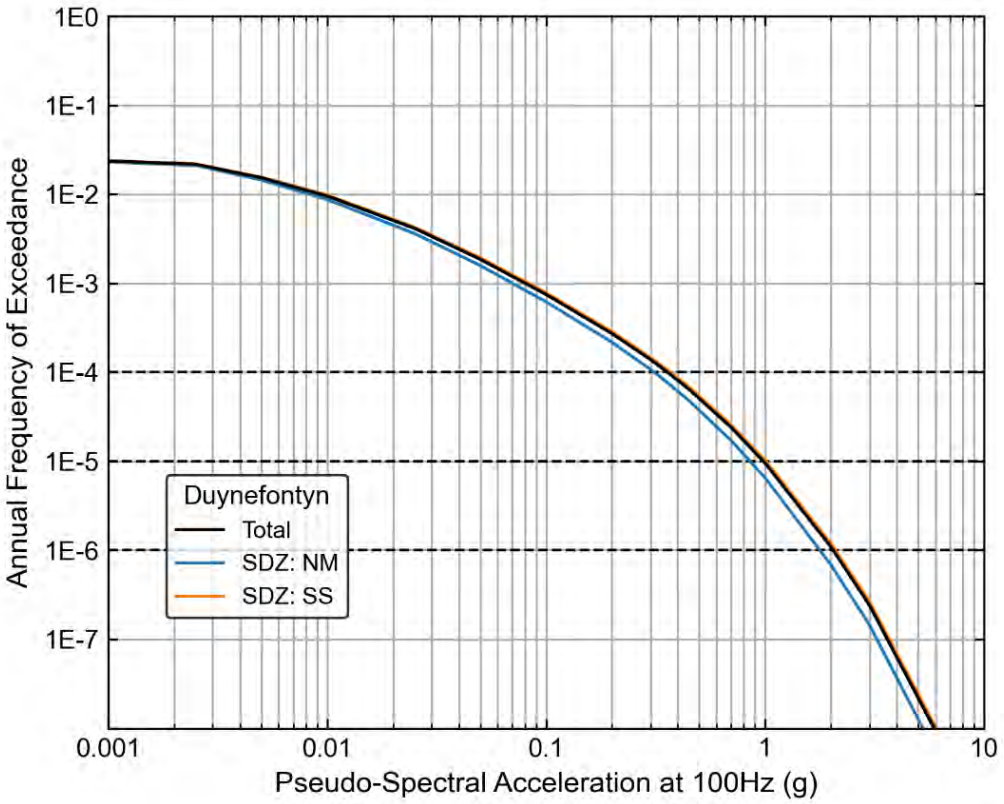

Figure 10-55. Hazard sensitivity for 100 Hz to fault mechanism in the host zone for the new build site at Duynefontyn.

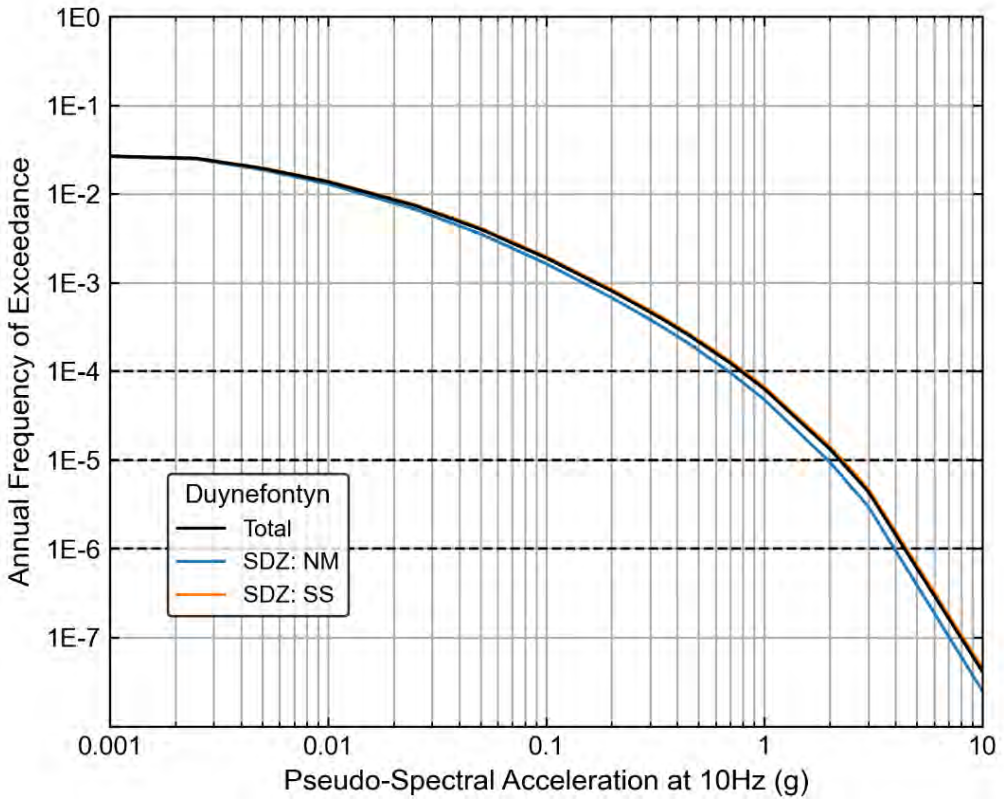

Figure 10-56. Hazard sensitivity for 10 Hz to fault mechanism in the host zone for the new build site at Duynefontyn.

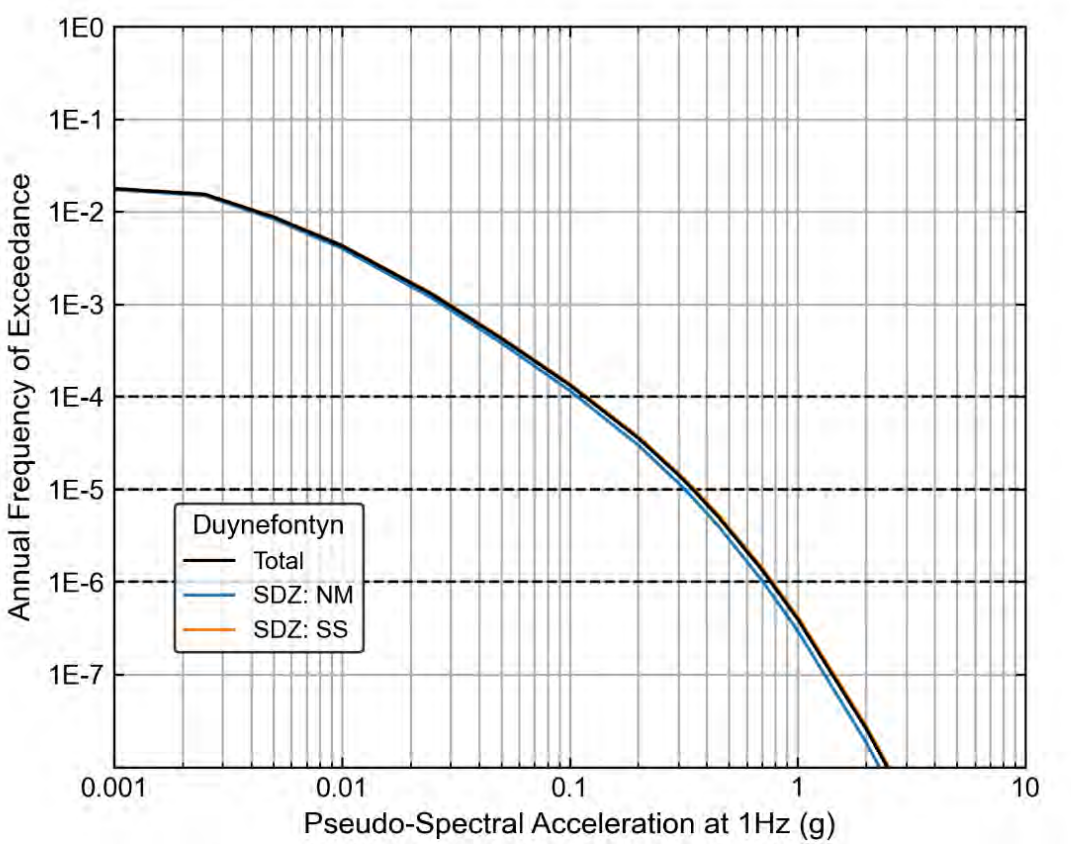

Figure 10-57. Hazard sensitivity for 1 Hz to fault mechanism in the host zone for the new build site at Duynefontyn.

10.3.2.2.5 Sensitivity to epistemic uncertainty in regional b-Value calculation method

Two methods were used to estimate the *b*-values for the source zones as described in Section 8.2.10. The first is the maximum likelihood method (LL) and the second is the *b*-positive method (BP). The hazard curves resulting from the different *b*-value calculation methods for oscillator frequencies of 100, 10, and 1 Hz are presented in Figure 10-58, Figure 10-59, and Figure 10-60, respectively. Hazard curves showing the sensitivity to the *b*-value calculation method for the remaining seven oscillator frequencies are presented in Appendix G. As demonstrated in the figures below, the hazard sensitivity at all frequencies shows insignificant variation due to *b*-value calculation method (approximately 1% above and below the mean).

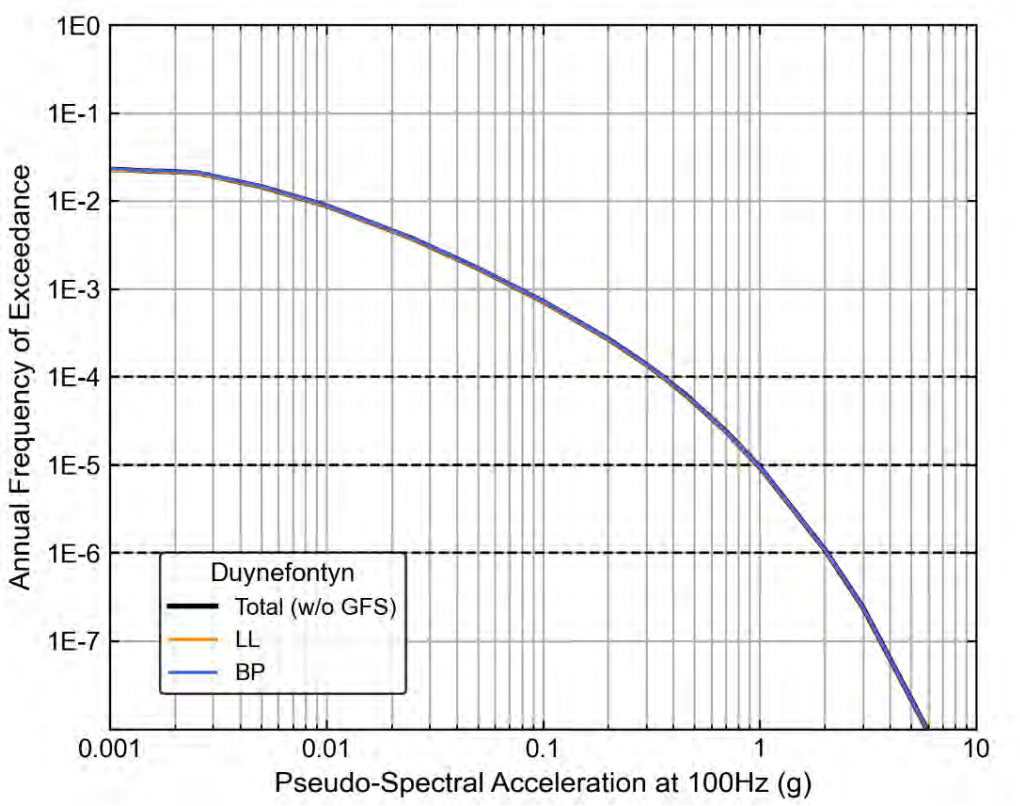

Figure 10-58. Hazard sensitivity to regional *b*-value calculation method for 100 Hz at the new build site at Duynefontyn

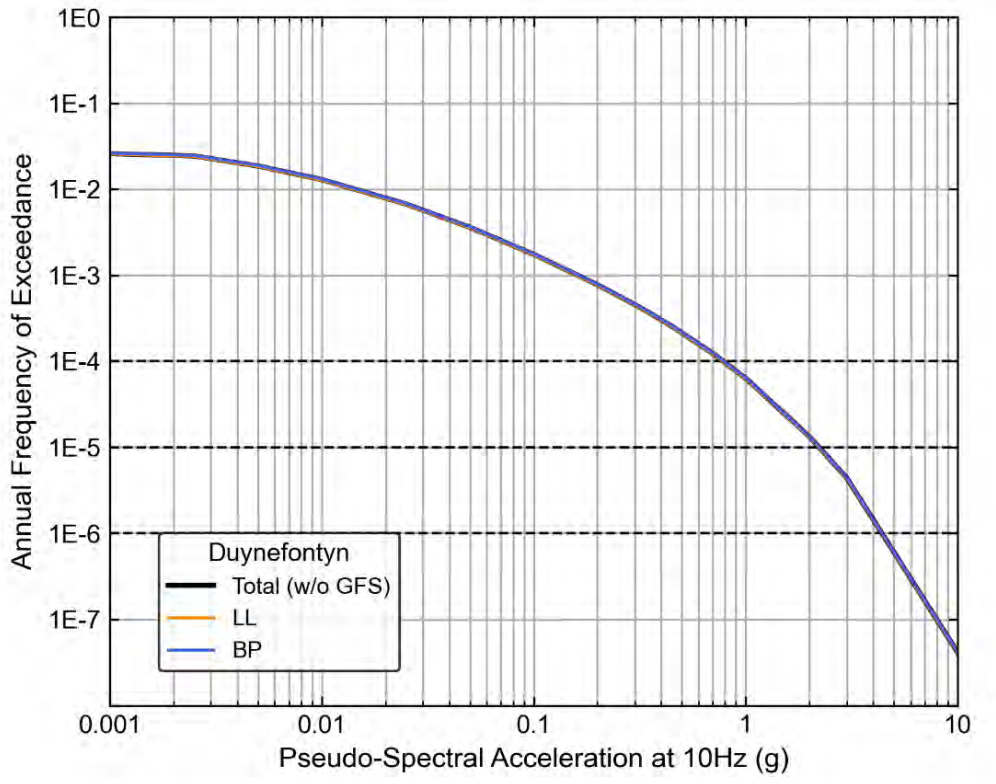

Figure 10-59. Hazard sensitivity to regional *b*-value calculation method for 10 Hz at the new build site at Duynefontyn.

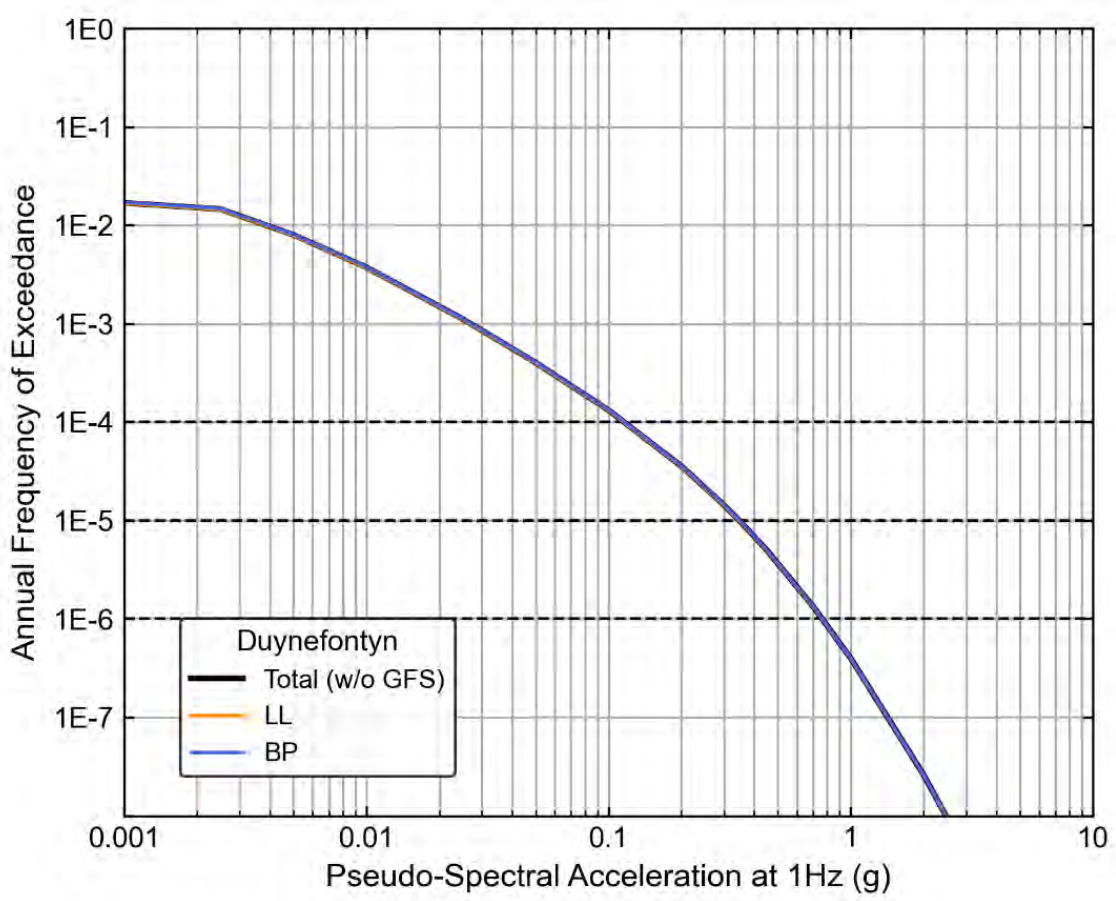

Figure 10-60. Hazard sensitivity to regional *b*-value calculation method for 1 Hz at the new build site at Duynefontyn.

10.4 KOEBERG NUCLEAR POWER STATION SEISMIC HAZARD RESULTS

The following sections provide figures of the hazard results at the KNPS for oscillator frequencies of 100, 10 and 1 Hz. The total mean seismic hazard curves and source contribution curves are presented for all ten oscillator frequencies. Three fractile hazard curves are presented at 100, 10, and 1 Hz for the host zone. The disaggregation results for magnitude-distance are presented at AFEs of 10^{-4}, 10^{-5}, and 10^{-6}, followed by the UHRS at AFEs from 10^{-3} to 10^{-8} and the DRS. Finally, sensitivity analyses are presented for the 100, 10, and 1 Hz for multiple parameters in the overarching model. The analyses of the hazard results and the sensitivities for KNPS are identical to those described for the KNPS at Duynefontyn in Section 10.3. Hazard curves showing the sensitivity for the remaining seven oscillator frequencies are presented in Appendix H.

10.4.1 Seismic hazard curves

Figure 10-61 depicts the total mean hazard curves for each of the ten oscillator frequencies. The grey dashed lines show the three AFE values used in the disaggregation.

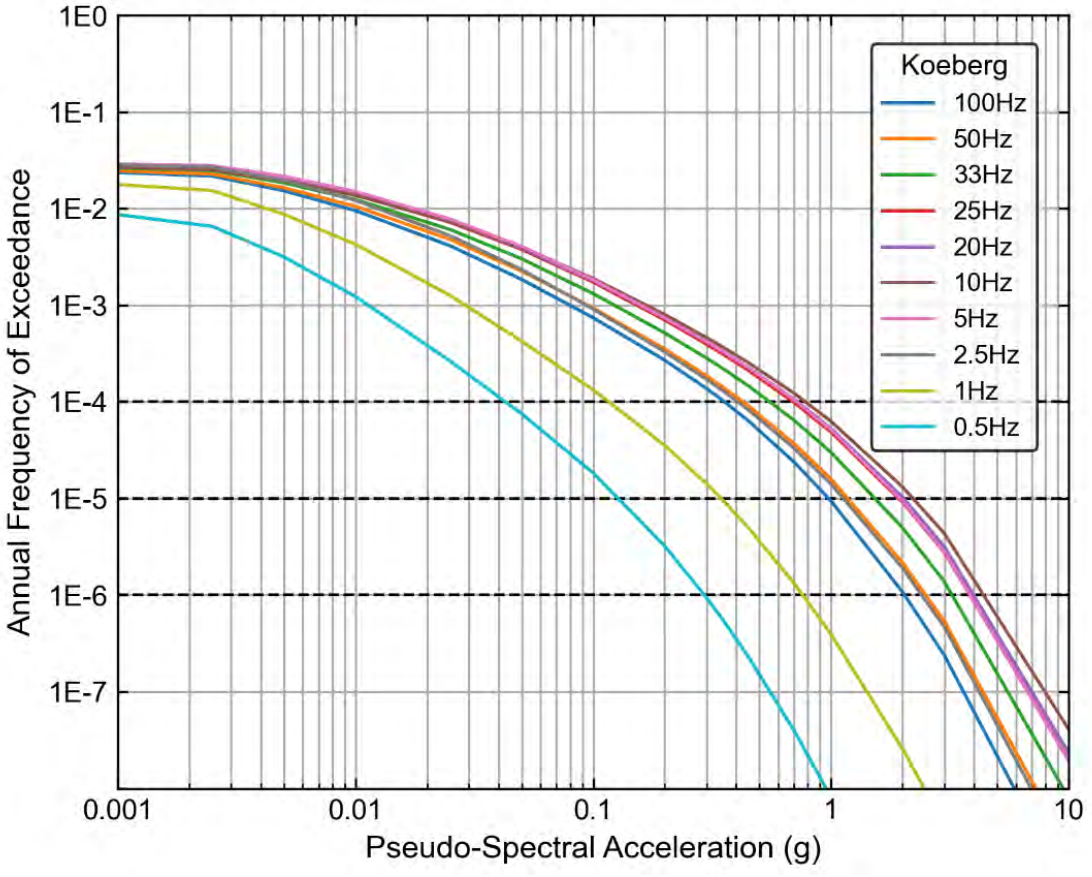

Figure 10-61. Hazard results for the KNPS.

10.4.1.1 Fractiles

Figure 10-62 to Figure 10-64 depict the fractile results for the KNPS at Duynefontyn for 100, 10, and 1 Hz, respectively. The black line in each figure represents the median, the red line the mean, the dashed lines represent the 5th and 95th percentiles, and the dotted lines

represent the 15th and 85th percentiles. The pseudo-spectral acceleration values associated with each are presented in Table 10-9 for an AFE of 10^{-4}, which demonstrates the uncertainty in the pseudo-spectral acceleration values computed for the KNPS at Duynefontyn.

As is typical, the mean hazard curves approach higher fractiles as the AFEs increase. At both 100 Hz (Figure 10-62) and 10 Hz (Figure 10-63) the total mean hazard crosses the 85th percentile hazard curve at higher AFE values because there is larger epistemic uncertainty in the tails of the distribution at these frequencies. The slope of the mean hazard curve is a combination of the epistemic uncertainty and the aleatory variability, whereas the slope of the median is largely representative of the aleatory variability.

Table 10-9. Pseudo-spectral acceleration values for the presented fractiles at the KNPS for an AFE of 10^{-4}

Frequency (Hz)	5th	15th	Median	Mean	85th	95th
100	0.110	0.147	0.268	0.357	0.494	0.705
10	0.228	0.311	0.553	0.780	1.077	1.599
1	0.043	0.057	0.096	0.116	0.158	0.213

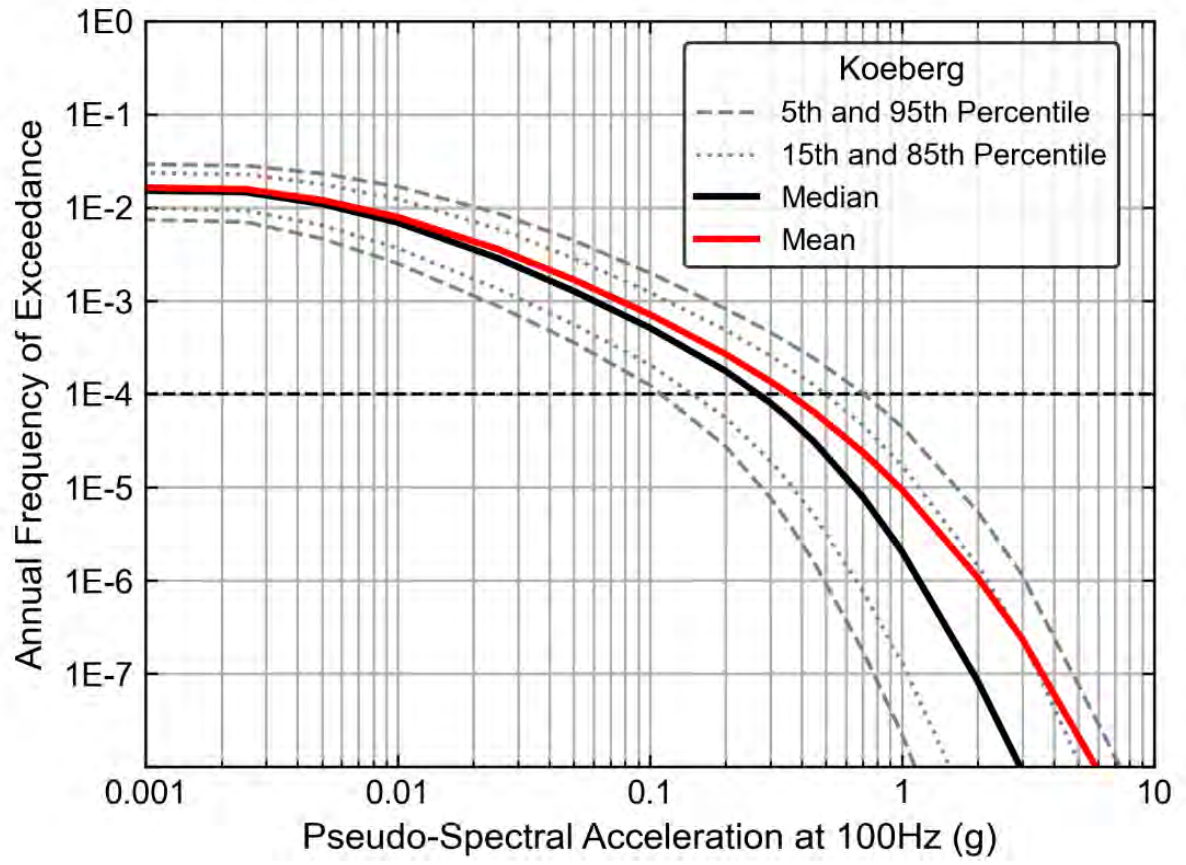

Figure 10-62. Fractile hazard curves for the host zone at 100 Hz at the KNPS.

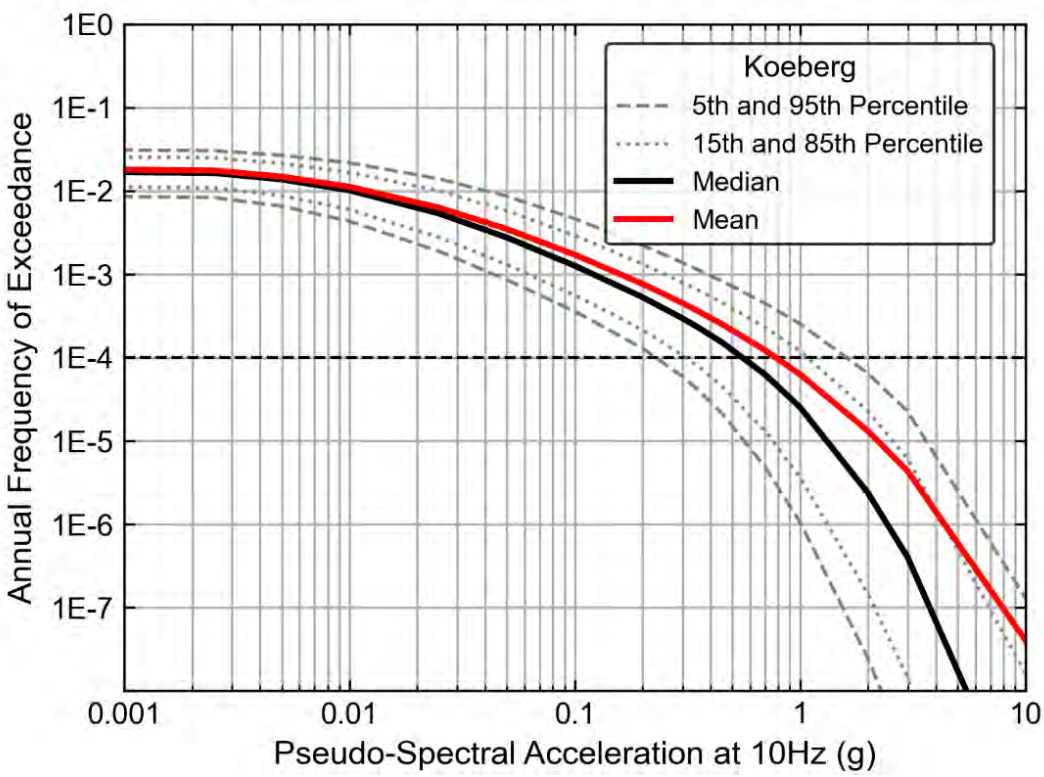

Figure 10-63. Fractile hazard curves for the host zone at 10 Hz at the KNPS.

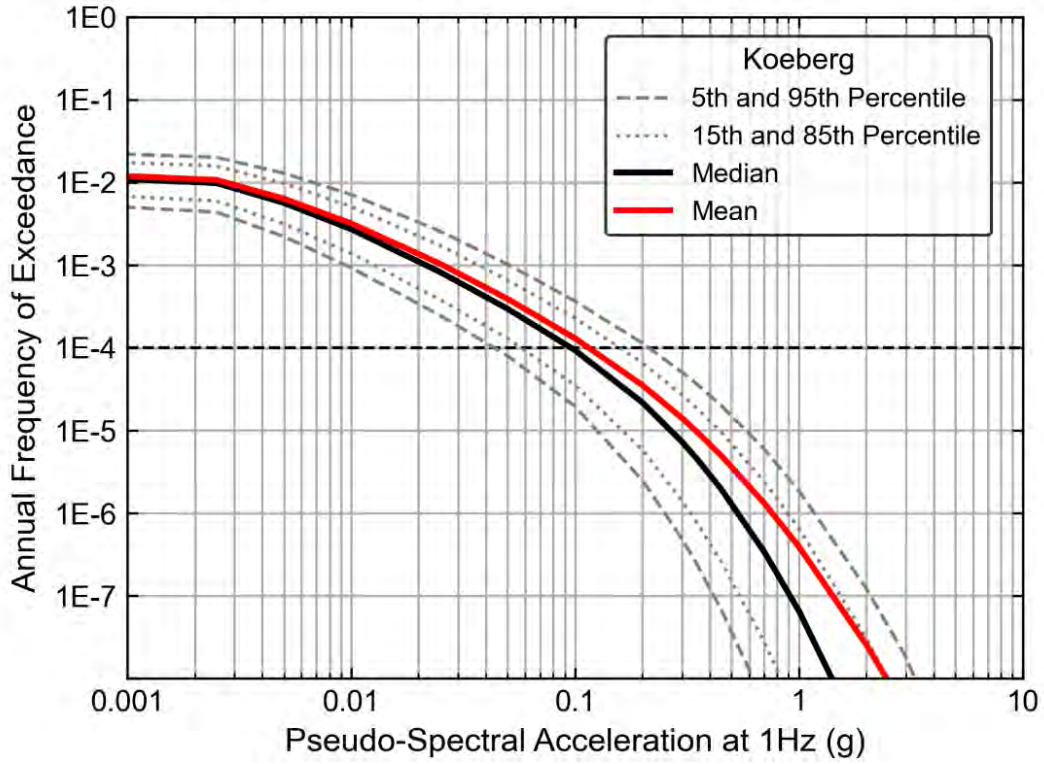

Figure 10-64. Fractile hazard curves for the host zone at 1 Hz at the KNPS.

10.4.1.2 Contributions by seismic source

The following section presents the hazard contribution from each seismic source at the KNPS at Duynefontyn for the ten oscillator frequencies. The KNPS at Duynefontyn is within the SDZ and approximately 50 km from the Groenhof Fault Source. Figure 10-65 to Figure 10-74 show the total mean hazard (black line), the Saldania Zone (SDZ, host zone, red), Olifants River Zone (ORZ, yellow), Agulhas Zone (AGZ, green), Orange Basin Zone (OBZ, blue), Combined Outer Zone (COZ, orange), and the Groenhof Fault Source (GFS, purple). For the KNPS at Duynefontyn, the largest contributing source is the SDZ followed by GFS for all oscillator frequencies.

As evident in these figures, the total hazard is dominated by the contribution from the SDZ at AFEs less than 10^{-2}. This is not surprising because the activity rate in the SDZ is higher than the other source zones and the earthquakes in this zone are closest to the site. For example, Figure 8-15 shows the highest concentration of earthquakes occur in the SDZ based on the adaptive kernel model for spatial smoothing. The small contribution of the Groenhof Fault Source reflects the minimal slip rate (mean slip rate of 0.01 mm/yr).

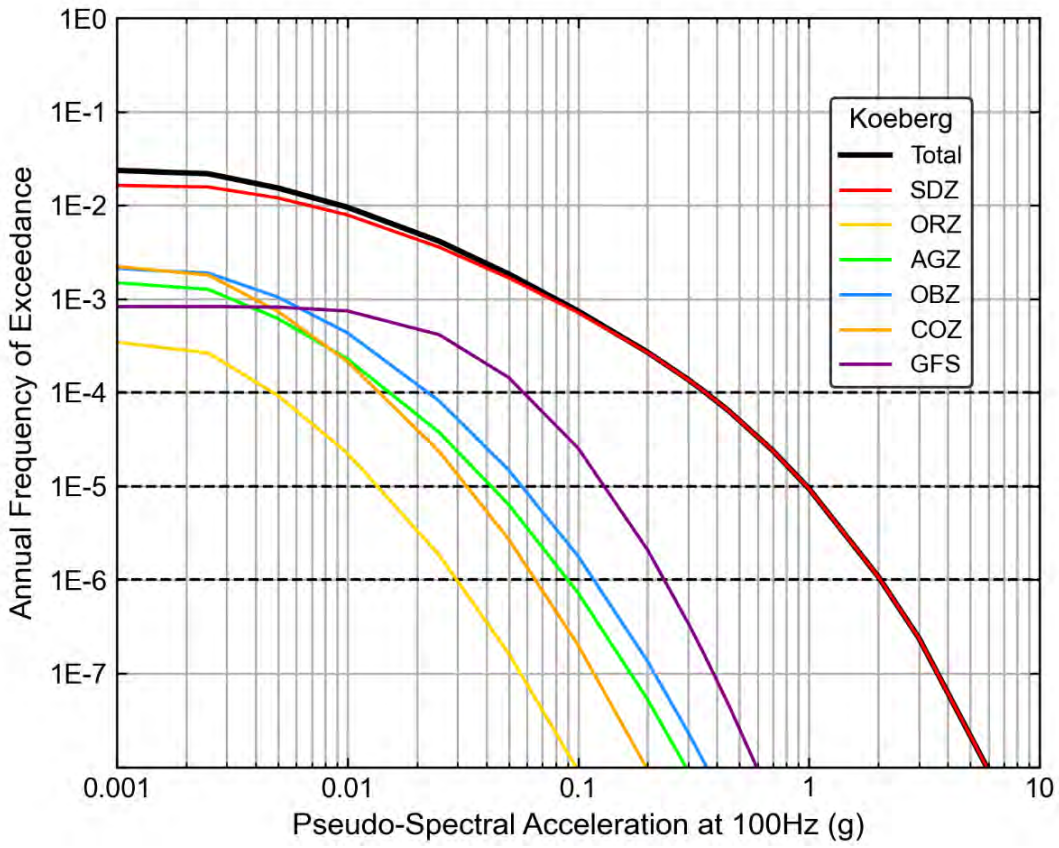

Figure 10-65. Source contribution hazard curves for 100 Hz at the KNPS.

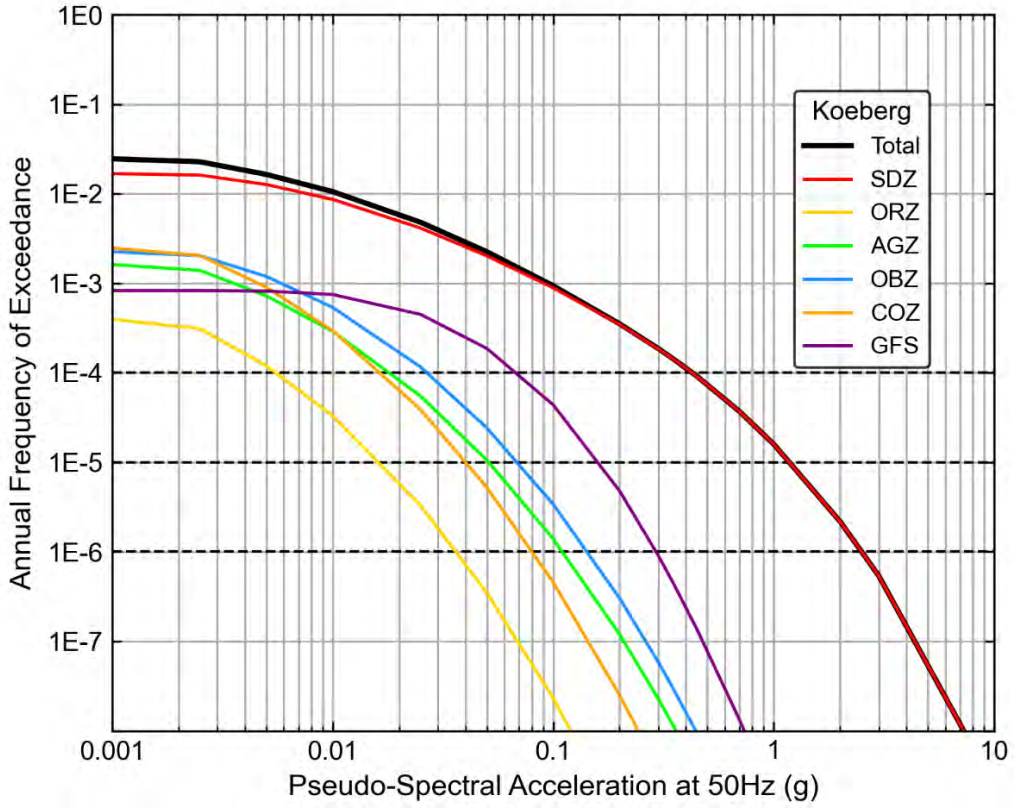

Figure 10-66. Source contribution hazard curves for 50 Hz at the KNPS.

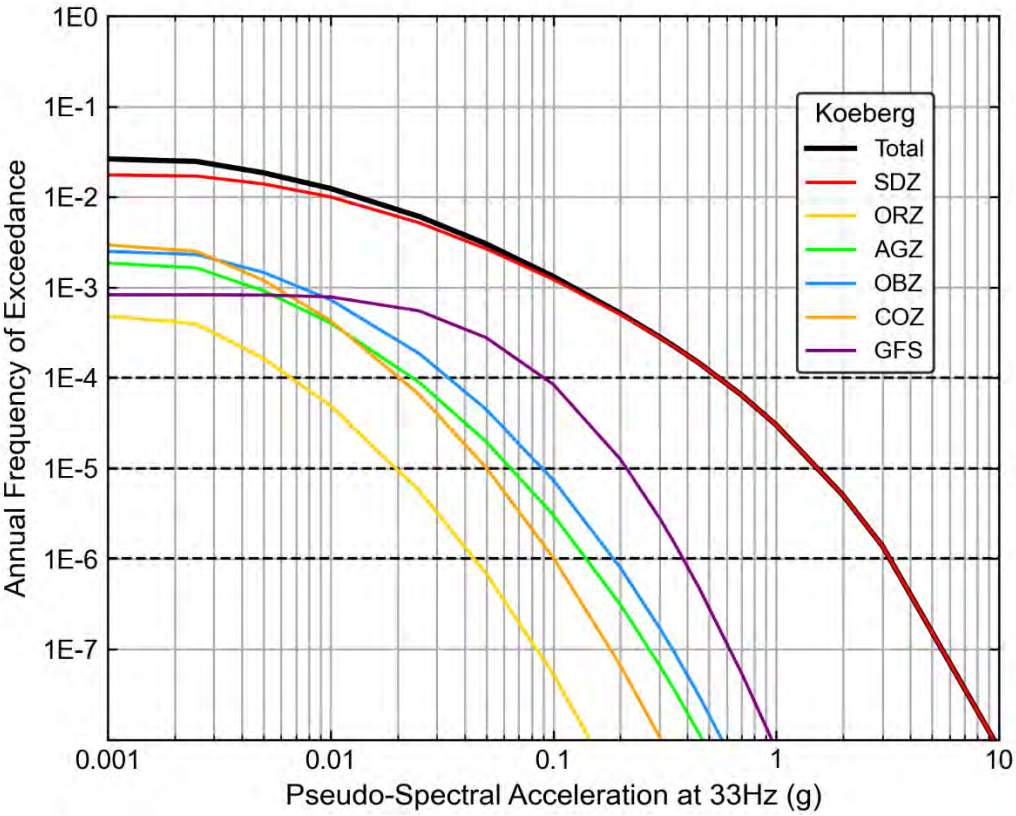

Figure 10-67. Source contribution hazard curves for 33 Hz at the KNPS.

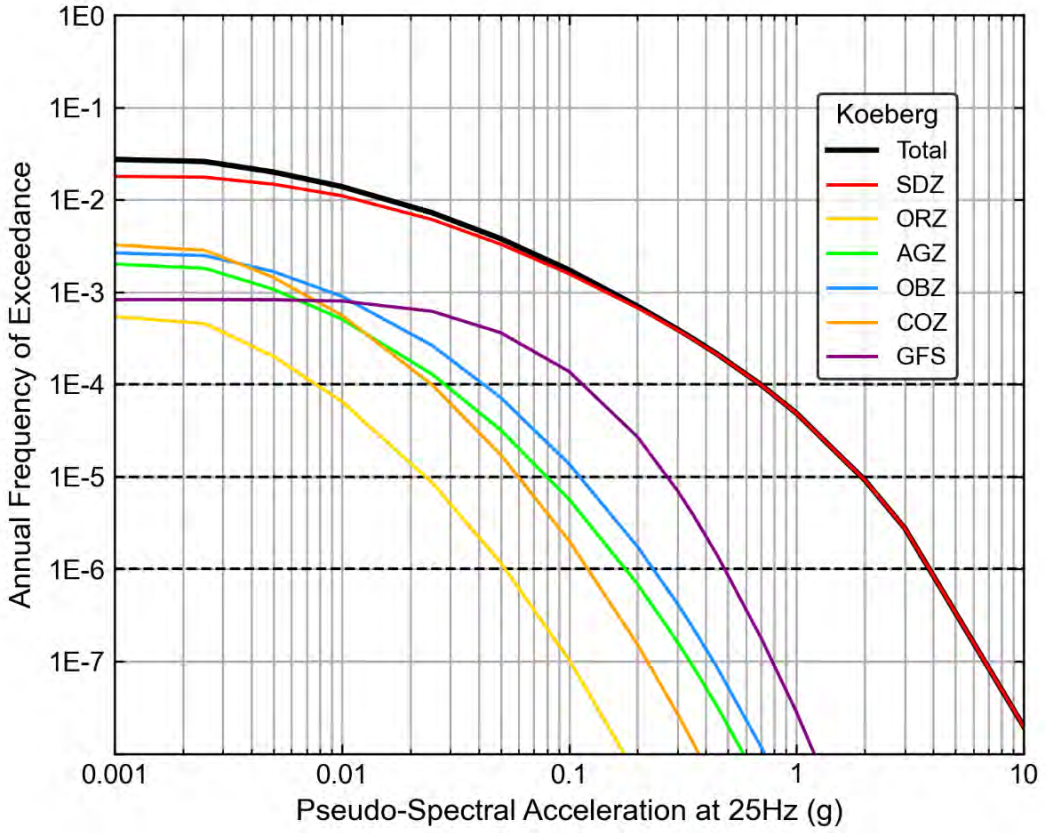

Figure 10-68. Source contribution hazard curves for 25 Hz at the KNPS.

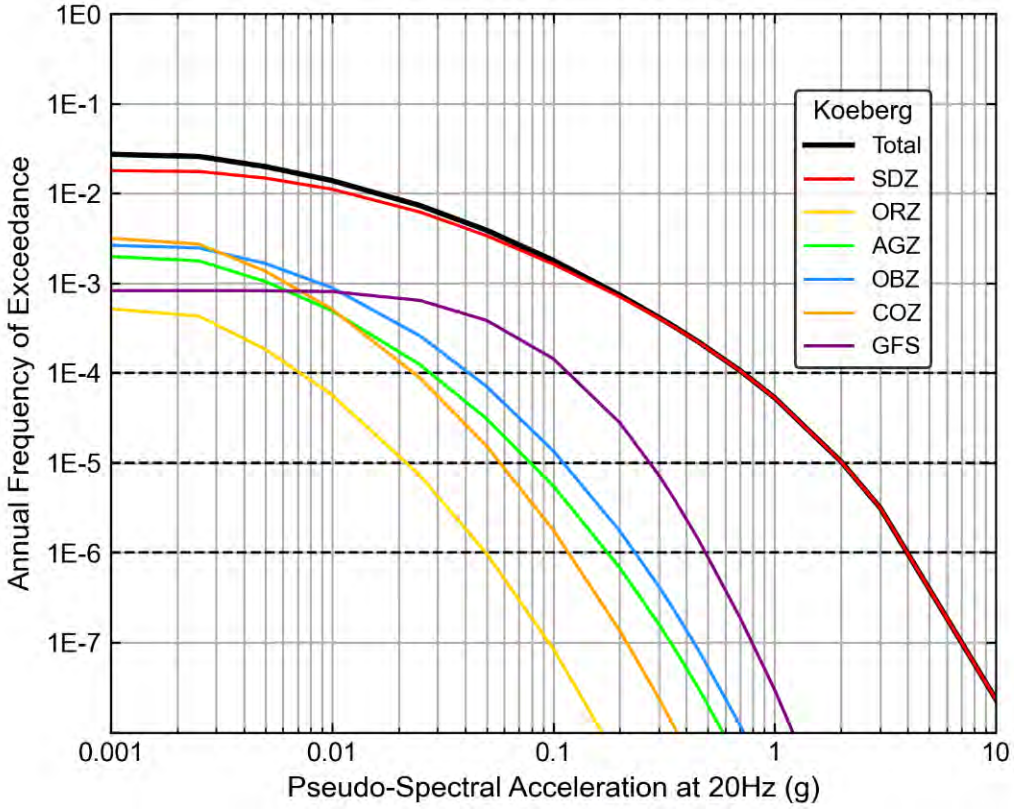

Figure 10-69. Source contribution hazard curves for 20 Hz at the KNPS.

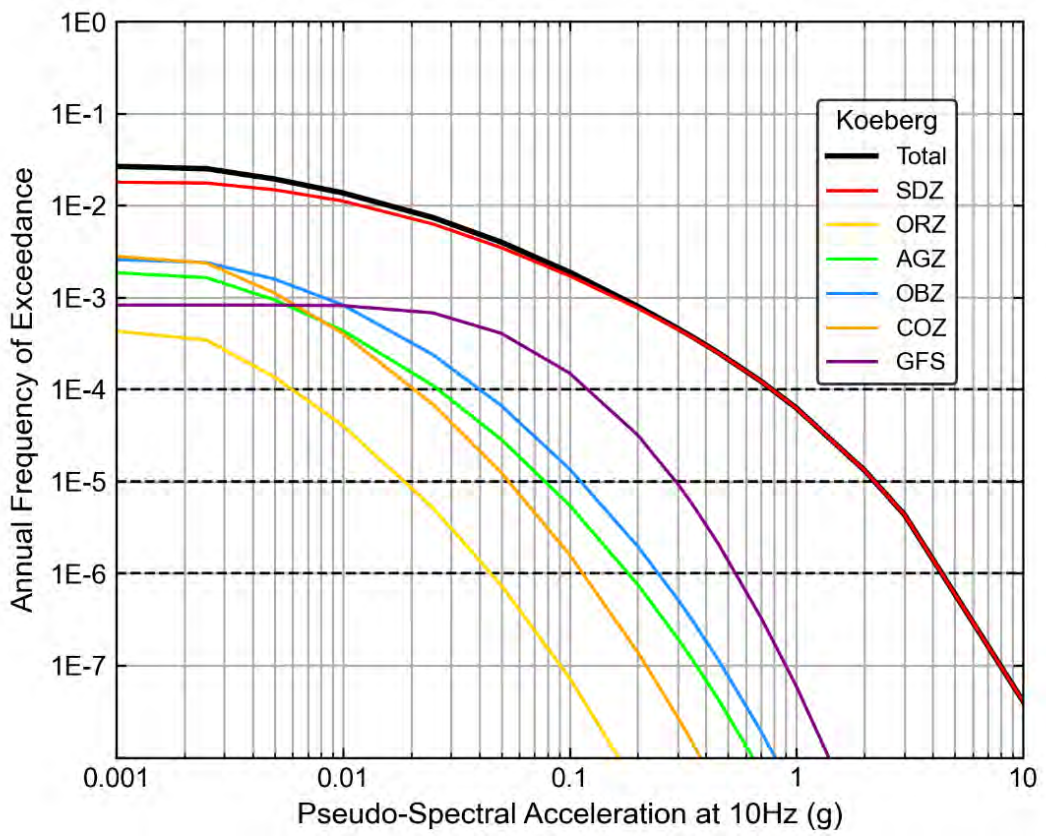

Figure 10-70. Source contribution hazard curves for 10 Hz at the KNPS.

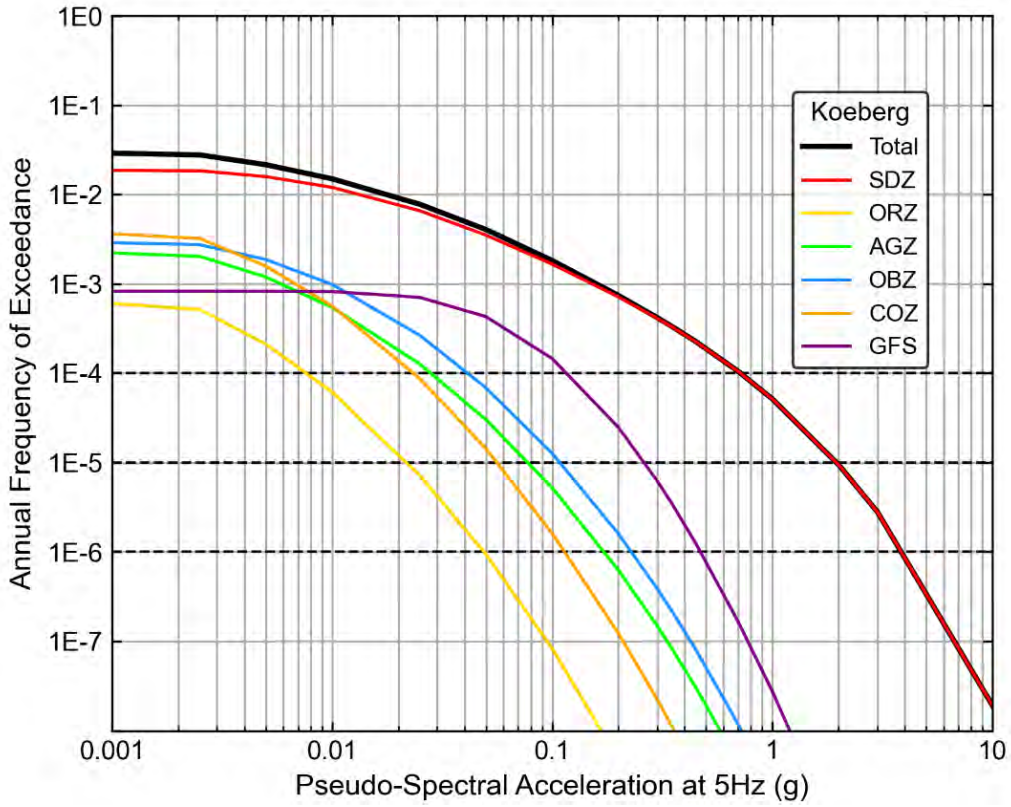

Figure 10-71. Source contribution hazard curves for 5 Hz at the KNPS.

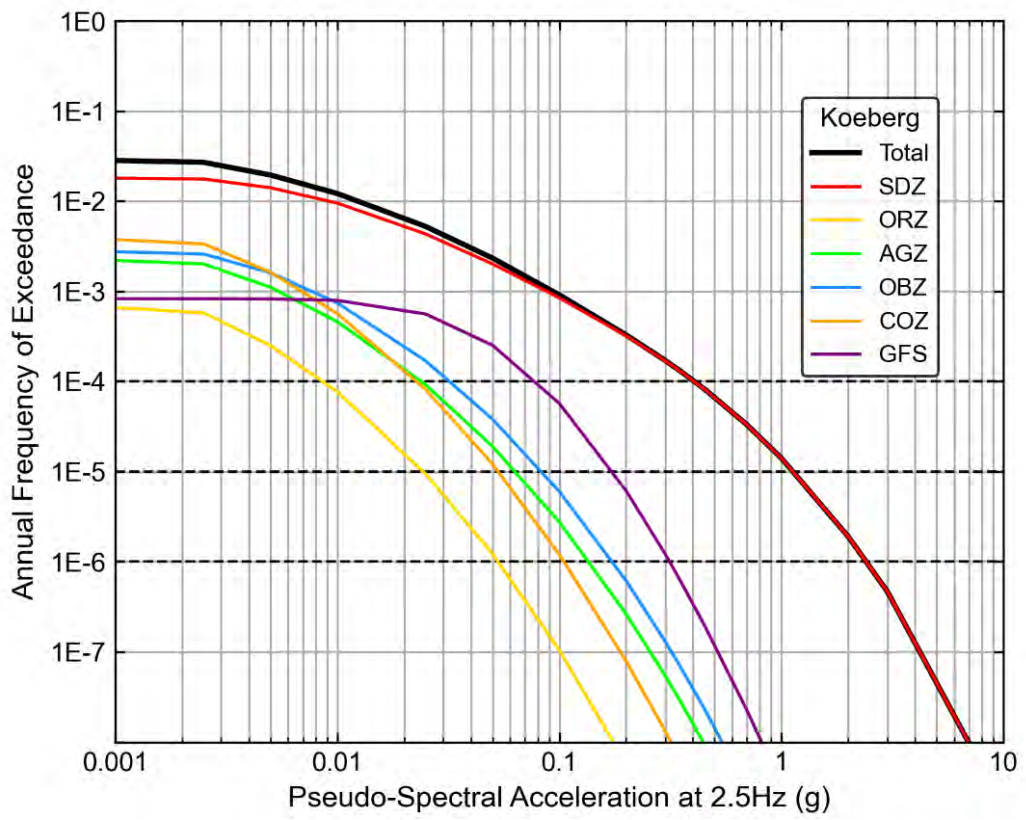

Figure 10-72. Source contribution hazard curves for 2.5 Hz at the KNPS.

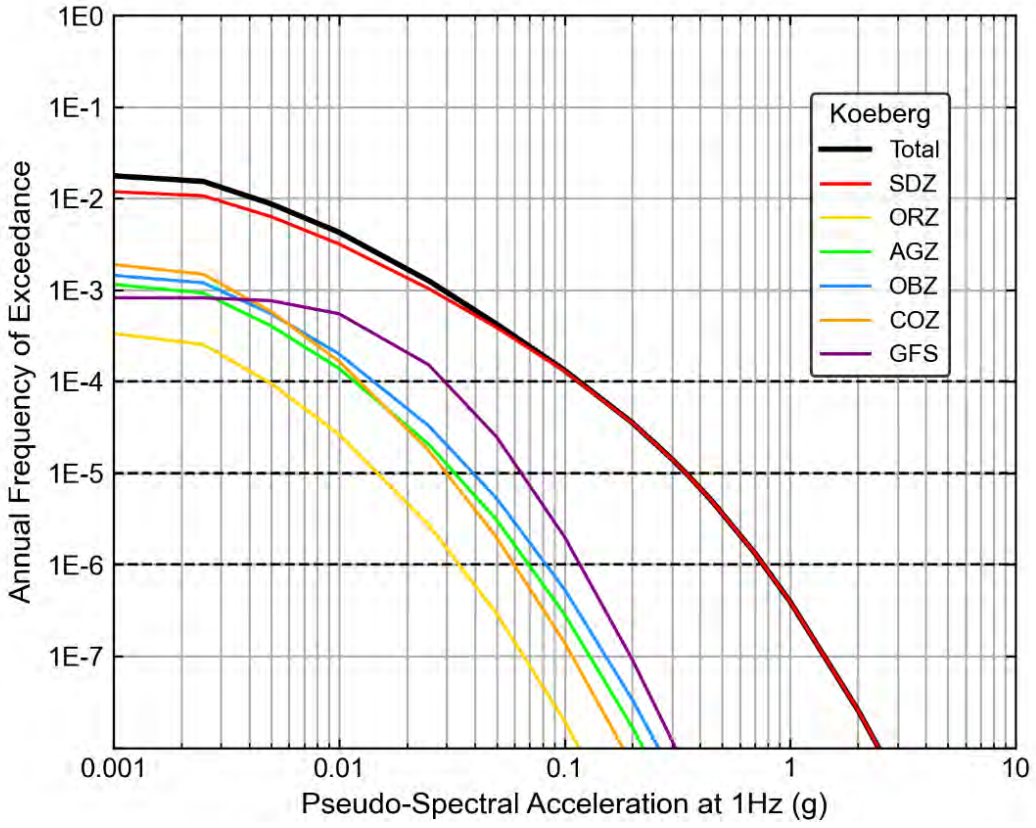

Figure 10-73. Source contribution hazard curves for 1 Hz at the KNPS.

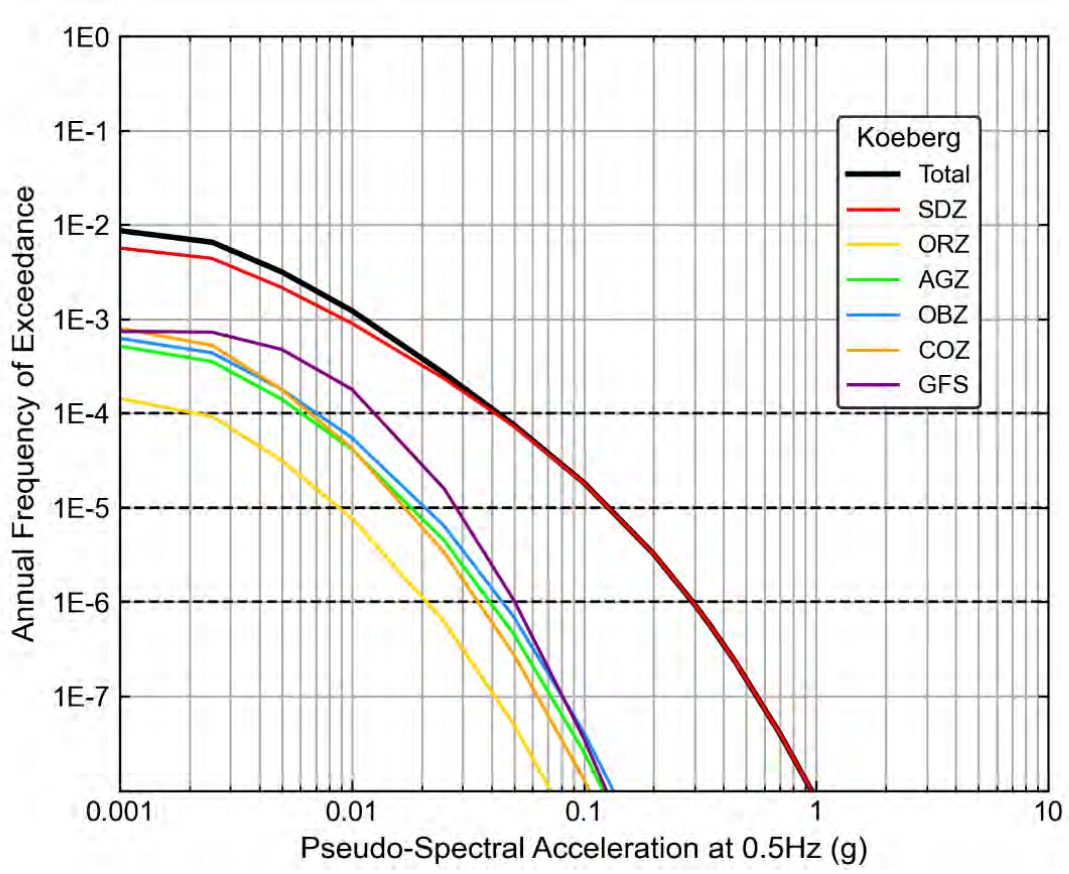

Figure 10-74. Source contribution hazard curves for 0.5 Hz at the KNPS.

10.4.1.3 Contributions by magnitude, distance and epsilon scenarios

The following section presents the disaggregation of the total mean hazard by magnitude and distance at the KNPS at Duynefontyn for the ten oscillator frequencies. The disaggregation was performed for AFEs of 10^{-4}, 10^{-5}, and 10^{-6}. Figure 10-75 to Figure 10-84 show the hazard disaggregation results at each of the three AFEs for various magnitude and distance pairs for all ten oscillator frequencies.

As demonstrated in the Figure 10-75 to Figure 10-84and

Table 10-10, earthquakes with approximately **M** 6 located close to the site are the dominant contributors to the hazard. For oscillator frequencies of 10 to 100 Hz the modal magnitude and distance is **M** 5.1 to 5.3 at 15 km. It should be noted that the modal magnitude and distance are taken as the centre of the disaggregation bins. For oscillator frequencies of 0.5 and 5 Hz the modal magnitude and distance ranges from **M** 5.5 to 6.3 at 15 km. The mean magnitudes are slightly higher than the mode, ranging from **M** 5.8 to 6.3 for 10^{-4}. For smaller oscillator frequencies, larger more distant earthquakes contribute slightly more to hazard, but this contribution is still minimal compared to the nearby earthquakes in the SDZ. The epsilon values for all oscillator frequencies at 10^{-4} range widely from less than negative two to above positive two. At lower AFEs, this changes to epsilons primarily greater than one for all oscillator frequencies.

Table 10-10. Modal and Mean magnitude and distance pairings for the KNPS.

Frequency (Hz)	10^{-4}				10^{-5}				10^{-6}			
	Mode		Mean		Mode		Mean		Mode		Mean	
	M	Dist. (km)	M	Dist. (km)	M	Dist. (km)	M	Dist. (km)	M	Dist. (km)	M	Dist. (km)
100	5.3	15	5.9	13.7	5.5	7.5	5.9	9.1	5.5	7.5	5.9	7.4
50	5.1	15	5.9	14.3	5.5	7.5	5.9	9.7	5.5	7.5	5.9	7.6
33	5.1	15	5.8	14.8	5.5	7.5	5.9	9.9	5.5	7.5	5.9	7.7
25	5.1	15	5.8	14.6	5.5	7.5	5.9	9.7	5.5	7.5	5.9	8.2
20	5.1	15	5.9	14.3	5.5	7.5	5.9	9.4	5.5	7.5	5.9	8.1
10	5.1	15	5.9	14.3	5.5	7.5	5.9	9.6	5.5	7.5	5.9	8.4
5	5.5	15	5.9	13.4	5.5	7.5	6.0	8.9	5.5	7.5	6.0	7.5
2.5	5.7	15	6.0	13.7	5.9	7.5	6.1	8.5	5.9	7.5	6.3	6.3
1	6.1	15	6.2	17.6	6.1	7.5	6.4	8.6	6.5	7.5	6.6	6.1
0.5	6.3	15	6.4	26.2	6.5	7.5	6.6	10.5	6.7	7.5	6.7	6.2

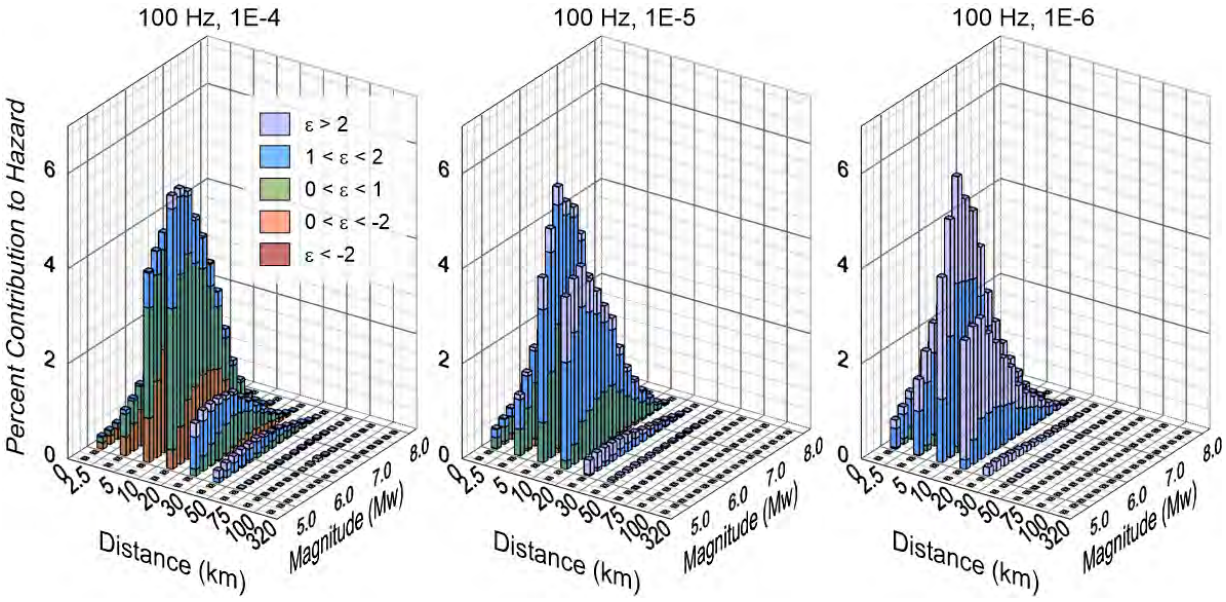

Figure 10-75. Disaggregation for three AFEs at 100 Hz at the KNPS.

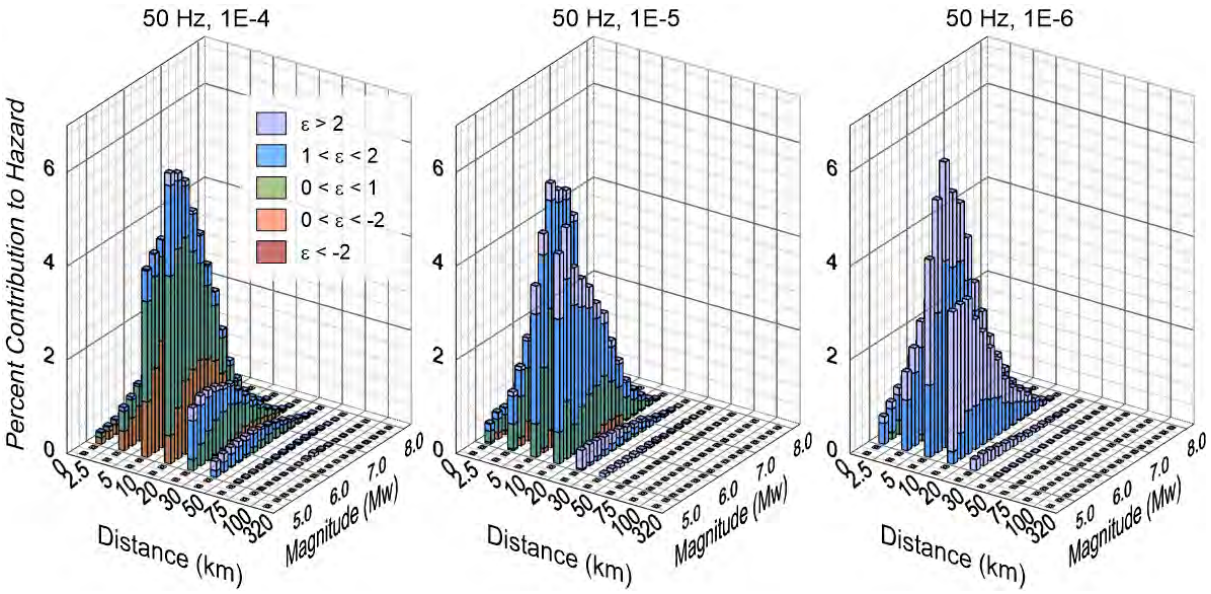

Figure 10-76. Disaggregation for three AFEs at 50 Hz at the KNPS.

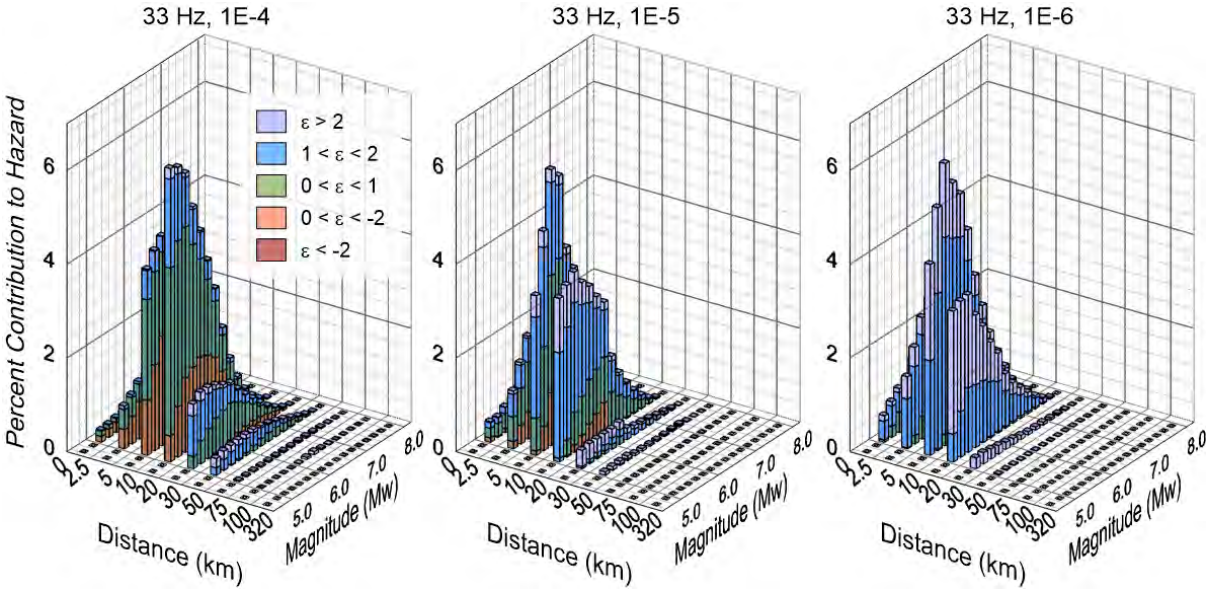

Figure 10-77. Disaggregation for three AFEs at 33 Hz at the KNPS.

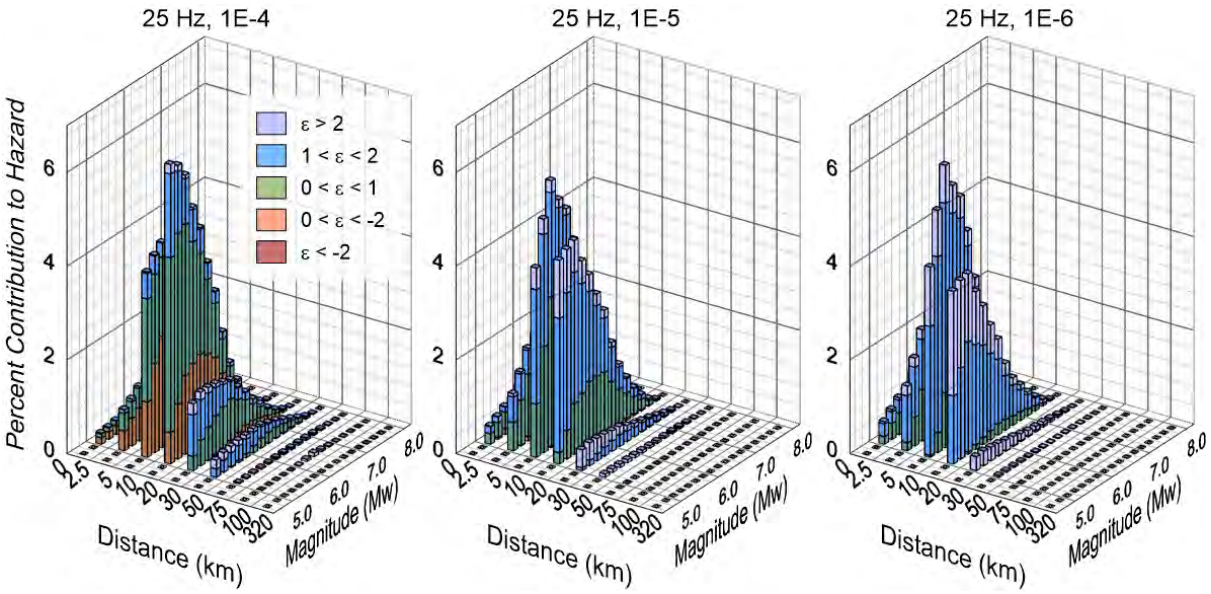

Figure 10-78. Disaggregation for three AFEs at 25 Hz at the KNPS.

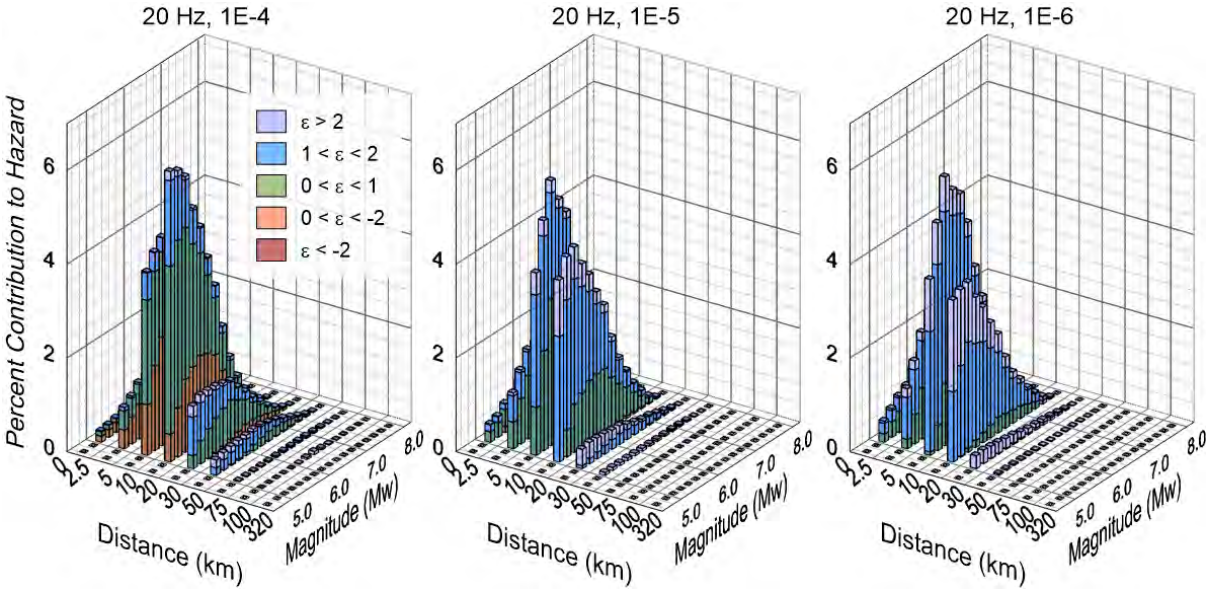

Figure 10-79. Disaggregation for three AFEs at 20 Hz at the KNPS.

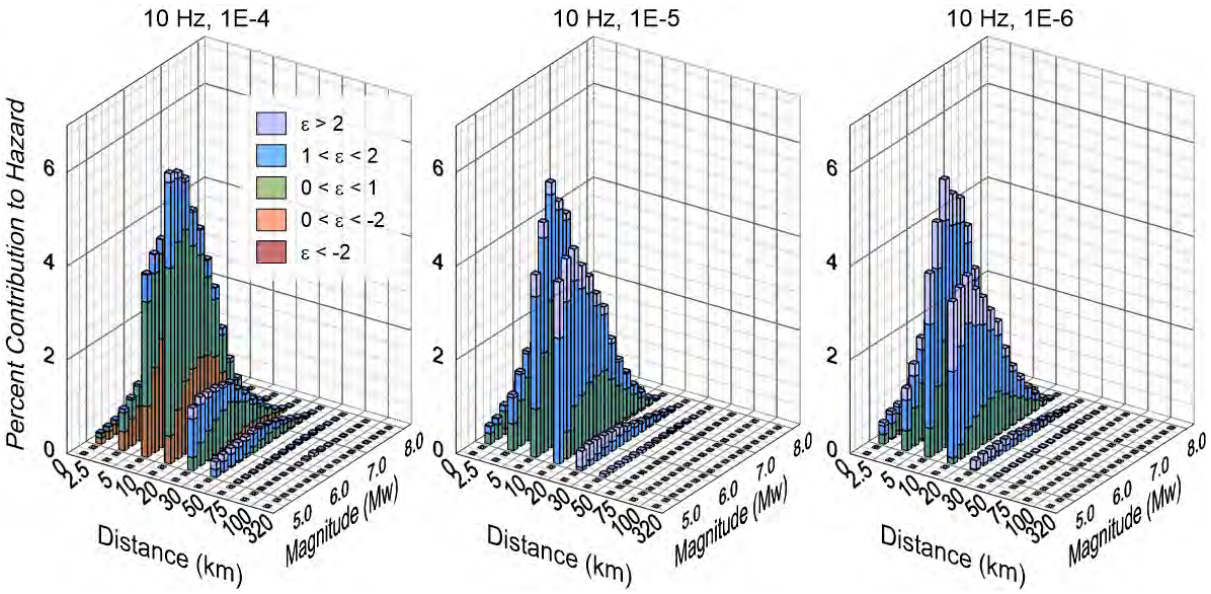

Figure 10-80. Disaggregation for three AFEs at 10 Hz at the KNPS.

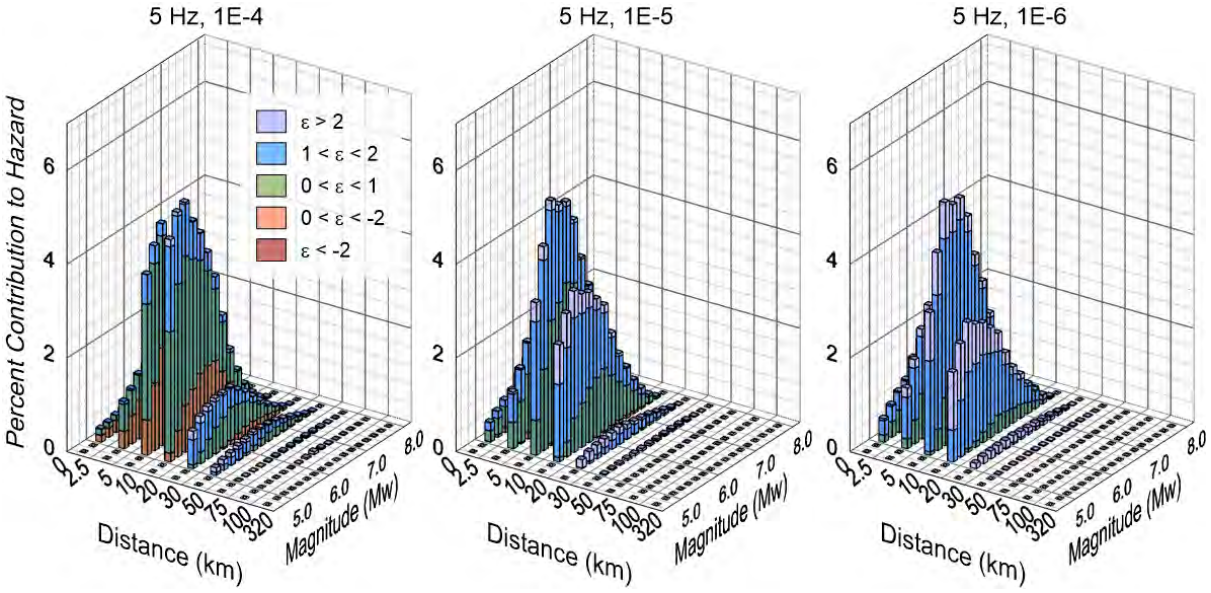

Figure 10-81. Disaggregation for three AFEs at 5 Hz at the KNPS.

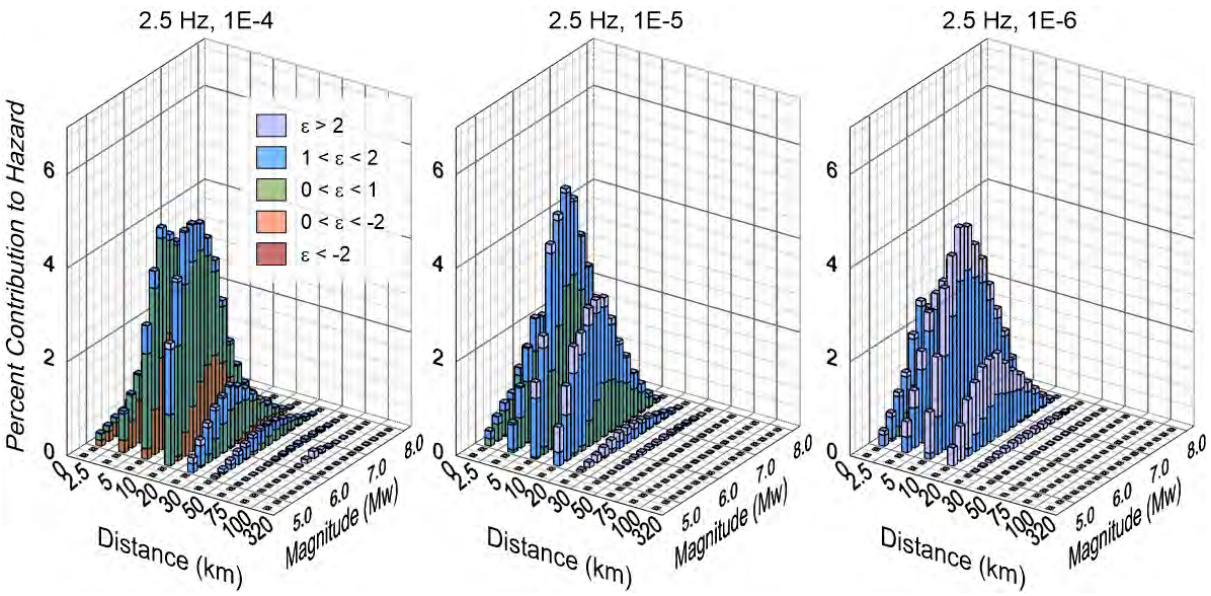

Figure 10-82. Disaggregation for three AFEs at 2.5 Hz at the KNPS.

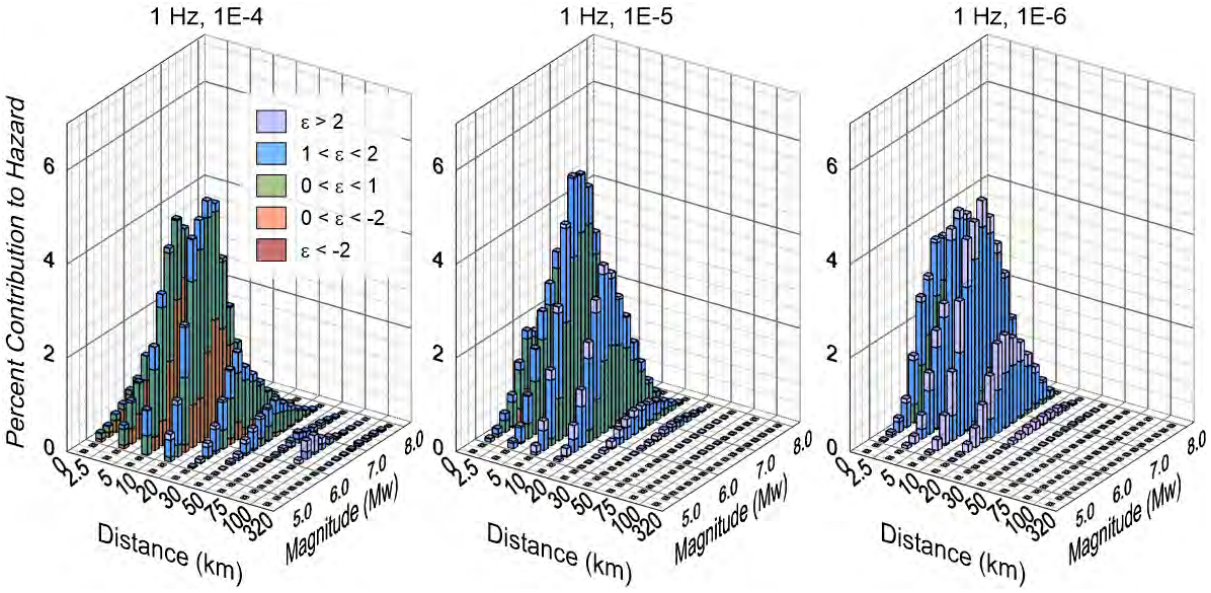

Figure 10-83. Disaggregation for three AFEs at 1 Hz at the KNPS.

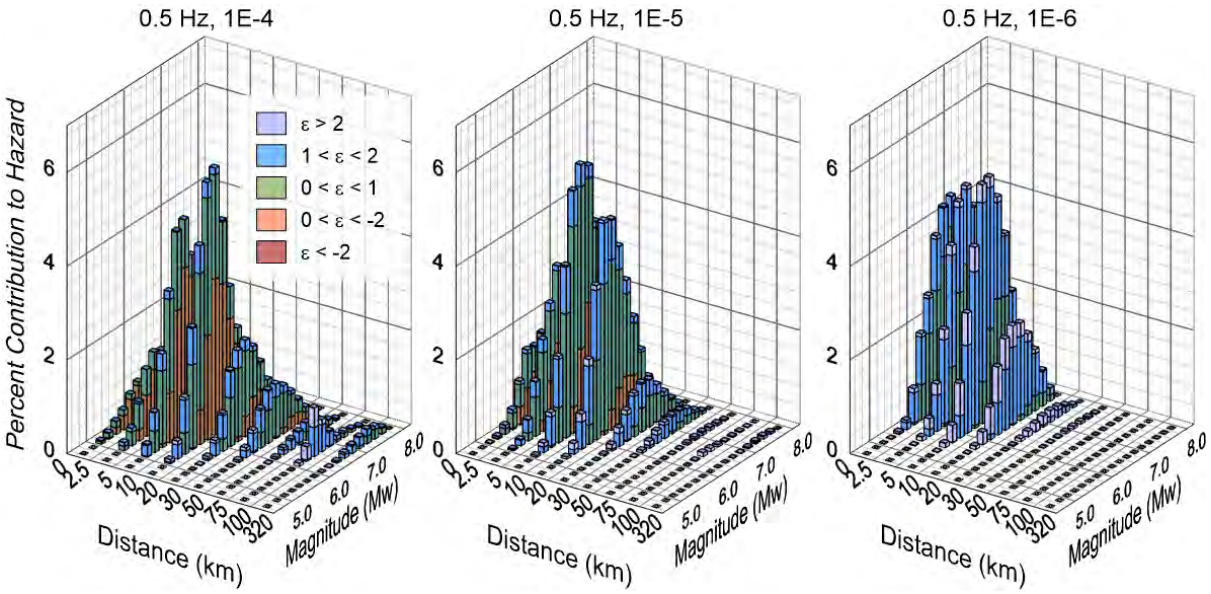

Figure 10-84. Disaggregation for three AFEs at 0.5 Hz at the KNPS.

10.4.1.4 Uniform Hazard Response Spectra

The UHRS represent the ground-motion at a specific AFE through the ten oscillator frequencies. The UHRS are calculated by interpolating the total mean hazard curves in log-space, at each period, at AFEs of 10^{-3}, 10^{-4}, 10^{-5}, 10^{-6}, 10^{-7}, and 10^{-8}. The six UHRS are depicted in Figure 10-85 and summarised in Table 10-11.

As shown in Figure 10-85, the shapes of the UHRS are relatively broad with the largest accelerations between 5 and 20 Hz. There are several contributing factors related to the complexity of the site geology that lead to the broad spectral shape. The large variability in the V_S profiles at the site contributes large epistemic uncertainty to the spectral accelerations between 5 and 20 Hz. The large variability in V_S is reflective of the complexity of the site as described in Sections 4.4 and 4.5. The broad shape captures the variability of more narrowly peaked spectra occurring at different frequencies. For example, in Figure 9-104 the highly variable contributions from eight borehole V_S profiles demonstrates this result. The largest variability is at 10 Hz, thus the UHRS peaks at this value for lower AFEs.

Additionally, the large spread in κ_0 contributes to the epistemic uncertainty in the high frequency ground motions above 10 Hz reflecting the limited earthquake data available to constrain κ_0. For example, Figure 9-105 shows a broad range of amplification at 25 Hz due to the epistemic uncertainty in κ_0.

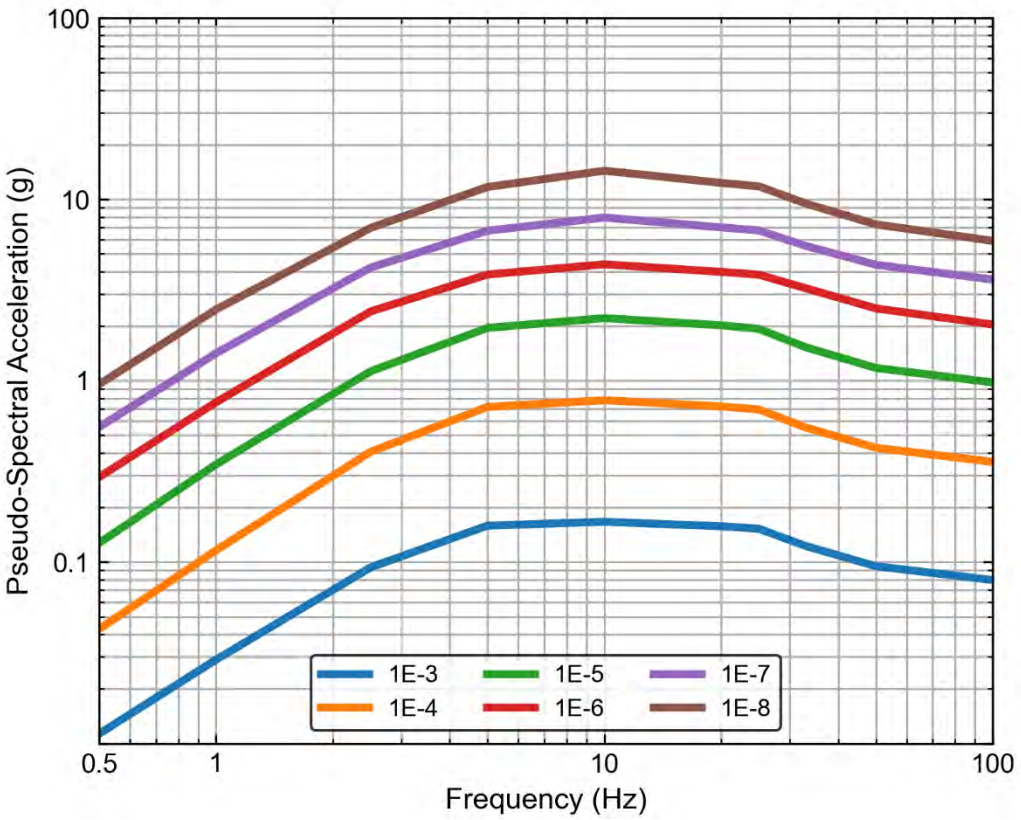

Figure 10-85. Uniform hazard spectra for the KNPS.

Table 10-11. Uniform hazard spectra and design spectrum results for the KNPS.

Frequency (Hz)	10^{-3}	10^{-4}	10^{-5}	10^{-6}	10^{-7}	10^{-8}
100	0.0796	0.3566	0.9781	2.0407	3.6106	5.9037
50	0.0949	0.4266	1.1757	2.5045	4.3586	7.2765
33	0.1226	0.5519	1.5293	3.2344	5.5388	9.4848
25	0.1526	0.6942	1.9302	3.8423	6.7323	11.7961
20	0.1576	0.7217	2.0211	3.9805	7.0016	12.3155
10	0.1668	0.7801	2.2124	4.3829	7.9395	14.3820
5.0	0.1587	0.7170	1.9549	3.8502	6.7113	11.6986
2.5	0.0935	0.4051	1.1263	2.4089	4.2045	6.9565
1.0	0.0289	0.1161	0.3455	0.7605	1.4171	2.4689
0.5	0.0113	0.0427	0.1273	0.2938	0.5546	0.9547

10.4.1.5 Ground-motion response spectrum

The ground-motion response spectrum (GMRS) was calculated in accordance with ASCE/SEI 43-19 Section 2.2, and detailed in Section 10.3.1.5.

A comparison of the GMRS with the UHRS for AFE of 10^{-4} through 10^{-5} is presented in Figure 10-86 below and the development of the GMRS is demonstrated in Table 10-12.

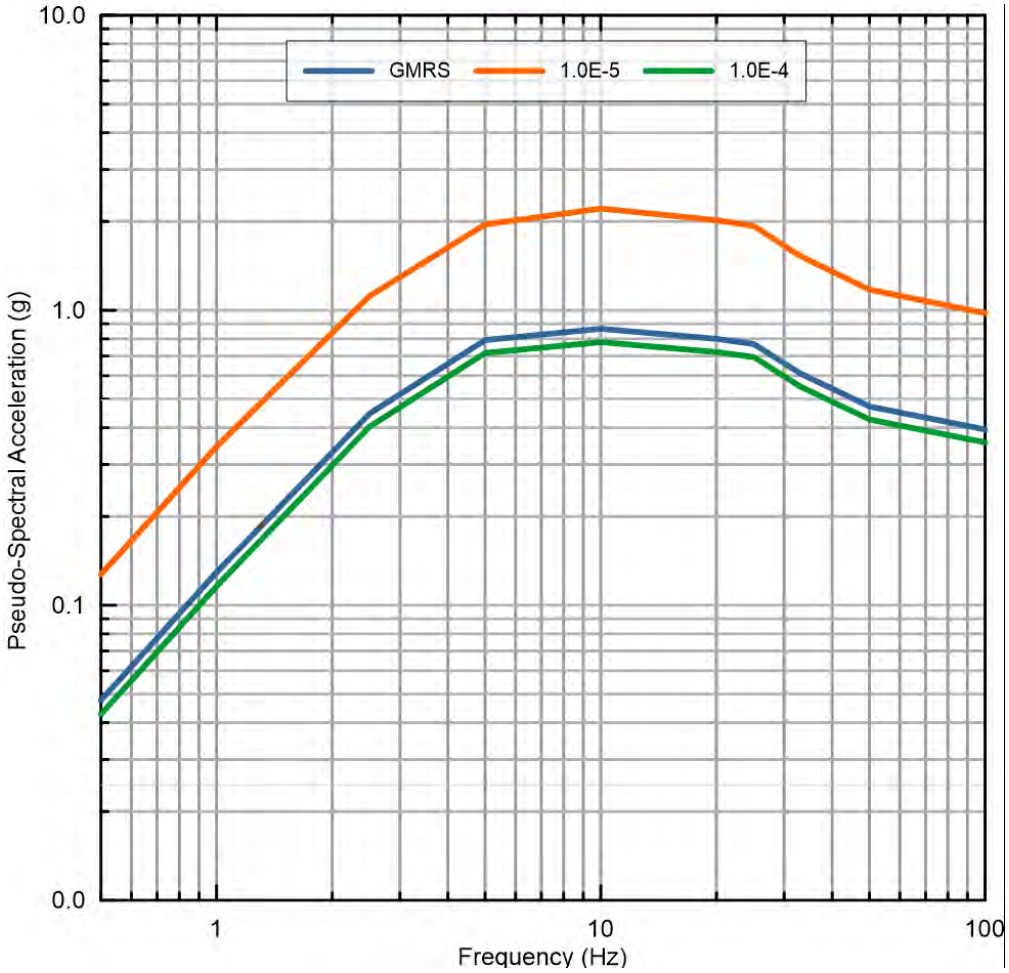

Figure 10-86. Design response spectrum for the KNPS.

Table 10-12. Ground-motion response spectrum results for the KNPS per ASCE/SEI 43-19.

Frequency (Hz)	$\frac{Sa10^{-4}}{Sa10^{-5}}$	$Ratio^{-0.1}$	$0.6 * Ratio^{0.2}$	0.45	GMRS
100	0.365	1.106	0.734	0.45	0.394
50	0.363	1.107	0.735	0.45	0.472
33	0.361	1.107	0.736	0.45	0.611
25	0.360	1.108	0.736	0.45	0.769
20	0.357	1.108	0.737	0.45	0.800
10	0.353	1.110	0.739	0.45	0.866
5.0	0.367	1.106	0.733	0.45	0.793
2.5	0.361	1.107	0.736	0.45	0.446
1.0	0.336	1.115	0.746	0.45	0.129
.5	0.336	1.115	0.746	0.45	0.048

10.4.2 Hazard sensitivities

The sensitivity analyses are presented for 100, 10, and 1 Hz representing the spread of frequencies for the KNPS at Duynefontyn. Sensitivity plots for the remaining seven oscillator frequencies are presented in Appendix H. The analyses are presented in two forms: (1) sensitivity tornado plots, and (2) sensitivity hazard curves. The sensitivity tornado plots are presented in this section. The following subsections include more detailed discussions of the

ground-motion variability due to each of the individual parameters summarised in the tornado plots below, as well as the associated hazard curves.

Each sensitivity analysis is done systematically by setting one branch on the respective logic tree to 1.0 and the others to 0.0. Figure 10-87 to Figure 10-89 show sensitivity tornado plots for 100, 10, and 1 Hz for annual frequency of exceedance values of 10^{-4} and 10^{-5}. Each tornado plot depicts parameters that changed the total mean ground motion at AFEs of 10^{-4} and 10^{-5} by more than 1%.

As shown in Figure 10-87 to Figure 10-89, the only logic-tree branches that contribute 1% or more to hazard sensitivities are within the GMM and the SDZ branches of the SSM. The single greatest contributor to hazard sensitivity is epistemic uncertainty in site amplification, represented by SAFs or Amp. Factors. This is consistent with the high epistemic uncertainty in the V_S profiles and κ_0 at the site. Overall, the epistemic uncertainty in the GMM has a higher contribution to the hazard sensitivity than the SSM. The most significant contributor to hazard sensitivity in the SSM is the smoothing methodology for the SDZ and Mmax at oscillator frequencies below 1 Hz. These sensitivities are explored in more detail in the following sections.

a)

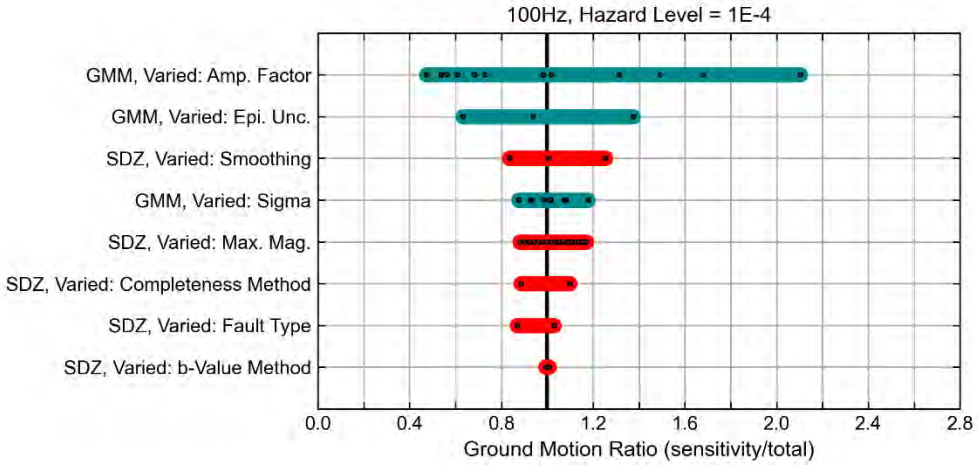

b)

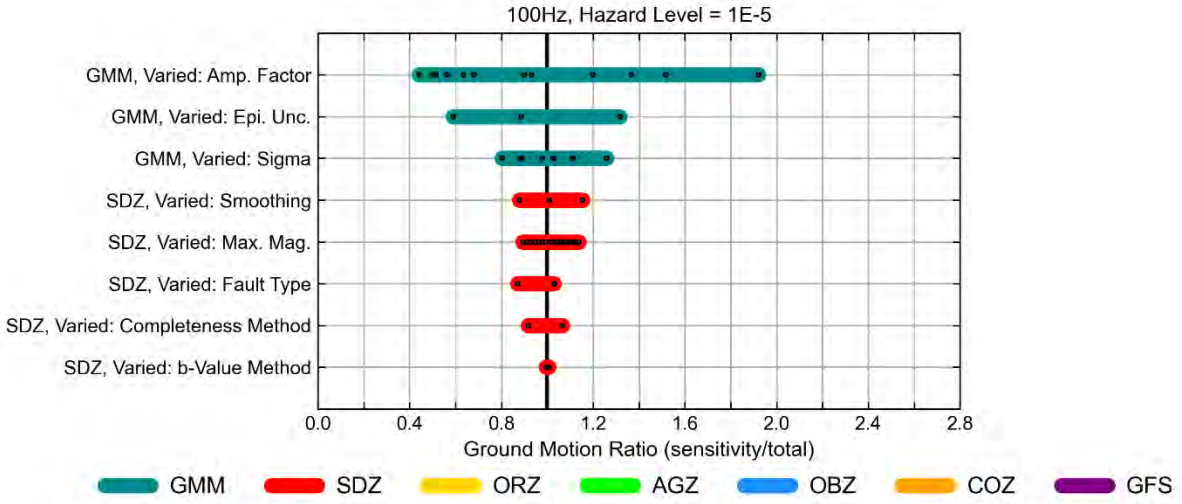

Figure 10-87. Hazard sensitivity tornado plots for AFEs of a) 10^{-4} and b) 10^{-5} at 100 Hz at the KNPS.

a)

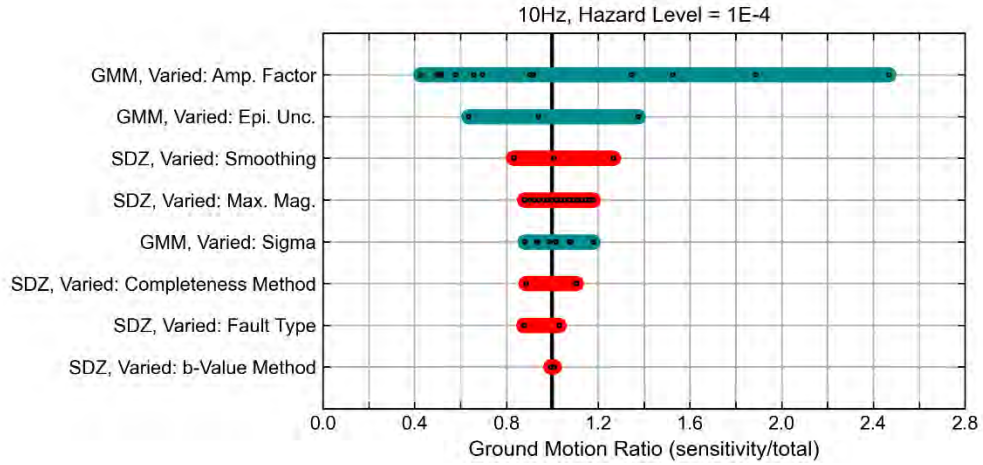

b)

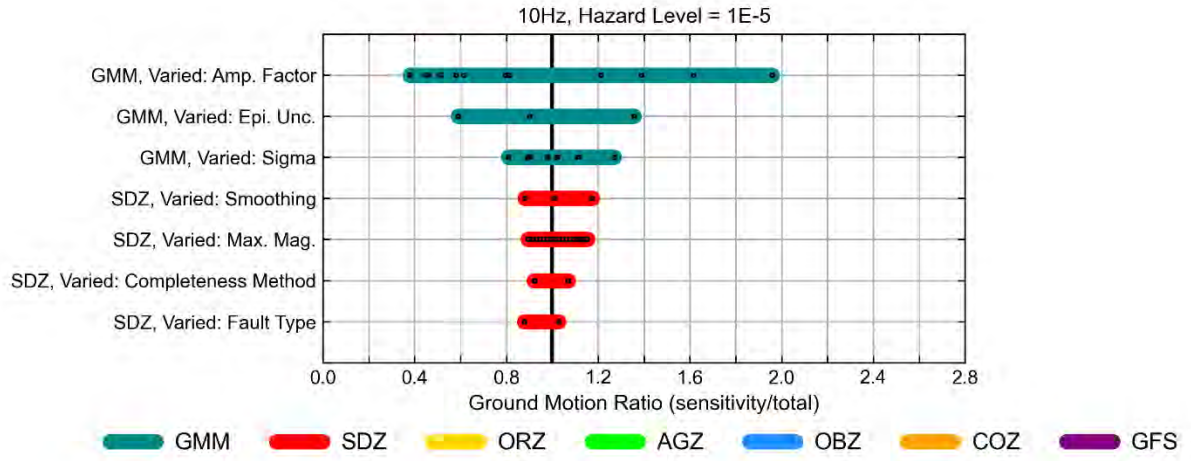

Figure 10-88. Hazard sensitivity tornado plots for AFEs of a) 10^{-4} and b) 10^{-5} at 10 Hz at the KNPS.

a)

b)

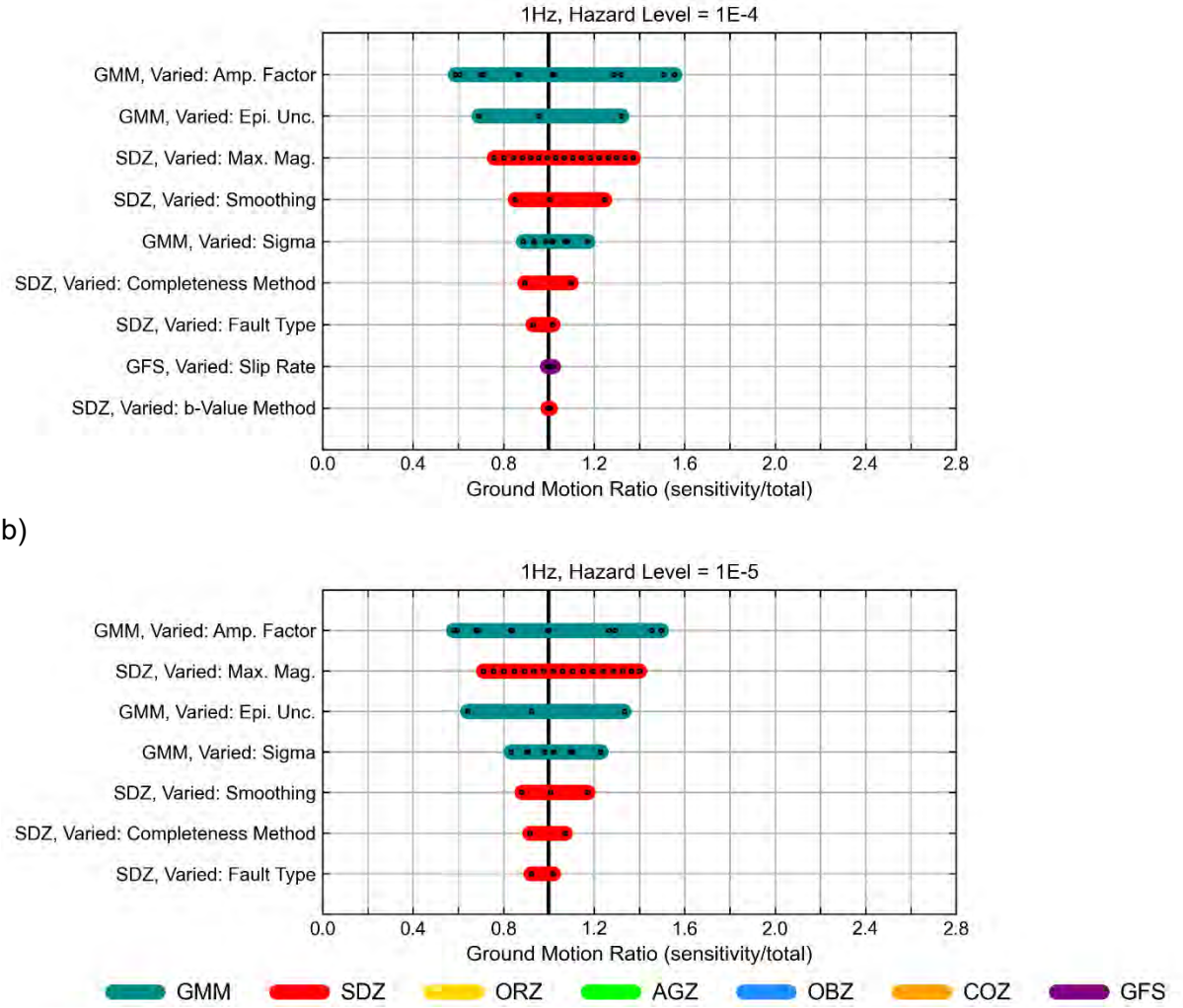

Figure 10-89. Hazard sensitivity tornado plots for AFEs of a) 10^{-4} and b) 10^{-5} at 1 Hz at the KNPS.

10.4.2.1 Sensitivity to ground-motion model

There are three main components of the GMM: the epistemic uncertainty branch, site-specific amplification branch, and aleatory variability branch. Further detail regarding the epistemic uncertainty branch and the aleatory variability branch can be found in Section 9.2.5 and 9.3, respectively. Details regarding the site-specific amplification branch are presented in Section 9.4.

10.4.2.1.1 Sensitivity to epistemic uncertainty in site adjustment factor

The first component of the GMM sensitivity and the parameter with the largest contribution to hazard sensitivity in the presented frequencies and AFEs, is the SAF. In total, there are twelve SAF values. These consist of two model groupings (denoted M1 and M2, below) of six SAF values (denoted SAF1 through SAF6, below). The two major groupings were developed to account for two methods of handling epistemic uncertainty. The six SAF values were resampled from the 408 site response branches. Details regarding the SAF values are presented in Section 9.4.

The final development of the SAFs (Section 9.4.9) shows a large range in uncertainty in SAF, particularly at high frequencies. This large uncertainty is due to the complicated geology at the site and its impact on the epistemic uncertainty of the V_S profiles and κ_0. This uncertainty leads to both large amplification and deamplification, shown in the spread of hazard curves presented in Figure 10-90 to Figure 10-92.

A comparison of the hazard curves resulting from the 12 different SAF models with the total mean hazard curve is presented in Figure 10-90, 10-91, and 10-92 for oscillator frequencies of 100, 10, and 1 Hz, respectively. Hazard curves showing the sensitivity to uncertainty in the SAF for the remaining seven frequencies are presented in Appendix H.

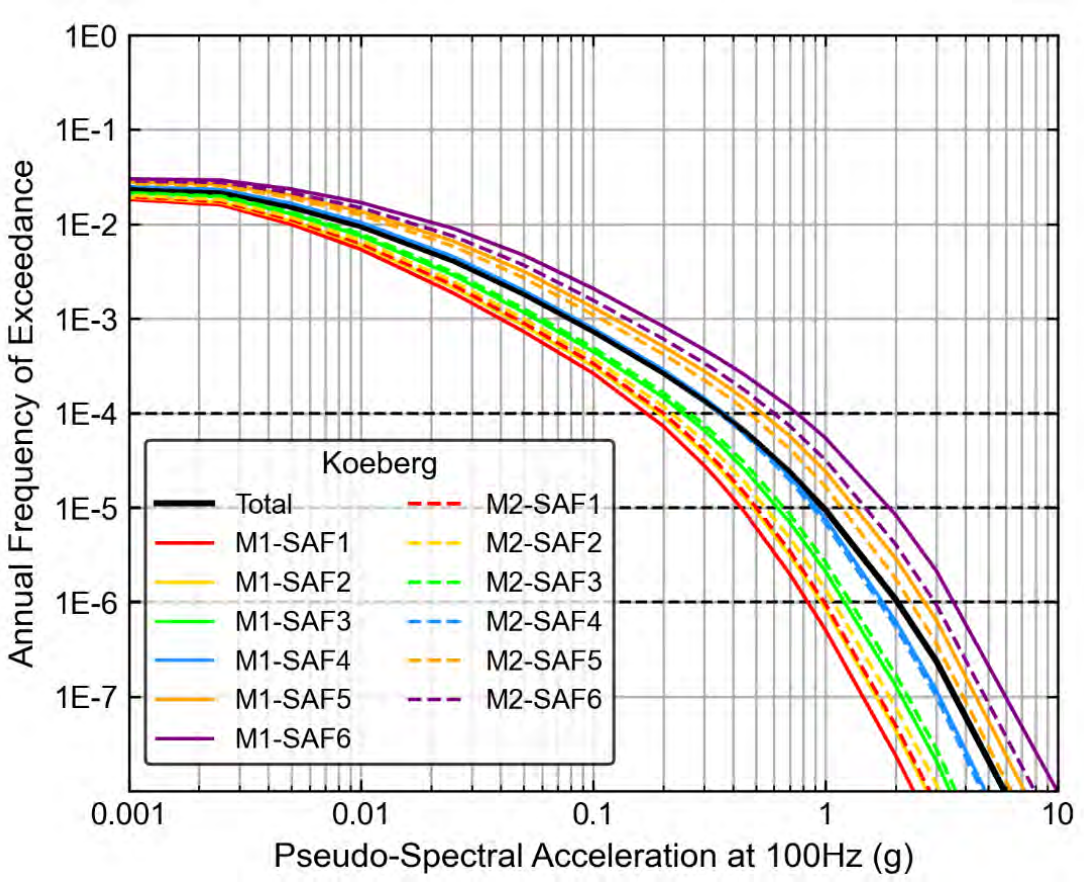

Figure 10-90. Hazard sensitivity to the site response branches for 100 Hz at the KNPS.

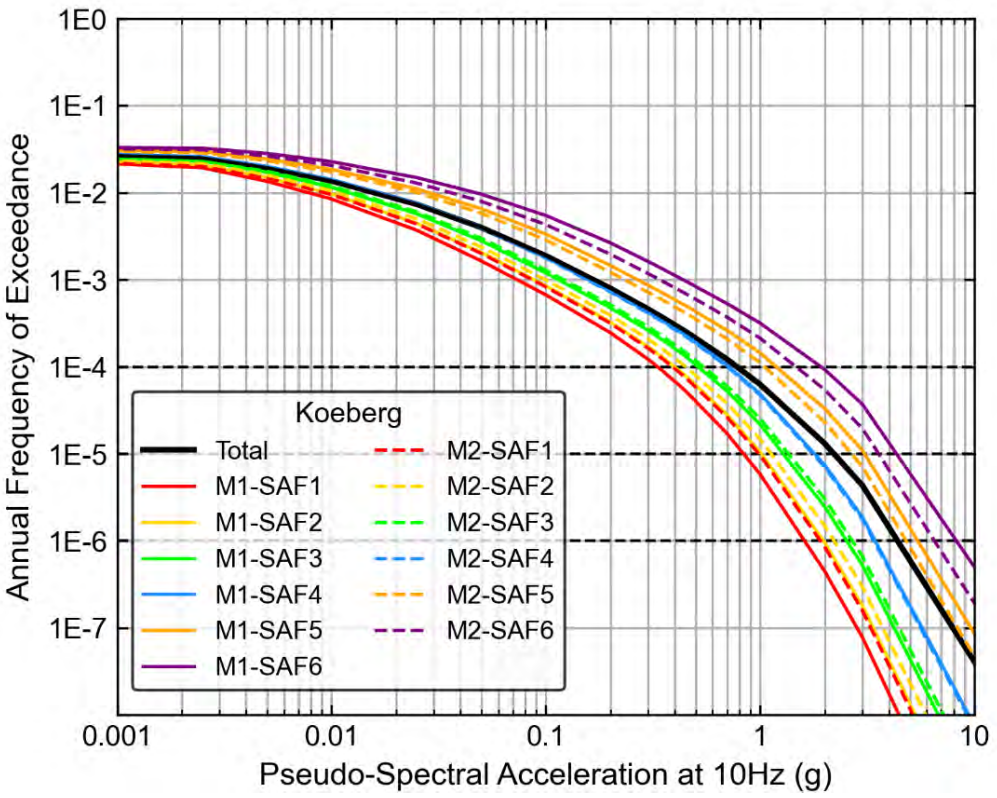

Figure 10-91. Hazard sensitivity to the site response branches for 10 Hz at the KNPS.

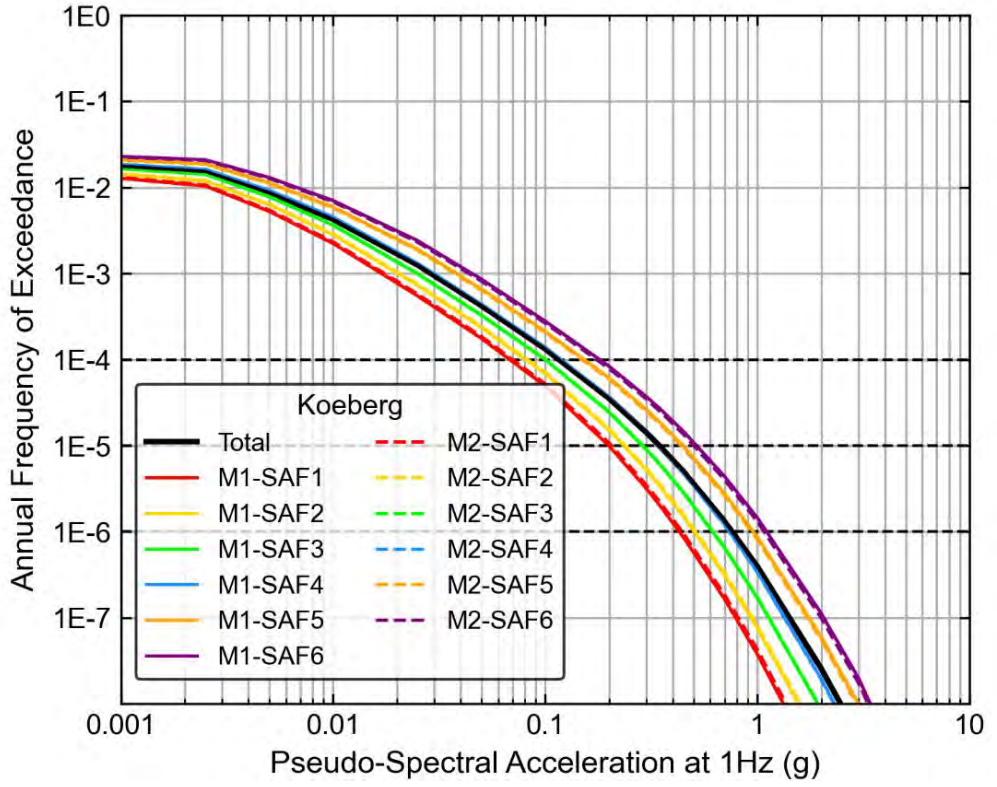

Figure 10-92. Hazard sensitivity to the site response branches for 1 Hz at the KNPS.

10.4.2.1.2 Sensitivity to epistemic uncertainty in the mean GMM

Epistemic uncertainty in the mean GMM was captured in the three-branch model developed for the project by the GMM TI Team. The GMM TI Team developed this model to capture the epistemic uncertainty in the seismic properties of South Africa based on the inversion results of the GMM TI Team and the specialty contractor Ben Edwards (Edwards, 2023). This model characterises the median (mean in log-space) ground-motion for each earthquake scenario (magnitude and distance), as well as the epistemic uncertainty in the median. As described in Section 9.2.5, a median spectral acceleration value was computed for each of the seven individual models (adjustments made to the CY14 GMPE) and a weighted average was then calculated to develop the spectral acceleration for the central (middle) model. The epistemic uncertainty in the median (mean in log-space), designated as $\sigma_{\mu ln,Sa,}$ was also computed to account for: 1) model-to-model differences from the seven individual models; 2) uncertainty due to near-source saturation; and 3) additional uncertainty.

The final model includes three branches: one with the weighted average GMM (middle branch); one where 1.28 is multiplied by $\sigma_{\mu ln,Sa}$, which is then added to the weighted average (upper branch); and one where 1.28 is multiplied by $\sigma_{\mu ln,Sa}$, which is then subtracted from the weighted average (lower branch).

A comparison of the hazard curves resulting from the three branches with the total mean hazard curve is presented in Figure 10-93, Figure 10-94, and Figure 10-95 for oscillator frequencies of 100, 10, and 1 Hz, respectively. Hazard curves showing the sensitivity to uncertainty in the mean GMM for the remaining seven frequencies are presented in Appendix H.

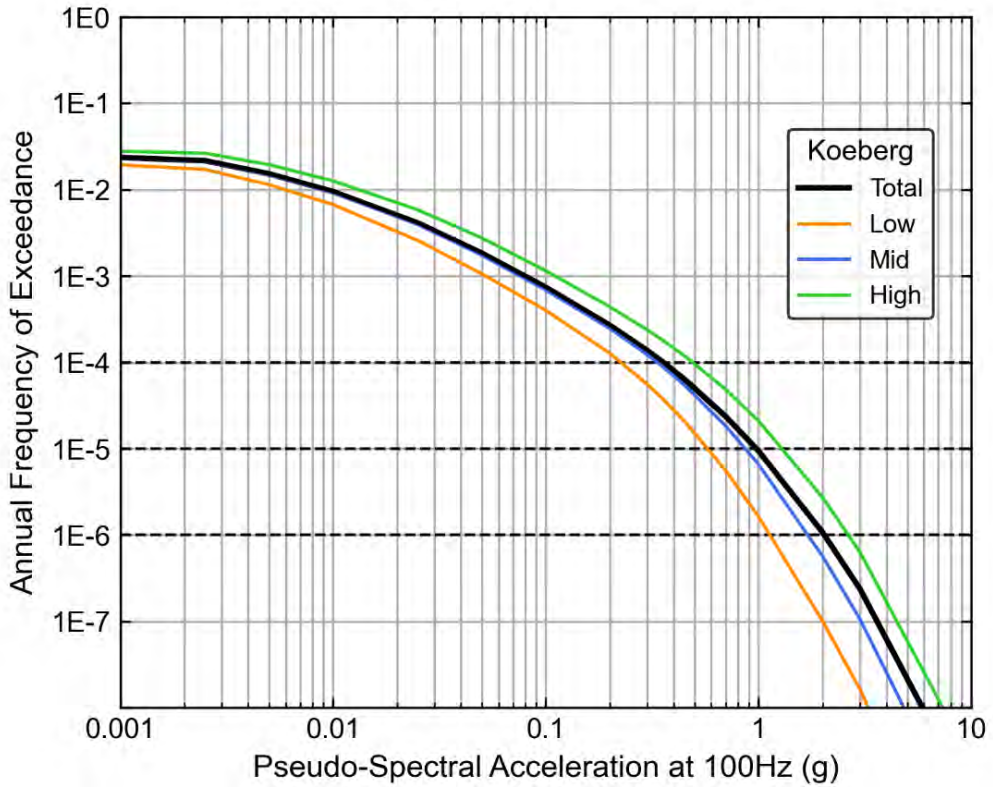

Figure 10-93. Hazard sensitivity to the epistemic uncertainty model for 100Hz at the KNPS.

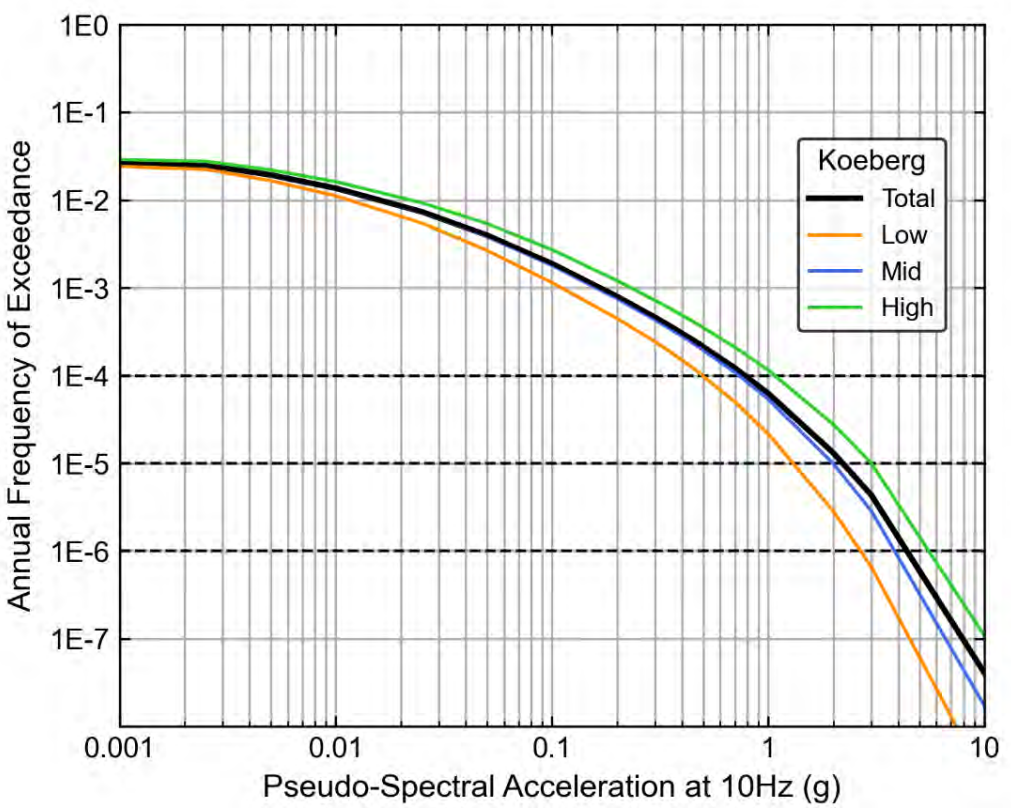

Figure 10-94. Hazard sensitivity to the epistemic uncertainty model for 10Hz at the KNPS.

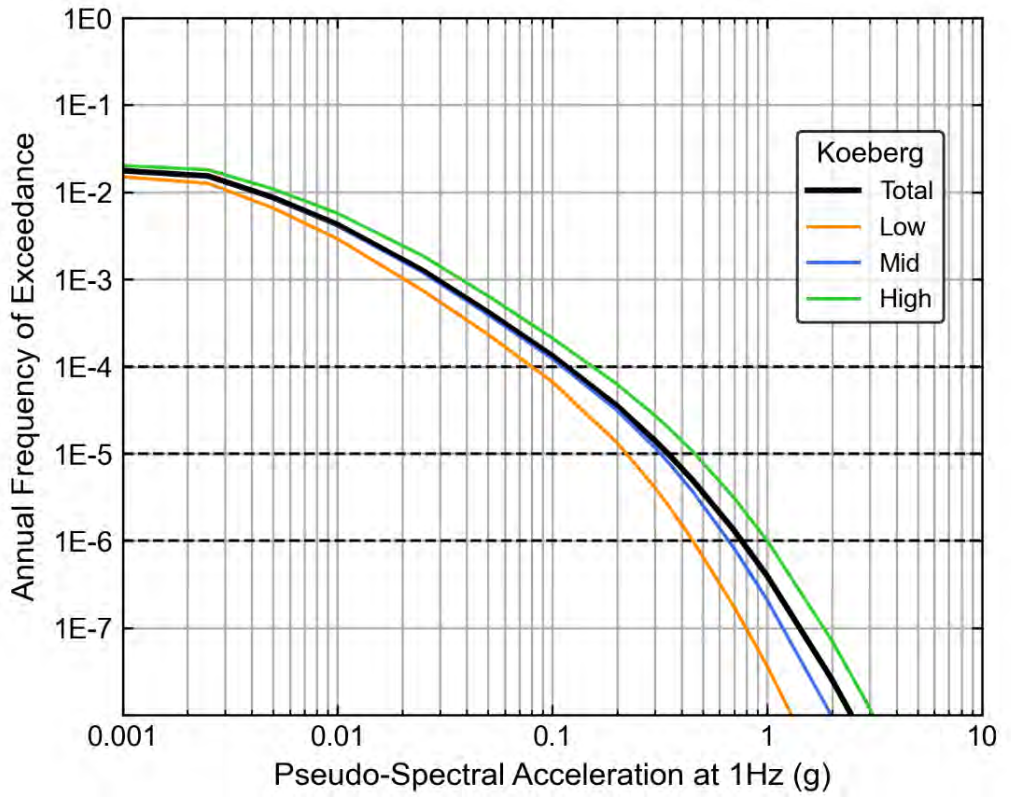

Figure 10-95. Hazard sensitivity to the epistemic uncertainty model for 1Hz at the KNPS.

10.4.2.1.3 Sensitivity to uncertainty in the GMM aleatory variability model

The uncertainty in the GMM includes aleatory variability branches as presented by Al Atik (2015) and discussed in Section 9.3. The logic-tree branches of the aleatory variability model capture the epistemic uncertainty in applying a single-station sigma model based on world-wide data to a single location that lacks sufficient data for its own single-station sigma evaluation. There are a total of nine standard deviation (σ) values (designated as S1 through S9) computed by varying three within-event variability (ϕ_{ss}, global) terms and three between-event variability (τ, global) terms, the branch pairings are described in Table 10-8. Figure 10-96, Figure 10-97, and Figure 10-98 demonstrates the spread in the hazard results due to variation in the aleatory variability used in the analysis for oscillator frequencies of 100, 10, and 1 Hz, respectively. Hazard sensitivity to the GMM aleatory variability for the remaining seven oscillator frequencies is presented in Appendix H.

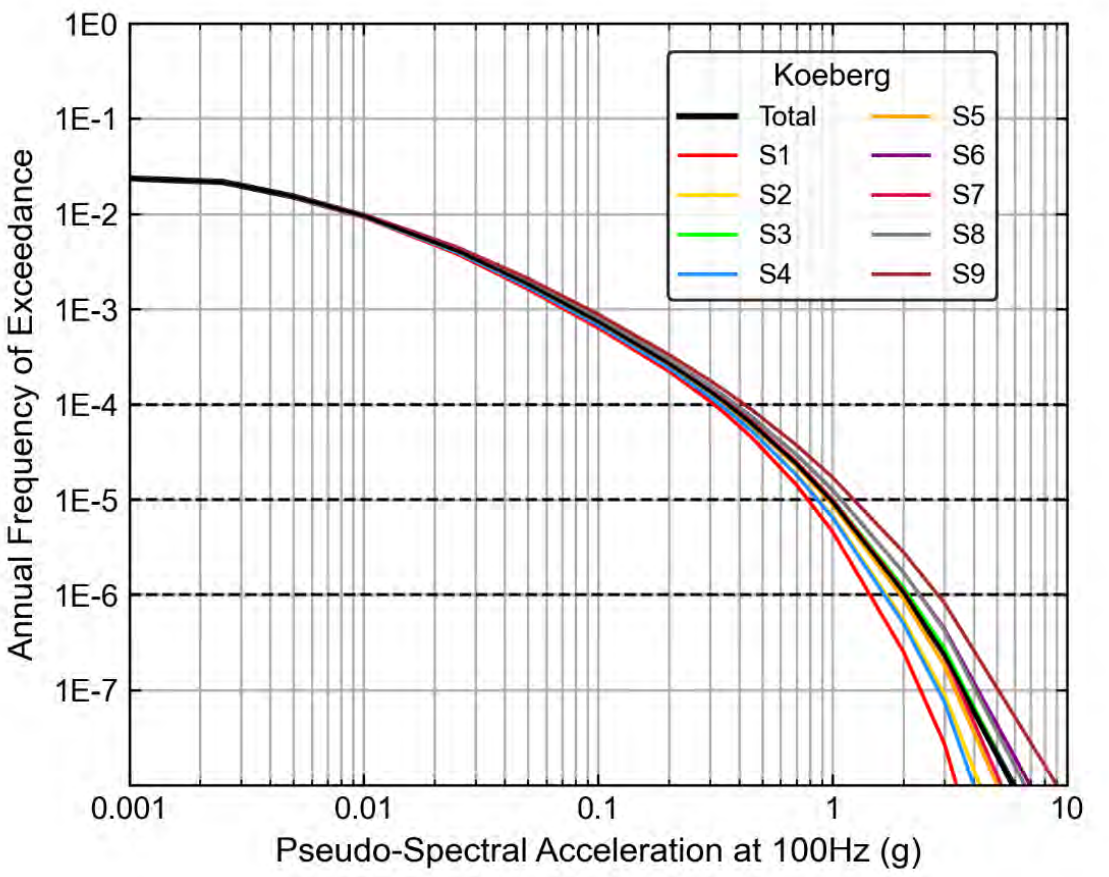

Figure 10-96. Hazard sensitivity to the aleatory variability branches for 100 Hz at the KNPS.

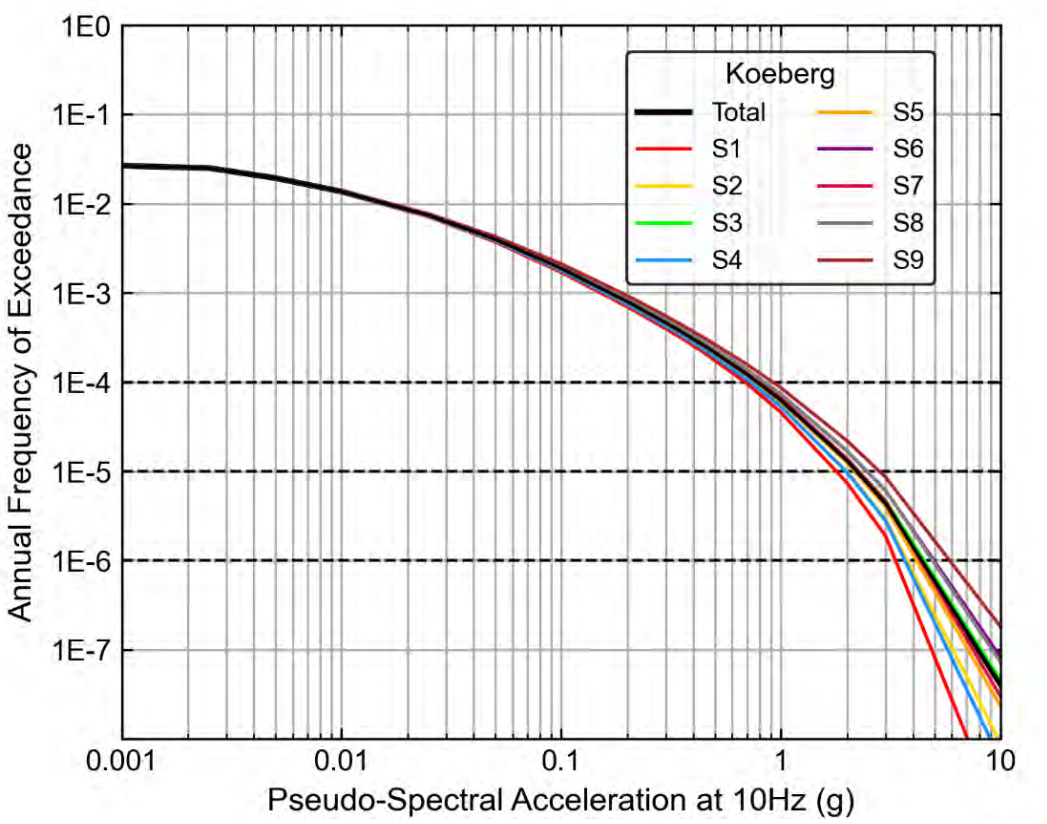

Figure 10-97. Hazard sensitivity to the aleatory variability branches for 10 Hz at the KNPS.

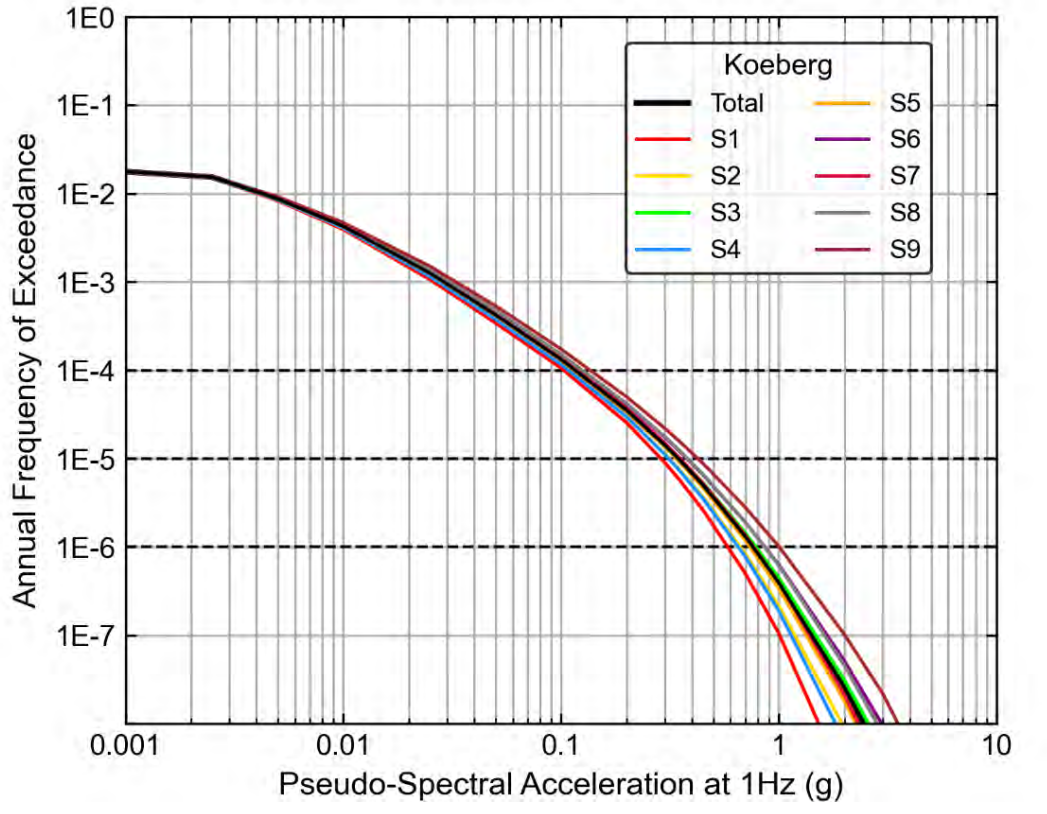

Figure 10-98. Hazard sensitivity to the aleatory variability branches for 1 Hz at the KNPS.

10.4.2.2 Sensitivity to SSM

This section presents results of sensitivity calculations performed for logic-tree nodes in the SSM including: spatial smoothing, completeness method, regional *b*-value calculation method, the maximum magnitude values and fault type.

10.4.2.2.1 Sensitivity to epistemic uncertainty in spatial smoothing models

The SSM utilised three methods for spatial smoothing of past earthquakes in the source zones. The three methods are uniform smoothing, an adaptive kernel method, and fixed kernel with a 100 km radius. These three alternatives were included in the SSM because the SSM TI Team could not establish the assumption of stationarity for future earthquakes. The SSM TI Team concluded that these three alternatives capture the epistemic uncertainty in the future location of earthquakes based on the spatial distribution of past earthquakes. The hazard curves resulting from the three smoothing types in the host zone for oscillator frequencies of 100, 10, and 1 Hz are presented in Figure 10-99, Figure 10-100, and Figure 10-101Figure 10-44, respectively. Hazard curves showing the sensitivity to spatial smoothing for the remaining seven oscillator frequencies are presented in Appendix H.

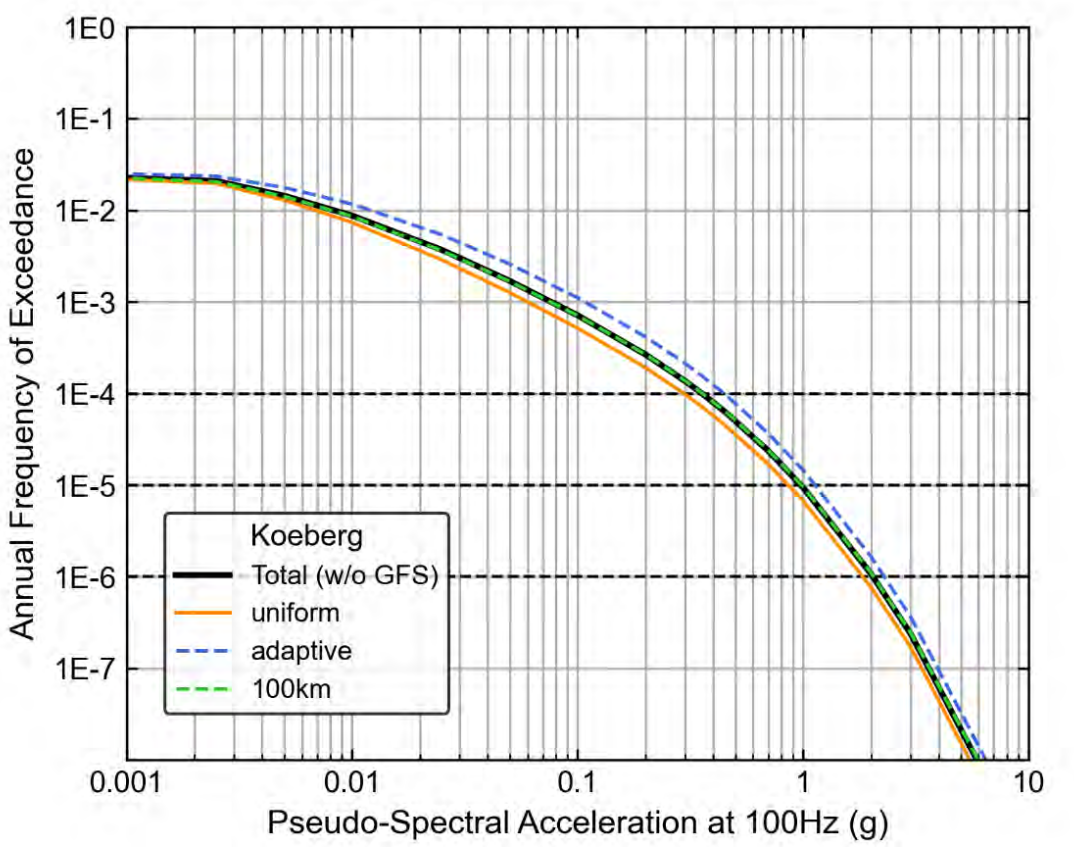

Figure 10-99. Hazard sensitivity for 100 Hz to spatial smoothing at the KNPS.

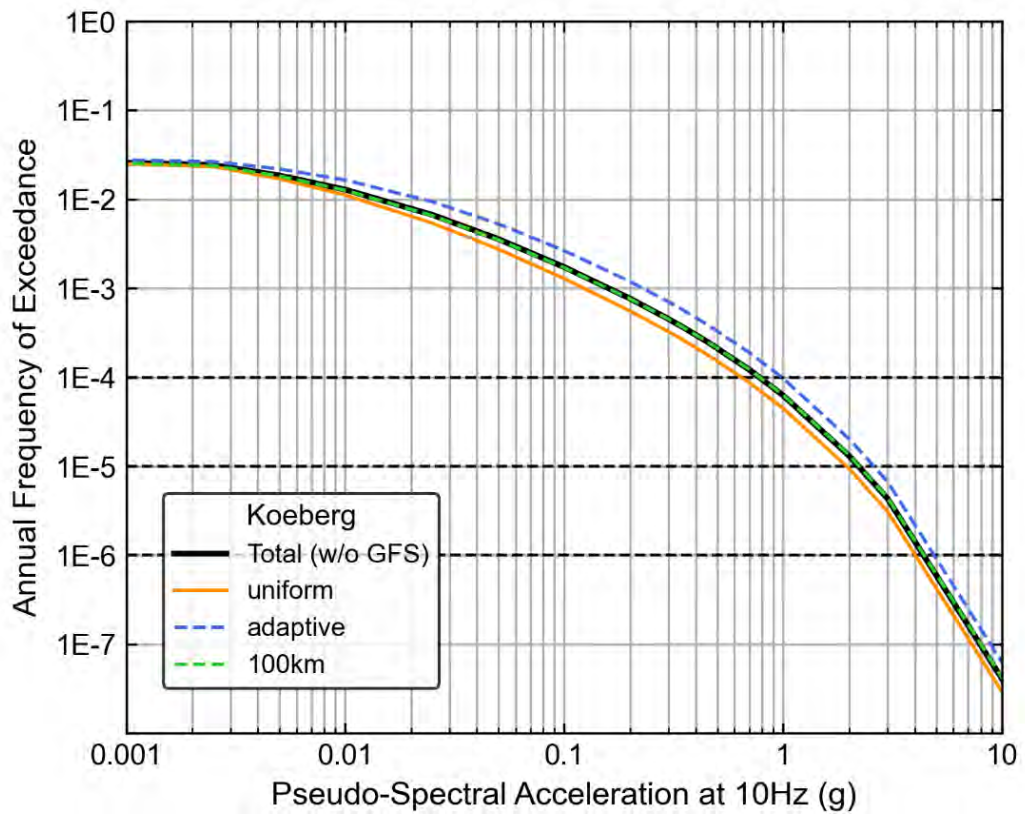

Figure 10-100. Hazard sensitivity for 10 Hz to spatial smoothing at the KNPS.

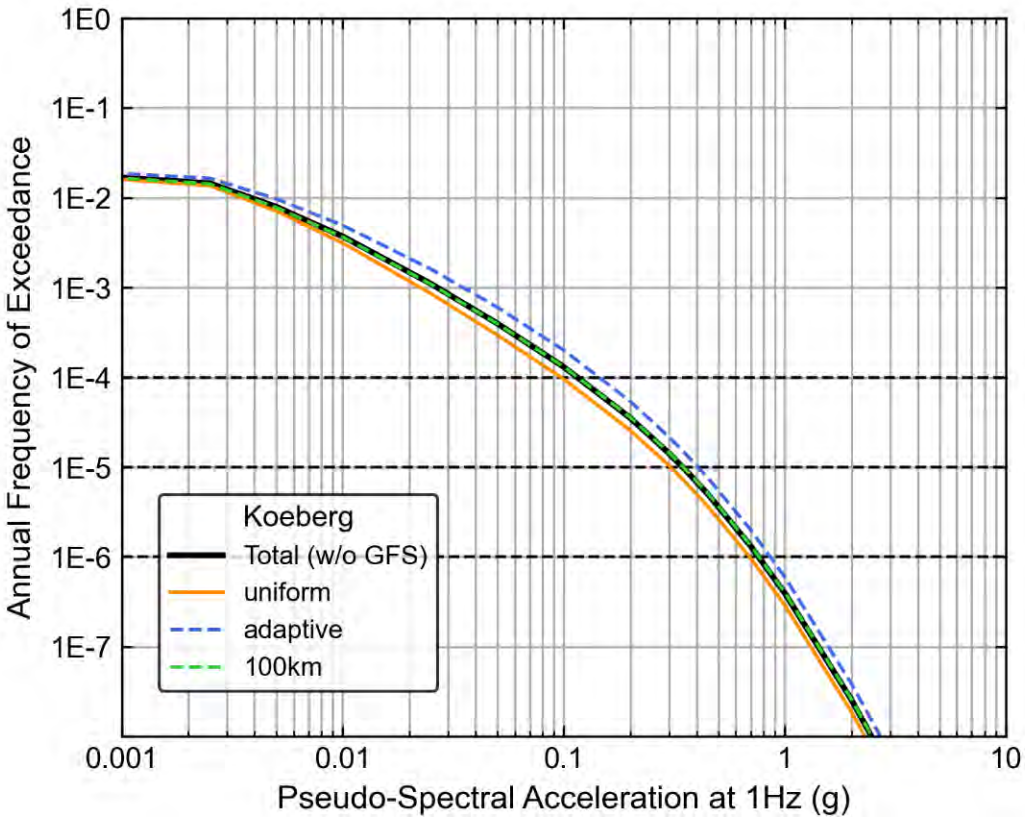

Figure 10-101. Hazard sensitivity for 1 Hz to spatial smoothing at the KNPS.

10.4.2.2.2 Sensitivity to epistemic uncertainty in Mmax

The SDZ parameters include 17 alternative estimates of Mmax from a fine sample of the continuous posterior Mmax distributions. Additional information about Mmax can be found in Section 8.2.9. The hazard curves resulting from the different Mmax for SDZ for oscillator frequencies of 100, 10, and 1 Hz are presented in Figure 10-102, Figure 10-103, and Figure 10-104, respectively. Hazard curves showing the sensitivity to Mmax for SDZ for the remaining seven oscillator frequencies are presented in Appendix H.

Similar to the Thyspunt PSHA (Bommer et al. 2013), the wide range of Mmax values starting at 6.2, not just the maximum, contributes to hazard sensitivity, but is relatively less important than spatial smoothing models and the epistemic uncertainty in the GMM. The larger epistemic uncertainty at low oscillator frequencies is due to the larger impact of magnitude on low oscillator frequencies as compared to high oscillator frequency, see Figures Figure 10-102 through Figure 10-104.

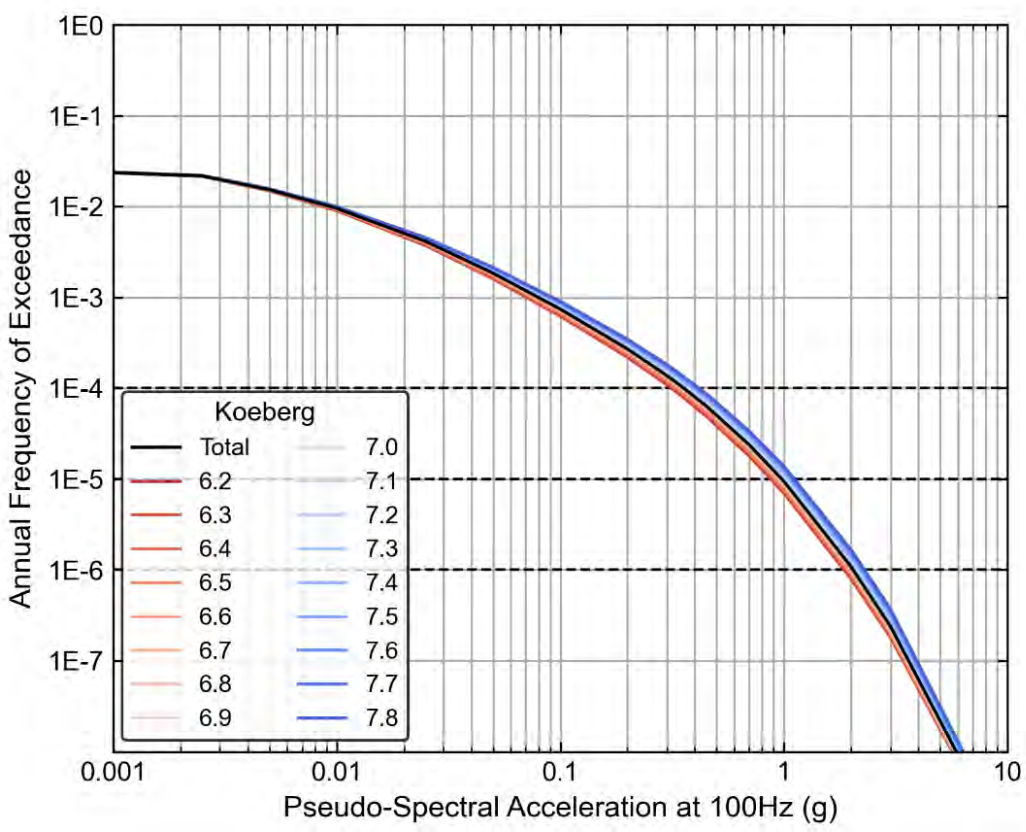

Figure 10-102. Hazard sensitivity for 100 Hz to the host zone maximum magnitude branches at the KNPS.

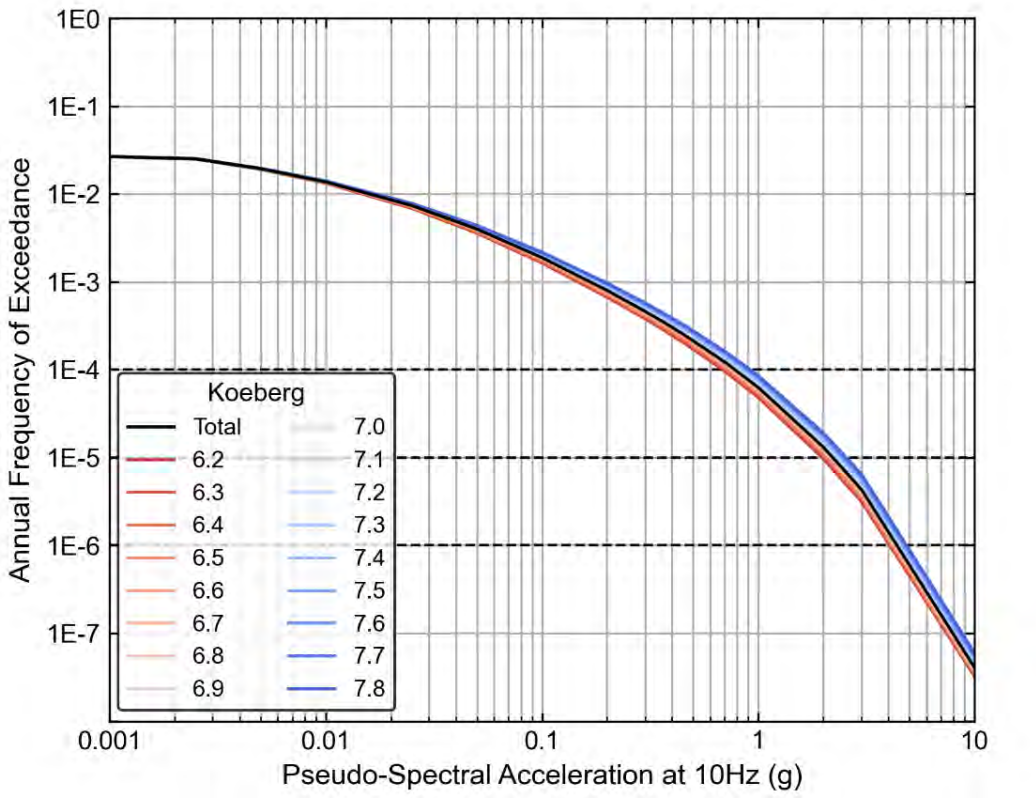

Figure 10-103. Hazard sensitivity for 10 Hz to the host zone maximum magnitude branches at the KNPS.

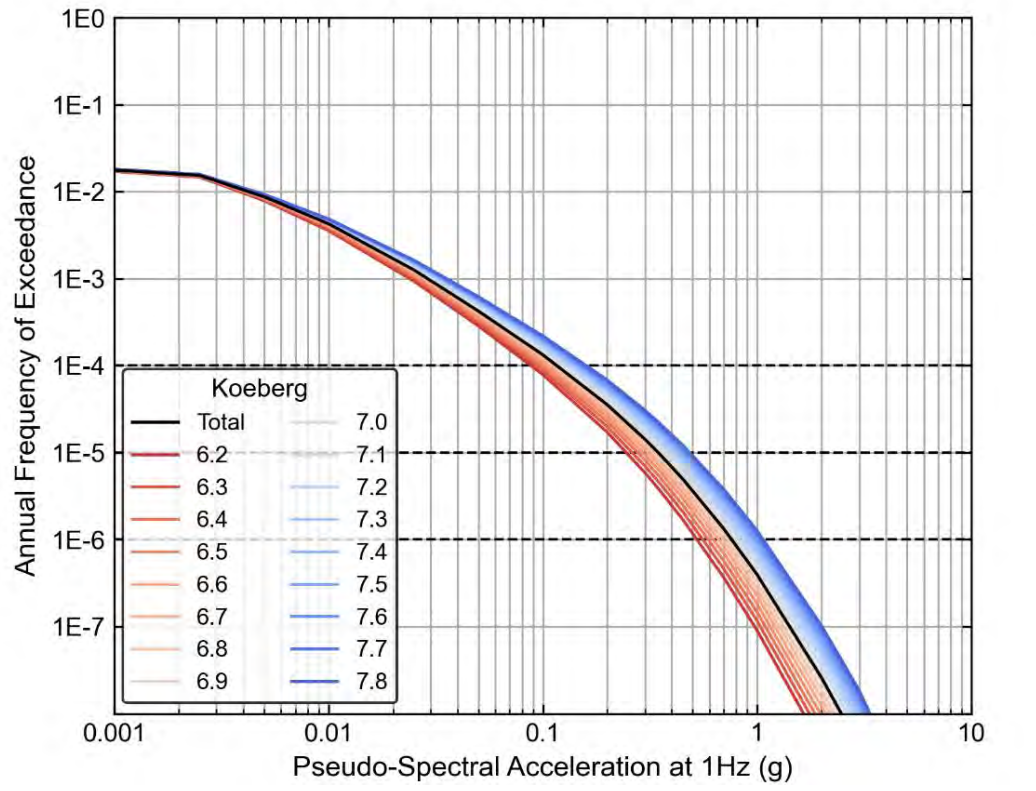

Figure 10-104. Hazard sensitivity for 1 Hz to the host zone maximum magnitude branches at the KNPS.

10.4.2.2.3 Sensitivity to epistemic uncertainty in completeness method

The SSM included two different completeness methods as described in Section 8.2.4. These are the probability of detection method (PD) and Stepp plot analysis (CC). The hazard curves resulting from the different completeness methods for oscillator frequencies of 100, 10, and 1 Hz are presented in Figure 10-105, Figure 10-106, and Figure 10-107, respectively. Hazard curves showing the sensitivity to completeness method for the remaining seven oscillator frequencies are presented in Appendix H. The mean presented in these figures removes the contribution of the GFS (indicated as w/out GFS) to directly compare the impact of completeness method on hazard results from the source zones. The completeness method effects the number, and thus rate, of small earthquakes and shows some spread in the hazard curve results for AFE above 10^{-2}.

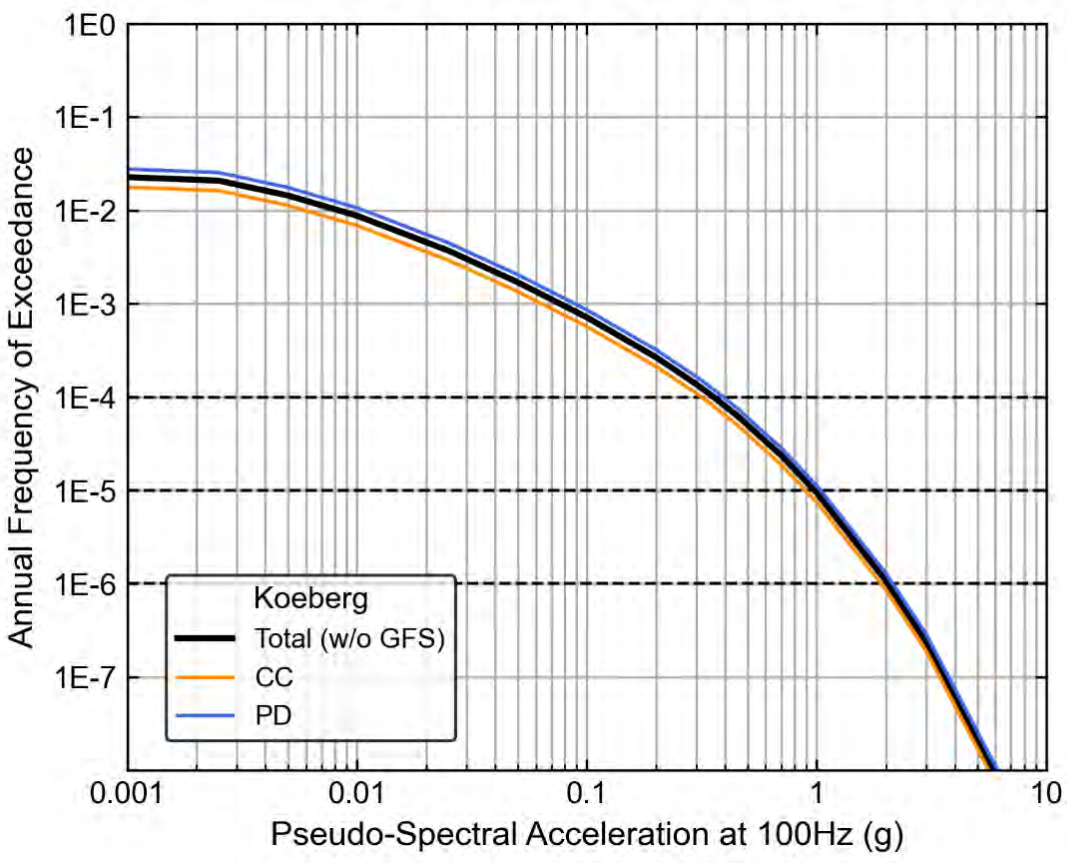

Figure 10-105. Hazard sensitivity for 100 Hz to completeness method branches at the KNPS.

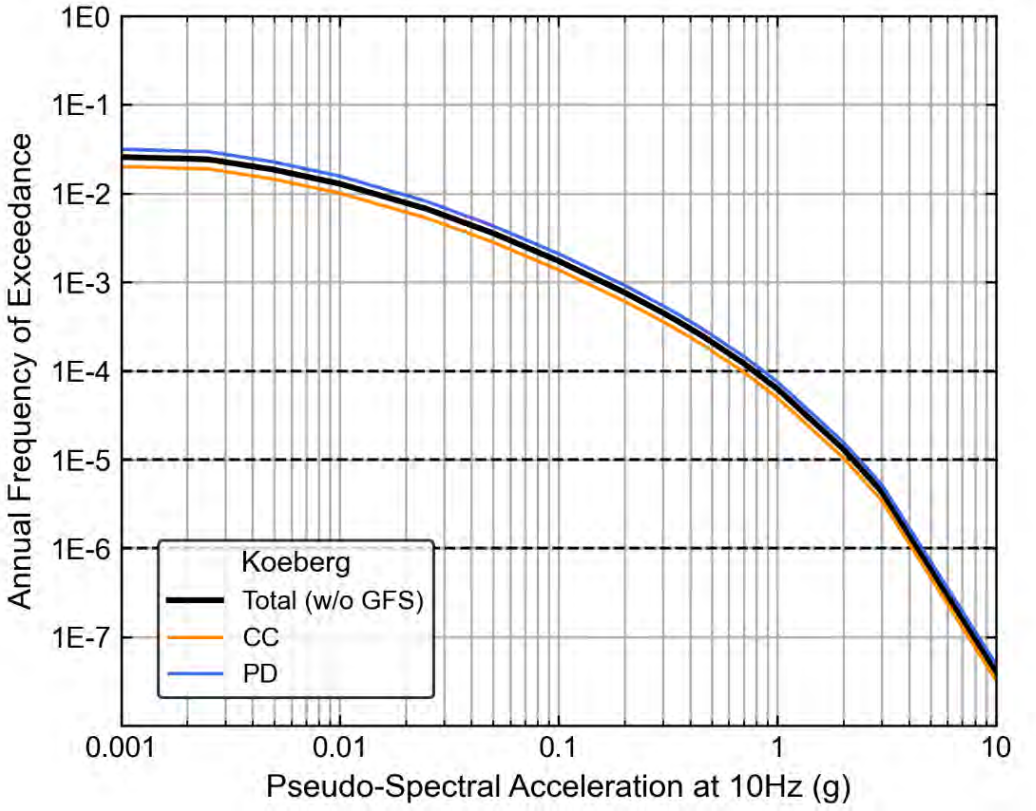

Figure 10-106. Hazard sensitivity for 10 Hz to completeness method branches at the KNPS.

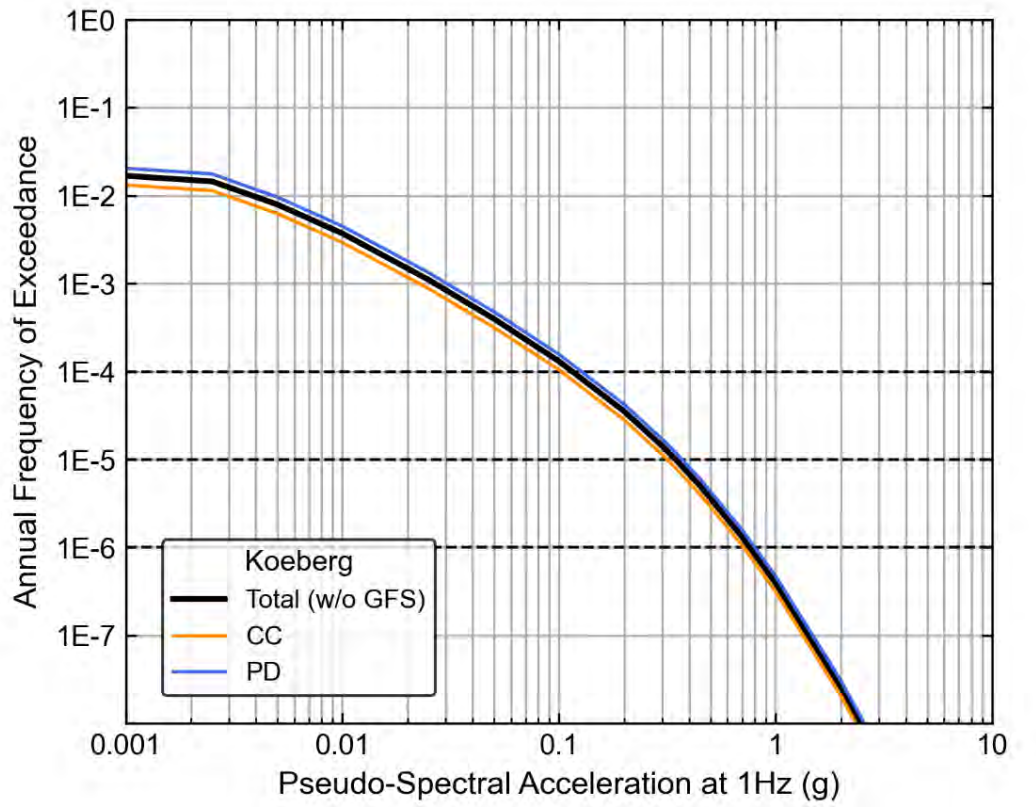

Figure 10-107. Hazard sensitivity for 1 Hz to completeness method branches at the KNPS.

10.4.2.2.4 Sensitivity to aleatory variability in SDZ rupture type

Virtual ruptures in the SDZ were modelled as a combination of strike-slip (SS) and normal (NM) earthquakes. The details are discussed in Section 8.2.5. The hazard curves resulting from the two different rupture types for oscillator frequencies of 100, 10, and 1 Hz are presented in Figure 10-108, Figure 10-109, and Figure 10-110, respectively. Hazard curves showing the sensitivity to SDZ fault type for the remaining seven oscillator frequencies are presented in Appendix H. Though not an element of epistemic uncertainty, sensitivity results for this analysis show that SS ruptures produce slightly larger ground-motions than NM earthquakes. This difference reflects the difference in GMM for these two styles of earthquake ruptures.

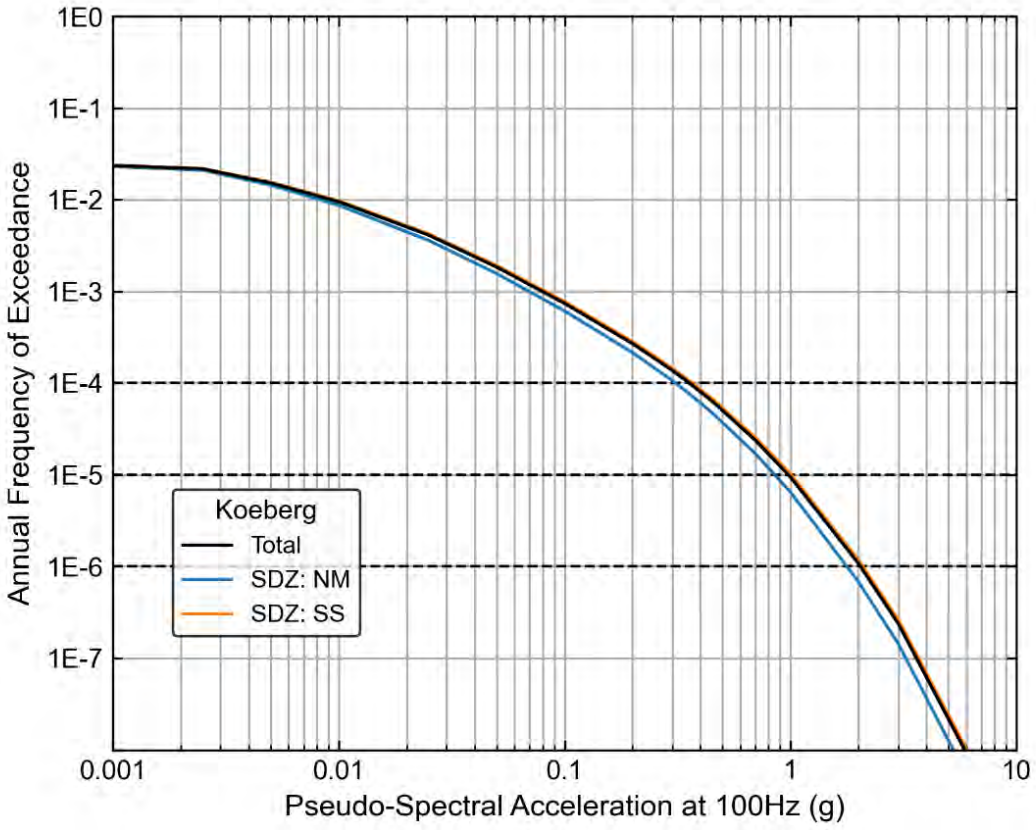

Figure 10-108. Hazard sensitivity for 100 Hz to fault mechanism in the host zone for the KNPS.

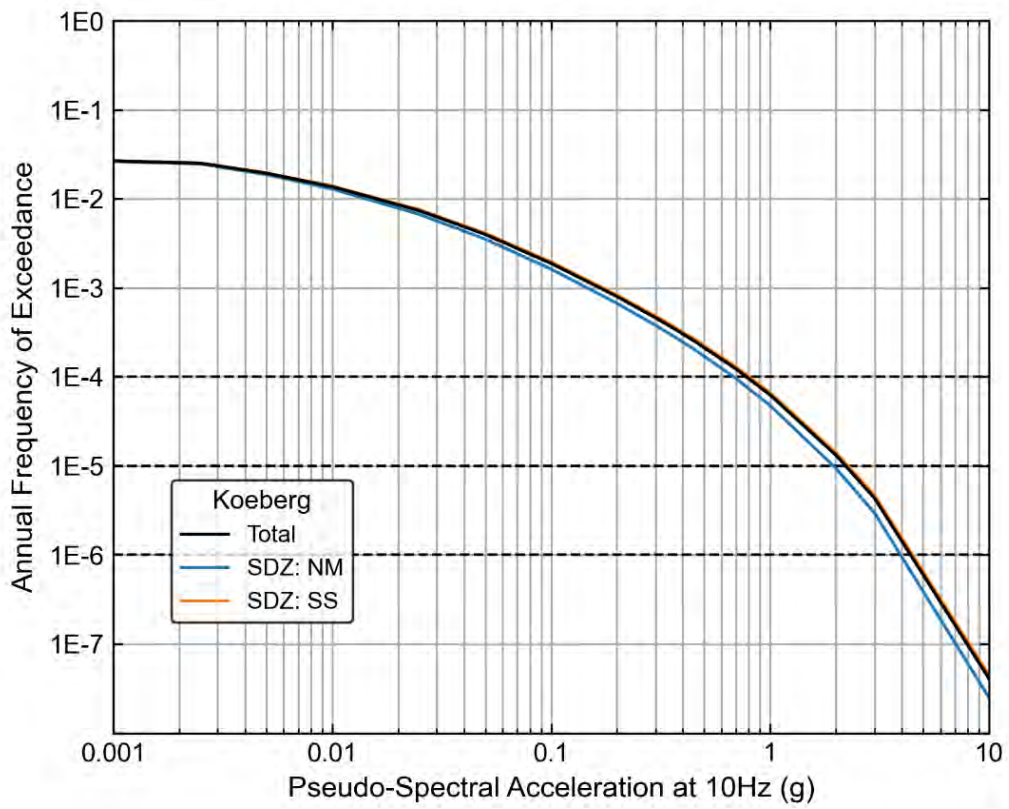

Figure 10-109. Hazard sensitivity for 10Hz to fault mechanism in the host zone for the KNPS.

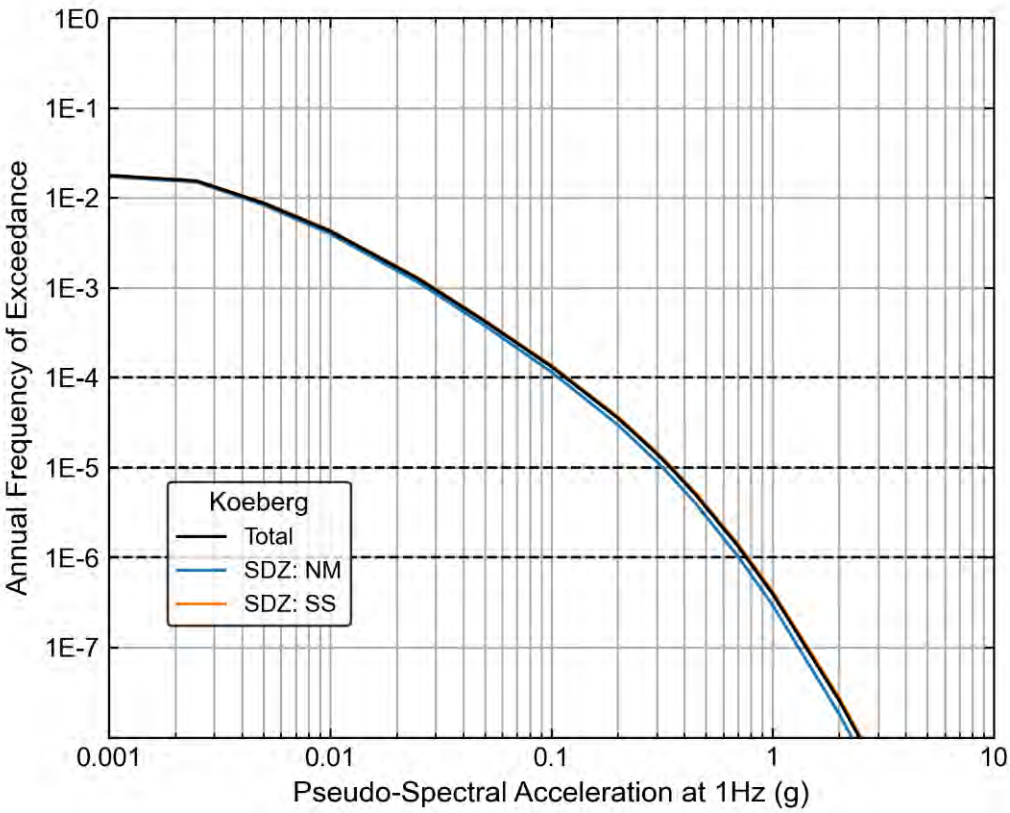

Figure 10-110. Hazard sensitivity for 1 Hz to fault mechanism in the host zone for the KNPS.

10.4.2.2.5 Sensitivity to epistemic uncertainty in regional b-Value calculation method

Two methods were used to estimate the *b*-values for the source zones as described in Section 8.2.10. The first is the maximum likelihood method (LL) and the second is the *b*-positive method (BP). The hazard curves resulting from the different *b*-value calculation methods for oscillator frequencies of 100, 10, and 1 Hz are presented in Figure 10-111, Figure 10-112, and Figure 10-113, respectively. Hazard curves showing the sensitivity to the *b*-value calculation method for the remaining seven oscillator frequencies are presented in Appendix H. As demonstrated in the figures below, the hazard sensitivity at all frequencies shows insignificant variation due to *b*-value calculation method (approximately 1% above and below the mean).

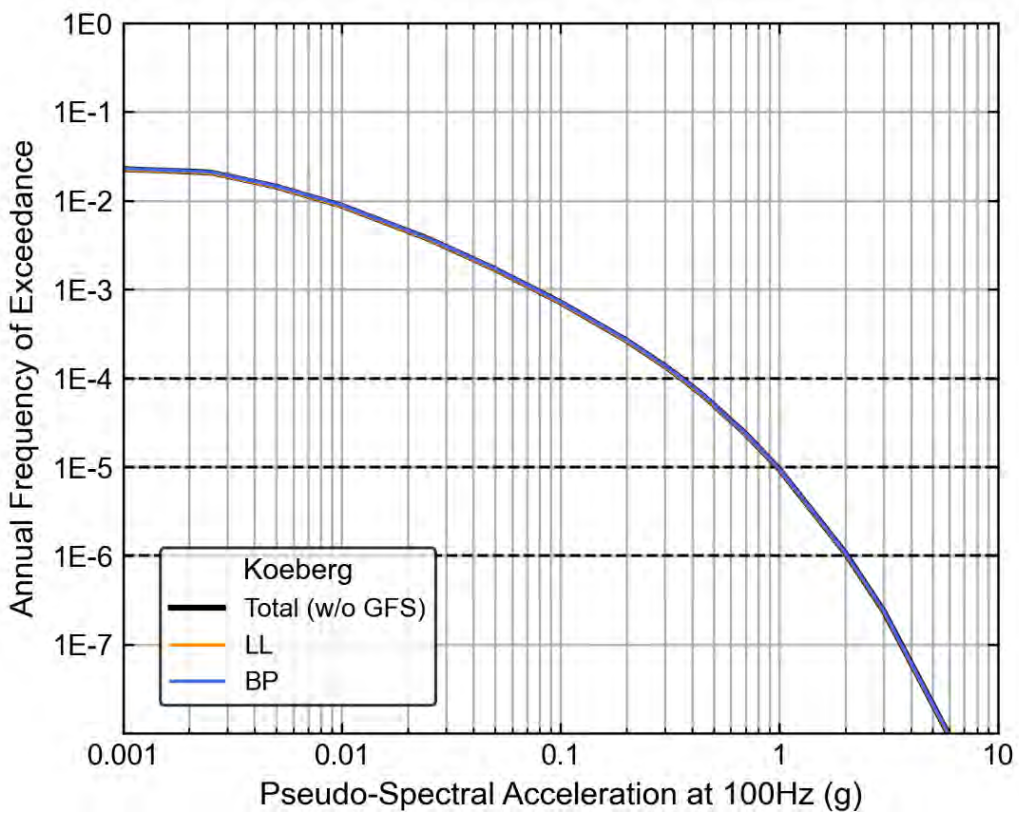

Figure 10-111. Hazard sensitivity to regional *b*-value calculation method for 100 Hz at the KNPS.

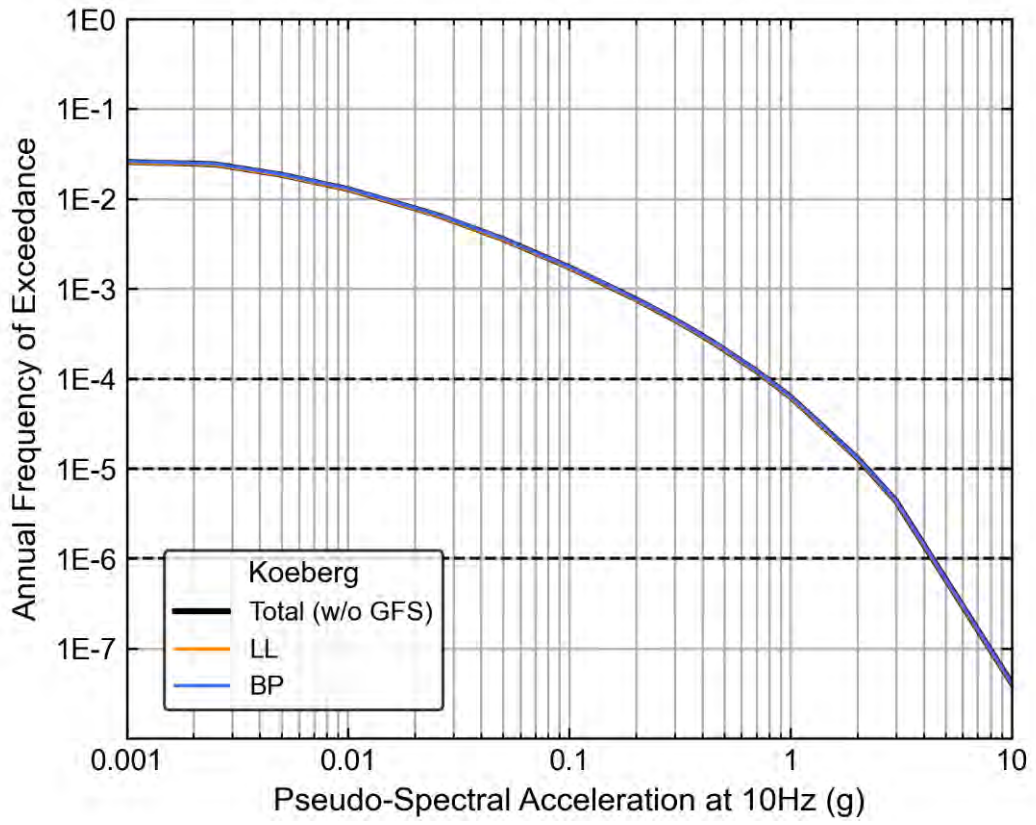

Figure 10-112. Hazard sensitivity to regional *b*-value calculation method for 10 Hz at the KNPS.

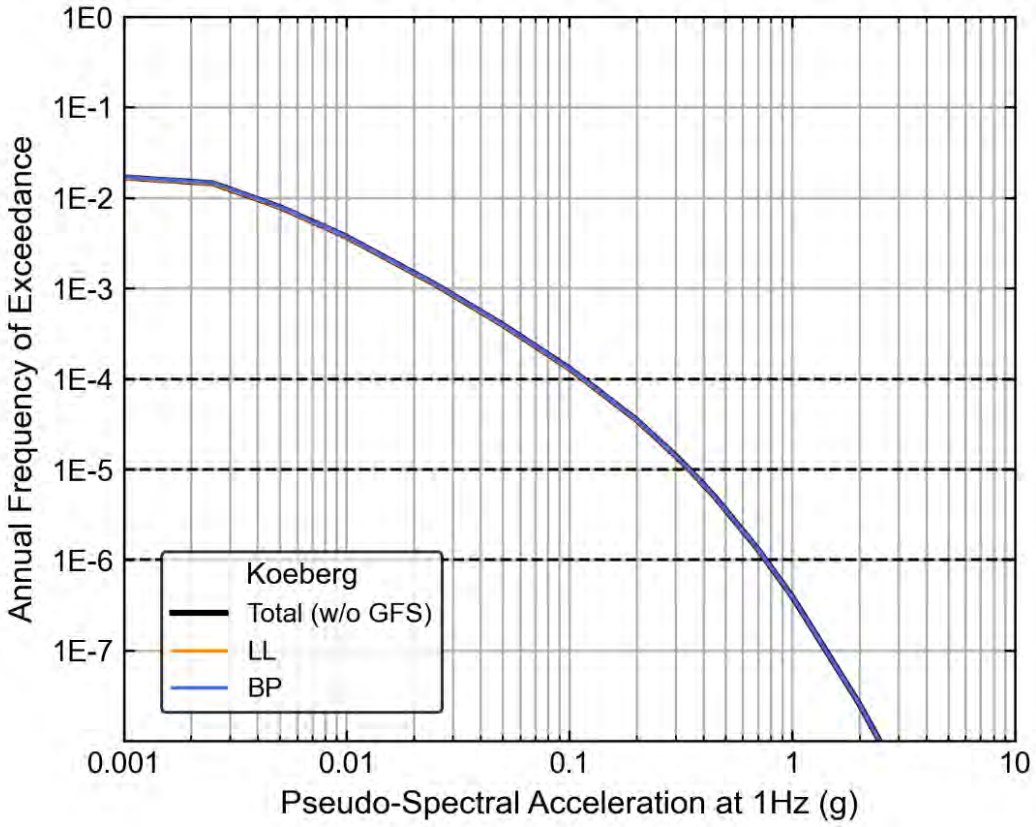

Figure 10-113. Hazard sensitivity to regional *b*-value calculation method for 1 Hz at the KNPS.

10.5 REFERENCES

Abrahamson, N. (2017). “HAZ” v45.2. Contributors: Hale, C.; Kottke, A.; Hsieh, P.S.; Murphy, D.G. and Gregor, N.J.

Al Atik, L. (2015). NGA-East: Ground-Motion Standard Deviation Models for Central and Eastern North America. PEER Report No. 2015/09. Pacific Earthquake Engineering Research Center, University of California, Berkeley, California, USA.

American Society of Civil Engineers (ASCE) (2019). ASCE/SEI 43-19 Seismic Design Criteria for Structures, Systems, and Components in Nuclear Facilities. Reston, Virginia, USA.

Bommer, J.J. and Stafford, P.J. (2020). Selecting Ground-Motion Models for Site-Specific PSHA: Adaptability Versus Applicability. Bulletin of the Seismological Society of America 110(6). 2801-2815.

Bommer, J.J., Coppersmith, K.J., Coppersmith, R., Hanson, K., Mangongolo, A., Neveling, J., Rathje, E., Rodriguez-Marek, A., Scherbaum, F., Shelembe, R., Stafford, P. and Strasser, F. (2013). Probabilistic Seismic Hazard Analysis for the Thyspunt Nuclear Site, South Africa. CGS Report 2013-0190. Council for Geoscience, Pretoria, South Africa.

Chiou, B.S.J. and Youngs, R.R. (2014). Update of the Chiou and Youngs NGA Model for the Average Horizontal Component of Peak Ground-Motion and Response Spectra. Earthquake Spectra 30. 1117-1153.

Cornell, C.A. (1968). Engineering Risk Analysis. Bulletin of the Seismological Society of America 58. 1583-1606.

Edwards, B. (2023). Final Report on ‘Inversion of ground-motion data to determine target source and path parameters for the development of the Ground Motion Model for Duynefontyn, South Africa. ISEIS-CGS-001.0.

Electric Power Research Institute (EPRI) (2015). High Frequency Program: Application Guidance for Functional Confirmation and Fragility Evaluation. Electric Power Research Institute, Palo Alto, California, USA.

GeoPentech (2015). Southwestern United States Ground-Motion Characterization SSHAC Level 3: Technical Report (Rev. 2). March 10.

Hale, C.; Abrahamson, N. and Bozorgnia, Y. (2018). Probabilistic Seismic Hazard Analysis Code Verification. Report No. 2018/03. Pacific Earthquake Engineering Research Center, University of California, Berkeley, California, USA.

Largent, M.; Williams, T.; Yust, M. and Montaldo-Falero, V. (2024). Virtual Rupture Generator Verification and Validation. CGS Report 2023-0201. Council for Geoscience,

Largent, M.; Williams, T.; Yust, M. and Shaw, K. (In Prep.). Verification and Validation for SSHAC-EL2 PSHA Inputs for the Duynefontyn Site and Koeberg Nuclear Power Station. CGS Report 2023-0196. Council for Geoscience, Pretoria, South Africa.

Osada, R.; Funkhouser, T.; Chazelle, B. and Dobkin, D. (2002). Shape Distributions. ACM Transactions on Graphics 21(4). 807-832.

Pacific Northwest National Laboratory (PNNL) (2014). Hanford Sitewide Probabilistic Seismic Hazard Analysis. Pacific Northwest National Laboratory Report PNNL-23361. Richland, Washington, USA.

Stafford, P. (2023). Personal Communication.

Stafford, P. (2014). Source-Scaling Relationships for the Simulation of Rupture Geometry within Probabilistic Seismic-Hazard Analysis. Bulletin of the Seismological Society of America 104(4). 1620-1635.

United States Nuclear Regulatory Commission (USNRC) (2001). Technical Basis for Revision of Regulatory Guidance on Design Ground Motions: Hazard- and Risk-Consistent Ground Motion Spectra Guidelines. NUREG/CR-6728. US Nuclear Regulatory Commission, Office of Nuclear Regulatory Research, Washington DC, USA.

United States Nuclear Regulatory Commission (USNRC) (2001). Design Response Spectra for Seismic Design of Nuclear Power Plants. Regulatory Guide 1.60 US Nuclear Regulatory Commission, Office of Nuclear Regulatory Research, Washington DC, USA.

United States Nuclear Regulatory Commission (USNRC) (2021). Seismic Hazard Evaluations for U.S. Nuclear Power Plants: Near-Term Task Force Recommendations 2.1 Results. NUREG/KM-0017. US Nuclear Regulatory Commission, Office of Nuclear Regulatory Research, Washington DC, USA.

Wooddell, K. and Watson-Lamprey, J. (2022). Verification and Validation Plan for the Senior Seismic Hazard Analysis Committee Enhanced Level-2 Probabilistic Seismic Hazard Analysis at the Duynefontyn Nuclear Site.

APPENDICES

APPENDIX A. BIOGRAPHIES OF KEY PROJECT PARTICIPANTS

TECHNICAL INTEGRATOR LEADS

John Stamatakos (Project Technical Integrator and SSM TI Lead), is a geologist and geophysicist who holds a MSc (1988) and PhD (1990) from Leigh University. He is based at the Southwest Research Institute, which he joined in 1995. Prior to that he held positions of visiting faculty at the University of Michigan and postdoctoral fellow at the Eidgenössische Technische Hochschule in Zurich, Switzerland. At the University of Michigan, Dr Stamatakos taught courses in field mapping, structural geology, geophysics, and tectonics.

Dr Stamatakos research experience includes basic and applied research in seismic sources characterisation for earthquake hazard studies; volcanic field characterisation for volcanic hazard analyses; kinematics of fault block rotations in active fault systems; effects of internal strain on the magnetic properties of deformed rocks; evolution of curvature in arcuate mountain belts; and age and sequence of deformation in folded and faulted mountain belts. He led and conducted investigations in the Basin and Range in the western United States, the northern and central Appalachians in the eastern United States and Canada, the coastal region of the United States, the Central United States, the Hercynian mountains in Germany and northern Spain, and the northern Cordilleran Mountains in Alaska.

Dr Stamatakos has been conducting seismic hazard studies and evaluations for more than 25 years, mainly for the United States Nuclear Regulatory Commission (USNRC) on commercial nuclear facilities, including expert testimony to the Atomic Safety and Licensing Board on seismic and volcanic hazard assessments. He participated in hazard assessments for nearly 20 commercial and governmental facilities, mainly in the United States, but also for other internationally-based facilities.

Dr Stamatakos co-authored several NRC seismic hazard documents, including NUREG-2213 updated guideline on SSHAC studies and the recent update to the American Nuclear Standard (ANSI/ANS-2.29-2020) titled "*Probabilistic Seismic Hazard Analysis*". He also has practical experience in the execution of SSHAC projects, having served on the Participatory Panel Review Panels (PPRP) for SSHAC Level 2 and Level-3 studies and participating as member of the Seismic Source TI Team for the Idaho National Laboratory SSHAC Level-3 study. He is currently serving on the Committee on Geotechnical and Geological Engineering (COGGE) at the United States National Academy of Sciences.

Jennie Watson-Lamprey (GMM Lead) is an engineering seismologist with over seventeen years of seismic hazard and ground motion characterisation experience for high consequence of failure projects, including nuclear power plants, dams, hospitals, and other high occupancy facilities. An expert in seismic hazard analysis and ground-motion model development, Dr Watson-Lamprey has worked in diverse seismotectonic settings. Past hazard projects include ground-motion and hazard assessment in Indonesia, Japan, Finland, France, the Continental United States, and Hawaii. In total, these projects include regions controlled by shallow, local earthquakes in active tectonic regions (central and southern California), earthquakes in volcanic environments (Hawaii), background seismicity (Intermountain United States), earthquakes in subduction zones (Japan), and earthquakes on high activity rate faults (central California).

Dr Watson-Lamprey developed ground motions to evaluate the potential liquefaction and deformation at three sites in Hawaii. Other notable time series selection and modification projects include developing ground-motions from shallow crustal tectonic environments (PEER NGA-West2) and subduction environments (NGA-Subduction) for the Columbia Nuclear Generating station. Recently, she modified the input ground motions for the structural upgrade of the Millennium Tower in downtown San Francisco.

She has experience developing site-specific ground motion characterisation models in areas of low seismicity and in areas where ground-motion prediction equations (GMPE) are unavailable. Dr Watson-Lamprey's orientation-independent measure of ground motion was used in the Next Generation Attenuation (NGA) West 1 project. Subsequently to that she worked with the NGA-West 2 developers to incorporate directivity into their suite of models based on directivity effects calculated with state-of-practice directivity models over a range of magnitudes, distances, hypocentres, and rupture types. She was also involved with developing GMPEs for the challenging tectonic settings of Hawaii, where seismicity is highly regionalised, and the complicated seismotectonic environment of Puerto Rico.

Past SSHAC projects include work on the Diablo Canyon, Palo Verde, and Blue Castle SSHAC Level 3 projects. Dr Watson-Lamprey was both a Resource Expert and Proponent Expert for the Diablo Canyon and Palo Verde SSHAC projects, and also served as Technical Integration staff and technical support for the ground motion characterisation. For the Blue Castle SSHAC, Dr Watson-Lamprey was a member of the Technical Integration team.

TECHNICAL INTEGRATION TEAM

Hayley Cawthra is a geologist employed by the Council for Geoscience (CGS), where she leads the marine geoscience programme. She is also a Research Associate in Nelson Mandela University's African Centre for Coastal Palaeoscience. Dr Cawtrha has over 17 years of experience in the acquisition, processing and interpretation of marine geologic and hydroacoustic data and is a qualified commercial diver. Hayley has research interests in Pleistocene sea-level change and reconstructing now-submerged terrestrial landscapes on the continental shelf. This is done by coastal- and offshore mapping, and studying markers of palaeoenvironmental and palaeoclimatic change over time. Hayley has led or been a co-investigator on several local and international projects, all with a focus on South African records. She has published more than 100 papers in peer-reviewed journals in the field of marine geology, and her work has received over 1900 citations to date.

Dr Cawthra completed a PhD in geologic science from the University of Cape Town (2014), carried out a post-doctoral research fellowship at the University of Bremen in 2016, and was a junior fellow of the Hanse-Wissenschaftskolleg in Germany from 2017-2019. She is a steering committee member of the South African Extended Continental Shelf Claim Project and a technical advisor on the South African delegation to the International Seabed Authority where she is assisting in the development of a sustainable deep seabed mining legislation for international waters under the auspices of the United Nations. Hayley is a Fellow of the Geological Society of South Africa and is a rated scientist by the National Research Foundation of South Africa. Her interests extend to geoheritage and geoscience education and she has worked on several initiatives in this regard.

Dr Cawthra was a team member supporting the marine geoscience investigations for the Duynefontyn, Thyspunt and Bantamsklip nuclear sites (responsible for the processing of side-scan sonar and sub-bottom profiling data) in 2006 and 2007. She also participated in the SSHAC Level 3 investigations that followed at Thyspunt. More recently she participated in studies characterised potential geologic tsunamigenic sources for the Duynefontyn nuclear site.

Debbie Claassen holds the position of Senior Geologist at the Council For Geoscience, boasting 17 years of extensive experience across a diverse range of geologic disciplines. She obtained a BSc Honours (2007) and MSc (2015) from the Nelson Mandela Metropolitan University. Ms Claassen led and participated in a variety of multidisciplinary mapping research projects focused on detailing the lithostratigraphy, sedimentology, structure sedimentology, geohydrology and mineral potential of rocks associated with the late Carboniferous to Jurassic Cape Fold Belt, Karoo Supergroup and near coastal environ deposits of the Cenozoic Algoa Group within the Eastern Cape Province. Mapping efforts also included investigations on alluvial diamonds in the Free State, Northwest and Northern Cape provinces during 2015-2017. In total she has published more than 20 detailed geologic maps and several extensive geoscience reports and publications on geology across South Africa, including a set of detailed alluvial diamond maps in the greater Douglas area. For her efforts she received the Council for Geoscience Award for Scientific Excellence in 2018. She continues to actively lead several geohazard studies, including investigations into land degradation and soil erosion in the development of hazardous gullying in the northern Eastern Cape as part of a PhD degree. She is also involved in several neotectonic investigations and site safety investigations in support of Seismic Hazard Analyses of the Thyspunt nuclear site in the Eastern Cape.

She is a registered Professional Natural Scientist with the South African Council for Natural Scientific Professions and an active member of multiple professional societies and committees, including the Geological Society of South Africa, Africa Earth Observatory Network - Earth Stewardship Research Institute and served as the Secretary of the Post-Karoo Working Group, South African Committee of Stratigraphy (SACS) from 2019-2021.

Ryan Coppersmith is a structural geologist who obtained his MS in structural geology from the University of Texas at Austin (2008). Since 2008 he has been active and specialising in probabilistic hazard analyses (e.g., for seismic and fault displacements hazards) and geologic investigations in highly regulated environments. These studies typically involve the characterisation of earth science data, and their associated uncertainties, for the purposes of quantifying vibratory ground motion and fault displacement hazard at new and existing sites. Geological studies carried out in these environments typically include both Quaternary and bedrock mapping, compiling and managing relational project and GIS databases, and interpreting site geologic data. Mr Coppersmith has managed large field campaigns and geospatial databases for domestic and international projects. These highly regulatory studies include clients from national laboratories, the USNRC, the USDOE, the USDOD, along with public utilities, state agencies, and oil companies.

He has significant experience in nuclear siting projects. This includes serving on the Technical Integration Teams for the SSHAC Level 3 PSHA for the Thyspunt nuclear site in South Africa, Hanford SSHAC Level 3 PSHA for the Hanford site (USA), SSHAC Level 3 PSHA for Nuclear Facilities in Spain and the SSHAC Level 3 PSHA for the Idaho National Laboratory Sitewide study. Mr Coppersmith is currently the SSC TI Lead for a SSHAC Augmented Level 2 study

for Los Alamos National Laboratory, and has also participated, in various roles, in the technical work for multiple PSHA and PFDHA studies of various regulatory levels over the past decade. In addition to being an SSC TI team member, he has a deep understanding of project and database management, often acting as the liaison between technical teams and management.

He has also been active in geologic investigations carried out in support of hazard studies. These included Quaternary and bedrock mapping, paleoseismic trenching, comprehensive geologic literature reviews, compiling project and GIS databases, interpreting site geologic data, and characterising seismic sources. Mr Coppersmith served as the field coordinator for multiple geologic field teams performing studies in the vicinity of the six nuclear power plant sites in Spain and established a centralised web-based system for storing and cataloging field data.

Courtney Johnson is an engineering geologist with degrees from the Pacific Lutheran University at Tacoma (BS, 2004) and The Pennsylvania State University (MS, 2006). She has over 17 years experience undertaking geotechnical, geologic hazard and seismic hazard projects for a variety of civil structures in the United States and abroad.

In addition to the assessment of earthquake-related geologic hazards (e.g., surface fault rupture, slope stability, liquefaction and related phenomena), Ms. Johnson has extensive experience in the development of earthquake catalogues, characterisation of seismic sources, and running computer models to calculate probabilistic ground motions and probabilistic fault rupture hazards. Ms. Johnson has worked with earthquake catalogues and developed seismic source zone characterisation parameters for crustal fault, subduction, and areal source zones, for project sites in central and eastern Canada, the eastern United States, Finland, and western Australia, as well as sites in active tectonic regions on every continent except Antarctica. The earthquake catalogue work has included assessment of available datasets, prioritisation mapping of reported origin time, location and magnitude for events, magnitude conversion, declustering, and completeness assessment. Seismic source characterisation work has included developing earthquake recurrence, spatial smoothing of the earthquake catalogue, and updates to crustal fault models including new segmentation models, updated fault extents, and updates to parameters such as fault dip, slip rate, recency of faulting, and characteristic magnitudes. Depending on owner and regulatory needs, the scope for these previous projects has included assessment and revision of previous models, compilation and development of a new seismic source model, or update and implementation of the Central and Eastern United States (CEUS) Seismic Source Characterisation model.

Brassnavy Manzunzu is a seismologist with degrees from the University of Zimbabwe (BSc Honours, 2006), National University of Science and Techncology (MSc, 2013) and the University of the Witwatersrand (PhD, 2021). He joined the Zimbabwe Meteorological Services in 2007, before moving to the Seismology Section in 2008 where he rose through the ranks to become the Seismology Manager in 2011.

Dr Manzunzu joined the Council for Geoscience in 2012 where he participated in several projects related to seismic hazard assessments in Africa. These involved commercial projects assessing seismic hazard and risk for sites of critical engineering structures such as dams, bridges, power stations, pipelines, buildings, etc. He has also worked on several statutory research projects including the development of the South African seismic hazard map, seismic hazard assessment for South Africa and the development of microzonation models for

Johannesburg and Kwa-Zulu Natal cities. In 2023 Brassnavy joined the National University of Science and Technology in Zimbabwe as a senior lecturer.

Brassnavy participated in almost all aspects of seismic hazard including the development of earthquake catalogues, seismotectonic modelling, seismic source characterisation, selection and ranking of ground motion prediction equations and seismic hazard calculations using a number of software including OpenQuake. He has published more than 20 papers in the peer-reviewed scientific literature.

Vunganai Midzi, is a seismologist who has been working at the Council for Geoscience since 2007. He obtained a BSc from the University of Zimbabwe (1990) and a MSc (1997) and Dr Scient. Degree (2000) in Seismology from the University of Bergen in Norway. Dr Midzi is a registered Professional Natural Scientist with the South African Council for Natural Scientific Professions.

Prior to joining the CGS, Dr Midzi was a senior lecturer at the National University of Science and Technology, Zimbabwe, where he worked for six years in the Applied Physics Department, concentrating mainly on teaching and supervising Geophysics postgraduate students. During this time he took the lead in undertaking a seismic hazard assessment for east and southern Africa. Since joining the CGS he focussed primarily on seismic hazard assessment and risk studies for commercial clients as well as research in relevant seismological topics, including the seismotectonics of the African continent. He played a key role in the development of the seismotectonic map of Africa, a project funded by UNESCO.

Dr Midzi was the technical lead of the CGS team responsible for developing the South African national hazard map. He has extensive experience in seismic hazard analyses, including large projects such as the SSHAC Level 3 PSHA for the Thyspunt nuclear site in South Africa.

Vunganai has published numerous scientific reports and more than 50 articles in peer-reviewed scientific journals and also serves as a reviewer for several international journals and examiner of postgraduate theses. He is an honorary lecturer at the School of Geosciences of the University of the Witwatersrand, South Africa, which allows him to contribute towards the training future scientists.

Valentina Montaldo Falero is an Assistant Vice Principal with WSP USA Environment & Infrastructure, Inc. (formerly Wood Environment & Infrastructure Solutions, Inc.). She has more than 20 years of research/consulting experience in probabilistic seismic hazard analysis and earthquake catalogue development. She received her MS (Laurea) in geology from Università degli Studi di Milano (Italy) in 2000, and her PhD from Università degli Studi di Milano-Bicocca (Italy) in 2006. Prior to moving to the United States, she was a researcher at Istituto Nazionale di Geofisica e Vulcanologia in Milan, Italy. There, she collaborated in developing the 2004 Italian national seismic hazard map and participated in projects funded by the Italian Emergency Management Agency (Protezione Civile).

She joined WSP (then Geomatrix Consultants) in 2007 and participated in several probabilistic seismic hazard studies for nuclear power, hydropower, oil/gas, and mining facilities. Her project portfolio comprises studies for nuclear power plants in the United States, including Combined Operating License Applications and Preliminary Safety Analyses Reports for proposed new nuclear reactors, seismic hazard studies for nuclear power plants and

repositories in Canada, including the siting of Canada's first small modular reactor and multiple SSHAC projects.

Dr Montaldo Falero's experience in SSHAC projects includes participating as the seismic hazard analyst in the SSHAC Level 3 Hanford Sitewide PSHA, the SSHAC Level 3 PSHA for Nuclear Power Plant Sites in Spain, and the Idaho National Laboratory (INL) SSHAC Level 3 Sitewide PSHA study. She was a specialty contractor for the development of the earthquake catalogue in the Central and Eastern United States Seismic Source Characterization for Nuclear Facilities SSHAC Level 3 project, the SSHAC Level 3 Hanford Sitewide PSHA study and the INL Sitewide PSHA study. She also was a member of the hazard calculation team in the BC Hydro SSHAC Level 3 study, contributed to the PEGASOS Refinement Project, and was the hazard analyst in the SSHAC Level 1 study for INL.

Dr Montaldo Falero is currently engaged as hazard analyst for the INL SSHAC Level 3 Sitewide Probabilistic Volcanic Hazard Study, as member of the Seismic Source Characterization Technical Integrator Team and seismic hazard analysis team for the Los Alamos National Laboratory Augmented SSHAC Level 2 study, and as seismic hazard analyst and specialty contractor (earthquake catalogue development) in a SSHAC Level 2 PSHA Study for a proposed new nuclear site in the eastern United States.

Thifhelimbilu F. Mulabisana is a geophysicist specialising in earthquake seismology. She obtained a BSc (2011), BSc Honours. (2012) and MSc (2016) from the University of Witwatersrand and a PhD (2023) from the University of Strasbourg (France). She has been based at the CGS since 2013 where she undertakes research on seismotectonics and seismic hazard. Dr Mulabisana has published 11 articles in peer-reviewed journals and contributed to numerous research reports. Project experience include participation in several international research projects such as the Global Earthquake Modelling (GEM) and IGCP-601, where she focused on developing seismic source models for hazard assessment of southern Africa and seismotectonics of southern Africa for the contribution to the Seismotectonics map of Africa, respectively. She has been part of CGS teams undertaking national seismic hazard projects (research and commercial), including the development of the South African national hazard curves and map. She is registered with the South African Council for Natural Scientific Professions as a Professional Natural Scientist, as well as involved in numerous earthquake seismology organisations such as IASPEI and AFSC.

Ellen M. Rathje is an engineer and currently the Janet S. Cockrell Centennial Chair in Engineering in the Department of Civil, Architectural, and Environmental Engineering at the University of Texas at Austin, and a Senior Research Scientist at the University of Texas Bureau of Economic Geology. She holds degrees from Cornell University (BS, Civil Engineering, 1993) and the University of California at Berkeley (MS, 1994; PhD, 1997) and is a Registered Professional Engineer and an Elected Fellow of the American Society of Civil Engineers.

Prof. Rathje has extensive experience and expertise in the areas of seismic site response analysis, seismic slope stability, liquefaction, field reconnaissance after earthquakes, and remote sensing. She led multiple research projects funded by the National Science Foundation and agencies such as the United States Nuclear Regulatory Commission, United States Geological Survey, Southern California Earthquake Center, other government departments

and industrial entities. Prof. Rathje has published more than 110 papers in peer-reviewed scientific journals, and also contributed to many technical reports.

Prof. Rathje is a founding member and previous Co-Chair of the Geotechnical Extreme Events Reconnaissance (GEER) Association, and currently the Principal Investigator for the DesignSafe-ci.org cyberinfrastructure for the NSF-funded Natural Hazards Engineering Research Infrastructure (NHERI). She has been honoured with the 2022 Peck Lecture Award from the ASCE Geo-Institute, the 2018 William B. Joyner Lecture Award from the Seismological Society of America and the Earthquake Engineering Research Institute, and the 2010 Huber Research Prize from the ASCE. She was elected Fellow of the American Society of Civil Engineers in 2016.

Her research in site response analysis has led to her involvement in seismic hazard assessment projects for nuclear facilities from around the world, including (e.g., US, Taiwan, United Kingdom, South Africa). She was a member of the Technical Integration teams for the SSHAC Level 2 project on the Site Response for Nuclear Facilities in the United States and the SSHAC Level 3 PSHA for the Thyspunt nuclear site in South Africa. She served on the Participatory Peer Review Panel for the SSHAC Level 3 probabilistic seismic hazard analysis for nuclear facilities at the Idaho National Laboratory.

Peter Stafford is an engineer who is currently Professor of Engineering Seismology at Imperial College, London. He holds a BE Honours. (2000), ME (2005) and PhD (2006) from the University of Canterbury in New Zealand. After stints in industry and as lecturer at the University of Canterbury, he joined the faculty of the Department of Civil & Environmental Engineering at Imperial College in 2007, where he contributes to teaching at late-stage MEng, MSc and PhD levels.

Prof. Stafford is an expert in ground-motion modelling, particularly for partially non-ergodic applications, but has a broad understanding of many aspects of seismic hazard and risk analysis, from seismic source modelling and seismicity analysis, through to the downstream geotechnical and structural engineering applications. He maintains active research interests in applications of probabilistic methods to engineering applications and applied structural dynamics of engineering structures, has contributed to more than 75 peer-reviwed papers in the academic literature, and co-authored the recently published textbook "*Seismic Hazard and Risk Analysis*".

In addition to his professional academic activities, Prof. Stafford remains actively involvement in industry, participating in numerous consulting projects related to probabilistic seismic hazard analyses and seismic risk analyses for critical infrastructure at locations throughout the world. These include serving on the Expert Panel on Natural Hazards of the Office for Nuclear Regulation (UK), and his involvement in the SSHAC Level 3 PSHAs for the Thyspunt nuclear site (South Africa), nuclear facilities in Spain and Idaho National Laboratories (USA) and the SSHAC Level 4 PEGASOS Refinement Project (Switzerland).

Kristin Ulmer is a Senior Research Engineer for the Southwest Research Institute (SwRI) specialising in geotechnical engineering and geotechnical earthquake engineering. She obtained a BS in Civil and Environmental Engineering and MS in Civil Engineering from Brigham Young University and was awarded a PhD in Civil Engineering from the Virginia Polytechnic Institute and State University in 2019. Her doctoral research focused on the

development of an energy-based procedure for evaluating liquefaction and incorporation of epistemic uncertainty in site response analyses in a probabilistic seismic hazard analysis (PSHA). In 2017 Dr Ulmer received the EERI/FEMA NEHRP Graduate Fellowship in Earthquake Hazard Reduction.

Since joining SwRI, she has participated in several research projects evaluating hazards from earthquakes and seismic-induced liquefaction, including review of liquefaction analyses in seismic probabilistic risk assessment documents, developing models to update regulatory guidance to evaluate soil liquefaction, and writing regulatory documents for incorporating seismic isolation and other technologies in a risk-informed and performance-based framework.

Dr Ulmer became a member of the global Next Generation Liquefaction project in 2020 which aims to advance the state-of-the-art in liquefaction model development. In 2021, she supported the hazard analyst team as part of a Senior Seismic Hazards Analysis Committee (SSHAC) Level 2 project that documented the process for systematically identifying and propagating epistemic uncertainties in site response analyses within the SSHAC framework. Following the devastating earthquakes in Türkiye in 2023, she joined a reconnaissance team through the Geotechnical Extreme Events Reconnaissance (GEER) association to document ground deformations and damage to foundations in the region with the goal of improving our understanding of liquefaction initiation and its effects.

HAZARD ANALYSIS TEAM

Micaela Largent is a Project Engineer with Slate Geotechnical Consultants, Inc. with six years of geotechnical, seismic hazard, and ground motion characterisation experience. Past hazard projects include ground-motion and hazard assessments in Finland, Hawaii, and California. Ms Largent performs seismic hazard analyses, develops site-specific design ground-motions using deterministic, probabilistic approaches and performs site response analysis.

She also has expertise in time-history selection and modification. Her practice includes linear scaling and spectral matching to select and modify records for dynamic analysis, fragility development, and risk analysis. Notable time-history selection and modification projects include developing a suite of two-component as recorded ground-motions from shallow crustal tectonic environments (PEER NGA-West2) to evaluate the performance of liquefaction and deformation, for three conditional mean spectra, at three sites in Hawaii. She also selected and modified suites of recorded ground-motions for a series of 11 hospitals in different regions of California per ASCE/SEI 7-16 for use in dynamic analyses.

Ms Largent was part of an engineering support team for an expert witness for the Mediation of Millennium Tower, calculating one-dimensional settlement and contributing to the development and presentation of a new framework for secondary settlement that capture the behaviour at time. Her professional interests are focused on seismic hazard analyses and time-history selection and modification.

Tessa Williams is a Senior Engineer with Slate Geotechnical Consultants, Inc. with nine years of geotechnical, seismic hazard, and ground motion characterisation experience. Past hazard projects include ground-motion and hazard assessments internationally, but primarily in California. Ms Williams performs seismic hazard analyses, develops site-specific design

ground-motions using deterministic and probabilistic approaches and performs site response analysis. She also has experience developing time series, including scaling and spectral matching. Notable projects include performing a ground motion hazard analysis and developing acceleration time series for inputs into the dynamic model for the Transbay Terminal Downtown Extension Tunnel project in San Francisco, performing a ground motion hazard analysis and 1-D equivalent-linear site response analysis for new structures in Vietnam, and performing a ground motion hazard analysis for a tailings storage facility in Canada.

Ms Williams has also authored papers with Dr Norman Abrahamson presenting the V_s Correction Methodology (also referred to as the One-Step Approach) for site response analysis, which has been used on previous SSHAC projects. Ms Williams has also published a paper demonstrating a method for developing suites of acceleration time-series (conditional scenario spectra) to be used for developing hazard curves for engineering demand parameters, which can be particularly useful for structures where spectral acceleration does not adequately capture the dynamic behaviour (e.g., displacement hazard curves for earth structures).

Kelley Shaw is an engineering geologist who obtained BS degrees in Geology and Environmental Science from the University of California at Davis. She was awarded a MS in geophysics by the University of Nevada, Reno in 2018. In her professional career she performed seismic hazard studies, geological mapping, geotechnical investigations, geomorphological interpretation, and geophysical studies for a variety of projects located throughout the United States, and abroad. Her project responsibilities have included catalog compilation and processing, characterisation of seismic sources and executing models to calculate probabilistic ground motions and fault rupture hazards. Ms Shaw worked on a number of fault rupture studies, as well as other studies focussed on geological hazards throughout the western United States. She has managed large-scale, multi-year geotechnical projects, leading large teams composed of numerous sub-consultants and subcontractors.

PARTICIPATORY PEER REVIEW PANEL

Julian Bommer (PPRP Chair) is a Chartered Civil Engineer, Fellow of the UK Institution of Civil Engineers, and Fellow of the Royal Academy of Engineering, holding a Masters' degree in Geotechnical Engineering and a PhD in Engineering Seismology. Dr Bommer was formerly Professor of Earthquake Risk Assessment at Imperial College London, where he now holds the position of Senior Research Investigator. He has published extensively on topics related to ground motion, seismic hazard analysis and earthquake risk assessment in relation to both natural and induced seismicity, and currently has more than 150 publications listed on *Web of Science* with over 14,000 citations and an *h*-index of 64 (74 on *Research Gate* and 77 on *Google Scholar*). He has also served on the editorial boards of many of the leading journals in this field, including *Bulletin of the Seismological Society of America, Bulletin of Earthquake Engineering, Engineering Geology, Soil Dynamics & Earthquake Engineering, and Structural Dynamics & Earthquake Engineering*.

Dr Bommer has undertaken field investigations of damaging earthquakes around the world, including Algeria, Armenia, California, Colombia, El Salvador, Greece, Italy, Japan, Mozambique, Turkey, and Peru. He has also worked extensively as a consultant in the areas of earthquake hazard and risk assessment for major engineering projects worldwide, including

dams, bridges, and pipelines, as well as serving on the Seismic Advisory Board for the Panama Canal expansion. Julian has served as a consultant on seismic hazard studies for nuclear facilities in Brazil, California, Romania, Switzerland, and the United Arab Emirates. He served as Project Technical Integrator and GMC TI Lead in the SSHAC Level 3 PSHA for the Thyspunt site and as GMC TI Lead in PSHA studies for nuclear sites in Idaho, Spain, and Washington. He is currently serving as PPRP chair for a SSHAC Level 2 PSHA for tailings dams in Minas Gerais, Brazil, and in the same role in a SSHAC Level 3 PSHA for a new-build nuclear site in Poland. He was a contributing author to the NUREG-2117 and NUREG-2213 guidelines on the Senior Seismic Hazard Analysis Committee (SSHAC) process for conducting such studies developed by the US Nuclear Regulatory Commission. In the UK, he led the Expert Panel on Seismic Hazard of the Office for Nuclear Regulation (ONR) for over a decade, reviewing all seismic hazard assessments for existing and new-build nuclear facilities. Dr Bommer also works extensively on hazard and risk assessments for induced seismicity with many engagements in Europe, Australia, and North, South and Central America, as well as advising the Oil & Gas Authority in the UK on induced seismicity related to hydraulic fracturing.

Recently Dr Bommer's contributions to the fields of Engineering Seismology and Earthquake Engineering have been recognised in two major awards. He was selected as the 2021 Joyner Memorial Lecturer by both the Seismological Society of America (SSA) and the Earthquake Engineering Research Institute (EERI), one of only four recipients (among 20) from outside the United States. He was also chosen by the UK Society for Earthquake and Civil Engineering Dynamics (SECED) to deliver the 17th Mallet-Milne lecture in 2022 on the subject of "Earthquake hazard and risk analysis for natural and induced seismicity: Towards objective assessments in the face of uncertainty".

Jon Ake is a seismologist specialising in seismic hazard and risk assessment for critical facilities. He holds a Masters degree (1984) and PhD (1988) in geophysics, both awarded by the New Mexico Institute of Mining and Technology. He previously was a Senior–Level Advisor for Seismic Engineering at the United States Nuclear Regulatory Commission (USNRC) and Senior Technical Specialist in Seismotectonics and Geophysics Group at the United States Bureau of Reclamation. He participated in the seismic review or analysis of the existing US nuclear fleet, new-build nuclear projects as well as more than a 100 dam sites.

As part of his duties he operated and analysed data from seismic networks deployed to study seismicity induced by reservoir impoundment and deep-well injection. Dr Ake also served on the expert panel for Mmax in the Groningen gas field. Dr Ake has extensive experience with hazard analyses using the SSHAC methodology. He was a member of the Seismic Source Characterisation expert panel for the Yucca Mountain PSHA, one of the earliest applications of the SSHAC framework. He participated as a member of the TI Team for the NRC SSHAC Level 2 site response project. Dr Ake also served on the PPRP for the Central and Eastern United States (CEUS) Seismic Source Characterisation SSHAC Level 3 project, the NGA-East SSHAC Level 3 project and the TerraPower SSHAC Level 3 Nuclear Reactor Siting Study. He was a contributing author to SSHAC guidelines published as NUREG-2117 and NUREG-2213.

Dr Ake was a member of development committees for ANS/ANSI Standards 2.27 (Criteria for Investigations of Nuclear Facilities Sites for Seismic Hazard Assessments), 2.29 (Probabilistic Seismic Hazard Analysis), and 2.20 (Seismic Instrumentation for Nuclear Facilities). He also

served as peer reviewer for the University of California Campus Earthquake Safety Program, British Columbia Hydroelectric, US Army Corps of Engineers, US Department of Energy, California Department of Water Resources, Federal Energy Regulatory Commission, and the Unites States Geological Survey, among others.

Raymond Durrheim is geophysicist specialising in seismology. He holds degrees from the University of Stellenbosch (BSc, 1977), University of the Witwatersrand (BSc Honours, 1978; PhD, 1989), University of Pretoria (MSc, 1984) and University of South Africa (BA, 1984). He recently retired as Professor from the University of the Witwatersrand with whom he had a long association (1983–1993 and 2007–present) and has been appointed as an Emeritus Professor, continuing to research, teach and consult. In between he was employed by the Council for Scientific and Industrial research to conduct research in seismology and mining safety. In 2007 Prof Durrheim was appointed as the South Africa Research Chair in Exploration, Earthquake & Mining Seismology, hosted by the University of the Witwatersrand.

His research interests are wide-ranging, but a major focus has been the risk that seismic events in gold mining districts pose to miners, mines, and the public. He was instrumental in the establishment of the AfricaArray research and capacity-building program (co-director, 2007 – present), which deployed a backbone array of 50 seismographs in 20 countries in Sub-Saharan Africa and more than 100 seismographs in various temporary arrays to investigate geodynamic process, resources and geohazards.

Prof. Durrheim has more than 190 refereed scientific publications, with over 4,500 citations and an h-index of 34. He has supervised numerous MSc (15) and PhD (13) studies, as well as seven postdoctoral fellows. Highlights include his involvement in: observational studies in South African mines to mitigate seismic risks (Japan-South African collaborative project, 2010-2015); Proponent Expert participating in the SSHAC Level 3 PSHA for Thyspunt nuclear site in South Africa (2011-2013); GEM seismic hazard model for sub-Saharan Africa (2016-2018); ISRM Working Groups on microseismic monitoring (2014-16) and deep mining (2019-present); ICDP research project drilling into seismogenic zones of M2.0-M5.5 earthquakes in deep SA gold mines (2016-present). He also participated in several Strategic Environmental Assessments as integrating author of the geohazard component of SEAs that address the risks associated with shale gas development (2016), gas pipelines (2019), electricity grid infrastructure (2019).

Honours include the following: South African Institute of Rock Engineering (SANIRE) *Salamon Prize* (1998), CSIR *Outstanding Achiever Award* (1999), SA Institute of Mining & Metallurgy Silver Medal (2003), Society of Exploration Geophysicists *Best Paper in Geophysics Award* (2012), SA Geophysical Association *Rudolf Krahmann Memorial Medal* (2015), NSTF-South32 *Lifetime Award* (2021), NSTF-South32 *Data for Research Award* (2021).

Marc Goedhart is a geologist who holds degrees from the University of Cape Town (BSc, 1987; BSc Honours, 1988), University of Illinois at Chicago (MSc,1991) and the Nelson Mandela University (PhD, 2019). His research interests are wide-ranging including sedimentary processes, mineralisation (especially the origin of the Wits gold), the deep crustal structure to cover sediments of the Cape Fold Belt and adjacent areas, soils on various geomorphic terraces and the 3D geometry of large fault systems using a variety of geophysical techniques and drilling investigations. Marc has 31 publications including conference

proceedings. He has reviewed and edited a wide variety of manuscripts and produced >100 technical reports for industry.

Dr Goedhart taught graduate sedimentology at the University of the Western Cape, before joining the Geological Survey of South Africa (later to become the Council for Geoscience [CGS]) in 1992. While there he conducted extensive field mapping in the Cape Fold Belt and adjacent Karoo and served as manager of the Eastern Cape regional office (1998–2004). He played a founding role for both the CGS's Groundwater Unit and what would later become the Nuclear Geohazards Group at the CGS. He was an active participant in the regional-to-site evaluation of new nuclear sites in South Africa, which included conducting the country's first detailed palaeoseismic trench investigation to determine Holocene reactivation of the Kango Fault. This large body of work formed the basis of his PhD research thesis. Dr Goedhart was the lead geologist for the onshore and offshore geologic investigations for the Thyspunt nuclear site in the Eastern Cape Province of South Africa. He supported technical review teams from Eskom, Areva and Westinghouse and technical meetings between Eskom, CGS and the National Nuclear Regulator. He served as the SA representative on the INQUA TERPRO commission on Palaeoseismology and Active Tectonics and on the Nelson Mandela Bay Disaster Management advisory committee. He was a contributing author to several chapters of the QA system that formed the basis of the CGS's Integrated Management System for nuclear projects.

In November 2010 Dr Goedhart founded Kainos South Africa. Notable projects have included participating as Resource Expert and a Proponent Expert in the SSHAC Level 3 PSHA for the Thyspunt nuclear site, and a PSHA sensitivity analysis for the Port of Ngqura. Kainos SA also played a key role in locating and drilling South Africa's highest yielding water borehole for the city of Gqeberha. He was also approached to teach short courses in Palaeoseismology to students of the Africa Array program at the University of the Witwatersrand.

Thomas Rockwell is a geologist who achieved international recognition for his work in paleoseismology and structural geology. He published over 190 articles in major international journals, coauthored a number of book chapters, published over 40 papers in conference proceedings and guidebooks, and coauthored several hundred papers presented at professional meetings. He is a professor at San Diego State University in Geological Sciences, having joined the faculty in 1983.

He served as Geology Group Leader and on the Planning Committee for the Southern California Earthquake Center for many years and is now on the Board of Directors. He is an expert on the tectonics and earthquake hazards of southern California and Baja California, has conducted extensive trenching programs to date earthquakes on faults in the western US, South and Central America, Europe, the Middle East and Asia, and routinely uses soil stratigraphy and geomorphology combined with various radiometric dating techniques to assess rates of fault activity, determine recency of faulting, and date past earthquakes. In the last two decades, he initiated a number of ground-breaking studies on fault zone architecture and processes in southern California and Baja California. New work on fault zone damage, pulverisation, and fluid processes has resulted in over two dozen well-cited papers on this topic since 2006. His other research focuses on understanding earthquake occurrence in time and space.

Current projects include the characterisation of fault systems behaviour by understanding patterns of past recurrence of large earthquakes on faults in southern California, northern Mexico, Portugal, Spain, the Czech Republic, and Germany. This work includes resolving information on slip per event, as it relates to understanding the controls on segmentation and rupture termination. Current work on fault zone processes initially focused on damage characteristics, but has shifted to the role of fluids and the processes that produce the damage. He has also worked extensively on the effects of tectonism on the landscape, and using geomorphology to constrain rates and timing of tectonic events. Included in this latter aspect are detailed mapping and dating of marine terraces along the west coast of North America and assessment of paleosea level during the late Quaternary.

As a consultant, he has worked on numerous critical facilities worldwide, including seismic hazard characterisation studies of dams, LNG facilities, nuclear power plants, the Panama Canal Expansion project, and US Government facilities (LANL). He has served on the PPRP for several SSHAC3 Seismic Source Characterisation studies (Diablo Canyon, Palo Verde, Korea) and one GMC study (SWUS), served on the TI team for the SSHAC3 for Natrium, and worked with the IAEA in evaluation of nuclear sites in Turkey, Armenia and Chile. He served on the Board of Consultants for utility companies in California, including Pacific Gas & Electric and Los Angeles Department of Water and Power, and has joined the Advisory Panel for Geotechnical Extreme Events Reconnaissance (GEER) Association, which coordinates National Science Foundation responses to extreme events, such as earthquakes, and the earthquake expert Board for the Los Angeles Metro.

Jonathan P. Stewart is an engineer and currently a Professor in the Samueli School of Engineering at University of California at Los Angeles (UCLA), where he has been a faculty member since 1996. He served as Chair of the Civil & Environmental Engineering Department from 2012-2018. He holds several degrees (BS, 1990; MS, 1992; PhD, 1996) from the University of California at Berkeley.

Prof. Stewart's technical expertise is in geotechnical earthquake engineering and engineering seismology, with emphases on soil-structure interaction, ground motion and ground failure hazard characterisation, and seismic risk analysis for levees and other distributed infrastructure. Several current research endeavours include his leadership of the Next-Generation Liquefaction project, development of site amplification and ground motion models for diverse global and region-specific applications, development and application of non-ergodic site response analysis methods for use in probabilistic seismic hazard analysis, and development of soil-structure interaction-based procedures for evaluating seismic earth pressures on retaining structures.

The work of his research group has impacted the US National Seismic Hazard Maps, the Global Earthquake Model, building code documents (NEHRP Provisions and ASCE-7); and guidelines documents for tall buildings (Tall Buildings Initiative project), existing structures (ASCE-41), soil-structure interaction (NIST, 2012), and landslide hazards (SCEC, 2002). His work has been recognised with a Fulbright Scholarship, the UCLA Distinguished Teaching Award, the Bruce Bolt Medal and the Joyner Lecture from the Earthquake Engineering Research Institute and Seismological Society of America, the Huber Prize and Casagrande Award from ASCE, the NSF CAREER Award, and two best paper awards and membership in the United States National Academy of Engineering.

He is a former Chief Editor for the ASCE *Journal of Geotechnical and Geoenvironmental Engineering* and former Editor of *Earthquake Spectra*. He is co-PI of the Geotechnical Extreme Events Reconnaissance Association and has led post-event deployments in California, Italy, Greece, and Lebanon. He currently serves on several committees that set or impact policy related to the identification or mitigation of earthquake risk, including the University of California Seismic Advisory Board, the Building Seismic Safety Council Provisions Update Committee (responsible for drafting the NEHRP Provisions and Commentary), the USGS National Seismic Hazard Model Steering Committee, and the Advisory Committee on Earthquake Hazards Reduction (provides input to and reviews NEHRP federal agencies).

He has participated in impactful professional activities, recent examples of which include: (1) Chair, Ground Motion Assurance Review Panel for Groningen Gas Field Seismic Hazard and Risk Study, The Netherlands; (2) Member, advisory panel for the New Zealand ground motion national hazard model; (3) Reviewer, Seismic Hazard Model for application to dams in British Columbia, Canada (BC Hydro); (4) Expert testimony and engineering team lead, Millennium Tower foundation performance, San Francisco, CA; (5) Expert witness, Champlain Tower South collapse, Surfside, FL; (6) Member, Technical Review Panel, Delta Conveyance Project, California Department of Water Resources; and (7) Member, Project Participatory Review Panel, SSHAC Level 2 probabilistic seismic hazard analysis for Los Alamos National Lab, New Mexico.

APPENDIX B. PPRP CONCURRENCE LETTER

7th March 2024

Mr Israel Sekoko
Nuclear Analysis and Siting Department
Koeberg Operating Unit
Eskom Holdings SOC Ltd. Reg. No. 2002/015527/30
R27 Trunk Road, Melkbosstrand 7440
South Africa
Email: sekokoi@eskom.co.za

PPRP Review of the Enhanced SSHAC Level 2 Probabilistic Seismic Hazard Analysis (PSHA) for the Duynefontyn Site, South Africa

This document constitutes the final consensus letter report from the Participatory Peer Review Panel (PPRP, hereafter "the Panel") for the Enhanced SSHAC Level 2 Probabilistic Seismic Hazard Analysis (PSHA) for the Duynefontyn site in South Africa.

Background

The PSHA for the Duynefontyn site in the Western Cape Province has produced estimates of the ground shaking hazard for both the operating Koeberg Nuclear Power Station (KNPS) and the Duynefontyn new-build site located just to the north of the KNPS site. The PSHA commissioned by Eskom has been executed by the Council for Geoscience (CGS) supported by teams of international experts.

The fundamental objective of the PSHA was to determine the seismic hazard in terms of vibratory ground-motion at the top of bedrock for specified locations at the Duynefontyn and KNPS sites. The ground-motion hazard was to be characterised in terms of the horizontal component of 5%-damped pseudo-acceleration response spectral ordinates, for oscillator frequencies between 0.5 and 100 Hz. The key deliverables were uniform hazard response spectra (UHRS) for annual frequencies of exceedance (AFE) from 10^{-2} to 10^{-8}, and ground-motion response spectra (GMRS) as specified in Regulatory Guide 1.208 issued by the United States Nuclear Regulatory Commission (USNRC).

The PSHA was to be executed as an enhanced SSHAC (Senior Seismic Hazard Analysis Committee) Level 2 process, following the specifications in NUREG-2213, published by the USNRC in 2018. A key requirement of the SSHAC process is the appointment of a PPRP to conduct process and technical review throughout the course of the study. The six members of the PPRP appointed for this project, through our individual and collective experience of PSHA studies and the SSHAC process, in addition to our proven subject-matter expertise, fully satisfy the requirements for this role as defined in Sections 2.6.8 and 2.6.9 of NUREG-2213. Evidence for this statement is provided in our brief biographical summaries in Appendix A of the final PSHA report. We are grateful to Eskom as the project sponsor for placing their trust in the Panel to undertake this review on your behalf.

We note that prior to the commencement of the Enhanced SSHAC Level 2 study, a Baseline PSHA study was conducted by the CGS, with three members of the PPRP serving as a participatory review panel. However, this letter, as a consensus report and closing statement of the PPRP focuses exclusively on the Enhanced SSHAC Level 2 PSHA study executed between February 2022 and March 2024.

Before presenting the Panel's assessment of the project within the framework of the SSHAC requirements, we would like to express our great appreciation of the work done by the Project Manager, Dr Johann Neveling, and his team at the CGS. We appreciate that the project has faced many challenges, including many logistical and administrative obstacles to be surmounted, and we believe that Dr Neveling and his colleagues deserve a very special mention for navigating the project through all these difficulties with equanimity and professionalism. We would also like to express our gratitude to the CGS team for facilitating the work of the Panel throughout the project, especially with regards to the excellent organisation of the Workshops and the hospitality extended to us on each visit to South Africa. Similarly, we would also like to express our appreciation to Eskom for facilitating the execution of our review, and in particular for enabling the Panel to meet in person to compile our review comments on the draft final report.

Objectives of the PPRP Review

As specified in NUREG-2213, participatory peer review is one of the five essential features of the SSHAC process. The role of the PPRP in a SSHAC project is to conduct process and technical review to ensure that the project meets the other four essential requirements of the process: (i) appointment of suitably qualified individuals to each of the specified roles within the project and compliance with the requirements of those roles; (ii) objective and impartial evaluation of all the potentially relevant data, methods and models to characterise the future seismicity of the region and the resulting ground motions at the target site; (iii) integration of the outcomes from this evaluation to develop logic trees for the characterisation of seismic sources and ground motions, including local site effects, that capture the centre, body and range of technically defensible interpretations (CBR of TDI); and (iv), comprehensive documentation of the evaluation and integration phases, including clear technical justifications for all features of the final models, together with the seismic hazard results for the target locations.

The purpose of this letter is to record the Panel's assessment of the project with regards to these four key requirements. We first explain how our review was conducted and then present our assessments of the process and of the technical outcomes. Although the distinction between process and technical review is often not clear-cut, we broadly address items (i) and (ii) under the heading of our process review and items (iii) and (iv) under the heading of our technical review.

Following the summaries of our process and technical review, we close with a summary of our findings and our concluding statements regarding the project and its deliverables. This

letter is the final contribution of the PPRP to the Enhanced SSHAC Level 2 PSHA study for the Duynefontyn site and it is to be included as an appendix to the final report.

Conduct of the PPRP Review

The Panel conducted its review via a series of engagements throughout the entire duration of the project, which enabled us to observe the process at many stages and also to provide feedback to the TI (Technical Integration) Teams in a timely manner. In the following sub-sections, we record the key activities involved in our review.

Review of the Project Execution Plan

At an early stage of the project, the Panel undertook a review of the Project Execution Plan (PEP). The overall assessment of the Panel was that the PEP was a clear and complete blueprint for the execution of the Enhanced SSHAC Level 2 PSHA study, but the PPRP did have some concerns regarding the technical qualification and SSHAC experience of some members of TI Teams. Specifically, the concern was whether the SSM (Seismic Source Model) and GMM (Ground Motion Model) TI Teams collectively satisfied the requirements for the attributes specified in NUREG-2213.

These concerns were raised with the Project Technical Integrator (PTI) and TI Leads through the Project Manager. In response to these concerns, some personnel changes were implemented, and new TI Team members were recruited.

Although not strictly part of the PEP, it is also pertinent to note under this heading that the PPRP was provided the opportunity to review the draft agenda for Workshop 2. The PPRP provided feedback in terms of topics to be addressed and specifically in terms of potential Resource and Proponent Experts to be invited to present at the Workshop.

PPRP Presence at Project Meetings

An indispensable element of the PPRP's role is to observe the three Workshops and the formal Working Meetings that form the backbone of the SSHAC process. The table below records the meetings that were attended by members of the PPRP, including an indication of which members of the Panel were present at each of these events.

At the Working Meetings, the PPRP observers provided informal feedback at various points, including the close of each day. At Workshops 1 and 2, the PPRP were present as observers but provided comments from the floor in open session at the end of each day and then gave more detailed feedback in closed meetings with the TI Leads and the Project Manager. At Workshop 3, in accordance with the SSHAC guidelines, the PPRP were active participants rather than simply observers since the third workshop provides an opportunity for the Panel to interrogate the TI Teams regarding the preliminary SSM and GMM, as well as on the

hazard sensitivity results. Since the Panel interacted with the TI Teams throughout the sessions of Workshop 3, there were no closed meetings with the TI Leads at the end of each day. An additional interaction between the PPRP and the TI Teams was the PPRP Briefing, which is discussed below.

Meeting	Dates	Location	PPRP Members
Workshop 1	23-24 February 2022	Cape Town, RSA	All
SSM Working Meeting 1	2-5 May 2022	Walnut Creek, CA, USA	RJD, TKR
GMM Working Meeting 1	2-5 May 2022	Walnut Creek, CA, USA	JPA, JJB, JPS
Workshop 2	20-24 June 2022	Stellenbosch, RSA	All
SSM Working Meeting 2	10-14 October 2022	Pretoria, RSA	RJD, MLG
GMM Working Meeting 2	10-14 October 2022	Pretoria, RSA	JJB
SSM Working Meeting 3	23-27 January, 2023	San Antonio, TX, USA	JPA, TKR
GMM Working Meeting 3	23-27 January, 2023	San Antonio, TX, USA	JJB, JPS
Workshop 3	19-23 June 2023	Stellenbosch, RSA	All
SSM Working Meeting 4*	July-August 2023	Virtual (online)	JPA, JJB, RJD, TKR
GMM Working Meeting 4	10-14 July 2023	Virtual (online)	JJB, JPA, JPS

* SSM WM4 was held in South Lake Tahoe, CA, USA, 28 August to 1 September 2023, but there was no PPRP attendance because the meeting was devoted to report writing; between WS3 and WM4, the SSM TI Team met online a few times and PPRP members participated in those calls (as observers) as indicated.

Following all three workshops, the Panel members remained at the meeting location for an additional day in order to compile and discuss our report on the Workshop, which was then submitted to the Project Manager prior to returning to our respective bases. The comments to the TI Leads provided overall feedback on the conduct of the Workshop and the engagement of the TI Team members in the discussions, as well as raising issues for their consideration during the ongoing work of evaluation and integration. The issues raised in these comments addressed elements of both the evaluation and integration processes, bringing to the attention of the TI Teams additional sources of information, concerns regarding the technical bases of modelling decisions, and suggestions regarding additional sensitivity analyses that could shed light on the relative impact of decisions being made in model-building process. The comments, particularly following Workshop 3, also highlighted where the Panel believed particular attention would need to be paid to documentation of the evaluation and integration stages that resulted in particular components of the final logic trees. The TI Leads were required to respond in writing to each of these comments, but there was no further formal follow-up since the purpose of the feedback after each workshop is precisely to raise issues ahead of the SSM and GMM being finalised.

Review of White Papers and PPRP Briefing

The SSHAC guidelines in NUREG-2213 only specify requirements for the review of two documents by the PPRP, namely the PEP and the draft final PSHA report. However, in this project, the TI Teams responded positively to a suggestion from the PPRP to issue White Papers outlining their evaluations and the emerging approaches to be adopted for the integration. Copies of the first drafts of these White Papers were shared with the PPRP prior to Working Meeting 2, which the Panel members found very informative. The PPRP

observers present at the Working Meetings in Pretoria in October 2022 were then able to provide feedback, informally, on these draft documents, including comments from the Panel members who did not attend.

The White Papers were updated and expanded as the work continued, and a revised version of the SSM White Paper was shared with the Panel in December 2022, in response to which we provided written comments for consideration by the SSM TI Team.

NUREG-2213 recommends that after completion of the final SSM and GMM following Working Meeting 4, a PPRP Briefing should be held in which the TI Leads, possibly supported by some or all members of their respective teams, present the models to the Panel. The PPRP Briefing was an innovation introduced to the SSHAC guidelines in NUREG-2213 based on lessons learned from high-level SSHAC projects, particularly the SSHAC Level 3 study for the Thyspunt site. The PPRP Briefing was introduced to bridge the potentially long period between the full PPRP's engagement in Workshop 3 and the review of the draft final report. The primary objective of the Briefing is to provide an opportunity for the PPRP to become familiar with the final models and their technical bases, and to provide feedback to the TI Leads regarding issues that will require particular attention in the documentation phase, possibly even including recommendations for sensitivity analyses (but it is not expected that the models would change following the Briefing). The intention is that the feedback from the PPRP at the Briefing pre-empts comments that would otherwise be made during the review of the draft final report.

The standard format for the PPRP Briefing is a series of presentations by TI Teams members summarising the evaluation and integration processes for both the SSM and GMM. For the Duynefontyn project, an alternative format was adopted following discussions between the PPRP and the TI Leads, facilitated by the Project Manager. This alternative approach was designed to be more efficient (which was an important consideration in view of the tight schedule for completion of this project) and potentially to meet the objectives of this meeting more effectively. This format was for the TI Teams to produce updated versions of the White Papers that presented and explained the key features of the final SSM and GMM logic trees. These documents were provided to the PPRP who then provided feedback in online meetings held on 21-22 September 2023.

Review of the Final PSHA Report

The final product of the PSHA project is the report documenting all aspects of the study from database compilation and new data collection, the evaluation of these databases and of available models, the development of logic trees capturing the CBR of TDI, and the final hazard results. The draft final report, consisting of ten chapters issued in effect as standalone reports, were provided to the PPRP in parts between 31 October and 7 November 2023.

The Panel members individually reviewed the submitted chapters and provided comments to the PPRP chair, who compiled the comments into a table for each chapter. The Panel then met in San Diego (California, USA) from 11 to14 December 2023. During this meeting, we

classified the comments as either ‘editorial’ or ‘technical’, removed or reconciled duplicate comments, and resolved comments on which there was not initially a consensus view among the Panel members. The comments were then submitted to the Project Manager and the TI Leads immediately following the meeting. There were around 3,500 editorial comments, provided in an Excel spreadsheet, and 472 technical comments provided in tabular form in a PDF file. The covering email from the PPRP clarified that written responses from the TI Teams were required for the technical comments but not for the editorial comments. The email also highlighted the technical comments of greatest importance.

The PPRP received the TI Teams’ responses to the technical review comments and several revised chapters of the report on 15 February 2024, with other elements (including the Executive Summary, the List of Abbreviations and Appendices) being delivered in the ensuing period up to 28 February. Once again, the PPRP members undertook individual reviews of the comment responses and of the revised report, providing comments to the Panel Chair for compilation. We then met online on 1 March 2024 to finalise the comments, which were then submitted to the Project Manager and the TI Leads on the same day. The comments were provided in an Excel file, with one sheet for each chapter or other element of the report, this time making no distinction between editorial and technical feedback. This final round of feedback included 440 comments, the majority being editorial in nature (and half of which corresponded to parts of the report that had not been previously reviewed, such as the Executive Summary), but a few refer to responses that the Panel did not feel had fully addressed our original concerns or for which we felt additional clarification was required.

In order to have assurance that due consideration was given by the TI Teams to the final comments from the PPRP, it was requested that written responses to the comments be provided prior to issue of this closure letter. These comments, which satisfied the Panel that the final report would be acceptable, were duly received on 6 March.

Process Assessment

On the basis of the review conducted as described above, the PPRP concludes that the Duynefontyn PSHA study has satisfied the requirements of the SSHAC process, both in terms of procedure and evaluation of the available data, method and models.

SSHAC Procedural Requirements

The final composition of the TI Teams satisfied the requirements of the SSHAC process in terms of the collective technical expertise and relevant experience of the team members, for both the SSM and GMM TI Teams. Moreover, the PPRP is of the view that TI Teams adhered to the requirement of acting as impartial and objective evaluators of the available data, methods, and models.

The Duynefontyn PSHA project has also met and exceeded the requirements of an Enhanced SSHAC Level 2 process in conducting a Kick-Off meeting, three formal workshops, four

formal working meetings of each TI Team, and a PPRP briefing. The PPRP has been able to evaluate the process through observation or participation in all these meetings and to provide timely feedback to the TI Teams. It is our view that the project actually satisfies the requirements of a SSHAC Level 3 study, and we recommend that it be classified as such.

Evaluation of Data, Methods and Models

The SSM and GMM databases assembled for the Duynefontyn PSHA project have included all relevant data for the seismic characterisation of the region and of the site. The compilation of existing datasets was complemented by extensive new data collection activities that have all contributed to better constrained hazard input models: retrieval and analysis of historical accounts of earthquakes and identification of the completeness of the historical record; re-evaluation of the earthquake catalogue for the syntaxis region; systematic analysis of the earthquake catalogue to identify and remove events of anthropogenic origin (mainly quarry blasts); evaluation of new offshore geophysical surveys; evaluation of marine terrace studies for evidence of displacements on faults crossing the coastline; studies of major known and postulated geological faults, including the inferred Milnerton fault; geochronology analyses to support the geological investigations; retrieval and analysis of borehole breakout and other data sets for the regional tectonic stress field; measurements of shear-wave velocities (V_S) at the target sites using borehole and non-invasive (surface-wave based) techniques; analysis of weak-motion recordings to estimate regional source and path parameters, which was complemented by V_S measurements at some of the recording stations; analysis of recordings from seismic arrays close to the site, including from newly installed borehole instruments on the Duynefontyn site, to infer dynamic response characteristics—especially the high-frequency attenuation parameter, κ_0—for the sites. These data collection, compilation and analysis activities were carried out by teams comprised of TI Team members and Specialty Contractors.

The information assembled in the project database was also supplemented by presentations at Workshop 1 made by Resource Experts, some of whom were TI Team members or Specialty Contractors engaged for the data collection and analysis activities. At Workshop 2, an impressive line-up of presentations was made by both Resource and Proponent Experts, providing excellent exposure to data, methods, and models for the TI Teams, who actively engaged with each of the presenters.

In our view, the SSM and GMM TI Teams were able to examine abundant and valuable datasets to inform their evaluations, and that they made these evaluations with due impartiality. Critically, these evaluations addressed the inevitable limitations of many of the datasets, which are a direct consequence of the low levels of seismicity in South Africa and the consequently sparse nature of the seismic data. The TI Teams made appropriate expert judgements regarding the degree of epistemic uncertainty associated with each of the key input models to the PSHA through these evaluations.

We conclude that in terms of the stipulations of assembling comprehensive databases and subjecting these to impartial evaluation, the project has satisfied the SSHAC process

requirements. We also conclude that the databases and their evaluation have been adequately documented in the final project report.

Technical Assessment

The PPRP believes that both the SSM and GMM capture the CBR of TDI with regards to characterising the seismic hazard at the Duynefontyn site. Concretely, this means that these models are, respectively, appropriate representations of the most likely patterns of future seismicity in the region and of the ground-motion amplitudes that would occur at the Duynefontyn site as a result of each possible future earthquake. The models also reflect the degree of uncertainty associated with these representations in the light of the current state of knowledge and the limitations of the available data. In the sub-sections below, we briefly summarise our assessment of the SSM and GMM.

The available information indicates that the SSM and GMM were correctly implemented in the hazard code, which itself has undergone appropriate quality assurance, hence we conclude that the hazard results are also reliable. The hazard results reflect the appreciable levels of epistemic uncertainty captured in the input models, and the disaggregation and sensitivity results suggest that the dominant influences on the hazard estimates are consistent with these models.

Seismic Source Model (SSM)

The final SSM consists of a number of seismic source zones and a single fault zone, namely the Groenhof Fault Source (GFS), which is the source of 1969 Ceres earthquake. The available geological and seismological data led the TI Team to conclude that all other mapped geological faults in the region, including the postulated Milnerton fault or lineament, are not seismogenic structures.

The hazard is almost entirely controlled by the seismicity within the host Saldania source zone (SDZ) that encloses the Duynefontyn site. The SSM captures the uncertainty in the spatial distribution of future seismicity within the SDZ through modelling both uniform activity across the source zone and also different degrees of spatial smoothing of the earthquake catalogue, with the latter reflecting the possibility of spatial stationarity (i.e., future earthquakes are more likely to occur at the locations of past earthquakes). Uncertainty in the average earthquake recurrence rates was captured through the use of different approaches to the calculation of these rates and the application of two different approaches to estimate the length of the catalogue completeness intervals for earthquakes of different magnitudes.

The assignment of zero probability of seismogenicity on all the mapped geological faults (apart from the GFS) does not preclude fault ruptures occurring at any location within the source zones. Indeed, the PSHA calculations generate virtual fault ruptures (VFRs) for each earthquake scenario in order to allow the correct calculation of the source-to-site distance metrics used in the GMM. The project has set new standards in visualising the VFRs

generated within the SDZ, whereas common practice is to simply generate the ruptures and calculate the corresponding distances within subroutines of the PSHA code without examining the nature of the ruptures. Through such visualisations, the project team arrived at the defensible decision to model each earthquake as a point source within all other source zones and to only generate VFRs within the host SDZ.

Ground Motion Model (GMM)

The GMM was constructed using the concept of an adaptable backbone ground-motion prediction equation (GMPE), which is consistent with the current state-of-practice. Two inversions, using different approaches, were performed on the database of ground-motion recordings from South Africa, to estimate parameters that characterise the strength of earthquake sources and the degree of attenuation experienced by seismic waves as they propagate through the crust. The TI Team made appropriate assessments of the epistemic uncertainties associated with these parameter estimates as a result of the recordings being predominantly from smaller-magnitude earthquakes recorded at large distances, whereas the hazard is controlled by events of moderate magnitude occurring relatively close to the site. Uncertainty also arises due to the limited dynamic characterisation of the recording sites. The ranges of source and path parameters were used to adjust the selected backbone GMPE for differences between the characteristics of the host region of the GMPE and the target region (i.e., the Western Cape). Additional epistemic uncertainty was included to capture the full range of possible ground-motion amplitudes in this region of South Africa, especially for larger earthquakes at short distances. The outcome was a GMM that is tuned to the seismic characteristics of South Africa (centre) while also reflecting the uncertainty in these characteristics (body and range). It is also important to note, however, that in developing the final distribution of median predictions, correlations between different elements were accounted for that avoided inflation of epistemic uncertainty. The implicit site response characteristics of the backbone GMPE were retained and then a host-to-target site adjustment made in one step using the full site profiles at the target locations, as described below. Since epistemic uncertainty was fully accounted for in the site adjustments, the model appropriately adopted a partially non-ergodic (or single-station) sigma model for the aleatory variability, to prevent double counting of the site-to-site variability.

The site adjustments were based on a characterisation of the dynamic properties of the target horizons (top of bedrock) at Duynefontyn and KNPS in terms of V_S profiles determined from both borehole and non-invasive measurements and damping profiles obtained from estimates of κ_0. Epistemic uncertainty was fully captured in logic trees developed for the site response analyses, in particular to incorporate the range of possible V_S values given the limited borehole data and the difficulties posed for non-invasive measurements due to the thick sand layers overlying the target bedrock. Uncertainty in the rock damping and the non-linear characteristics of the rock profile were also accounted for in the site response analyses. Recognising the steeply inclined layers of intensely folded turbidite rock below the site, the Team also explored possible 2D effects through modelling and new acoustic measurements of V_S in the layers. The conclusion was that any 2D effects would be sufficiently small to be neglected in the site response modelling.

The site adjustment factors were applied to the site- and path-adjusted models for ground motions inside the hazard integral, effectively creating site-specific GMPEs, which would therefore be classified by USNRC as Approach 4, the most rigorous method for incorporating site response into PSHA.

Conclusions

In closing, the conclusions of the PPRP, which represent the consensus view of the entire Panel, are summarised as follows:

- The Duynefontyn PSHA project has satisfied the requirements of a high-level SSHAC study and can be classified as a SSHAC Level 3 study.
- The PPRP concurs that the full ranges of relevant data, models, and methods were duly considered in the TI Teams' assessments.
- The PPRP concurs that the assessments and decisions defining the Seismic Source Model and Ground Motion Model, and their implementation in a carefully executed PSHA, are adequately defended and justified in the Final Report.
- The PPRP concurs, based on its observation of the implementation of the SSHAC Level 3 process and its review of the technical bases and justifications provided by the TI Teams for their representations of the centre, body, and range (CBR) of technically defensible interpretations (TDI), that the final PSHA for the Duynefontyn and Koeberg sites appropriately captures the CBR of TDI.

In the light of these conclusions, we believe that the results can be accepted with confidence as a reliable representation of the ground-shaking hazard at the Duynefontyn and Koeberg sites. These new hazard results supersede prior seismic hazard assessments for these sites, since none of these earlier studies conforms to the requirements of a modern site-specific PSHA. We believe that the new hazard estimates that have been generated by this study provide Eskom with a reliable basis for developing the safety case to support the application for an extension of the operation license for the KNPS and any new-build nuclear facility on the Duynefontyn site.

Julian J Bommer
Chair

Jon P Ake

Raymond J Durrheim

Marc L Goedhart

Thomas K Rockwell

Jonathan P Stewart

cc. Dr Johann Neveling, Project Manager, E: jneveling@geoscience.org.za
Dr John Stamatakos, Project Technical Integrator, E: john.stamatakos@swri.org

APPENDIX C. PROJECT CATALOGUE

Note: Lower magnitude limit is E[M] = 3.3

eqID	srcID	year	mon	day	hr	min	sec	lat	lon	dep	depFix	E[M]	sigEM	Nstar
9	TNS0008	1809	12	4	20	8	0	-33.905	18.409	20	F	6.12	0.242	1.133
37	TNS0034	1899	9	15	10	23	0	-33.905	18.409	20		4.66	0.231	1.121
43	TNS0040	1908	9	26	21	7	0	-28.7	25.8			4.66	0.231	1.121
47	TNS0044	1910	10	21	18	42	0	-30.55	24.7			4.66	0.231	1.121
49	TNS0046	1912	2	20	13	3	0	-29.5	25			6.05	0.108	1.025
63	TNS0059	1921	10	9	13	20	0	-33.3	19.1			4.66	0.231	1.121
74	TNS0070	1936	1	16	9	38	0	-29.8	25.3			4.66	0.231	1.121
85	CGS0078	1950	9	30	16	56	56	-30.5	18	0	F	5.2	0.233	1.124
88	CGS0081	1951	6	13	14	8	18	-31.9	23.2	0	F	4.36	0.23	1.12
89	CGS0082	1951	9	16	16	33	8	-33	22.5	0	F	4.27	0.23	1.12
96	CGS0089	1952	1	28	16	41	22	-32.9	20.5	0	F	5.09	0.232	1.123
103	CGS0096	1953	5	1	1	7	2	-29	17	0	F	5.53	0.235	1.126
107	CGS0100	1955	5	20	6	23	40	-29.3	25.3	0	F	4.77	0.231	1.121
111	CGS0104	1957	9	20	3	38	0	-34	18.2	0	F	3.89	0.229	1.119
112	CGS0105	1957	9	30	0	0	0	-34	18.2	0	F	3.89	0.229	1.119
113	CGS0106	1960	8	29	5	35	0	-33.448	18.373	20		4.46	0.23	1.12
114	CGS0107	1963	8	27	0	48	0	-33.44	19.229	20		4.66	0.231	1.121
116	CGS0109	1964	2	21	0	0	0	-34.1	18	0	F	3.98	0.229	1.12
117	CGS0110	1964	6	9	20	1	18	-29	25	0	F	4.66	0.231	1.121
118	CGS0111	1965	9	28	14	45	0	-33.9	22	0	F	3.98	0.229	1.12
119	ISC0002	1966	1	4	16	25	2	-28	26	0		3.38	0.229	1.119
120	ISC0003	1966	2	18	11	42	48.01	-29.057	25.449	10	F	3.95	0.162	1.058
121	CGS0113	1966	3	1	0	4	0	-34.1	18	0	F	3.98	0.229	1.12
122	CGS0114	1966	7	31	20	2	15	-30	19	0	F	3.95	0.162	1.058
123	CGS0115	1966	8	25	1	27	38	-28.4	19.3	0	F	3.51	0.162	1.058
124	CGS0116	1967	6	16	14	51	35	-30.4	18.4	0	F	4.04	0.162	1.058
125	CGS0117	1967	7	12	22	36	22	-30	20	0	F	3.51	0.162	1.058
126	CGS0118	1967	8	9	23	10	29	-31.3	23.3	0	F	3.43	0.162	1.058
128	ISC0010	1968	1	12	1	0	7.95	-33.126	23.704	10	F	5.25	0.165	1.06
129	CGS0120	1968	2	24	2	23	48	-30.2	20	0	F	3.43	0.162	1.058
131	CGS0121	1968	8	31	13	13	32	-29.6	25.9	0	F	4.08	0.229	1.12
134	ISC0016	1969	3	4	19	3	49.36	-29.951	25.842	14	F	3.71	0.229	1.119
135	ISC0017	1969	9	11	21	45	18.35	-33.807	18.714	20		4.93	0.164	1.059
138	ISC0018	1969	9	29	20	3	30.8	-33.265	19.281	16.7		6.16	0.14	1.043
162	ISC0024	1969	9	30	11	40	44.81	-32.801	19.969	10	F	4.13	0.162	1.058
175	ISC0030	1969	10	6	20	26	19.88	-33.838	19.972	10	F	3.63	0.229	1.119
179	CGS0165	1969	10	8	23	14	50	-32.2	19.2	0	F	3.8	0.229	1.119
180	ISC0032	1969	10	8	23	15	5.02	-32.59	20.281	10	F	3.8	0.229	1.119
181	ISC0033	1969	10	10	18	34	54.14	-33.924	20.391	10	F	4.52	0.163	1.058
189	ISC0035	1969	11	6	20	5	16.68	-34.352	19.254	10	F	3.99	0.162	1.058
191	ISC0036	1969	11	8	12	23	59.82	-32.475	19.742	10	F	3.99	0.162	1.058
216	ISC0045	1969	11	13	11	3	19.85	-33.126	20.815	10	F	3.86	0.162	1.058
232	CGS0214	1971	7	29	3	15	40.4	-31.7	25.8	30	F	3.77	0.263	1.16
233	ISC0054	1971	7	29	3	15	47.74	-31.691	25.213	10	F	3.63	0.229	1.119
234	ISC0055	1971	9	28	17	1	9.28	-32.451	20.859	10	F	4.27	0.23	1.12
235	TNS0171	1972	3	9	8	29	0	-31.796	25.049			3.43	0.162	1.058
236	ISC0057	1972	7	19	17	35	21.84	-31.695	25.393	10	F	3.86	0.162	1.058
237	TNS0173	1972	9	21	23	26	0	-29.531	25.649			4.42	0.163	1.058
239	TNS0174	1973	1	12	5	27	0	-33.327	19.103			4.18	0.162	1.058
240	ISC0060	1974	10	11	12	3	42.03	-30.667	23.883	10	F	4.62	0.163	1.059
241	CGS0220	1974	12	19	9	17	54.1	-33.294	19.25	5	F	3.38	0.229	1.119
242	CGS0221	1974	12	23	17	23	3.2	-33.386	18.843	5	F	3.54	0.229	1.119
243	TNS0178	1975	1	5	17	48	0	-32.37	23.343			3.46	0.229	1.119
245	ISC0062	1975	6	8	18	32	50.71	-29.452	25.156	8	F	4.32	0.162	1.058
247	ISC0063	1976	7	1	11	24	3.3	-29.596	24.994	11.9		5.7	0.149	1.049
273	CGS0249	1977	1	25	23	1	22.2	-28	16.9	10	F	4.08	0.229	1.12
274	ISC0071	1977	3	2	4	54	58.98	-32.658	19.251	10	F	5.09	0.164	1.06
288	ISC0072	1977	5	24	7	47	1	-31	26	0		3.71	0.229	1.119
289	ISC0073	1977	6	7	20	19	31.12	-33.259	19.357	10	F	5.04	0.164	1.059
290	CGS0265	1977	6	7	20	20	48.2	-29.7	24.4	10	F	4.17	0.23	1.12
313	ISC0076	1978	6	2	11	16	44.55	-29.494	25.147	8	F	3.56	0.162	1.058
324	ISC0077	1979	2	21	10	58	58.58	-29.418	21.121	10	F	4.52	0.163	1.058
327	ISC0080	1979	8	4	9	31	10.93	-29.571	20.948	10	F	3.86	0.162	1.058
329	ISC0082	1979	8	11	3	59	56.37	-29.238	20.61	10	F	3.4	0.162	1.058
330	ISC0083	1979	8	17	1	9	39.45	-29.262	20.065	10	F	3.86	0.162	1.058
333	ISC0085	1980	8	1	10	16	42.5	-30.14	19.6	10		3.54	0.229	1.119
334	ANS0005	1980	8	28	14	37	51.3	-30.697	24.399	33		4.94	0.263	1.16
336	CGS0309	1981	3	20	22	46	18.4	-30.72	21.95	10	F	3.38	0.229	1.119
337	GSO0001	1981	8	24	1	27	0.1	-33.305	18.994	15	F	4.32	0.162	1.058

350	GSO0006	1983	2	24	6	46	51.4	-32.467	19.342	10	F	4.27	0.23	1.12
352	ISC0094	1983	7	31	0	35	35.78	-31.115	23.911	10	F	3.54	0.229	1.119
355	ISC0095	1983	9	5	0	33	32.05	-29.355	25.056	8	F	4.27	0.23	1.12
360	ISC0099	1985	4	30	19	6	20.09	-29.298	19.906	10	F	3.89	0.229	1.119
361	ISC0100	1985	5	8	11	35	43.84	-29.285	24.832	7	F	4.87	0.231	1.122
365	ISC0103	1985	8	26	12	31	50.9	-29.249	20.051	10.4		4.27	0.23	1.12
366	ISC0104	1985	11	21	0	56	10.08	-29.364	23.993	10	F	3.63	0.229	1.119
369	ISC0106	1986	3	23	5	3	49.28	-29.334	24.672	8	F	3.46	0.229	1.119
373	ISC0107	1986	9	13	11	5	54.77	-30.773	23.922	10	F	3.54	0.229	1.119
375	ISC0108	1987	2	14	6	21	33.04	-29.493	24.744	8	F	3.86	0.162	1.058
382	ISC0112	1987	4	27	6	52	55.41	-29.811	19.79	10	F	4.27	0.23	1.12
392	CGS0364	1987	8	26	6	31	29	-29.48	25.04	5	F	3.3	0.229	1.119
394	GSO0009	1987	9	26	17	5	43.1	-30.168	18.472	10	F	3.31	0.162	1.058
404	ISC0117	1987	11	15	13	58	18.16	-29.486	25.135	8	F	4.5	0.133	1.039
405	ISC0118	1987	12	11	1	49	23.5	-29.5	19.79	10		3.47	0.162	1.058
413	CGS0383	1988	8	5	5	0	58.7	-29.46	19.96	10	F	3.55	0.162	1.058
425	CGS0395	1989	11	6	4	59	35.8	-29.23	25.32	10	F	3.8	0.229	1.119
428	ISC0122	1990	7	29	0	58	33	-28.7	24.8	0		3.38	0.229	1.119
434	ISC0123	1991	1	25	17	55	46.5	-30.09	22.5	5		3.06	0.229	1.119
436	CGS0403	1991	4	13	8	33	11.59	-33.982	18.188	5	F	3.26	0.14	1.043
439	CGS0404	1991	6	10	15	11	52.69	-33.335	19.352	288.1		2.91	0.229	1.119
440	CGS0405	1991	6	18	17	11	59.39	-29.785	22.406	10	F	3.51	0.132	1.038
441	CGS0406	1991	6	24	12	34	38.79	-30.049	18.749	10	F	3.29	0.132	1.038
442	CGS0407	1991	8	11	22	12	15.19	-30.668	19.048	10	F	3.73	0.132	1.038
443	CGS0408	1991	8	17	23	41	12.69	-29.396	22.119	10	F	3.43	0.162	1.058
446	GSO0011	1991	10	31	13	36	29.1	-33.255	19.31	5	F	4.06	0.14	1.043
449	CGS0414	1992	2	16	2	28	32.69	-28.051	17.092	10	F	3.46	0.229	1.119
453	CGS0418	1992	8	27	4	12	17.99	-31.533	22.798	38.8		3.54	0.229	1.119
454	CGS0419	1992	9	3	10	42	43.09	-28.461	25.123	199.7		3.38	0.229	1.119
455	CGS0420	1992	9	8	19	25	12.09	-32.651	18.056	0		3.63	0.229	1.119
456	CGS0421	1992	10	24	1	46	41.19	-30.012	25.464	10	F	3.01	0.162	1.058
457	CGS0422	1992	11	2	10	55	17.09	-31.576	23.059	10	F	3.31	0.162	1.058
458	ISC0133	1992	11	19	8	32	10.29	-30.346	24.959	10	F	3.73	0.115	1.029
459	CGS0424	1992	12	17	15	32	27.49	-29.165	25.824	339		3.14	0.229	1.119
460	ISC0134	1993	3	11	20	5	51.61	-29.195	18.805	10	F	4.74	0.133	1.039
461	CGS0426	1993	4	17	21	12	13.79	-31.054	24.932	5		2.91	0.229	1.119
462	PRE0008	1993	4	29	2	39	4.8	-34.356	18.292	5	F	3.36	0.14	1.043
463	ISC0135	1993	6	3	4	45	13	-29.395	17.897	10	F	3.82	0.132	1.038
470	ISC0136	1993	11	20	9	20	52.3	-29.68	19.42	10		3.3	0.229	1.119
473	CGS0431	1994	3	10	2	34	9.69	-29.833	19.566	38		2.99	0.229	1.119
475	CGS0432	1994	3	22	18	44	27.49	-29.488	25.116	10	F	3.43	0.162	1.058
481	CGS0433	1994	7	14	17	22	27.69	-30.337	17.216	41.6		3.14	0.229	1.119
482	CGS0434	1994	7	19	9	9	1.59	-29.671	25.333	10	F	3.16	0.162	1.058
483	PRE0021	1994	8	12	9	47	37.4	-33.117	18.619	5	F	2.96	0.14	1.043
484	CGS0435	1994	11	6	23	1	10.79	-29.379	18.743	0.1		3.46	0.229	1.119
485	ISC0139	1994	12	31	22	9	56.46	-30.379	20.867	10	F	4.54	0.133	1.039
487	CGS0437	1995	1	17	22	19	40.39	-29.432	19.245	41.3		3.38	0.229	1.119
488	ISC0140	1995	2	27	8	15	4.3	-29.58	18.51	10		3.82	0.132	1.038
491	CGS0440	1995	9	2	4	55	37.69	-29.34	19.928	39.5		2.99	0.229	1.119
492	CGS0441	1995	9	29	14	26	5.19	-28.573	24.611	237.4		4.08	0.229	1.12
493	CGS0442	1995	11	25	4	5	48.89	-30.629	21.761	2	F	5.31	0.234	1.124
495	CGS0444	1996	2	4	20	52	35.9	-32.635	20.585	5	F	3.51	0.162	1.058
496	CGS0445	1996	4	26	9	31	26.7	-29.31	19.607	10	F	3.6	0.162	1.058
497	CGS0446	1996	6	20	1	27	43.4	-29.576	25.222	10	F	2.9	0.162	1.058
498	PRE0024	1996	8	16	15	25	0.9	-33.353	19.282	5	F	3.26	0.14	1.043
499	CGS0447	1996	9	15	20	37	4.5	-30.09	19.599	10	F	4.51	0.133	1.039
501	PRE0026	1997	1	30	17	24	45.3	-33.537	19.656	5	F	3.16	0.14	1.043
513	CGS0451	1997	10	19	8	56	4.49	-29.813	19.535	5	F	3.06	0.229	1.119
516	CGS0452	1998	4	24	11	44	14.19	-28.306	20.471	5	F	3.73	0.162	1.058
517	CGS0453	1998	5	9	11	57	0.59	-30.288	24.248	2	F	3.3	0.229	1.119
519	CGS0454	1998	6	22	11	33	34.49	-31.846	23.294	5	F	3.23	0.162	1.058
521	PRE0038	1998	6	30	18	10	1.6	-33.576	20.061	5	F	2.99	0.229	1.119
522	CGS0455	1998	7	15	22	53	27.09	-30.065	24.444	5	F	2.97	0.162	1.058
533	GSO0013	1998	10	5	22	40	16.6	-31.641	21.987	5	F	3.4	0.162	1.058
534	PRE0048	1998	10	24	19	48	42.1	-32.72	20.378	5	F	2.91	0.229	1.119
538	CGS0462	1999	2	4	2	2	11.69	-30.134	24.919	5	F	3.76	0.14	1.043
541	CGS0464	1999	6	21	9	18	19.29	-29.594	25.296	5	F	3.08	0.162	1.058
542	ISC0152	1999	7	3	20	53	1.32	-29.39	24.611	7	F	3.83	0.132	1.038
544	CGS0466	2000	3	8	17	3	55	-32.767	20.247	5	F	3.06	0.229	1.119
545	ISC0153	2000	3	8	17	4	35.6	-28.28	17.959	5	F	3.14	0.229	1.119
547	CGS0468	2000	6	3	17	21	43.9	-31.559	20.809	5	F	3.14	0.229	1.119
549	CGS0470	2000	7	12	3	46	32.2	-32.295	23.934	5	F	3.16	0.162	1.058

550	TNS0283	2000	8	27	19	34	0	-28.874	19.737			3.63	0.229	1.119
551	CGS0471	2000	8	27	19	34	42.5	-30.88	19.014	5	F	3.06	0.229	1.119
560	CGS0486	2001	1	4	16	58	55.2	-30.769	23.688	2	F	3.06	0.229	1.119
561	ISC0158	2001	1	8	19	3	17	-29.967	25.418	2	F	3.63	0.229	1.119
562	CGS0487	2001	3	24	20	40	40.1	-29.868	18.516	5	F	4	0.162	1.058
563	CGS0488	2001	4	6	19	42	43	-29.689	19.623	5	F	3.94	0.133	1.039
564	CGS0489	2001	4	6	20	58	56.2	-28.405	19.965	5	F	4.13	0.162	1.058
567	CGS0491	2001	9	1	22	5	57.1	-33.556	24.409	5	F	3.35	0.162	1.058
568	CGS0492	2001	10	25	2	30	30.4	-30.883	22.784	2	F	3.22	0.229	1.119
569	CGS0493	2001	10	28	22	48	30.8	-33.706	22.465	5	F	3.91	0.162	1.058
571	ANS0017	2002	1	8	5	32	19.33	-29.268	24.112	5		4.24	0.133	1.038
572	ISC0167	2002	2	14	23	59	47.7	-29.203	18.538	5	F	3.86	0.162	1.058
580	CGS0495	2002	10	5	7	26	57	-34.278	22.338	5	F	3.82	0.162	1.058
582	ISC0177	2002	11	18	6	59	32.2	-33.217	19.62	5	F	2.99	0.229	1.119
587	ISC0182	2003	3	6	3	32	53	-33.27	19.386	5	F	2.51	0.229	1.119
590	ISC0185	2003	4	2	5	39	59	-30.55	25.615	5	F	2.32	0.229	1.119
591	ISC0186	2003	4	14	23	6	20.4	-33.34	19.338	5	F	2.27	0.229	1.119
592	PRE0053	2003	4	15	19	56	36.1	-32.03	15.639	5	F	3.26	0.14	1.043
594	CGS0496	2003	4	22	1	49	17.8	-30.382	19.274	5	F	2.38	0.229	1.119
595	CGS0497	2003	4	24	11	8	54.6	-32.389	20.806	0		2.64	0.229	1.119
596	ISC0188	2003	4	25	15	23	28.2	-30.804	25.659	5	F	2.32	0.229	1.119
597	CGS0498	2003	5	4	2	58	43.5	-29.513	25.267	5	F	2.76	0.162	1.058
599	ISC0191	2003	5	5	12	53	27.1	-29.225	23.261	5	F	2.84	0.229	1.119
600	ISC0192	2003	5	8	21	26	14.4	-29.852	24.617	5	F	2.64	0.229	1.119
601	ISC0193	2003	5	12	13	10	0.9	-29.379	25.729	5	F	3.3	0.229	1.119
602	ISC0194	2003	5	13	14	20	23.3	-28.988	24.139	5	F	3.22	0.229	1.119
603	CGS0500	2003	5	19	7	0	53.9	-33.452	18.532	5	F	3.26	0.14	1.043
604	GSO0015	2003	5	19	7	0	55.7	-33.775	18.81	5	F	3.26	0.14	1.043
605	ISC0197	2003	5	22	1	36	3.1	-33.401	19.262	5	F	2.51	0.229	1.119
606	ISC0198	2003	6	1	7	23	15.5	-30.713	25.983	5	F	2.27	0.229	1.119
608	ISC0200	2003	7	5	1	21	59.5	-33.362	19.315	5	F	2.26	0.14	1.043
609	ISC0201	2003	7	19	0	2	35	-33.375	19.307	5	F	1.96	0.14	1.043
611	ISC0203	2003	7	31	8	13	2.9	-33.369	19.303	5	F	2.06	0.14	1.043
612	ISC0204	2003	8	2	20	48	21.4	-30.216	24.431	5	F	2.77	0.229	1.119
613	CGS0501	2003	8	20	1	45	10.2	-31.925	23.347	5	F	2.38	0.229	1.119
614	ISC0205	2003	8	20	1	45	20.6	-30.852	25.126	5	F	2.7	0.229	1.119
616	CGS0502	2003	9	3	7	36	12.5	-33.352	24.191	5	F	3.31	0.162	1.058
617	ISC0208	2003	9	3	11	20	23.9	-32.925	23.466	5	F	2.32	0.229	1.119
619	CGS0503	2003	9	7	15	8	31.1	-31.298	23.455	5	F	2.38	0.229	1.119
620	ISC0210	2003	9	7	16	57	51.6	-31.031	19.993	5	F	2.38	0.229	1.119
621	ISC0211	2003	9	9	1	5	51.1	-28.399	19.925	5	F	2.64	0.229	1.119
622	ISC0212	2003	9	11	19	40	4.7	-30.136	24.848	5	F	2.38	0.229	1.119
623	CGS0504	2003	9	12	10	50	2.1	-31.775	23.388	5	F	2.44	0.229	1.119
624	ISC0213	2003	9	12	10	51	6.4	-33.372	20.451	5	F	3.16	0.14	1.043
627	ISC0216	2003	9	12	21	32	45.3	-33.327	19.269	5	F	1.96	0.14	1.043
629	ISC0218	2003	9	19	1	6	46.8	-33.39	19.331	5	F	2.46	0.14	1.043
630	ISC0219	2003	9	23	4	23	42.4	-33.201	19.186	5	F	2.27	0.229	1.119
632	ISC0221	2003	9	27	11	46	21.2	-30.057	24.041	5	F	2.7	0.229	1.119
633	ISC0222	2003	9	28	8	10	40	-30.811	24.2	5	F	2.7	0.229	1.119
634	CGS0506	2003	9	30	0	50	10.9	-30.393	21.191	5	F	3.01	0.162	1.058
640	PRE0055	2003	10	22	9	4	5.9	-33.382	19.318	5	F	3.28	0.244	1.136
641	CGS0508	2003	10	22	21	36	54.7	-28.654	25.062	5	F	3.01	0.162	1.058
647	ISC0236	2003	11	8	22	32	34.1	-33.876	24.629	5	F	2.84	0.229	1.119
648	ISC0237	2003	11	9	7	26	3.7	-28.298	18.272	5	F	2.44	0.229	1.119
649	CGS0509	2003	11	10	17	0	7.5	-30.323	25.723	5	F	2.66	0.162	1.058
652	ISC0241	2003	12	11	22	23	28.9	-29.971	18.707	5	F	2.57	0.229	1.119
654	ISC0243	2003	12	12	19	44	38.2	-33.179	19.226	5	F	3.16	0.14	1.043
656	CGS0511	2003	12	12	19	44	9.8	-32.5	20.518	5	F	3.16	0.14	1.043
657	CGS0512	2003	12	12	19	44	51.9	-29.256	18.32	5	F	1.66	0.14	1.043
658	PRE0057	2003	12	22	1	18	58.3	-34.104	19.267	5	F	2.77	0.229	1.119
659	ISC0244	2004	1	4	5	28	24.3	-29.849	17.424	5	F	2.38	0.229	1.119
660	ISC0245	2004	1	6	6	58	32.1	-33.356	19.288	5	F	2.26	0.14	1.043
661	ISC0246	2004	1	30	9	29	16.3	-30.014	18.253	5	F	2.32	0.229	1.119
664	ISC0249	2004	4	23	23	17	41.1	-34.551	20.887	5	F	2.91	0.229	1.119
665	CGS0514	2004	4	23	23	18	5.3	-32.781	20.091	5	F	2.32	0.229	1.119
666	CGS0515	2004	5	11	17	23	56.3	-29.442	20.79	5	F	2.44	0.229	1.119
667	ISC0250	2004	5	21	4	48	10	-33.365	19.305	5	F	1.96	0.14	1.043
669	CGS0516	2004	6	17	18	18	38.9	-30.32	23.298	5	F	2.38	0.229	1.119
670	ISC0252	2004	6	17	18	19	6.2	-28.775	20.131	5	F	2.64	0.229	1.119
671	ISC0253	2004	6	18	3	1	30.2	-33.313	19.415	5	F	2.06	0.14	1.043
672	ISC0254	2004	6	20	10	53	48.8	-31.006	25.97	5	F	3.22	0.229	1.119
673	ISC0255	2004	6	23	14	25	58.7	-34.342	25.968	5	F	2.27	0.229	1.119

674	ISC0256	2004	6	26	11	57	27.5	-34.044	25.394	5	F	2.32	0.229	1.119
675	ISC0257	2004	7	1	4	4	25.5	-30.2	21.419	5	F	2.84	0.229	1.119
676	ISC0258	2004	7	6	13	43	5.9	-29.926	21.819	5	F	2.38	0.229	1.119
677	ISC0259	2004	7	7	23	59	50.2	-33.643	16.62	5	F	2.51	0.229	1.119
678	ISC0260	2004	7	8	18	41	0.1	-28.537	23.909	5	F	2.27	0.229	1.119
679	ISC0261	2004	7	9	10	5	10.6	-29.684	20.167	5	F	2.77	0.229	1.119
680	ISC0262	2004	7	16	13	35	44.1	-29.246	24.26	5	F	2.32	0.229	1.119
681	ISC0263	2004	7	16	13	52	37.9	-33.218	24.146	5	F	2.51	0.229	1.119
682	CGS0517	2004	7	17	2	1	21.1	-32.322	23.351	5	F	2.32	0.229	1.119
683	ISC0264	2004	7	17	3	55	45.6	-31.662	23.994	5	F	2.84	0.229	1.119
684	ISC0265	2004	7	17	4	16	42.2	-29.235	17.722	5	F	2.27	0.229	1.119
685	ISC0266	2004	7	18	3	11	38.3	-29.713	19.744	5	F	2.32	0.229	1.119
686	ISC0267	2004	7	21	13	55	50	-31.413	19.512	5	F	2.38	0.229	1.119
687	ISC0268	2004	7	21	17	37	0.2	-33.286	20.321	5	F	2.27	0.229	1.119
688	CGS0518	2004	7	22	6	12	20.5	-32.361	24.708	5	F	2.38	0.229	1.119
689	ISC0269	2004	7	22	8	40	56.5	-29.612	18.726	5	F	2.38	0.229	1.119
690	ISC0270	2004	7	24	2	55	50.4	-30.602	19.331	5	F	2.27	0.229	1.119
691	ISC0271	2004	7	27	11	30	24.5	-30.667	15.489	5	F	2.44	0.229	1.119
692	PRE0059	2004	7	27	11	30	40.1	-33.987	18.52	5	F	2.46	0.14	1.043
693	ISC0273	2004	7	27	12	49	27.6	-32.762	19.13	5	F	2.26	0.14	1.043
694	ISC0274	2004	7	29	3	54	31.5	-29.68	17.905	5	F	2.51	0.229	1.119
695	CGS0519	2004	7	30	12	17	12	-29.693	21.495	5	F	2.51	0.229	1.119
696	ISC0275	2004	7	30	12	17	15.1	-32.669	17.497	5	F	2.7	0.229	1.119
697	ISC0276	2004	7	30	12	55	5.8	-31.014	18.731	5	F	2.84	0.229	1.119
698	ISC0277	2004	7	31	1	25	32.6	-33	24.973	5	F	2.32	0.229	1.119
699	ISC0278	2004	7	31	11	38	27.6	-31.253	22.071	5	F	2.44	0.229	1.119
700	ISC0279	2004	7	31	11	45	10.4	-29.067	18.146	5	F	2.32	0.229	1.119
701	CGS0520	2004	8	3	11	4	31.1	-30.51	17.799	5	F	2.6	0.162	1.058
702	ISC0281	2004	8	4	4	2	51.4	-30.476	25.221	5	F	3.06	0.229	1.119
703	ISC0282	2004	8	5	12	34	30.1	-32.916	23.332	5	F	2.32	0.229	1.119
704	GSO0020	2004	8	9	7	38	59.8	-31.206	19.832	5	F	2.91	0.229	1.119
705	CGS0522	2004	8	14	8	49	37.6	-29.628	19.68	5	F	2.32	0.229	1.119
706	ISC0284	2004	8	14	8	49	42.4	-32.14	21.538	5	F	2.44	0.229	1.119
707	ISC0285	2004	8	24	6	43	4.1	-28.592	19.575	5	F	2.32	0.229	1.119
708	ISC0286	2004	8	24	16	37	4.6	-28.534	20.617	5	F	2.44	0.229	1.119
709	ISC0287	2004	8	30	17	13	29.6	-31.155	24.151	5	F	2.57	0.229	1.119
710	ISC0288	2004	8	31	5	55	5.4	-30.248	21.737	5	F	2.32	0.229	1.119
711	ISC0289	2004	8	31	6	34	7.6	-30.11	17.799	5	F	2.32	0.229	1.119
712	ISC0290	2004	9	1	9	55	29.2	-31.034	19.135	5	F	2.91	0.229	1.119
713	ISC0291	2004	9	2	22	34	43.4	-28.699	16.692	5	F	2.77	0.229	1.119
714	ISC0292	2004	9	3	3	19	24.1	-29.732	19.384	5	F	2.44	0.229	1.119
715	ISC0293	2004	9	3	9	54	35.4	-30.339	18.559	5	F	2.27	0.229	1.119
717	ISC0295	2004	9	3	13	14	3	-28.801	23.082	5	F	2.91	0.229	1.119
718	ISC0296	2004	9	6	8	42	18.9	-30.678	20.23	5	F	2.44	0.229	1.119
721	ISC0299	2004	9	15	10	56	5	-28.766	22.909	5	F	2.91	0.229	1.119
722	CGS0523	2004	9	16	10	45	2.9	-30.057	21.007	5	F	3.08	0.162	1.058
723	ISC0301	2004	9	17	13	21	3.7	-31.003	21.939	5	F	2.64	0.229	1.119
724	ISC0302	2004	9	17	18	29	8.4	-31.449	21.055	5	F	2.99	0.229	1.119
725	CGS0524	2004	9	18	18	4	57.5	-30.046	19.22	5	F	2.44	0.229	1.119
726	ISC0303	2004	9	18	18	5	1.1	-30.744	21.137	5	F	2.64	0.229	1.119
727	ISC0304	2004	9	21	16	31	28.2	-31.451	18.387	5	F	2.27	0.229	1.119
728	CGS0525	2004	9	25	0	38	0.1	-28.227	23.485	0	F	2.6	0.162	1.058
729	CGS0526	2004	9	27	7	2	11.3	-33.265	19.216	5	F	2.16	0.14	1.043
730	ISC0307	2004	10	2	11	47	56.6	-31.365	24.302	5	F	2.38	0.229	1.119
731	ISC0308	2004	10	4	11	39	38.7	-30.995	21.89	5	F	2.44	0.229	1.119
732	ISC0309	2004	10	5	13	16	58.9	-30.686	21.75	5	F	2.27	0.229	1.119
733	ISC0310	2004	10	7	3	30	33.8	-32.824	19.977	5	F	2.38	0.229	1.119
734	ISC0311	2004	10	7	19	11	28.5	-29.997	21.719	5	F	2.57	0.229	1.119
735	CGS0527	2004	10	7	19	13	53.1	-29.779	23.916	5	F	2.35	0.162	1.058
736	ISC0313	2004	10	8	9	55	0.1	-29.313	22.854	5	F	2.38	0.229	1.119
737	ISC0314	2004	10	8	14	7	56.4	-29.975	20.378	5	F	3.14	0.229	1.119
738	ISC0315	2004	10	10	5	30	42.8	-32.712	18.187	5	F	3.38	0.229	1.119
741	ISC0317	2004	10	13	0	32	48.6	-31.365	23.393	5	F	2.77	0.229	1.119
742	ISC0318	2004	10	13	10	43	36.5	-32.24	22.487	5	F	3.06	0.229	1.119
743	CGS0529	2004	10	13	10	46	39.2	-30.724	25.3	5	F	2.57	0.229	1.119
745	ISC0320	2004	10	14	3	53	21.2	-33.248	19.365	5	F	2.16	0.14	1.043
746	ISC0321	2004	10	14	10	44	21.4	-31.5	18.415	5	F	2.57	0.229	1.119
749	ISC0324	2004	10	18	9	35	47	-31.044	21.076	5	F	2.91	0.229	1.119
750	ISC0325	2004	10	18	11	41	22.4	-30.495	23.989	5	F	2.32	0.229	1.119
751	ISC0326	2004	10	19	0	49	55.1	-30.023	18.426	5	F	2.57	0.229	1.119
752	ISC0327	2004	10	21	3	54	58.6	-31.228	18.713	5	F	2.32	0.229	1.119
754	ISC0329	2004	10	21	10	14	17.2	-29.664	21.527	5	F	2.64	0.229	1.119

755	GSO0021	2004	10	22	21	24	27.9	-32.914	17.742	5	F	2.56	0.14	1.043
757	ISC0330	2004	10	24	2	45	9.9	-31.586	20.487	5	F	2.27	0.229	1.119
758	ISC0331	2004	10	25	7	31	51.6	-33.184	19.414	5	F	2.44	0.229	1.119
759	GSO0022	2004	10	27	10	21	12.9	-33.218	19.103	5	F	3.26	0.14	1.043
760	ISC0333	2004	10	27	15	44	5.1	-33.408	19.658	5	F	2.66	0.14	1.043
761	ISC0334	2004	10	28	11	39	14.8	-29.667	21.822	5	F	2.84	0.229	1.119
763	ISC0336	2004	10	29	8	54	14.1	-29.664	24	5	F	2.57	0.229	1.119
764	ISC0337	2004	10	29	19	55	33.8	-33.755	24.509	5	F	2.99	0.229	1.119
765	ISC0338	2004	10	29	21	43	16.9	-34.797	25.581	5	F	2.64	0.229	1.119
767	ISC0340	2004	10	30	22	34	9	-32.113	17.543	5	F	2.77	0.229	1.119
768	CGS0532	2004	10	31	12	12	35.8	-33.02	24.711	5	F	2.27	0.229	1.119
769	ISC0341	2004	11	4	2	5	24.5	-33.288	24.754	5	F	2.84	0.229	1.119
770	ISC0342	2004	11	4	3	5	42.4	-32.603	20.332	5	F	2.84	0.229	1.119
771	ISC0343	2004	11	6	1	16	21.4	-32.35	19.302	5	F	2.44	0.229	1.119
772	ISC0344	2004	11	6	3	51	36.6	-30.849	18.498	5	F	2.91	0.229	1.119
773	ISC0345	2004	11	6	14	49	12.5	-32.311	19.821	5	F	2.38	0.229	1.119
774	ISC0346	2004	11	8	12	33	33.6	-30.396	20.666	5	F	2.91	0.229	1.119
775	ISC0347	2004	11	11	11	38	31.8	-33.667	19.256	5	F	2.27	0.229	1.119
776	ISC0348	2004	11	12	13	5	38.1	-30.611	21.452	5	F	2.51	0.229	1.119
777	ISC0349	2004	11	13	12	26	25	-33.26	25.6	5	F	2.57	0.229	1.119
778	ISC0350	2004	11	15	13	6	52.2	-28.071	24.559	5	F	2.57	0.229	1.119
779	ISC0351	2004	11	15	14	41	46.2	-30.098	20.434	5	F	2.57	0.229	1.119
782	ISC0354	2004	11	18	11	26	46.7	-32.44	25.479	5	F	2.32	0.229	1.119
783	ISC0355	2004	11	18	13	1	35.5	-31.066	23.662	5	F	2.44	0.229	1.119
784	ISC0356	2004	11	18	14	36	41.2	-29.932	21.171	5	F	2.44	0.229	1.119
785	ISC0357	2004	11	19	6	30	24.6	-33.357	19.293	5	F	2.16	0.14	1.043
786	ISC0358	2004	11	19	11	40	11.7	-31.147	22.643	5	F	2.32	0.229	1.119
787	ISC0359	2004	11	20	11	26	25.3	-33.982	24.991	5	F	2.84	0.229	1.119
788	ISC0360	2004	11	22	13	43	21.7	-33.982	19.178	5	F	2.38	0.229	1.119
789	ISC0361	2004	11	22	19	26	35.6	-31.86	19.165	5	F	3.22	0.229	1.119
791	ISC0363	2004	11	27	6	1	23.2	-33.534	19.785	5	F	2.36	0.14	1.043
792	CGS0533	2004	11	28	1	25	36.6	-36.91	25.49	5	F	2.77	0.229	1.119
793	CGS0535	2004	11	30	5	57	51.3	-29.476	25.125	5	F	4.18	0.162	1.058
794	ISC0365	2004	11	30	6	19	14.3	-34.367	19.773	5	F	2.91	0.229	1.119
795	ISC0366	2004	11	30	14	0	20	-33.684	19.6	5	F	2.44	0.229	1.119
796	ISC0367	2004	11	30	16	53	52.7	-33.008	19.186	5	F	2.7	0.229	1.119
797	ISC0368	2004	12	1	13	7	45.3	-28.965	16.69	5	F	2.64	0.229	1.119
798	ISC0369	2004	12	2	10	22	0.5	-33.582	18.567	5	F	2.57	0.229	1.119
800	ISC0371	2004	12	7	10	55	50	-33.053	20.097	5	F	2.91	0.229	1.119
801	ISC0372	2004	12	7	21	46	50.7	-33.357	19.295	5	F	2.27	0.229	1.119
802	ISC0373	2004	12	10	9	24	4.1	-33.059	19.579	5	F	2.38	0.229	1.119
803	ISC0374	2004	12	11	22	25	15	-33.042	19.011	5	F	2.27	0.229	1.119
804	ISC0375	2004	12	20	4	35	32.6	-33.247	19.297	5	F	2.32	0.229	1.119
805	ISC0376	2004	12	22	7	46	20.2	-31.771	19.351	5	F	2.32	0.229	1.119
807	ISC0378	2005	1	5	4	37	21.2	-33.369	19.293	5	F	1.96	0.14	1.043
810	ISC0381	2005	1	11	5	44	29.7	-33.362	19.294	5	F	1.96	0.14	1.043
811	ISC0382	2005	1	11	6	6	34.5	-33.207	19.108	5	F	2.27	0.229	1.119
814	ISC0385	2005	1	17	6	8	41.1	-29.757	19.931	5	F	2.57	0.229	1.119
815	CGS0537	2005	1	17	11	52	38.2	-31.41	20.509	5	F	2.83	0.162	1.058
816	ISC0387	2005	1	18	12	10	6.8	-34.106	25.529	5	F	2.64	0.229	1.119
817	ISC0388	2005	1	26	9	32	56.4	-31.799	18.859	5	F	2.51	0.229	1.119
818	ISC0389	2005	2	1	11	40	37.3	-34.269	25.725	5	F	2.44	0.229	1.119
819	ISC0390	2005	2	6	6	5	16	-33.367	19.293	5	F	2.32	0.229	1.119
820	ISC0391	2005	2	6	20	10	18.7	-32.783	19.932	5	F	2.64	0.229	1.119
823	ISC0394	2005	2	9	12	28	1.9	-34.262	25.816	5	F	2.32	0.229	1.119
824	ISC0395	2005	2	16	12	5	17.8	-33.049	19.143	5	F	2.7	0.229	1.119
825	ISC0396	2005	2	18	21	10	57.1	-29.698	19.405	5	F	3.22	0.229	1.119
827	ISC0398	2005	2	20	2	48	51.9	-32.298	17.818	5	F	3.22	0.229	1.119
829	ISC0400	2005	2	23	0	4	39.2	-33.399	19.314	5	F	2.76	0.14	1.043
831	ISC0402	2005	2	25	22	45	14.1	-33.743	19.386	5	F	2.44	0.229	1.119
833	ISC0403	2005	2	27	0	54	38.2	-33.411	19.669	5	F	3.14	0.229	1.119
834	CGS0539	2005	3	2	22	16	24.5	-31.379	21.074	5	F	2.86	0.162	1.058
835	ISC0405	2005	3	25	11	3	7.6	-30.996	21.326	5	F	2.38	0.229	1.119
836	ISC0406	2005	3	30	6	33	45.9	-28.898	24.38	5	F	2.44	0.229	1.119
837	ISC0407	2005	4	4	23	21	27.2	-29.943	19.855	5	F	2.77	0.229	1.119
839	CGS0540	2005	4	11	12	33	25.9	-33.791	21.972	5	F	2.77	0.162	1.058
841	CGS0542	2005	4	26	5	20	36.6	-29.731	23.713	5	F	2.27	0.229	1.119
842	CGS0543	2005	5	5	6	14	22	-28.121	16.747	5	F	2.57	0.229	1.119
843	CGS0544	2005	5	19	20	59	38.1	-28.534	17.439	5	F	2.32	0.229	1.119
845	CGS0546	2005	6	11	10	6	25.9	-29.699	19.713	5	F	2.69	0.162	1.058
846	CGS0547	2005	7	1	10	10	58.4	-30.151	18.597	5	F	2.7	0.229	1.119
847	ISC0413	2005	7	1	10	11	6.6	-31.411	21.181	5	F	2.77	0.229	1.119

849	ISC0415	2005	8	12	14	27	54.1	-30.452	23.803	5	F	2.27	0.229	1.119
850	ISC0416	2005	8	16	11	20	19.1	-28.15	22.355	5	F	2.27	0.229	1.119
851	ISC0417	2005	8	17	13	32	13.8	-29.544	24.267	5	F	2.32	0.229	1.119
853	CGS0549	2005	8	22	6	38	5.4	-30.278	20.136	5	F	2.44	0.162	1.058
856	ISC0421	2005	9	1	10	30	4.3	-30.253	25.945	5	F	2.7	0.229	1.119
857	ISC0422	2005	9	3	20	42	59.2	-32.385	18.708	5	F	2.27	0.229	1.119
860	ISC0425	2005	9	11	21	51	2.6	-31.63	22.058	5	F	2.27	0.229	1.119
861	ISC0426	2005	9	14	10	33	58.2	-34.037	19.298	5	F	2.38	0.229	1.119
862	CGS0553	2005	9	15	0	37	39.5	-30.372	19.112	5	F	2.32	0.229	1.119
864	ISC0428	2005	9	15	16	14	2.8	-29.743	21.215	5	F	2.27	0.229	1.119
865	GSO0023	2005	9	18	21	45	27.2	-33.357	19.15	6.7		2.38	0.162	1.058
866	ISC0430	2005	9	19	13	57	44	-31.188	22.474	5	F	2.27	0.229	1.119
867	CGS0555	2005	9	19	22	21	16.9	-29.377	24.83	5	F	2.83	0.162	1.058
869	ISC0433	2005	9	29	15	38	44.9	-33.174	21.163	5	F	2.64	0.229	1.119
870	ISC0434	2005	9	30	10	6	52.7	-34.645	20.006	5	F	2.51	0.229	1.119
871	CGS0556	2005	10	9	1	13	15.3	-32.929	22.139	5	F	2.38	0.229	1.119
873	ISC0436	2005	10	19	10	59	24.9	-28.538	22.375	5	F	2.27	0.229	1.119
874	ISC0437	2005	10	19	11	0	2.1	-28.026	21.18	5	F	2.77	0.229	1.119
875	CGS0558	2005	10	20	0	30	51	-30.2	18.459	5	F	2.47	0.162	1.058
876	CGS0559	2005	10	25	21	33	23	-29.607	22.251	5	F	2.6	0.162	1.058
877	CGS0560	2005	11	3	16	58	42.9	-30.132	19.736	5	F	2.66	0.162	1.058
879	ISC0441	2005	11	15	13	30	14.2	-28.998	23.487	5	F	2.27	0.229	1.119
880	CGS0562	2005	11	25	14	53	8.2	-29.038	20.401	5	F	2.63	0.162	1.058
881	CGS0563	2005	12	2	3	55	3.8	-29.033	25.056	5	F	2.38	0.162	1.058
882	CGS0564	2005	12	6	13	43	46.8	-34.041	23.152	5	F	2.64	0.229	1.119
883	CGS0565	2005	12	9	5	15	37.9	-29.249	23.945	5	F	2.38	0.162	1.058
885	ISC0446	2005	12	17	19	8	1.3	-31.027	21.451	5	F	2.27	0.229	1.119
886	CGS0566	2005	12	18	8	51	17.4	-30.113	18.067	5	F	2.63	0.162	1.058
887	ISC0448	2005	12	23	11	29	43.9	-32.255	21.041	5	F	2.27	0.229	1.119
890	CGS0568	2006	1	26	10	16	25.9	-30.605	23.528	5	F	3.01	0.162	1.058
893	CGS0571	2006	1	26	23	56	17.1	-29.417	25.03	5	F	2.44	0.162	1.058
895	ISC0453	2006	3	30	14	22	59.9	-29.531	18.554	5	F	2.32	0.229	1.119
896	CGS0573	2006	4	11	20	53	22.2	-30.772	25.881	5	F	3.24	0.162	1.058
897	ISC0455	2006	4	14	3	39	16.3	-28.737	23.93	5	F	2.32	0.229	1.119
898	CGS0574	2006	4	14	18	6	48.7	-30.169	19.752	5	F	2.5	0.162	1.058
900	CGS0576	2006	4	29	20	48	34.2	-32.417	22.221	5	F	2.76	0.162	1.058
901	CGS0577	2006	6	2	7	51	6.6	-29.422	24.35	5	F	2.79	0.162	1.058
902	CGS0578	2006	6	11	19	51	13.5	-30.275	24.618	5	F	2.47	0.162	1.058
904	CGS0580	2006	7	28	10	50	39.3	-30.461	22.415	5	F	2.44	0.162	1.058
905	CGS0581	2006	8	7	1	18	42.2	-29.564	25.033	5	F	2.79	0.162	1.058
906	ISC0462	2006	8	23	4	56	31.7	-29.033	20.45	5	F	2.32	0.229	1.119
907	CGS0582	2006	8	31	3	59	28.1	-29.807	19.433	5	F	2.41	0.162	1.058
908	CGS0583	2006	9	10	2	39	21.4	-28.55	21.747	5	F	2.5	0.162	1.058
909	ISC0465	2006	9	17	6	50	51.7	-31.182	20.341	5	F	2.38	0.229	1.119
910	CGS0584	2006	9	21	19	57	36.3	-28.082	24.365	5	F	2.38	0.162	1.058
911	CGS0585	2006	9	22	3	16	21.6	-29.763	25.294	5	F	2.41	0.162	1.058
912	CGS0586	2006	9	23	5	14	57.9	-28.352	19.817	5	F	2.41	0.162	1.058
913	CGS0587	2006	9	24	21	19	13.7	-30.281	21.849	5	F	2.93	0.162	1.058
914	GSO0024	2006	9	27	21	53	23.5	-33.422	19.017	5		2.66	0.14	1.043
915	ISC0471	2006	10	4	10	23	54.4	-29.062	22.986	5	F	2.27	0.229	1.119
917	CGS0589	2006	10	20	13	57	43.1	-30.096	24.04	5	F	2.47	0.162	1.058
918	CGS0590	2006	11	6	2	48	37.1	-30.645	19.637	5	F	2.41	0.162	1.058
919	CGS0591	2006	11	25	0	0	42.1	-33.522	23.724	5	F	2.6	0.162	1.058
921	ISC0476	2006	11	29	1	50	9.4	-29.703	19.53	5	F	2.27	0.229	1.119
922	CGS0593	2006	12	22	9	21	30.6	-29.524	22.914	5	F	2.5	0.162	1.058
923	ISC0478	2006	12	28	19	58	14.2	-29.786	17.982	5	F	2.38	0.229	1.119
924	CGS0594	2007	1	3	6	26	41.7	-30.817	19.256	5	F	2.56	0.162	1.058
925	CGS0595	2007	1	3	17	29	54	-32.258	23.603	5	F	2.8	0.162	1.058
926	ISC0481	2007	1	6	11	53	50.6	-32.536	23.654	5	F	2.27	0.229	1.119
927	CGS0596	2007	1	8	8	19	44.2	-32.015	21.322	5	F	2.41	0.162	1.058
928	GSO0025	2007	1	21	1	35	7.9	-32.801	17.801	5.8		2.27	0.162	1.058
929	GSO0026	2007	1	31	6	30	48.1	-34.171	19.992	6.4		2.26	0.14	1.043
930	CGS0598	2007	2	2	10	54	14.6	-32.963	22.184	5	F	2.5	0.162	1.058
932	ISC0485	2007	3	25	19	43	40.9	-32.705	17.939	5	F	2.27	0.229	1.119
933	GSO0027	2007	3	31	11	41	19	-33.089	17.795	5.1		2.27	0.229	1.119
934	CGS0600	2007	4	19	15	3	52.8	-28.547	23.331	0	F	2.27	0.229	1.119
936	CGS0601	2007	5	1	8	9	18.5	-32.789	22.094	5	F	2.5	0.162	1.058
937	ISC0488	2007	5	7	4	53	16.8	-30.158	18.88	5	F	2.32	0.229	1.119
938	ISC0489	2007	5	25	19	7	57.8	-30.331	19.04	5	F	2.51	0.229	1.119
939	CGS0602	2007	6	24	5	26	27.2	-30.862	18.849	5	F	2.6	0.162	1.058
941	CGS0604	2007	7	1	7	28	26.4	-28.661	18.013	5	F	2.47	0.162	1.058
943	ISC0492	2007	7	20	22	8	32	-29.816	20.499	5	F	2.27	0.229	1.119

944	CGS0606	2007	8	18	15	39	51.4	-29.838	19.241	5	F	2.6	0.162	1.058
945	CGS0607	2007	8	20	19	17	43.1	-30.389	24.652	5	F	3.36	0.162	1.058
946	ISC0495	2007	9	5	14	36	18.3	-31.163	22.868	5	F	2.27	0.229	1.119
947	CGS0608	2007	9	5	19	9	54.7	-31.596	19.231	5	F	2.44	0.162	1.058
948	CGS0609	2007	9	6	14	51	12	-28.149	24.129	0	F	2.51	0.229	1.119
949	CGS0610	2007	9	9	10	24	19.3	-29.814	19.301	5	F	2.38	0.162	1.058
951	CGS0611	2007	9	17	20	3	33.7	-29.928	18.781	5	F	3.44	0.162	1.058
952	CGS0612	2007	9	18	14	59	26.3	-33.855	20.168	5	F	2.8	0.162	1.058
953	ISC0501	2007	9	19	23	52	59.1	-29.962	25.11	20	F	2.51	0.229	1.119
954	CGS0613	2007	10	12	9	17	58.9	-28.301	18.315	5	F	2.41	0.162	1.058
955	ISC0503	2007	10	23	21	51	3.9	-31.189	20.348	5	F	2.27	0.229	1.119
957	CGS0615	2007	10	27	5	42	37.2	-32.507	24.653	5	F	2.87	0.162	1.058
960	CGS0616	2007	10	30	14	34	46.3	-30.3	19.259	5	F	2.9	0.162	1.058
961	CGS0617	2007	11	1	7	47	39.3	-30.634	20.509	5	F	2.38	0.162	1.058
962	CGS0618	2007	11	3	9	3	53.6	-32.793	22.023	5	F	3.91	0.162	1.058
963	CGS0619	2007	11	14	5	20	52.3	-29.516	25.215	5	F	2.35	0.162	1.058
964	ISC0511	2007	11	18	14	14	49.8	-32.068	20.749	5	F	2.38	0.229	1.119
965	CGS0620	2007	12	21	17	16	52.9	-30.272	25.805	5	F	2.44	0.162	1.058
966	ISC0513	2007	12	24	1	41	11.3	-29.456	19.641	5	F	2.32	0.229	1.119
967	ISC0514	2008	1	19	8	53	7.1	-30.257	25.259	5	F	2.32	0.229	1.119
968	ISC0515	2008	1	26	12	36	41.3	-30.586	19.112	5	F	2.27	0.229	1.119
969	CGS0621	2008	2	19	20	15	8.7	-29.52	18.284	5	F	3.16	0.162	1.058
970	CGS0622	2008	2	21	1	1	20.7	-35.625	25.561	5	F	2.94	0.162	1.058
971	CGS0623	2008	3	3	15	44	26.6	-28.305	17.857	5	F	2.69	0.162	1.058
972	CGS0624	2008	3	11	21	4	1.8	-30.157	19.907	5	F	2.53	0.162	1.058
973	ISC0520	2008	3	17	21	43	57.3	-32.869	22.063	5	F	2.32	0.229	1.119
974	CGS0625	2008	3	20	13	6	41.6	-28.683	22.187	0	F	2.38	0.229	1.119
975	CGS0626	2008	3	27	1	59	30.5	-36.212	23.313	0		2.51	0.229	1.119
976	CGS0627	2008	4	17	0	5	10.6	-30.526	20.271	5	F	2.42	0.144	1.046
977	CGS0628	2008	4	27	2	2	32.2	-31.864	23.244	5	F	2.56	0.162	1.058
978	CGS0629	2008	5	19	9	16	18.6	-29.966	18.957	5	F	2.44	0.162	1.058
979	CGS0630	2008	6	1	17	56	36.4	-30.355	23.281	5	F	2.6	0.162	1.058
980	CGS0631	2008	6	26	20	59	7.6	-28.878	19.343	5	F	2.53	0.162	1.058
981	ISC0526	2008	6	28	0	29	8.6	-28.901	20.245	5	F	2	0.144	1.046
982	CGS0632	2008	7	9	15	1	22.6	-29.465	21.902	5	F	2.46	0.132	1.038
983	ISC0528	2008	7	20	5	30	24.6	-29.8	19.803	5	F	2.41	0.162	1.058
985	GSO0028	2008	8	11	11	41	34.9	-32.596	17.512	6.5		2.56	0.14	1.043
986	CGS0635	2008	8	14	3	22	37.8	-30.371	20.986	5	F	2.41	0.162	1.058
987	CGS0636	2008	8	14	18	38	50.1	-30.079	25.74	5	F	2.42	0.132	1.038
988	CGS0637	2008	8	23	13	42	48.9	-29.323	23.053	5	F	2.4	0.132	1.038
990	CGS0639	2008	8	25	20	25	57.2	-32.794	22.059	5	F	2.76	0.162	1.058
992	CGS0641	2008	8	26	18	22	28.5	-30.599	18.419	5	F	2.41	0.162	1.058
994	TNS0432	2008	8	27	13	7	0	-29.991	18.18			2.32	0.229	1.119
995	ISC0534	2008	8	30	15	16	24.4	-30.324	25.824	5	F	2.41	0.162	1.058
996	CGS0643	2008	9	2	22	25	50.3	-30.509	20.402	5	F	2.5	0.162	1.058
998	CGS0645	2008	9	8	14	33	34	-30.425	19.527	5	F	2.63	0.132	1.038
999	GSO0030	2008	9	10	19	17	4.5	-33.065	17.715	5.5		2.7	0.162	1.058
1001	TNS0438	2008	9	15	1	56	0	-29.82	18.079			2.27	0.229	1.119
1002	TNS0439	2008	9	22	2	8	0	-29.971	18.728			2.32	0.229	1.119
1003	TNS0440	2008	9	27	10	35	0	-28.982	18.458			2.27	0.229	1.119
1004	CGS0647	2008	9	30	11	21	31.6	-29.954	19.826	5	F	2.6	0.162	1.058
1005	GSO0031	2008	10	4	11	18	9.1	-32.929	17.833	7		2.41	0.162	1.058
1006	CGS0649	2008	10	9	16	51	48.8	-32.887	22.153	5	F	2.76	0.162	1.058
1008	CGS0651	2008	10	19	21	13	18	-28.907	19.715	5	F	2.9	0.162	1.058
1009	CGS0652	2008	10	20	5	32	47.4	-29.533	24.865	5	F	2.44	0.132	1.038
1010	GSO0032	2008	11	7	2	19	49.2	-32.989	17.747	7.1		2.44	0.229	1.119
1011	ISC0541	2008	11	15	2	27	26.6	-28.193	18.352	5	F	2.32	0.229	1.119
1012	CGS0654	2008	11	19	10	5	22.4	-31.7	24.478	5	F	3.12	0.162	1.058
1013	ISC0543	2008	11	20	13	5	59.2	-31.889	22.4	5	F	2.32	0.229	1.119
1014	CGS0655	2008	11	20	21	2	42.2	-29.485	24.528	5	F	2.6	0.162	1.058
1015	ISC0545	2008	12	16	0	36	36.9	-29.648	18.512	5	F	2.27	0.229	1.119
1016	ISC0546	2008	12	23	5	20	16.7	-29.743	18.776	5	F	2.32	0.229	1.119
1017	CGS0656	2008	12	28	5	21	51.4	-32.523	25.209	5	F	2.69	0.162	1.058
1018	ISC0548	2009	1	4	3	33	33	-32.873	22.056	5	F	2.27	0.229	1.119
1020	CGS0658	2009	1	24	10	50	51	-32.835	19.236	0		2.44	0.162	1.058
1021	GSO0034	2009	1	25	6	58	4.3	-34.573	18.674	6.4		2.57	0.229	1.119
1022	CGS0660	2009	1	26	13	4	12.4	-28.247	22	2	F	2.77	0.229	1.119
1024	CGS0662	2009	1	28	4	27	15.4	-28.582	18.591	10	F	3.65	0.162	1.058
1025	GSO0035	2009	2	14	21	40	5.7	-33.248	19.114	7.1		2.56	0.14	1.043
1026	ISC0553	2009	2	18	9	41	32.2	-29.801	19.018	5	F	2.35	0.162	1.058
1027	ISC0554	2009	3	8	3	23	46.6	-33.163	21.846	5	F	2.41	0.162	1.058
1028	GSO0036	2009	3	8	21	10	18	-32.723	20.23	5.8		2.86	0.14	1.043

1029	CGS0665	2009	3	17	12	15	41.8	-33.647	20.873	5	F	2.76	0.132	1.038
1030	GSO0037	2009	3	20	0	37	33.3	-33.421	19.297	5.3		2.16	0.14	1.043
1031	CGS0667	2009	4	21	10	22	46.6	-29.83	18.882	5	F	2.44	0.162	1.058
1032	ISC0559	2009	5	7	0	43	45.4	-30.31	18.136	5	F	2.44	0.229	1.119
1033	ISC0560	2009	5	25	20	57	15.1	-29.655	17.843	5	F	2.27	0.229	1.119
1034	CGS0668	2009	6	8	0	8	34.6	-32.836	22.068	5	F	2.87	0.162	1.058
1035	ISC0562	2009	6	29	16	12	6	-32.16	23.118	5	F	2.38	0.229	1.119
1036	CGS0669	2009	7	9	2	38	2.4	-28.857	20.198	5	F	3.2	0.162	1.058
1040	CGS0671	2009	7	13	12	53	1	-29.496	19.806	5	F	3.73	0.162	1.058
1041	GSO0038	2009	7	13	18	0	12	-34.507	18.343	6.7		2.56	0.14	1.043
1042	ISC0569	2009	7	21	20	51	58.6	-30.107	25.863	5	F	2.27	0.229	1.119
1044	CGS0674	2009	7	24	12	49	0.6	-28.581	17.461	5	F	2.41	0.162	1.058
1045	CGS0675	2009	7	30	1	52	16.3	-28.875	19.639	10	F	2.9	0.162	1.058
1046	CGS0676	2009	8	11	4	30	17.5	-32.794	22.049	5	F	3.07	0.119	1.031
1047	CGS0677	2009	8	14	11	36	24.9	-29.51	19.768	5	F	2.38	0.162	1.058
1049	ISC0576	2009	8	24	23	12	20	-31.816	18.244	5	F	2.44	0.229	1.119
1050	CGS0679	2009	8	31	13	14	28.3	-28.932	20.384	5	F	2.69	0.162	1.058
1051	CGS0680	2009	9	3	6	33	1.5	-32.849	22.046	5	F	3.2	0.162	1.058
1052	CGS0681	2009	9	27	14	9	19.8	-28.779	20.149	5	F	2.47	0.162	1.058
1054	CGS0683	2009	10	16	18	35	48.8	-31.297	20.671	5	F	3.52	0.162	1.058
1056	ISC0583	2009	10	30	7	2	3.5	-28.904	20.237	5	F	2.32	0.229	1.119
1057	CGS0685	2009	11	4	22	14	11.5	-31.572	24.943	5	F	3.08	0.162	1.058
1061	CGS0688	2009	11	13	5	36	59.6	-30.223	18.849	5	F	2.83	0.162	1.058
1062	CGS0689	2009	11	16	5	43	45.5	-30.892	18.768	5	F	2.47	0.162	1.058
1063	GSO0039	2009	12	2	17	9	24.1	-33.076	18.036	6.2		2.96	0.14	1.043
1064	CGS0691	2009	12	8	23	21	39.5	-32.788	22.135	5	F	3.87	0.162	1.058
1066	ISC0593	2009	12	11	12	8	6	-31.616	18.429	5	F	2.27	0.229	1.119
1068	CGS0693	2010	2	19	7	23	14.8	-28.497	20.045	5	F	2.54	0.162	1.058
1069	GSO0040	2010	3	10	23	27	46.8	-33.444	19.371	6.2		2.5	0.162	1.058
1070	CGS0695	2010	3	11	15	6	37.4	-30.364	25.995	5	F	3.24	0.162	1.058
1071	GSO0041	2010	3	29	8	54	44	-33.581	19.312	5.2		2.99	0.229	1.119
1072	CGS0697	2010	4	8	6	39	40.3	-29.46	19.787	5	F	3.01	0.162	1.058
1073	CGS0698	2010	4	9	22	34	2.3	-28.284	23.041	0		2.64	0.229	1.119
1074	CGS0699	2010	4	21	11	28	47.6	-29.567	18.325	5	F	2.69	0.162	1.058
1075	CGS0700	2010	4	22	12	36	8.5	-29.453	19.89	5	F	2.63	0.162	1.058
1077	ISC0600	2010	5	13	20	22	1.8	-33.305	19.443	5	F	2.27	0.229	1.119
1078	GSO0042	2010	5	18	13	32	54	-32.589	17.577	5.4		2.16	0.14	1.043
1080	CGS0704	2010	5	25	1	14	25	-29.787	25.591	5	F	2.33	0.119	1.031
1083	CGS0707	2010	6	21	1	17	59.8	-28.682	20.435	5	F	2.54	0.162	1.058
1084	CGS0708	2010	6	22	22	53	7.4	-28.717	22.119	5	F	2.69	0.162	1.058
1085	CGS0709	2010	6	24	10	6	26.7	-28.721	20.805	5	F	3.52	0.162	1.058
1086	CGS0710	2010	6	24	10	20	36.8	-28.507	19.004	5	F	2.8	0.162	1.058
1087	ISC0607	2010	6	24	11	2	43.1	-30.154	21.533	5	F	2.32	0.229	1.119
1089	ISC0609	2010	6	25	20	41	14.9	-28.831	23.598	5	F	2.38	0.229	1.119
1090	CGS0712	2010	6	29	2	7	0.4	-28.38	20.014	5	F	3.24	0.162	1.058
1094	ISC0613	2010	7	15	10	32	11.8	-29.823	18.72	5	F	2.41	0.162	1.058
1095	ISC0614	2010	7	19	15	3	28.3	-28.877	25.819	5	F	2.32	0.229	1.119
1096	CGS0718	2010	7	24	12	4	35.3	-33.342	22.022	5	F	2.6	0.162	1.058
1097	CGS0719	2010	7	26	14	24	19.2	-28.79	20.407	5	F	3.64	0.162	1.058
1100	CGS0722	2010	8	4	5	12	47.2	-28.991	20.63	5	F	2.66	0.162	1.058
1102	CGS0724	2010	8	6	0	15	2.2	-28.67	20.006	5	F	2.38	0.229	1.119
1104	ISC0622	2010	8	20	16	31	2.3	-29.541	21.339	5	F	2.32	0.229	1.119
1105	CGS0727	2010	8	23	23	38	50.6	-29.981	18.783	5	F	2.38	0.162	1.058
1106	ISC0624	2010	8	25	5	11	45.3	-28.771	20.17	5	F	2.5	0.162	1.058
1107	ISC0625	2010	8	25	12	14	53.3	-29.616	23.036	5	F	2.77	0.229	1.119
1108	ISC0626	2010	8	26	22	25	14.9	-28.379	20.355	5	F	2.38	0.229	1.119
1109	ISC0627	2010	9	9	20	21	7.6	-28.787	20.445	5	F	2.32	0.229	1.119
1110	ISC0628	2010	9	10	4	49	54.6	-32.233	20.256	5	F	2.32	0.229	1.119
1112	CGS0729	2010	9	17	15	55	7.7	-29.142	18.412	5	F	2.53	0.162	1.058
1113	CGS0730	2010	9	18	11	2	11.9	-30.403	25.274	5	F	2.57	0.162	1.058
1114	CGS0731	2010	9	27	3	28	52.4	-33.341	22.198	5	F	2.53	0.162	1.058
1115	ISC0632	2010	10	2	17	12	1.1	-33.066	18.002	5	F	2.27	0.229	1.119
1117	ISC0634	2010	10	7	0	52	8.7	-28.566	20.426	5	F	3.24	0.132	1.038
1119	CGS0736	2010	10	8	13	16	5.3	-28.78	20.577	5	F	2.56	0.162	1.058
1121	TNS0538	2010	10	15	16	32	0	-30.499	21.073			2.91	0.229	1.119
1123	ISC0639	2010	10	31	2	26	52.4	-30.876	23.616	5	F	2.41	0.162	1.058
1124	ISC0640	2010	11	1	15	19	58.2	-30.615	21.095	5	F	3.26	0.132	1.038
1125	ISC0641	2010	11	12	17	46	34.2	-29.211	25.08	5	F	2.41	0.162	1.058
1127	CGS0740	2010	11	14	13	34	9.2	-29.306	22.215	0		2.91	0.229	1.119
1129	CGS0741	2010	11	15	7	22	50.6	-29.176	19.149	5	F	2.89	0.132	1.038
1130	CGS0742	2010	11	15	14	12	35.9	-29.16	19.637	5	F	2.57	0.229	1.119
1136	CGS0749	2010	11	26	13	10	19.6	-28.364	21.244	0		2.32	0.229	1.119

1137	ISC0649	2010	12	5	5	2	36	-30.774	25.959	5	F	2.32	0.229	1.119
1157	ISC0669	2011	1	4	2	10	53.4	-30.115	21.624	5	F	1.98	0.144	1.046
1164	CGS0773	2011	1	7	15	58	18.1	-30.608	20.47	5	F	2.44	0.162	1.058
1179	CGS0787	2011	1	12	6	14	21	-28.69	20.348	5	F	4.41	0.133	1.039
1229	CGS0829	2011	1	23	9	14	38	-29.996	19.679	5	F	2.35	0.162	1.058
1239	ISC0750	2011	1	27	1	20	31.5	-28.104	20.105	5	F	2.27	0.229	1.119
1250	ISC0761	2011	1	31	10	6	10.5	-30.314	18.73	5	F	2.27	0.229	1.119
1266	CGS0863	2011	2	5	12	43	15.2	-29.105	24.912	5	F	2.66	0.162	1.058
1275	GSO0043	2011	2	9	2	44	28.4	-33.115	17.483	6.4		2.46	0.14	1.043
1282	CGS0878	2011	2	13	5	20	30.8	-32.03	19.905	5	F	2.44	0.162	1.058
1284	CGS0880	2011	2	13	23	45	3.2	-30.787	21.103	5	F	2.41	0.162	1.058
1285	CGS0881	2011	2	14	5	21	18.4	-29.218	20.953	5	F	2.41	0.162	1.058
1299	CGS0894	2011	2	25	12	40	13.1	-32.863	22.135	5	F	3.01	0.162	1.058
1315	CGS0906	2011	3	11	17	57	41.8	-30.479	24.555	5	F	2.38	0.162	1.058
1325	CGS0912	2011	3	18	7	17	22.7	-29.679	24.542	5	F	2.5	0.162	1.058
1326	CGS0913	2011	3	18	20	42	58.4	-32.069	24.745	5	F	3.04	0.162	1.058
1332	CGS0918	2011	3	22	2	59	53.7	-28.987	20.889	5	F	2.92	0.132	1.038
1337	CGS0920	2011	4	5	22	12	41.3	-28.411	20.288	5	F	2.47	0.162	1.058
1339	CGS0921	2011	4	6	23	34	52.8	-28.747	20.46	5	F	3.8	0.132	1.038
1343	CGS0925	2011	4	12	11	35	2.3	-30.23	24.036	5	F	2.53	0.162	1.058
1354	CGS0934	2011	5	3	19	45	57.5	-28.447	16.077	5	F	2.53	0.162	1.058
1356	CGS0936	2011	5	4	9	59	1.2	-28.461	20.386	5	F	3.35	0.162	1.058
1358	CGS0938	2011	5	4	12	44	8.5	-28.243	16.474	5	F	3.31	0.162	1.058
1361	CGS0941	2011	5	5	10	38	20.9	-28.543	19.982	5	F	3.01	0.162	1.058
1371	CGS0950	2011	5	14	14	10	41.7	-32.78	22.139	5	F	4.12	0.133	1.038
1372	CGS0951	2011	5	14	16	26	12.7	-28.756	20.493	5	F	3.82	0.162	1.058
1374	CGS0952	2011	5	16	8	32	3.8	-29.671	19.747	5	F	2.59	0.162	1.058
1392	ISC0902	2011	6	7	19	38	13	-28.949	20.25	5	F	2.27	0.229	1.119
1404	CGS0975	2011	6	22	21	2	50.6	-28.57	20.437	5	F	3.55	0.132	1.038
1405	ISC0914	2011	6	22	21	4	5.6	-29.618	23.07	5	F	3.22	0.229	1.119
1407	ISC0916	2011	6	22	21	11	19.7	-29.667	22.798	5	F	3.46	0.229	1.119
1412	CGS0980	2011	6	25	13	38	22.7	-30.167	17.9	5	F	3.77	0.132	1.038
1413	CGS0981	2011	6	30	22	0	32.5	-31.067	18.119	5	F	2.66	0.162	1.058
1414	ISC0923	2011	7	1	7	8	12.1	-31.374	20.128	5	F	2.32	0.229	1.119
1415	ISC0924	2011	7	2	5	13	52.2	-28.287	20.226	5	F	2.27	0.229	1.119
1416	CGS0982	2011	7	2	5	24	39	-28.385	23.527	0	F	2.32	0.229	1.119
1419	CGS0984	2011	7	7	15	26	53	-28.585	23.373	0	F	2.38	0.229	1.119
1421	CGS0986	2011	7	16	8	27	16.7	-28.893	20.197	5	F	2.93	0.162	1.058
1423	CGS0987	2011	7	18	15	23	25.9	-28.643	22.409	5	F	2.38	0.162	1.058
1424	CGS0988	2011	7	20	14	22	46.3	-28.102	22.712	0	F	2.44	0.229	1.119
1425	CGS0989	2011	7	21	16	20	19.4	-33.533	17.34	5	F	2.88	0.132	1.038
1427	TNS0773	2011	7	24	15	37	0	-28.7	20.456			2.32	0.229	1.119
1429	CGS0992	2011	7	31	19	8	4.4	-29.807	20.572	5	F	2.44	0.162	1.058
1430	CGS0993	2011	7	31	20	48	47.8	-31.246	24.678	5	F	2.6	0.162	1.058
1432	CGS0995	2011	8	7	20	22	49.6	-30.078	21.051	5	F	2.5	0.162	1.058
1435	CGS0998	2011	8	9	10	10	50.8	-28.228	25.142	5	F	2.47	0.162	1.058
1436	CGS0999	2011	8	9	10	57	4.6	-31.1	22.973	5	F	2.8	0.162	1.058
1438	CGS1001	2011	8	10	12	19	15.8	-30.012	21.378	5	F	2.5	0.162	1.058
1442	CGS1004	2011	8	13	18	51	21.8	-30.913	18.268	5	F	3.04	0.162	1.058
1444	CGS1006	2011	8	13	18	53	6.5	-29.802	19.219	5	F	2.44	0.162	1.058
1445	CGS1007	2011	8	13	19	33	28.7	-28.446	20.36	5	F	3.12	0.162	1.058
1448	CGS1008	2011	8	13	19	48	7.6	-29.909	18.717	5	F	2.56	0.162	1.058
1450	CGS1009	2011	8	13	21	13	48.9	-28.701	20.436	5	F	2.44	0.132	1.038
1451	CGS1010	2011	8	13	23	3	54.8	-28.682	20.388	5	F	2.44	0.162	1.058
1456	CGS1013	2011	8	25	15	23	46.9	-30.971	20.472	5	F	2.44	0.162	1.058
1460	CGS1015	2011	8	27	1	0	11.3	-28.751	20.565	5	F	3.12	0.162	1.058
1467	CGS1019	2011	8	29	12	6	9.5	-30.129	23.567	5	F	2.56	0.162	1.058
1470	CGS1022	2011	8	30	12	26	57.5	-28.862	22.906	0	F	2.38	0.229	1.119
1471	CGS1023	2011	9	2	23	43	5.3	-30.113	17.262	5	F	2.6	0.162	1.058
1472	CGS1024	2011	9	4	3	1	50.9	-32.079	20.819	5	F	2.6	0.162	1.058
1473	CGS1025	2011	9	5	22	1	3.2	-31.912	20.98	5	F	2.56	0.162	1.058
1485	CGS1036	2011	9	15	14	45	2.1	-28.624	23.719	0	F	2.27	0.229	1.119
1487	ISC0969	2011	9	17	1	23	49.1	-30.114	19.156	5	F	2.27	0.229	1.119
1489	CGS1039	2011	9	22	19	26	56	-28.794	17.825	5	F	2.73	0.162	1.058
1490	CGS1040	2011	9	24	1	39	13.2	-28.695	20.445	5	F	2.63	0.162	1.058
1497	ISC0975	2011	10	6	11	8	35	-29.745	23.63	5	F	2.38	0.229	1.119
1499	ISC0976	2011	10	6	21	23	39.6	-30.983	21.04	5	F	2.32	0.229	1.119
1500	CGS1047	2011	10	8	22	47	36.2	-28.878	20.45	5	F	2.44	0.162	1.058
1502	CGS1048	2011	10	9	9	40	30.4	-34.297	15.529	5	F	2.77	0.162	1.058
1503	ISC0980	2011	10	10	12	18	34.9	-31.236	19.106	5	F	2.32	0.229	1.119
1506	ISC0981	2011	10	13	15	32	28.2	-29.609	20.363	5	F	2.27	0.229	1.119
1508	CGS1052	2011	10	14	13	1	50.8	-29.725	23.944	5	F	2.44	0.162	1.058

1509	ISC0983	2011	10	17	1	11	18.3	-30.508	25.136	5	F	2.32	0.229	1.119
1516	CGS1054	2011	10	17	18	8	1.3	-30.898	20.191	5	F	2.63	0.162	1.058
1519	CGS1056	2011	10	17	23	41	59.4	-28.652	20.417	5	F	2.63	0.162	1.058
1522	CGS1059	2011	10	18	18	33	24.3	-28.946	16.93	5	F	2.38	0.162	1.058
1523	CGS1060	2011	10	18	21	54	10.4	-28.752	17.654	5	F	2.79	0.162	1.058
1524	ISC0996	2011	10	20	15	18	1.4	-29.481	22.767	5	F	2.38	0.229	1.119
1525	CGS1061	2011	10	21	12	32	39.8	-29.001	21.684	5	F	2.47	0.162	1.058
1530	TNS0838	2011	11	3	5	29	0	-29.586	24.852			2.27	0.229	1.119
1532	ISC1001	2011	11	4	14	10	40.2	-28.723	25.106	5	F	2.38	0.229	1.119
1534	CGS1066	2011	11	10	15	39	57.3	-30.884	23.793	5	F	2.35	0.162	1.058
1538	CGS1070	2011	11	22	6	21	37.8	-29.235	23.481	5	F	2.38	0.162	1.058
1539	ISC1008	2011	11	29	1	42	49.7	-28.824	20.17	5	F	2.27	0.229	1.119
1540	CGS1071	2011	11	29	5	41	42.5	-29.034	20.408	5	F	3.12	0.162	1.058
1543	CGS1074	2011	12	2	17	5	20.7	-30.019	20.446	5	F	2.56	0.162	1.058
1545	ISC1011	2011	12	6	18	31	46.3	-28.873	20.213	5	F	2.27	0.229	1.119
1546	ISC1012	2011	12	7	21	24	13.7	-29.508	21.081	5	F	2.27	0.229	1.119
1547	GSO0044	2011	12	8	19	28	44.8	-32.83	17.645	5.2		2.56	0.14	1.043
1549	CGS1077	2011	12	15	5	45	29	-29.769	21.902	5	F	2.63	0.162	1.058
1550	CGS1078	2011	12	18	13	28	49.8	-29.383	20.637	5	F	2.83	0.162	1.058
1552	CGS1080	2011	12	18	18	7	5.7	-28.474	20.489	5	F	4.26	0.14	1.043
1558	CGS1084	2011	12	21	21	45	27.2	-31.327	21.607	5	F	2.53	0.162	1.058
1560	CGS1085	2011	12	23	7	51	8.1	-29.683	18.475	5	F	3.23	0.162	1.058
1562	CGS1087	2011	12	27	2	39	30.1	-28.738	17.443	5	F	2.59	0.162	1.058
1563	CGS1088	2011	12	27	3	56	52.5	-29.171	20.998	5	F	2.97	0.162	1.058
1567	CGS1091	2011	12	29	8	6	56.8	-28.244	23.597	0	F	2.32	0.229	1.119
1571	CGS1095	2012	1	1	0	44	35.9	-30.433	16.876	5	F	2.38	0.229	1.119
1572	CGS1096	2012	1	4	0	52	55.5	-28.622	20.181	5	F	2.7	0.229	1.119
1574	CGS1098	2012	1	6	14	19	29.6	-28.263	20.194	5	F	2.57	0.229	1.119
1575	CGS1099	2012	1	13	10	17	0.9	-30.031	19.159	5	F	2.99	0.229	1.119
1578	CGS1102	2012	1	25	0	44	29.9	-31.843	25.647	0		3.38	0.229	1.119
1579	CGS1103	2012	1	25	8	17	13.9	-28.007	19.913	0		2.84	0.229	1.119
1581	CGS1105	2012	1	25	23	38	56.6	-30.326	19.16	5	F	3.46	0.229	1.119
1582	CGS1106	2012	1	27	0	42	53.4	-32.162	19.603	5	F	2.66	0.144	1.046
1585	CGS1109	2012	1	27	14	44	28.9	-28.778	23.677	0	F	2.64	0.229	1.119
1596	CGS1120	2012	2	9	14	52	54.6	-28.529	23.208	0	F	2.38	0.229	1.119
1600	GSO0045	2012	2	19	16	53	47.1	-33.914	18.149	6.3		2.77	0.229	1.119
1601	CGS1124	2012	3	2	3	32	52	-32.24	16.359	5	F	2.44	0.229	1.119
1603	CGS1126	2012	3	9	7	18	18.9	-28.708	20.338	5	F	3.14	0.229	1.119
1604	GSO0046	2012	3	11	14	20	42	-33.786	18.038	1.8		2.77	0.229	1.119
1610	CGS1133	2012	3	20	18	35	47.4	-29.905	21.459	5	F	2.27	0.229	1.119
1611	CGS1134	2012	3	21	11	45	1.8	-29.971	19.372	5	F	2.64	0.229	1.119
1616	CGS1139	2012	3	30	20	6	43.7	-33.196	22.032	5	F	3.44	0.144	1.046
1617	CGS1140	2012	3	30	20	18	14.4	-33.413	21.885	5	F	2.7	0.229	1.119
1618	CGS1141	2012	3	31	3	13	51.7	-30.082	18.574	5	F	4.08	0.229	1.12
1619	CGS1142	2012	4	1	12	18	47.8	-29.549	20.61	5	F	2.38	0.162	1.058
1620	CGS1143	2012	4	2	2	36	4.2	-28.837	20.107	5	F	3.17	0.144	1.046
1622	CGS1145	2012	4	9	4	34	18.6	-29.671	21.268	5	F	2.41	0.162	1.058
1624	CGS1147	2012	4	11	23	42	5.3	-28.566	20.53	5	F	2.38	0.229	1.119
1625	CGS1148	2012	4	12	8	20	59.8	-28.8	23.043	0	F	2.38	0.229	1.119
1626	CGS1149	2012	4	19	13	39	58.4	-30.643	24.151	5	F	2.35	0.162	1.058
1629	CGS1152	2012	4	21	7	24	14.1	-28.067	23.003	0	F	2.27	0.229	1.119
1630	CGS1153	2012	4	25	8	21	1.6	-28.518	23.573	0	F	2.51	0.229	1.119
1631	CGS1154	2012	4	25	10	41	55.7	-28.994	22.668	0	F	2.38	0.229	1.119
1632	CGS1155	2012	4	27	13	13	51.6	-28.676	22.911	0	F	2.38	0.229	1.119
1636	CGS1159	2012	5	6	0	12	16.3	-28.745	20.301	5	F	2.41	0.162	1.058
1638	CGS1161	2012	5	10	14	23	6.5	-28.693	22.976	0	F	2.57	0.229	1.119
1639	CGS1162	2012	5	12	19	32	25.8	-31.112	20.735	5	F	2.5	0.162	1.058
1642	CGS1165	2012	5	13	13	58	11.2	-28.493	20.536	5	F	2.83	0.162	1.058
1645	CGS1168	2012	5	13	21	58	53.2	-28.28	20.183	5	F	2.38	0.229	1.119
1647	CGS1170	2012	5	14	0	24	42.4	-29.631	16.735	5	F	2.29	0.144	1.046
1649	CGS1172	2012	5	14	14	42	47.2	-28.705	20.448	5	F	2.44	0.229	1.119
1650	CGS1173	2012	5	17	7	52	37.2	-29.961	18.728	5	F	2.38	0.229	1.119
1651	CGS1174	2012	5	20	0	35	18.6	-28.457	24.451	5	F	2.47	0.162	1.058
1652	CGS1175	2012	5	20	4	26	10.5	-29.316	24.671	5	F	2.69	0.162	1.058
1655	CGS1178	2012	5	21	8	20	24.1	-28.283	23.346	0	F	2.51	0.229	1.119
1658	CGS1181	2012	5	26	6	36	28.3	-29.364	18.236	5	F	3.16	0.162	1.058
1660	CGS1183	2012	5	27	5	54	8.3	-28.862	20.238	5	F	2.38	0.229	1.119
1661	CGS1184	2012	5	27	9	0	5.9	-28.706	20.341	5	F	2.32	0.229	1.119
1662	CGS1185	2012	5	28	9	16	30	-28.716	20.416	5	F	2.32	0.229	1.119
1663	CGS1186	2012	5	30	3	23	33.5	-29.56	25.194	5	F	2.56	0.162	1.058
1666	CGS1189	2012	6	1	3	29	37.9	-28.918	18.48	5	F	2.32	0.229	1.119
1667	CGS1190	2012	6	1	12	44	36.4	-28.705	22.935	0	F	2.32	0.229	1.119

1668	CGS1191	2012	6	2	12	8	22.5	-29.592	19.965	5	F	2.32	0.229	1.119
1669	CGS1192	2012	6	3	5	4	8.5	-28.857	20.208	5	F	2.47	0.162	1.058
1670	CGS1193	2012	6	3	14	46	43.6	-28.869	19.744	5	F	2.32	0.229	1.119
1671	CGS1194	2012	6	10	13	3	21.3	-30.064	17.119	5	F	3.12	0.162	1.058
1672	CGS1195	2012	6	10	17	8	18.9	-28.542	20.489	5	F	2.63	0.162	1.058
1675	CGS1198	2012	6	18	21	2	55.9	-28.656	20.316	5	F	2.69	0.162	1.058
1677	CGS1200	2012	6	19	6	20	0.4	-32.005	21.777	5	F	2.6	0.162	1.058
1679	CGS1202	2012	6	26	8	29	7.9	-28.408	22.901	0	F	2.32	0.229	1.119
1680	CGS1203	2012	6	29	8	0	20.2	-28.638	22.829	0	F	2.32	0.229	1.119
1681	CGS1204	2012	6	29	12	1	46.9	-30.736	24.246	5	F	2.72	0.162	1.058
1684	CGS1207	2012	7	5	11	30	14.7	-29.788	23.597	5	F	2.32	0.229	1.119
1685	CGS1208	2012	7	10	15	39	29.5	-28.717	23.115	5	F	2.27	0.229	1.119
1686	CGS1209	2012	7	11	13	34	52.7	-30.983	23.928	5	F	2.7	0.229	1.119
1687	CGS1210	2012	7	17	6	50	18.4	-28.353	23.074	0	F	2.38	0.229	1.119
1689	CGS1212	2012	7	24	6	12	36.9	-28.645	20.482	5	F	2.32	0.229	1.119
1691	CGS1214	2012	7	30	20	28	23.2	-29.719	25.973	5	F	3.46	0.229	1.119
1695	CGS1218	2012	8	14	12	48	52.4	-28.864	22.825	0	F	2.27	0.229	1.119
1697	CGS1220	2012	8	31	13	56	42.8	-28.958	23.418	5	F	2.64	0.229	1.119
1699	CGS1222	2012	9	8	11	45	40.5	-36.724	18.216	5	F	2.51	0.229	1.119
1700	CGS1223	2012	9	14	3	26	56	-32.853	22.031	5	F	2.57	0.229	1.119
1702	CGS1225	2012	9	27	12	59	47.8	-30.281	20.971	5	F	2.27	0.229	1.119
1704	CGS1227	2012	10	6	20	52	17.5	-31.203	21.198	5	F	2.44	0.229	1.119
1706	ISC1105	2012	10	10	12	19	32.5	-32.487	19.036	44.1		2.51	0.229	1.119
1707	CGS1229	2012	10	12	13	2	47.1	-28.015	22.283	0	F	2.51	0.229	1.119
1708	CGS1230	2012	10	14	2	42	20.8	-29.592	19.42	5	F	2.51	0.229	1.119
1709	CGS1231	2012	10	15	20	37	19.1	-31.93	21.964	5	F	2.51	0.229	1.119
1710	CGS1232	2012	10	15	22	23	48.4	-31.614	20.668	5	F	2.84	0.229	1.119
1712	CGS1234	2012	10	21	19	12	43.8	-30.408	16.942	5	F	2.38	0.229	1.119
1715	CGS1237	2012	10	29	14	36	29.4	-28.632	20.26	5	F	2.27	0.229	1.119
1717	CGS1239	2012	11	28	6	29	3.8	-28.264	22.891	0	F	2.27	0.229	1.119
1718	CGS1240	2012	12	1	9	20	18.8	-28.501	18.203	5	F	2.99	0.229	1.119
1719	CGS1241	2012	12	11	16	25	13.7	-31.678	19.91	5	F	2.7	0.229	1.119
1722	CGS1244	2012	12	13	6	15	11.3	-28.512	20.237	5	F	2.77	0.229	1.119
1725	CGS1247	2013	1	6	19	51	32.4	-31.963	22.839	5	F	2.7	0.229	1.119
1727	CGS1249	2013	1	27	23	18	57.1	-30.025	25.482	5	F	2.91	0.229	1.119
1728	CGS1250	2013	1	28	15	10	19.2	-28.619	25.231	0	F	2.44	0.229	1.119
1729	CGS1251	2013	1	29	13	39	25.8	-32.317	22.16	5	F	2.57	0.229	1.119
1731	CGS1253	2013	2	26	3	26	54.5	-30.039	19.432	5	F	2.13	0.144	1.046
1733	CGS1255	2013	3	21	7	12	20.5	-30.159	19.033	5	F	2.32	0.229	1.119
1734	CGS1256	2013	3	27	20	53	16.9	-32.588	24.89	5	F	2.32	0.229	1.119
1735	CGS1257	2013	3	31	9	25	22	-28.443	20.578	5	F	2.27	0.229	1.119
1736	CGS1258	2013	5	15	21	19	21	-31.179	19.651	5	F	2.27	0.229	1.119
1737	CGS1259	2013	5	23	12	29	53.2	-29.051	23.172	5	F	2.27	0.229	1.119
1739	CGS1261	2013	6	12	13	3	19.4	-29.527	23.971	5	F	2.27	0.229	1.119
1741	CGS1263	2013	6	19	13	49	36.2	-32.677	24.29	5	F	3.06	0.229	1.119
1743	CGS1265	2013	6	26	9	55	2.2	-28.921	23.582	5	F	2.27	0.229	1.119
1744	CGS1266	2013	7	4	20	16	24.9	-28.112	24.484	5	F	2.27	0.229	1.119
1750	CGS1272	2013	7	30	8	13	8.6	-30.208	17.833	5	F	2.44	0.229	1.119
1752	CGS1274	2013	8	8	16	19	55.4	-29.518	19.699	5	F	2.44	0.229	1.119
1753	CGS1275	2013	8	10	18	56	53.3	-31.211	23.275	5	F	2.38	0.229	1.119
1755	CGS1277	2013	8	13	11	33	30.3	-28.656	22.963	0	F	2.38	0.229	1.119
1760	CGS1282	2013	8	31	3	20	8.5	-30.811	19.251	5	F	2.44	0.229	1.119
1761	CGS1283	2013	9	7	18	11	3.6	-30.6	23.901	5	F	2.27	0.229	1.119
1762	CGS1284	2013	9	17	3	23	55.7	-30.423	21.026	5	F	2.44	0.229	1.119
1763	CGS1285	2013	9	18	0	19	49.5	-31.036	20.529	5	F	2.51	0.229	1.119
1765	CGS1287	2013	9	30	1	4	12.3	-28.052	18.28	5	F	2.44	0.229	1.119
1766	CGS1288	2013	10	7	1	24	50.9	-30.48	19.059	5	F	2.27	0.229	1.119
1767	CGS1289	2013	10	8	18	37	44.1	-29.803	18.83	5	F	2.27	0.229	1.119
1772	CGS1294	2013	11	14	3	9	15.3	-28.609	20.443	5	F	2.27	0.229	1.119
1774	CGS1296	2013	11	21	16	18	47.3	-28.191	24.057	5	F	2.27	0.229	1.119
1775	CGS1297	2013	11	29	18	55	52	-29.218	20.637	5	F	2.27	0.229	1.119
1777	CGS1298	2013	12	17	14	5	11.8	-28.666	23.023	0	F	2.27	0.229	1.119
1778	CGS1299	2014	1	12	8	57	25.9	-28.597	20.346	5	F	2.32	0.229	1.119
1779	CGS1300	2014	1	13	10	53	7.4	-30.225	24.556	5	F	2.38	0.229	1.119
1780	CGS1301	2014	1	16	1	53	12.4	-31.687	25.447	5	F	2.7	0.144	1.046
1781	CGS1302	2014	1	20	22	5	47.1	-29.156	20.603	5	F	2.38	0.229	1.119
1783	CGS1304	2014	1	23	11	55	48.6	-29.28	21.903	0		2.91	0.229	1.119
1784	CGS1305	2014	1	28	13	23	33.9	-28.661	20.509	5	F	2.38	0.229	1.119
1785	CGS1306	2014	2	7	10	58	22.9	-28.737	20.333	5	F	2.32	0.229	1.119
1787	CGS1308	2014	2	17	15	18	33.7	-28.664	20.328	5	F	2.27	0.229	1.119
1789	CGS1310	2014	2	23	17	26	20.3	-29.676	18.69	5	F	2.57	0.229	1.119
1790	CGS1311	2014	2	28	8	35	21.3	-28.837	23.915	5	F	2.38	0.229	1.119

1791	CGS1312	2014	3	1	13	20	49.7	-28.233	20.369	5	F	2.38	0.229	1.119
1792	CGS1313	2014	3	3	8	16	21.4	-28.3	22.979	0	F	2.32	0.229	1.119
1794	ISC1152	2014	3	4	15	42	58.2	-28.219	20.614	5	F	2.27	0.229	1.119
1796	CGS1316	2014	3	6	23	9	56.3	-28.603	20.348	5	F	2.32	0.229	1.119
1798	CGS1318	2014	3	14	4	47	14.3	-28.41	22.253	5	F	2.32	0.229	1.119
1802	CGS1322	2014	3	23	15	54	51.4	-28.733	20.43	5	F	2.32	0.229	1.119
1803	CGS1323	2014	3	24	8	28	19.9	-30.106	19.976	5	F	2.43	0.16	1.057
1804	CGS1324	2014	3	25	9	25	16.6	-29.811	21.028	5	F	2.32	0.229	1.119
1806	CGS1326	2014	3	28	11	50	51.3	-28.542	22.644	0	F	2.84	0.229	1.119
1809	CGS1329	2014	4	9	12	44	3.6	-30.486	18.342	5	F	2.57	0.229	1.119
1811	ISC1162	2014	4	23	10	36	49.6	-28.699	22.671	5	F	2.38	0.229	1.119
1812	CGS1331	2014	4	24	4	16	30.4	-28.673	20.455	5	F	2.12	0.144	1.046
1816	CGS1335	2014	5	9	15	3	18.2	-28.411	22.928	0	F	2.84	0.229	1.119
1817	CGS1336	2014	5	23	11	53	9.4	-28.567	23.158	0	F	2.7	0.229	1.119
1818	CGS1337	2014	5	23	13	19	56.1	-32.1	22.932	5	F	2.08	0.144	1.046
1819	CGS1338	2014	5	23	14	22	23.8	-28.995	23.959	5	F	2.32	0.229	1.119
1821	CGS1340	2014	5	29	15	31	26.6	-28.62	20.262	5	F	2.44	0.229	1.119
1822	CGS1341	2014	5	29	15	44	54.6	-28.367	20.41	5	F	2.83	0.144	1.046
1823	CGS1342	2014	5	29	16	50	32.3	-28.454	20.148	5	F	2.57	0.229	1.119
1824	CGS1343	2014	5	30	10	37	58.7	-28.949	24.592	5	F	2.32	0.229	1.119
1826	CGS1345	2014	6	7	8	54	13.2	-28.724	20.407	5	F	2.38	0.229	1.119
1829	CGS1348	2014	6	22	22	49	53.8	-28.797	16.105	5	F	2.27	0.229	1.119
1833	CGS1352	2014	6	27	6	7	42.9	-32.098	23.322	5	F	2.36	0.144	1.046
1834	CGS1353	2014	6	30	23	36	41.9	-30.172	18.974	5	F	2.51	0.229	1.119
1835	CGS1354	2014	7	3	11	20	57.5	-29.106	22.109	5	F	2.38	0.229	1.119
1836	CGS1355	2014	7	3	12	23	0.2	-28.722	20.436	5	F	2.38	0.229	1.119
1837	CGS1356	2014	7	5	19	53	12.7	-31.635	23.112	5	F	2.66	0.144	1.046
1838	CGS1357	2014	7	6	16	32	60	-30.181	18.745	5	F	2.57	0.229	1.119
1839	CGS1358	2014	7	7	16	18	15.8	-28.406	20.215	5	F	2.64	0.229	1.119
1841	CGS1360	2014	7	10	18	49	31.4	-28.706	20.419	5	F	2.38	0.229	1.119
1850	CGS1369	2014	8	22	23	48	42.1	-32.01	23.424	5	F	2.32	0.229	1.119
1854	CGS1373	2014	8	31	3	30	13.7	-28.728	20.31	5	F	2.4	0.119	1.031
1856	CGS1375	2014	9	2	12	21	8	-29.922	22.448	5	F	2.38	0.229	1.119
1858	CGS1377	2014	9	4	14	16	39	-30.218	22.93	5	F	2.64	0.229	1.119
1859	CGS1378	2014	9	8	7	12	0.8	-30.677	19.059	5	F	2.32	0.229	1.119
1860	CGS1379	2014	9	26	8	48	21.2	-28.123	22.944	0	F	2.27	0.229	1.119
1862	CGS1381	2014	9	29	8	42	57.5	-28.609	22.836	0	F	2.38	0.229	1.119
1864	CGS1383	2014	10	5	22	13	36.7	-30.2	18.743	5	F	2.32	0.229	1.119
1865	CGS1384	2014	10	9	6	23	54.6	-31.048	20.334	5	F	2.31	0.119	1.031
1867	CGS1386	2014	10	14	12	50	48	-28.492	20.37	5	F	2.32	0.229	1.119
1869	CGS1388	2014	10	26	6	22	58	-28.751	20.324	5	F	2.44	0.229	1.119
1873	CGS1392	2014	11	8	21	2	10.9	-28.772	20.426	5	F	2.32	0.229	1.119
1874	CGS1393	2014	11	8	21	39	6.1	-30.248	18.94	5	F	2.47	0.144	1.046
1877	CGS1396	2014	11	28	2	4	52.4	-30.264	17.368	5	F	3.06	0.229	1.119
1878	CGS1397	2014	11	29	17	6	30.5	-30.644	18.99	5	F	2.49	0.144	1.046
1879	CGS1398	2014	12	7	5	10	18.6	-28.922	20.482	5	F	2.38	0.229	1.119
1882	CGS1401	2014	12	15	18	14	30.1	-28.632	20.457	5	F	2.32	0.229	1.119
1883	CGS1402	2014	12	22	17	12	33.5	-28.781	20.5	5	F	2.32	0.229	1.119
1887	CGS1406	2015	1	4	5	33	48.3	-30.682	19.213	5	F	2.32	0.229	1.119
1888	CGS1407	2015	1	9	5	57	0.2	-28.284	23.556	0	F	2.32	0.229	1.119
1890	CGS1409	2015	1	23	8	10	55.3	-29.688	19.246	5	F	2.27	0.229	1.119
1891	CGS1410	2015	2	5	2	5	9.2	-30.179	23.882	5	F	2.18	0.144	1.046
1892	CGS1411	2015	2	5	9	30	31.9	-29.277	22.908	5	F	2.3	0.05	1.005
1894	CGS1413	2015	2	26	5	27	19.2	-28.345	23.521	0	F	2.32	0.229	1.119
1895	CGS1414	2015	2	28	17	53	24.6	-30.285	18.913	5	F	2.51	0.229	1.119
1901	CGS1420	2015	4	11	4	8	13	-36.289	22.945	5	F	2.89	0.144	1.046
1902	CGS1421	2015	4	29	8	21	33.7	-28.384	22.963	0	F	2.51	0.229	1.119
1903	CGS1422	2015	5	26	5	51	18.8	-30.336	18.85	5	F	2.48	0.119	1.031
1906	CGS1425	2015	6	12	8	26	19.4	-29.58	19.37	5	F	2.51	0.229	1.119
1909	CGS1428	2015	6	21	16	15	28.6	-30.819	24.405	5	F	2.39	0.144	1.046
1912	CGS1431	2015	6	27	22	34	48.7	-32.295	22.974	5	F	2.13	0.144	1.046
1915	CGS1434	2015	7	13	5	44	53.7	-30.433	22.041	5	F	2.35	0.162	1.058
1917	CGS1436	2015	8	2	20	51	28.4	-29.56	23.72	5	F	2.27	0.229	1.119
1921	CGS1440	2015	8	13	13	23	58.5	-28.804	24.8	5	F	2.53	0.162	1.058
1922	CGS1441	2015	8	14	12	16	11.5	-29.637	23.974	5	F	2.51	0.229	1.119
1925	CGS1444	2015	8	27	9	19	28.6	-31.018	18.497	5	F	2.96	0.12	1.031
1927	GSO0048	2015	8	30	13	22	37.1	-33.208	17.782	5.6		2.57	0.229	1.119
1928	CGS1447	2015	8	31	21	25	35.4	-30.117	19.282	5	F	2.66	0.162	1.058
1929	CGS1448	2015	9	1	7	38	49.4	-31.625	17.501	5	F	2.57	0.229	1.119
1935	CGS1454	2015	9	5	10	8	21.7	-28.778	20.581	5	F	2.44	0.229	1.119
1937	CGS1456	2015	9	8	13	46	41	-28.861	22.891	0	F	2.38	0.229	1.119
1940	CGS1459	2015	9	12	2	5	20	-32.295	21.863	5	F	2.25	0.144	1.046

1942	CGS1461	2015	10	1	12	33	36.8	-28.557	22.699	0	F	2.32	0.229	1.119
1943	CGS1462	2015	10	1	20	15	1.3	-29.517	24.697	5	F	3.42	0.144	1.046
1944	CGS1463	2015	10	2	23	23	31.3	-30.741	22.903	5	F	2.32	0.229	1.119
1947	CGS1466	2015	10	9	4	10	11.6	-30.897	24.739	5	F	2.41	0.144	1.046
1948	CGS1467	2015	10	13	7	38	1	-29.79	19.848	5	F	2.27	0.229	1.119
1950	CGS1469	2015	10	14	12	3	24.9	-28.781	22.586	5	F	2.32	0.229	1.119
1951	CGS1470	2015	10	19	10	18	15.9	-28.894	23.052	0	F	2.32	0.229	1.119
1954	CGS1473	2015	10	22	22	38	24.2	-32.029	21.391	5	F	2.46	0.144	1.046
1960	CGS1479	2015	11	19	12	31	4.7	-28.014	22.619	0	F	2.44	0.229	1.119
1963	CGS1482	2015	11	22	2	31	45.8	-28.709	20.387	5	F	2.32	0.229	1.119
1964	GSO0049	2015	12	2	7	14	53.9	-33.221	19.063	9.7		3.6	0.106	1.024
1965	CGS1484	2015	12	4	23	44	0.8	-30.736	19.897	5	F	3.13	0.116	1.029
1967	CGS1486	2015	12	5	18	34	2.2	-30.143	17.211	5	F	2.44	0.229	1.119
1970	CGS1489	2015	12	17	11	48	55.6	-29.76	22.705	5	F	2.27	0.229	1.119
1974	CGS1493	2016	1	6	12	34	18.2	-29.243	21.989	5	F	2.32	0.229	1.119
1977	CGS1496	2016	1	27	1	50	24.8	-32.895	22.066	5	F	2.43	0.144	1.046
1978	GSO0050	2016	1	27	11	46	46.7	-32.711	21.399	5.4		2.44	0.229	1.119
1979	CGS1498	2016	1	28	13	55	48.2	-29.338	22.881	5	F	2.51	0.229	1.119
1981	CGS1500	2016	2	27	9	44	11	-30.117	19.834	5	F	2.32	0.229	1.119
1982	CGS1501	2016	3	10	1	18	20.4	-31.368	21.361	5	F	3.45	0.104	1.023
1984	GSO0051	2016	3	16	4	16	11.2	-32.463	21.366	5.5		2.31	0.144	1.046
1986	CGS1505	2016	3	22	13	28	2.1	-29.279	23.491	5	F	2.57	0.229	1.119
1988	CGS1507	2016	3	24	16	42	14.9	-28.386	22.293	5	F	2.38	0.229	1.119
1989	CGS1508	2016	4	8	8	38	52.8	-28.465	22.976	0	F	2.27	0.229	1.119
1993	CGS1512	2016	5	2	5	24	57.6	-30.741	16.688	5	F	2.66	0.162	1.058
1994	CGS1513	2016	5	5	2	30	14	-33.345	19.425	5	F	2.32	0.229	1.119
1995	CGS1514	2016	5	5	8	5	34.1	-28.28	23.495	0	F	2.27	0.229	1.119
1997	CGS1516	2016	5	14	5	53	18.8	-28.177	23.464	0	F	2.27	0.229	1.119
1999	CGS1518	2016	5	20	13	3	10.6	-29.084	23.213	5	F	2.51	0.229	1.119
2000	CGS1519	2016	5	24	8	55	5.5	-29.961	18.737	5	F	2.72	0.162	1.058
2001	CGS1520	2016	5	26	11	44	9.2	-28.854	23.122	0	F	2.54	0.12	1.031
2003	CGS1522	2016	5	26	12	27	12.5	-28.632	23.119	0	F	2.44	0.229	1.119
2004	CGS1523	2016	5	26	13	48	41.8	-32.928	22.026	5	F	2.02	0.144	1.046
2006	CGS1525	2016	6	5	13	40	57.4	-32.784	21.996	5	F	2.25	0.144	1.046
2007	CGS1526	2016	6	10	9	41	37	-29.436	21.225	5	F	3.02	0.144	1.046
2010	CGS1529	2016	6	28	0	41	22.2	-32.783	21.985	5	F	1.98	0.144	1.046
2011	CGS1530	2016	7	2	12	44	21	-31.012	16.921	5	F	2.32	0.229	1.119
2012	CGS1531	2016	7	6	6	4	37.9	-28.321	24.049	5	F	2.56	0.119	1.031
2013	CGS1532	2016	7	7	14	8	29	-30.368	18.31	5	F	2.57	0.05	1.005
2015	CGS1534	2016	7	9	21	12	30.5	-28.02	24.394	5	F	2.38	0.229	1.119
2016	CGS1535	2016	7	10	4	51	18.3	-29.466	21.172	5	F	2.32	0.229	1.119
2020	CGS1539	2016	7	15	1	36	5	-28.047	24.255	5	F	2.27	0.229	1.119
2022	CGS1541	2016	7	17	10	17	35.9	-32.847	22.047	5	F	2.27	0.229	1.119
2024	CGS1543	2016	7	21	16	3	21.5	-30.924	21.057	5	F	2.32	0.229	1.119
2026	GSO0052	2016	7	29	0	55	39.5	-32.605	17.819	5.9		2.7	0.229	1.119
2036	CGS1555	2016	9	5	16	4	25.5	-28.546	23.276	0	F	2.51	0.229	1.119
2039	CGS1558	2016	9	9	9	54	25	-29.239	21.862	0	F	2.57	0.229	1.119
2040	CGS1559	2016	9	15	8	57	27.2	-28.486	22.922	0	F	2.32	0.229	1.119
2045	CGS1564	2016	9	27	21	43	23.2	-29.14	21.27	5	F	2.38	0.229	1.119
2047	CGS1566	2016	10	7	11	5	10.9	-28.653	22.762	0	F	2.44	0.229	1.119
2049	CGS1568	2016	10	10	18	22	33.8	-28.41	18.417	5	F	2.44	0.229	1.119
2052	CGS1571	2016	10	18	6	25	31.6	-33.325	22.361	5	F	3.8	0.076	1.012
2053	CGS1572	2016	10	21	10	18	0.6	-28.466	22.438	0	F	2.84	0.229	1.119
2054	CGS1573	2016	10	22	11	25	16.5	-33.708	21.977	5	F	2.51	0.229	1.119
2057	CGS1576	2016	10	27	18	6	23.3	-29.287	24.5	5	F	2.27	0.229	1.119
2058	CGS1577	2016	10	28	16	45	24	-30.516	24.86	5	F	2.8	0.081	1.014
2066	CGS1585	2016	11	4	12	37	25.6	-29.461	18.74	5	F	2.51	0.229	1.119
2074	CGS1593	2016	11	18	11	21	35.4	-28.614	22.729	0	F	2.51	0.229	1.119
2075	CGS1594	2016	11	18	15	6	27.2	-35.734	25.079	5	F	2.77	0.229	1.119
2077	CGS1596	2016	11	21	9	19	51	-28.566	23.32	0	F	2.51	0.229	1.119
2083	CGS1602	2016	11	30	14	18	13.7	-30.727	23.938	5	F	2.27	0.229	1.119
2084	CGS1603	2016	12	1	12	52	2	-30.862	15.377	5	F	2.57	0.229	1.119
2089	CGS1608	2016	12	15	8	14	51.2	-28.162	18.409	5	F	2.44	0.229	1.119
2091	CGS1610	2016	12	22	16	54	27.4	-32.864	17.837	5	F	2.42	0.119	1.031
2092	GSO0055	2017	1	14	1	20	21.1	-31.631	20.581	3		2.15	0.071	1.011
2095	GSO0056	2017	1	31	14	3	52.2	-34.069	22.029	6.3		2.32	0.229	1.119
2096	CGS1614	2017	2	10	14	57	11.5	-28.708	23.037	0	F	2.32	0.229	1.119
2098	CGS1616	2017	2	27	18	41	59.5	-30.36	20.796	5	F	2.23	0.112	1.027
2099	CGS1617	2017	3	2	2	30	17.3	-29.239	22.347	5	F	2.32	0.229	1.119
2102	CGS1620	2017	3	2	13	55	29	-28.339	22.565	0	F	2.38	0.229	1.119
2103	GSO0057	2017	3	2	16	10	7.5	-33.169	17.94	5.7		2.14	0.144	1.046
2104	GSO0058	2017	3	3	4	8	11.1	-33.289	22.331	6.2		2.29	0.08	1.014

2110	CGS1628	2017	3	22	20	0	28.7	-28.192	24.447	5	F	2.53	0.162	1.058
2114	CGS1632	2017	4	1	11	39	0.4	-30.784	20.122	5	F	2.3	0.154	1.052
2115	CGS1633	2017	4	4	12	48	50.4	-28.524	22.699	0	F	2.38	0.229	1.119
2116	CGS1634	2017	4	5	23	1	6	-28.723	20.501	5	F	2.32	0.229	1.119
2118	GSO0059	2017	4	9	10	1	53.3	-32.85	22.73	5.8		2.87	0.067	1.01
2119	CGS1636	2017	4	10	13	46	38.6	-28.412	22.3	0	F	2.44	0.229	1.119
2121	CGS1638	2017	4	14	5	13	15.2	-28.587	19.428	5	F	2.45	0.144	1.046
2122	CGS1639	2017	4	18	14	38	22.1	-28.563	18.772	5	F	2.5	0.162	1.058
2124	CGS1641	2017	4	23	20	28	52.4	-28.71	19.512	5	F	2.16	0.144	1.046
2126	CGS1643	2017	4	28	6	55	17.8	-28.683	19.542	5	F	2.22	0.144	1.046
2130	CGS1647	2017	5	8	8	47	4	-31.35	22.47	5	F	2.44	0.081	1.014
2138	CGS1655	2017	5	26	14	50	27.4	-28.441	22.639	0	F	2.38	0.229	1.119
2139	CGS1656	2017	5	30	10	24	11.7	-28.527	19.923	5	F	2.48	0.104	1.023
2140	CGS1657	2017	6	1	15	23	35.3	-28.722	25.723	5	F	2.27	0.229	1.119
2141	CGS1658	2017	6	8	8	15	28.3	-29.104	18.806	5	F	2.27	0.229	1.119
2143	CGS1660	2017	6	10	8	40	2.1	-29.228	18.952	5	F	2.27	0.229	1.119
2144	CGS1661	2017	6	10	12	53	8.6	-30.94	21.389	5	F	2.37	0.104	1.023
2145	CGS1662	2017	6	12	8	33	41.3	-28.905	18.638	5	F	2.27	0.229	1.119
2151	CGS1668	2017	6	30	12	26	57.7	-28.751	23.154	0	F	2.32	0.229	1.119
2152	ISC1312	2017	7	1	10	0	23.3	-31.005	17.133	5	F	2.51	0.229	1.119
2156	CGS1672	2017	7	15	9	9	14.7	-36.379	19.075	5	F	2.56	0.144	1.046
2158	GSO0060	2017	7	22	12	20	13.1	-32.112	21.937	3.7		2.3	0.075	1.012
2160	CGS1676	2017	7	27	14	34	55.7	-28.71	18.647	5	F	2.32	0.229	1.119
2161	CGS1677	2017	8	4	10	23	56.7	-30.265	20.352	5	F	2.79	0.095	1.02
2163	CGS1679	2017	8	10	8	43	9.7	-29.189	18.883	5	F	2.27	0.229	1.119
2164	CGS1680	2017	8	10	18	9	1	-31.068	18.477	5	F	2.11	0.144	1.046
2165	CGS1681	2017	8	16	16	29	0.3	-29.764	18.404	5	F	2.38	0.229	1.119
2166	CGS1682	2017	8	17	5	7	0.7	-32.57	24.621	5	F	2.49	0.061	1.008
2168	ISC1318	2017	8	22	14	7	45.89	-28.451	23.078	0	F	2.32	0.229	1.119
2170	CGS1685	2017	9	2	12	35	4	-28.824	18.261	5	F	2.32	0.229	1.119
2173	CGS1688	2017	9	12	11	43	46.6	-28.039	22.78	0	F	2.27	0.229	1.119
2174	ISC1319	2017	9	16	12	37	48.3	-28.067	16.223	5	F	2.27	0.229	1.119
2175	CGS1689	2017	9	20	9	21	39.2	-28.49	23.416	0	F	2.32	0.229	1.119
2179	CGS1693	2017	10	5	13	45	59.1	-28.293	22.956	0	F	2.44	0.162	1.058
2185	CGS1699	2017	10	31	1	33	11.8	-34.468	20.054	5	F	2.32	0.229	1.119
2187	CGS1701	2017	11	3	7	43	33.2	-29.163	18.799	5	F	2.38	0.229	1.119
2188	CGS1702	2017	11	4	11	39	21.5	-30.519	18.194	5	F	2.32	0.229	1.119
2192	CGS1706	2017	11	13	8	22	56.7	-29.065	18.687	5	F	2.38	0.229	1.119
2193	CGS1707	2017	11	15	16	28	2.2	-29.476	18.682	5	F	2.27	0.229	1.119
2197	ISC1326	2017	12	2	11	5	39.7	-28.477	19.735	15		2.99	0.229	1.119
2199	CGS1712	2017	12	14	8	20	51.7	-29.227	18.877	5	F	2.72	0.04	1.003
2204	CGS1717	2018	1	2	15	13	31.7	-29.278	21.37	5	F	2.44	0.229	1.119
2210	CGS1723	2018	1	18	15	37	6.4	-32.927	21.133	5	F	2.51	0.229	1.119
2211	CGS1724	2018	1	19	11	44	27.8	-28.82	22.167	0	F	2.32	0.229	1.119
2212	CGS1725	2018	1	19	14	18	41.4	-32.074	21.454	0	F	2.64	0.229	1.119
2213	CGS1726	2018	1	19	21	45	22.6	-28.333	20.176	5	F	3.26	0.094	1.019
2215	CGS1728	2018	1	20	2	10	21	-28.166	20.375	5	F	2.37	0.104	1.023
2217	CGS1730	2018	2	3	5	45	23	-28.543	20.314	5	F	3.46	0.075	1.012
2247	CGS1760	2018	2	27	8	30	42.8	-28.188	23.172	0	F	2.51	0.229	1.119
2249	CGS1762	2018	3	3	7	54	3.3	-28.281	23.545	0	F	2.27	0.229	1.119
2251	CGS1764	2018	3	13	9	44	14.3	-28.839	18.897	5	F	3.45	0.04	1.003
2253	CGS1766	2018	3	15	21	28	7.3	-28.7	20.924	5	F	2.55	0.104	1.023
2254	CGS1767	2018	3	15	22	50	34.3	-28.651	20.656	5	F	2.47	0.162	1.058
2256	CGS1769	2018	3	17	12	58	43.3	-28.43	23.361	0	F	2.27	0.229	1.119
2258	CGS1771	2018	3	24	11	50	25.5	-29.103	20.291	5	F	2.23	0.144	1.046
2261	CGS1774	2018	3	29	8	36	0.3	-28.234	22.997	0	F	2.38	0.229	1.119
2264	CGS1777	2018	4	1	13	25	17.3	-28.642	20.342	5	F	3.45	0.106	1.024
2268	CGS1781	2018	4	2	0	6	22.8	-28.941	19.926	5	F	2.54	0.12	1.031
2272	CGS1785	2018	4	8	15	40	23.7	-28.746	20.663	5	F	2.27	0.229	1.119
2274	CGS1787	2018	4	11	15	26	0.4	-28.688	23.141	0	F	2.38	0.229	1.119
2277	CGS1790	2018	4	15	0	21	50	-31.946	22.863	5	F	2.1	0.071	1.011
2278	CGS1791	2018	4	17	13	53	3.3	-29.394	18.85	5	F	2.27	0.229	1.119
2280	CGS1793	2018	4	18	11	33	17.3	-28.743	20.711	5	F	2.53	0.162	1.058
2281	CGS1794	2018	4	20	4	35	47	-33.244	22.542	5	F	2.09	0.071	1.011
2282	CGS1795	2018	4	21	12	52	11.5	-28.355	20.33	5	F	2.44	0.1	1.022
2285	CGS1798	2018	4	25	15	12	49.5	-35.69	20.862	5	F	2.32	0.229	1.119
2287	CGS1800	2018	4	25	23	30	15.6	-28.545	20.482	5	F	2.41	0.086	1.016
2294	CGS1807	2018	4	28	19	21	38.4	-28.724	20.574	5	F	2.83	0.089	1.017
2296	CGS1809	2018	5	10	1	31	17.5	-28.525	20.35	5	F	2.73	0.09	1.018
2302	CGS1815	2018	5	18	2	33	57.8	-29.199	24.447	5	F	2.84	0.068	1.01
2304	CGS1817	2018	5	20	22	8	10	-30.196	19.367	5	F	2	0.144	1.046
2306	CGS1819	2018	5	24	12	37	18.3	-28.325	21.753	5	F	2.27	0.229	1.119

2307	CGS1820	2018	5	26	18	9	24.3	-28.7	20.537	5	F	2.39	0.12	1.031
2313	CGS1825	2018	6	10	21	29	36.8	-28.399	20.301	5	F	2.67	0.08	1.014
2314	CGS1826	2018	6	12	14	29	35.1	-32.182	19.052	0	F	2.57	0.229	1.119
2315	CGS1827	2018	6	14	9	19	33.1	-28.732	20.433	5	F	2.54	0.12	1.031
2316	CGS1828	2018	6	14	12	7	31.5	-29.147	22.755	38		2.27	0.229	1.119
2317	CGS1829	2018	6	15	4	54	45.6	-28.759	20.775	5	F	2.23	0.111	1.027
2318	CGS1830	2018	6	16	10	20	7.9	-28.626	25.262	0	F	2.32	0.229	1.119
2319	CGS1831	2018	6	18	8	31	5.8	-28.192	23.148	0	F	2.38	0.229	1.119
2321	CGS1833	2018	6	21	16	17	57.8	-28.913	22.45	5	F	2.29	0.05	1.005
2322	CGS1834	2018	6	23	15	10	55	-30.035	17.966	5	F	2.35	0.162	1.058
2323	CGS1835	2018	6	25	8	52	34.8	-30.107	19.161	5	F	2.38	0.229	1.119
2324	GSO0061	2018	7	1	13	18	22.7	-32.506	21.108	6.8		2.38	0.086	1.016
2325	CGS1837	2018	7	2	11	18	55.1	-28.685	23.365	0	F	2.32	0.229	1.119
2328	CGS1840	2018	7	16	15	2	41.8	-30.917	16.974	5	F	2.27	0.229	1.119
2329	CGS1841	2018	7	19	11	9	31.1	-28.785	20.573	5	F	2.38	0.229	1.119
2333	CGS1845	2018	7	30	8	37	23.3	-28.706	20.434	5	F	2.27	0.229	1.119
2336	CGS1848	2018	8	4	16	24	27.4	-30.45	19.04	5	F	2.28	0.119	1.031
2337	CGS1849	2018	8	5	7	30	8.1	-28.758	20.375	5	F	2.17	0.111	1.027
2341	CGS1853	2018	8	24	18	7	7	-33.13	25.808	5	F	2.57	0.229	1.119
2342	CGS1854	2018	8	29	14	19	6.4	-28.147	25.585	5	F	3	0.05	1.005
2344	CGS1856	2018	9	1	13	25	13.2	-29.42	18.661	5	F	2.32	0.229	1.119
2345	CGS1857	2018	9	4	9	21	19.5	-28.585	19.93	5	F	2.27	0.229	1.119
2346	CGS1858	2018	9	7	8	28	55.8	-30.545	18.76	5	F	2.7	0.094	1.019
2347	CGS1859	2018	9	8	8	51	51.3	-29.029	18.805	5	F	2.38	0.229	1.119
2349	CGS1861	2018	9	11	18	56	39	-28.556	20.455	5	F	2.32	0.12	1.031
2350	CGS1862	2018	9	18	9	30	23.8	-28.561	20.346	5	F	2.32	0.086	1.016
2351	CGS1863	2018	9	21	16	22	10.8	-29.1	18.942	0	F	2.59	0.162	1.058
2352	CGS1864	2018	9	29	4	30	8.7	-29.58	19.01	5	F	2.57	0.075	1.012
2354	CGS1866	2018	10	3	14	0	20.9	-28.63	23.1	5	F	2.38	0.229	1.119
2361	CGS1873	2018	10	21	1	45	45.9	-30.082	24.796	5	F	2.32	0.229	1.119
2362	CGS1874	2018	10	25	11	54	47.4	-30.234	22.874	5	F	2.27	0.229	1.119
2364	CGS1876	2018	10	29	23	55	40.9	-29.542	19.059	5	F	2.21	0.134	1.039
2366	CGS1878	2018	11	20	12	30	47.5	-29.932	20.889	5	F	2.38	0.229	1.119
2371	CGS1882	2018	12	9	1	48	56.1	-28.121	17.454	5	F	2.25	0.16	1.057
2376	CGS1887	2018	12	20	16	52	8.2	-29.194	25.68	5	F	2.32	0.05	1.005
2377	CGS1888	2018	12	24	5	6	28.9	-31.085	24.944	5	F	2.22	0.086	1.016
2379	CGS1890	2019	1	9	16	12	27.1	-30.083	18.703	5	F	2.99	0.229	1.119
2380	CGS1891	2019	1	10	20	9	8	-31.006	17.597	5	F	2.84	0.229	1.119
2383	CGS1894	2019	1	28	15	10	42	-30.21	19.026	5	F	2.27	0.229	1.119
2384	CGS1895	2019	2	5	18	23	11.9	-30.956	24.663	5	F	2.91	0.229	1.119
2385	GSO0062	2019	2	6	16	55	44.5	-32.68	21.245	5.9		2.32	0.229	1.119
2386	CGS1897	2019	2	20	9	26	13.2	-28.424	19.672	5	F	2.27	0.229	1.119
2388	CGS1899	2019	2	20	9	44	43.6	-28.654	20.4	5	F	2.7	0.229	1.119
2390	CGS1901	2019	3	4	14	7	8.8	-28.076	18.192	5	F	2.94	0.144	1.046
2391	GSO0063	2019	3	6	14	17	23.4	-32.675	18.362	5.3		2.27	0.229	1.119
2394	CGS1905	2019	3	10	8	29	2.4	-29.333	23.036	5	F	2.57	0.229	1.119
2395	GSO0064	2019	3	19	12	32	32.2	-32.321	20.439	6.9		2.46	0.14	1.043
2397	CGS1908	2019	3	20	5	4	48.1	-28.494	20.355	5	F	2.51	0.229	1.119
2404	ISC1442	2019	4	18	14	56	42.1	-30.144	22.754	0		3.06	0.229	1.119
2408	CGS1918	2019	5	16	4	15	47.7	-30.527	21	5	F	2.32	0.229	1.119
2409	CGS1919	2019	5	19	4	57	44.3	-28.343	17.605	5	F	2.91	0.229	1.119
2411	CGS1921	2019	5	19	10	18	54.9	-28.51	17.936	5	F	2.27	0.229	1.119
2412	CGS1922	2019	5	19	14	3	27.1	-32.198	17.372	5	F	2.7	0.229	1.119
2414	CGS1924	2019	5	24	22	2	24.6	-29.476	24.58	5	F	2.94	0.144	1.046
2415	CGS1925	2019	5	25	22	41	7.3	-31.151	23.851	5	F	2.27	0.229	1.119
2417	CGS1927	2019	5	31	14	19	9.6	-31.232	18.229	5	F	2.27	0.229	1.119
2419	CGS1929	2019	6	18	21	16	32.4	-30.44	20.737	5	F	2.44	0.229	1.119
2422	CGS1932	2019	8	1	12	50	25.2	-29.107	18.322	5	F	2.38	0.229	1.119
2425	CGS1935	2019	8	9	0	7	21.9	-29.986	18.141	5	F	3.14	0.229	1.119
2428	CGS1938	2019	8	15	23	42	14	-29.09	25.047	5	F	2.91	0.229	1.119
2432	GSO0065	2019	9	1	9	38	13.7	-32.457	17.745	7.2		2.44	0.229	1.119
2433	CGS1943	2019	9	4	10	7	7.9	-29.481	24.706	5	F	2.57	0.229	1.119
2434	CGS1944	2019	9	5	15	16	48.1	-29.057	21.839	5	F	2.27	0.229	1.119
2436	CGS1946	2019	9	13	0	57	3.1	-29.521	24.636	5	F	2.38	0.229	1.119
2437	ISC1475	2019	9	13	0	57	11.49	-27.976	22.571	10	F	2.7	0.229	1.119
2441	CGS1950	2019	10	1	13	44	6.9	-29.609	17.974	5	F	2.64	0.229	1.119
2445	CGS1954	2019	10	8	9	0	6.1	-31.913	21.282	5	F	2.38	0.229	1.119
2452	CGS1961	2019	11	15	2	33	6.6	-28.609	20.305	5	F	2.59	0.144	1.046
2455	CGS1964	2019	11	30	15	48	14.5	-28.492	20.475	5	F	2.51	0.229	1.119
2458	CGS1966	2019	12	6	20	24	27.8	-29.779	18.9	5	F	2.32	0.229	1.119
2459	CGS1967	2019	12	7	0	13	0.5	-28.677	20.445	5	F	2.46	0.144	1.046
2464	CGS1972	2019	12	27	17	26	18.9	-28.714	20.411	5	F	2.18	0.144	1.046

2467	GSO0066	2020	1	5	7	48	44.4	-33.145	17.687	6.2		2.86	0.14	1.043
2468	CGS1976	2020	1	15	21	12	6.5	-29.783	24.338	5	F	2.32	0.229	1.119
2469	CGS1977	2020	1	20	1	31	1.1	-28.2	20.743	5	F	2.57	0.229	1.119
2471	CGS1979	2020	1	30	17	47	57.1	-32.572	22.601	5	F	2.32	0.229	1.119
2479	CGS1987	2020	3	4	23	30	35.6	-32.473	25.147	5	F	2.98	0.162	1.058
2484	CGS1992	2020	3	19	15	14	26.9	-28.676	18.566	5	F	2.32	0.229	1.119
2486	CGS1994	2020	4	3	23	7	28.5	-28.181	20.27	5	F	2.51	0.229	1.119
2489	CGS1997	2020	4	4	6	36	35.8	-34.616	23.065	5	F	2.38	0.229	1.119
2490	CGS1998	2020	4	4	9	4	10.9	-28.604	20.376	5	F	2.44	0.229	1.119
2491	ISC1529	2020	4	25	23	10	29.7	-28.247	17.559	0		2.64	0.229	1.119
2493	CGS2000	2020	5	21	3	20	50.3	-28.865	20.705	5	F	2.27	0.229	1.119
2495	CGS2002	2020	5	25	11	16	51.9	-29.564	25.798	5	F	2.51	0.229	1.119
2504	CGS2011	2020	7	14	13	49	42.4	-30.135	17.587	5	F	2.38	0.229	1.119
2507	CGS2014	2020	7	24	14	59	53.4	-29.489	17.882	5	F	2.27	0.229	1.119
2508	CGS2015	2020	7	25	17	7	57	-30.273	19.617	5	F	2.38	0.229	1.119
2509	ISC1547	2020	8	9	10	34	22.8	-29.668	23.229	0		2.91	0.229	1.119
2510	CGS2016	2020	8	12	13	50	35.6	-30.483	18.033	5	F	2.51	0.229	1.119
2512	CGS2018	2020	8	17	2	26	44	-31.147	18.168	5	F	2.84	0.229	1.119
2514	CGS2020	2020	8	26	19	50	4.7	-28.687	20.496	5	F	2.38	0.229	1.119
2515	CGS2021	2020	8	28	7	42	8.4	-29.833	19.121	5	F	2.32	0.229	1.119
2516	CGS2022	2020	8	31	12	41	57.3	-29.689	19.317	5	F	2.27	0.229	1.119
2517	CGS2023	2020	8	31	21	51	43.3	-32.202	15.75	5	F	2.57	0.229	1.119
2518	CGS2024	2020	9	18	13	43	34.3	-28.147	24.13	5	F	2.51	0.229	1.119
2520	CGS2026	2020	9	23	13	8	45.1	-28.909	19.757	5	F	2.44	0.229	1.119
2522	CGS2027	2020	9	25	13	47	13.1	-28.338	25.494	5	F	2.7	0.229	1.119
2524	GSO0068	2020	9	27	7	12	51.7	-33.755	18.683	5.4		2.46	0.14	1.043
2525	CGS2030	2020	10	3	10	24	16	-29.507	24.868	5	F	3.19	0.162	1.058
2527	CGS2031	2020	10	5	15	21	54.5	-32.849	22.118	5	F	2.44	0.229	1.119
2528	CGS2032	2020	10	5	16	16	44.8	-33.422	21.934	5	F	2.64	0.229	1.119
2529	CGS2033	2020	10	6	23	21	20.3	-28.702	20.471	5	F	2.44	0.229	1.119
2532	CGS2036	2020	10	11	12	42	0.3	-29.647	19.386	5	F	2.27	0.229	1.119
2533	CGS2037	2020	10	13	15	16	17.1	-28.978	17.752	5	F	2.51	0.229	1.119
2534	CGS2038	2020	10	15	14	1	56.5	-28.762	23.416	5	F	2.38	0.229	1.119
2538	ISC1576	2020	10	28	16	30	48.9	-28.389	22.688	64.3		2.27	0.229	1.119
2539	ISC1577	2020	11	6	11	55	14.5	-28.425	22.087	287.6		2.51	0.229	1.119
2541	ANS0031	2020	11	16	22	27	3.219	-33.43	17.897	5		3.38	0.229	1.119
2543	ISC1581	2020	12	2	10	12	5.5	-29.423	19.149	0.1		2.99	0.229	1.119
2545	ISC1583	2020	12	2	12	42	21.4	-29.751	20.619	38.7		3.38	0.229	1.119
2547	ISC1585	2020	12	3	15	20	34.4	-28.058	19.737	0		2.38	0.229	1.119
2548	ISC1586	2020	12	4	11	52	12.6	-28.053	21.286	0		2.38	0.229	1.119
2549	ISC1587	2020	12	8	14	31	46.8	-28.793	23.25	0		2.84	0.229	1.119
2551	CGS2044	2020	12	10	15	35	19.2	-28.355	22.065	5	F	2.44	0.229	1.119
2553	ISC1591	2020	12	19	8	6	44.9	-28.895	24.052	5		2.77	0.229	1.119
2554	CGS2046	2020	12	20	9	54	9.1	-28.672	20.714	5	F	2.38	0.229	1.119
2556	CGS2048	2021	1	9	7	27	23.7	-29.232	19.369	5	F	2.32	0.229	1.119
2557	ISC1595	2021	1	13	12	35	48.6	-28.121	17.695	9.1		3.63	0.229	1.119
2561	ISC1599	2021	1	14	19	12	23.7	-28.505	17.943	0		2.57	0.229	1.119
2562	ISC1600	2021	1	17	0	34	52.3	-28.041	17.401	0		2.57	0.229	1.119
2564	ISC1602	2021	1	18	0	48	23.4	-28.891	17.9	38.7		2.51	0.229	1.119
2565	CGS2051	2021	1	18	5	7	46.5	-31.234	20.032	5	F	2.44	0.229	1.119
2566	ISC1604	2021	1	20	10	55	31.7	-28.065	19.797	5		3.3	0.229	1.119
2567	ISC1605	2021	1	21	7	8	21.9	-28.227	17.379	38.1		2.57	0.229	1.119
2568	CGS2052	2021	1	27	13	54	8.8	-28.121	21.999	5	F	2.57	0.229	1.119
2569	CGS2053	2021	1	31	1	51	2.8	-30.092	20.351	5	F	2.59	0.162	1.058
2570	ISC1608	2021	2	2	16	2	23.6	-30.981	19.985	35.1		2.77	0.229	1.119
2573	ISC1611	2021	2	6	7	23	25.4	-29.033	22.959	0		2.57	0.229	1.119
2574	ISC1612	2021	2	16	13	50	11.7	-28.057	19.747	0		3.63	0.229	1.119
2575	ISC1613	2021	2	19	11	54	42.5	-29.77	18.341	0		2.51	0.229	1.119
2576	ISC1614	2021	2	19	15	3	30.1	-28.179	22.315	0		2.7	0.229	1.119
2578	CGS2057	2021	2	23	20	11	54.9	-30.56	23.507	5	F	2.32	0.229	1.119
2579	CGS2058	2021	3	1	8	34	55.8	-28.971	19.041	5	F	2.27	0.229	1.119
2580	CGS2059	2021	3	2	12	19	39.8	-28.418	17.191	5	F	2.44	0.229	1.119
2582	CGS2061	2021	3	13	7	5	55.7	-28.188	23.021	0	F	2.38	0.229	1.119
2585	CGS2064	2021	3	21	22	36	3.8	-30.855	24.581	5	F	2.64	0.229	1.119
2586	CGS2065	2021	3	26	19	41	22.2	-32.712	20.524	5	F	2.44	0.229	1.119
2589	CGS2068	2021	4	4	18	59	6.7	-28.78	20.39	5	F	2.38	0.229	1.119
2591	ISC1617	2021	4	21	4	15	17.1	-29.137	23.051	0.1		2.51	0.229	1.119
2592	CGS2070	2021	4	22	15	9	12.7	-28.016	22.768	0	F	2.44	0.229	1.119
2597	CGS2075	2021	5	21	8	38	16.7	-28.322	23.28	0	F	2.38	0.229	1.119
2598	CGS2076	2021	5	23	8	51	16.9	-31.153	24.439	5	F	2.27	0.229	1.119
2600	CGS2078	2021	5	31	5	8	3.1	-29.614	17.519	5	F	2.6	0.162	1.058
2601	CGS2079	2021	5	31	14	27	55.4	-29.621	18.888	0	F	2.27	0.229	1.119

2602	ISC1619	2021	6	1	15	16	13.8	-28.781	21.288	0		2.7	0.229	1.119
2603	ISC1620	2021	6	4	14	47	30.3	-29.502	19.332	0		2.51	0.229	1.119
2606	ISC1621	2021	7	1	14	27	17.6	-28.522	23.063	0.1		3.14	0.229	1.119
2609	CGS2084	2021	7	5	19	26	13.1	-30.693	18.893	5	F	2.51	0.229	1.119
2610	CGS2085	2021	7	5	23	39	7.9	-29.755	18.177	5	F	4.09	0.162	1.058
2611	CGS2086	2021	7	8	5	21	33.6	-30.483	25.008	5	F	2.27	0.229	1.119
2614	ISC1623	2021	7	27	14	43	13.9	-29.589	19.326	0		2.44	0.229	1.119
2615	CGS2089	2021	7	29	15	21	36.4	-28.068	22.597	0	F	2.32	0.229	1.119
2616	CGS2090	2021	7	30	16	8	24.9	-28.826	19.201	5	F	2.47	0.162	1.058
2619	CGS2092	2021	8	6	15	0	51.3	-28.586	23	0	F	2.27	0.229	1.119
2620	CGS2093	2021	8	7	12	50	29.4	-28.16	22.527	0	F	2.27	0.229	1.119
2621	CGS2094	2021	8	13	12	24	7.5	-28.795	23.28	0	F	2.32	0.229	1.119
2624	CGS2097	2021	8	20	15	37	39	-28.404	22.635	0	F	2.7	0.229	1.119
2625	ISC1627	2021	8	23	6	13	27.6	-31.608	19.999	5		2.51	0.229	1.119
2627	CGS2099	2021	8	31	13	17	51.7	-28.678	22.183	0	F	2.27	0.229	1.119
2628	ISC1629	2021	8	31	21	54	19.6	-28.821	18.592	0.1		2.44	0.229	1.119
2630	CGS2101	2021	9	6	14	23	40.3	-29.127	18.501	0	F	2.27	0.229	1.119
2631	CGS2102	2021	9	7	0	36	14.9	-30.608	25.319	5	F	2.44	0.229	1.119
2632	CGS2103	2021	9	8	20	14	29.2	-29.383	18.214	5	F	2.27	0.229	1.119
2642	ISC1633	2021	11	22	14	57	10.6	-29.391	19.241	0		2.51	0.229	1.119
2645	ISC1634	2021	12	1	12	5	8.7	-29.627	19.366	0.1		2.44	0.229	1.119
2650	CGS2119	2021	12	20	17	18	34	-29.405	18.796	0	F	2.44	0.229	1.119
2651	CGS2120	2021	12	21	0	33	13.2	-30.995	23.519	5	F	2.32	0.229	1.119
2652	CGS2121	2021	12	24	13	16	5.6	-28.761	18.698	10	F	2.32	0.229	1.119
2653	CGS2122	2021	12	25	11	51	38.4	-35.411	22.309	5	F	2.32	0.229	1.119
2654	CGS2123	2021	12	30	14	57	53.9	-28.836	22.687	5	F	2.32	0.229	1.119

Note: Lower magnitude limit is E[M] = 3.3

eqID	srcID	year	mon	day	hr	min	sec	lat	lon	dep	depFix	E[M]	sigEM	Nstar
9	TNS0008	1809	12	4	20	8	0	-33.905	18.409	20	F	6.12	0.242	1.133
22	TNS0021	1857	8	14	21	30	0	-33.508	18.776	20	F	4.66	0.231	1.121
37	TNS0034	1899	9	15	10	23	0	-33.905	18.409	20		4.66	0.231	1.121
40	TNS0037	1903	8	3	0	0	0	-29.4	25			3.98	0.229	1.12
42	TNS0039	1908	8	18	3	0	0	-29	26			3.71	0.229	1.119
43	TNS0040	1908	9	26	21	7	0	-28.7	25.8			4.66	0.231	1.121
44	TNS0041	1908	12	30	0	20	0	-29.7	17.9			3.71	0.229	1.119
2655	IDP0001	1909	12	9	19	20	0	-33.661	19.509	20		4.09	0.23	1.12
47	TNS0044	1910	10	21	18	42	0	-30.55	24.7			4.66	0.231	1.121
48	TNS0045	1911	7	6	20	15	0	-33.583	22.2			3.71	0.229	1.119
49	TNS0046	1912	2	20	13	3	0	-29.5	25			6.05	0.108	1.025
63	TNS0059	1921	10	9	13	20	0	-33.3	19.1			4.66	0.231	1.121
72	TNS0068	1926	8	11	0	0	0	-33.4	18.4			3.71	0.229	1.119
74	TNS0070	1936	1	16	9	38	0	-29.8	25.3			4.66	0.231	1.121
78	TNS0074	1940	10	13	13	45	0	-32.5	24			3.98	0.229	1.12
81	TNS0077	1941	10	24	18	30	0	-31	17.7			3.98	0.229	1.12
82	TNS0078	1943	11	24	22	45	0	-30	23			3.98	0.229	1.12
85	CGS0078	1950	9	30	16	56	56	-30.5	18	0	F	5.2	0.233	1.124
86	CGS0079	1950	11	19	0	0	0	-34	18	0	F	3.89	0.229	1.119
87	CGS0080	1951	1	19	6	15	21	-29.5	24.5	0	F	3.63	0.229	1.119
88	CGS0081	1951	6	13	14	8	18	-31.9	23.2	0	F	4.36	0.23	1.12
89	CGS0082	1951	9	16	16	33	8	-33	22.5	0	F	4.27	0.23	1.12
96	CGS0089	1952	1	28	16	41	22	-32.9	20.5	0	F	5.09	0.232	1.123
100	CGS0093	1952	2	26	19	45	0	-34	20.4	0	F	3.89	0.229	1.119
102	CGS0095	1953	2	26	9	14	17	-30	21	0	F	4.08	0.229	1.12
103	CGS0096	1953	5	1	1	7	2	-29	17	0	F	5.53	0.235	1.126
107	CGS0100	1955	5	20	6	23	40	-29.3	25.3	0	F	4.77	0.231	1.121
108	CGS0101	1955	10	28	13	17	16	-29.5	25.5	0	F	3.71	0.229	1.119
109	CGS0102	1956	6	26	9	9	52	-30	26	0	F	3.3	0.229	1.119
110	CGS0103	1956	10	23	21	21	3	-31.2	22.2	0	F	3.3	0.229	1.119
111	CGS0104	1957	9	20	3	38	0	-34	18.2	0	F	3.89	0.229	1.119
112	CGS0105	1957	9	30	0	0	0	-34	18.2	0	F	3.89	0.229	1.119
113	CGS0106	1960	8	29	5	35	0	-33.448	18.373	20		4.46	0.23	1.12
114	CGS0107	1963	8	27	0	48	0	-33.44	19.229	20		4.66	0.231	1.121
116	CGS0109	1964	2	21	0	0	0	-34.1	18	0	F	3.98	0.229	1.12
117	CGS0110	1964	6	9	20	1	18	-29	25	0	F	4.66	0.231	1.121
118	CGS0111	1965	9	28	14	45	0	-33.9	22	0	F	3.98	0.229	1.12
119	ISC0002	1966	1	4	16	25	2	-28	26	0		3.38	0.229	1.119
120	ISC0003	1966	2	18	11	42	48.01	-29.057	25.449	10	F	3.95	0.162	1.058
121	CGS0113	1966	3	1	0	4	0	-34.1	18	0	F	3.98	0.229	1.12
122	CGS0114	1966	7	31	20	2	15	-30	19	0	F	3.95	0.162	1.058
123	CGS0115	1966	8	25	1	27	38	-28.4	19.3	0	F	3.51	0.162	1.058
124	CGS0116	1967	6	16	14	51	35	-30.4	18.4	0	F	4.04	0.162	1.058
125	CGS0117	1967	7	12	22	36	22	-30	20	0	F	3.51	0.162	1.058
126	CGS0118	1967	8	9	23	10	29	-31.3	23.3	0	F	3.43	0.162	1.058
128	ISC0010	1968	1	12	1	0	7.95	-33.126	23.704	10	F	5.25	0.165	1.06
129	CGS0120	1968	2	24	2	23	48	-30.2	20	0	F	3.43	0.162	1.058
131	CGS0121	1968	8	31	13	13	32	-29.6	25.9	0	F	4.08	0.229	1.12
134	ISC0016	1969	3	4	19	3	49.36	-29.951	25.842	14	F	3.71	0.229	1.119
135	ISC0017	1969	9	11	21	45	18.35	-33.807	18.714	20		4.93	0.164	1.059
138	ISC0018	1969	9	29	20	3	30.8	-33.265	19.281	16.7		6.16	0.14	1.043
162	ISC0024	1969	9	30	11	40	44.81	-32.801	19.969	10	F	4.13	0.162	1.058
175	ISC0030	1969	10	6	20	26	19.88	-33.838	19.972	10	F	3.63	0.229	1.119
179	CGS0165	1969	10	8	23	14	50	-32.2	19.2	0	F	3.8	0.229	1.119
180	ISC0032	1969	10	8	23	15	5.02	-32.59	20.281	10	F	3.8	0.229	1.119
181	ISC0033	1969	10	10	18	34	54.14	-33.924	20.391	10	F	4.52	0.163	1.058
189	ISC0035	1969	11	6	20	5	16.68	-34.352	19.254	10	F	3.99	0.162	1.058
191	ISC0036	1969	11	8	12	23	59.82	-32.475	19.742	10	F	3.99	0.162	1.058
216	ISC0045	1969	11	13	11	3	19.85	-33.126	20.815	10	F	3.86	0.162	1.058
232	CGS0214	1971	7	29	3	15	40.4	-31.7	25.8	30	F	3.77	0.263	1.16
233	ISC0054	1971	7	29	3	15	47.74	-31.691	25.213	10	F	3.63	0.229	1.119
234	ISC0055	1971	9	28	17	1	9.28	-32.451	20.859	10	F	4.27	0.23	1.12
235	TNS0171	1972	3	9	8	29	0	-31.796	25.049			3.43	0.162	1.058
236	ISC0057	1972	7	19	17	35	21.84	-31.695	25.393	10	F	3.86	0.162	1.058
237	TNS0173	1972	9	21	23	26	0	-29.531	25.649			4.42	0.163	1.058
239	TNS0174	1973	1	12	5	27	0	-33.327	19.103			4.18	0.162	1.058
240	ISC0060	1974	10	11	12	3	42.03	-30.667	23.883	10	F	4.62	0.163	1.059
241	CGS0220	1974	12	19	9	17	54.1	-33.294	19.25	5	F	3.38	0.229	1.119
242	CGS0221	1974	12	23	17	23	3.2	-33.386	18.843	5	F	3.54	0.229	1.119

243	TNS0178	1975	1	5	17	48	0	-32.37	23.343			3.46	0.229	1.119
245	ISC0062	1975	6	8	18	32	50.71	-29.452	25.156	8	F	4.32	0.162	1.058
247	ISC0063	1976	7	1	11	24	3.3	-29.596	24.994	11.9		5.7	0.149	1.049
273	CGS0249	1977	1	25	23	1	22.2	-28	16.9	10	F	4.08	0.229	1.12
274	ISC0071	1977	3	2	4	54	58.98	-32.658	19.251	10	F	5.09	0.164	1.06
288	ISC0072	1977	5	24	7	47	1	-31	26	0		3.71	0.229	1.119
289	ISC0073	1977	6	7	20	19	31.12	-33.259	19.357	10	F	5.04	0.164	1.059
290	CGS0265	1977	6	7	20	20	48.2	-29.7	24.4	10	F	4.17	0.23	1.12
313	ISC0076	1978	6	2	11	16	44.55	-29.494	25.147	8	F	3.56	0.162	1.058
324	ISC0077	1979	2	21	10	58	58.58	-29.418	21.121	10	F	4.52	0.163	1.058
327	ISC0080	1979	8	4	9	31	10.93	-29.571	20.948	10	F	3.86	0.162	1.058
329	ISC0082	1979	8	11	3	59	56.37	-29.238	20.61	10	F	3.4	0.162	1.058
330	ISC0083	1979	8	17	1	9	39.45	-29.262	20.065	10	F	3.86	0.162	1.058
333	ISC0085	1980	8	1	10	16	42.5	-30.14	19.6	10		3.54	0.229	1.119
334	ANS0005	1980	8	28	14	37	51.3	-30.697	24.399	33		4.94	0.263	1.16
336	CGS0309	1981	3	20	22	46	18.4	-30.72	21.95	10	F	3.38	0.229	1.119
337	GSO0001	1981	8	24	1	27	0.1	-33.305	18.994	15	F	4.32	0.162	1.058
350	GSO0006	1983	2	24	6	46	51.4	-32.467	19.342	10	F	4.27	0.23	1.12
352	ISC0094	1983	7	31	0	35	35.78	-31.115	23.911	10	F	3.54	0.229	1.119
355	ISC0095	1983	9	5	0	33	32.05	-29.355	25.056	8	F	4.27	0.23	1.12
360	ISC0099	1985	4	30	19	6	20.09	-29.298	19.906	10	F	3.89	0.229	1.119
361	ISC0100	1985	5	8	11	35	43.84	-29.285	24.832	7	F	4.87	0.231	1.122
365	ISC0103	1985	8	26	12	31	50.9	-29.249	20.051	10.4		4.27	0.23	1.12
366	ISC0104	1985	11	21	0	56	10.08	-29.364	23.993	10	F	3.63	0.229	1.119
369	ISC0106	1986	3	23	5	3	49.28	-29.334	24.672	8	F	3.46	0.229	1.119
373	ISC0107	1986	9	13	11	5	54.77	-30.773	23.922	10	F	3.54	0.229	1.119
375	ISC0108	1987	2	14	6	21	33.04	-29.493	24.744	8	F	3.86	0.162	1.058
382	ISC0112	1987	4	27	6	52	55.41	-29.811	19.79	10	F	4.27	0.23	1.12
392	CGS0364	1987	8	26	6	31	29	-29.48	25.04	5	F	3.3	0.229	1.119
394	GSO0009	1987	9	26	17	5	43.1	-30.168	18.472	10	F	3.31	0.162	1.058
404	ISC0117	1987	11	15	13	58	18.16	-29.486	25.135	8	F	4.5	0.133	1.039
405	ISC0118	1987	12	11	1	49	23.5	-29.5	19.79	10		3.47	0.162	1.058
413	CGS0383	1988	8	5	5	0	58.7	-29.46	19.96	10	F	3.55	0.162	1.058
425	CGS0395	1989	11	6	4	59	35.8	-29.23	25.32	10	F	3.8	0.229	1.119
428	ISC0122	1990	7	29	0	58	33	-28.7	24.8	0		3.38	0.229	1.119
440	CGS0405	1991	6	18	17	11	59.39	-29.785	22.406	10	F	3.51	0.132	1.038
442	CGS0407	1991	8	11	22	12	15.19	-30.668	19.048	10	F	3.73	0.132	1.038
443	CGS0408	1991	8	17	23	41	12.69	-29.396	22.119	10	F	3.43	0.162	1.058
446	GSO0011	1991	10	31	13	36	29.1	-33.255	19.31	5	F	4.06	0.14	1.043
449	CGS0414	1992	2	16	2	28	32.69	-28.051	17.092	10	F	3.46	0.229	1.119
453	CGS0418	1992	8	27	4	12	17.99	-31.533	22.798	38.8		3.54	0.229	1.119
454	CGS0419	1992	9	3	10	42	43.09	-28.461	25.123	199.7		3.38	0.229	1.119
455	CGS0420	1992	9	8	19	25	12.09	-32.651	18.056	0		3.63	0.229	1.119
457	CGS0422	1992	11	2	10	55	17.09	-31.576	23.059	10	F	3.31	0.162	1.058
458	ISC0133	1992	11	19	8	32	10.29	-30.346	24.959	10	F	3.73	0.115	1.029
460	ISC0134	1993	3	11	20	5	51.61	-29.195	18.805	10	F	4.74	0.133	1.039
462	PRE0008	1993	4	29	2	39	4.8	-34.356	18.292	5	F	3.36	0.14	1.043
463	ISC0135	1993	6	3	4	45	13	-29.395	17.897	10	F	3.82	0.132	1.038
470	ISC0136	1993	11	20	9	20	52.3	-29.68	19.42	10		3.3	0.229	1.119
475	CGS0432	1994	3	22	18	44	27.49	-29.488	25.116	10	F	3.43	0.162	1.058
484	CGS0435	1994	11	6	23	1	10.79	-29.379	18.743	0.1		3.46	0.229	1.119
485	ISC0139	1994	12	31	22	9	56.46	-30.379	20.867	10	F	4.54	0.133	1.039
487	CGS0437	1995	1	17	22	19	40.39	-29.432	19.245	41.3		3.38	0.229	1.119
488	ISC0140	1995	2	27	8	15	4.3	-29.58	18.51	10		3.82	0.132	1.038
492	CGS0441	1995	9	29	14	26	5.19	-28.573	24.611	237.4		4.08	0.229	1.12
493	CGS0442	1995	11	25	4	5	48.89	-30.629	21.761	2	F	5.31	0.234	1.124
495	CGS0444	1996	2	4	20	52	35.9	-32.635	20.585	5	F	3.51	0.162	1.058
496	CGS0445	1996	4	26	9	31	26.7	-29.31	19.607	10	F	3.6	0.162	1.058
499	CGS0447	1996	9	15	20	37	4.5	-30.09	19.599	10	F	4.51	0.133	1.039
516	CGS0452	1998	4	24	11	44	14.19	-28.306	20.471	5	F	3.73	0.162	1.058
517	CGS0453	1998	5	9	11	57	0.59	-30.288	24.248	2	F	3.3	0.229	1.119
533	GSO0013	1998	10	5	22	40	16.6	-31.641	21.987	5	F	3.4	0.162	1.058
538	CGS0462	1999	2	4	2	2	11.69	-30.134	24.919	5	F	3.76	0.14	1.043
542	ISC0152	1999	7	3	20	53	1.32	-29.39	24.611	7	F	3.83	0.132	1.038
550	TNS0283	2000	8	27	19	34	0	-28.874	19.737			3.63	0.229	1.119
561	ISC0158	2001	1	8	19	3	17	-29.967	25.418	2	F	3.63	0.229	1.119
562	CGS0487	2001	3	24	20	40	40.1	-29.868	18.516	5	F	4	0.162	1.058
563	CGS0488	2001	4	6	19	42	43	-29.689	19.623	5	F	3.94	0.133	1.039
564	CGS0489	2001	4	6	20	58	56.2	-28.405	19.965	5	F	4.13	0.162	1.058
567	CGS0491	2001	9	1	22	5	57.1	-33.556	24.409	5	F	3.35	0.162	1.058
569	CGS0493	2001	10	28	22	48	30.8	-33.706	22.465	5	F	3.91	0.162	1.058
571	ANS0017	2002	1	8	5	32	19.33	-29.268	24.112	5		4.24	0.133	1.038

572	ISC0167	2002	2	14	23	59	47.7	-29.203	18.538	5	F	3.86	0.162	1.058
580	CGS0495	2002	10	5	7	26	57	-34.278	22.338	5	F	3.82	0.162	1.058
601	ISC0193	2003	5	12	13	10	0.9	-29.379	25.729	5	F	3.3	0.229	1.119
616	CGS0502	2003	9	3	7	36	12.5	-33.352	24.191	5	F	3.31	0.162	1.058
738	ISC0315	2004	10	10	5	30	42.8	-32.712	18.187	5	F	3.38	0.229	1.119
793	CGS0535	2004	11	30	5	57	51.3	-29.476	25.125	5	F	4.18	0.162	1.058
945	CGS0607	2007	8	20	19	17	43.1	-30.389	24.652	5	F	3.36	0.162	1.058
951	CGS0611	2007	9	17	20	3	33.7	-29.928	18.781	5	F	3.44	0.162	1.058
962	CGS0618	2007	11	3	9	3	53.6	-32.793	22.023	5	F	3.91	0.162	1.058
1024	CGS0662	2009	1	28	4	27	15.4	-28.582	18.591	10	F	3.65	0.162	1.058
1040	CGS0671	2009	7	13	12	53	1	-29.496	19.806	5	F	3.73	0.162	1.058
1054	CGS0683	2009	10	16	18	35	48.8	-31.297	20.671	5	F	3.52	0.162	1.058
1064	CGS0691	2009	12	8	23	21	39.5	-32.788	22.135	5	F	3.87	0.162	1.058
1085	CGS0709	2010	6	24	10	6	26.7	-28.721	20.805	5	F	3.52	0.162	1.058
1097	CGS0719	2010	7	26	14	24	19.2	-28.79	20.407	5	F	3.64	0.162	1.058
1179	CGS0787	2011	1	12	6	14	21	-28.69	20.348	5	F	4.41	0.133	1.039
1339	CGS0921	2011	4	6	23	34	52.8	-28.747	20.46	5	F	3.8	0.132	1.038
1356	CGS0936	2011	5	4	9	59	1.2	-28.461	20.386	5	F	3.35	0.162	1.058
1358	CGS0938	2011	5	4	12	44	8.5	-28.243	16.474	5	F	3.31	0.162	1.058
1371	CGS0950	2011	5	14	14	10	41.7	-32.78	22.139	5	F	4.12	0.133	1.038
1372	CGS0951	2011	5	14	16	26	12.7	-28.756	20.493	5	F	3.82	0.162	1.058
1404	CGS0975	2011	6	22	21	2	50.6	-28.57	20.437	5	F	3.55	0.132	1.038
1407	ISC0916	2011	6	22	21	11	19.7	-29.667	22.798	5	F	3.46	0.229	1.119
1412	CGS0980	2011	6	25	13	38	22.7	-30.167	17.9	5	F	3.77	0.132	1.038
1552	CGS1080	2011	12	18	18	7	5.7	-28.474	20.489	5	F	4.26	0.14	1.043
1578	CGS1102	2012	1	25	0	44	29.9	-31.843	25.647	0		3.38	0.229	1.119
1581	CGS1105	2012	1	25	23	38	56.6	-30.326	19.16	5	F	3.46	0.229	1.119
1616	CGS1139	2012	3	30	20	6	43.7	-33.196	22.032	5	F	3.44	0.144	1.046
1618	CGS1141	2012	3	31	3	13	51.7	-30.082	18.574	5	F	4.08	0.229	1.12
1691	CGS1214	2012	7	30	20	28	23.2	-29.719	25.973	5	F	3.46	0.229	1.119
1943	CGS1462	2015	10	1	20	15	1.3	-29.517	24.697	5	F	3.42	0.144	1.046
1964	GSO0049	2015	12	2	7	14	53.9	-33.221	19.063	9.7		3.6	0.106	1.024
1982	CGS1501	2016	3	10	1	18	20.4	-31.368	21.361	5	F	3.45	0.104	1.023
2052	CGS1571	2016	10	18	6	25	31.6	-33.325	22.361	5	F	3.8	0.076	1.012
2217	CGS1730	2018	2	3	5	45	23	-28.543	20.314	5	F	3.46	0.075	1.012
2251	CGS1764	2018	3	13	9	44	14.3	-28.839	18.897	5	F	3.45	0.04	1.003
2264	CGS1777	2018	4	1	13	25	17.3	-28.642	20.342	5	F	3.45	0.106	1.024
2541	ANS0031	2020	11	16	22	27	3.219	-33.43	17.897	5		3.38	0.229	1.119
2545	ISC1583	2020	12	2	12	42	21.4	-29.751	20.619	38.7		3.38	0.229	1.119
2557	ISC1595	2021	1	13	12	35	48.6	-28.121	17.695	9.1		3.63	0.229	1.119
2566	ISC1604	2021	1	20	10	55	31.7	-28.065	19.797	5		3.3	0.229	1.119
2574	ISC1612	2021	2	16	13	50	11.7	-28.057	19.747	0		3.63	0.229	1.119
2610	CGS2085	2021	7	5	23	39	7.9	-29.755	18.177	5	F	4.09	0.162	1.058

APPENDIX D. FINAL HAZARD INPUT DOCUMENT (HID)

FINAL HAZARD INPUT DOCUMENT (HID)
DUYNEFONTYN SSHAC EL-2 PSHA
14 September 2023

The Hazard Input Document (HID) describes the Seismic Source Model (SSM) and Ground Motion Model (GMM) for the Duynefontyn SSHAC EL-2 PSHA study. The goal of the HID is to provide sufficient information for the hazard analyst to unequivocally implement the SSM and GMM into the hazard code for calculations, by outlining the models developed by the SSM TI Team and GMM TI Team. To avoid making the document unnecessarily bulky, large tables defining model elements are included as appendices (with active links). The SSM is presented in its entirety below, followed by the GMM.

The following document is for the hazard analysis to be performed at two locations, one at the Duynefontyn site (-33.661108, 18.428319) and the other at the Koeberg Power Generation Station (-33.676894, 18.431397).

SEISMIC SOURCE MODEL (SSM)

The SSM developed by the SSM TI Team is presented in the following pages. SSM figures, tables, and attachments are listed below for reference.

List of SSM Figures:

List of SSM Tables:

List of SSM Attachments:

SSM_Source_Points_HID_2023_0726_v1.xlsx
SSM_HID_recurrence_inputs_2023_0801.xlsx
SSM_HID_Mmax_Distributions_2023_0802.zip
Spatial_smoothing_files_HID_2023_0807.zip
SDZ_Strike_Dist.xlsx
SSM_HID_Rupture_Area_Scaling_2023_0807.xlsx

DESCRIPTION OF SEISMIC SOURCES AND APPLICATION INSTRUCTIONS

Two types of seismic sources are identified in the model: seismic source zones and one fault. The names and acronyms for each source are the following:

Seismic Source Zones:

- Saldania (SDZ)
- Orange Basin (OBZ)
- Olifants River (ORZ)
- Agulhas (AGZ)
- Combined Outer Zone (COZ)

Fault Source:

- Groenhof Fault Source (GFS)

Source zone SDZ will be modeled using virtual ruptures. All other source zones ruptures are modeled using point sources. The geographical coordinates for all sources, including the Groenhof Fault Source, are in SSM_Source_Points_HID_2023_0726_v1.xlsx, included as an attachment.

The seismic sources zones are shown on Figure 1. The Saldania Zone is also referred to as the "host zone."

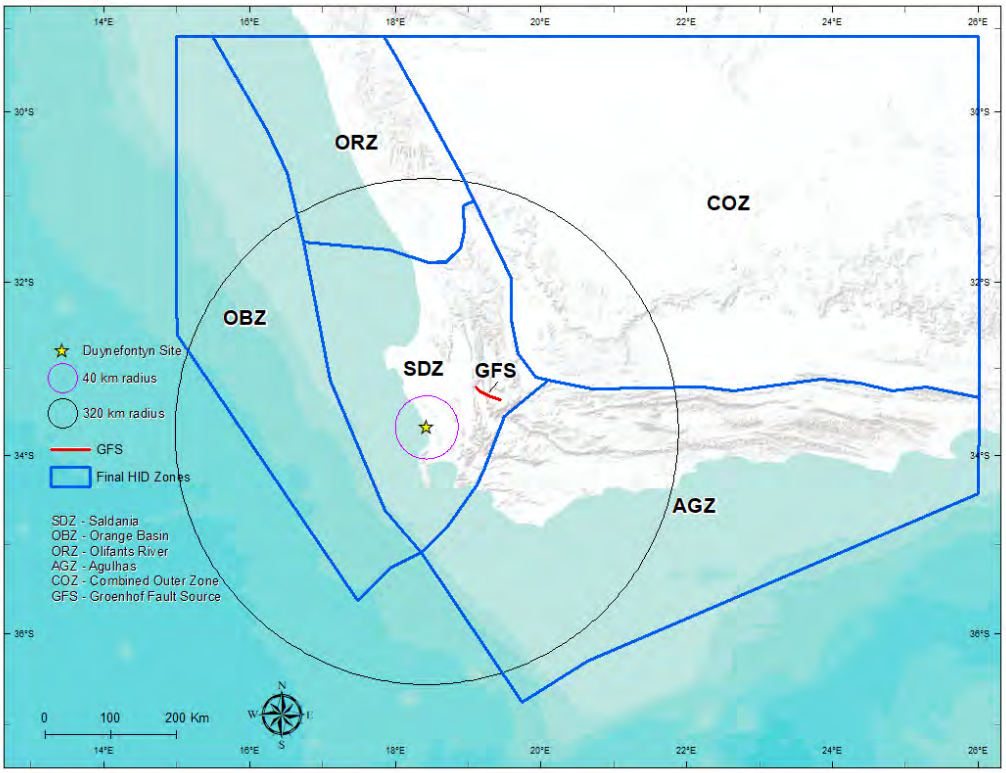

Figure 1. Seismic sources of the SSM

COMMON HAZARD INPUTS FOR ALL SOURCE ZONES

This section includes elements of the SSM model that are common to all seismic source zones.

Seismogenic Thickness

The SSM considers three seismogenic crustal thicknesses of 15 [0.2], 17 [0.6], and 22 [0.2] kilometers. The seismogenic thickness node logic tree is shown in Figure 2.

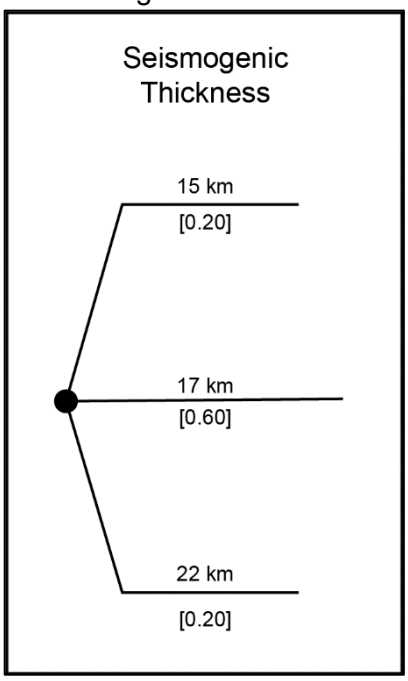

Figure 2. Seismogenic thickness logic tree

Focal Depth Distribution for Future Earthquakes

The focal depth distribution of future earthquakes is given in Table 1, Table 2, and Table 3 as a function of the seismogenic crustal thickness.

Table 1. DNSP focal depth distribution for a seismogenic crustal thickness of 15 km

H_i[1]	PDF[2]	CDF[3]
0.5	0	0
1.5	0.0155	0.0155
2.5	0.0302	0.0457
3.5	0.0487	0.0944
4.5	0.0628	0.1572
5.5	0.0783	0.2355
6.5	0.1030	0.3385
7.5	0.1154	0.4539
8.5	0.1270	0.5809
9.5	0.1062	0.6871
10.5	0.0821	0.7692
11.5	0.0705	0.8396

12.5	0.0605	0.9001
13.5	0.0534	0.9535
14.5	0.0465	1.0000

[1] Depth bin centers (1.0 km wide bins).
[2] Probability density function derived based on renormalized NGA East distribution.
[3] Cumulative density function derived based on PDF.

Table 2. DNSP focal depth distribution for a seismogenic crustal thickness of 17 km

H_i[1]	PDF[2]	CDF[3]
0.5	0	0
1.5	0.0145	0.0145
2.5	0.0283	0.0428
3.5	0.0457	0.0885
4.5	0.0588	0.1473
5.5	0.0733	0.2206
6.5	0.0965	0.3171
7.5	0.1081	0.4252
8.5	0.1190	0.5442
9.5	0.0995	0.6437
10.5	0.0769	0.7206
11.5	0.0660	0.7866
12.5	0.0567	0.8433
13.5	0.0500	0.8933
14.5	0.0435	0.9368
15.5	0.0393	0.9761
16.5	0.0239	1.0000

[1] Depth bin centers (1.0 km wide bins)
[2] Probability density function derived based on renormalized NGA East distribution.
[3] Cumulative density function derived based on PDF.

Table 3. DNSP focal depth distribution for a seismogenic crustal thickness of 22 km

H_i[1]	PDF[2]	CDF[3]
0.5	0	0
1.5	0.0133	0.0133
2.5	0.0258	0.0390
3.5	0.0416	0.0806
4.5	0.0536	0.1342
5.5	0.0668	0.2010
6.5	0.0879	0.2890
7.5	0.0985	0.3875
8.5	0.1084	0.4959
9.5	0.0906	0.5865
10.5	0.0701	0.6566
11.5	0.0601	0.7167

12.5	0.0516	0.7684
13.5	0.0456	0.8140
14.5	0.0397	0.8536
15.5	0.0358	0.8894
16.5	0.0218	0.9112
17.5	0.0204	0.9316
18.5	0.0192	0.9507
19.5	0.0178	0.9685
20.5	0.0164	0.9849
21.5	0.0151	1.0000

[1] Depth bin centers (1.0 km wide bins)
[2] Probability density function derived based on renormalized NGA East distribution.
[3] Cumulative density function derived based on PDF.

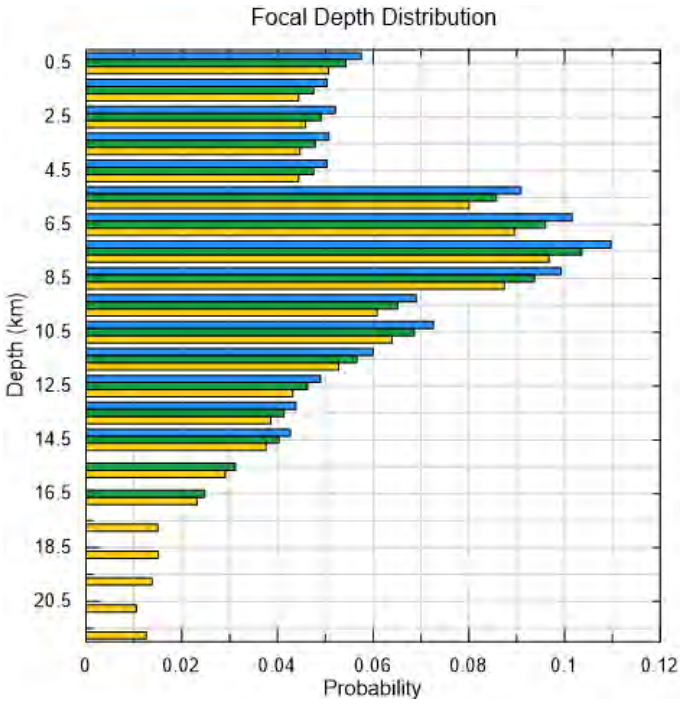

Figure 3. Focal depth distribution

FAULT SOURCE HAZARD INPUTS AND APPLICATION INSTRUCTIONS

The hazard inputs for the Groenhof Fault Source (GFS) are provided in Table 4. Summary of Groenhof Fault source (GFS). Logic trees and application instructions are provided in the following sections.

Mchar Magnitude Scaling

Values for the characteristic magnitude (Mchar) were calculated using the relationship for strike-slip faults developed by Thingbaijam et al. (2017), as provided in Equation 1 and are given in Table 5. Rupture areas are calculated using the seismogenic thickness and characteristic rupture lengths from Table 4. A value of 0.25 magnitude units should be applied on either side of the Mchar value in the application of the recurrence method. The Thingbaijam et al. (2017) equation is given below with appropriate a- and b-values for strike-slip faulting.

$$Log(RA) = a + b * \boldsymbol{M} \qquad \text{Equation 1}$$

Strike-slip faults for source zones (a= -3.486, b= 0.942)

Table 4. Summary of Groenhof Fault source (GFS) hazard inputs

Name	Groenhof Fault Source
Scaling relation for Mchar	Thingbaijam et al. (2017) [1.0]
Seismogenic probability, p[S]	p[S] = 1 [1.0]
Style of faulting	Strike-slip [1.0]
Dip	90 [0.5] 75 [0.5] Simplified dip of 82.5 [1.0] may be used in hazard run.
Dip Direction	N [0.5] S [0.5] Applies only to non-vertical dip
Seismogenic Thickness (km)	15 km [0.2] 17 km [0.6] 22 km [0.2]
Characteristic rupture length (km)	15 [0.2] 20 [0.6] 35 [0.2]
Slip Rate	0.035 mm/yr [0.1] 0.01 mm/yr [0.5] 0.0007 mm/yr [0.4]
Recurrence Approach	Maximum Magnitude Model (Wesnousky, 1986) [1.0]

The SSM TI Team assessment of dip shows that the variable dips have minimal impact on rupture area. Therefore, the SSM TI Team decided to simplify the logic tree for hazard calculations to a single dip of 82.5 (average of 75 and 90).

Table 5. Summary of GSF Mchar distribution

Rupture Length (km)	Length Weight	Seismogenic Thickness (km)	Thickness Weight	Dip[1] (°)	Dip Weight	Mchar Rupture Area (km2)	Mchar	Resultant Mchar Weight
15	0.2	15	0.2	82.5	1	226.9	6.20	0.04
15	0.2	17	0.6	82.5	1	257.2	6.26	0.12
15	0.2	22	0.2	82.5	1	332.9	6.38	0.04
20	0.6	15	0.2	82.5	1	302.6	6.33	0.12
20	0.6	17	0.6	82.5	1	342.9	6.39	0.36
20	0.6	22	0.2	82.5	1	443.8	6.51	0.12
35	0.2	15	0.2	82.5	1	529.3	6.59	0.04
35	0.2	17	0.6	82.5	1	600.1	6.65	0.12
35	0.2	22	0.2	82.5	1	776.6	6.77	0.04
Limited to the average dip for hazard calculation input.								

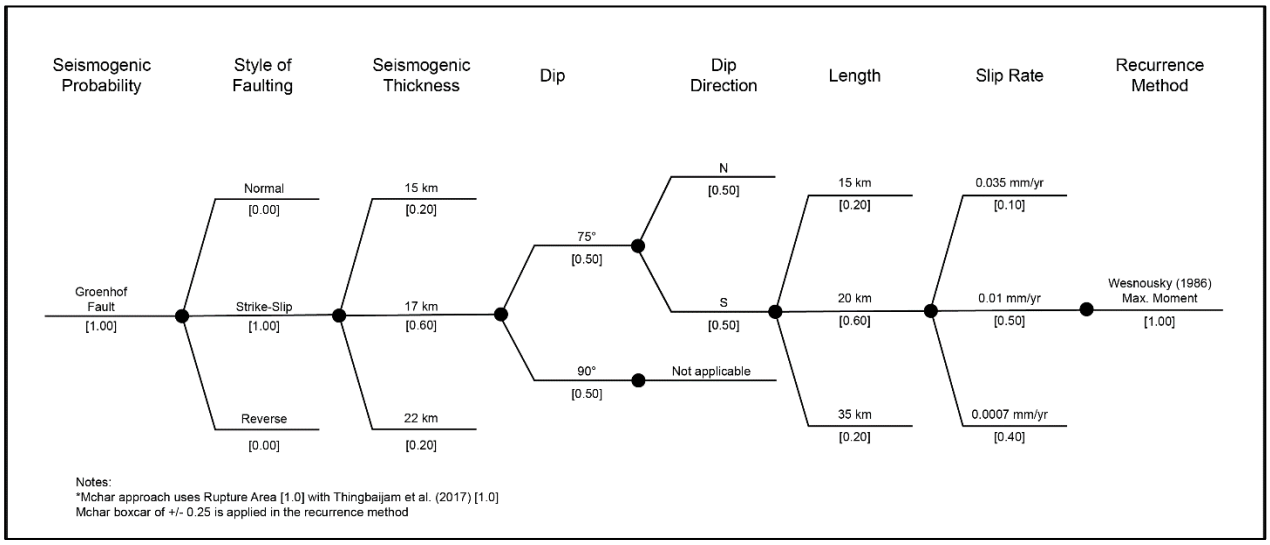

Figure 4. Fault source logic tree. A simplified dip of 82.5 degrees with weight of 1.0 may be used in the hazard calculation.

SOURCE ZONE HAZARD INPUTS

The hazard inputs for all source zones are found in Table 6. Summary of seismic source zone hazard inputs. Logic trees and application instructions are provided in the sections that follow.

Table 6. Summary of seismic source zone hazard inputs

Characteristic	SDZ	ORZ	AGZ	OBZ	COZ
Seismogenic Thickness (km)	15 km [0.2] 17 km [0.6] 22 km [0.2]	15 km [0.2] 17 km [0.6] 22 km [0.2]	15 km [0.2] 17 km [0.6] 22 km [0.2]	15 km [0.2] 17 km [0.6] 22 km [0.2]	15 km [0.2] 17 km [0.6] 22 km [0.2]
Style of Faulting	Normal (20%) Strike slip (80%)	Normal (50%) Strike slip (50%)	Normal (90%) Strike slip (10%)	Normal (100%)	Normal (50%) Strike slip (50%)
Strike Aleatory Distributions	All faults 130º +/- 25º (normal distribution[2]) (s = 6)	Point Source	Point source	Point source	Point source
Dip Aleatory Distributions	**Normal** faults dip to south (100%) Dip values 45º (20%) 65º (60%) 85º (20%) **Strike slip** faults (dip south (50%) or north (50%)) Dip Values 75º (40%) 90º (60%)	**Normal** Dip values 45º (20%) 65º (60%) 85º (20%) **Strike slip** Dip Values 75º (40%) 90º (60%)	**Normal** Dip values 45º (20%) 65º (60%) 85º (20%) **Strike slip** Dip Values 75º (40%) 90º (60%)	**Normal** Dip values 45º (20%) 65º (60%) 85º (20%)	**Normal** Dip values 45º (20%) 65º (60%) 85º (20%) **Strike slip** Dip Values 75º (40%) 90º (60%)
Mmax Bayesian Prior	NMESE [1.0]	NMESE [1.0]	MESE [1.0]	MESE [1.0]	NMESE [1.0]
Max Observed	E[**M**] 6.2 1969-09-29	E[**M**] 5.2 1950-09-30	E[**M**] 4.9 1969-09-11 Or E[**M**] 4.5 1969-10-10	E[**M**] 3.3 2003-04-15	E[**M**] 6.1 1912-02-20

[1] Epistemic weights are given in [brackets].
[2] Normal distribution sampled at 5 degree increments

APPLICATION INSTRUCTIONS FOR SOURCE ZONE HAZARD INPUTS

Zone Condition Alternatives

Numerous earthquake catalogue conditions or calculation methods considered and assessed by the SSM TI Team were selected for implementation as alternatives in the SSM. These conditions are included as alternatives in the SSM, and result in a total of 4 sets of recurrence parameters for each zone – each with three a- and b-value pairs. The branches are identified here to assist with application of branch weights and to note any dependencies for implementation.

Location of 1969/9/11 Event

The 11 September 1969 event occurred in the AGZ zone or SDZ zone. The two locations were considered as alternatives with equal weight by the SSM TI Team. Both alternatives are included in logic tree figures, showing the uncertainty in event location. Based on sensitivity studies, the 11 September 1969 event location may be simplified to a single location. Therefore, a single location within the host zone should be used in the hazard calculation. This simplification of the event location node is reflected in the SSM attachments.

Completeness Catalogue

Two completeness methods are used by the SSM TI Team, resulting in two final catalogues. Equal weight is assigned to each completeness method. A suffix of “cc” or “pd” immediately follows the zone acronym to indicate the completeness catalogue in use.

Regional b-Value Method

Two methods of b-value calculation are used, with equal weight assigned to each method. A prefix of “bp” or “ll” is used to indicate which b-value calculation method is in use.

Spatial Density Model

Two types of spatial density models are considered for the SSM for the application of recurrence: uniform density and spatial smoothing. The figure below illustrates the spatial density logic tree, with the first two branches representing the four earthquake catalogues used as inputs for the spatial density model.

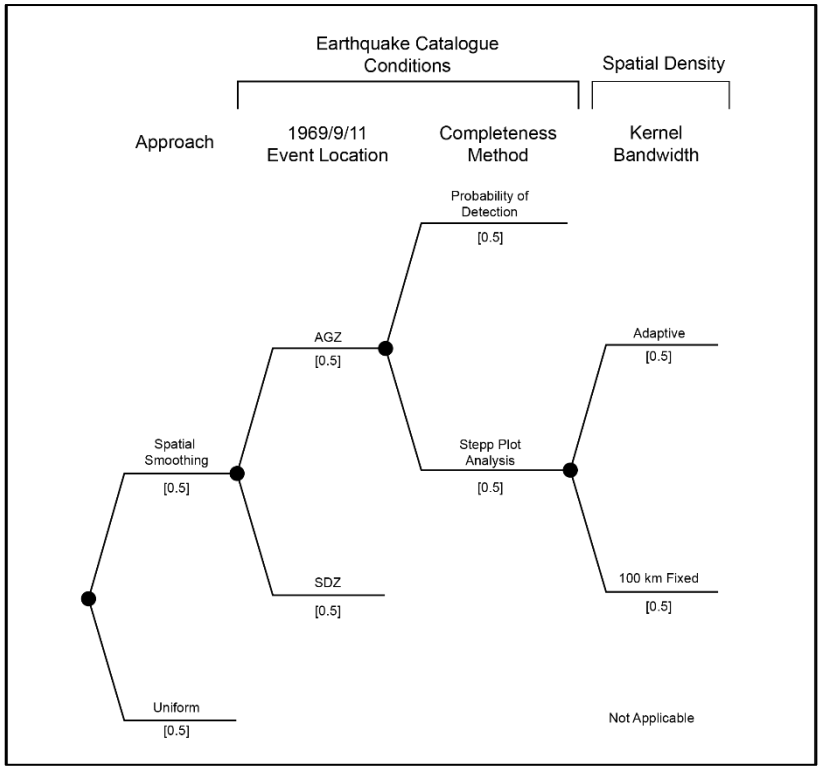

Figure 5. Spatial density logic tree. Note that, based on sensitivity studies, the 1969/9/11 Event Location node should be simplified to a single branch using the location within the host zone (SDZ) with a weight of 1.0.

Uniform Density Model

Uniform density is to be applied to all zone sources.

Spatial Smoothing Model

Two spatial smoothing branches are considered for the SSM: 1) smoothing with an adaptive kernel bandwidth and 2) smoothing with a 100-kilometer fixed kernel bandwidth. Smoothing was conducted for the entire region, then density partitioned within each zone. The project earthquake catalogues are used as inputs for the spatial smoothing process. Conditions included as different alternatives in the earthquake catalogue include the location of the 11 September 1969 event (in AGZ or SDZ), and the method used to evaluate catalogue completeness (probability of detection and Stepp plot analysis). These alternatives result in four different earthquake catalogues as inputs for spatial smoothing.

Spatial smoothing grids are provided for each branch and represent spatial density distributions for smoothed activity rates (a-values) only. The coordinates for spatial smoothing are provided in the file Spatial_smoothing_files_HID_2023_0808r1.zip, included as an attachment. The spatial smoothing coordinates include latitude, longitude, and density value by zone. **Error! Reference source not found.** shows the spatial smoothing logic tree, including branches showing the earthquake catalogue alternatives.

Faulting Mechanism

Faulting mechanism is applied as an aleatory parameter, with source zones containing a combination of strike-slip and/or normal ruptures. The percentage contributions for faulting mechanisms are found in Table 6 and must be applied in both regions where virtual ruptures and point sources are used.

Maximum Earthquake Magnitude

Maximum magnitude (Mmax) distributions are zone specific, calculated following a Bayesian process using the largest observed magnitude within the zone, b-value, and a posterior prior distribution appropriate to the zone crustal type. The two crustal types are Mesozoic extended (MESE) and non-Mesozoic extended (NMESE) crust. An Mmax distribution has been developed for each b-value and ranges up to magnitude 7.8. Consistent with the approach to recurrence values, the ORZ b-values were adopted for zone OBZ to develop maximum magnitude distributions for that zone. Source-specific priors are given in Table 7. Mmax prior weights for areal sources
6, indicating MESE or NMESE crustal type, and the resulting Mmax distributions are given in SSM_HID_Mmax_distributions_2023_0807r1.zip. Each Mmax distribution should be run only for the applicable zone conditions and b-values indicated.

Table 7. Mmax prior weights for areal sources

PRIOR DISTRIBUTIONS	PRIORS	SDZ	ORZ	AGZ	OBZ	COZ
Two Priors: MESE and NMESE	MESE	0	0	1.0	1.0	0
	NMESE	1.0	1.0	0	0	1.0

Recurrence Parameters

Recurrence for all seismic source zones is to be implemented using the doubly-truncated exponential model (Gutenberg and Richter, 1954; Cornell and Van Marke, 1969). Required recurrence parameters for the truncated exponential model include maximum magnitude, a-value, and b-value. Distributions of maximum earthquake magnitude were developed for each source zone, as described above. The a- and b-values are presented below.

The sparsity of events in the earthquake catalogue prevents the development of zone-specific recurrence parameters. Therefore, regional b-values were developed using the project earthquake catalogue falling within the seismic source zones. Two completeness methods were used to evaluate completeness of the project earthquake catalogue: 1) Stepp plot method, and 2) Probability of Detection method. These alternatives for completeness result in two alternative earthquake catalogues to use as inputs for developing recurrence parameters.

The alternative earthquake catalogues were used as inputs for two methods to calculate regional b-values: 1) b-positive (van der Elst, 2021), and 2) log-likelihood (Weichert, 1980). This results in eight mean regional b-values. The mean regional b-values were used as b-priors and fitted to each zone, using events of E[**M**] 3.3 and larger within the given zone to determine fit. The resultant set of four b-values for each zone are hereafter referred to as the zone-applied b-values.

The regional b-value sigma was applied to the mean zone-applied b-values to capture uncertainty in the slope of the rate. The process by while b-prior were applied to the zones produced sigma values of activity rates at E[**M**] 3.3, which was used to capture rate uncertainty. Using the zone-applied a- and b-values and respective sigma values, three recurrence rate curves were developed for each branch of the seismic source zone model: 1) Mean rate, 2) High rate, and 3) Low rate. Each curve is zone-specific and represented by paired a- and b-values.

We note that no events of E[**M**] 3.3 or larger and within the complete earthquake catalogues fall within the OBZ. Therefore, recurrence from the ORZ was adopted directly for the OBZ. The ORZ is the neighboring zone and of comparable size to the OBZ.

The logic tree illustrating recurrence rate development is provided in Figure 5. Zone recurrence logic tree. SSM hazard inputs for activity rates and b-value are provided in SSM_HID_recurrence_inputs_2023_0801r1.xlsx.

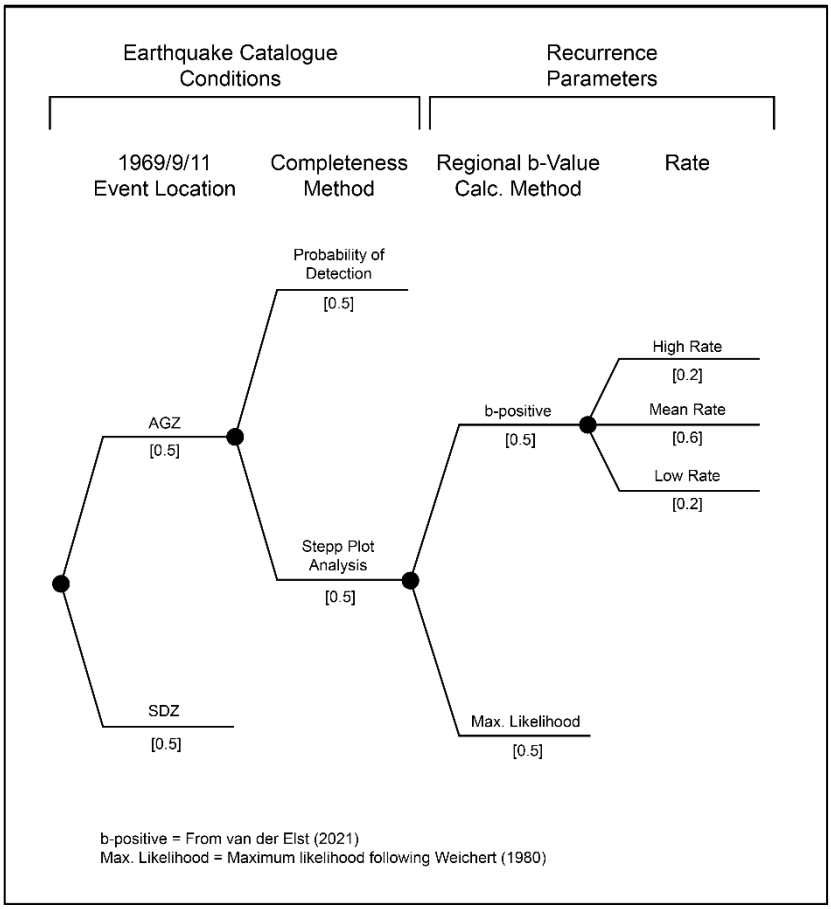

Figure 6. Zone recurrence logic tree. In the hazard calculation, the 1969/9/11 Event Location node should be simplified to a single branch with location in SDZ and weight of 1.0.

Rupture Orientation and Dip

Rupture geometries for virtual ruptures in source zones apply to the SDZ zone. The aleatory strike and dip of these ruptures for the SDZ are shown in Table 6. A distribution for strike was developed and given in SDZ_Strike_Dist.xlsx.

Future earthquake ruptures in zones AGZ, OBZ, ORZ, and COZ are modeled as point sources, given their great distances from the site. In these cases, the event-to-site distances provided to the GMPEs are based on epicentral location rather than shortest path to a rupture plane. Dip values for these sources are shown in Table 4.

Aspect Ratio and Hypocentral Depth Ratio

Rupture aspect ratio (AR) and hypocentral depth ratio (HDR) for virtual ruptures generated for the SDZ should follow the equations from the NGA-East project (Goulet et al., 2018), as provided below. Aspect ratio is equal to length over width, until the seismogenic thickness (width) is saturated and becomes fixed. The hypocenter is placed at the middle (center) of the rupture along strike. The hypocentral depth ratio is the depth of the hypocentre below the top of the rupture plane divided by the total depth extent of the rupture.

The aspect ratio model for normal faulting is provided in Equation 2, with the model for strike-slip faulting provided in Equation 3.

$$\ln(AR) = \max(0, -3.814 + 0.666 * \boldsymbol{M}), \sigma_{\ln(\mathrm{AR})} = 0.285 \quad \text{Equation 2}$$

$$\ln(AR) = \max(0, -4.254 + 0.785 * \boldsymbol{M}), \sigma_{\ln(\mathrm{AR})} = 0.395 \quad \text{Equation 3}$$

The aspect ratio model is used only in the "RA, AR" branch of the logic tree shown in Figure 7.

The equation for HDR is provided below in Equation 4.

$$HDR = \frac{(Z_{Hypocenter} - Z_{TOR})}{(Z_{BOR} - Z_{TOR})} \quad \text{Equation 4}$$

Where the Z terms are depth terms for hypocentral depth, top of rupture (TOR), and base of rupture (BOR).

In conjunction with Equation 4, the distribution in Table 8 (originally Table 13-8 in Goulet et al. (2018) will be used to define the HDR cumulative distribution for normal and strike-slip faulting.

Table 8. Hypocentral depth ratio distribution as defined in Goulet et al. (2018)

HDR	Normal	Strike-Slip
0	0	0
0.1	0	0.025
0.2	0	0.05
0.3	0	0.09
0.4	0	0.15
0.5	0	0.24
0.6	0.05	0.35
0.7	0.1	0.53
0.8	0.25	0.72
0.9	0.5	0.86
1.0	1	1

Rupture Dimensions

Rupture dimensions are developed for virtual ruptures within the SDZ for each magnitude used in the hazard integration. Two alternative methods are used to obtain rupture dimensions. The first method consists in the direct application of Stafford (2014) equations for rupture area (RA) and rupture width (RW). When this approach is followed, there is no aspect ratio model because the method requires the use of seismogenic thickness and dip of rupture and is already accounting for the aspect ratio. The model is implemented using the following equations:

$$ln(RW) = \beta_0 + \beta_1 M_w \quad \text{Equation 5}$$

$$ln(RA) = \begin{cases} \gamma_0 + ln(10)M_w & for\ M_w \leq M_{w,crit} \\ \gamma_0 + ln(10)M_w - \frac{ln(10)}{4}(M_w - M_{w.crit}) & for\ M_w > M_{w,crit} \end{cases} \quad \text{Equation 6}$$

$$M_{w,crit} = \frac{ln(RW_{max}) - \beta_0}{\beta_1}$$ Equation 7

RW_{max} in Equation 7 is the seismogenic thickness divided by sin(dip). Rupture length is calculated as the ratio of RA and RW. RW should be extended until meeting RW_{max} where the seismogenic thickness is saturated.

Table 9 presents the coefficients to use for Equations 5 through 7 for normal and strike-slip style of faulting.

Table 9. Coefficients of Equations 5 through 7 (Stafford, 2014)

Style-of-Faulting	β_0	β_1	γ_0
Strike-slip	-2.3000	0.7167	-9.3137
Normal	-4.1055	1.0370	-9.2483

The second approach is to obtain RA using a weighted average of relationships for rupture area derived from magnitudes 4.5 to 7.8 for normal and strike-slip faulting. Relationships from four publications were used: 1) Thingbaijam et al. (2017), 2) Wells and Coppersmith (1994), 3) Hanks and Bakun (2002), and 4) Leonard (2014). The relationship weights differ by magnitude based on applicability limits specified by the authors.

An uncertainty value of 0.35 was multiplied by the weighted average at each magnitude to develop uncertainty bounds, resulting in three branches to be used for rupture area – magnitude relationships: 1) weighted average [weight = 0.6], 2) weighted average plus uncertainty [weight = 0.2], and 3) weighted average minus uncertainty [weight = 0.2].

Tables of values of rupture area per magnitude for each of the three branches, for normal and strike-slip faulting, are given in SSM_HID_Rupture_Area_Scaling_2023_0807.xlsx.

When this approach is selected, the rupture width is computed as follows:

$$RW = \min\left(\sqrt{\frac{RA}{AR}}, RW_{max}\right)$$ Equation 8

Where RW_{max} is the seismogenic thickness divided by sin(dip). Rupture length is calculated as the ratio of RA and RW.

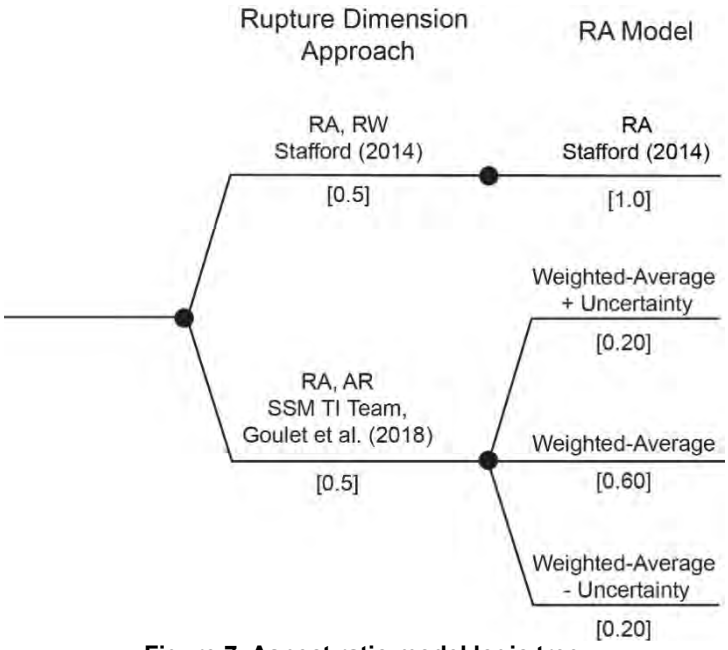

Figure 7. Aspect ratio model logic tree

SSM REFERENCES

Cornell, C.A. and Van Marke, E.H. (1969). The major influences on seismic risk. Proceedings of the Third World Conference on Earthquake Engineering, Santiago, Chile A-1, 69-93.

Gutenberg, B. and Richter, C.F. (1954). Seismicity of the earth and associated phenomena. Second edition. Princeton University Press. Princeton, NJ.

Goulet, C., Bozorgnia, Y., Abrahamson, N., Kuehn, N., Al Atik, L., Youngs, R., Graves, R., and Atkinson, G. (2018). Central and Eastern North America Ground-Motion Characterization, NGA-East Final Report. Pacific Earthquake Engineering Research Center, PEER Report No. 2018/08.

Hanks, T.C. & Bakun, W.H. (2002). A bilinear source-scaling model for M-log A observations of continental earthquakes. Bulletin of the Seismological Society of America 92, 1841-1846.

Leonard, M. (2014). Self-consistent earthquake fault-scaling relations: update and extension to stable continental strike-slip faults. Bulletin of the Seismological Society of America 104(6), 2953-2965.

Stafford, P. (2014). Source-scaling relationships for the simulation of rupture geometry within probabilistic seismic-hazard analysis. Bulletin of the Seismological Society of America, 104(4), 1620-1635.

Thingbaijam, K.K.S., Mai, P.M., and Goda, K., 2017, New empirical earthquake source-scaling laws. Bulletin of the Seismological Society of America, v. 107, pp. 2225-2246.

van der Elst, N.J. (2021). B-positive: A robust estimator of aftershock magnitude distribution in transiently incomplete catalogs. Journal of Geophysical Research: Solid Earth 126(2).

Weichert, D. H. (1980). Estimation of the earthquake recurrence parameters for unequal observation periods for different magnitudes. Bulletin of the Seismological Society of America, 70(4), pp. 1337-1346.

Wells, D.L. & Coppersmith, K.J. (1994). New empirical relationships among magnitude, rupture length, rupture width, rupture area, and surface displacement. Bulletin of the Seismological Society of America 84(4), 974-1002.

Wesnousky, S.G. (1986). Earthquakes, quaternary faults, and seismic hazard in California. Journal of Geophysical Research: Solid Earth 91(B12), 12587-12631.

GROUND MOTION MODEL (GMM)

MEDIAN GROUND MOTION MODEL

Backbone Model

The Ground Motion Model (GMM) is defined as a three-branch meta model that characterizes the best estimate of median ground-motion levels $\widehat{Sa}$ (via the mean logarithmic ground-motion level, $\mu_{\ln Sa}$) for each rupture scenario, rup, of interest along with epistemic uncertainty in the mean logarithmic ground-motion level, $\sigma_{\mu_{\ln Sa}}$.

The three branches of the meta model are then defined via Equation 9:

$$\mu_{\ln Sa}^{(i)} = \mu_{\ln Sa} + \varepsilon^{(i)}\sigma_{\mu_{\ln Sa}} \quad \text{Equation 9}$$

where the nodes, $\varepsilon^{(i)}$, are specified in Table 10 along with the associated weights that are assigned to each branch.

Table 10. Nodes and weights defining the three branches of the meta model for the mean logarithmic ground-motion level (equivalently the median ground-motion level)

Branch	Node	Weight
Upper	+1.28	0.3
Central	0.0	0.4
Lower	-1.28	0.3

Definition of the Central Model, $\mu_{\ln Sa}$

The central model is equivalent to $\mu_{\ln Sa}$ within Equation 10. This model is obtained as the weighted average of seven individual models that each represent an adjusted version of the Chiou and Youngs (2014, CY14) GMM. These different models reflect differences in source and path scaling, as implied by inversions of South African data.

The central model is thus defined via Equation 3.

$$\mu_{\ln Sa} = \sum_j^7 w_j \times \ln Sa_j \quad \text{Equation 10}$$

The first four models, $j \in \{1, \ldots, 4\}$, correspond to the inversions from Peter Stafford, while the final three models, $j \in \{5, \ldots, 7\}$, correspond to the inversions from Ben Edwards. The weights for the individual models are defined in Table 11.

Table 11. Weights for the individual models used within Equation 10.

Model Index j	Underlying Inversion	Weight, w_j	Collective Weight
1	Stafford 1	0.143	0.571
2	Stafford 2	0.143	
3	Stafford 3	0.143	
4	Stafford 4	0.143	
5	Edwards L	0.086	0.429
6	Edwards C	0.256	
7	Edwards U	0.086	

These individual models share many characteristics but have key differences in terms of their path adjustments. Each individual model represents an adjustment to the Chiou and Youngs (2014, CY14) GMM, but the adjustments are made to a version of CY14 that only includes linear site response effects for a reference site condition of $V_{S,30} = 760$ m/s. The specific adjustments that are made relate to stress parameter differences and path scaling differences (incorporating geometric spreading, anelastic attenuation and duration effects).

The overall structure of each individual model is the same and can be represented in pseudo-code as in Listing 1. Within that listing, parameter T is the oscillator period, while rup is not strictly a variable, but rather represents the collection of variables that define a given rupture scenario, such as magnitude, rupture distance, depth to the top of rupture, *etc*.

Listing 1. Overall structure of an individual model for $ln\,Sa_j$ used within Equation 10

```
function south_africa_inversion_model(T, rup)
    # stress drop for this inversion model
    Δσ = stress_parameter_for_inversion_model(rup)
    # linear prediction of lnSa from CY14 with the stress parameter adjustment
    lnSa_cy = chiou_youngs_2014_linear(T, Δσ, rup)
    # distance scaling adjustment (geometric, anelastic and duration effects)
    δlnSaR = distance_adjustment_for_inversion_model(T, rup)
    # source-corrected CY14 prediction and distance adjustment in lnSa space
    lnSa = lnSa_cy + δlnSaR
    # return the actual spectral acceleration level Sa space
    return exp(lnSa)
end
```

The core function within each of the individual models is the Chiou and Youngs (2014) prediction for linear site effects (`chiou_youngs_2014_linear` in Listing 1). This function is mathematically defined in Equation 11, with relevant model coefficients available in Chiou and Youngs (2014). Within Equation 11, the elements that are adjusted from the published version of

Chiou and Youngs (2014) are highlighted in red font. Those changes relate to the enforcement of linear site response for a reference shear-wave velocity of $V_{S,30} = 760$ m/s, and a stress parameter adjustment that is made through the coefficient Δc_M.

$$\begin{aligned}\ln Sa_{CY} = c_1 &+ \left\{c_{1a} + \frac{c_{1c}}{\cosh[2\max(\boldsymbol{M} - 4.5, 0)]}\right\} F_{RV} + \left\{c_{1b} + \frac{c_{1d}}{\cosh[2\max(\boldsymbol{M} - 4.5, 0)]}\right\} F_{NM} \\ &+ \left\{c_7 + \frac{c_{7b}}{\cosh[2\max(\boldsymbol{M} - 4.5, 0)]}\right\} \Delta Z_{TOR} \\ &+ \left\{c_{11} + \frac{c_{11b}}{\cosh[2\max(\boldsymbol{M} - 4.5, 0)]}\right\} (\cos\delta)^2 + c_2(\boldsymbol{M} - 6) \\ &+ \frac{c_2 - c_3}{c_n} \ln\left[1 + e^{c_n(c_M + \Delta c_M - \boldsymbol{M})}\right] - (c_2 - c_3)\Delta c_M \\ &+ c_4 \ln\{R_{RUP} + c_5 \cosh[c_6 \max(\boldsymbol{M} - c_{HM}, 0)]\} + (c_{4a} - c_4) \ln\left(\sqrt{R_{RUP}^2 + c_{RB}^2}\right) \\ &+ \left\{c_{\gamma 1} + \frac{c_{\gamma 2}}{\cosh[\max(\boldsymbol{M} - c_{\gamma 3}, 0)]}\right\} R_{RUP} \\ &+ c_9 F_{HW} \cos\delta \left[c_{9a} + (1 - c_{9a}) \tanh\left(\frac{R_X}{c_{9b}}\right)\right] \left(1 - \frac{\sqrt{R_{JB}^2 - Z_{TOR}^2}}{R_{RUP} + 1}\right) \\ &+ \phi_1 \ln\left(\frac{760}{1130}\right)\end{aligned}$$

Equation 11

Note that other standard requirements regarding the application of the CY14 model remain in place. Specifically, for periods less than or equal to 0.3 seconds, if the spectral acceleration predicted by Equation 11 falls below the corresponding level of peak ground acceleration, then the peak ground acceleration value should be used.

Stress parameter adjustments

The adjustment for stress parameter effects that appears in Equation 4 via Δc_M is defined in two steps. First, we define the change $\Delta c_{M,FS}$ that would theoretically apply in the Fourier spectral domain. This change is found from Equation 12:

$$\Delta c_{M,FS} = \frac{2}{3} \log_{10}\left(\frac{\Delta\sigma_{SA}}{\Delta\sigma_{CY}}\right) \qquad \text{Equation 12}$$

where $\Delta\sigma_{SA}$ is the estimate of target region (South Africa) stress parameter that is consistent with one of the individual models arising from the inversions of South African data, and $\Delta\sigma_{CY}$ is the level of stress parameter implicit within the Chiou and Youngs (2014) GMM. This latter value was found by Stafford *et al*. (2022) to be a function of magnitude according to Equation 13.

$$\ln \Delta\sigma_{CY} = 4.5994 + 0.46241 \min(\boldsymbol{M} - 5.0, 0.0) \qquad \text{Equation 13}$$

The values of $\Delta\sigma_{SA}$ to be used within Equation 5 are defined in Table 12, and the theoretical change to c_M in the Fourier domain is also provided as $\Delta c_{M,FS}$.

Table 12. Values of stress parameter $\Delta\sigma_{SA}$ associated with individual models for use in Equation 12. All of these values are constant when used for magnitudes of 5 and above.

Model Index j	Underlying Inversion	Stress parameter, $\Delta\sigma_{SA}$ (bar)	Parameter change in Fourier domain $\Delta\mathbf{c}_{\mathbf{M,FS}}$
1	Stafford 1	99.4	0.0000
2	Stafford 2	105.1	0.0161
3	Stafford 3	99.4	0.0000
4	Stafford 4	98.7	-0.0020
5	Edwards L	38.7	-0.2731
6	Edwards C	77.4	-0.0724
7	Edwards U	154.8	0.1283

The values in Table 12 relate to the case where magnitudes are at least 5, and, in this case, we just have constant adjustment terms. More generally, the stress parameters in the target region, $\Delta\sigma_{SA}$, are computed as:

$$\Delta\sigma_{SA} = \psi_0 \exp[4.5994 + \psi_1 \min(\boldsymbol{M} - 5.0, 0.0)] \qquad \text{Equation 13a}$$

Table 12a provides the values of ψ_0 and ψ_1 for the seven different models.

Table 12a. Parameters of Equation 13a, used to specify target stress parameter values for the seven individual models. Note that for magnitudes of at least 5, these parameters lead to stress parameter values that match those in Table 12.

Model Index j	Underlying Inversion	Parameter ψ_0	Parameter ψ_1
1	Stafford 1	1.0	0.46241
2	Stafford 2	1.05743	0.46241
3	Stafford 3	1.0	0.25596
4	Stafford 4	0.99283	0.46241
5	Edwards L	0.38930	0.46241
6	Edwards C	0.77860	0.46241
7	Edwards U	1.55719	0.46241

The second step in defining Δc_M for use in Equation 11, is to then adjust the values of $\Delta c_{M,FS}$ for the Fourier domain (in Table 12) to their corresponding values in the response spectral domain. For that process we require the coefficients c_2 and c_3 from CY14 (the same coefficients that are used in Equation 11). Note that the first of these is period independent and equal to $c_2 = 1.06$ while c_3 varies with period as tabulated in Chiou and Youngs (2014).

Using these values of c_2 and c_3, we can then define:

$$\Delta c_M = \chi \times \Delta c_{M,FS} \qquad \text{Equation 14}$$

where χ is found from Equation 8:

$$\chi = \begin{cases} \frac{c_{3,FS} - c_2}{c_3 - c_2} & \text{for } \Delta c_{M,FS} < 0 \\ \frac{c_{3,FS} - c_{2,FS}}{c_3 - c_{2,FS}} & \text{for } \Delta c_{M,FS} \geq 0 \end{cases} \qquad \text{Equation 15}$$

in which $c_{2,FS}$ and $c_{3,FS}$ are the theoretical values of these parameters in the Fourier spectral domain with values equal to $c_{2,FS} = \frac{1}{2}\ln(10) = 1.15$ and $c_{3,FS} = \frac{3}{2}\ln(10) = 3.45$. Again, the values of c_2 and c_3 in Equation 8 are the published values from Chiou and Youngs (2014) that used in Equation 4.

As we are only interested in magnitude of at least 5 for the hazard calculations, the function `stress_parameter_for_inversion_model` in Listing 1 that appears as a function of rupture characteristics is just the lookup table represented in Table 12. That is, for each individual model we simply obtain the relevant constant stress parameter from this table and either compute $\Delta c_{M,FS}$ using Equations 12 and 13, or equivalently just use the pre-computed value of $\Delta c_{M,FS}$ provided in Table 12. The value of Δc_M to be used within Equation 11 (inside the function `chiou_youngs_2014_linear` from Listing 1) is then found from Equations 14 and 15.

Distance-scaling Adjustments

The next key component is the distance scaling adjustments that represent apparent differences in geometric spreading, anelastic attenuation and duration. These adjustments are collectively represented by `distance_adjustment_for_inversion_model` in Listing 1.

Listing 2. Psuedo-code showing structure of function for defining the overall distance-scaling adjustments for individual models. Note that this listing represents a single line within Listing 1.

```
function distance_adjustment_for_inversion_model(T, rup)
    # target FAS parameters from inversion model
    Δσ_t = stress_parameter_for_inversion_model(rup)
    γ1_t = …; Q0_t = …; η_t = …;
    # CY14 optimal host parameters from Stafford et al. (2022)
    Δσ_h = stress_parameter_for_CY14(rup) # HID, Equation 6
    γ1_h = 1.1611
    Q0_h = 205.36
```

```
    η_h = anelastic_exponent_for_CY14(rup) # HID, Equation 9
    # equivalent point-source distance
    sat_exponent = 1
    r_ps = point_source_distance(rup, sat_exponent)
    # excitation duration adjustment
    ΔlnDe = excitation_duration_adjustment(m, r_ps, Δσ_h, Δσ_t)
    # geometric spreading adjustment
    Δlng = geometric_spreading_adjustment(r_ps, rrup, γ1_h, γi_t)
    # anelastic attenuation adjustment
    Δlnq = anelastic_attenuation_adjustment(rrup, Q0_h, η_h, Q0_t, η_t)
    # combined adjustment (geometric, anelastic and duration effects)
    return Δlng + Δlnq + ΔlnDe
end
```

Listing 2 shows the general structure of all `distance_adjustment_for_inversion_model` functions, regardless of the underlying inversion model. Within these functions, the host FAS parameters never change, as these relate to the implied CY14 parameters from the Stafford *et al*. (2022) inversions. The function defining the stress parameter for CY14 was previous defined in Equation 13. The near-field geometric spreading rate and quality factor are specified explicitly in Listing 2, and the remaining FAS parameter requiring definition is the quality exponent, which is defined below in Equation 16 as a function of magnitude.

$$\eta(\boldsymbol{M}) = 0.6882 + 0.13537\tanh(\boldsymbol{M} - 5.1278) \qquad \text{Equation 16}$$

The complete sets of target region FAS parameters that are specified at the start of the distance adjustment functions are provided in Table 13.

Table 13 Target region FAS parameters for all individual models used within the distance_adjustment_for_inversion_model functions of Listings 1 and 2. Under the 'Duration model' column, 'BT15' corresponds to Boore and Thompson (2015), with 'SCR' identifying their path duration model for stable crustal regions. The four geometric spreading rates apply within the intervals defined by the five reference distances, i.e., the first rate of 1.0 applies between reference distances of 1-10km, while the last rate of 0.905 applies from reference distance 150-∞ km.

Model Index j	Underlying Inversion	Stress parameter, $\Delta\sigma_{CY}$ (bar)	Duration model	Reference distances, $R_{ref,i}$	Geometric spreading rates, γ_i	Quality factor, Q_0	Quality exponent, η
1	Stafford 1	99.4	BT15, SCR	--	1.0799	579.34	0.46097
2	Stafford 2	105.1	BT15, SCR	--	1.0	377.34	0.75890
3	Stafford 3	99.4	BT15, SCR	--	1.0	381.02	0.71826

4	Stafford 4	98.7	BT15, SCR	--	1.0843	1,979.64	0.0
5	Edwards L	38.7	Edwards	[1, 10, 60, 150, ∞]	[1.0, 1.06, 0.67, 0.905]	10,413.0	0.0
6	Edwards C	77.4	Edwards	[1, 10, 60, 150, ∞]	[1.0, 1.06, 0.67, 0.905]	10,413.0	0.0
7	Edwards U	154.8	Edwards	[1, 10, 60, 150, ∞]	[1.0, 1.06, 0.67, 0.905]	10,413.0	0.0

Equivalent point-source distances

Listing 2 shows that some adjustments make use of an equivalent point-source distance. This point-source distance is defined using Equation 17, with the saturation length $h(\boldsymbol{M})$ coming either from the Stafford *et al*. (2022) inversions of CY14 or from the finite-fault factor of Boore and Thompson (2015).

$$R_{PS} = [R_{RUP}^{n} + h^{n}(\boldsymbol{M})]^{\frac{1}{n}} \qquad \text{Equation 17}$$

Listing 2 shows that the saturation exponent (`sat_exponent` in Listing 2), which is equivalent to n in Equation 17, is equal to $n = 1$. That example in Listing 2 is always valid for all duration corrections within the individual models. That is, the saturation exponent of $n = 1$ is always used for the duration corrections for models $j \in \{1, \dots, 7\}$, and the Stafford *et al*. (2022) saturation model defined in Equation 18 is also always used for defining the point-source distances within the duration correlations.

$$\ln h(\boldsymbol{M}) = \alpha_h + \beta_h \boldsymbol{M} + \frac{\beta_h - \gamma_h}{\delta_h} \ln\left[1 + e^{-\delta_h(\boldsymbol{M} - \varepsilon_h)}\right] \qquad \text{Equation 18}$$

In Equation 11, the parameters are $\alpha_h = -0.87117$, $\beta_h = 0.44515$, $\gamma_h = 1.1513$, $\delta_h = 5.0948$ and $\varepsilon_h = 7.2725$.

However, the equivalent point-source distance used for the geometric spreading adjustments differ between the individual models corresponding to the Stafford, $j \in \{1, \dots, 4\}$, and Edwards, $j \in \{5, \dots, 7\}$, inversions. Specifically, the saturation length for models $j \in \{1, \dots, 4\}$ is always defined by Equation 11, with the saturation exponent of $n = 1$ being used in Equation 10. In contrast, for models $j \in \{5, \dots, 7\}$, a saturation exponent of $n = 2$ is used in Equation 17, along with the saturation length from Boore and Thompson (2015) reproduced here in Equation 19.

$$\log_{10} h(\boldsymbol{M}) = \begin{cases} \alpha_1 + \beta_1(\boldsymbol{M} - M_{t1}) & \boldsymbol{M} \le M_{t1} \\ \alpha_2 + \beta_2(\boldsymbol{M} - M_{t2}) & \boldsymbol{M} \ge M_{t2} \\ \alpha_1 + \beta_1(\boldsymbol{M} - M_{t1}) + \gamma_1(\boldsymbol{M} - M_{t1})^2 & \text{otherwise} \end{cases} \qquad \text{Equation 19}$$

In Equation 12, the threshold magnitudes are $M_{t1} = 5.744$ and $M_{t2} = 7.744$, and the parameters are $\alpha_1 = 0.7497$, $\beta_1 = 0.43$, $\alpha_2 = 1.4147$, $\beta_2 = 0.235$, $\gamma_1 = -0.04875$.

Table 11 summarises the above text associated with the definitions of the equivalent point-source distances used within the duration adjustments or geometric spreading adjustments.

Table 14. Summary of the model components used to define equivalent point-source distances in different parts of the overall distance adjustment procedure outlined in Listing 2.

Model indices, j	Underlying inversion	Excitation duration		Geometric spreading	
		Saturation length, $h(\boldsymbol{M})$	Saturation exponent, n	Saturation length, $h(\boldsymbol{M})$	Saturation exponent, n
1, 2, 3, 4	Stafford	Eq. 11	1	Eq. 11	1
5, 6, 7	Edwards	Eq. 11	1	Eq. 12	2

Excitation Duration Adjustments

As noted in the previous section, the adjustments for excitation duration make use of the equivalent point-source distance defined using the components of Table 14.

The adjustment for host-to-target differences in the excitation duration, $\Delta \ln D_{ex}$, is defined in two steps. In the first step, a nominal adjustment, $\Delta \ln D_{ex}^{*}$, is identified:

$$\Delta \ln D_{ex}^{*} = \frac{1}{2} \ln \left(\frac{D_{ex,h}}{D_{ex,t}} \right) \quad \text{Equation 20}$$

The second step then imposes the constraint:

$$\Delta \ln D_{ex} = \begin{cases} 0.0 & R_{PS} < 50 \text{ km and } \Delta \ln D_{ex}^{*} > 0 \\ \Delta \ln D_{ex}^{*} & \text{otherwise} \end{cases} \quad \text{Equation 21}$$

Within Equation 20, the excitation durations D_{ex} are always defined using the sum of a source, D_{src}, and path, D_{path}, duration.

$$D_{ex} = D_{src} + D_{path} \quad \text{Equation 22}$$

The source duration is generically defined as:

$$D_{src} = \frac{1}{f_c(\boldsymbol{M};\Delta\sigma)} \quad \text{Equation 23}$$

The corner frequency is generically found from:

$$f_c = (4.9058 \times 10^{6}) \beta_s \left(\frac{\Delta\sigma}{M_0} \right)^{\frac{1}{3}} \quad \text{Equation 24}$$

where $\Delta\sigma$ is defined in units of bars and the seismic moment M_0 takes units of dyne-cm, and comes from:

$$\log_{10} M_0 = \frac{3}{2}\boldsymbol{M} + 16.05 \qquad \text{Equation 25}$$

The host region excitation duration, $D_{ex,h}$ is always defined using the Boore and Thompson (2015) path duration model for active crustal regions (ACR) along with a source duration equal to the reciprocal of the source corner frequency. To define $D_{src,h}$, we have $\Delta\sigma = \Delta\sigma_{CY}$ from Equation 13, and this is used within Equation 24 (and hence Equation 23). The path duration model of Boore and Thompson (2015) is reproduced here in Table 15.

Table 15. Path duration model for active crustal regions from Boore and Thompson (2015). Values of the path duration for distances not defined in the table are found from linear interpolation of both distance and duration. For distances beyond the last tabulated R_{last}, the path duration is defined as: $D_{path} = D_{path}(R_{last}) + 0.156(R_{PS} - R_{last})$.

Point-source distance, R_{PS} [km]	Path duration, D_{path} [s]
0.0	0.0
7.0	2.4
45.0	8.4
125.0	10.9
175.0	17.4
270.0	34.2

For the target region models, the same framework above is used, but for each individual model, the corresponding value of stress parameter from Table 13 is adopted to define the source duration. The path durations are defined differently depending upon the individual model.

For models $j \in \{1, \ldots, 4\}$, the Boore and Thompson (2015) model for stable crustal regions (SCR) is used. This model is reproduced in Table 16.

Table 16. Path duration model for stable crustal regions from Boore and Thompson (2015). Values of the path duration for distances not defined in the table are found from linear interpolation of both distance and duration. For distances beyond the last tabulated R_{last}, the path duration is defined as: $D_{path} = D_{path}(R_{last}) + 0.111(R_{PS} - R_{last})$.

Point-source distance, R_{PS} [km]	Path duration, D_{path} [s]
0.0	0.0
15.0	2.6

35.0	17.5
50.0	25.1
125.0	25.1
200.0	28.5
392.0	46.0
600.0	69.1

For models $j \in \{5, \ldots, 7\}$, the path duration is defined simply as:

$$D_{path} = 0.13R_{PS} \quad \text{Equation 26}$$

Geometric Spreading Adjustments

Differences in geometric spreading are defined as:

$$\Delta \ln g = \ln g_t - \ln g_h \quad \text{Equation 27}$$

The host region geometric spreading function is defined as:

$$\ln g_h = -\gamma_{1,h} \ln R_{PS} + \frac{(\gamma_{1,h} - \gamma_{f,h})}{2} \ln \left(\frac{R_{RUP}^2 + r_t^2}{r_0^2 + r_t^2} \right) \quad \text{Equation 28}$$

with $r_0 = 1$ km, $r_t = 50$ km, $\gamma_{f,h} = 0.5$ and $\gamma_{1,h} = 1.611$.

The target region geometric spreading is defined using a similar function (and identical values of r_0, r_t and γ_f) for the Stafford inversions, models $j \in \{1, \ldots, 4\}$, but using a piecewise segmented function for the Edwards inversions, model $j \in \{5, \ldots, 7\}$.

As models $j \in \{1, \ldots, 4\}$ use the same functional form as in Equation 28 (along with common parameter values), the geometric spreading adjustment for those models is simply:

$$\Delta \ln g = -\Delta\gamma_1 \ln R_{PS} + \frac{\Delta\gamma_1}{2} \ln \left(\frac{R_{RUP}^2 + r_t^2}{r_0^2 + r_t^2} \right) \quad \text{Equation 29}$$

with $\Delta\gamma_1 = \gamma_{1,t} - \gamma_{1,h}$

However, for models $j \in \{5, \ldots, 7\}$, the target-region geometric spreading function is defined as:

$$g_t(R_{PS}) = \begin{cases} \left(\frac{R_{ref,1}}{\max[R_{PS}, R_{ref,1}]} \right)^{\gamma_1} & R_{PS} < R_{ref,2} \\ g(R_{ref,2}) \left(\frac{R_{ref,2}}{R_{PS}} \right)^{\gamma_2} & R_{ref,2} \le R_{PS} \le R_{ref,3} \\ \vdots & \\ g(R_{ref,n}) \left(\frac{R_{ref,n}}{R_{PS}} \right)^{\gamma_n} & R_{PS} \ge R_{ref,n} \end{cases} \quad \text{Equation 30}$$

For models $j \in \{5, \ldots, 7\}$, the relevant reference distances and geometric spreading rates are provided in Table 13.

Anelastic Attenuation Adjustments

The anelastic attenuation adjustment is comprised of two parts: (1) a theoretical approximation and (2) an empirical/data-driven correction. Technically, this second component also absorbs any deviations from theory that arise from the duration and geometric spreading elements. However, it is overwhelmingly related to anelastic attenuation.

For a given oscillator period, T, the corresponding oscillator frequency is first defined as $f_n = 1/T$. An initial adjustment for differences in anelastic attenuation is first made using:

$$\Delta \ln q_0 = -\frac{\pi f_n R_{RUP}}{\beta_s \left(\frac{1}{Q_{0,t} f_n^{\eta_t}} - \frac{1}{Q_{0,h} f_n^{\eta_h}} \right)} \quad \text{Equation 31}$$

with $\beta_s = 3.5$ km/s. Target region values of the quality factor and quality exponent for the individual models are provided in Table 10. The host region quality factor was previously provided in Listing 2 as $Q_{0,h} = 205.36$, while the host region quality exponent is defined by Equation 13.

The complete adjustment for anelastic attenuation effects is then defined as:

$$\Delta \ln q = \Delta \ln q_0 - \delta\gamma_q \times R_{RUP} \quad \text{Equation 32}$$

with $\delta\gamma_q$ defined by a separate function with parameters that differ for each individual model. The function defining $\delta\gamma_q$ depends upon period and magnitude through Equation 33.

$$\delta\gamma_q(T, \boldsymbol{M}) = \beta_M(\boldsymbol{M}) \exp\left[-\beta_5 \ln\left(\frac{T}{0.01}\right)\right] + \beta_6 + \beta_7 \tanh[\beta_8(\boldsymbol{M} - \beta_9)] \quad \text{Equation 33}$$

In Equation 33, the first term $\beta_M(\boldsymbol{M})$ is its own function of magnitude as specified in Equation 34.

$$\beta_M(\boldsymbol{M}) = \beta_1 + \frac{\beta_2}{1 + \exp[-\beta_4(\boldsymbol{M} - \beta_3)]} \quad \text{Equation 34}$$

The parameters for Equations 33 and 34 for each of the seven individual models are provided in Table 17.

Table 17. Model parameters for the anelastic attenuation correction defined through Equations 33 and 34

$\boldsymbol{\beta_i}$	**Individual Model Index, j**						
	$\boldsymbol{j = 1}$	$\boldsymbol{j = 2}$	$\boldsymbol{j = 3}$	$\boldsymbol{j = 4}$	$\boldsymbol{j = 5}$	$\boldsymbol{j = 6}$	$\boldsymbol{j = 7}$

β_1	0.0093246	0.015448	0.015028	-0.017576	-0.0021433	-0.0019286	-0.0016799
β_2	-0.018101	-0.014822	-0.014326	-0.018907	-0.016334	-0.016575	-0.016871
β_3	4.8799	4.9293	4.8938	4.7881	4.7957	4.7912	4.7821
β_4	2.7549	3.1261	3.3810	2.2447	2.4132	2.3907	2.3552
β_5	0.93194	0.9680	0.99014	1.5298	1.8052	1.8109	1.8134
β_6	-0.00017736	-0.002213	-0.0017315	0.00033613	0.00039617	0.00039302	0.00039768
β_7	0.00011394	0.0037614	0.0030441	0.00011596	0.00010975	0.00098946	0.00087575
β_8	0.57743	0.31348	0.3674	3.8524	1.2166	1.2723	1.3640
β_9	3.7991	2.2479	2.5628	2.7907	2.9621	2.9653	2.9647

Overall Distance-scaling Adjustments

The total distance-scaling adjustment ($\delta \ln Sa_R$ from Listing 1) is ultimately defined as:

$$\delta \ln Sa_R = \Delta \ln D_{ex} + \Delta \ln g + \Delta \ln q \qquad \text{Equation 35}$$

Final Individual Model Prediction

The complete prediction for an individual model $\ln Sa_j$ to be used within Equation 10 is finally defined as:

$$\ln Sa_j(T, rup) = \ln Sa_{CY}\left(T, rup; \Delta\sigma_j\right) + \delta \ln Sa_R(T, rup; \Delta\sigma_j, Q_{0,t,j}, \eta_{t,j}) \qquad \text{Equation 36}$$

Epistemic Uncertainty Model, $\sigma_{\mu_{\ln Sa}}$

The epistemic uncertainty in the mean logarithmic ground-motion level is defined in terms of three contributions:

- Model-to-model differences among the seven individual model predictions (σ_{M2M});
- Conditional uncertainty due to near-source saturation effects (σ_{CSAT}); and
- Additional epistemic uncertainty (σ_{ADD}).

These three contributions are combined according to Equation 37:

$$\sigma_{\mu_{\ln Sa}} = \zeta_{COR}\sqrt{\sigma_{M2M}^2 + \sigma_{CSAT}^2 + \sigma_{ADD}^2} \qquad \text{Equation 37}$$

in which ζ_{COR} is a reduction factor to account for the correlation of epistemic uncertainty across rupture scenarios. This reduction factor is a function of period and is defined as:

$$\zeta_{COR} = \begin{cases} 0.95 & T \leq 0.4 \\ 0.95 \exp\left[-0.1 \ln\left(\frac{T}{0.4}\right)\right] & \text{otherwise} \end{cases}$$

The variance arising from model-to-model differences among the seven individual model predictions arising from Equation 36 is defined as the weighted variance in Equation 38. The relevant weights for use in this equation were previously provided in Table 8.

$$\sigma_{M2M}^2 = \sum_j^7 w_j \times \left(\ln Sa_j - \mu_{\ln Sa}\right)^2 \quad \text{Equation 38}$$

The contribution from near-source saturation involves a function of magnitude and distance that is defined through Equations 39 and 40:

$$\sigma_{SAT} = \psi(\boldsymbol{M}) - \frac{\psi(\boldsymbol{M})}{1+\exp\left[-\frac{\ln R_{RUP} - \psi_3}{\psi_4}\right]} \quad \text{Equation 39}$$

and

$$\psi(\boldsymbol{M}) = \psi_1 + \psi_2[\min(\boldsymbol{M}, 7) - 6] \quad \text{Equation 40}$$

The parameters of Equations 39 and 40 are the same for all individual models and are defined as: $\psi_1 = 0.6543$, $\psi_2 = -0.17$, $\psi_3 = 1.246$ and $\psi_4 = 1.388$.

Equation 39 defines the unconditional uncertainty associated with near-source saturation effects. However, that uncertainty is correlated with the model-to-model uncertainty. The conditional uncertainty due to saturation effects is defined by:

$$\sigma_{CSAT} = \sigma_{SAT}\sqrt{1 - \rho_{M2M,SAT}^2} \quad \text{Equation 41}$$

with a correlation value of $\rho_{M2M,SAT} = 0.7$.

Finally, the additional epistemic uncertainty is a constant fixed at $\sigma_{ADD} = 0.1$.

Three-branch Meta Model

The final three-branch meta model is a single logic tree node with three branches is shown in Figure 8.

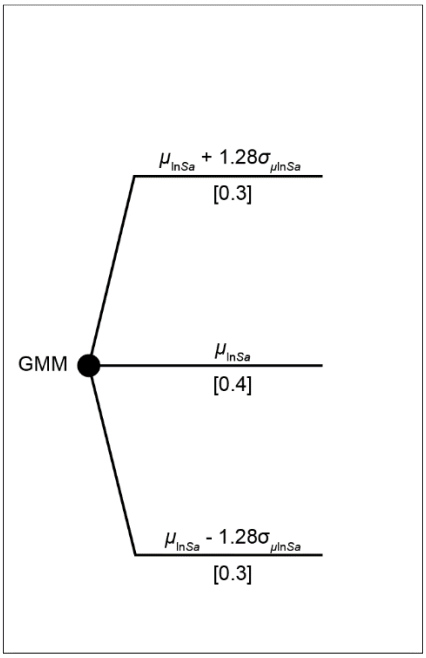

Figure 8. Backbone Model Logic Tree

Site Amplification Model

The site amplification model represents the combined effect of the target at the top of hard rock and site profile alternatives. The overall logic tree described further in the final report, ends in 408 combinations of parameters (i.e., branch). For each branch, there are 60 randomizations of the Vs profile to capture aleatory variability. The final site response model gives six resampled models of site adjustment factors (SAF). For each of these six resampled models, there are two alternatives to incorporate model error: 1) model error as additional uncertainty and 2) model error as minimum epistemic uncertainty (Rodriguez-Marek et al. 2021). Thus, there are 12 total site response models that are given as tables. Weights for these site response models are shown in Figure 9 per Miller & Rice (1983) 6-point discrete distribution. Each SAF is based on a reference (i.e., unmodified CY14) spectral acceleration (Sa,ref), magnitude, and oscillator frequency. The tables of SAFs can be found here by magnitude: *allSAF_alt1.csv* and *allSAF_alt2.csv*.

Interpolation should be logarithmic between Sa,ref values, linear between magnitude, and logarithmic between SAF values. When above and below the magnitude thresholds, the magnitudes should be set to the upper or lower bounds (5.5 and 7.5).

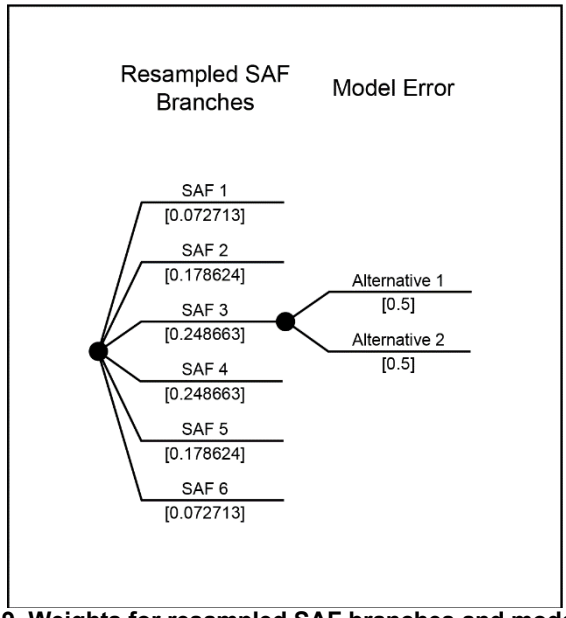

Figure 9. Weights for resampled SAF branches and model error

ALEATORY VARIABILITY MODEL

Al Atik (2015) is used for the aleatory variability model for this project, both for ϕ_{ss} and τ. Each model has a central, high, and low branch representing the median, 95th, and 5th percentile. The single-station intraevent term is represented in Equation 42 and Table 18. The interevent term is represented in Equation 43 and Table 19.

$$\varphi_{ss} = \begin{cases} a \; for \; M \leq 5.0 \\ a + (M - 5.0) * \frac{(b-a)}{1.5} for \; M \leq 6.5 \\ b \; for \; M > 6.5 \end{cases} \quad \text{Equation 42}$$

Table 18 Coefficients for the global ϕ_{ss} model (Originally Table 5.11 in Al Atik 2015)

Period (sec)	Frequency (Hz)	Central		High		Low	
		a	***b***	***a***	***b***	***a***	***b***
0.01	100	0.5423	0.3439	0.6553	0.4446	0.4367	0.2525
0.02	50	0.5410	0.3438	0.6537	0.4452	0.4357	0.2518
0.03	33.33	0.5397	0.3437	0.6521	0.4459	0.4347	0.2510
0.04	25	0.5382	0.3436	0.6503	0.4466	0.4334	0.2503
0.05	20	0.5371	0.3435	0.6489	0.4473	0.4326	0.2496
0.075	13.33	0.5339	0.3433	0.6450	0.4489	0.4301	0.2478
0.1	10	0.5308	0.3431	0.6412	0.4505	0.4277	0.2461
0.15	6.67	0.5247	0.3466	0.6338	0.4561	0.4229	0.2478
0.2	5	0.5189	0.3585	0.6266	0.4673	0.4182	0.2600
0.25	4	0.5132	0.3694	0.6196	0.4776	0.4137	0.2712
0.3	3.33	0.5077	0.3808	0.6129	0.4879	0.4093	0.2831

0.4	2.5	0.4973	0.4004	0.6002	0.5057	0.4010	0.3037
0.5	2	0.4875	0.4109	0.5884	0.5161	0.3932	0.3142
0.75	1.33	0.4658	0.4218	0.5622	0.5264	0.3757	0.3253
1	1	0.4475	0.4201	0.5403	0.5217	0.3607	0.3263
1.5	0.67	0.4188	0.4097	0.5068	0.4985	0.3367	0.3271
2	0.5	0.3984	0.3986	0.4836	0.4818	0.3189	0.3208
3	0.33	0.3733	0.3734	0.4565	0.4556	0.2958	0.2969
4	0.25	0.3604	0.3604	0.4436	0.4437	0.2832	0.2831
5	0.2	0.3538	0.3537	0.4374	0.4381	0.2764	0.2757
7.5	0.13	0.3482	0.3481	0.4325	0.4337	0.2703	0.2691
10	0.1	0.3472	0.3471	0.4317	0.4329	0.2692	0.2679

$$\tau = \begin{cases} \tau_1 \; for \; M \leq 4.5 \\ \tau_1 + (\tau_2 - \tau_1) * \frac{(M-4.5)}{0.5} for \; M \leq 5.0 \\ \tau_2 + (\tau_3 - \tau_2) * \frac{(M-5.0)}{0.5} for \; M \; \leq 5.5 \\ \tau_3 + (\tau_4 - \tau_3) * \frac{(M-5.5)}{1.0} for \; M \leq 6.5 \\ \tau_4 \; for \; M > 6.5 \end{cases}$$ Equation 43

Table 19 Coefficients for tau global model (original 5.15)

		τ_1	τ_2	τ_3	τ_4
Central	*F* 0.1 to 100 Hz	0.4436	0.4169	0.3736	0.3415
Low	*F* 0.1 to 100 Hz	0.3280	0.2928	0.2439	0.2343
High	*F* 0.1 to 100 Hz	0.5706	0.5551	0.5214	0.4618

A mixture model of two equally weighted normal distributions was adopted similar to PNNL 2014, Geopentech 2015, and many other SSHAC projects. These two normal distributions use 0.8 and 1.2ϕ_{ss}

$$P(Z > z) = \; 0.5\left\{1 - \Phi\frac{(z-\mu)}{\sigma_{mix1}}\right\} + 0.5\left\{1 - \Phi\frac{(z-\mu)}{\sigma_{mix2}}\right\}$$ Equation 44

Where,
σ_{mix1} and σ_{mix2} are the standard deviations obtained by using 0.8 and 1.2ϕ_{ss} with the interevent standard deviation, τ.

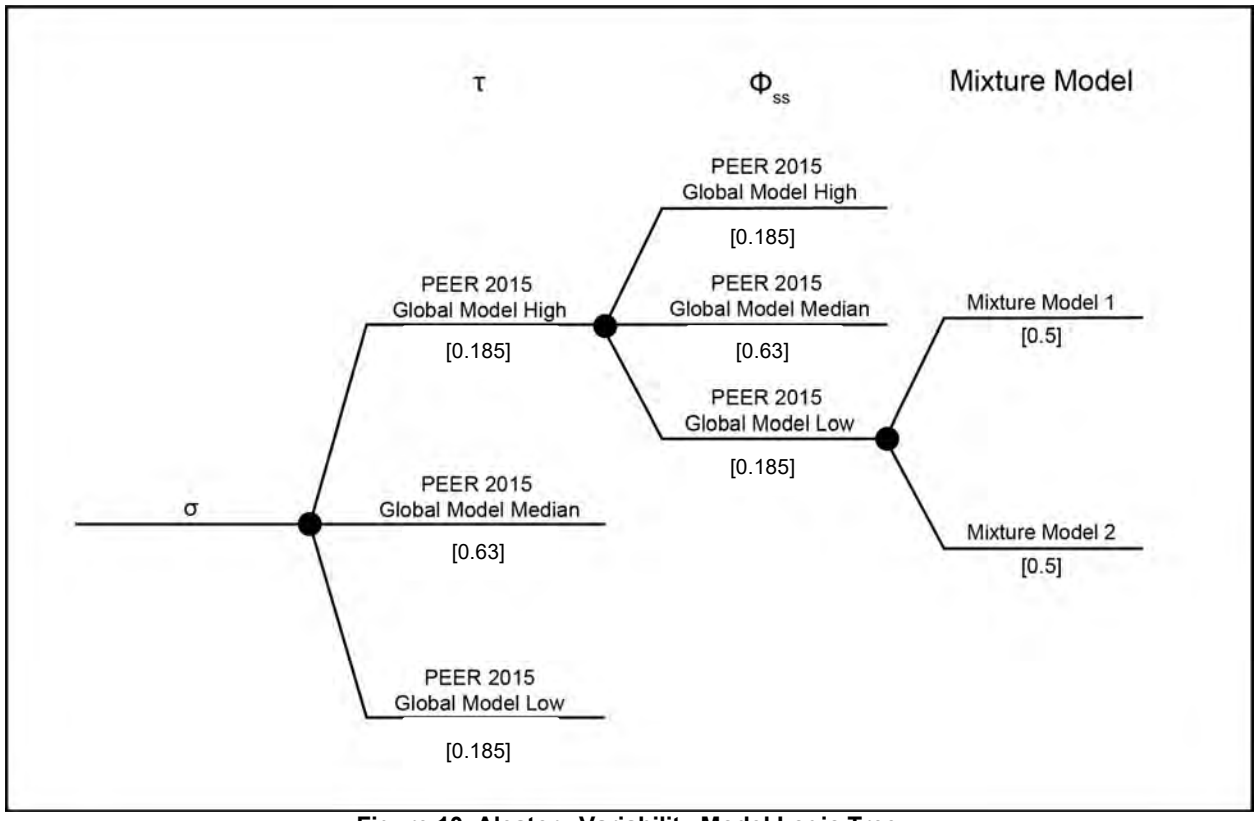

Figure 10. Aleatory Variability Model Logic Tree

References

Al Atik, L. (2015). “NGA-East: Ground motion standard deviation models for Central and Eastern North America.” *PEER Report No. 2015/09,* Pacific Earthquake Engineering Research Center, University of California, Berkeley, CA.

Boore, D. and EM, Thompson (2015). Revisions to come parameters used in stochastic-method simulations of ground motion. Bulletin of Seismological Society of America 105(2A): 1029-1041

Chiou, B.S.J., and Youngs, R.R. (2014) “Update of the Chiou and Youngs NGA Model for the Average Horizontal Component of Peak Ground Motion and Response Spectra.” *Earthquake Spectra* 30(3): 1117-1153.

Miller, A., and Rice, T. (1983). “Discrete approximations of probability distributions.” Management Science. 29(3): 352-362.

Rodriguez-Marek, A., Ake, J., Munson, C., Rathje, E., Stovall, S., Weaver, T., Ulmer, K., and Juckett, M. (2021). Documentation report for SSHAC Level 2: Site response. *U.S. Nuclear Regulatory Commission, Office of Nuclear Regulatory Research*. RIL 2021-15. https://www.nrc.gov/docs/ML2132/ML21323A056

Pacific Northwest National Laboratory (PNNL). (2014). Hanford Sitewide Probabilistic Seismic Hazard Analysis: Pacific Northwest National Laboratory Report PNNL-23361, Richland, Washinton

Stafford, P.J., Boore, D.M., Youngs, R.R., and Bommer, J.J. (2022) “Host-region Parameters for an Adjustable Model for Crustal Earthquakes to Facilitate the Implementation of the Backbone Approach to Building Ground-Motion Logic Trees in Probabilistic Seismic Hazard Analysis.” *Earthquake Spectra*, doi: 10.1177/87552930211062331

APPENDIX E. LIST OF SUPPORTING REPORTS AND PRESENTATIONS.

DUYNEFONTYN DATA COLLECTION REPORTS

Syntaxis Investigation (DDC2)

1. Saunders I. (2024). Review and homogenization of an Earthquake Catalogue for the Ceres area. CGS Report 2023-0162 (Rev.0), 60pp.

Palaeoliquefaction Investigation (DDC3)

2. Cawthra, H.C., MacHutchon, M.R. and Van Zyl, W. (2019). Cruise Report: Pinger and Boomer sub-bottom profiling surveys on Rietvlei. CGS Report 2019-0109 (Rev.1), Council for Geoscience, Pretoria, South Africa , 19 pp.

Historical Seimicity Investigation (DDC4)

3. Albini, P. and Flint, N. (2023). Investigating the Earthquake Records from 1620 to 1969 of interest for the Duynefontyn area, South Africa. CGS Report 2022-0127 Rev.0, Council for Geoscience, Pretoria, South Africa, 400 pp.

Marine Terrace Investigation (DDC5)

4. Chirenje, E., Nxantsiya, Z., Sebothoma, S., Sekiba, Sethobya, M and Netsianda, A. (2018). Report on the reconnaissance ground geophysical surveys at Duynefontyn, Western Cape, South Africa. CGS Report 2018-01260 (Rev.0), Council for Geoscience, Pretoria, South Africa, 37 pp.
5. Chirenje, E., Nxantsiya, Z., Sebothoma, S., Sekiba, M., Netsianda, A., Sethobya, M. and Claassen, D. (2019). Report on the seismic refraction and resistivity surveys for marine terrace and bedrock mapping at Duynefontyn, Western Cape, South Africa. CGS Report 2018-0264 (Rev.0), Council for Geoscience, Pretoria, South Africa, 42 pp.
6. Claassen, D., Mthembi, P. and Black, D.E. (2024). Marine Terrace Studies. CGS Report 2022-0140 (Rev.0), Council for Geoscience, Pretoria, South Africa, 148 pp.

Fault Investigations (DDC6 and DDC7)

7. Cawthra, H.C. and Van Zyl, F.W. (2023). Duynefontyn Data Collection for Offshore Faults. CGS Report 2023-0116 (Rev.0), Council for Geoscience, Pretoria, South Africa, 126 pp.
8. Coppersmith, R.; Slack, C.; Moabi, N.; Dhansay, T.; Cawthra, H.; Claassen, D. and Sethobya, M. (2024). Duynefontyn Onshore Fault Mapping Investigation, DDC6. CGS Report 2023-0001. Council for Geoscience, Pretoria, South Africa, Council for Geoscience, Pretoria, South Africa, 67 pp.
9. Mulabisana, T. (2023). Temporary network along the Colenso fault. CGS Report 2023-0082 (rev. 0), Council for Geoscience, Pretoria, South Africa, 16 pp.
10. Bierman, P.R. (2023). Cosmogenic ^{10}Be and ^{26}Al analysis of Western Cape sediment samples, South Africa. Report prepared by Dr Paul Bierman, Geologist and Geochronologist for the Council for Gesocience, 2023/12/22.

Stress Investigation (DDC8)

11. Smart, K.J., Cawood, A.J. and Ferrill, D.A. (2023). Geological Stress Analyses to Support a Probabilistic Seismic Hazard Analysis (PSHA) for a Critical Site in South Africa. SwRI® Project No. 15.27360, 23 pp.

Site Response Investigation (DDC9)

12. Cox, B.R., Abbas, A., Mulabisana, T., Jele, V., Mantsha, R., Sethobya, Sebothoma, S. and Nxantsiya, Z. (2024). Deep shear wave velocity profiling using MASW and MAM Surface Wave Methods,: Duynefontyn site, South Africa. CGS Report 2023-0203 (Rev.0), Council for Geoscience, Pretoria, South Africa, 33 pp.
13. Matamela, J. and Cox, B.R. (2024). PS Logging in support of Probabilistic Seismic Hazard Analyses for Duynefontyn. CGS Report 2023-0185 (Rev.0), Council for Geoscience, Pretoria, South Africa.
14. Mulabisana, T. and Cox, B.R. (2024). Verification and validation of surface wave processing using SWPROCESS. CGS Report 2024-0006, Council for Geoscience, Pretoria, South Africa, 5 pp.

Micro-seismic Monitoring (DDC10)

15. Jele, V., Tabane, L. and Mantsha, R. (2024). Report on the installation of a vertical array at Duynefontyn, Western Cape, Souith Africa. CGS Report 2023-0198 (Rev.0). Council for Geoscience, Pretoria, South Africa.

DUYNEFONTYN BASELINE PSHA REPORTS

1. Manzunzu, B. and Sebothoma, S. (2023). Determination of shear-wave velocity profile at South African Seismic National Seismograph Network stations using multi-channel analysis of surface waves. CGS Report 2022-0001 (Rev. 0), Council for Geoscience, Pretoria, South Africa, 32 pp.
2. Stamatakos, J., Watson-Lamprey, J., Cawthra, H., Claassen, D., Coppersmith, R., Johnson, C. Largent, M., Manzunzu, B., Midzi, V., Mulabisana, T., Murphy, D., Rathje, E., and Wooddell, K. (2022). Baseline PSHA for the Duynefontyn site and the Koeberg nuclear power station. CGS Report 2022-0009 (Rev.1), Council for Geoscience, Pretoria, South Africa, 75 pp.
3. Wooddell, K. and Watson-Lamprey, J. (2022). Validation and Verification for Baseline PSHA inputs for the Duynefontyn Site and Koeberg Nuclear Power Station. CGS Report 2022-0074 (Rev.0), Council for Geoscience, Pretoria, South Africa, 112pp.

SPECIALTY CONTRACTOR REPORTS

1. Barker, O. (2023). KOEBERG – 1976 TO 1978 – Memories, observations and ideas. BANZI GEOTECHNICS cc, Job No: 214-01-2023-Koeberg Consultations CGS, 29 pp.

2. Buthelezi, M. and Nxantsiya, Z. (2023). Magnetotelluric Survey Test for mapping geological layers at the Koeberg Nature Reserve, Cape Town, South Africa. CGS Report 2023-0023 (Rev.1), 29 pp.
3. Chirenje, E. and Sekiba, M. (2022). Report on the ground magnetic surveys conducted across False Bay dolerite dykes, Western Cape, South Africa. CGS Report 2022-0134, (Rev.0), Council for Geoscience, Pretoria, South Africa, 27pp.
4. Cole, J.(2023). 3D Magnetic Modelling of dykes in the area around Duynefontyn. CGS Report 2023-0002 (Rev.0), Council for Geoscience, Pretoria, South Africa, 34pp.
5. De la Torre, C.A. and Bradley, B.A. (2023). 2D Site Response at the Proposed Duynefontyn Nuclear Power Plant Site: The Influence of Steeply Inclined Interbedded Rock Layers. Bradley Seismics, 23 pp.
6. Edwards, B. (2023).Inversion of ground-motion data to determine target source and path parameters for the development of the Ground Motion Model for Duynefontyn, South Africa. Intraseis. Report Number: ISEIS-CGS-001.0, 27 pp.
7. Kijko, A. (2023). Assessment of earthquake recurrence parameters for Duynentein area, Western Cape. University of Pretoria Natural Hazard Centre, 29 pp.
8. Maré, L. (2022a). Acoustic velocity analyses of Tygerberg Formation sediments in support of probabilistic seismic hazard analyses for Duynefontyn. CGS Report 2022-0151 (Rev.2), Council for Geoscience, Pretoria, South Africa, 28 pp.
9. Maré, L. (2022b). Magnetic remanence study of the False Bay dolerite suite in support of geophysical modelling of existing Duynefontyn high resolution aeromagnetic data. CGS Report 2022-0152 (Rev.0), Council for Geoscience, Pretoria, South Africa, 24 pp.
10. Quiros, D. and Sloan, A. (2023). Estimation of kappa values in the coastal plain between Cape Town and Saldanha Bay. University of Cape Town, RFQ SAS060, 72 pp.

DUYNEFONTYN PSHA SUPPORTING REPORTS

1. Largent, M., Williams, T., Yust, M., and Montaldo-Falero, V. (2024). Virtual Rupture Generator Verification and Validation. CGS Report 2023-0201 (Rev.0), Council for Geoscience, Pretoria, South Africa, 28pp.
2. Largent, M. and Williams, T. (2024). Duynefontyn PSHA Verification and Validation Report. CGS Report 2024-0011, Council for Geoscience, Pretoria, South Africa.

PRESENTATIONS

Number	Speaker	Title
DNSP-PST-076	Johann Neveling	Kick-Off Meeting: Welcome
DNSP-PST-077	Johann Neveling & Emmanuel Chirenje	Kick-Off Meeting: Project Overview
DNSP-PST-078	John Stamatakos	Kick-Off Meeting: SSHAC Process
DNSP-PST-079	Julian Bommer	Kick-Off Meeting: PPRP Overview
DNSP-PST-080	John Stamatakos	Kick-Off Meeting: PEP
DNSP-PST-081	Jennie Watson-Lamprey	Kick-Off Meeting: Hazard Calculations
DNSP-PST-082	Annabel Percy-Lancaster	Kick-Off Meeting: QA
DNSP-PST-083	Kwena Komape	Kick-Off Meeting: Nuclear Safety Culture
DNSP-PST-084	Vunganai Midzi	Kick-Off Meeting: Past Koeberg SHAs
DNSP-PST-085	John Stamatakos	Kick-Off Meeting: Summary of Baseline Study
DNSP-PST-086	Neil Foster	Eskom / PSHA integration
DNSP-PST-087	John Stamatakos	Day 1 Recap
DNSP-PST-088	Debbie Claassen & Ryan Coppersmith	Fault Sources
DNSP-PST-089	Vunganai Midzi	Earthquake Catalogue
DNSP-PST-090	Courtney Johnson	Source Zones
DNSP-PST-091	Thifhe Mulabisana & John Stamatakos	Crustal Structure
DNSP-PST-092	John Stamatakos	3D Stress
DNSP-PST-093	Ian Saunders	Syntaxis
DNSP-PST-094	Paola Albini & Nicky Flint	Historical
DNSP-PST-095	Debbie Claassen	Marine Terraces
DNSP-PST-096	Neo Moabi & Taufeeq Dhansay	Fault Studies
DNSP-PST-097	Michael McHutchon	Marine Survey
DNSP-PST-098	Jennie Watson-Lamprey	GMM
DNSP-PST-099	Katie Wooddell	Baseline GM data
DNSP-PST-100	Brassnavy Manzunzu	MASW-Ceres
DNSP-PST-101	Debra Murphy	Site Profile
DNSP-PST-102	Katie Wooddell	GMM Database
DNSP-PST-103	Jennie Watson-Lamprey	Additional data

Number	Speaker	Title
DNSP-PST-104	Brassnavy Manzunzu	MASW-Elim / MAJT
DNSP-PST-105	Ellen Rathje & Brady Cox	Site Characterisation
DNSP-PST-113	Kwena Komape	NGG Safety Culture Committee
DNSP-PST-114	Johann Neveling	Project Overview
DNSP-PST-115	John Stamatakos	Workshop Overview
DNSP-PST-116	John Stamatakos	SSHAC Primer
DNSP-PST-117	Alex Kisters	Geology and structure of Pan-African basement rocks in the Western Cape
DNSP-PST-118	Janine Cole	Geophysical investigations of structures in the western Cape Fold Belt
DNSP-PST-119	Alistair Sloan	Geomorphological and seismological investigations of potential neotectonic faults in South Africa and Namibia
DNSP-PST-120	Marco Andreoli	The neotectonics of South Africa
DNSP-PST-121	Kwena Komape	Behavioural Safety
DNSP-PST-122	Laura Gulia	b-values and feature extraction
DNSP-PST-123	Laura Gulia	Challenges and possible solutions for the host zone
DNSP-PST-124	Ian Saunders	Host zone clusters
DNSP-PST-125	Martin Brandt	The Ceres events: a seismic cluster rather than a classic main shock–aftershock series
DNSP-PST-126	Thomas Weaver	Spatial smoothing options
DNSP-PST-127	Gabriel Toro	Areal sources and spatial smoothing
DNSP-PST-128	Anthony Tankard	Basement-involved structural framework and dynamics in the western Cape
DNSP-PST-129	Kwena Komape	Knowledge & Skills transfer
DNSP-PST-130	Douglas Paton	Can (should?) Thick/Thin skinned tectonics concepts be applied to understanding the Western Cape?
DNSP-PST-131	Martin Brandt	South Africa: a modified stable continental area
DNSP-PST-132	Olga Ktenidou	Considerations relating to the estimation of kappa from seismic data
DNSP-PST-133	Ben Edwards	Site damping (Kappa0) from ambient seismic noise and its potential for application at the Duynefontyn NPP
DNSP-PST-134	Peter Stafford	Inversion of response-spectral ground-motion models to identify host-region Fourier-spectral parameters
DNSP-PST-135	Linda Al Atik	Host-Region Site Characteristics of GMPEs (GMPE Vs Profile Inversion)
DNSP-PST-136	Linda Al Atik	Sigma models

Number	Speaker	Title
DNSP-PST-137	Kwena Komape	Importance of incident reporting
DNSP-PST-138	Ellen Rathje	Host-to-target site response methodologies
DNSP-PST-139	Brady Cox	What we know so far about Vs and its uncertainty ath the Duynefontyn site
DNSP-PST-140	Vunganai Midzi	An overview of SA intensity data
DNSP-PST-141	Norm Abrahamson	Uses of intensity data to constrain GMMs
DNSP-PST-142	Norm Abrahamson	Emperical constraints on Kappa scaling of ground-motion amplitudes
DNSP-PST-143	Kwena Komape	Nuclear Regulators
DNSP-PST-144	Andreas Rietbrock	GM Data Inversion Methodology based on weak motions: Estimates for South Africa
DNSP-PST-145	Peter Stafford	Direct inversion of response-spectral data to identify target-region Fourier-spectral parameters
DNSP-PST-146	Ben Edwards	Inversion of ground motion data for seismological source-, path- and site-effects, with example application to the Groningen Gas Field, Netherlands
DNSP-PST-147	John Stamatakos & Jennie Watson-Lamprey	Wrap Up
DNSP-PST-148	Paola Albini & Nicky Flint	Investigating the Seismicity of the Duynefontyn area from 1620 to 1970
DNSP-PST-159	Ellen Rathje	Site response approaches (working meeting)
DNSP-PST-160	John Stamatakos	WM2 Agenda / Background
DNSP-PST-161	Kristin Ulmer	Discussion: 2D Site Response Analyses
DNSP-PST-162	Micaela Largent	GMPE Vs Profile Inversion
DNSP-PST-163	Peter Stafford	Sensitivty of CY14 inversions to variations in parameter space
DNSP-PST-164	Peter Stafford	Consideration of alternative source modelling assumptions and the implications for interpretations of kappa
DNSP-PST-165	Kristin Ulmer	Site Response Sensitivities
DNSP-PST-166	Ellen Rathje, Brady Cox, Kristin Ulmer	Update on Vs Characterization
DNSP-PST-167	Peter Stafford	Correlation of Epistemic Uncertainty Within Scaled Backbone Models
DNSP-PST-168	Ryan Coppersmith	Onshore Fault Mapping
DNSP-PST-169	Hayley Cawthra	Marine geoscience updates (fault studies offshore)
DNSP-PST-170	Debbie Claassen	Marine Terrace Studies – DDC5 Update
DNSP-PST-171	Kevin Smart	3DStress Overview
DNSP-PST-172	Kevin Smart	Present day stress state estimation for Duynefontyn region
DNSP-PST-173	Adam Cawood	Regional Assessment of Offshore Faults
DNSP-PST-174	Taufeeq Dhansay	Western Cape Fault / Stress Update

DNSP-PST-175	Nicky Flint	Investigating the Earthquake Records from 1620 to 1969 of interest to the Duynefontyn area, South Africa
DNSP-PST-176	Ian Saunders	DDC2: Syntaxis Studies
DNSP-PST-177	Courtney Johnson	Earthquake Catalogue Update
DNSP-PST-178	Hayley Cawthra	Low slip rate strike slip faults in other areas
DNSP-PST-179	Thifhe Mulabisana	Geothermal Gradient
DNSP-PST-180	Thifhe Mulabisana	Ceres Cluster
DNSP-PST-183	Janine Cole	Magnetic modelling of dykes in the area around Duynefontyn
DNSP-PST-188	Neil Foster	Koeberg lessons learned from Fukushima
DNSP-PST-189	John Stamatakos	Overview: a. Objective of Workshop 3; b. SSHAC Process and Workshop Rules; c. Project Schedule
DNSP-PST-190	John Stamatakos	Overview of the SSM
DNSP-PST-191	Vunganai Midzi	Prior PSHA and DSHA results
DNSP-PST-192	John Stamatakos	SEISMOTECTONIC FRAMEWORK: a. Tectonic Models; b. Strain Analysis; c. Geodetic Analyses
DNSP-PST-193	Courtney Johnson, Laura Gulia, Vunganai Midzi	Earthquake Catalogue: a. Data Summary; b. Data Processing; c. Historical Events
DNSP-PST-194	Debbie Claassen	Marine Terrace Studies
DNSP-PST-195	Hayley Cawthra	Offshore Fault Studies
DNSP-PST-196	Ryan Coppersmith	Onshore Fault Studies
DNSP-PST-197	John Stamatakos	Preliminary Hazard Results with a focus on the SSM
DNSP-PST-198	Hayley Cawthra, Ryan Coppersmith, Thifhelimbilu Mulabisana	Source Zones (1): a. Identification of Source Zones and Justification for Source Zone Boundaries; b. Crustal Types and Mmax; c. Seismogenic Thickness
DNSP-PST-199	Courtney Johnson, Laura Gulia, Thifhelimbilu Mulabisana	Source Zones (2): d. Stationarity and Clusters; e. Smoothing; f. Activity Rates and b-Values; g. Source Zone Logic Tree
DNSP-PST-200	Ryan Coppersmith, Debbie Claassen	Fault Sources: a. Fault Sources no Longer in the SSM and Justifications; b. Groenhof Seismicity Corridor and Technical Basis; c. Recurrence and Magnitude Frequency Distribution; d. Logic tree
DNSP-PST-201	John Stamatakos	Summary of the SSM: a. Identification of SSM Elements that Require; Additional Consideration; b. Actions to Finalise SSM
DNSP-PST-199	Courtney Johnson, Laura Gulia, Thifhe Mulabisana	Source Zones (2): d. Stationarity and Clusters; e. Smoothing; f. Activity Rates and b-Values; g. Source Zone Logic Tree
DNSP-PST-200	Ryan Coppersmith, Debbie Claassen	Fault Sources: a. Fault Sources no Longer in the SSM & Justifications; b. Groenhof Seismicity Corridor & Technical Basis; c. Recurrence & Magnitude Frequency Distribution; d. Logic tree

Number	Speaker	Title
DNSP-PST-201	John Stamatakos	Summary of the SSM: a. Identification of SSM Elements that Require; Additional Consideration; b. Actions to Finalise SSM
DNSP-PST-202	John Stamatakos, Ryan Coppersmith, Jennie Watson-Lamprey	SSM-GMM Overlap Issues: a. Duynefontyn Site Geology; b. Virtual Faults; c. Virtual Fault Model
DNSP-PST-203	Jennie Watson-Lamprey	Overview of the GMM (mean and sigma)
DNSP-PST-204	Jennie Watson-Lamprey	GMM Ground Motion Data: a. Inversion Database; b. Kappa0 Database; c. Processing
DNSP-PST-205	Peter Stafford	GMM Inversions: a. Stafford Methodology; b. Edwards Methodology
DNSP-PST-206	Peter Stafford	GMM Inversions: c. GMPE Adjustments
DNSP-PST-207	Jennie Watson-Lamprey	GMM Kappa_0: a. K_disp; b. K_noise; b. K_0 Model
DNSP-PST-208	Ellen Rathje	GMM Site Data and Site Response Logic Tree: a. MASM; b. Down-hole; c. Site Characterisation
DNSP-PST-209	Kristin Ulmer	GMM Site Response Model: a. Site Response Calculations; b. Site Amplification Model; c. 2D Model
DNSP-PST-210	Jennie Watson-Lamprey	Summary of the GMM: a. Identification of GMM Elements that Require Additional Consideration; b. Actions to Finalise GMM
DNSP-PST-211	Kwena Komape	NGG Nuclear Safety Culture
DNSP-PST-212	Courtney Johnson	SSM Source Zone b-values
DNSP-PST-215	Hayley Cawthra	Cenozoic Sites
DNSP-PST-216	Thifhelimbilu Mulabisana	Seismogenic depth stationarity
DNSP-PST-217	Valentina Montaldo	Catalogue DNSP
DNSP-PST-218	Courtney Johnson	Reanalysis historical events
DNSP-PST-219	Courtney Johnson	Catalogue Updates
DNSP-PST-220	Laura Gulia	Mine events
DNSP-PST-221	Courtney Johnson	SSM HID
DNSP-PST-222	Micaela Largent	Al-Atik & Abrahamson recreation
DNSP-PST-223	Brady Cox	What We Know So Far About Vs and its Uncertainty at the Duynefontyn Site
DNSP-PST-224	Ellen Rathje and Kristin Ulmer	Site Response Sensitivities
DNSP-PST-225	Valentina Montaldo	b positive
DNSP-PST-226	Courtney Johnson	b values

APPENDIX F. HAZARD INPUT GMM TABLE

APPENDIX F. HAZARD INPUT – GMM INPUT TABLE

GMM No.	jcalc	GMM Weight	Description
1	550101	0.00037329	Lower GMM Branch, Sigma 1, SAF Model 1
2	550102	0.000917011	Lower GMM Branch, Sigma 1, SAF Model 2
3	550103	0.001276574	Lower GMM Branch, Sigma 1, SAF Model 3
4	550104	0.001276574	Lower GMM Branch, Sigma 1, SAF Model 4
5	550105	0.000917011	Lower GMM Branch, Sigma 1, SAF Model 5
6	550106	0.00037329	Lower GMM Branch, Sigma 1, SAF Model 6
7	550107	0.00037329	Lower GMM Branch, Sigma 1, SAF Model 7
8	550108	0.000917011	Lower GMM Branch, Sigma 1, SAF Model 8
9	550109	0.001276574	Lower GMM Branch, Sigma 1, SAF Model 9
10	550110	0.001276574	Lower GMM Branch, Sigma 1, SAF Model 10
11	550111	0.000917011	Lower GMM Branch, Sigma 1, SAF Model 11
12	550112	0.00037329	Lower GMM Branch, Sigma 1, SAF Model 12
13	550201	0.001271205	Lower GMM Branch, Sigma 2, SAF Model 1
14	550202	0.003122794	Lower GMM Branch, Sigma 2, SAF Model 2
15	550203	0.004347251	Lower GMM Branch, Sigma 2, SAF Model 3
16	550204	0.004347251	Lower GMM Branch, Sigma 2, SAF Model 4
17	550205	0.003122794	Lower GMM Branch, Sigma 2, SAF Model 5
18	550206	0.001271205	Lower GMM Branch, Sigma 2, SAF Model 6
19	550207	0.001271205	Lower GMM Branch, Sigma 2, SAF Model 7
20	550208	0.003122794	Lower GMM Branch, Sigma 2, SAF Model 8
21	550209	0.004347251	Lower GMM Branch, Sigma 2, SAF Model 9
22	550210	0.004347251	Lower GMM Branch, Sigma 2, SAF Model 10
23	550211	0.003122794	Lower GMM Branch, Sigma 2, SAF Model 11
24	550212	0.001271205	Lower GMM Branch, Sigma 2, SAF Model 12
25	550301	0.00037329	Lower GMM Branch, Sigma 3, SAF Model 1
26	550302	0.000917011	Lower GMM Branch, Sigma 3, SAF Model 2
27	550303	0.001276574	Lower GMM Branch, Sigma 3, SAF Model 3
28	550304	0.001276574	Lower GMM Branch, Sigma 3, SAF Model 4
29	550305	0.000917011	Lower GMM Branch, Sigma 3, SAF Model 5
30	550306	0.00037329	Lower GMM Branch, Sigma 3, SAF Model 6
31	550307	0.00037329	Lower GMM Branch, Sigma 3, SAF Model 7
32	550308	0.000917011	Lower GMM Branch, Sigma 3, SAF Model 8
33	550309	0.001276574	Lower GMM Branch, Sigma 3, SAF Model 9
34	550310	0.001276574	Lower GMM Branch, Sigma 3, SAF Model 10
35	550311	0.000917011	Lower GMM Branch, Sigma 3, SAF Model 11
36	550312	0.00037329	Lower GMM Branch, Sigma 3, SAF Model 12
37	550401	0.001271205	Lower GMM Branch, Sigma 4, SAF Model 1
38	550402	0.003122794	Lower GMM Branch, Sigma 4, SAF Model 2
39	550403	0.004347251	Lower GMM Branch, Sigma 4, SAF Model 3
40	550404	0.004347251	Lower GMM Branch, Sigma 4, SAF Model 4

GMM No.	jcalc	GMM Weight	Description
41	550405	0.003122794	Lower GMM Branch, Sigma 4, SAF Model 5
42	550406	0.001271205	Lower GMM Branch, Sigma 4, SAF Model 6
43	550407	0.001271205	Lower GMM Branch, Sigma 4, SAF Model 7
44	550408	0.003122794	Lower GMM Branch, Sigma 4, SAF Model 8
45	550409	0.004347251	Lower GMM Branch, Sigma 4, SAF Model 9
46	550410	0.004347251	Lower GMM Branch, Sigma 4, SAF Model 10
47	550411	0.003122794	Lower GMM Branch, Sigma 4, SAF Model 11
48	550412	0.001271205	Lower GMM Branch, Sigma 4, SAF Model 12
49	550501	0.004328968	Lower GMM Branch, Sigma 5, SAF Model 1
50	550502	0.01063438	Lower GMM Branch, Sigma 5, SAF Model 2
51	550503	0.014804152	Lower GMM Branch, Sigma 5, SAF Model 3
52	550504	0.014804152	Lower GMM Branch, Sigma 5, SAF Model 4
53	550505	0.01063438	Lower GMM Branch, Sigma 5, SAF Model 5
54	550506	0.004328968	Lower GMM Branch, Sigma 5, SAF Model 6
55	550507	0.004328968	Lower GMM Branch, Sigma 5, SAF Model 7
56	550508	0.01063438	Lower GMM Branch, Sigma 5, SAF Model 8
57	550509	0.014804152	Lower GMM Branch, Sigma 5, SAF Model 9
58	550510	0.014804152	Lower GMM Branch, Sigma 5, SAF Model 10
59	550511	0.01063438	Lower GMM Branch, Sigma 5, SAF Model 11
60	550512	0.004328968	Lower GMM Branch, Sigma 5, SAF Model 12
61	550601	0.001271205	Lower GMM Branch, Sigma 6, SAF Model 1
62	550602	0.003122794	Lower GMM Branch, Sigma 6, SAF Model 2
63	550603	0.004347251	Lower GMM Branch, Sigma 6, SAF Model 3
64	550604	0.004347251	Lower GMM Branch, Sigma 6, SAF Model 4
65	550605	0.003122794	Lower GMM Branch, Sigma 6, SAF Model 5
66	550606	0.001271205	Lower GMM Branch, Sigma 6, SAF Model 6
67	550607	0.001271205	Lower GMM Branch, Sigma 6, SAF Model 7
68	550608	0.003122794	Lower GMM Branch, Sigma 6, SAF Model 8
69	550609	0.004347251	Lower GMM Branch, Sigma 6, SAF Model 9
70	550610	0.004347251	Lower GMM Branch, Sigma 6, SAF Model 10
71	550611	0.003122794	Lower GMM Branch, Sigma 6, SAF Model 11
72	550612	0.001271205	Lower GMM Branch, Sigma 6, SAF Model 12
73	550701	0.00037329	Lower GMM Branch, Sigma 7, SAF Model 1
74	550702	0.000917011	Lower GMM Branch, Sigma 7, SAF Model 2
75	550703	0.001276574	Lower GMM Branch, Sigma 7, SAF Model 3
76	550704	0.001276574	Lower GMM Branch, Sigma 7, SAF Model 4
77	550705	0.000917011	Lower GMM Branch, Sigma 7, SAF Model 5
78	550706	0.00037329	Lower GMM Branch, Sigma 7, SAF Model 6
79	550707	0.00037329	Lower GMM Branch, Sigma 7, SAF Model 7
80	550708	0.000917011	Lower GMM Branch, Sigma 7, SAF Model 8
81	550709	0.001276574	Lower GMM Branch, Sigma 7, SAF Model 9
82	550710	0.001276574	Lower GMM Branch, Sigma 7, SAF Model 10

GMM No.	jcalc	GMM Weight	Description
83	550711	0.000917011	Lower GMM Branch, Sigma 7, SAF Model 11
84	550712	0.00037329	Lower GMM Branch, Sigma 7, SAF Model 12
85	550801	0.001271205	Lower GMM Branch, Sigma 8, SAF Model 1
86	550802	0.003122794	Lower GMM Branch, Sigma 8, SAF Model 2
87	550803	0.004347251	Lower GMM Branch, Sigma 8, SAF Model 3
88	550804	0.004347251	Lower GMM Branch, Sigma 8, SAF Model 4
89	550805	0.003122794	Lower GMM Branch, Sigma 8, SAF Model 5
90	550806	0.001271205	Lower GMM Branch, Sigma 8, SAF Model 6
91	550807	0.001271205	Lower GMM Branch, Sigma 8, SAF Model 7
92	550808	0.003122794	Lower GMM Branch, Sigma 8, SAF Model 8
93	550809	0.004347251	Lower GMM Branch, Sigma 8, SAF Model 9
94	550810	0.004347251	Lower GMM Branch, Sigma 8, SAF Model 10
95	550811	0.003122794	Lower GMM Branch, Sigma 8, SAF Model 11
96	550812	0.001271205	Lower GMM Branch, Sigma 8, SAF Model 12
97	550901	0.00037329	Lower GMM Branch, Sigma 9, SAF Model 1
98	550902	0.000917011	Lower GMM Branch, Sigma 9, SAF Model 2
99	550903	0.001276574	Lower GMM Branch, Sigma 9, SAF Model 3
100	550904	0.001276574	Lower GMM Branch, Sigma 9, SAF Model 4
101	550905	0.000917011	Lower GMM Branch, Sigma 9, SAF Model 5
102	550906	0.00037329	Lower GMM Branch, Sigma 9, SAF Model 6
103	550907	0.00037329	Lower GMM Branch, Sigma 9, SAF Model 7
104	550908	0.000917011	Lower GMM Branch, Sigma 9, SAF Model 8
105	550909	0.001276574	Lower GMM Branch, Sigma 9, SAF Model 9
106	550910	0.001276574	Lower GMM Branch, Sigma 9, SAF Model 10
107	550911	0.000917011	Lower GMM Branch, Sigma 9, SAF Model 11
108	550912	0.00037329	Lower GMM Branch, Sigma 9, SAF Model 12
109	560101	0.00049772	Middle GMM Branch, Sigma 1, SAF Model 1
110	560102	0.001222681	Middle GMM Branch, Sigma 1, SAF Model 2
111	560103	0.001702098	Middle GMM Branch, Sigma 1, SAF Model 3
112	560104	0.001702098	Middle GMM Branch, Sigma 1, SAF Model 4
113	560105	0.001222681	Middle GMM Branch, Sigma 1, SAF Model 5
114	560106	0.00049772	Middle GMM Branch, Sigma 1, SAF Model 6
115	560107	0.00049772	Middle GMM Branch, Sigma 1, SAF Model 7
116	560108	0.001222681	Middle GMM Branch, Sigma 1, SAF Model 8
117	560109	0.001702098	Middle GMM Branch, Sigma 1, SAF Model 9
118	560110	0.001702098	Middle GMM Branch, Sigma 1, SAF Model 10
119	560111	0.001222681	Middle GMM Branch, Sigma 1, SAF Model 11
120	560112	0.00049772	Middle GMM Branch, Sigma 1, SAF Model 12
121	560201	0.00169494	Middle GMM Branch, Sigma 2, SAF Model 1
122	560202	0.004163725	Middle GMM Branch, Sigma 2, SAF Model 2
123	560203	0.005796335	Middle GMM Branch, Sigma 2, SAF Model 3
124	560204	0.005796335	Middle GMM Branch, Sigma 2, SAF Model 4

GMM No.	jcalc	GMM Weight	Description
125	560205	0.004163725	Middle GMM Branch, Sigma 2, SAF Model 5
126	560206	0.00169494	Middle GMM Branch, Sigma 2, SAF Model 6
127	560207	0.00169494	Middle GMM Branch, Sigma 2, SAF Model 7
128	560208	0.004163725	Middle GMM Branch, Sigma 2, SAF Model 8
129	560209	0.005796335	Middle GMM Branch, Sigma 2, SAF Model 9
130	560210	0.005796335	Middle GMM Branch, Sigma 2, SAF Model 10
131	560211	0.004163725	Middle GMM Branch, Sigma 2, SAF Model 11
132	560212	0.00169494	Middle GMM Branch, Sigma 2, SAF Model 12
133	560301	0.00049772	Middle GMM Branch, Sigma 3, SAF Model 1
134	560302	0.001222681	Middle GMM Branch, Sigma 3, SAF Model 2
135	560303	0.001702098	Middle GMM Branch, Sigma 3, SAF Model 3
136	560304	0.001702098	Middle GMM Branch, Sigma 3, SAF Model 4
137	560305	0.001222681	Middle GMM Branch, Sigma 3, SAF Model 5
138	560306	0.00049772	Middle GMM Branch, Sigma 3, SAF Model 6
139	560307	0.00049772	Middle GMM Branch, Sigma 3, SAF Model 7
140	560308	0.001222681	Middle GMM Branch, Sigma 3, SAF Model 8
141	560309	0.001702098	Middle GMM Branch, Sigma 3, SAF Model 9
142	560310	0.001702098	Middle GMM Branch, Sigma 3, SAF Model 10
143	560311	0.001222681	Middle GMM Branch, Sigma 3, SAF Model 11
144	560312	0.00049772	Middle GMM Branch, Sigma 3, SAF Model 12
145	560401	0.00169494	Middle GMM Branch, Sigma 4, SAF Model 1
146	560402	0.004163725	Middle GMM Branch, Sigma 4, SAF Model 2
147	560403	0.005796335	Middle GMM Branch, Sigma 4, SAF Model 3
148	560404	0.005796335	Middle GMM Branch, Sigma 4, SAF Model 4
149	560405	0.004163725	Middle GMM Branch, Sigma 4, SAF Model 5
150	560406	0.00169494	Middle GMM Branch, Sigma 4, SAF Model 6
151	560407	0.00169494	Middle GMM Branch, Sigma 4, SAF Model 7
152	560408	0.004163725	Middle GMM Branch, Sigma 4, SAF Model 8
153	560409	0.005796335	Middle GMM Branch, Sigma 4, SAF Model 9
154	560410	0.005796335	Middle GMM Branch, Sigma 4, SAF Model 10
155	560411	0.004163725	Middle GMM Branch, Sigma 4, SAF Model 11
156	560412	0.00169494	Middle GMM Branch, Sigma 4, SAF Model 12
157	560501	0.005771958	Middle GMM Branch, Sigma 5, SAF Model 1
158	560502	0.014179173	Middle GMM Branch, Sigma 5, SAF Model 2
159	560503	0.019738869	Middle GMM Branch, Sigma 5, SAF Model 3
160	560504	0.019738869	Middle GMM Branch, Sigma 5, SAF Model 4
161	560505	0.014179173	Middle GMM Branch, Sigma 5, SAF Model 5
162	560506	0.005771958	Middle GMM Branch, Sigma 5, SAF Model 6
163	560507	0.005771958	Middle GMM Branch, Sigma 5, SAF Model 7
164	560508	0.014179173	Middle GMM Branch, Sigma 5, SAF Model 8
165	560509	0.019738869	Middle GMM Branch, Sigma 5, SAF Model 9
166	560510	0.019738869	Middle GMM Branch, Sigma 5, SAF Model 10

GMM No.	jcalc	GMM Weight	Description
167	560511	0.014179173	Middle GMM Branch, Sigma 5, SAF Model 11
168	560512	0.005771958	Middle GMM Branch, Sigma 5, SAF Model 12
169	560601	0.00169494	Middle GMM Branch, Sigma 6, SAF Model 1
170	560602	0.004163725	Middle GMM Branch, Sigma 6, SAF Model 2
171	560603	0.005796335	Middle GMM Branch, Sigma 6, SAF Model 3
172	560604	0.005796335	Middle GMM Branch, Sigma 6, SAF Model 4
173	560605	0.004163725	Middle GMM Branch, Sigma 6, SAF Model 5
174	560606	0.00169494	Middle GMM Branch, Sigma 6, SAF Model 6
175	560607	0.00169494	Middle GMM Branch, Sigma 6, SAF Model 7
176	560608	0.004163725	Middle GMM Branch, Sigma 6, SAF Model 8
177	560609	0.005796335	Middle GMM Branch, Sigma 6, SAF Model 9
178	560610	0.005796335	Middle GMM Branch, Sigma 6, SAF Model 10
179	560611	0.004163725	Middle GMM Branch, Sigma 6, SAF Model 11
180	560612	0.00169494	Middle GMM Branch, Sigma 6, SAF Model 12
181	560701	0.00049772	Middle GMM Branch, Sigma 7, SAF Model 1
182	560702	0.001222681	Middle GMM Branch, Sigma 7, SAF Model 2
183	560703	0.001702098	Middle GMM Branch, Sigma 7, SAF Model 3
184	560704	0.001702098	Middle GMM Branch, Sigma 7, SAF Model 4
185	560705	0.001222681	Middle GMM Branch, Sigma 7, SAF Model 5
186	560706	0.00049772	Middle GMM Branch, Sigma 7, SAF Model 6
187	560707	0.00049772	Middle GMM Branch, Sigma 7, SAF Model 7
188	560708	0.001222681	Middle GMM Branch, Sigma 7, SAF Model 8
189	560709	0.001702098	Middle GMM Branch, Sigma 7, SAF Model 9
190	560710	0.001702098	Middle GMM Branch, Sigma 7, SAF Model 10
191	560711	0.001222681	Middle GMM Branch, Sigma 7, SAF Model 11
192	560712	0.00049772	Middle GMM Branch, Sigma 7, SAF Model 12
193	560801	0.00169494	Middle GMM Branch, Sigma 8, SAF Model 1
194	560802	0.004163725	Middle GMM Branch, Sigma 8, SAF Model 2
195	560803	0.005796335	Middle GMM Branch, Sigma 8, SAF Model 3
196	560804	0.005796335	Middle GMM Branch, Sigma 8, SAF Model 4
197	560805	0.004163725	Middle GMM Branch, Sigma 8, SAF Model 5
198	560806	0.00169494	Middle GMM Branch, Sigma 8, SAF Model 6
199	560807	0.00169494	Middle GMM Branch, Sigma 8, SAF Model 7
200	560808	0.004163725	Middle GMM Branch, Sigma 8, SAF Model 8
201	560809	0.005796335	Middle GMM Branch, Sigma 8, SAF Model 9
202	560810	0.005796335	Middle GMM Branch, Sigma 8, SAF Model 10
203	560811	0.004163725	Middle GMM Branch, Sigma 8, SAF Model 11
204	560812	0.00169494	Middle GMM Branch, Sigma 8, SAF Model 12
205	560901	0.00049772	Middle GMM Branch, Sigma 9, SAF Model 1
206	560902	0.001222681	Middle GMM Branch, Sigma 9, SAF Model 2
207	560903	0.001702098	Middle GMM Branch, Sigma 9, SAF Model 3
208	560904	0.001702098	Middle GMM Branch, Sigma 9, SAF Model 4

GMM No.	jcalc	GMM Weight	Description
209	560905	0.001222681	Middle GMM Branch, Sigma 9, SAF Model 5
210	560906	0.00049772	Middle GMM Branch, Sigma 9, SAF Model 6
211	560907	0.00049772	Middle GMM Branch, Sigma 9, SAF Model 7
212	560908	0.001222681	Middle GMM Branch, Sigma 9, SAF Model 8
213	560909	0.001702098	Middle GMM Branch, Sigma 9, SAF Model 9
214	560910	0.001702098	Middle GMM Branch, Sigma 9, SAF Model 10
215	560911	0.001222681	Middle GMM Branch, Sigma 9, SAF Model 11
216	560912	0.00049772	Middle GMM Branch, Sigma 9, SAF Model 12
217	570101	0.00037329	Upper GMM Branch, Sigma 1, SAF Model 1
218	570102	0.000917011	Upper GMM Branch, Sigma 1, SAF Model 2
219	570103	0.001276574	Upper GMM Branch, Sigma 1, SAF Model 3
220	570104	0.001276574	Upper GMM Branch, Sigma 1, SAF Model 4
221	570105	0.000917011	Upper GMM Branch, Sigma 1, SAF Model 5
222	570106	0.00037329	Upper GMM Branch, Sigma 1, SAF Model 6
223	570107	0.00037329	Upper GMM Branch, Sigma 1, SAF Model 7
224	570108	0.000917011	Upper GMM Branch, Sigma 1, SAF Model 8
225	570109	0.001276574	Upper GMM Branch, Sigma 1, SAF Model 9
226	570110	0.001276574	Upper GMM Branch, Sigma 1, SAF Model 10
227	570111	0.000917011	Upper GMM Branch, Sigma 1, SAF Model 11
228	570112	0.00037329	Upper GMM Branch, Sigma 1, SAF Model 12
229	570201	0.001271205	Upper GMM Branch, Sigma 2, SAF Model 1
230	570202	0.003122794	Upper GMM Branch, Sigma 2, SAF Model 2
231	570203	0.004347251	Upper GMM Branch, Sigma 2, SAF Model 3
232	570204	0.004347251	Upper GMM Branch, Sigma 2, SAF Model 4
233	570205	0.003122794	Upper GMM Branch, Sigma 2, SAF Model 5
234	570206	0.001271205	Upper GMM Branch, Sigma 2, SAF Model 6
235	570207	0.001271205	Upper GMM Branch, Sigma 2, SAF Model 7
236	570208	0.003122794	Upper GMM Branch, Sigma 2, SAF Model 8
237	570209	0.004347251	Upper GMM Branch, Sigma 2, SAF Model 9
238	570210	0.004347251	Upper GMM Branch, Sigma 2, SAF Model 10
239	570211	0.003122794	Upper GMM Branch, Sigma 2, SAF Model 11
240	570212	0.001271205	Upper GMM Branch, Sigma 2, SAF Model 12
241	570301	0.00037329	Upper GMM Branch, Sigma 3, SAF Model 1
242	570302	0.000917011	Upper GMM Branch, Sigma 3, SAF Model 2
243	570303	0.001276574	Upper GMM Branch, Sigma 3, SAF Model 3
244	570304	0.001276574	Upper GMM Branch, Sigma 3, SAF Model 4
245	570305	0.000917011	Upper GMM Branch, Sigma 3, SAF Model 5
246	570306	0.00037329	Upper GMM Branch, Sigma 3, SAF Model 6
247	570307	0.00037329	Upper GMM Branch, Sigma 3, SAF Model 7
248	570308	0.000917011	Upper GMM Branch, Sigma 3, SAF Model 8
249	570309	0.001276574	Upper GMM Branch, Sigma 3, SAF Model 9
250	570310	0.001276574	Upper GMM Branch, Sigma 3, SAF Model 10

GMM No.	jcalc	GMM Weight	Description
251	570311	0.000917011	Upper GMM Branch, Sigma 3, SAF Model 11
252	570312	0.00037329	Upper GMM Branch, Sigma 3, SAF Model 12
253	570401	0.001271205	Upper GMM Branch, Sigma 4, SAF Model 1
254	570402	0.003122794	Upper GMM Branch, Sigma 4, SAF Model 2
255	570403	0.004347251	Upper GMM Branch, Sigma 4, SAF Model 3
256	570404	0.004347251	Upper GMM Branch, Sigma 4, SAF Model 4
257	570405	0.003122794	Upper GMM Branch, Sigma 4, SAF Model 5
258	570406	0.001271205	Upper GMM Branch, Sigma 4, SAF Model 6
259	570407	0.001271205	Upper GMM Branch, Sigma 4, SAF Model 7
260	570408	0.003122794	Upper GMM Branch, Sigma 4, SAF Model 8
261	570409	0.004347251	Upper GMM Branch, Sigma 4, SAF Model 9
262	570410	0.004347251	Upper GMM Branch, Sigma 4, SAF Model 10
263	570411	0.003122794	Upper GMM Branch, Sigma 4, SAF Model 11
264	570412	0.001271205	Upper GMM Branch, Sigma 4, SAF Model 12
265	570501	0.004328968	Upper GMM Branch, Sigma 5, SAF Model 1
266	570502	0.01063438	Upper GMM Branch, Sigma 5, SAF Model 2
267	570503	0.014804152	Upper GMM Branch, Sigma 5, SAF Model 3
268	570504	0.014804152	Upper GMM Branch, Sigma 5, SAF Model 4
269	570505	0.01063438	Upper GMM Branch, Sigma 5, SAF Model 5
270	570506	0.004328968	Upper GMM Branch, Sigma 5, SAF Model 6
271	570507	0.004328968	Upper GMM Branch, Sigma 5, SAF Model 7
272	570508	0.01063438	Upper GMM Branch, Sigma 5, SAF Model 8
273	570509	0.014804152	Upper GMM Branch, Sigma 5, SAF Model 9
274	570510	0.014804152	Upper GMM Branch, Sigma 5, SAF Model 10
275	570511	0.01063438	Upper GMM Branch, Sigma 5, SAF Model 11
276	570512	0.004328968	Upper GMM Branch, Sigma 5, SAF Model 12
277	570601	0.001271205	Upper GMM Branch, Sigma 6, SAF Model 1
278	570602	0.003122794	Upper GMM Branch, Sigma 6, SAF Model 2
279	570603	0.004347251	Upper GMM Branch, Sigma 6, SAF Model 3
280	570604	0.004347251	Upper GMM Branch, Sigma 6, SAF Model 4
281	570605	0.003122794	Upper GMM Branch, Sigma 6, SAF Model 5
282	570606	0.001271205	Upper GMM Branch, Sigma 6, SAF Model 6
283	570607	0.001271205	Upper GMM Branch, Sigma 6, SAF Model 7
284	570608	0.003122794	Upper GMM Branch, Sigma 6, SAF Model 8
285	570609	0.004347251	Upper GMM Branch, Sigma 6, SAF Model 9
286	570610	0.004347251	Upper GMM Branch, Sigma 6, SAF Model 10
287	570611	0.003122794	Upper GMM Branch, Sigma 6, SAF Model 11
288	570612	0.001271205	Upper GMM Branch, Sigma 6, SAF Model 12
289	570701	0.00037329	Upper GMM Branch, Sigma 7, SAF Model 1
290	570702	0.000917011	Upper GMM Branch, Sigma 7, SAF Model 2
291	570703	0.001276574	Upper GMM Branch, Sigma 7, SAF Model 3
292	570704	0.001276574	Upper GMM Branch, Sigma 7, SAF Model 4

GMM No.	jcalc	GMM Weight	Description
293	570705	0.000917011	Upper GMM Branch, Sigma 7, SAF Model 5
294	570706	0.00037329	Upper GMM Branch, Sigma 7, SAF Model 6
295	570707	0.00037329	Upper GMM Branch, Sigma 7, SAF Model 7
296	570708	0.000917011	Upper GMM Branch, Sigma 7, SAF Model 8
297	570709	0.001276574	Upper GMM Branch, Sigma 7, SAF Model 9
298	570710	0.001276574	Upper GMM Branch, Sigma 7, SAF Model 10
299	570711	0.000917011	Upper GMM Branch, Sigma 7, SAF Model 11
300	570712	0.00037329	Upper GMM Branch, Sigma 7, SAF Model 12
301	570801	0.001271205	Upper GMM Branch, Sigma 8, SAF Model 1
302	570802	0.003122794	Upper GMM Branch, Sigma 8, SAF Model 2
303	570803	0.004347251	Upper GMM Branch, Sigma 8, SAF Model 3
304	570804	0.004347251	Upper GMM Branch, Sigma 8, SAF Model 4
305	570805	0.003122794	Upper GMM Branch, Sigma 8, SAF Model 5
306	570806	0.001271205	Upper GMM Branch, Sigma 8, SAF Model 6
307	570807	0.001271205	Upper GMM Branch, Sigma 8, SAF Model 7
308	570808	0.003122794	Upper GMM Branch, Sigma 8, SAF Model 8
309	570809	0.004347251	Upper GMM Branch, Sigma 8, SAF Model 9
310	570810	0.004347251	Upper GMM Branch, Sigma 8, SAF Model 10
311	570811	0.003122794	Upper GMM Branch, Sigma 8, SAF Model 11
312	570812	0.001271205	Upper GMM Branch, Sigma 8, SAF Model 12
313	570901	0.00037329	Upper GMM Branch, Sigma 9, SAF Model 1
314	570902	0.000917011	Upper GMM Branch, Sigma 9, SAF Model 2
315	570903	0.001276574	Upper GMM Branch, Sigma 9, SAF Model 3
316	570904	0.001276574	Upper GMM Branch, Sigma 9, SAF Model 4
317	570905	0.000917011	Upper GMM Branch, Sigma 9, SAF Model 5
318	570906	0.00037329	Upper GMM Branch, Sigma 9, SAF Model 6
319	570907	0.00037329	Upper GMM Branch, Sigma 9, SAF Model 7
320	570908	0.000917011	Upper GMM Branch, Sigma 9, SAF Model 8
321	570909	0.001276574	Upper GMM Branch, Sigma 9, SAF Model 9
322	570910	0.001276574	Upper GMM Branch, Sigma 9, SAF Model 10
323	570911	0.000917011	Upper GMM Branch, Sigma 9, SAF Model 11
324	570912	0.00037329	Upper GMM Branch, Sigma 9, SAF Model 12

APPENDIX G. EXPANDED HAZARD SENSITIVITY ANALYSIS FOR THE NEW BUILD SITE AT THE DUYNEFONTYN SITE.

APPENDIX G. EXPANDED HAZARD SENSITIVITY ANALYSES FOR NEW BUILD SITE AT DUYNEFONTYN

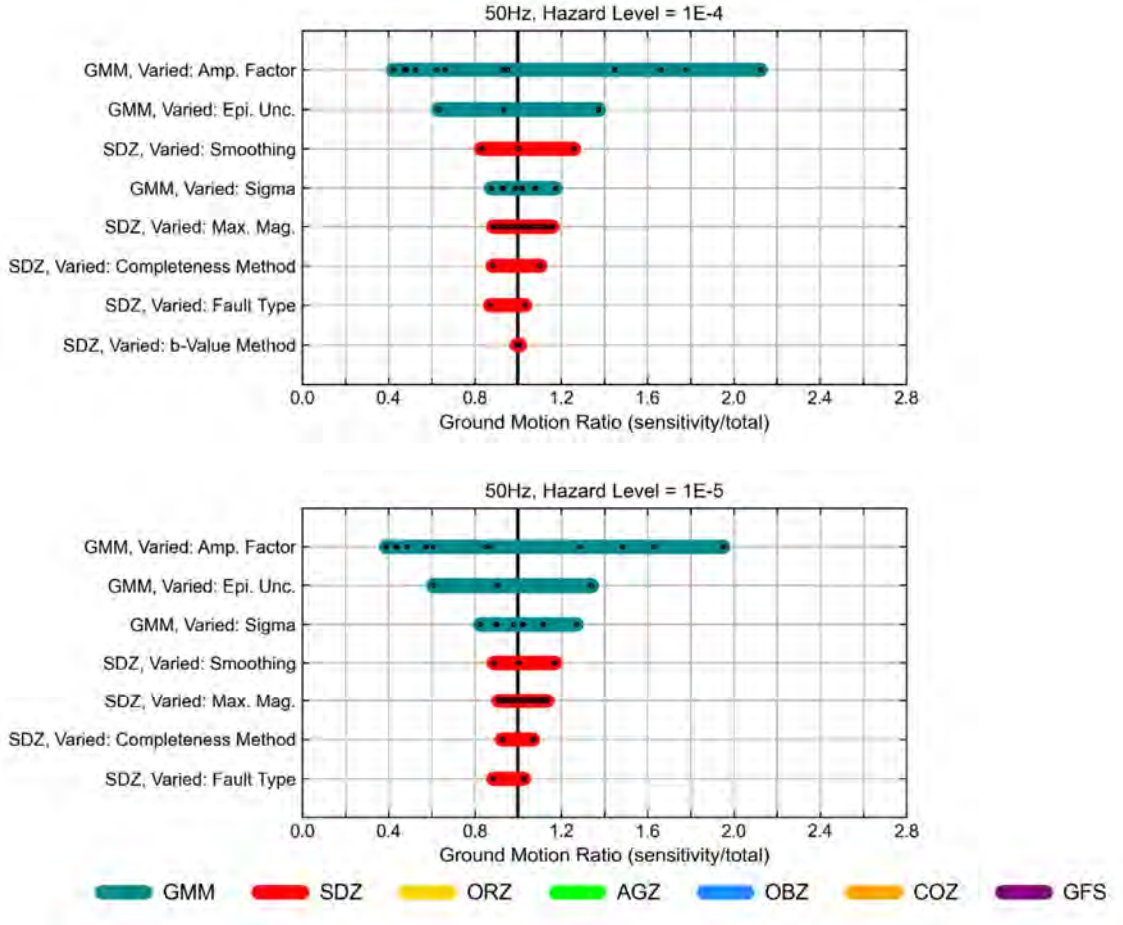

Figure 1

Figure G-1. Hazard sensitivity tornado plots at 50 Hz for the new build site at Duynefontyn.

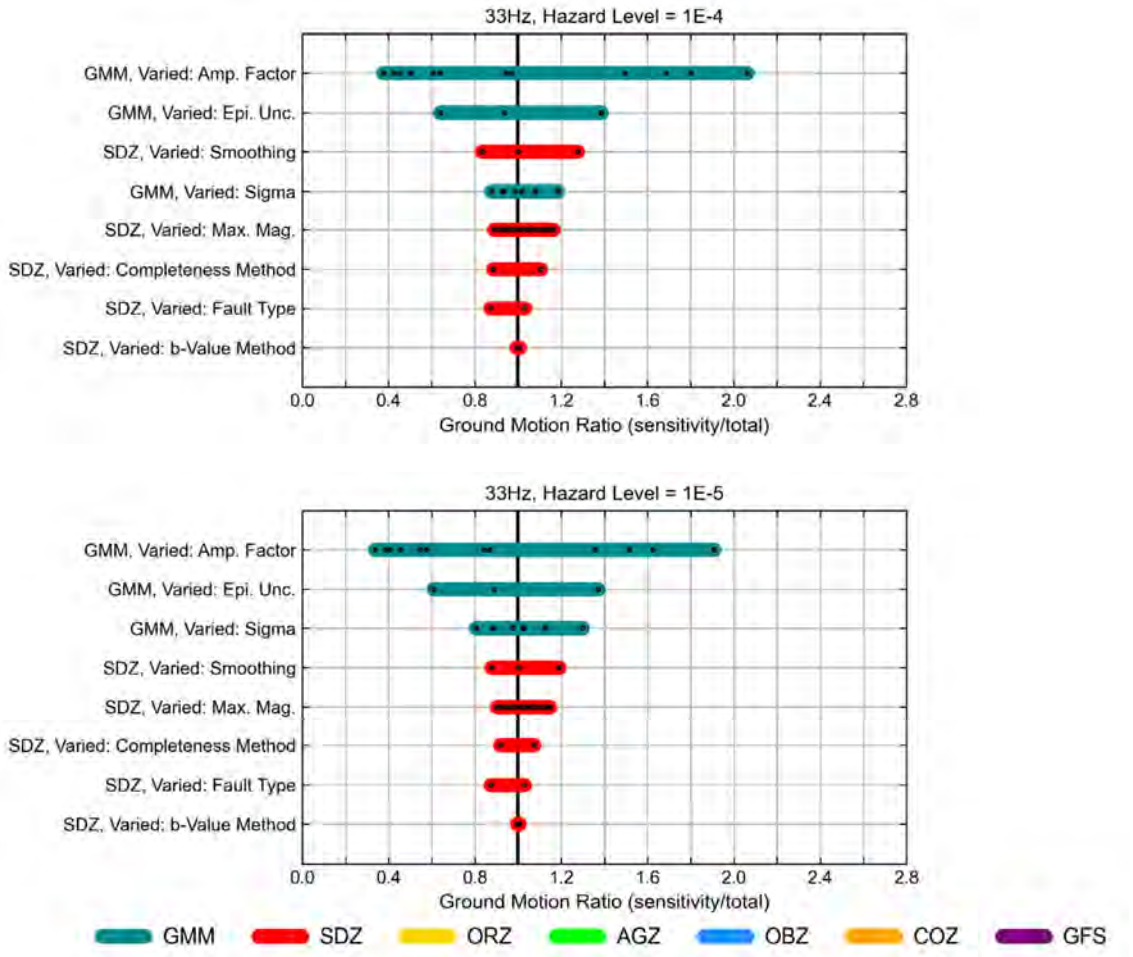

Figure G-2. Hazard sensitivity tornado plots at 33 Hz for the new build site at Duynefontyn.

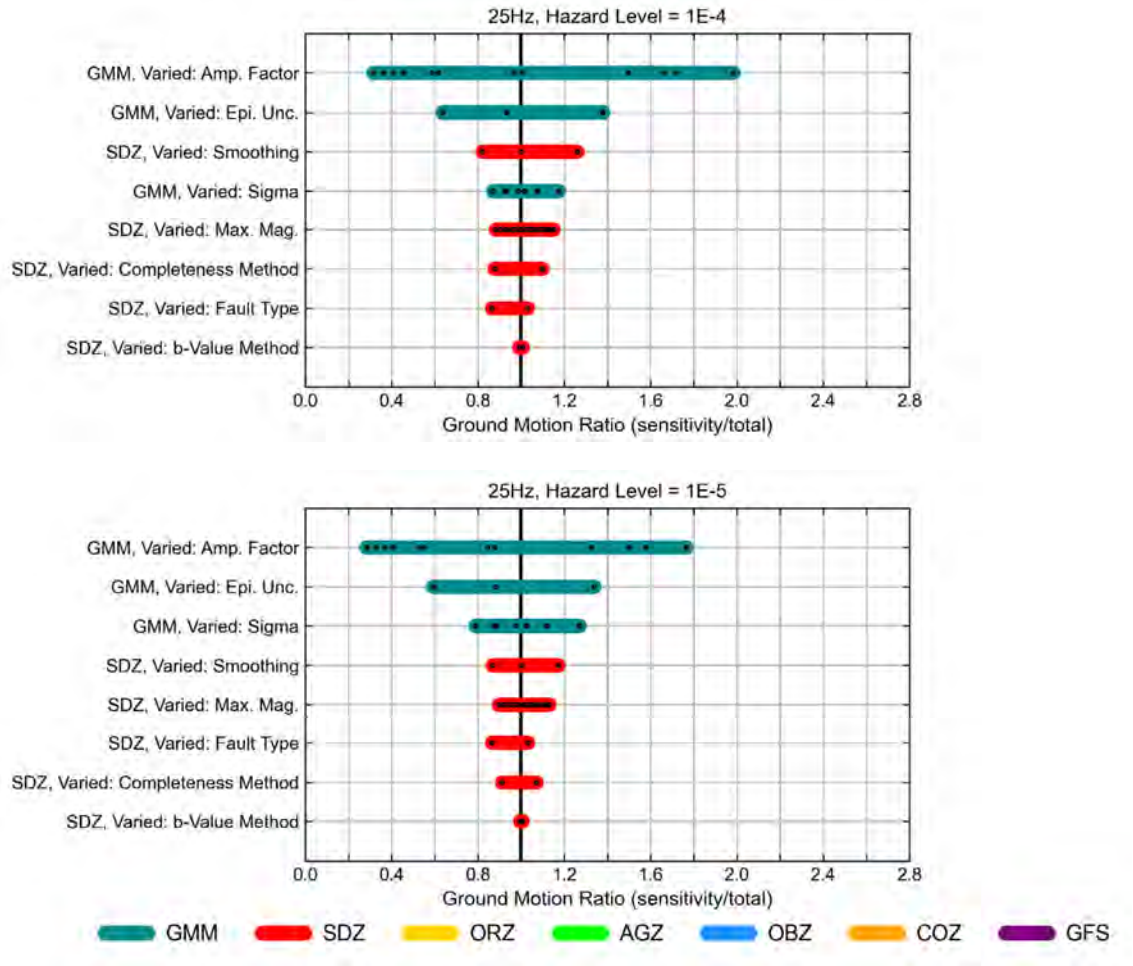

Figure G-3. Hazard sensitivity tornado plots at 25 Hz for the new build site at Duynefontyn.

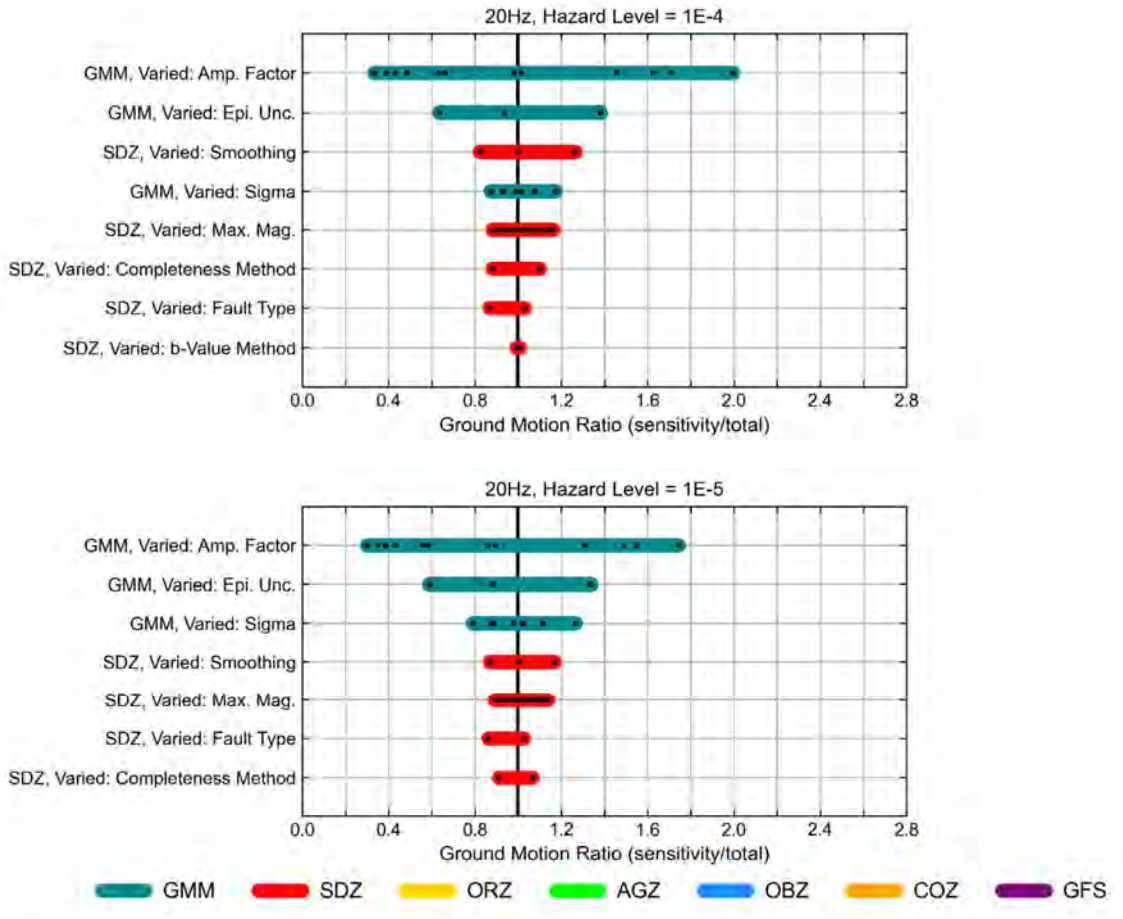

Figure G-4. Hazard sensitivity tornado plots at 20 Hz for the new build site at Duynefontyn.

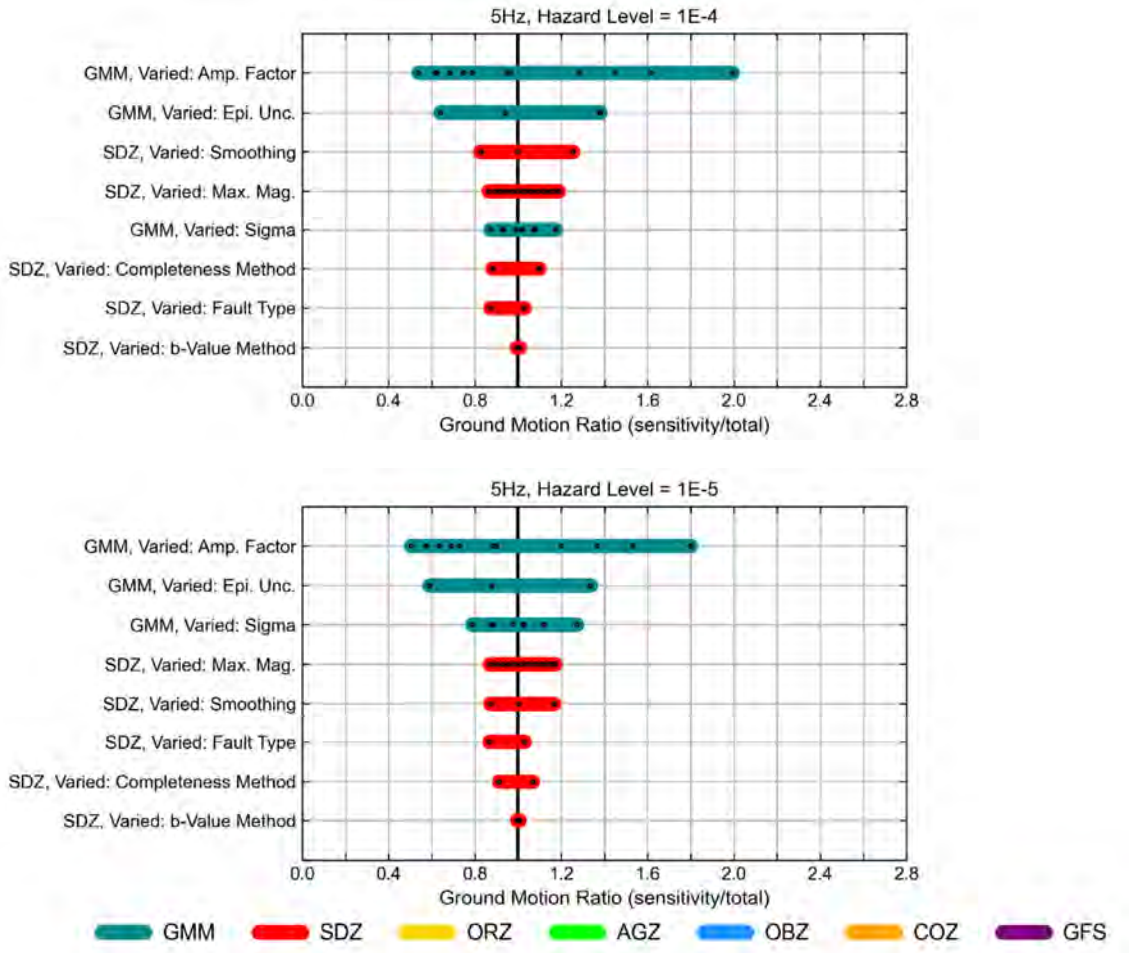

Figure G-5. Hazard sensitivity tornado plots at 5 Hz for the new build site at Duynefontyn.

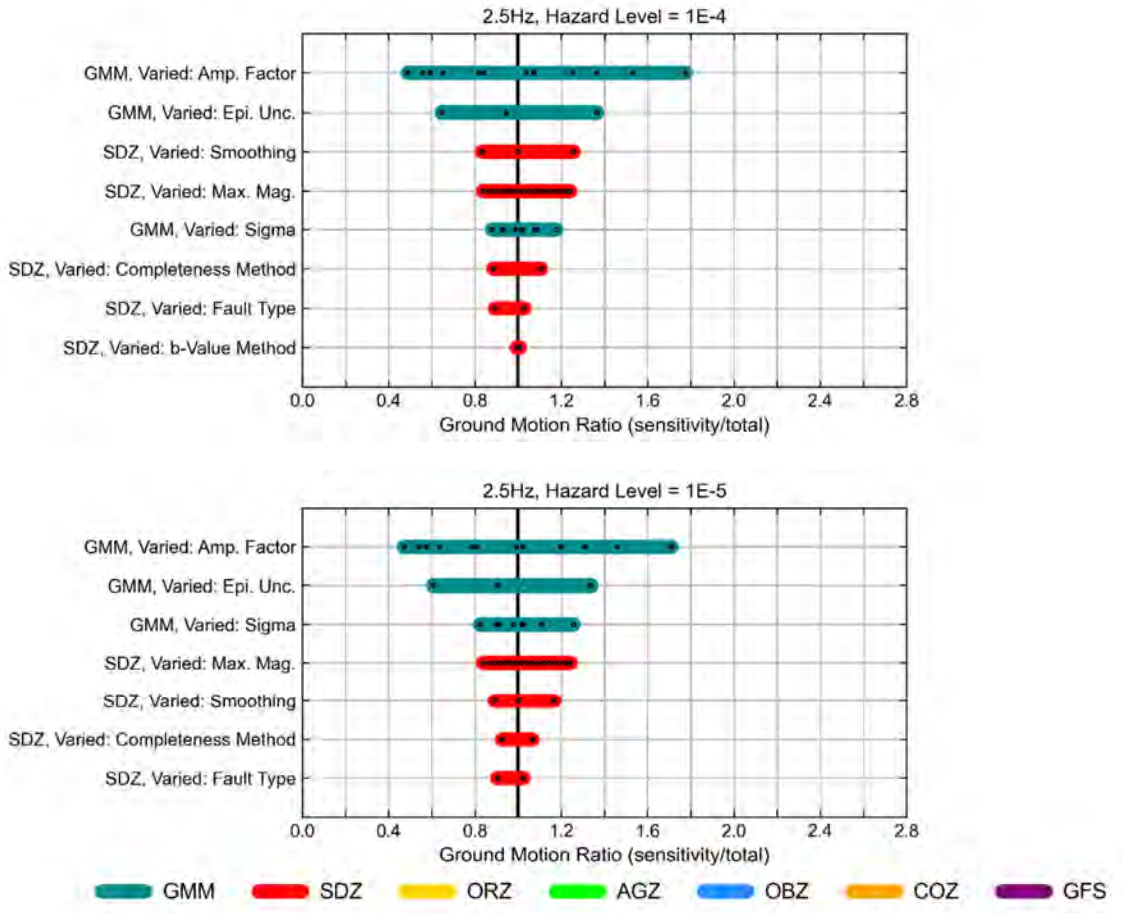

Figure G-6. Hazard sensitivity tornado plots at 2.5 Hz for the new build site at Duynefontyn.

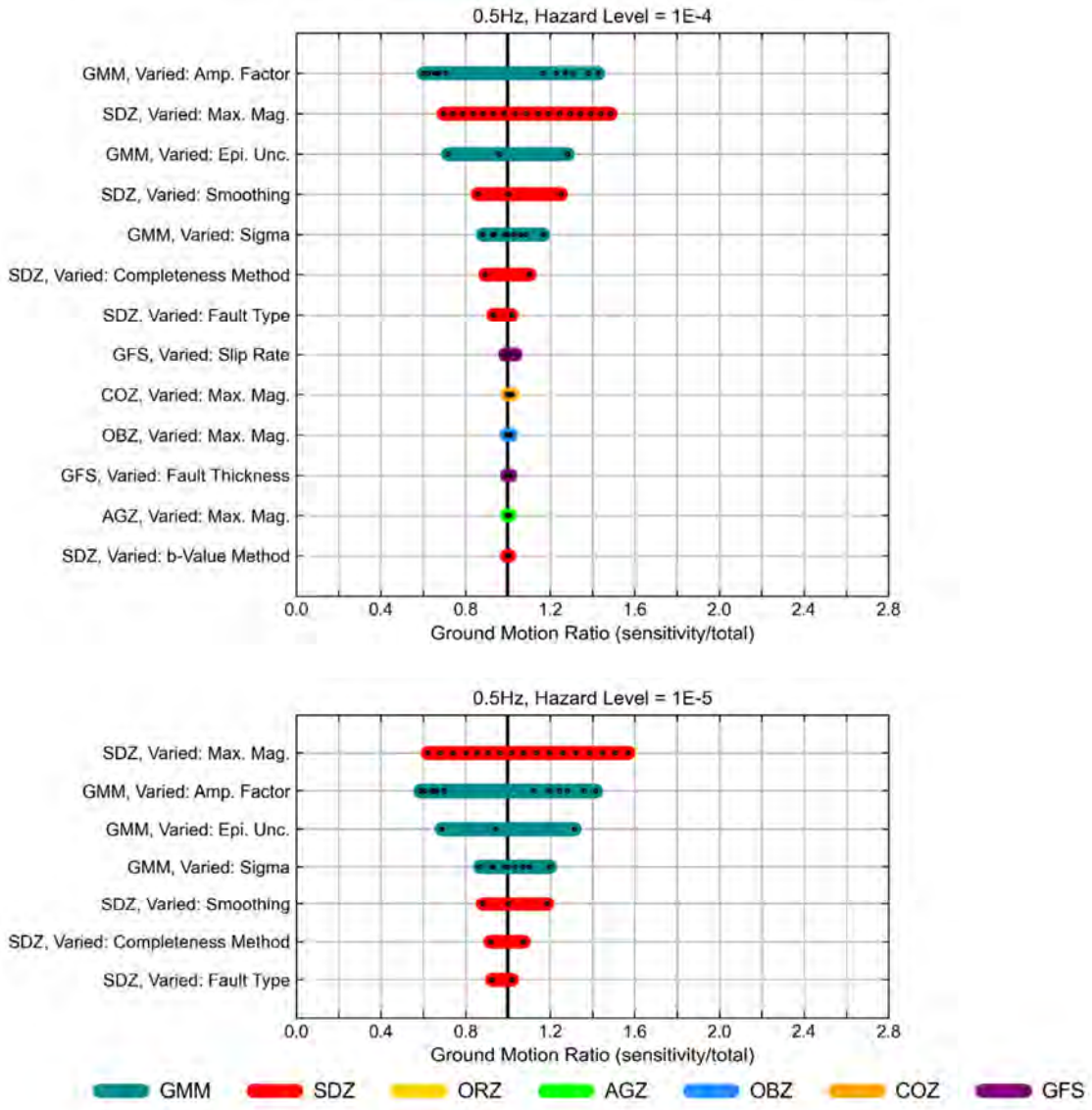

Figure G-7. Hazard sensitivity tornado plots at 0.5 Hz for the new build site at Duynefontyn.

G.1 SENSITIVITY TO GROUND-MOTION MODEL

Sensitivity to Site Adjustment Factor

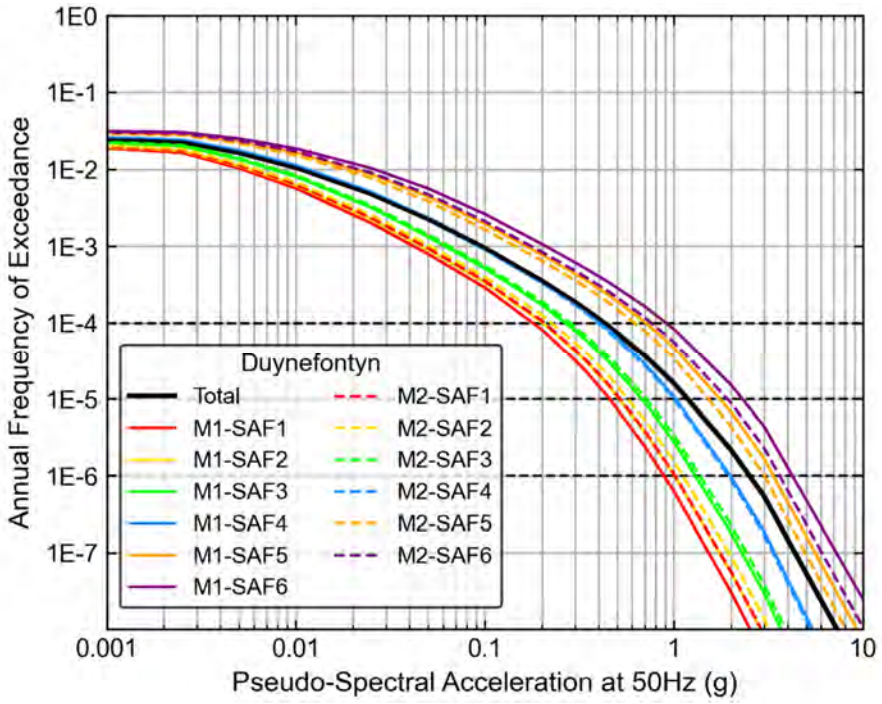

Figure G-8. Hazard sensitivity to the site response branches for 50 Hz at the new build site at Duynefontyn.

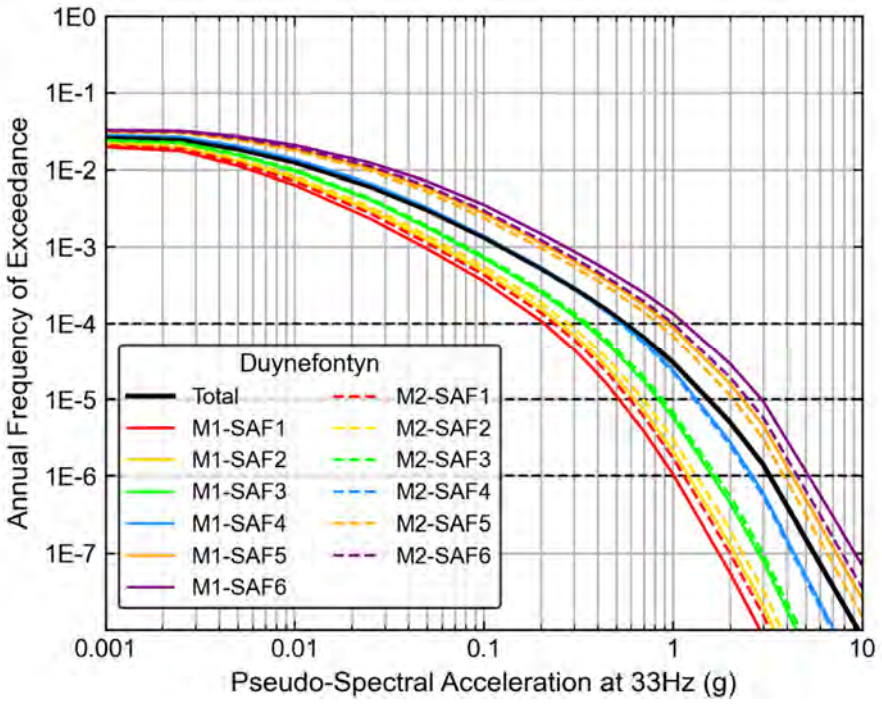

Figure G-9. Hazard sensitivity to the site response branches for 33 Hz at the new build site at Duynefontyn.

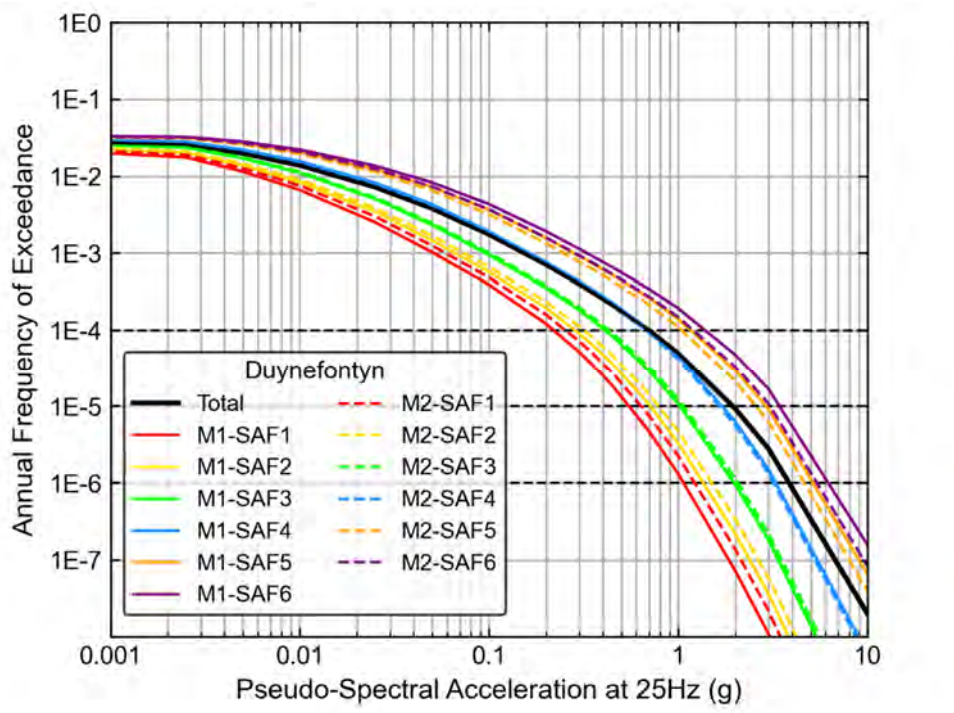

Figure G-10. Hazard sensitivity to the site response branches for 25 Hz at the new build site at Duynefontyn.

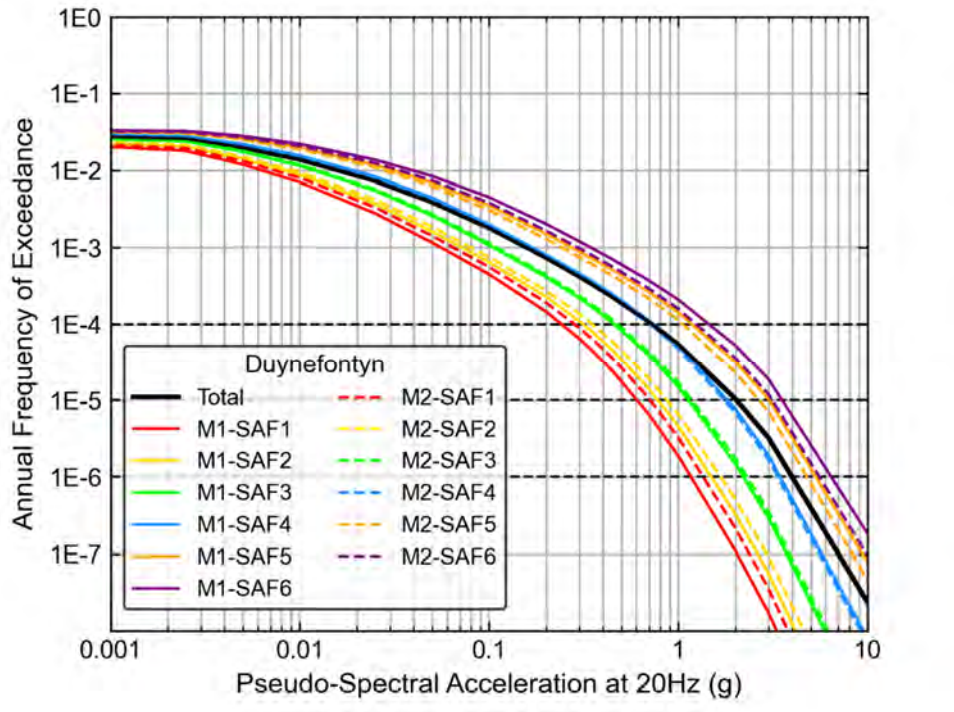

Figure G-11. Hazard sensitivity to the site response branches for 20 Hz at the new build site at Duynefontyn.

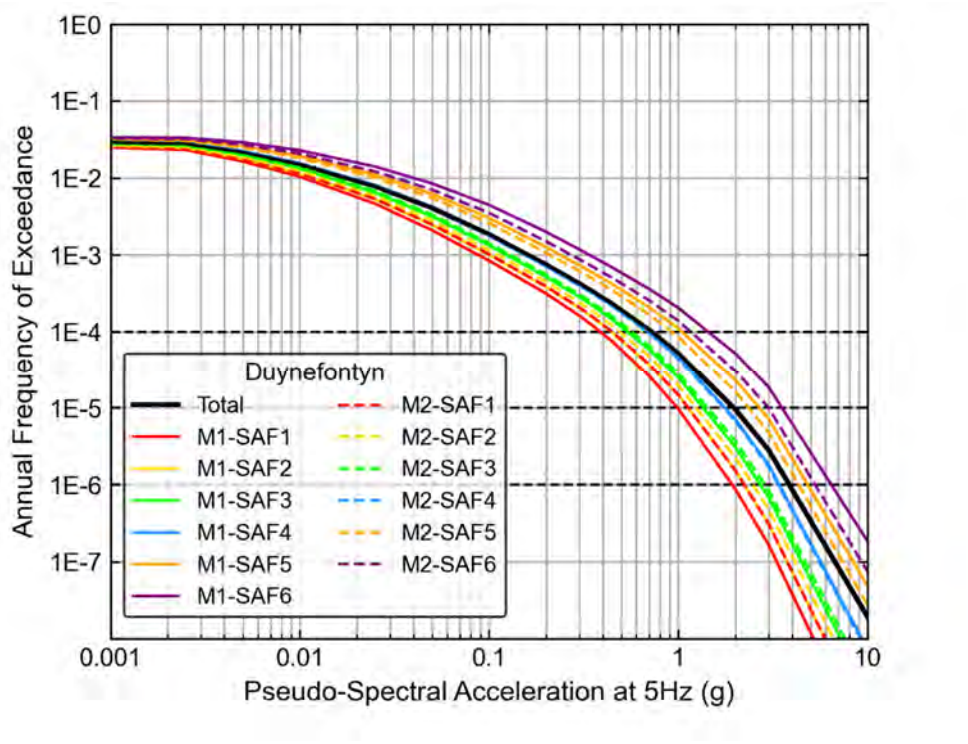

Figure G-12. Hazard sensitivity to the site response branches for 5 Hz at the new build site at Duynefontyn.

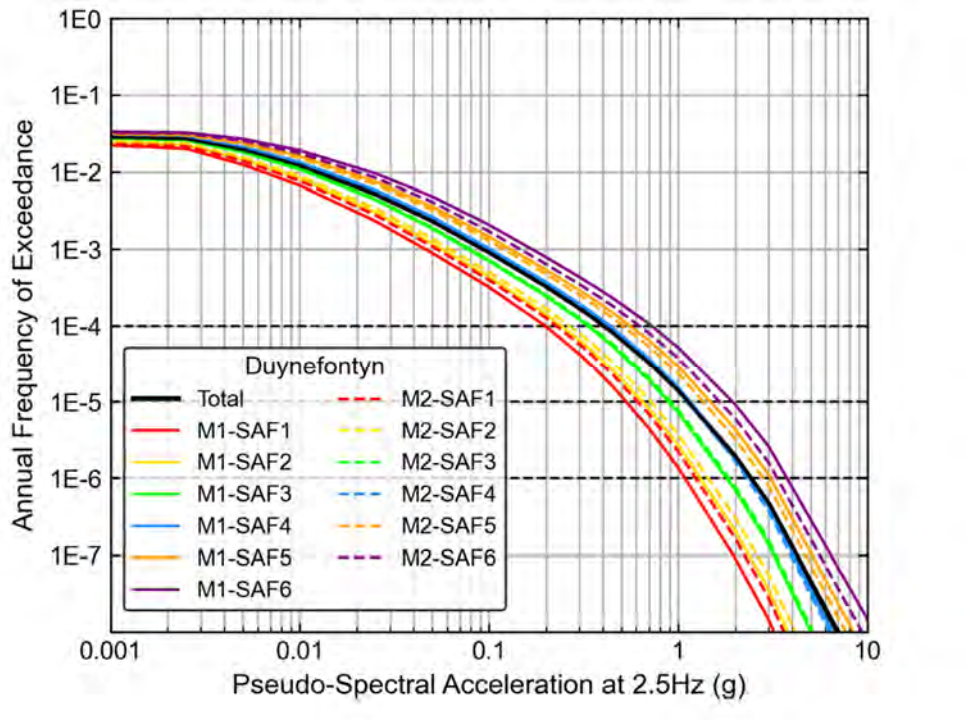

Figure G-13. Hazard sensitivity to the site response branches for 2.5 Hz at the new build site at Duynefontyn.

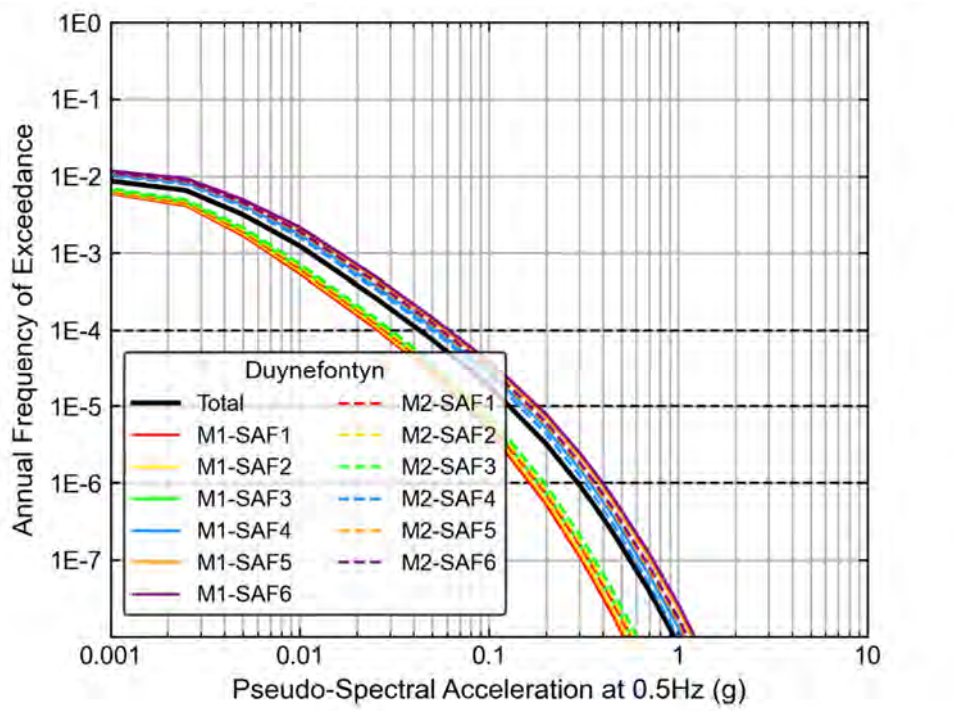

Figure G-14. Hazard sensitivity to the site response branches for 0.5 Hz at the new build site at Duynefontyn.

Sensitivity to GMM Epistemic Uncertainty Model

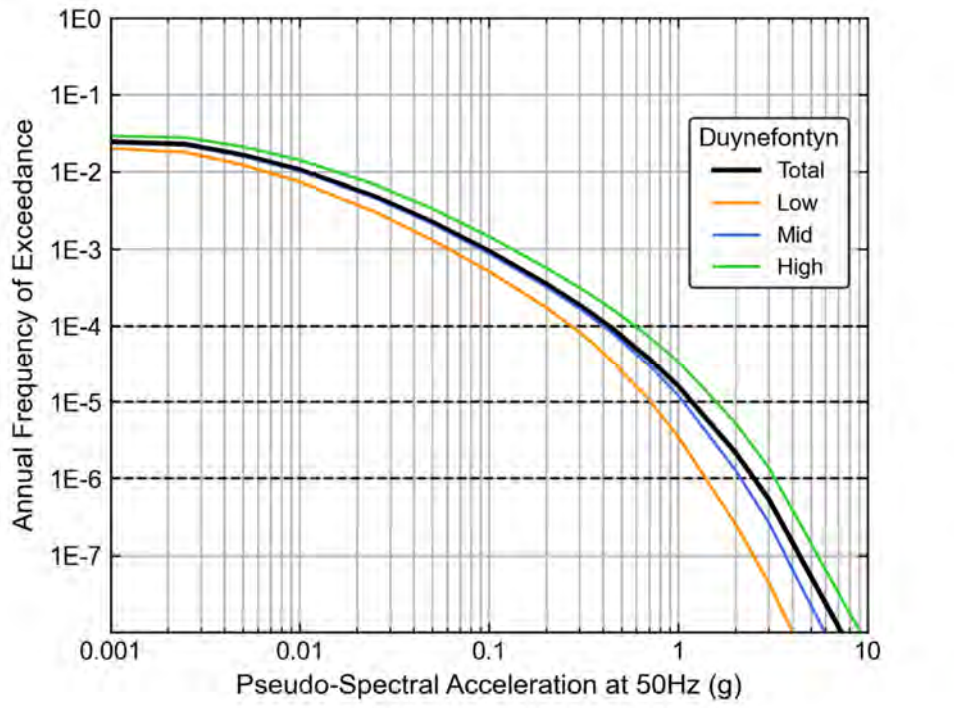

Figure G-15. Hazard sensitivity to the epistemic uncertainty model for 50 Hz at the new build site at Duynefontyn.

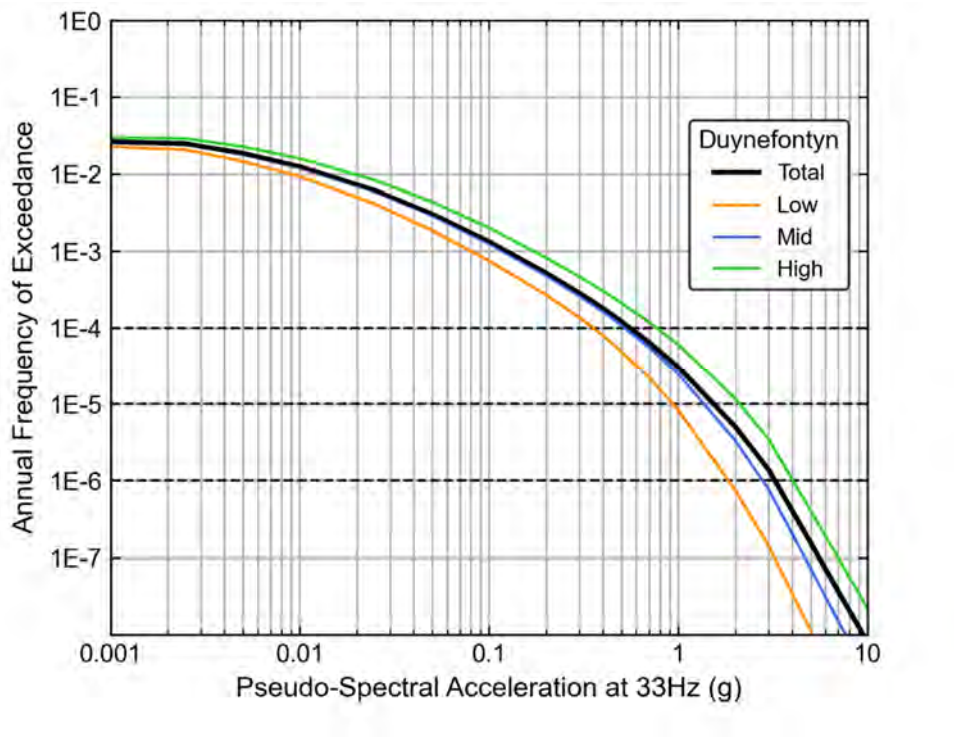

Figure G-16. Hazard sensitivity to the epistemic uncertainty model for 33 Hz at the new build site at Duynefontyn.

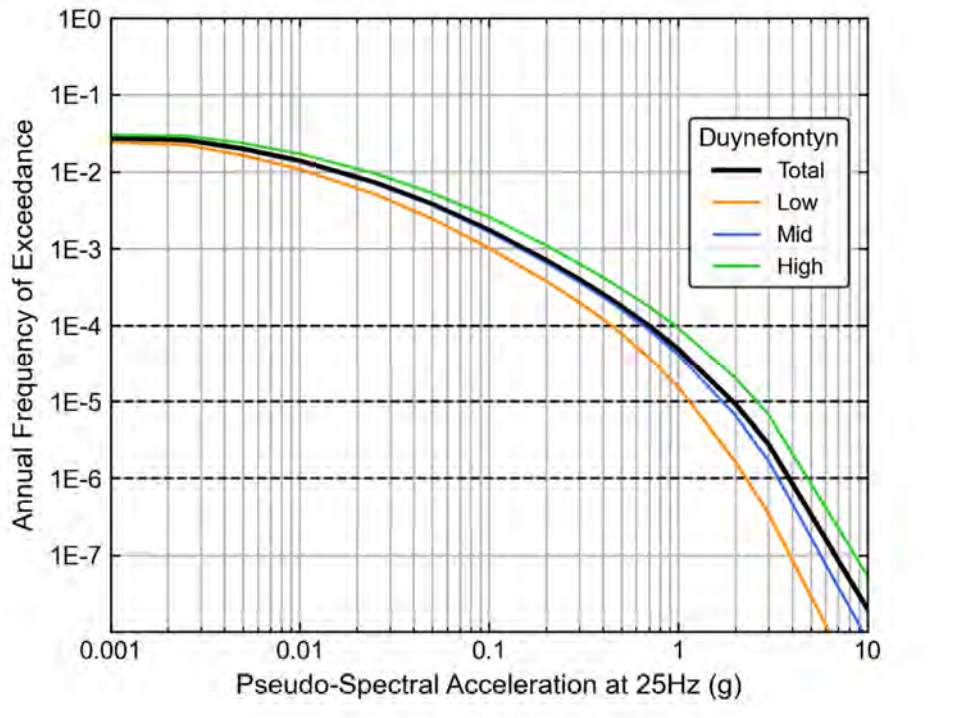

Figure G-17. Hazard sensitivity to the epistemic uncertainty model for 25 Hz at the new build site at Duynefontyn.

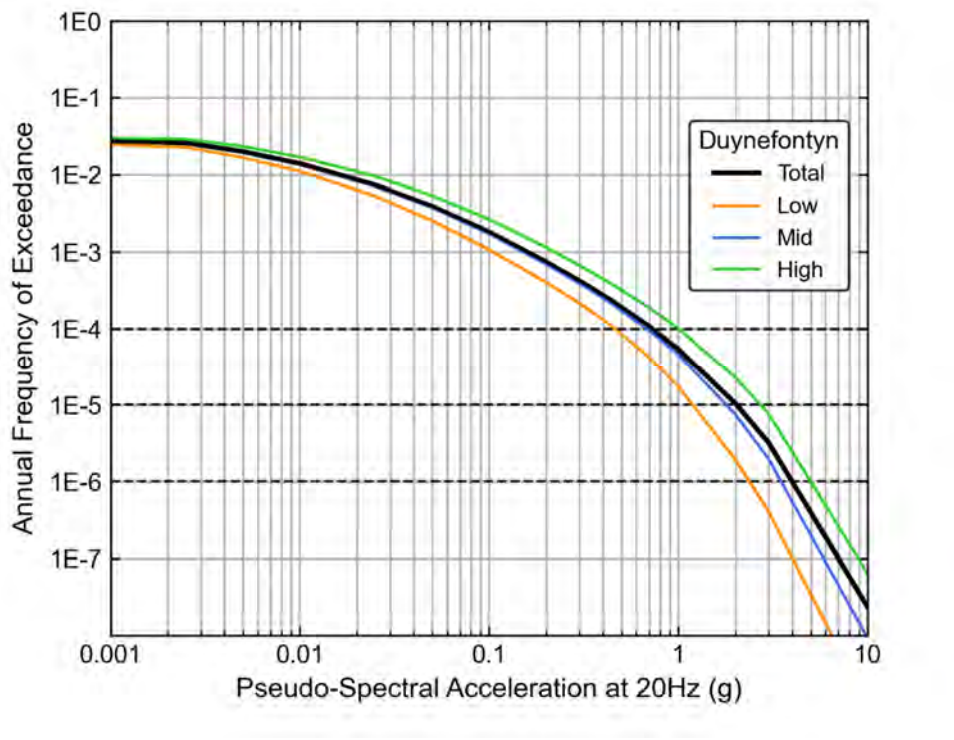

Figure G-18. Hazard sensitivity to the epistemic uncertainty model for 20 Hz at the new build site at Duynefontyn.

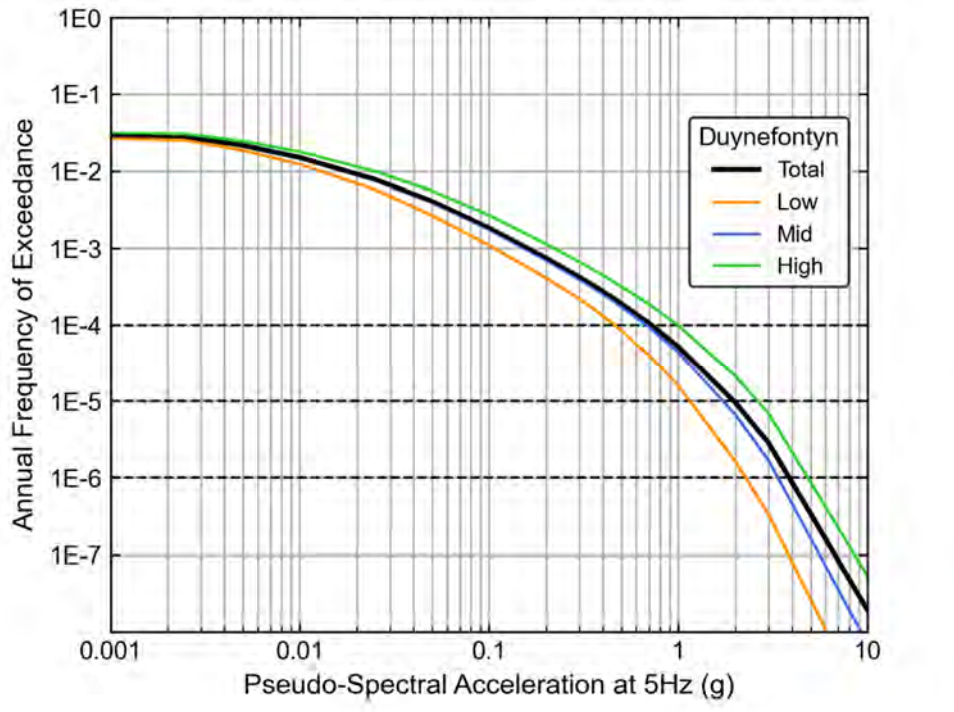

Figure G-19. Hazard sensitivity to the epistemic uncertainty model for 5 Hz at the new build site at Duynefontyn.

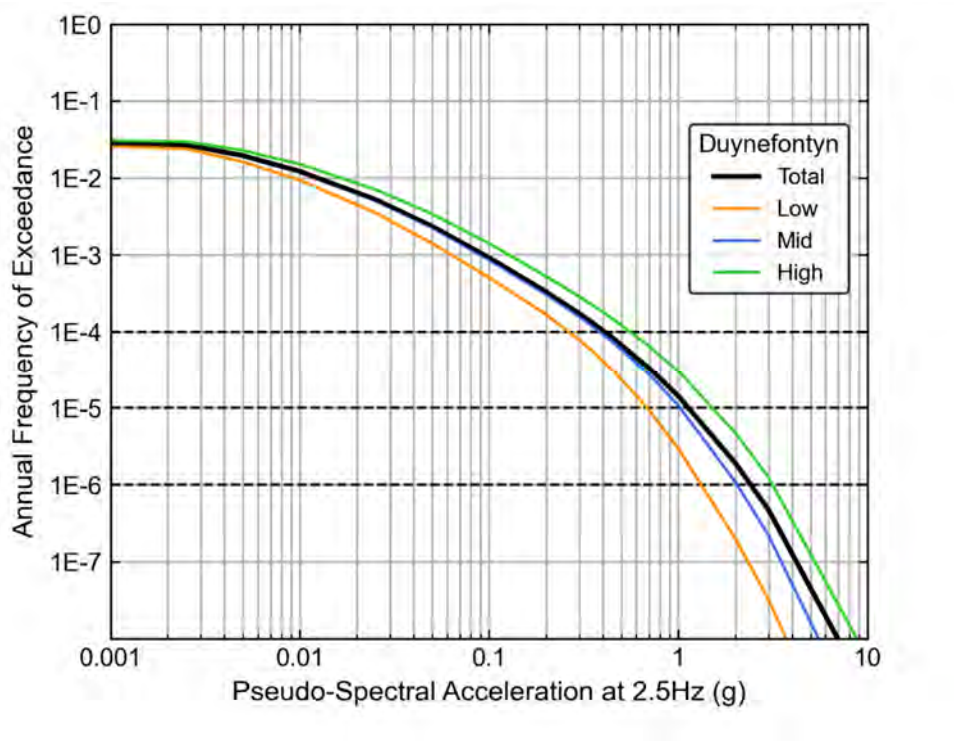

Figure G-20. Hazard sensitivity to the epistemic uncertainty model for 2.5 Hz at the new build site at Duynefontyn.

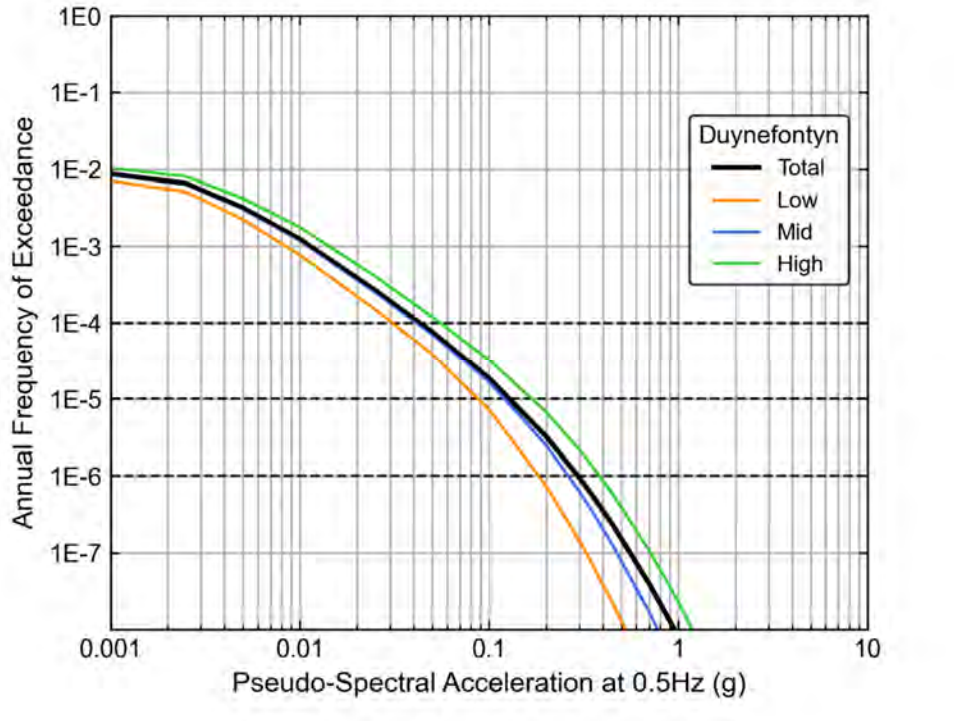

Figure G-21. Hazard sensitivity to the epistemic uncertainty model for 0.5 Hz at the new build site at Duynefontyn.

Sensitivity to Uncertainty in the GMM Aleatory Variability

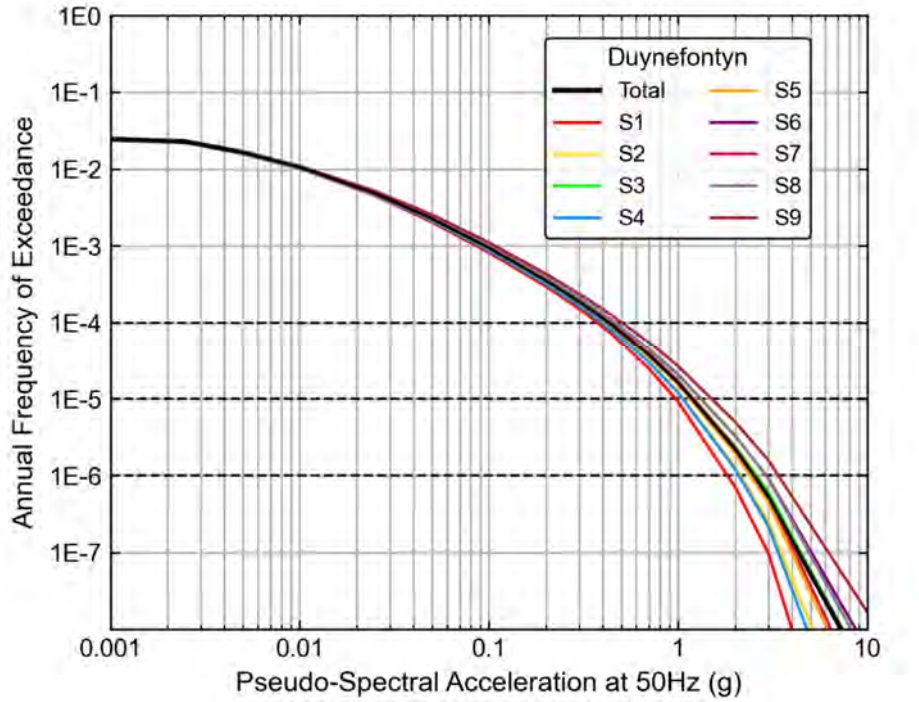

Figure G-22. Hazard sensitivity to the aleatory variability branches for 50 Hz at the new build site at Duynefontyn.

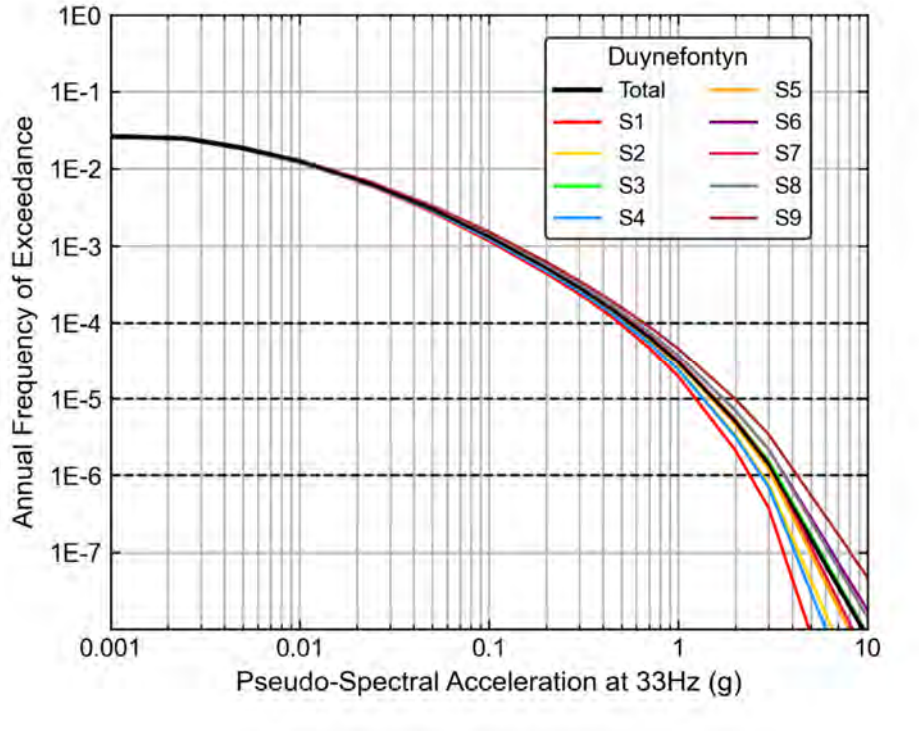

Figure G-23. Hazard sensitivity to the aleatory variability branches for 33 Hz at the new build site at Duynefontyn.

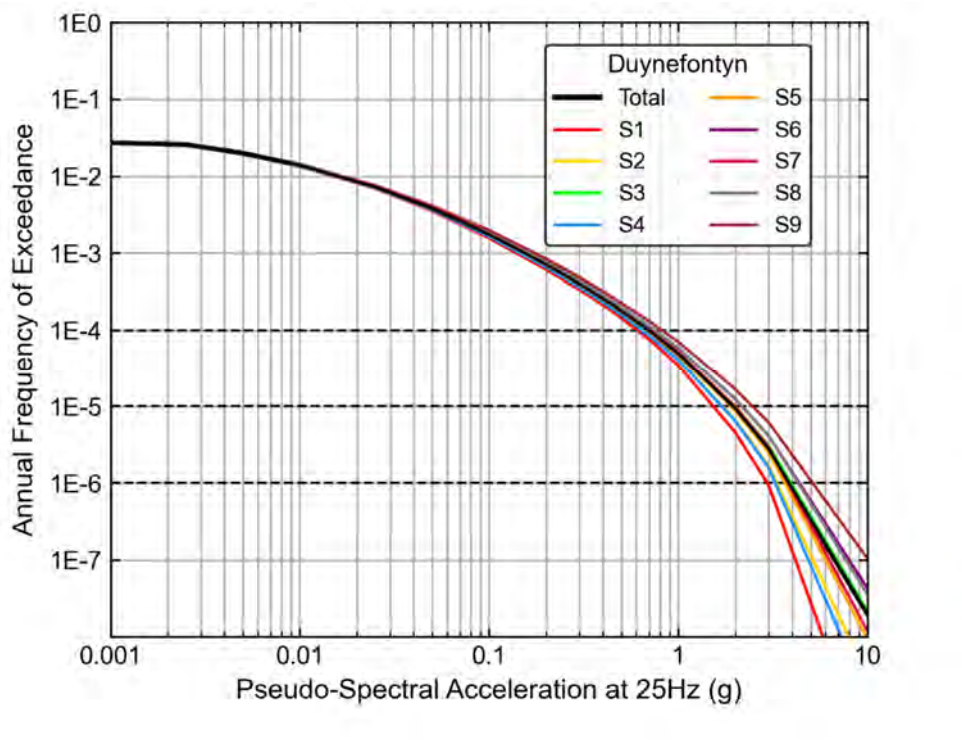

Figure G-24. Hazard sensitivity to the aleatory variability branches for 25 Hz at the new build site at Duynefontyn.

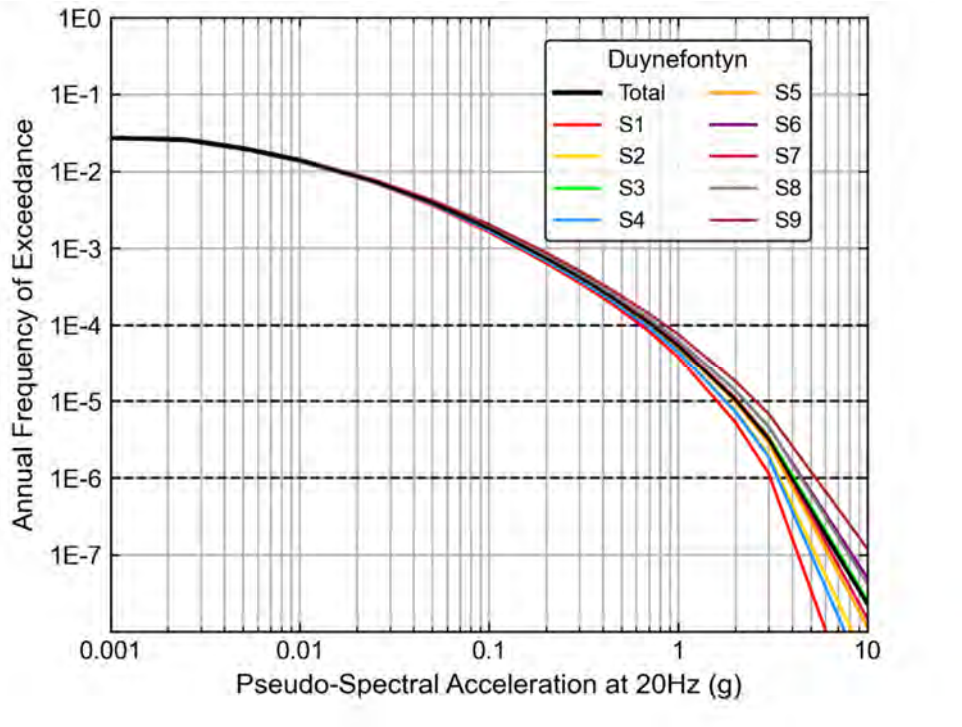

Figure G-25. Hazard sensitivity to the aleatory variability branches for 20 Hz at the new build site at Duynefontyn.

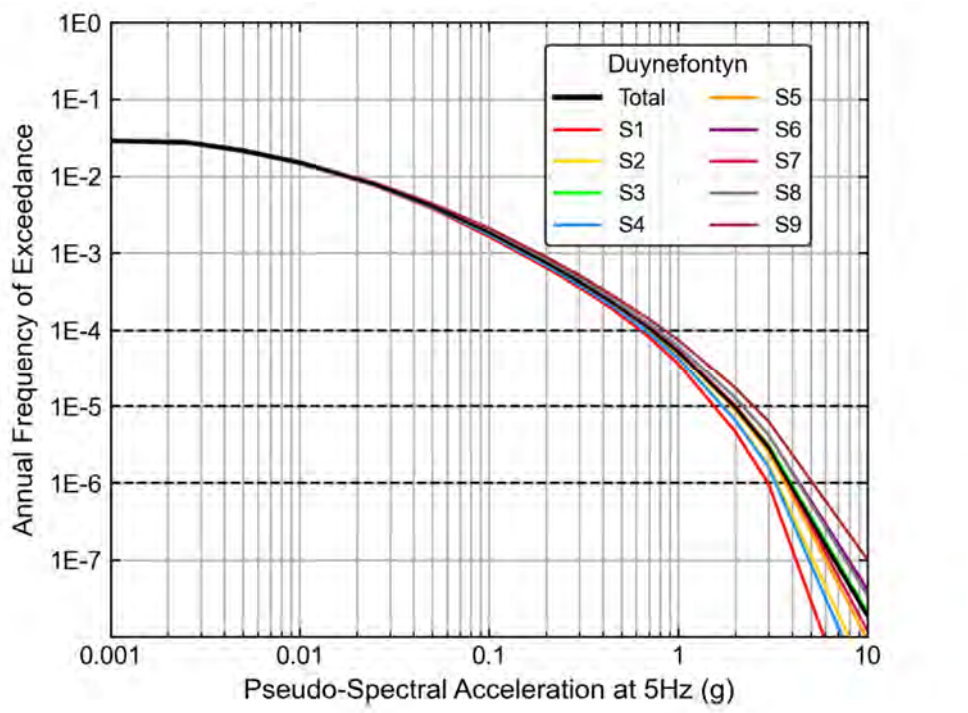

Figure G-26. Hazard sensitivity to the aleatory variability branches for 5 Hz at the new build site at Duynefontyn.

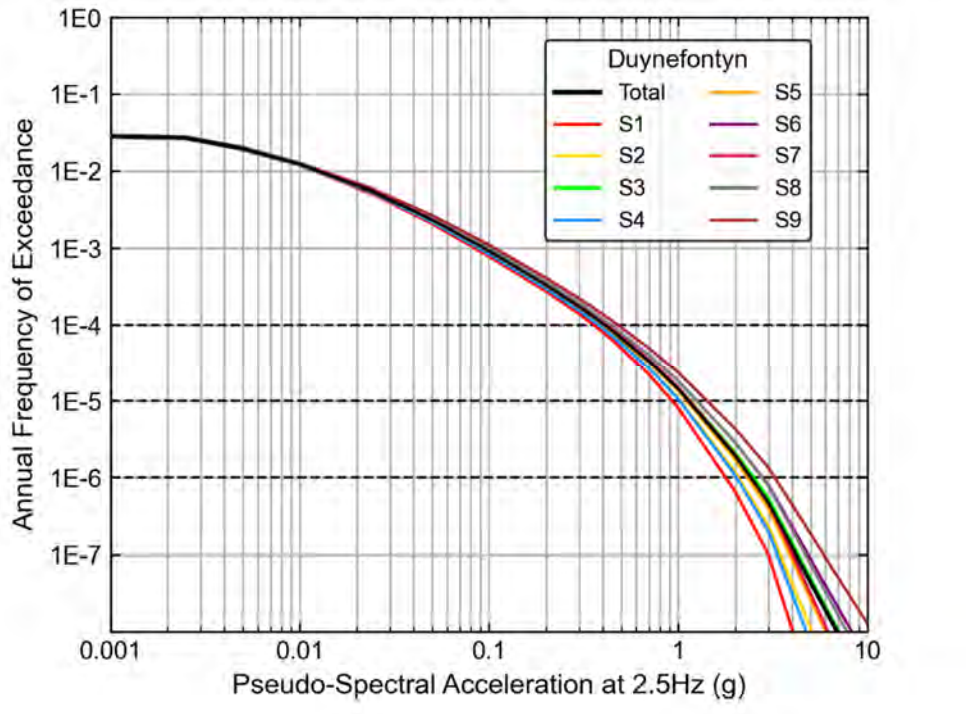

Figure G-27. Hazard sensitivity to the aleatory variability branches for 2.5 Hz at the new build site at Duynefontyn.

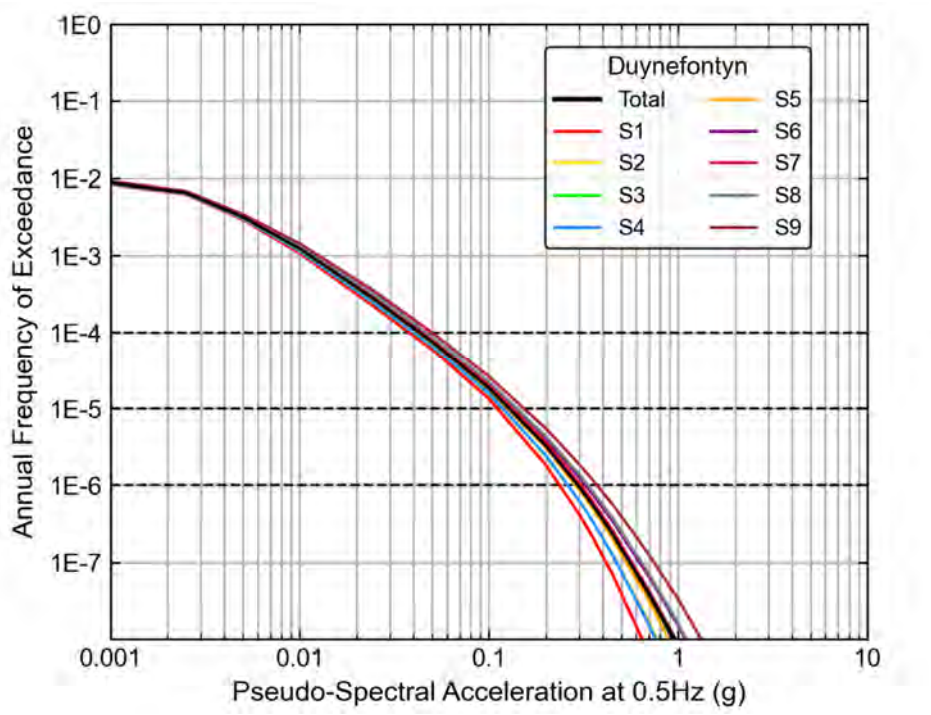

Figure G-28. Hazard sensitivity to the aleatory variability branches for 0.5 Hz at the new build site at Duynefontyn.

G.2 SENSITIVITY TO SEISMIC SOURCE MODEL

Sensitivity to Spatial Smoothing

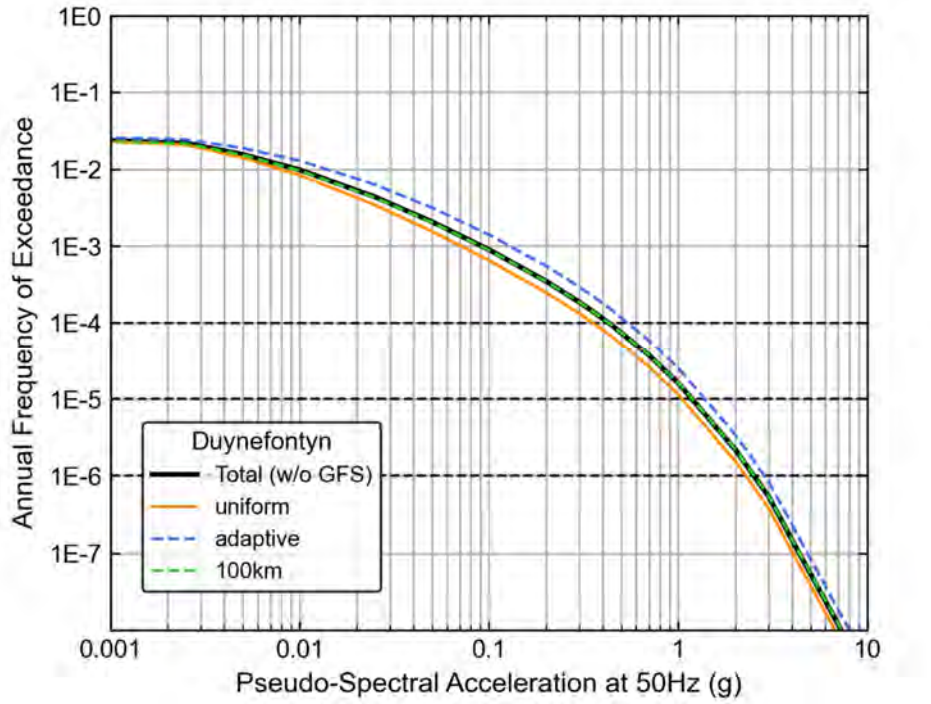

Figure G-29. Hazard sensitivity for 50 Hz to smoothed seismicity method branches at the new build site at Duynefontyn.

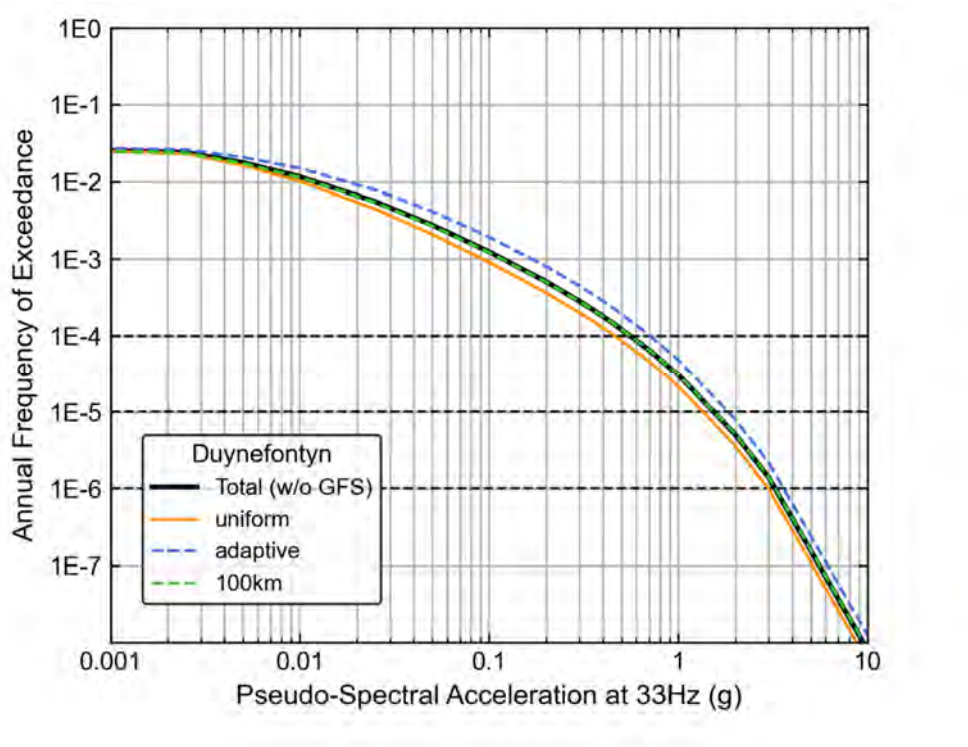

Figure G-30. Hazard sensitivity for 33 Hz to smoothed seismicity method branches at the new build site at Duynefontyn.

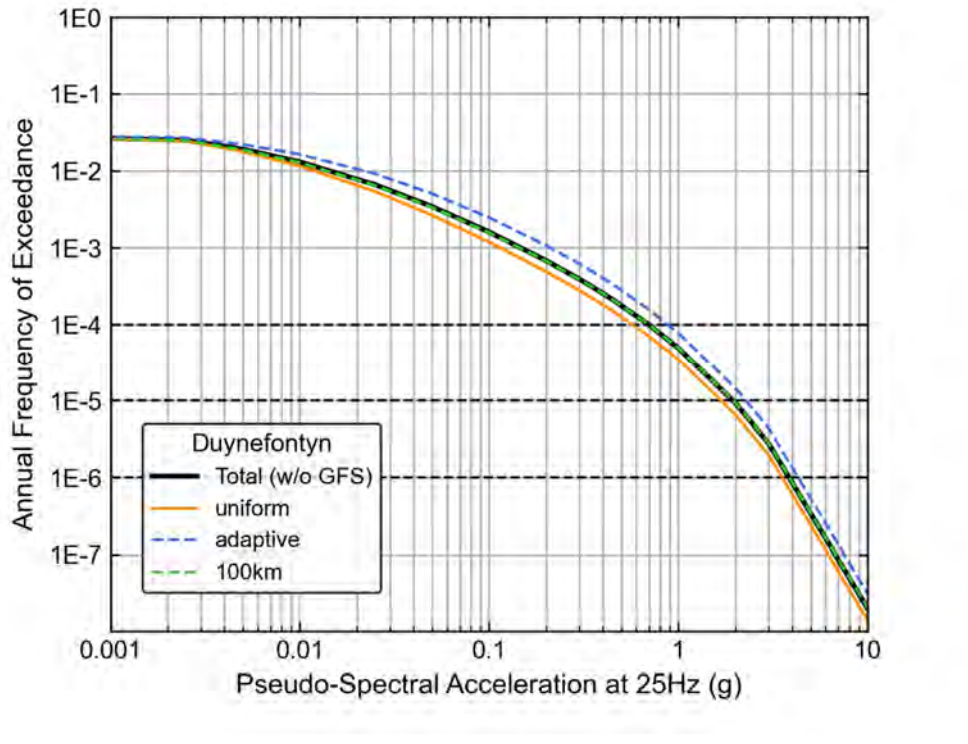

Figure G-31. Hazard sensitivity for 25 Hz to smoothed seismicity method branches at the new build site at Duynefontyn.

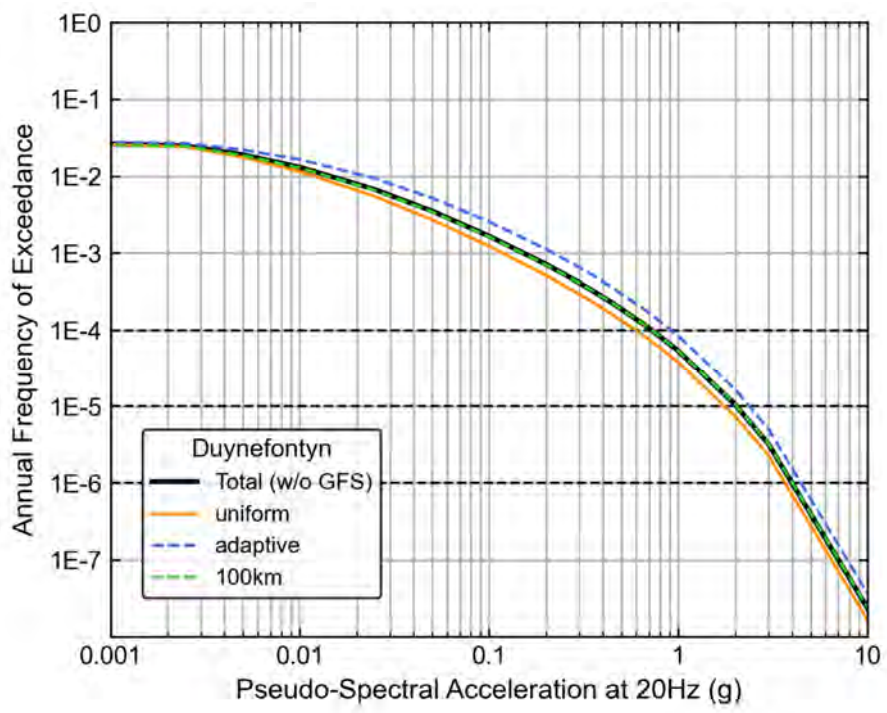

Figure G-32. Hazard sensitivity for 20 Hz to smoothed seismicity method branches at the new build site at Duynefontyn.

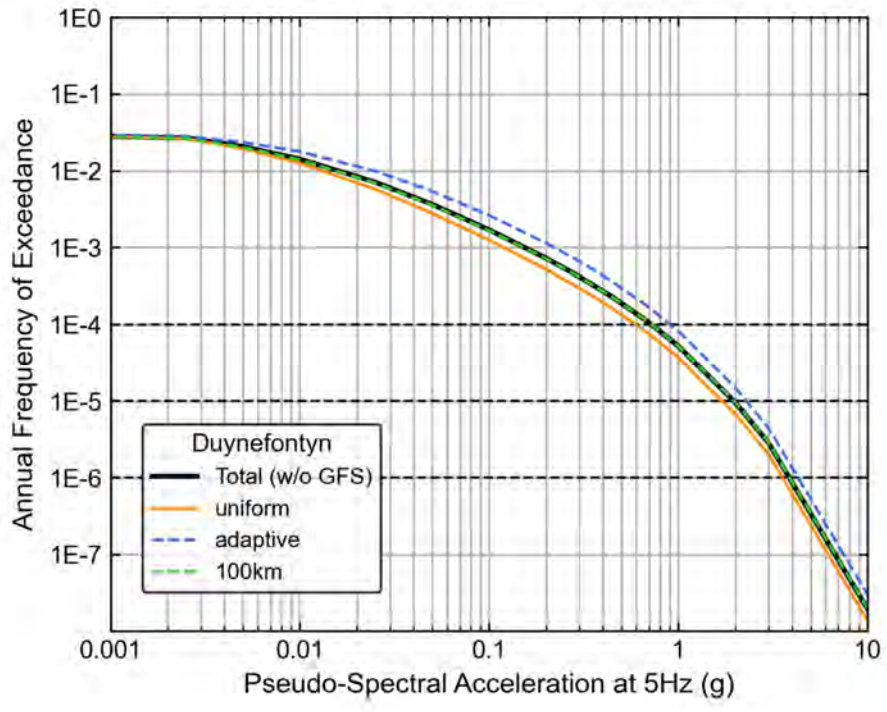

Figure G-33. Hazard sensitivity for 5 Hz to smoothed seismicity method branches at the new build site at Duynefontyn.

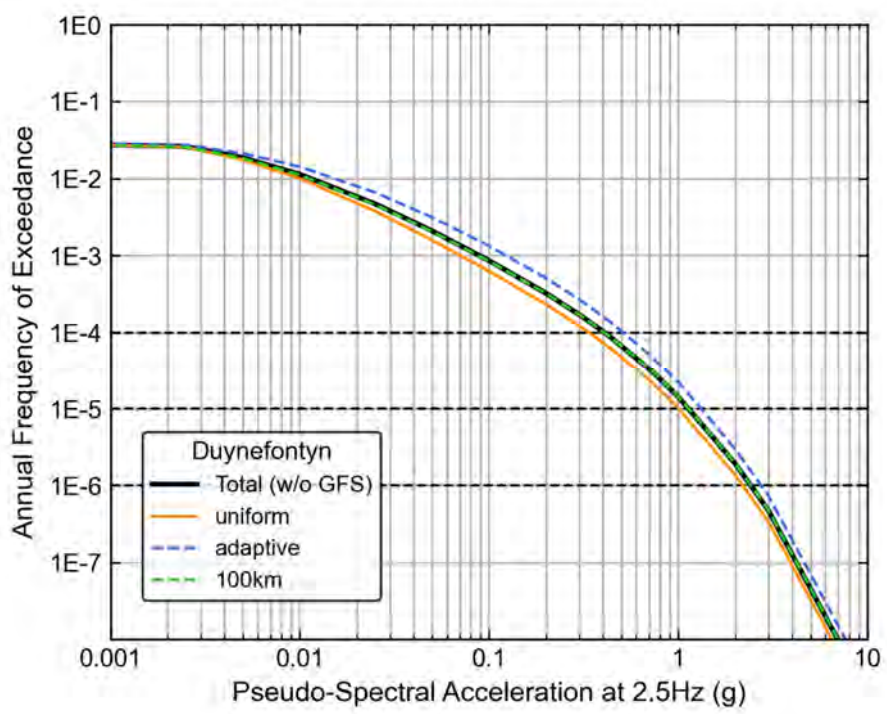

Figure G-34. Hazard sensitivity for 2.5 Hz to smoothed seismicity method branches at the new build site at Duynefontyn.

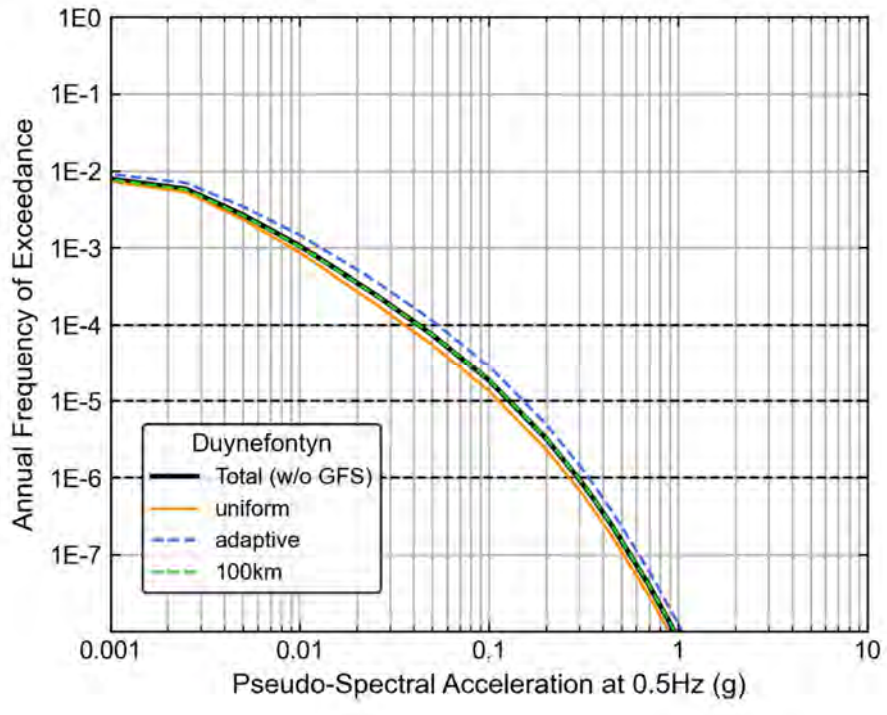

Figure G-35. Hazard sensitivity for 0.5 Hz to smoothed seismicity method branches at the new build site at Duynefontyn.

Sensitivity to Maximum Magnitude

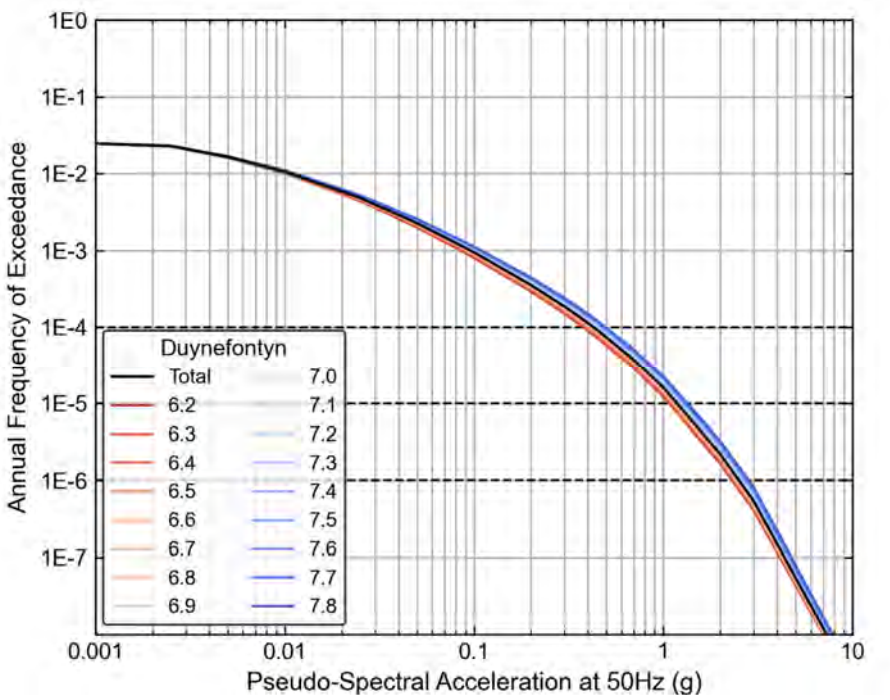

Figure G-36. Hazard sensitivity for 50 Hz to the host zone maximum magnitude branches at the new build site at Duynefontyn.

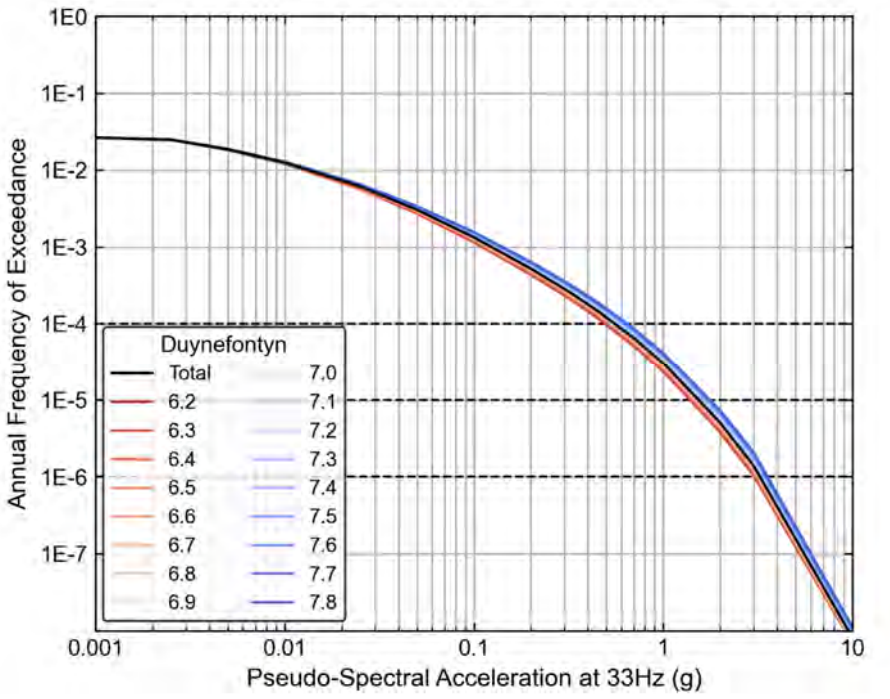

Figure G-37. Hazard sensitivity for 33 Hz to the host zone maximum magnitude branches at the new build site at Duynefontyn.

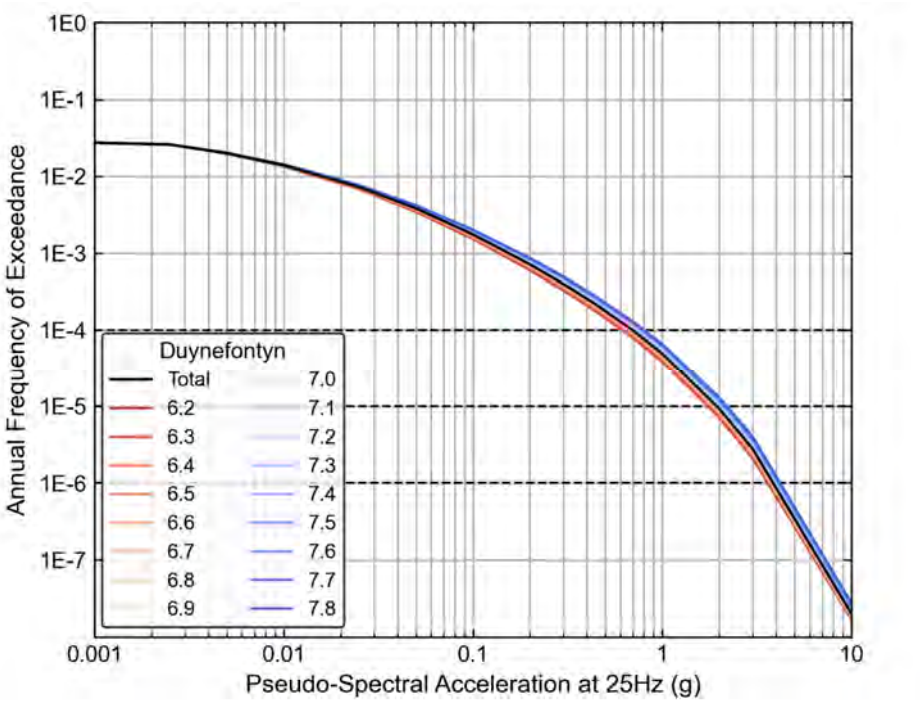

Figure G-38. Hazard sensitivity for 25 Hz to the host zone maximum magnitude branches at the new build site at Duynefontyn.

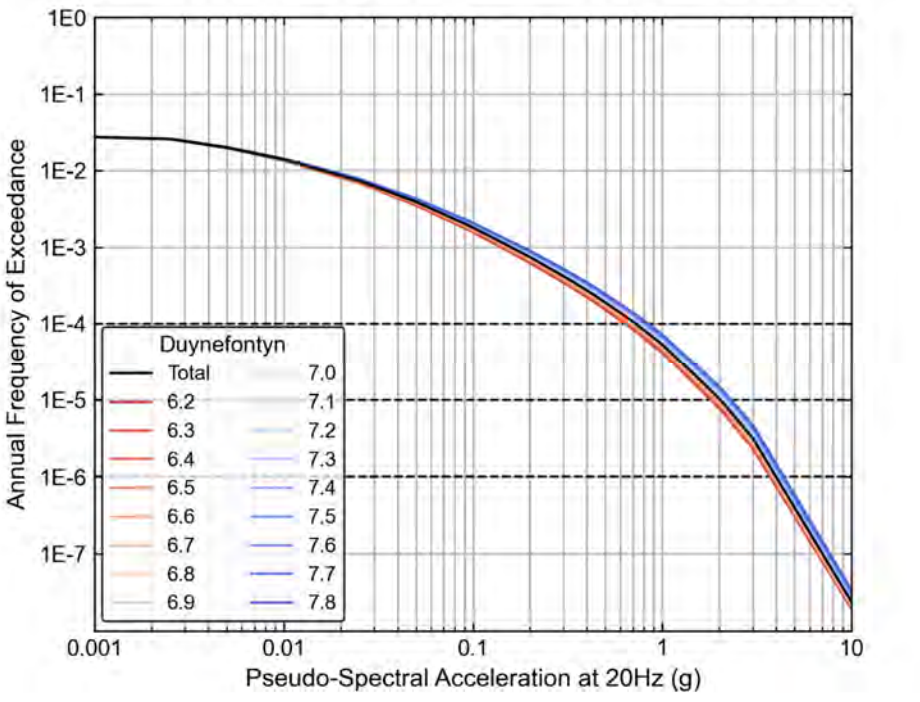

Figure G-39. Hazard sensitivity for 20 Hz to the host zone maximum magnitude branches at the new build site at Duynefontyn.

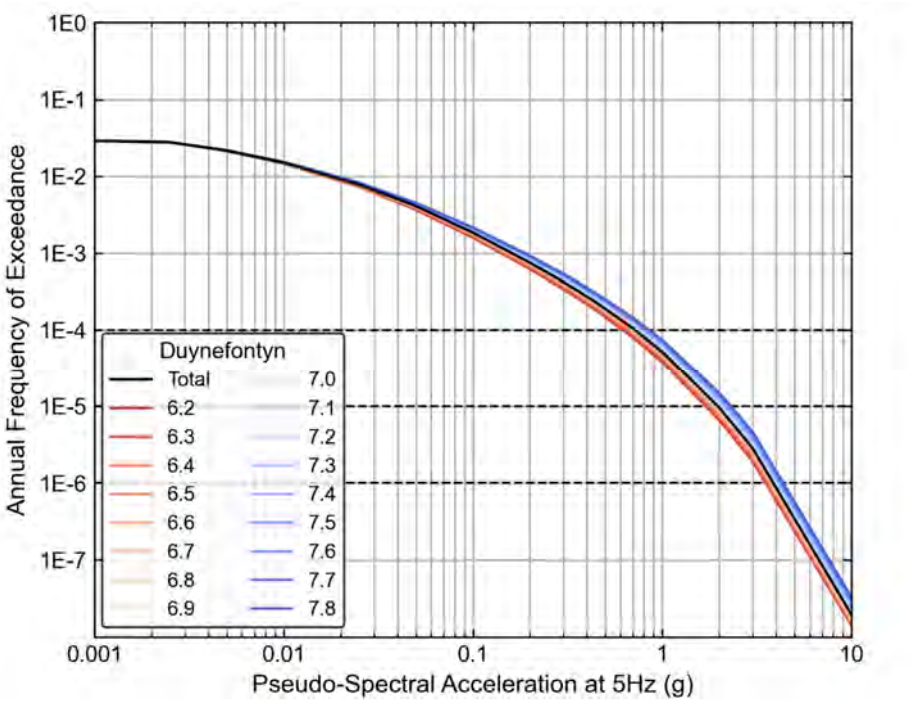

Figure G-40. Hazard sensitivity for 5 Hz to the host zone maximum magnitude branches at the new build site at Duynefontyn.

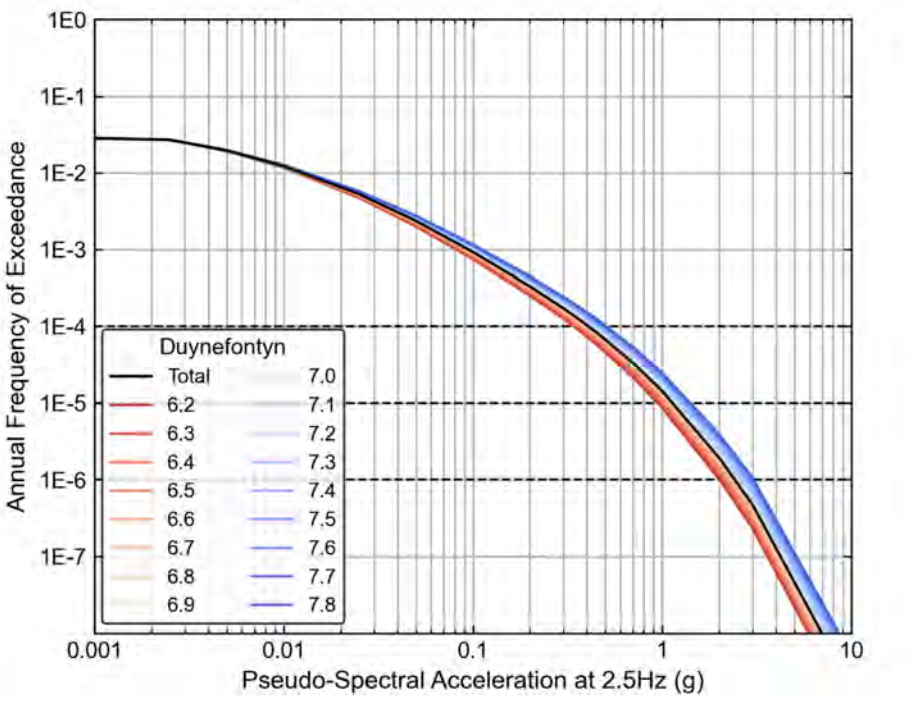

Figure G-41. Hazard sensitivity for 2.5 Hz to the host zone maximum magnitude branches at the new build site at Duynefontyn.

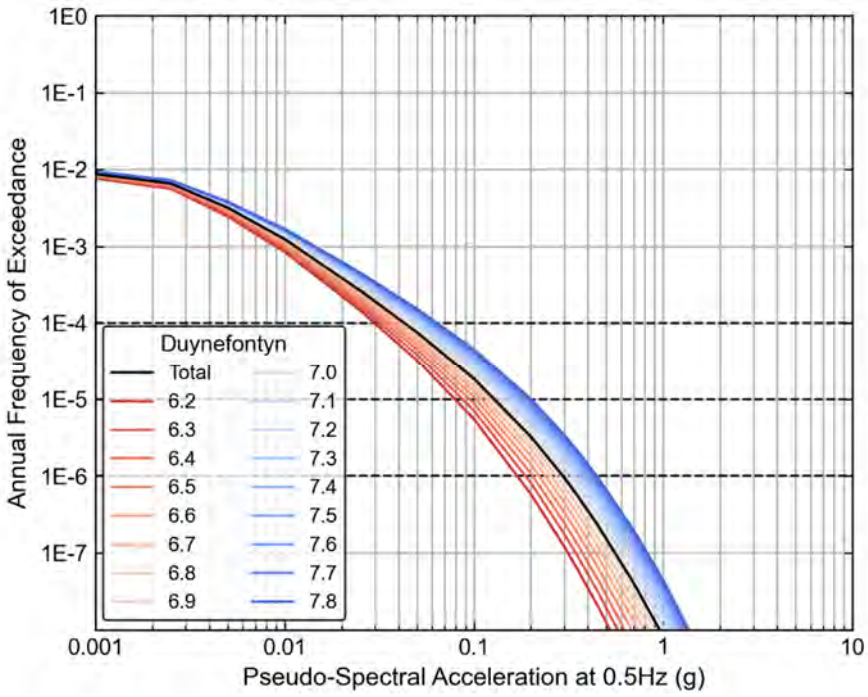

Figure G-42. Hazard sensitivity for 0.5 Hz to the host zone maximum magnitude branches at the new build site at Duynefontyn.

Sensitivity to Completeness Method

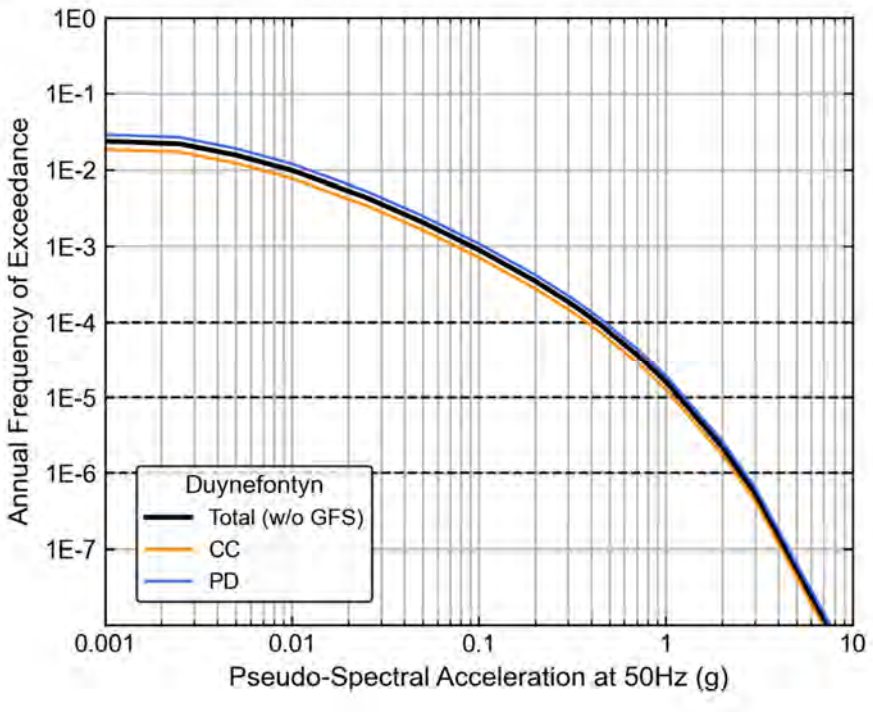

Figure G-43. Hazard sensitivity for 50 Hz to completeness method branches at the new build site at Duynefontyn.

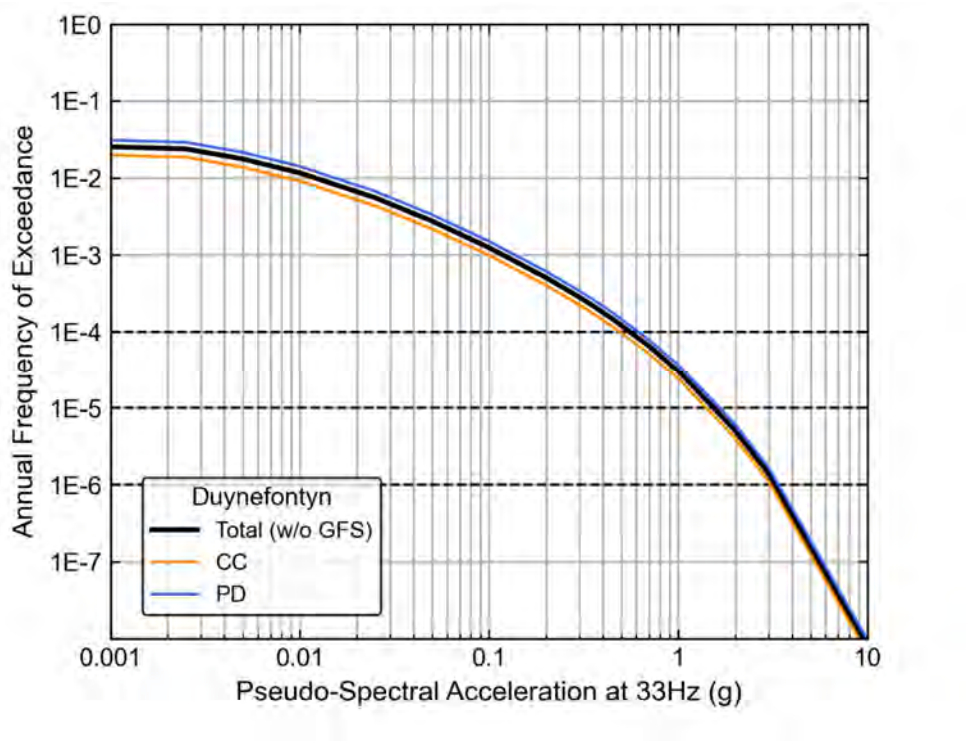

Figure G-44. Hazard sensitivity for 33 Hz to completeness method branches at the new build site at Duynefontyn.

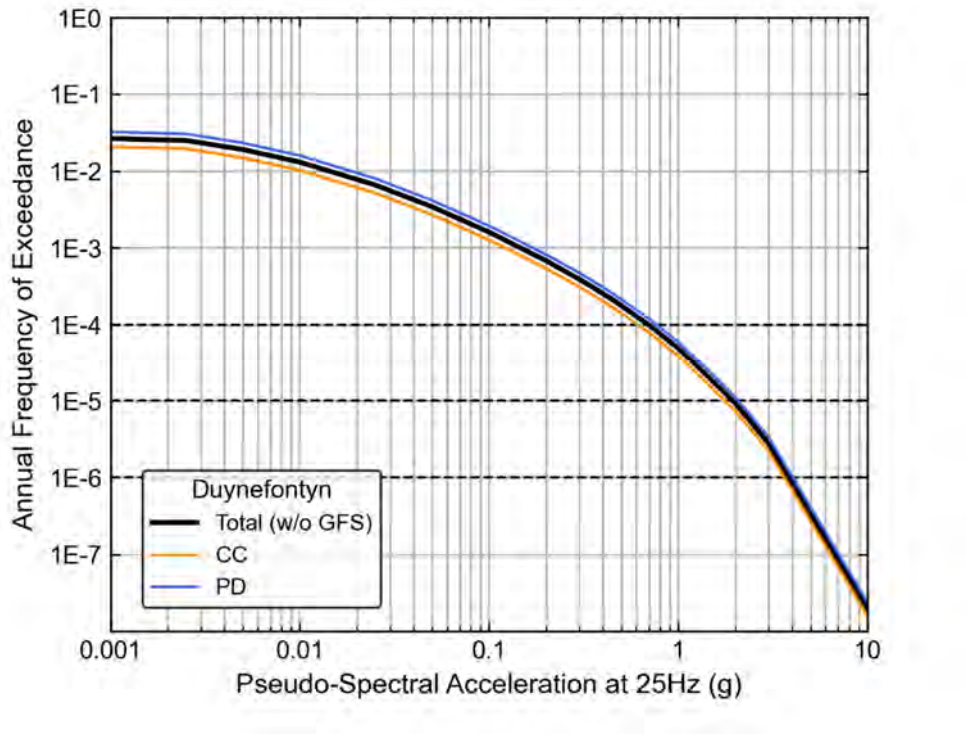

Figure G-45. Hazard sensitivity for 25 Hz to completeness method branches at the new build site at Duynefontyn.

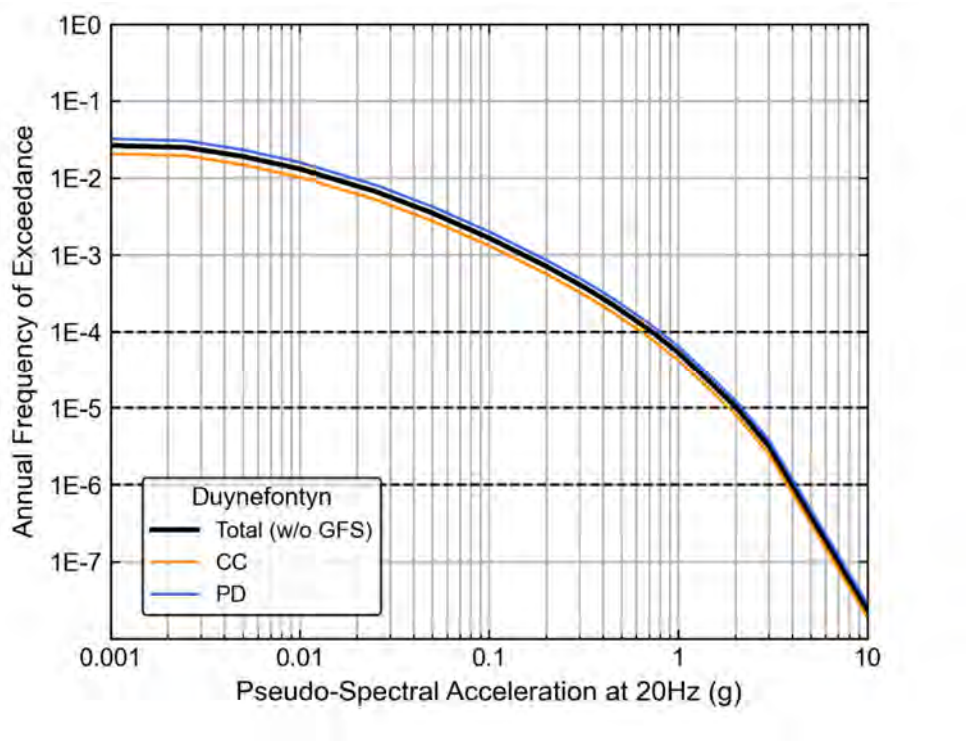

Figure G-46. Hazard sensitivity for 20 Hz to completeness method branches at the new build site at Duynefontyn.

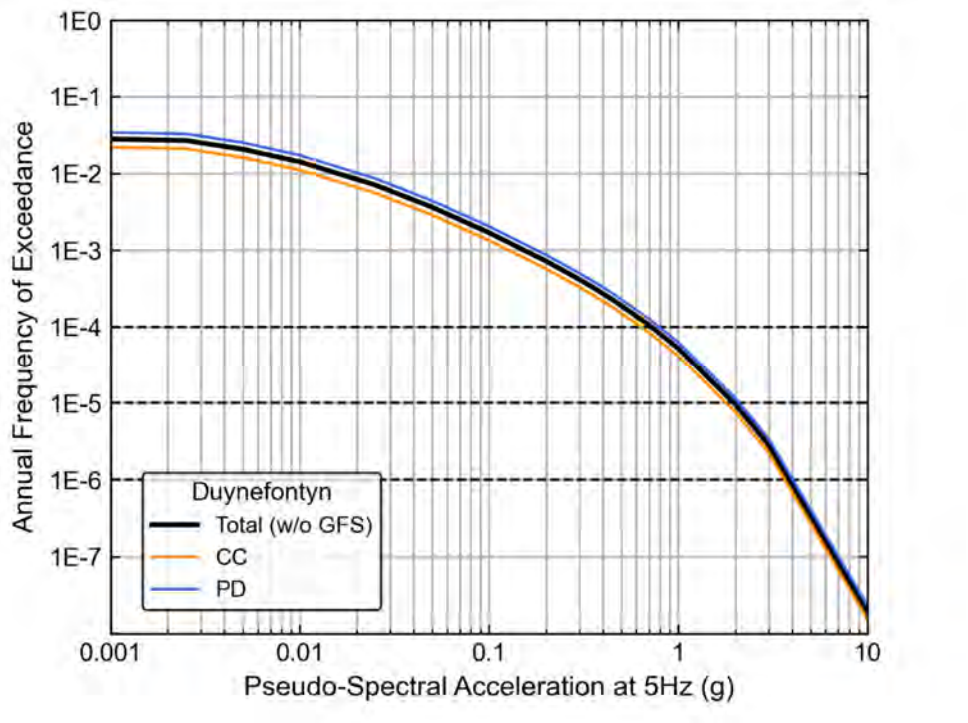

Figure G-47. Hazard sensitivity for 5 Hz to completeness method branches at the new build site at Duynefontyn.

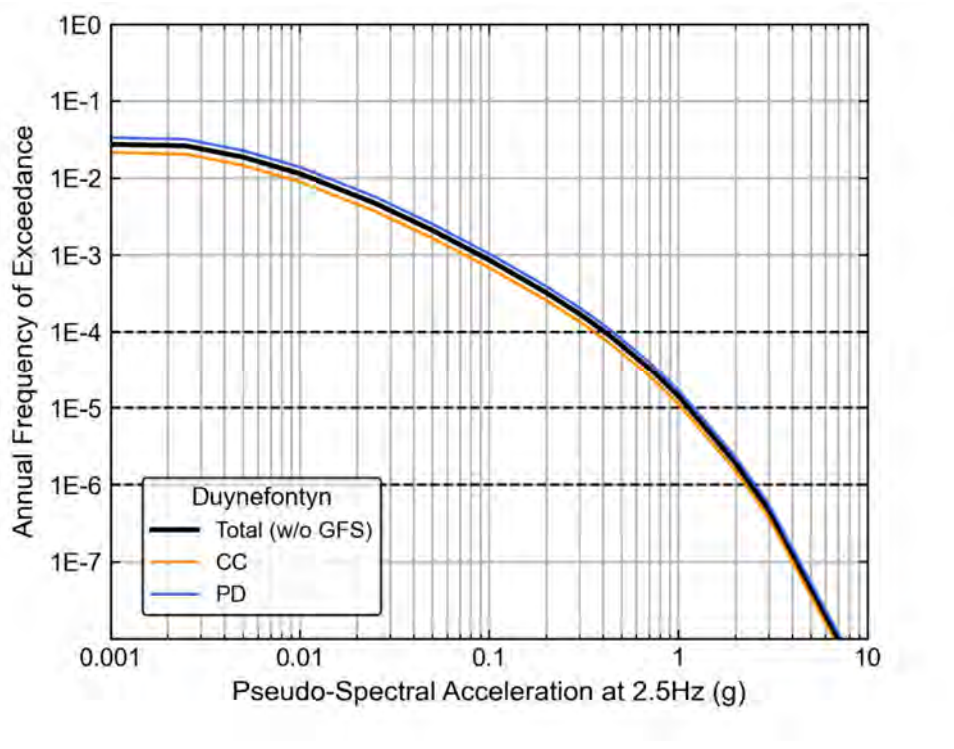

Figure G-48. Hazard sensitivity for 2.5 Hz to completeness method branches at the new build site at Duynefontyn.

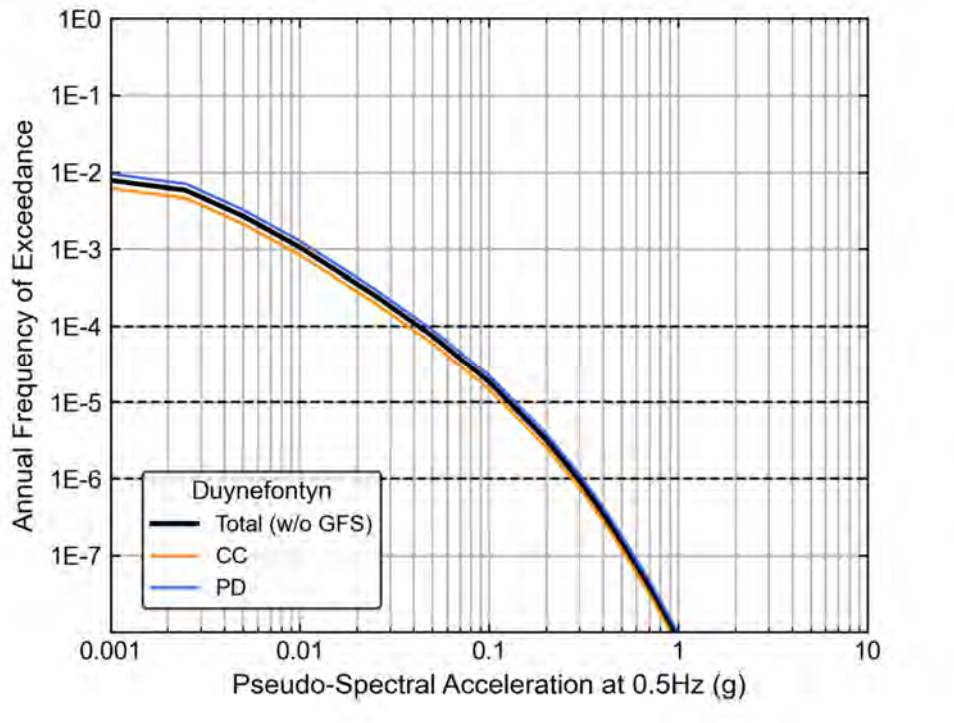

Figure G-49. Hazard sensitivity for 0.5 Hz to completeness method branches at the new build site at Duynefontyn.

Sensitivity to Host Zone Fault Type

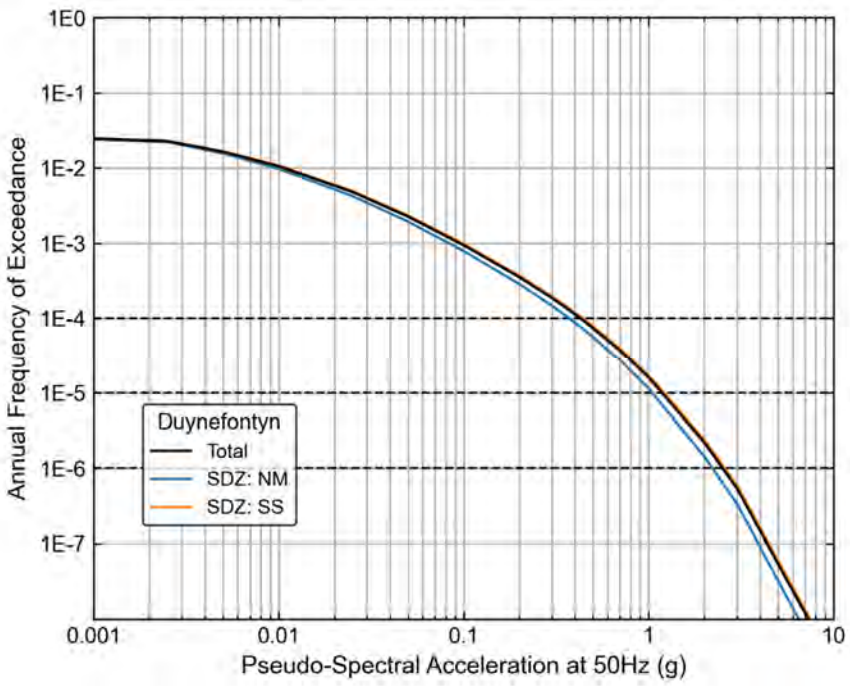

Figure G-50. Hazard sensitivity for 50 Hz to fault mechanism in the host zone for the new build site at Duynefontyn.

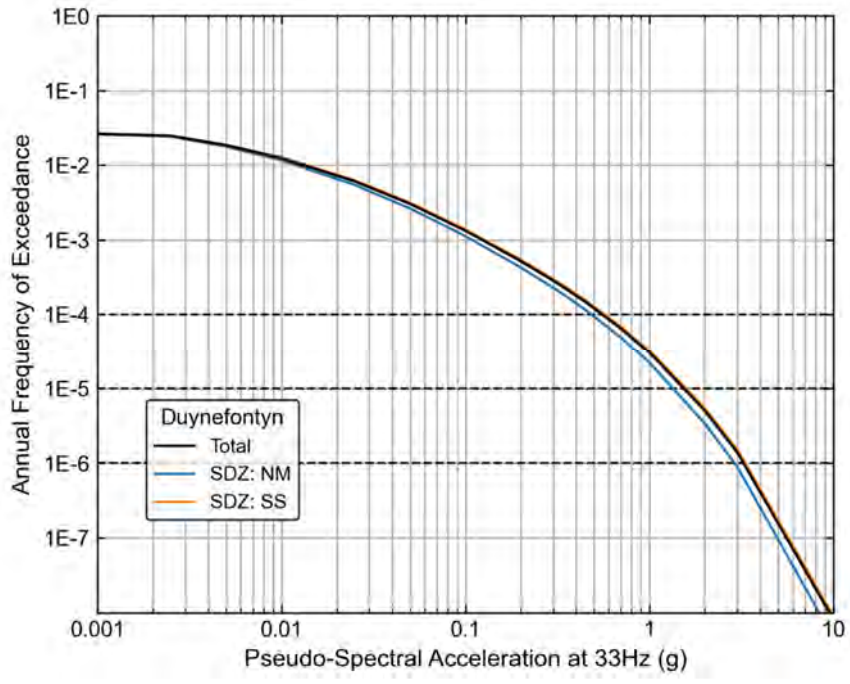

Figure G-51. Hazard sensitivity for 33 Hz to fault mechanism in the host zone for the new build site at Duynefontyn.

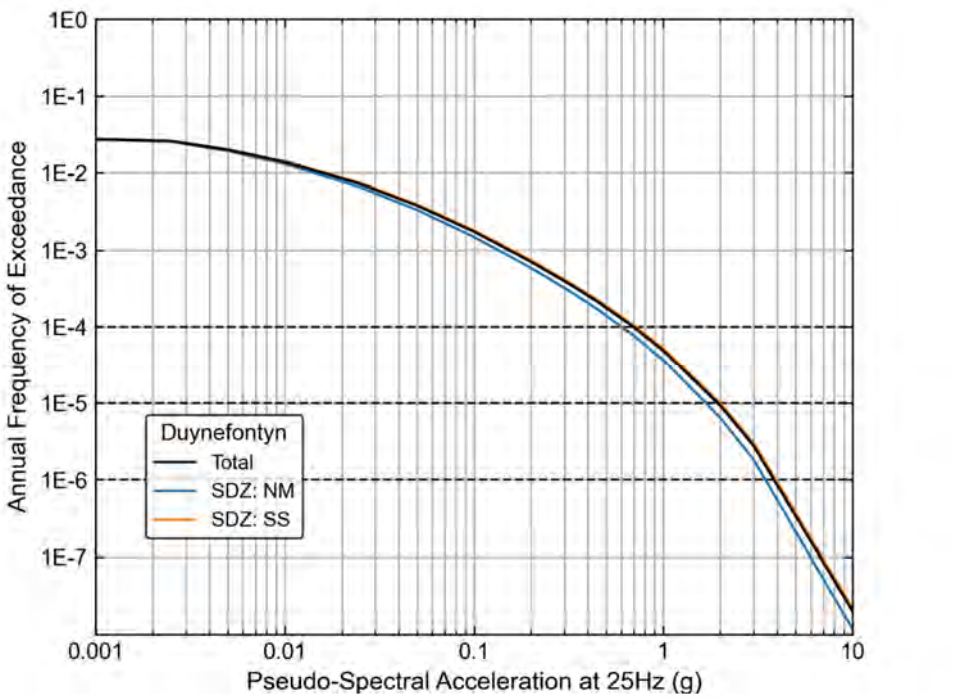

Figure G-52. Hazard sensitivity for 25 Hz to fault mechanism in the host zone for the new build site at Duynefontyn.

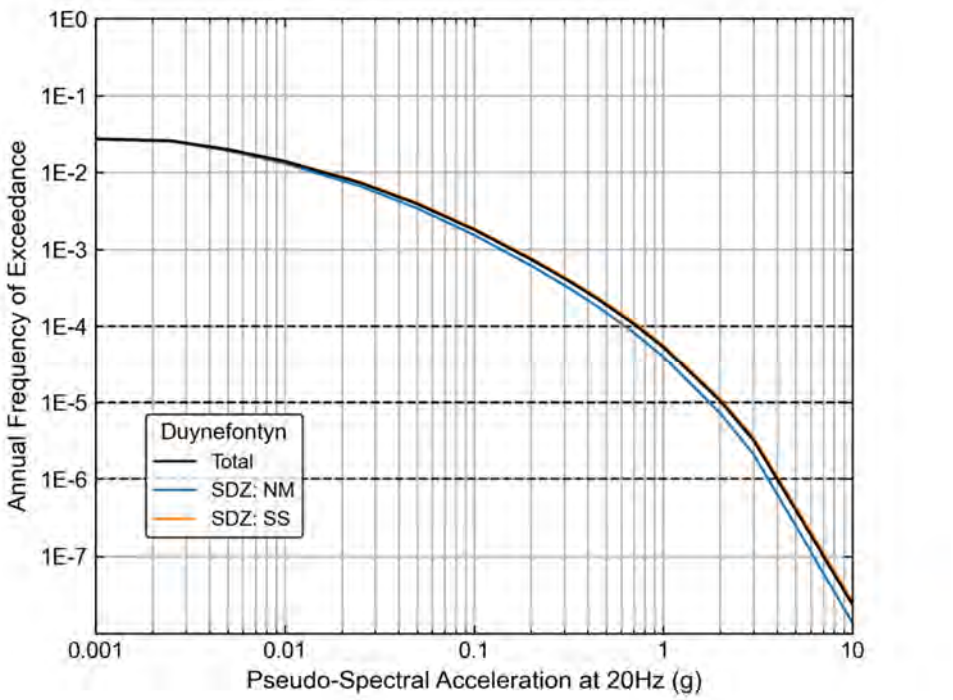

Figure G-53. Hazard sensitivity for 20 Hz to fault mechanism in the host zone for the new build site at Duynefontyn.

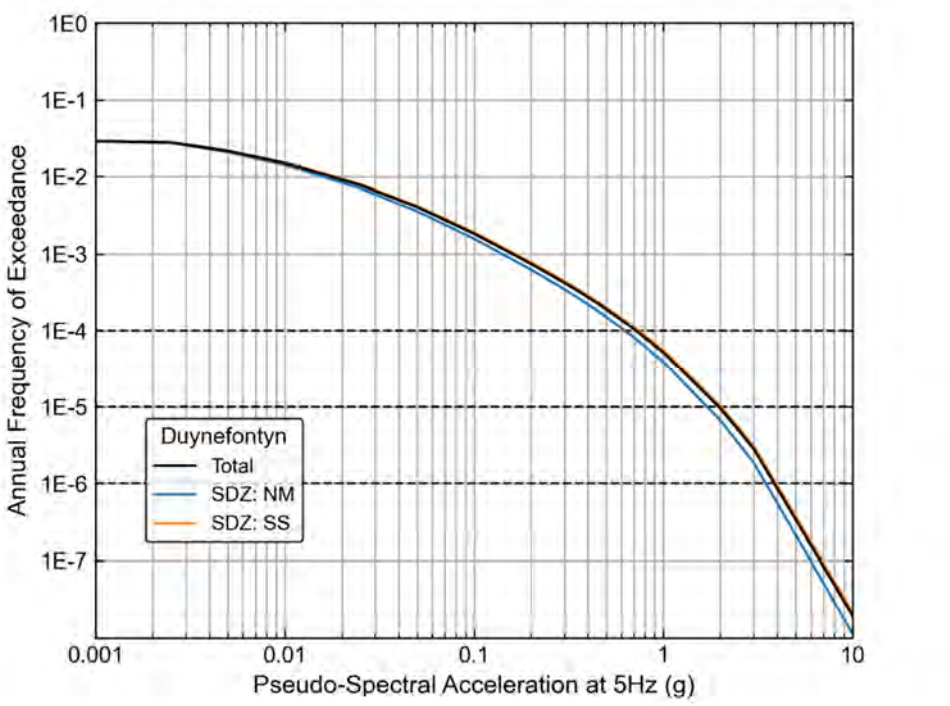

Figure G-54. Hazard sensitivity for 5 Hz to fault mechanism in the host zone for the new build site at Duynefontyn.

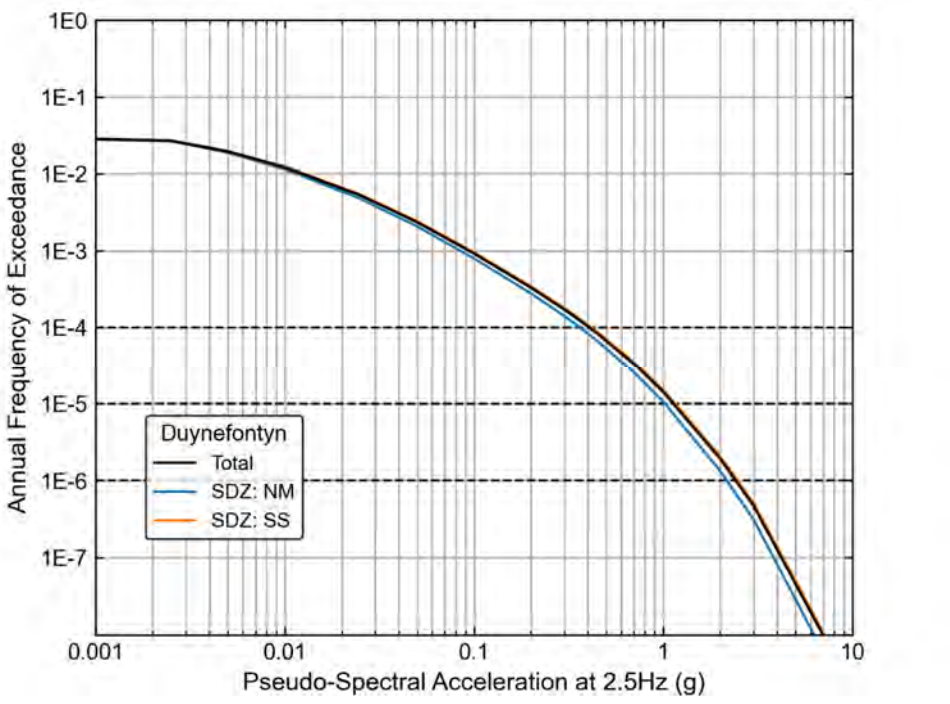

Figure G-55. Hazard sensitivity for 2.5 Hz to fault mechanism in the host zone for the new build site at Duynefontyn.

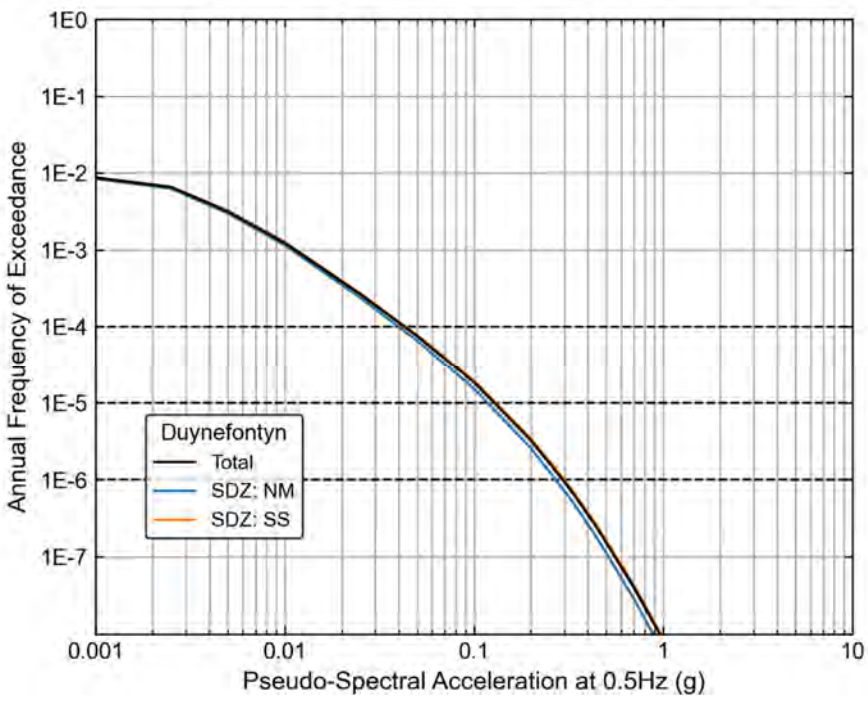

Figure G-56. Hazard sensitivity for 0.5 Hz to fault mechanism in the host zone for the new build site at Duynefontyn.

Sensitivity to Regional *b*-Value Calculation Method

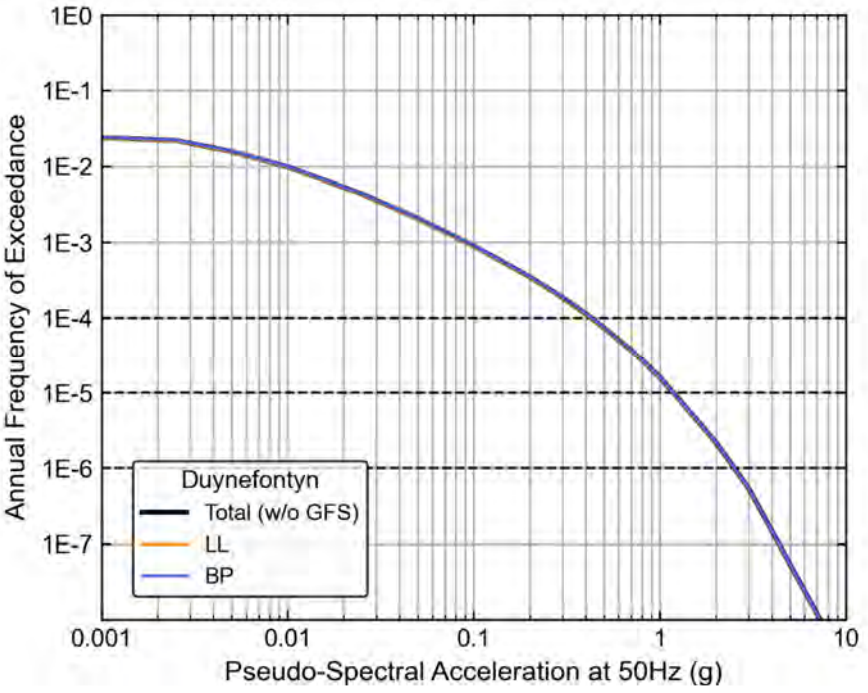

Figure G-57. Hazard sensitivity to regional *b*-value calculation method for 50 Hz at the new build site at Duynefontyn.

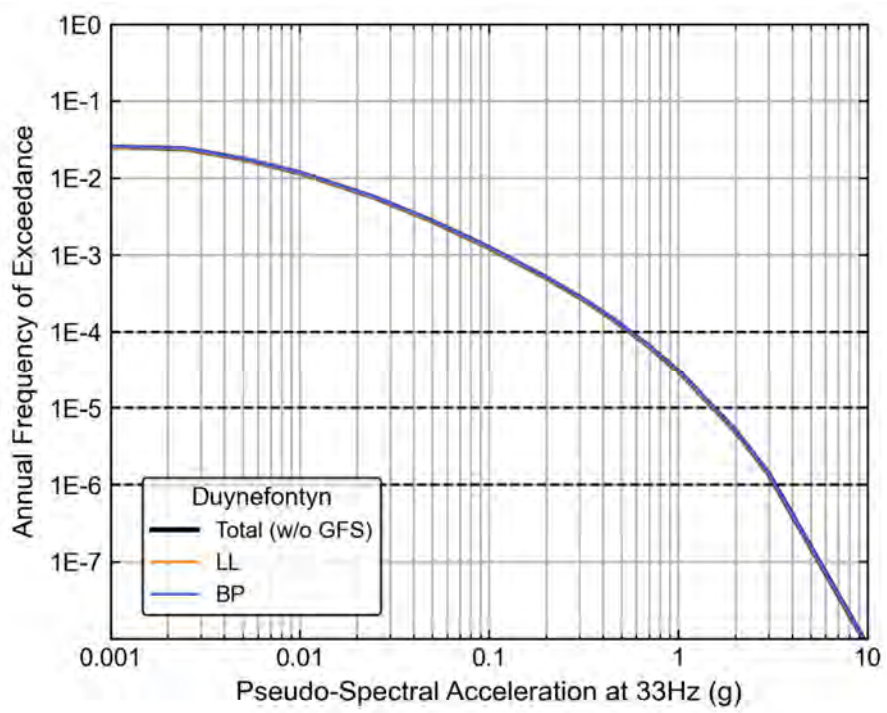

Figure G-58. Hazard sensitivity to regional *b*-value calculation method for 33 Hz at the new build site at Duynefontyn.

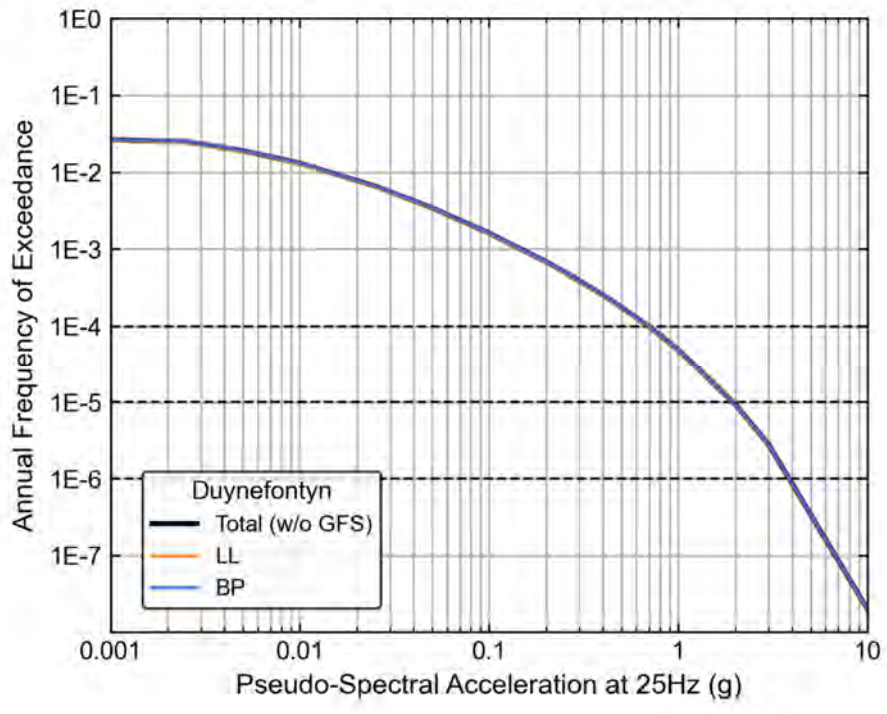

Figure G-59. Hazard sensitivity to regional *b*-value calculation method for 25 Hz at the new build site at Duynefontyn.

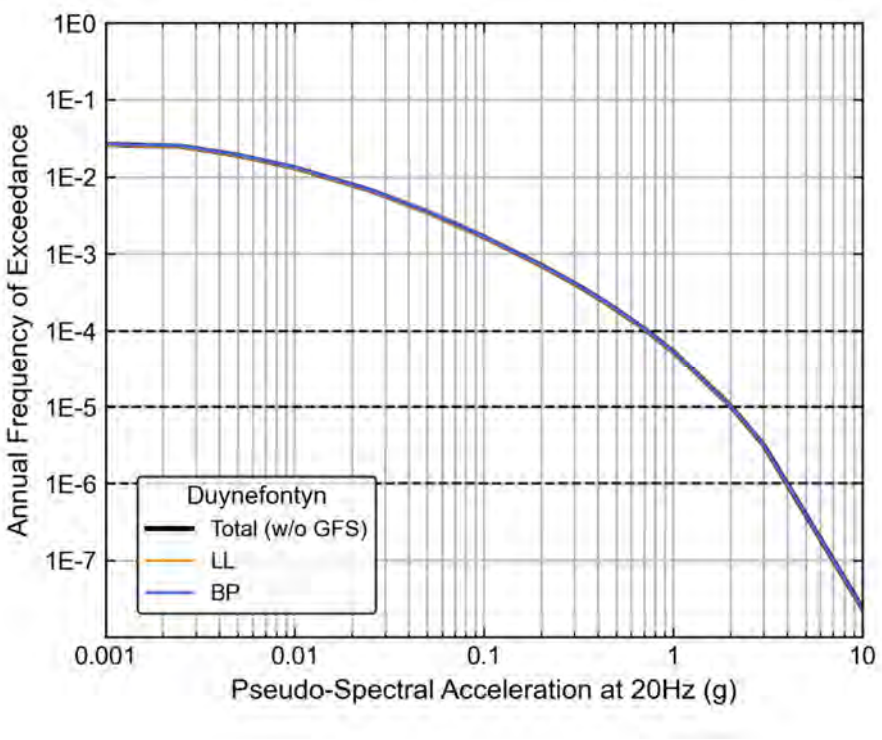

Figure G-60. Hazard sensitivity to regional *b*-value calculation method for 20 Hz at the new build site at Duynefontyn.

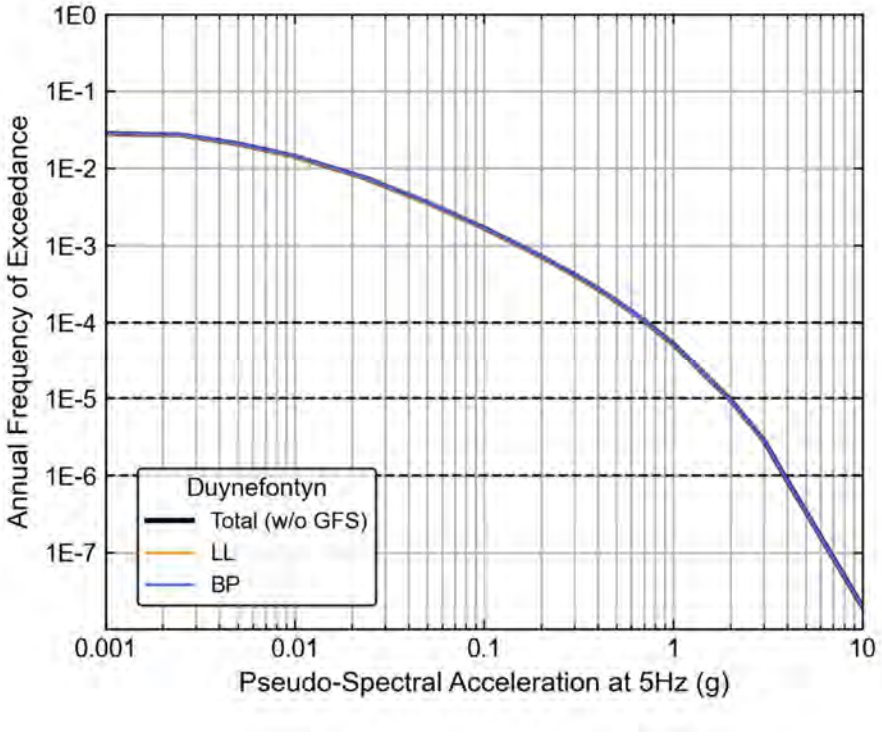

Figure G-61. Hazard sensitivity to regional *b*-value calculation method for 5 Hz at the new build site at Duynefontyn.

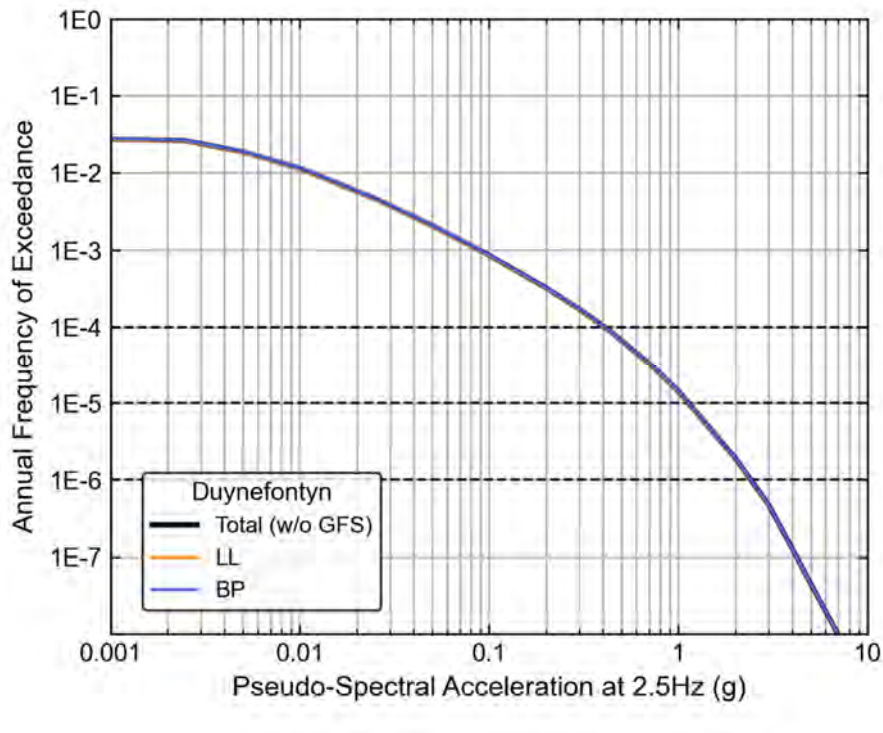

Figure G-62. Hazard sensitivity to regional *b*-value calculation method for 2.5 Hz at the new build site at Duynefontyn.

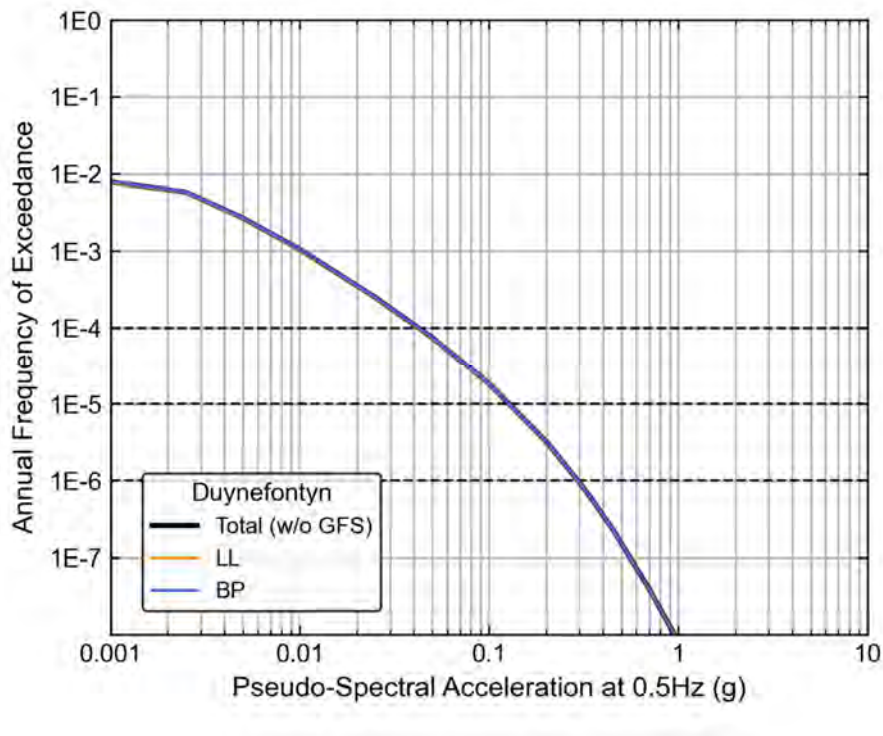

Figure G-63. Hazard sensitivity to regional *b*-value calculation method for 0.5 Hz at the new build site at Duynefontyn.

APPENDIX H. EXPANDED HAZARD SENSITIVITY ANALYSIS FOR THE KOEBERG NUCLEAR POWER STATION (KNPS) AT THE DUYNEFONTYN SITE.

APPENDIX H. EXPANDED HAZARD SENSITIVITY ANALYSES FOR KOEBERG NUCLEAR POWER STATION

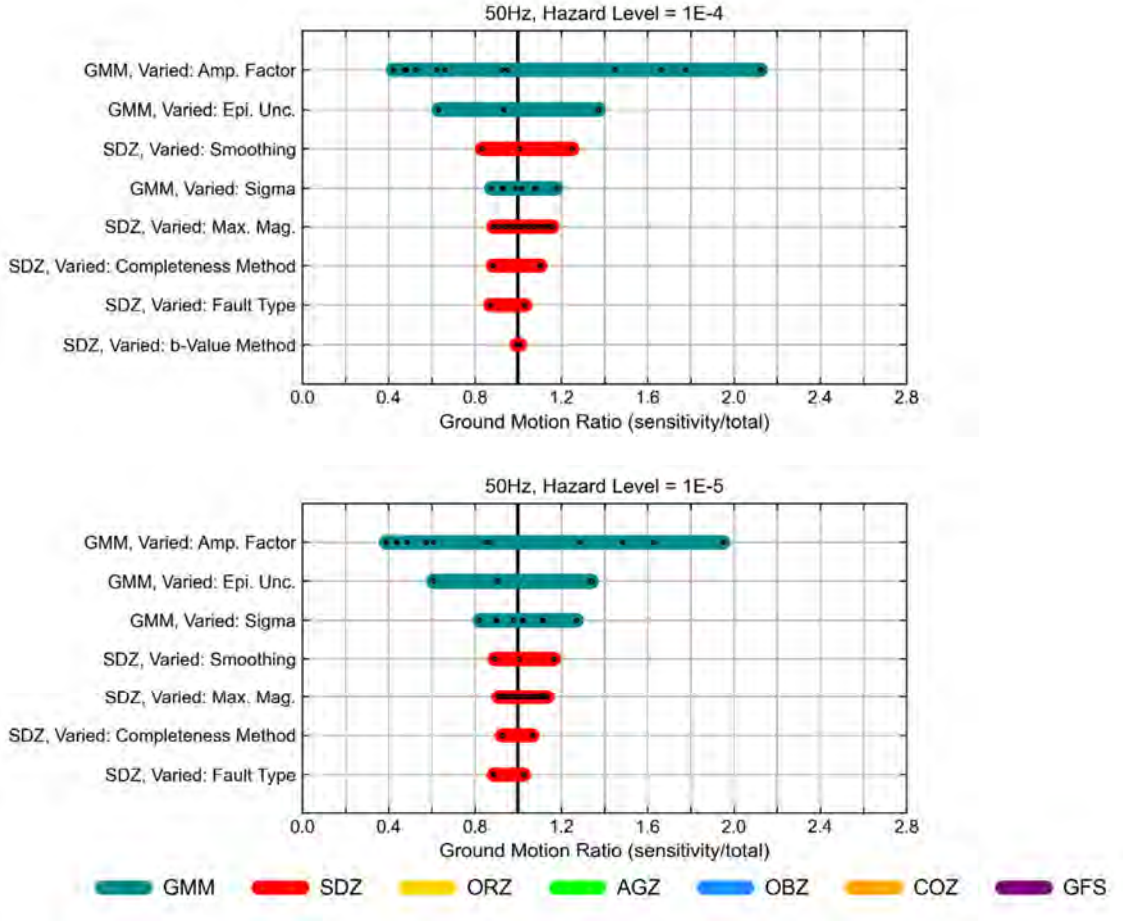

Figure H-1. Hazard sensitivity tornado plots at 50 Hz for the Koeberg Nuclear Power Station.

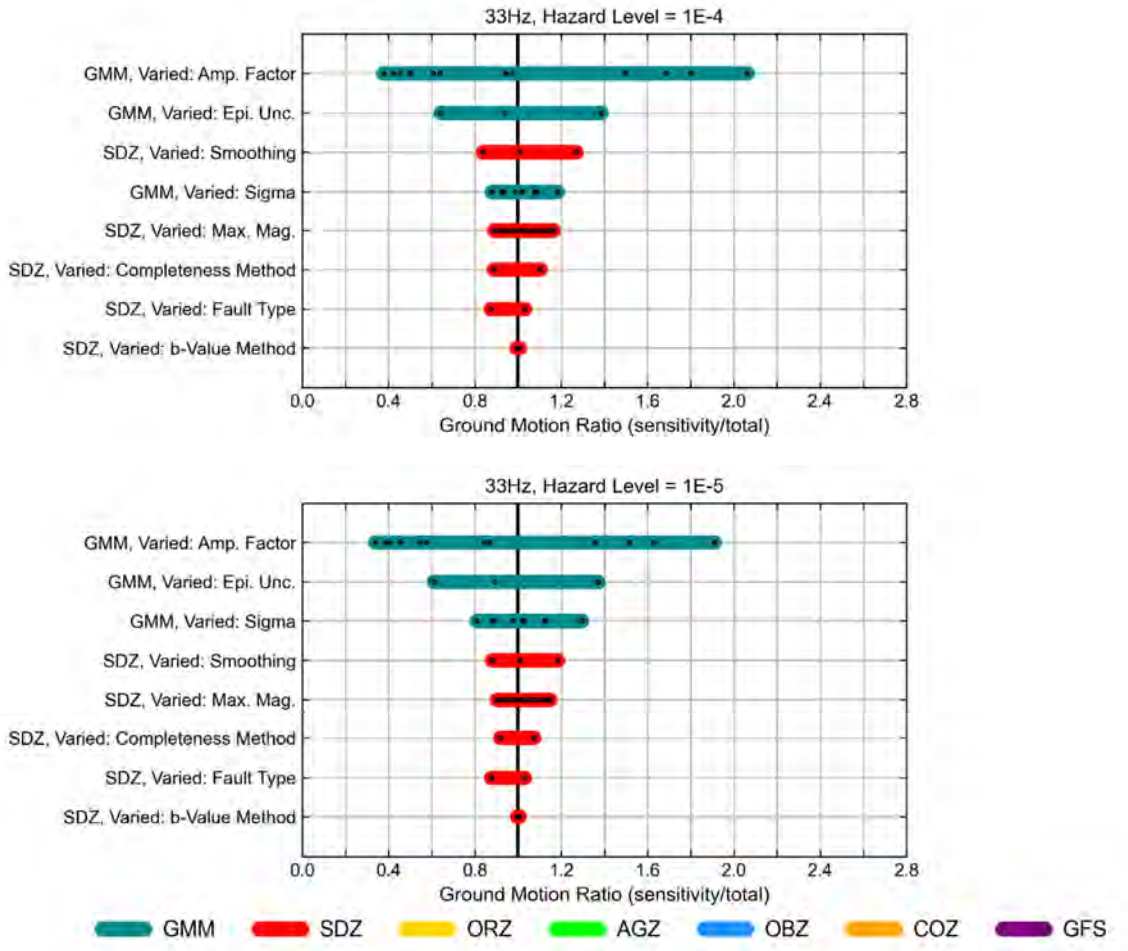

Figure H-2. Hazard sensitivity tornado plots at 33 Hz for the Koeberg Nuclear Power Station.

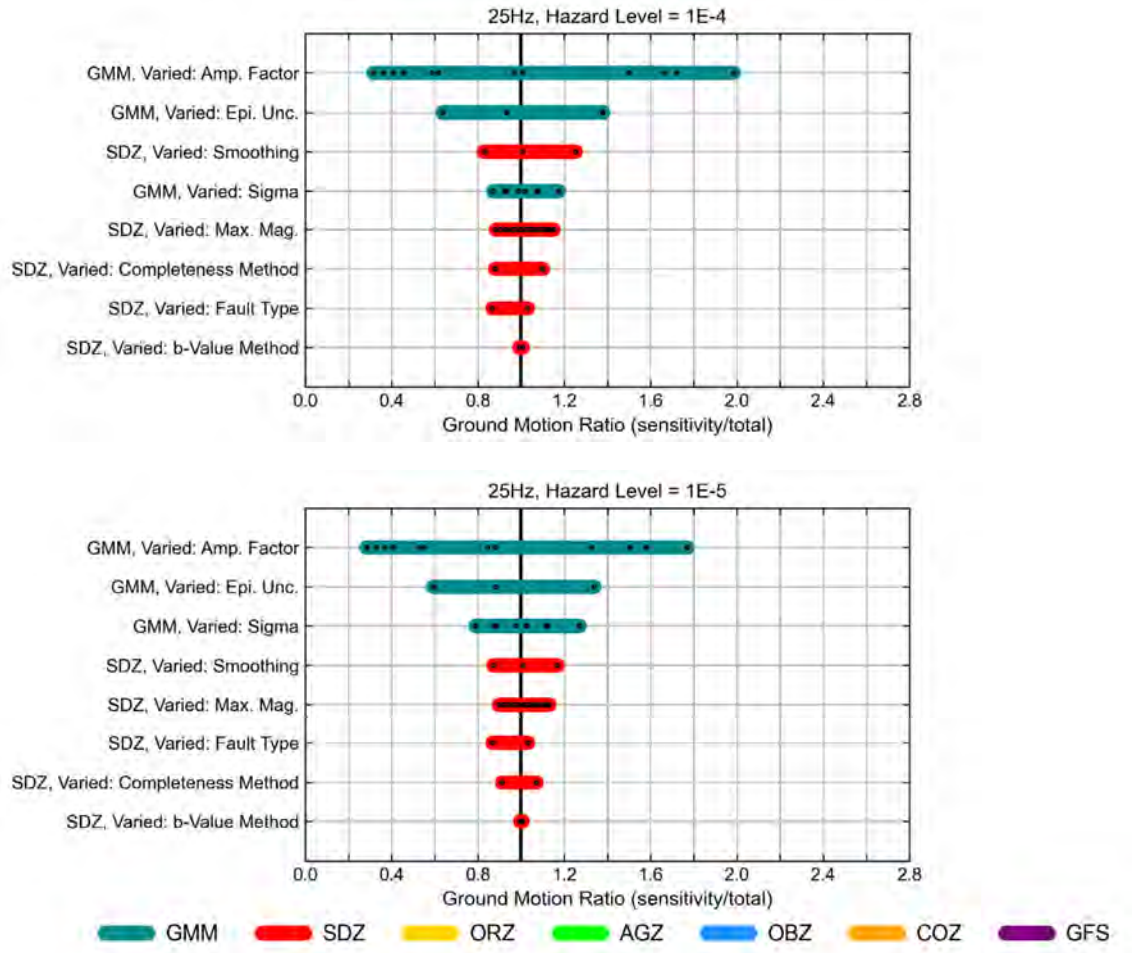

Figure H-3. Hazard sensitivity tornado plots at 25 Hz for the Koeberg Nuclear Power Station.

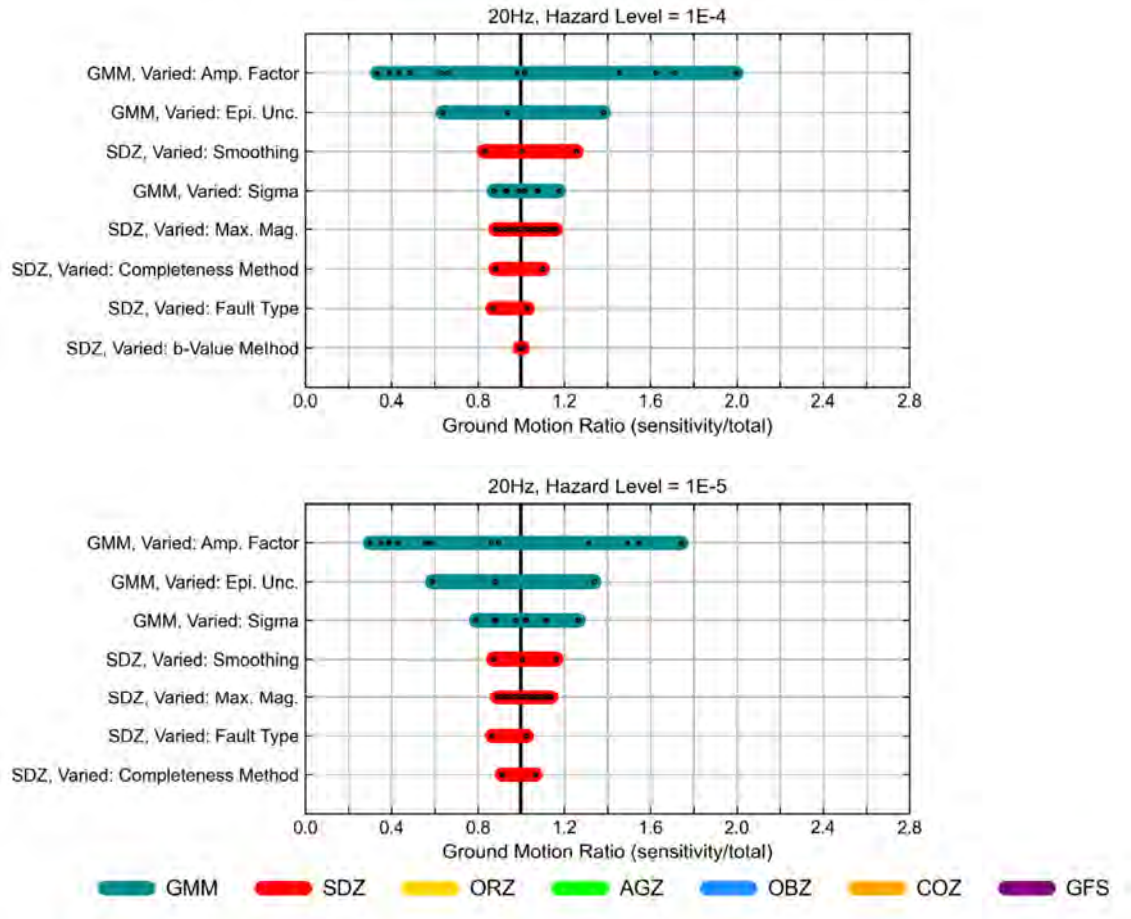

Figure H-4. Hazard sensitivity tornado plots at 20 Hz for the Koeberg Nuclear Power Station.

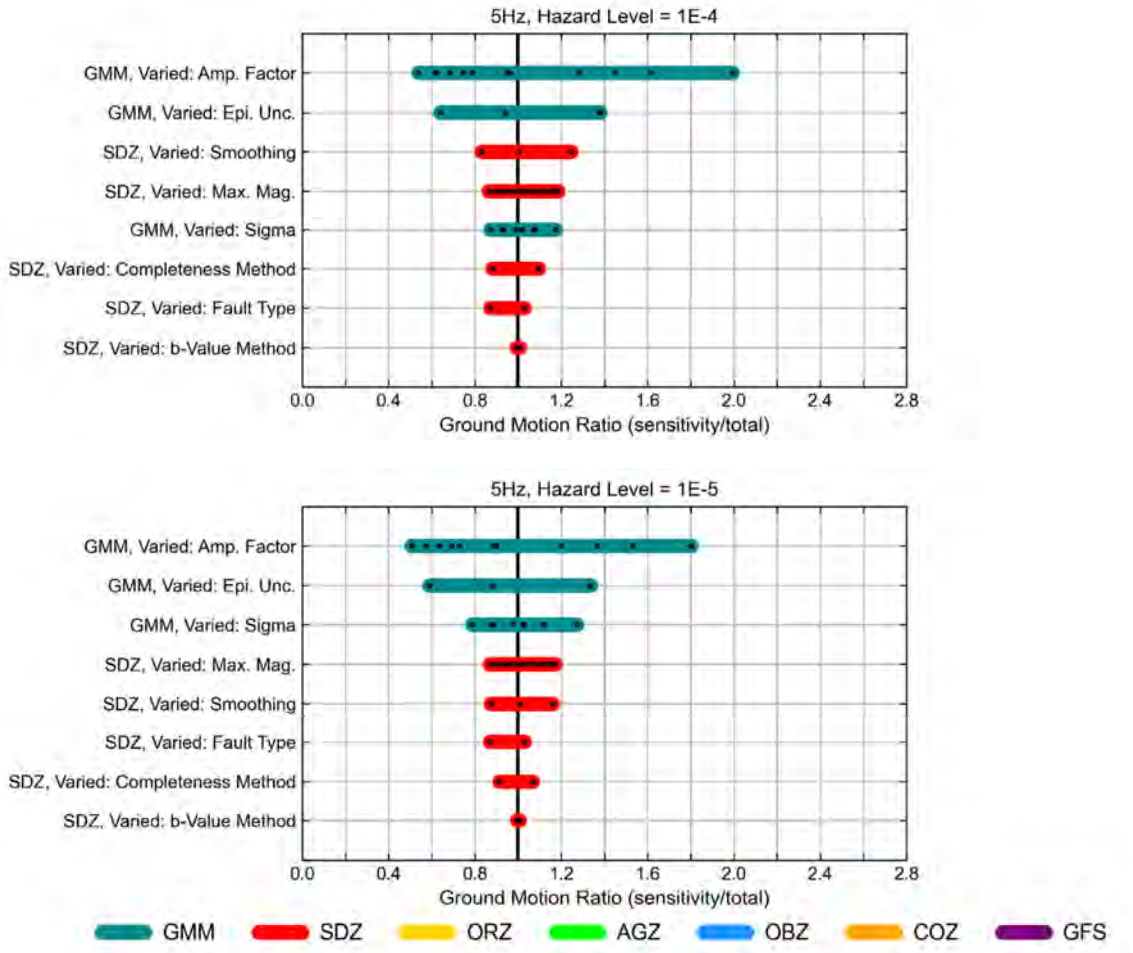

Figure H-5. Hazard sensitivity tornado plots at 5 Hz for the Koeberg Nuclear Power Station.

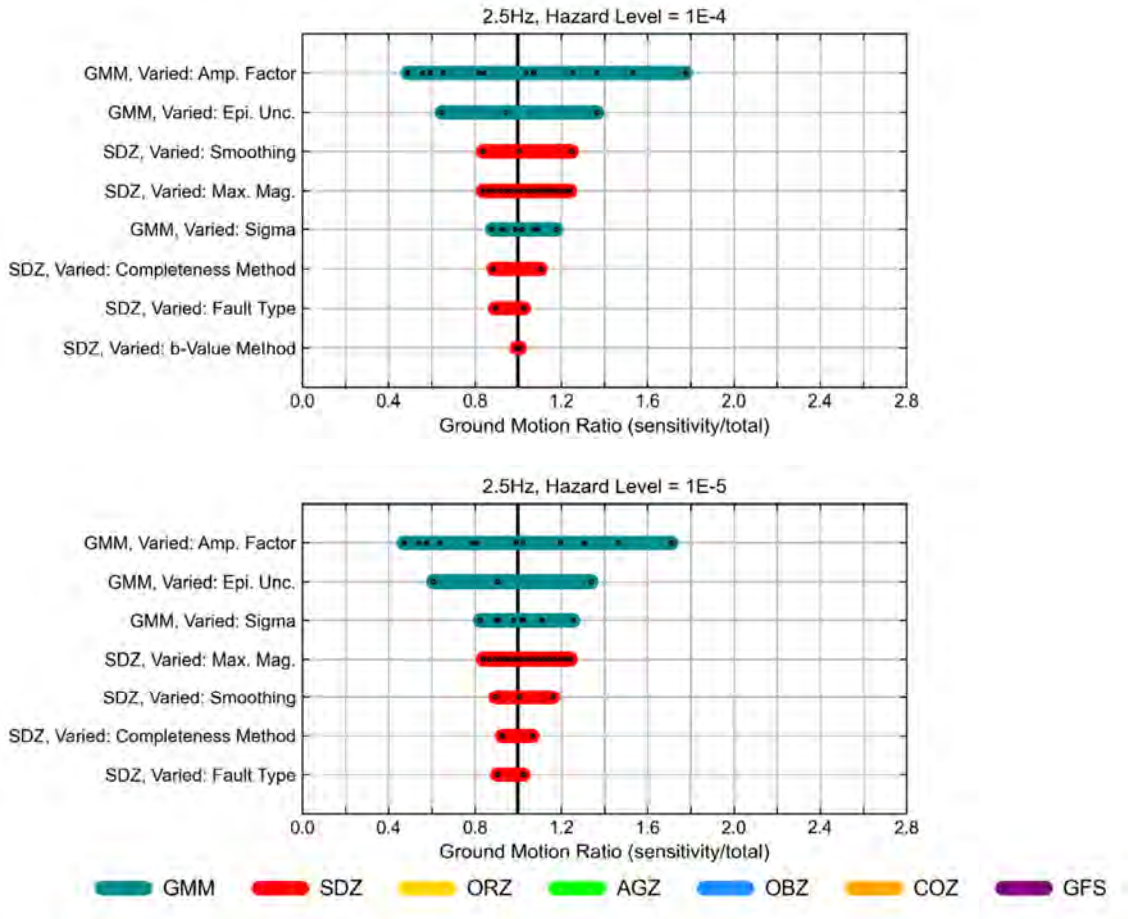

Figure H-6. Hazard sensitivity tornado plots at 2.5 Hz for the Koeberg Nuclear Power Station.

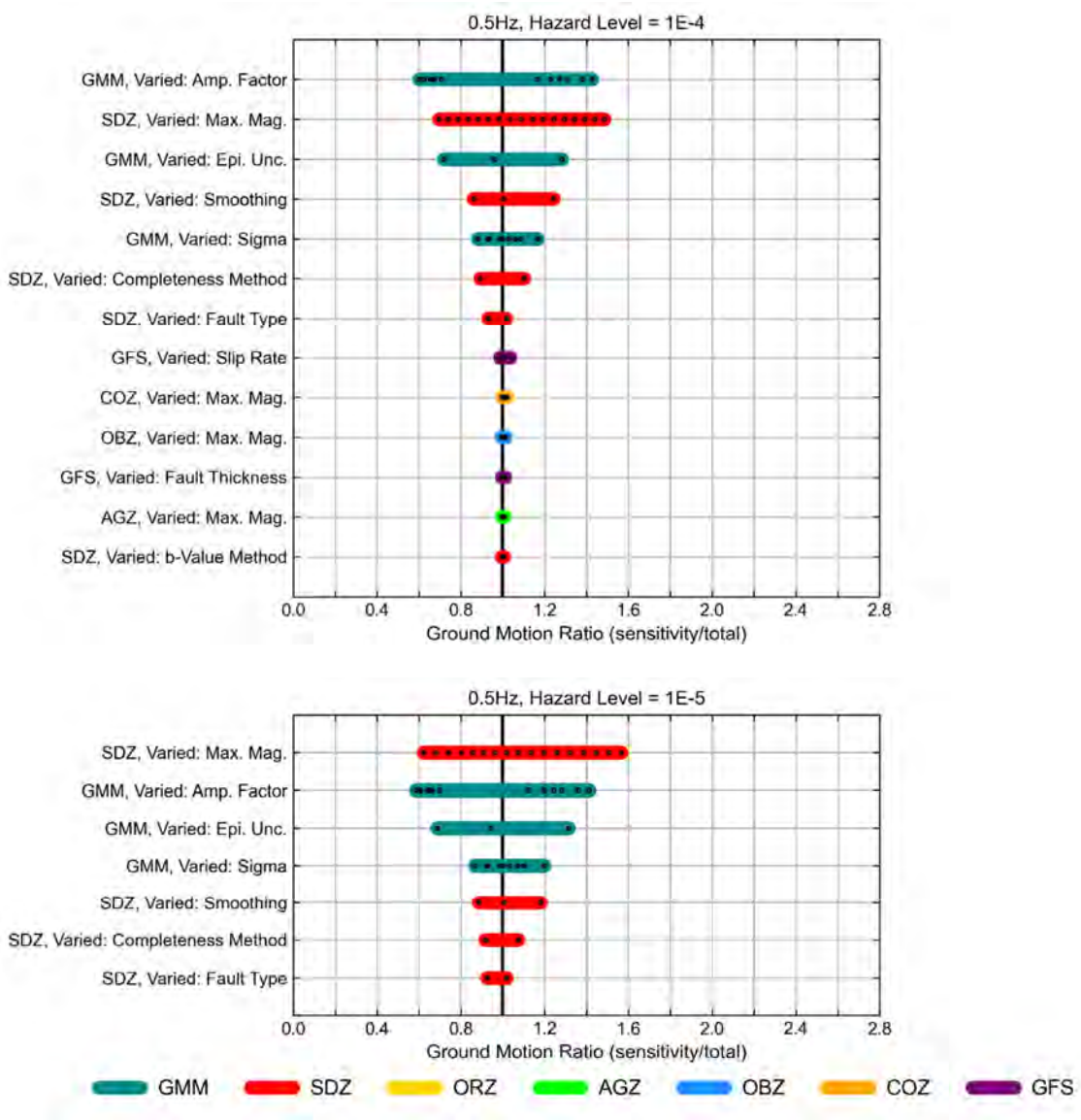

Figure H-7. Hazard sensitivity tornado plots at 0.5 Hz for the Koeberg Nuclear Power Station.

H.1 SENSITIVITY TO GROUND-MOTION MODEL

Sensitivity to Site Adjustment Factor

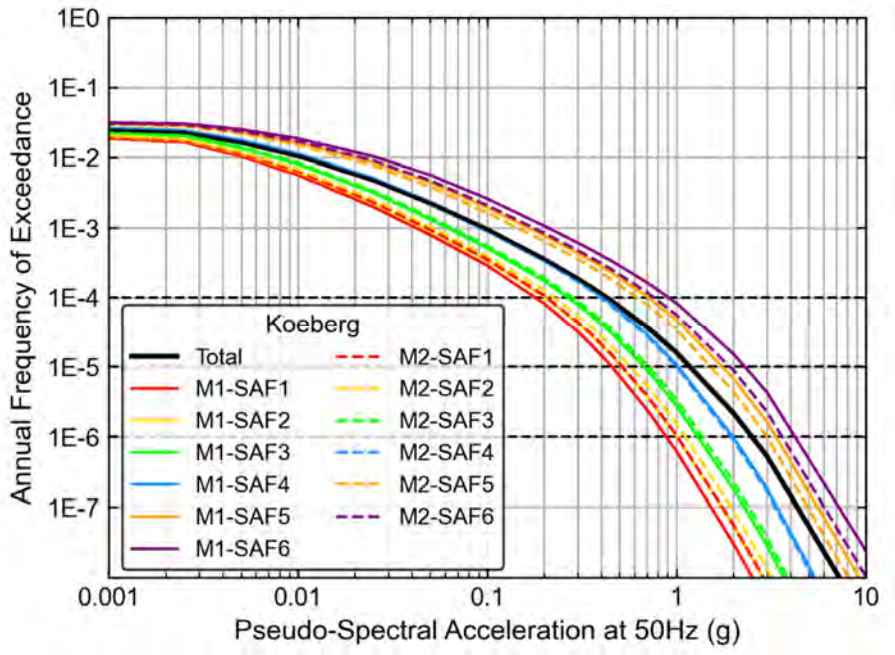

Figure H-8. Hazard sensitivity to the site response branches for 50 Hz at the Koeberg Nuclear Power Station.

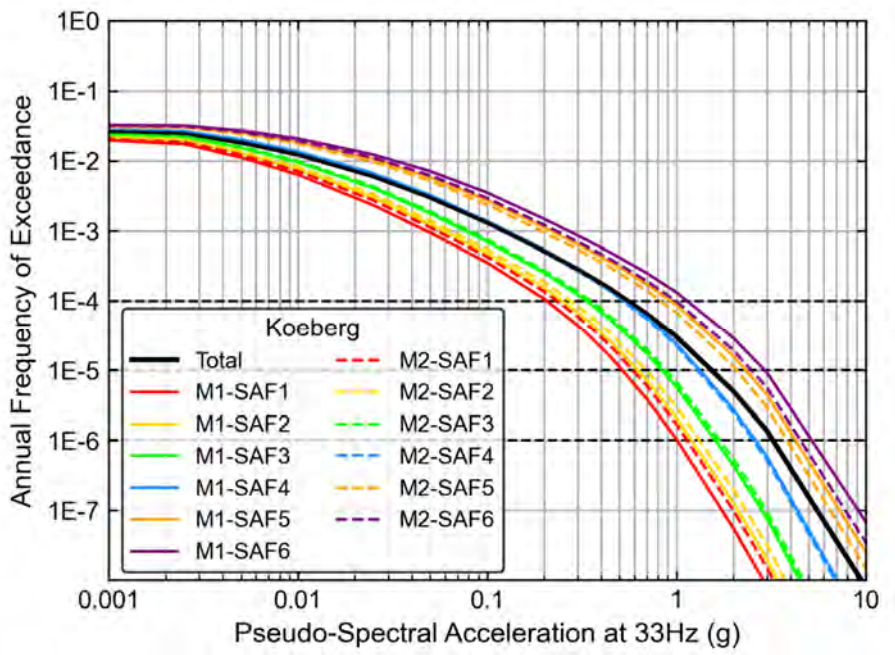

Figure H-9. Hazard sensitivity to the site response branches for 33 Hz at the Koeberg Nuclear Power Station.

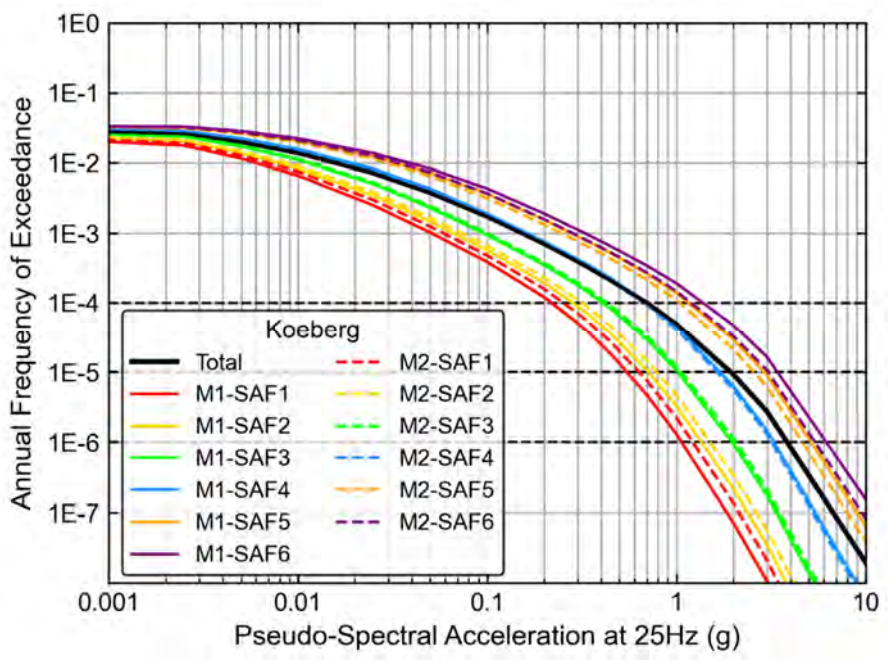

Figure H-10. Hazard sensitivity to the site response branches for 25 Hz at the Koeberg Nuclear Power Station.

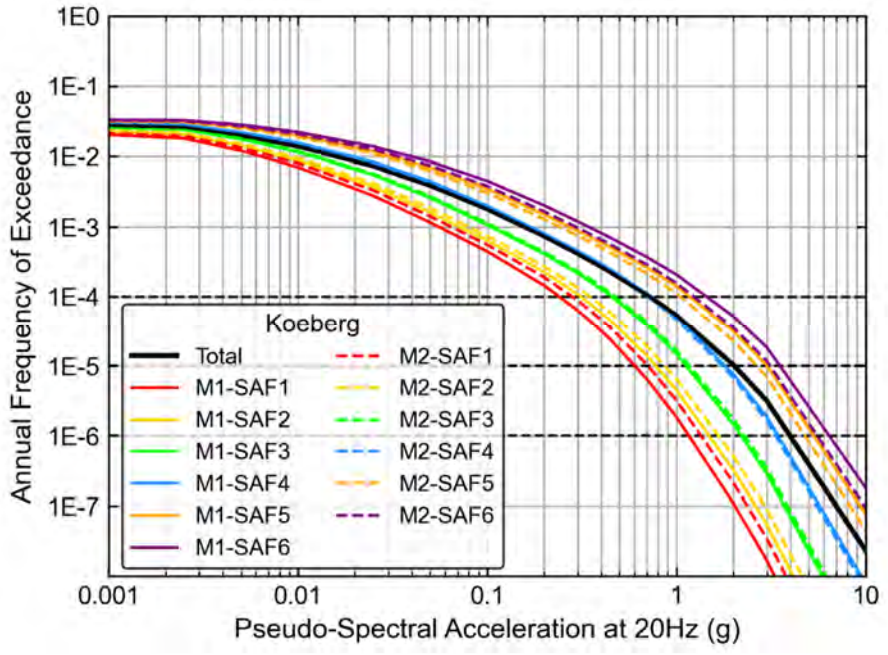

Figure H-11. Hazard sensitivity to the site response branches for 20 Hz at the Koeberg Nuclear Power Station.

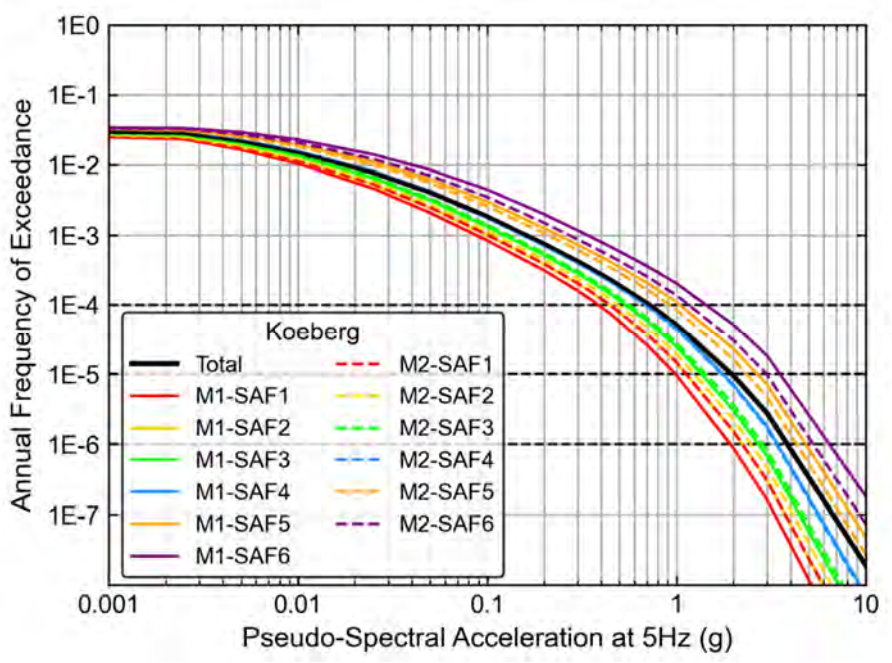

Figure H-12. Hazard sensitivity to the site response branches for 5 Hz at the Koeberg Nuclear Power Station.

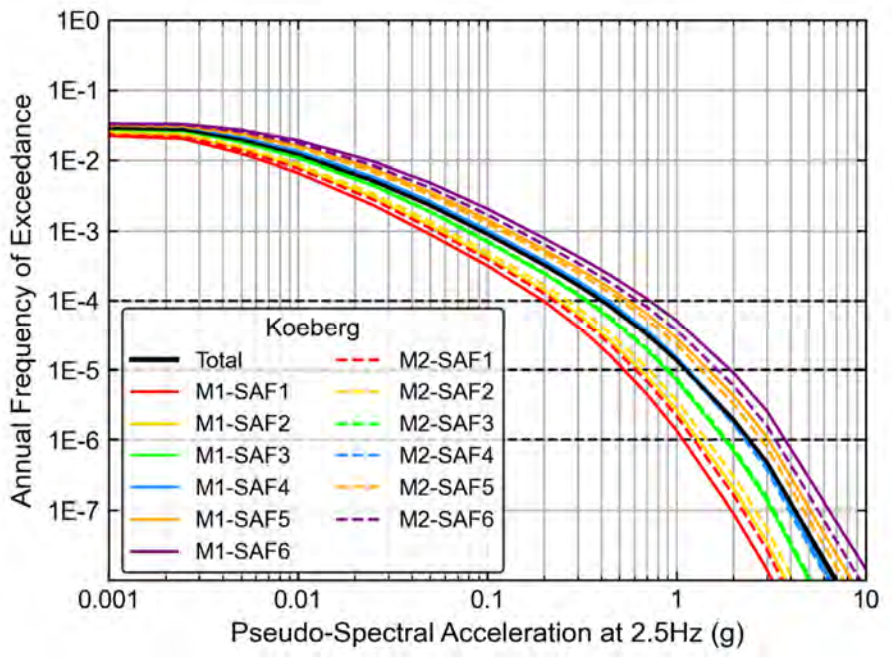

Figure H-13. Hazard sensitivity to the site response branches for 2.5 Hz at the Koeberg Nuclear Power Station.

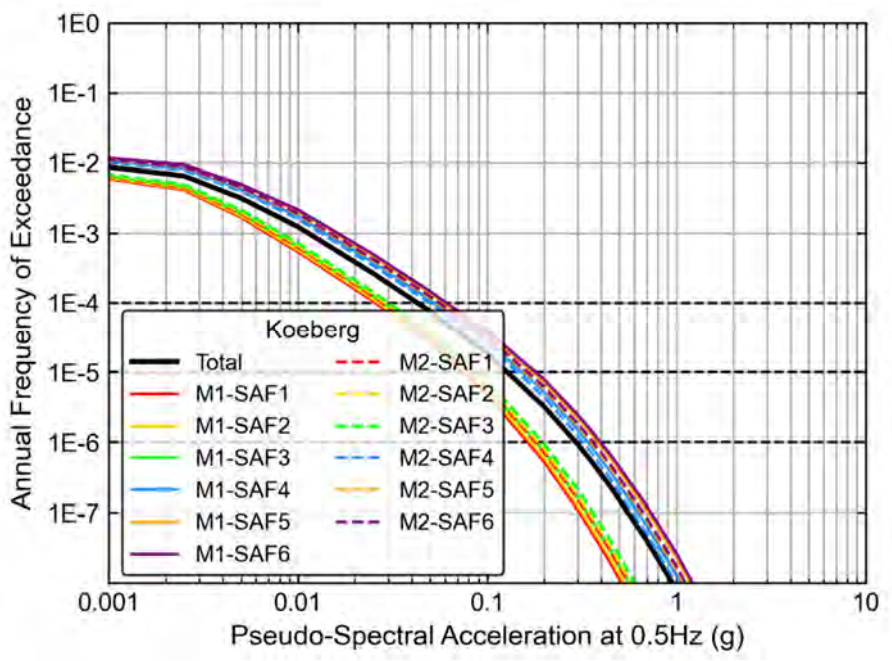

Figure H-14. Hazard sensitivity to the site response branches for 0.5 Hz at the Koeberg Nuclear Power Station.

Sensitivity to GMM Epistemic Uncertainty Model

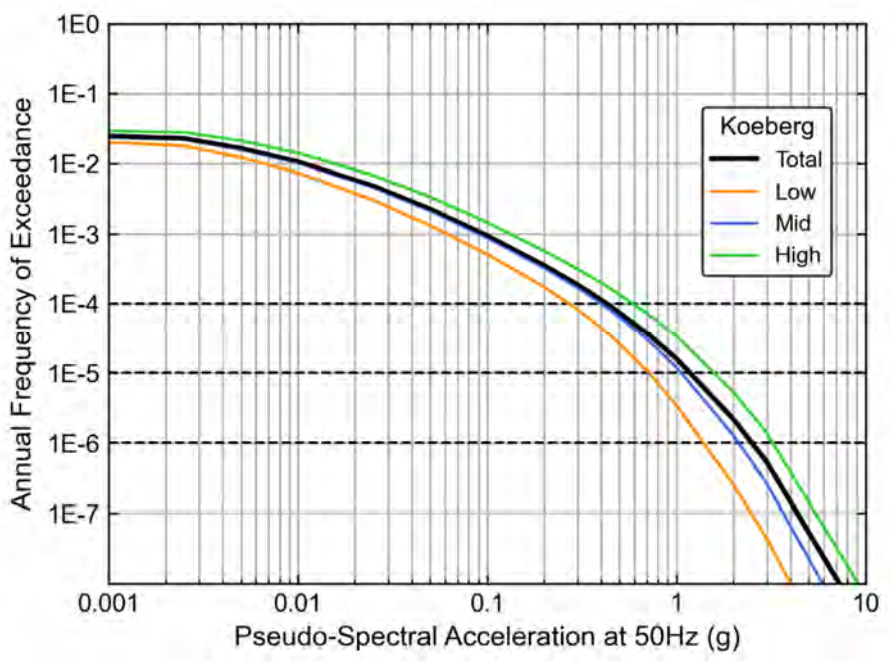

Figure H-15. Hazard sensitivity to the epistemic uncertainty model for 50 Hz at the Koeberg Nuclear Power Station.

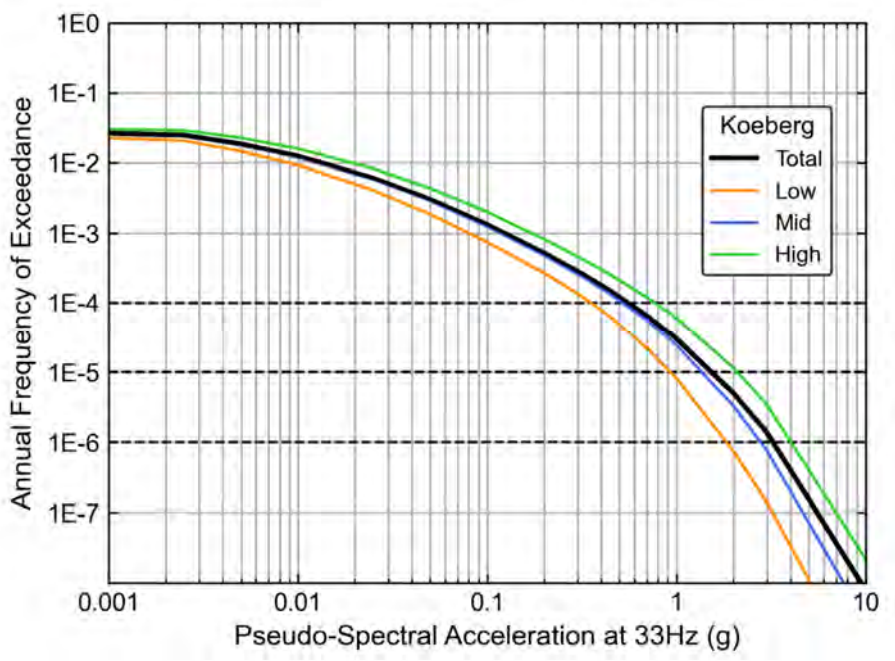

Figure H-16. Hazard sensitivity to the epistemic uncertainty model for 33 Hz at the Koeberg Nuclear Power Station.

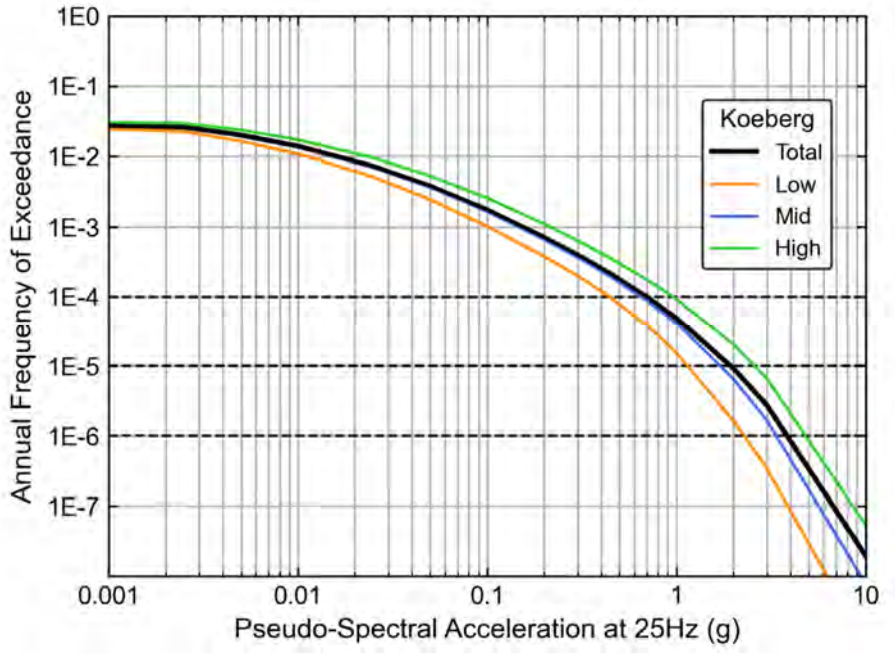

Figure H-17. Hazard sensitivity to the epistemic uncertainty model for 25 Hz at the Koeberg Nuclear Power Station.

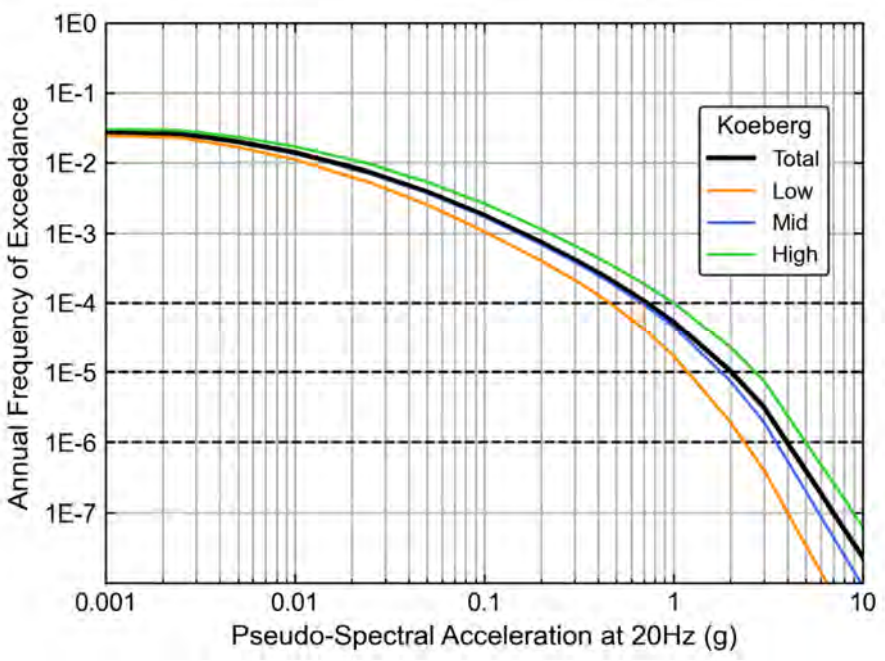

Figure H-18. Hazard sensitivity to the epistemic uncertainty model for 20 Hz at the Koeberg Nuclear Power Station.

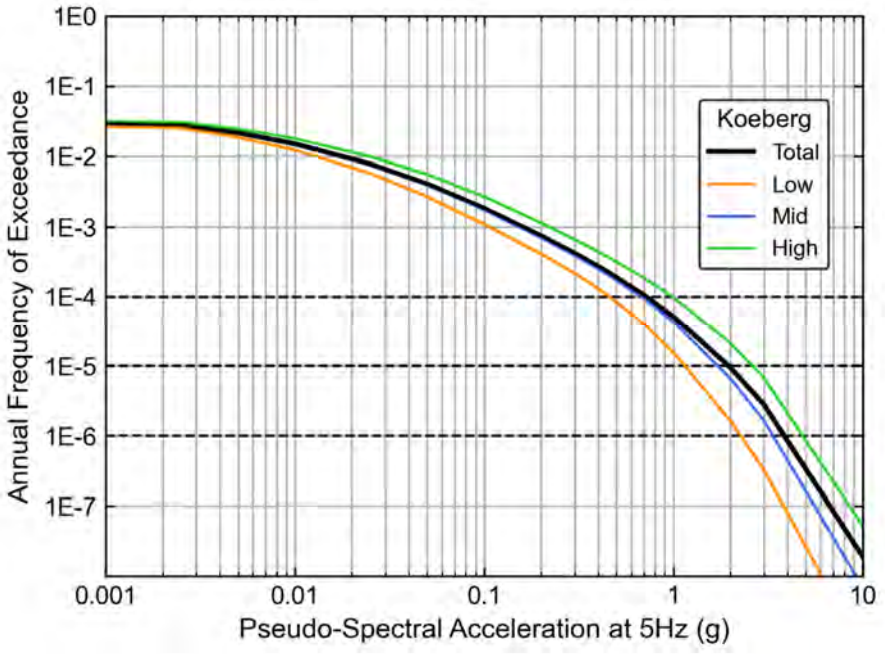

Figure H-19. Hazard sensitivity to the epistemic uncertainty model for 5 Hz at the Koeberg Nuclear Power Station.

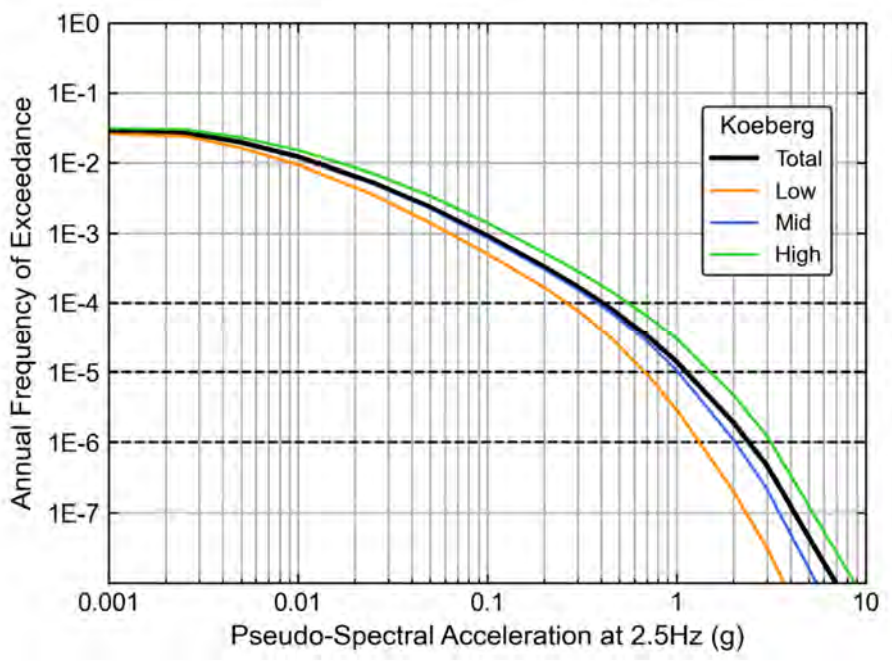

Figure H-20. Hazard sensitivity to the epistemic uncertainty model for 2.5 Hz at the Koeberg Nuclear Power Station.

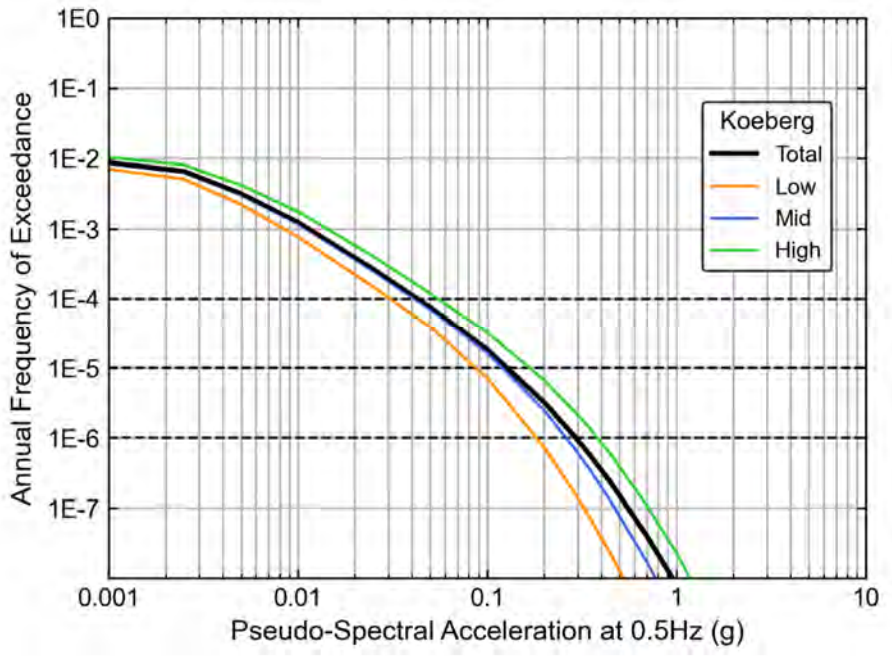

Figure H-21. Hazard sensitivity to the epistemic uncertainty model for 0.5 Hz at the Koeberg Nuclear Power Station.

Sensitivity to Uncertainty in the GMM Aleatory Variability

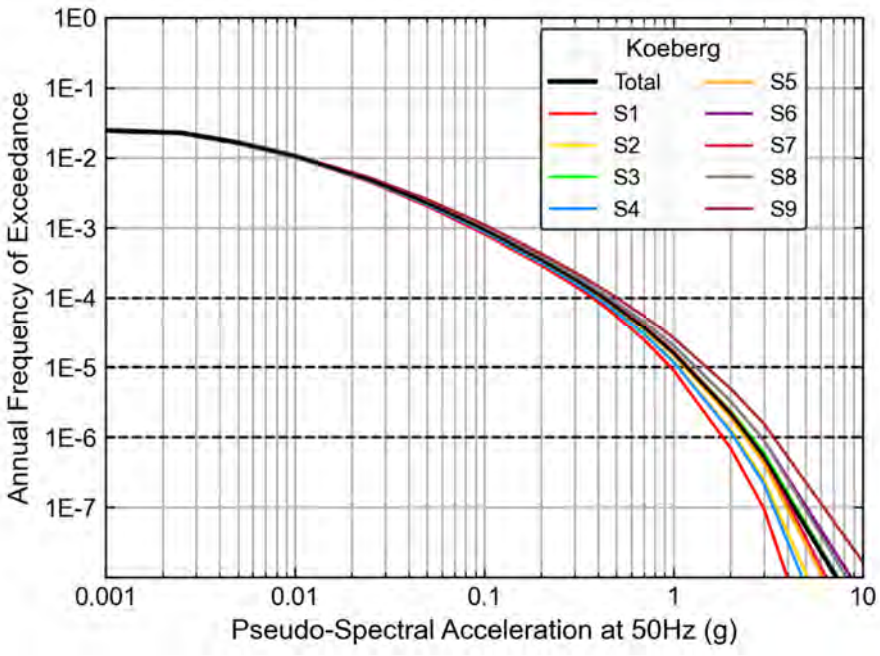

Figure H-22. Hazard sensitivity to the aleatory variability branches for 50 Hz at the Koeberg Nuclear Power Station.

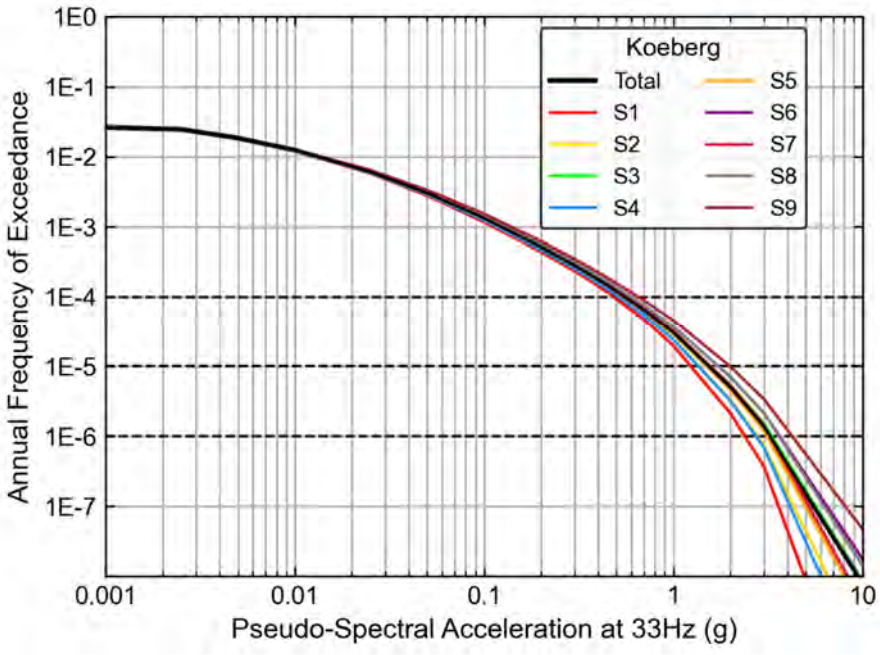

Figure H-23. Hazard sensitivity to the aleatory variability branches for 33 Hz at the Koeberg Nuclear Power Station.

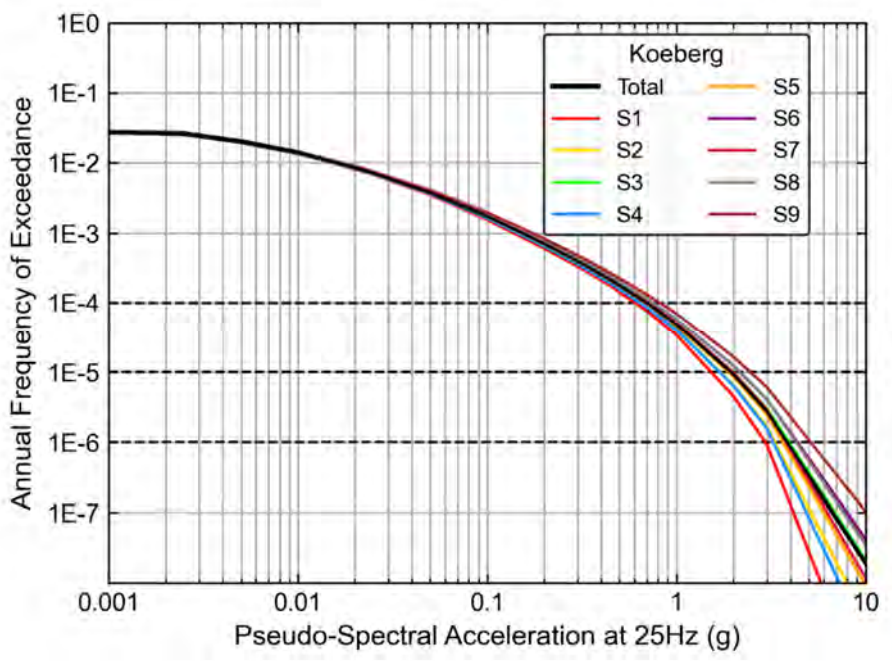

Figure H-24. Hazard sensitivity to the aleatory variability branches for 25 Hz at the Koeberg Nuclear Power Station.

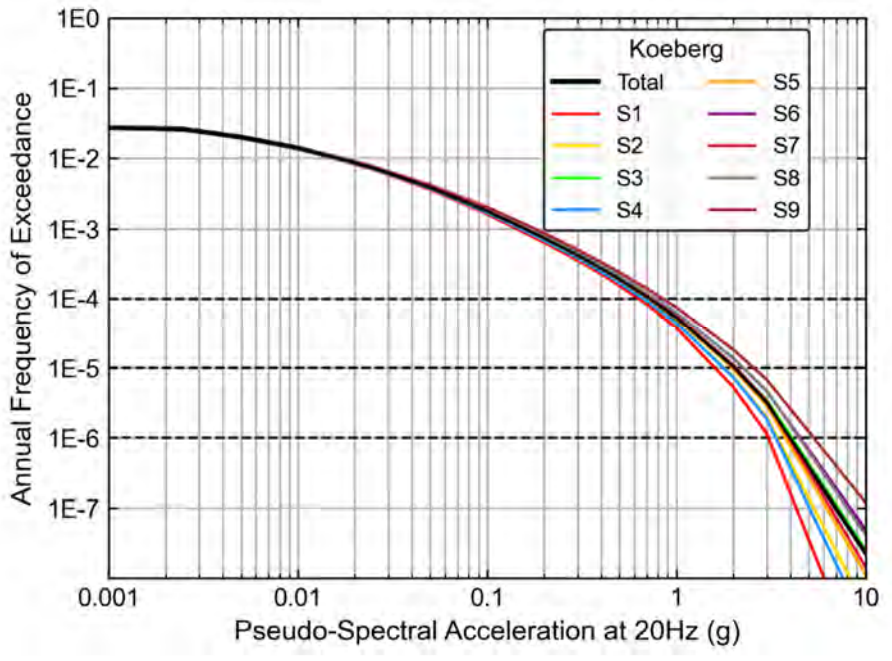

Figure H-25. Hazard sensitivity to the aleatory variability branches for 20 Hz at the Koeberg Nuclear Power Station.

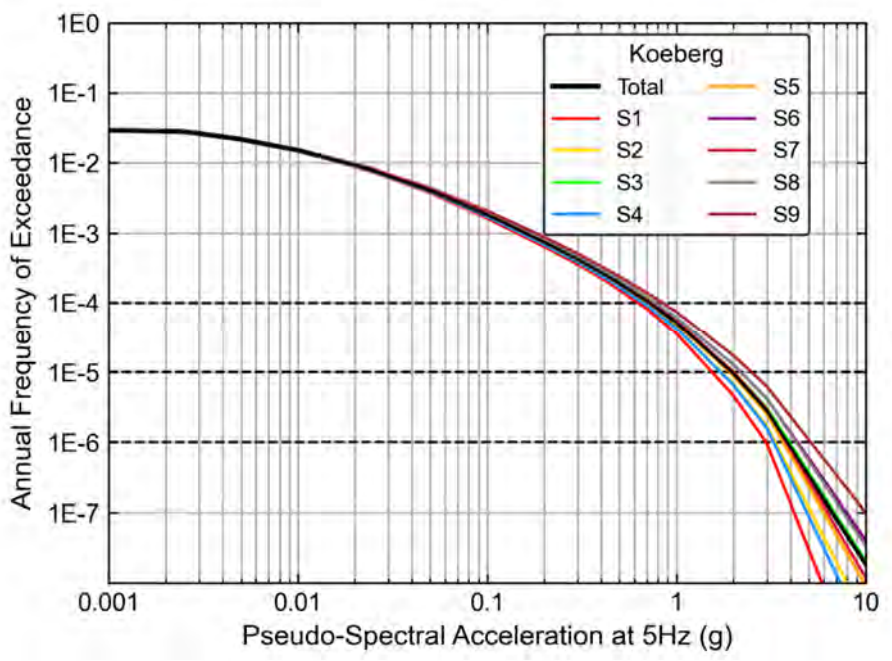

Figure H-26. Hazard sensitivity to the aleatory variability branches for 5 Hz at the Koeberg Nuclear Power Station.

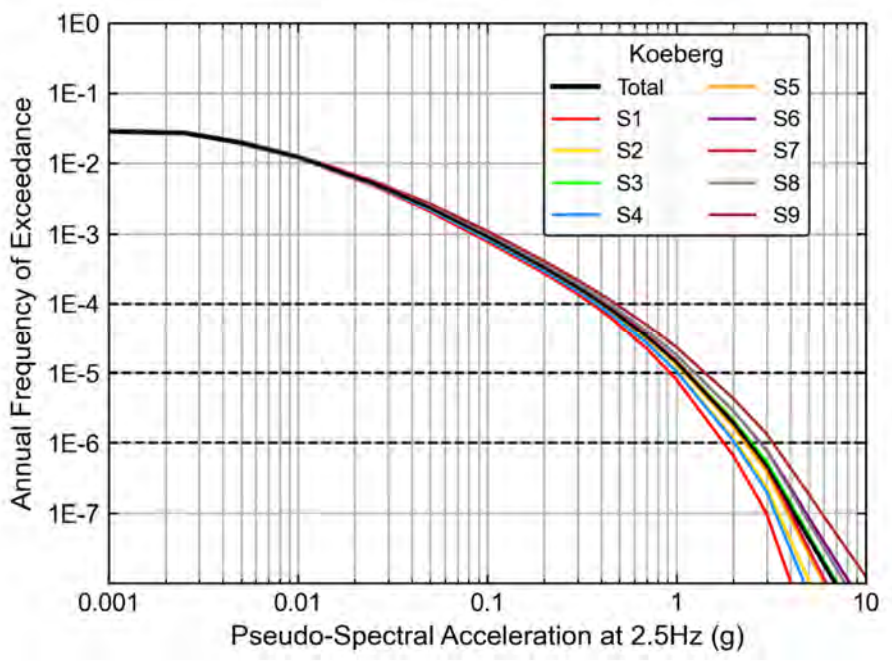

Figure H-27. Hazard sensitivity to the aleatory variability branches for 2.5 Hz at the Koeberg Nuclear Power Station.

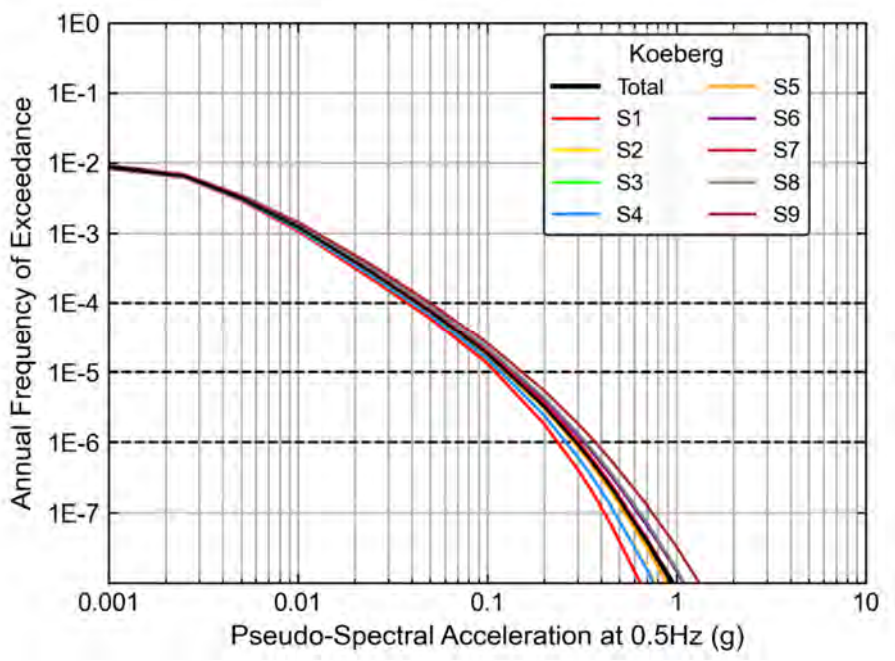

Figure H-28. Hazard sensitivity to the aleatory variability branches for 0.5 Hz at the Koeberg Nuclear Power Station.

H.2 SENSITIVITY TO SEISMIC SOURCE MODEL

Sensitivity to Spatial Smoothing

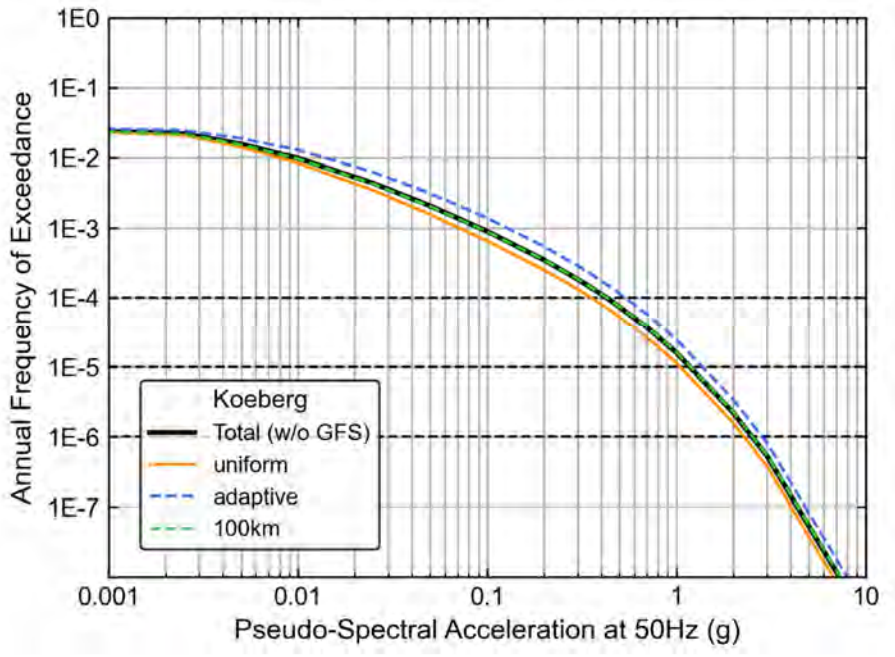

Figure H-29. Hazard sensitivity for 50 Hz to smoothed seismicity method branches at the Koeberg Nuclear Power Station.

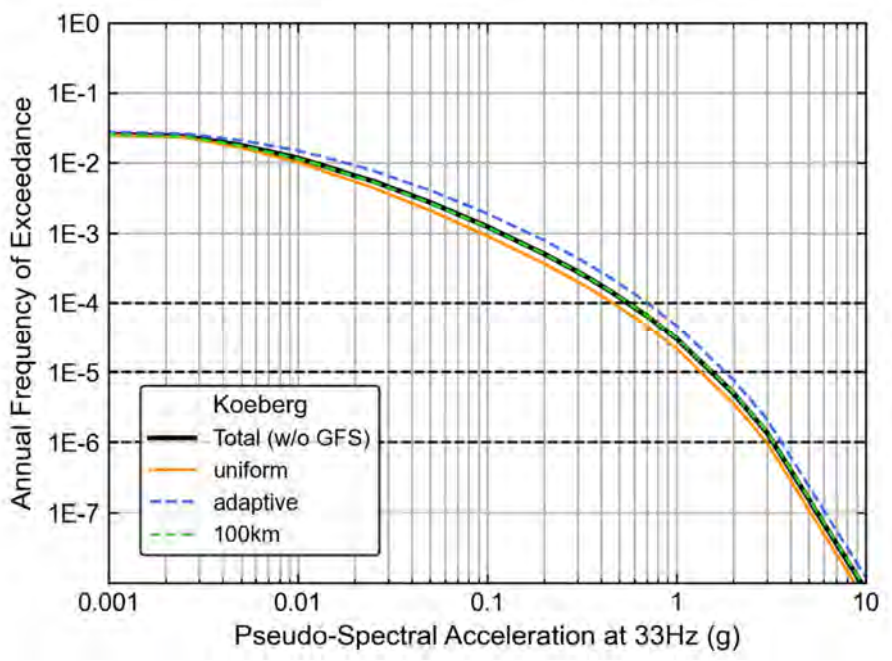

Figure H-30. Hazard sensitivity for 33 Hz to smoothed seismicity method branches at the Koeberg Nuclear Power Station.

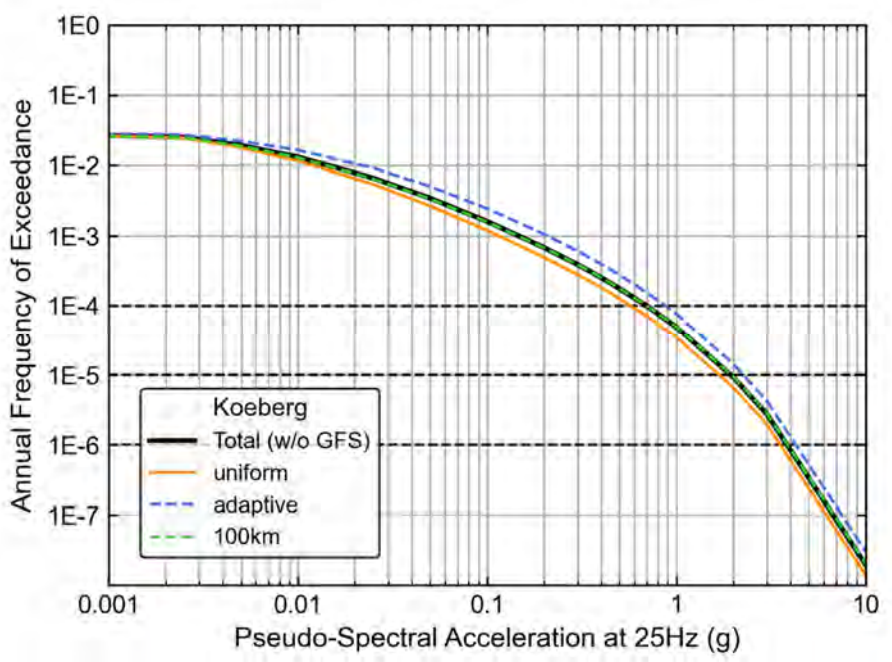

Figure H-31. Hazard sensitivity for 25 Hz to smoothed seismicity method branches at the Koeberg Nuclear Power Station.

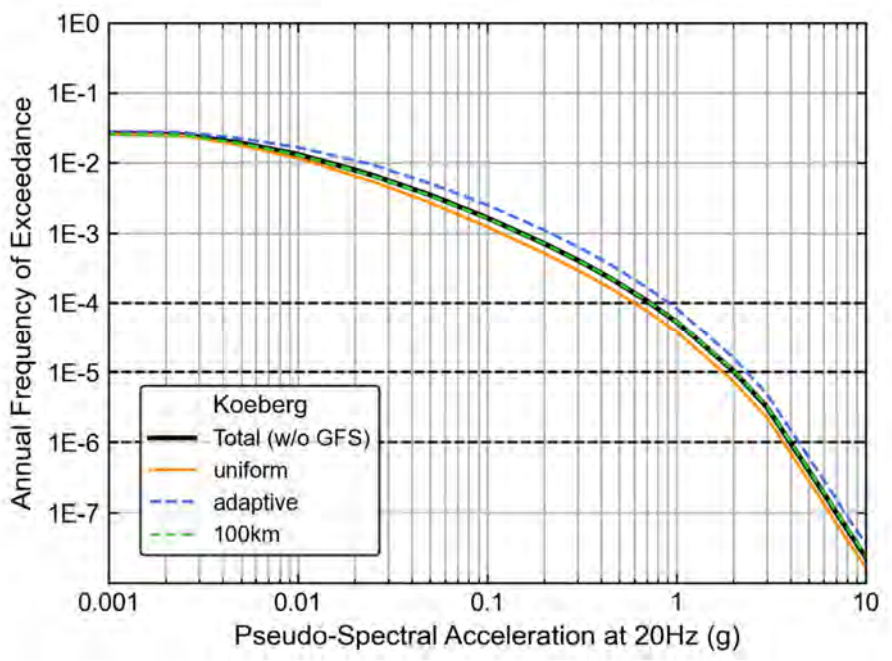

Figure H-32. Hazard sensitivity for 20 Hz to smoothed seismicity method branches at the Koeberg Nuclear Power Station.

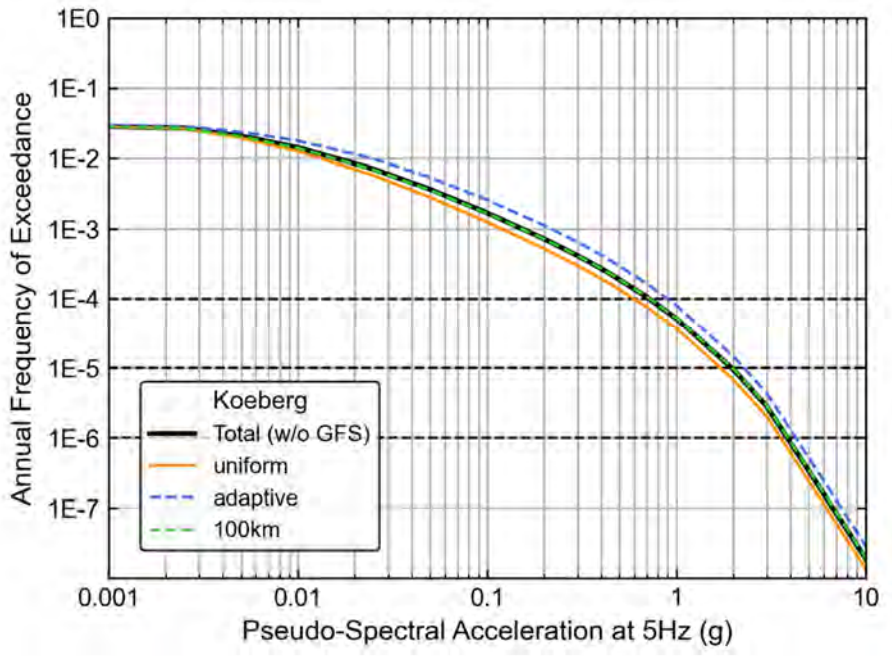

Figure H-33. Hazard sensitivity for 5 Hz to smoothed seismicity method branches at the Koeberg Nuclear Power Station.

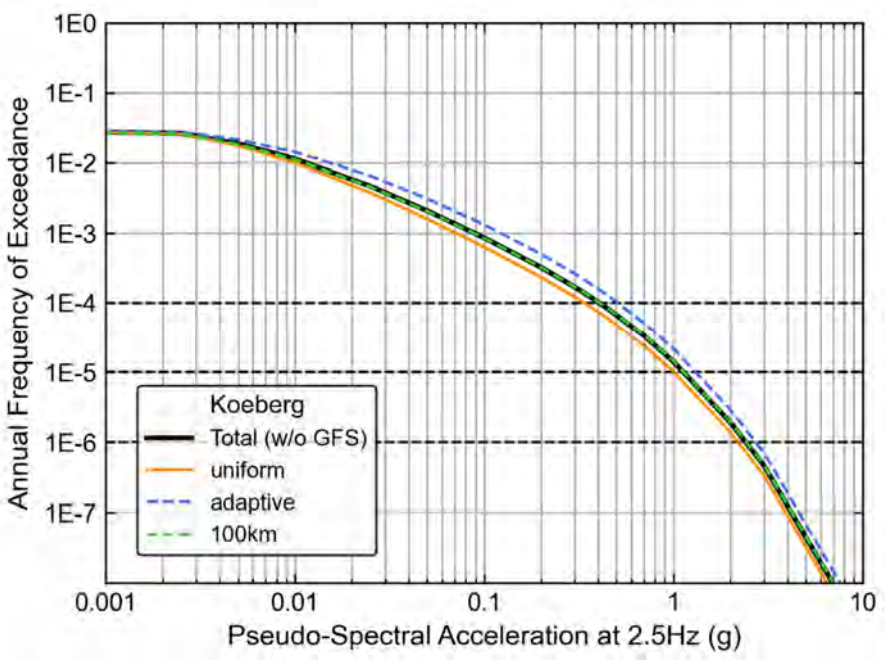

Figure H-34. Hazard sensitivity for 2.5 Hz to smoothed seismicity method branches at the Koeberg Nuclear Power Station.

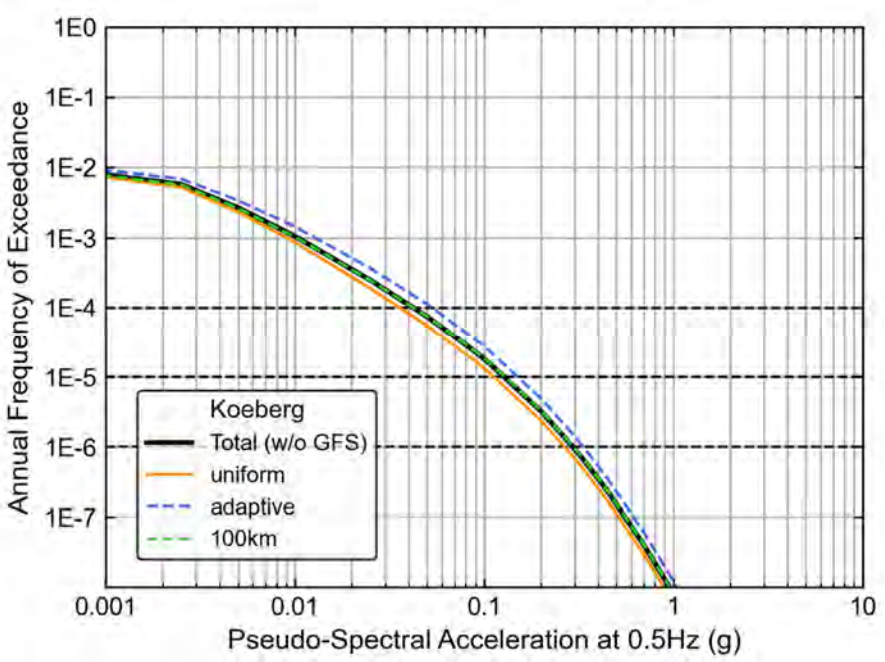

Figure H-35. Hazard sensitivity for 0.5 Hz to smoothed seismicity method branches at the Koeberg Nuclear Power Station.

Sensitivity to Maximum Magnitude

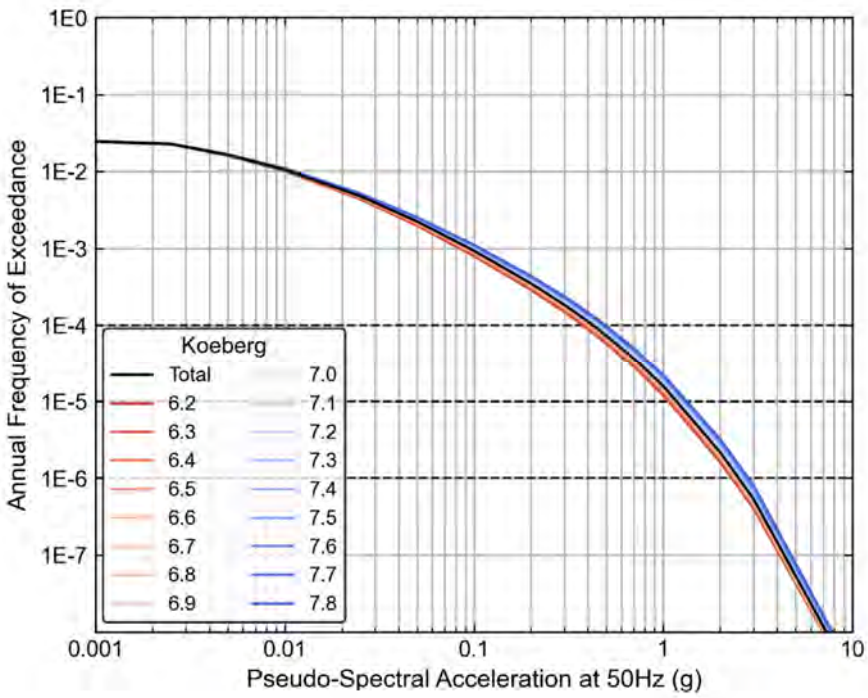

Figure H-36. Hazard sensitivity for 50 Hz to the host zone maximum magnitude branches at the Koeberg Nuclear Power Station.

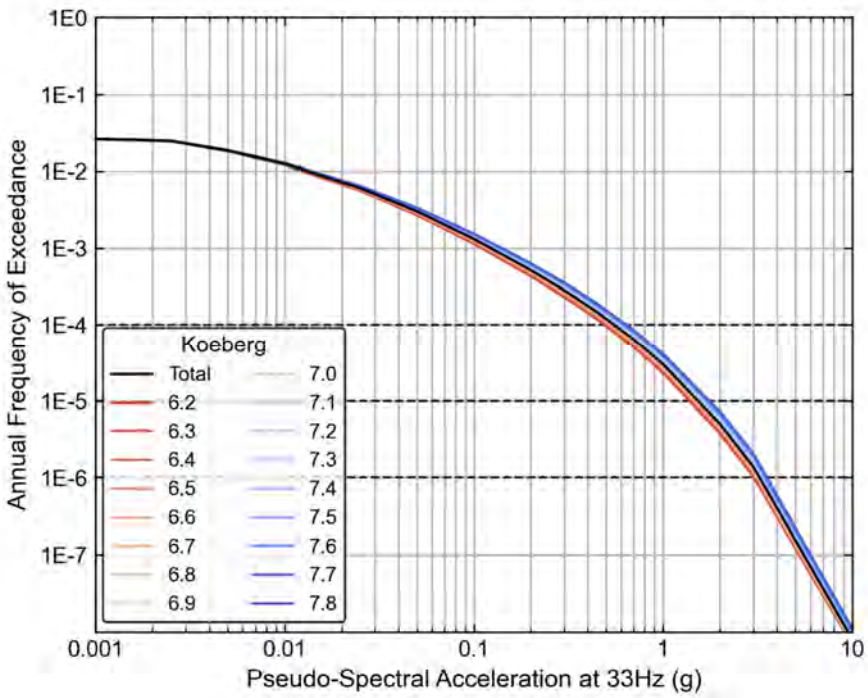

Figure H-37. Hazard sensitivity for 33 Hz to the host zone maximum magnitude branches at the Koeberg Nuclear Power Station.

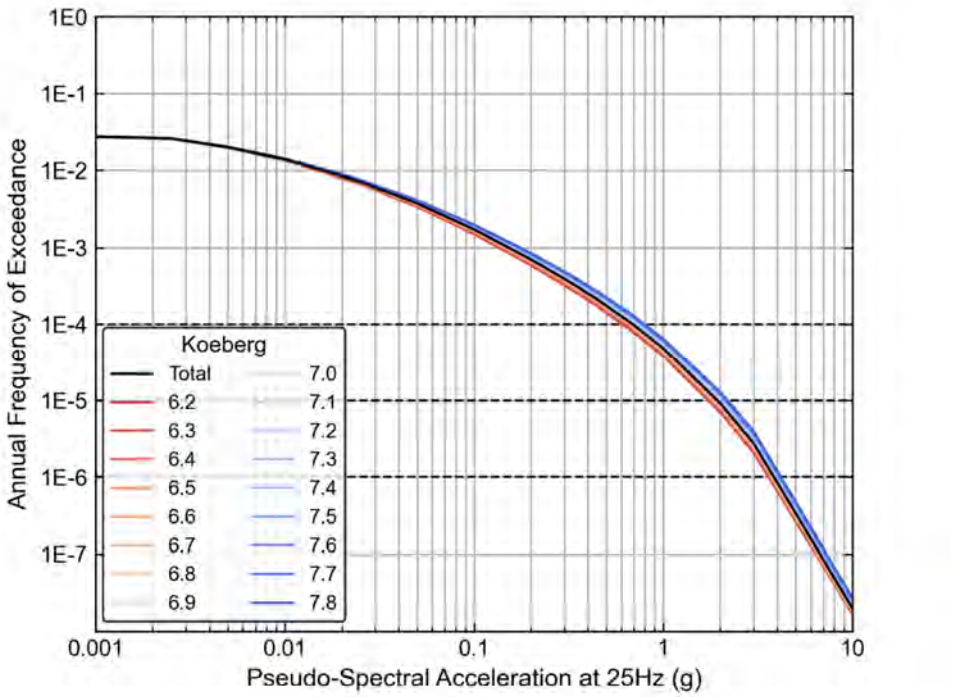

Figure H-38. Hazard sensitivity for 25 Hz to the host zone maximum magnitude branches at the Koeberg Nuclear Power Station.

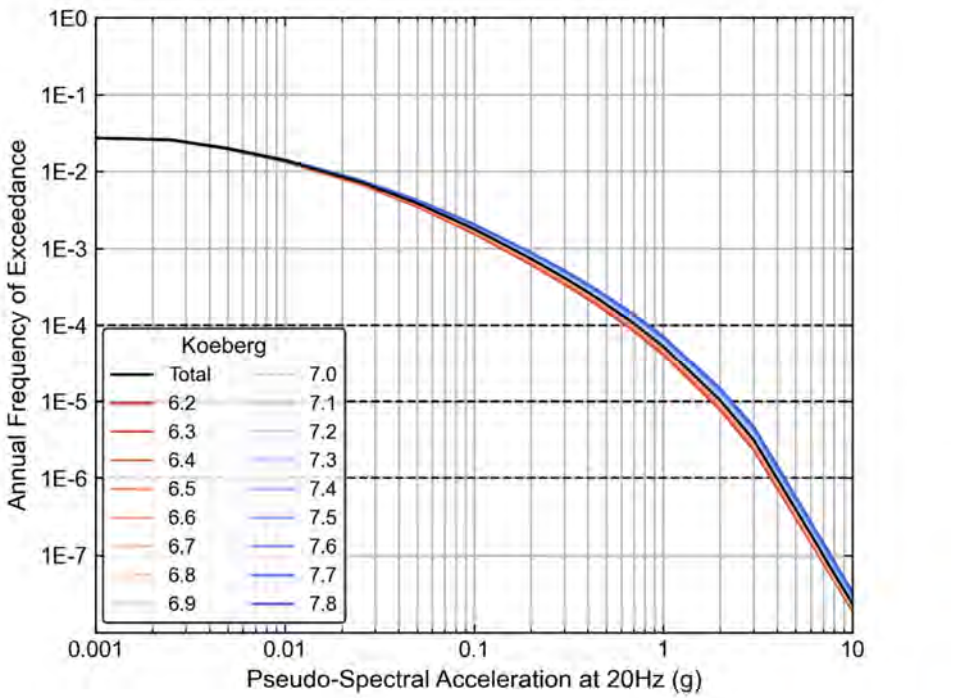

Figure H-39. Hazard sensitivity for 20 Hz to the host zone maximum magnitude branches at the Koeberg Nuclear Power Station.

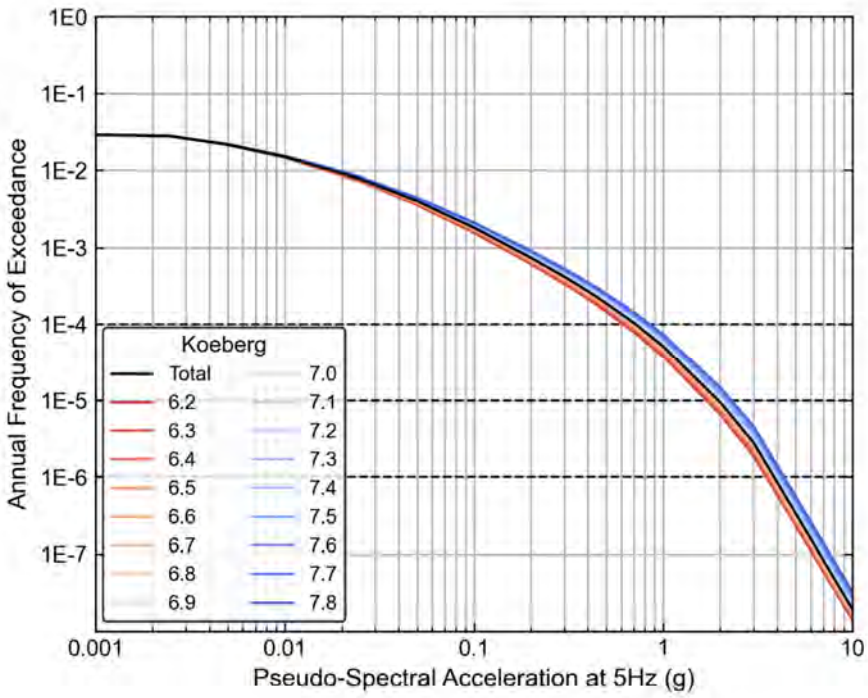

Figure H-40. Hazard sensitivity for 5 Hz to the host zone maximum magnitude branches at the Koeberg Nuclear Power Station.

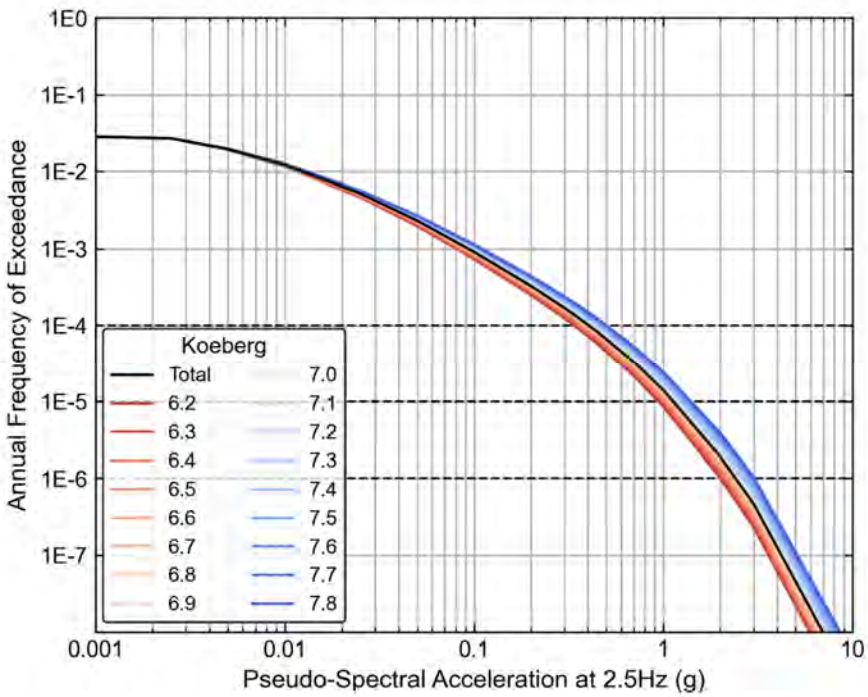

Figure H-41. Hazard sensitivity for 2.5 Hz to the host zone maximum magnitude branches at the Koeberg Nuclear Power Station.

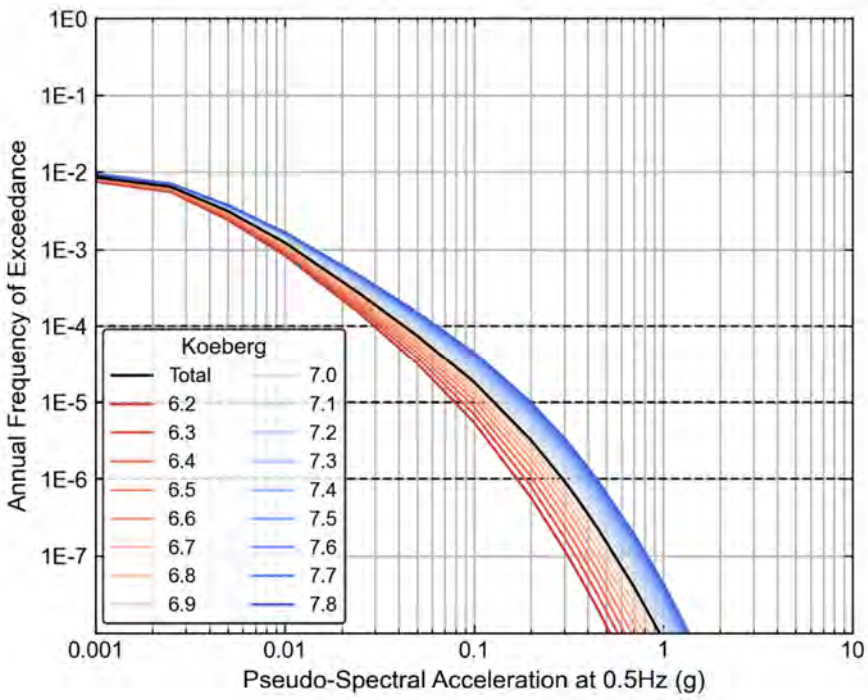

Figure H-42. Hazard sensitivity for 0.5 Hz to the host zone maximum magnitude branches at the Koeberg Nuclear Power Station.

Sensitivity to Completeness Method

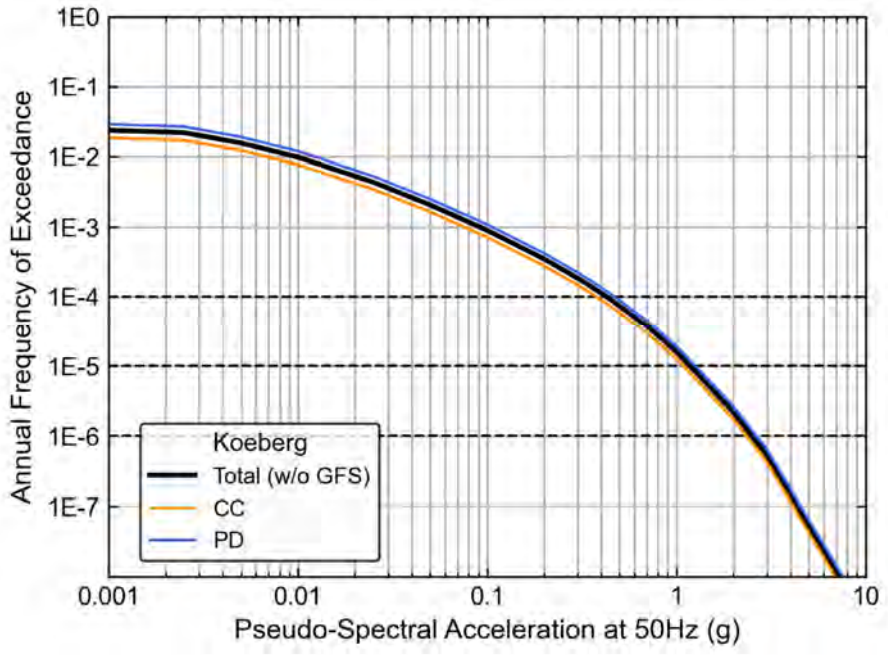

Figure H-43. Hazard sensitivity for 50 Hz to completeness method branches at the Koeberg Nuclear Power Station.

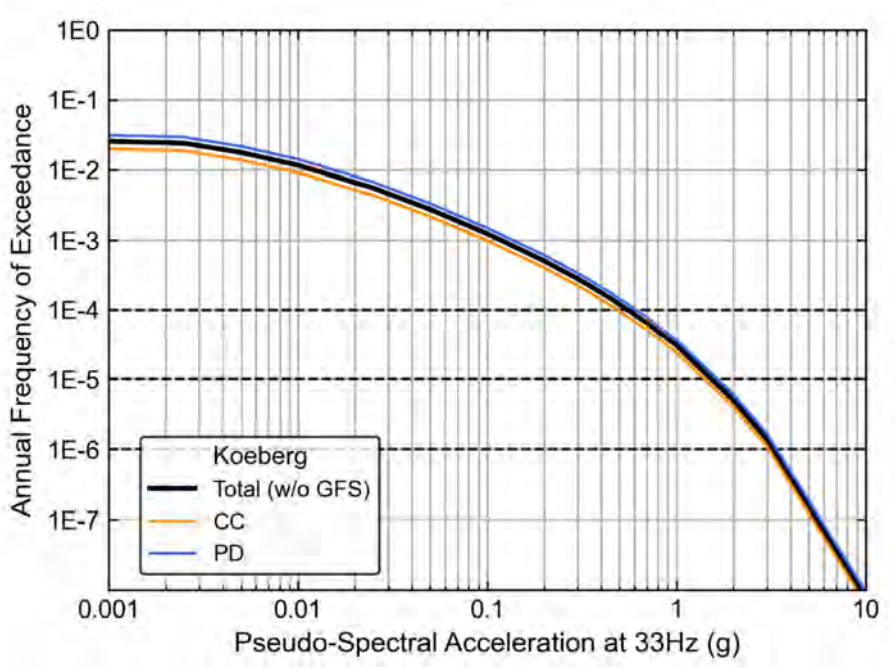

Figure H-44. Hazard sensitivity for 33 Hz to completeness method branches at the Koeberg Nuclear Power Station.

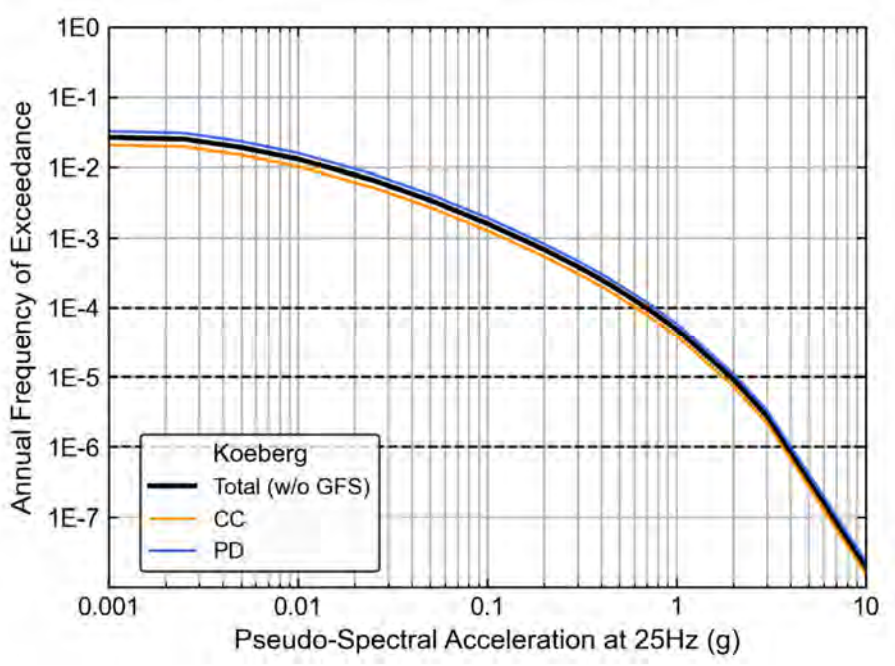

Figure H-45. Hazard sensitivity for 25 Hz to completeness method branches at the Koeberg Nuclear Power Station.

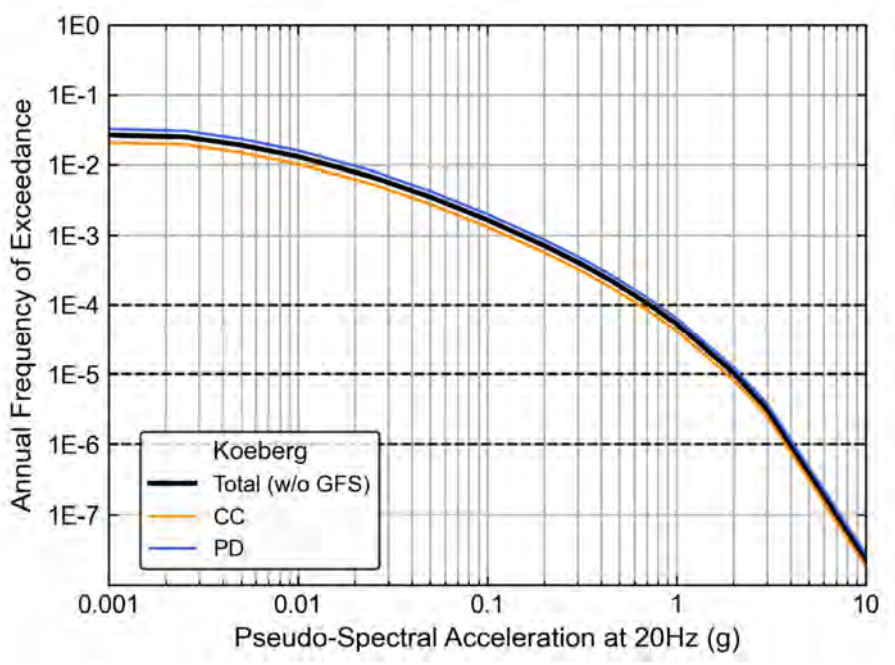

Figure H-46. Hazard sensitivity for 20 Hz to completeness method branches at the Koeberg Nuclear Power Station.

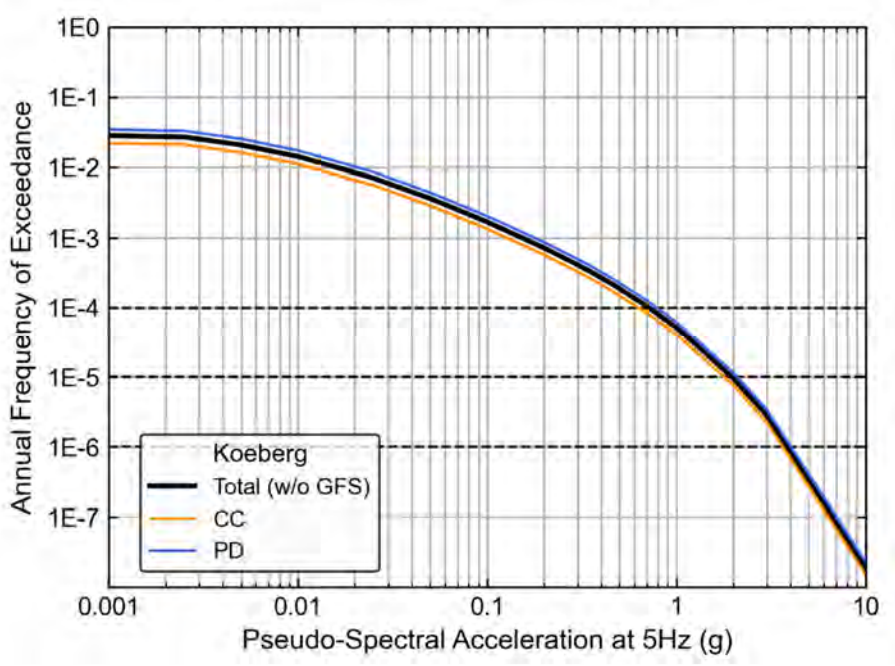

Figure H-47. Hazard sensitivity for 5 Hz to completeness method branches at the Koeberg Nuclear Power Station.

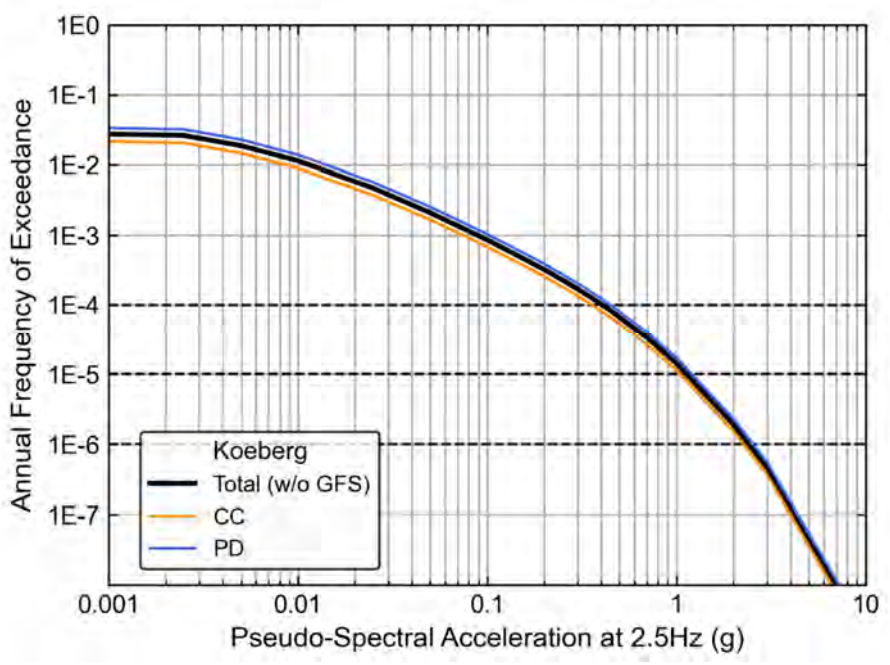

Figure H-48. Hazard sensitivity for 2.5 Hz to completeness method branches at the Koeberg Nuclear Power Station.

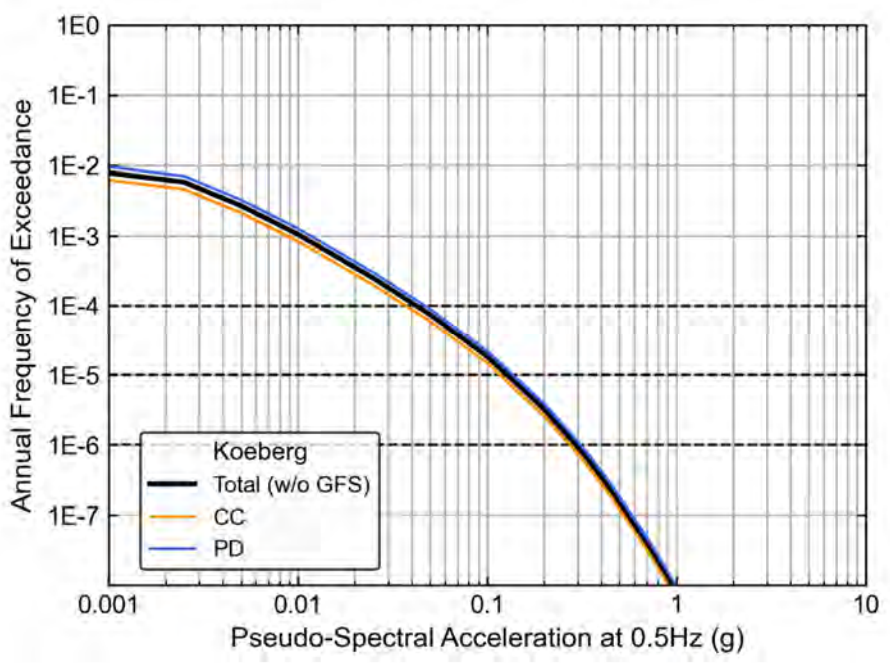

Figure H-49. Hazard sensitivity for 0.5 Hz to completeness method branches at the Koeberg Nuclear Power Station.

Sensitivity to Host Zone Fault Type

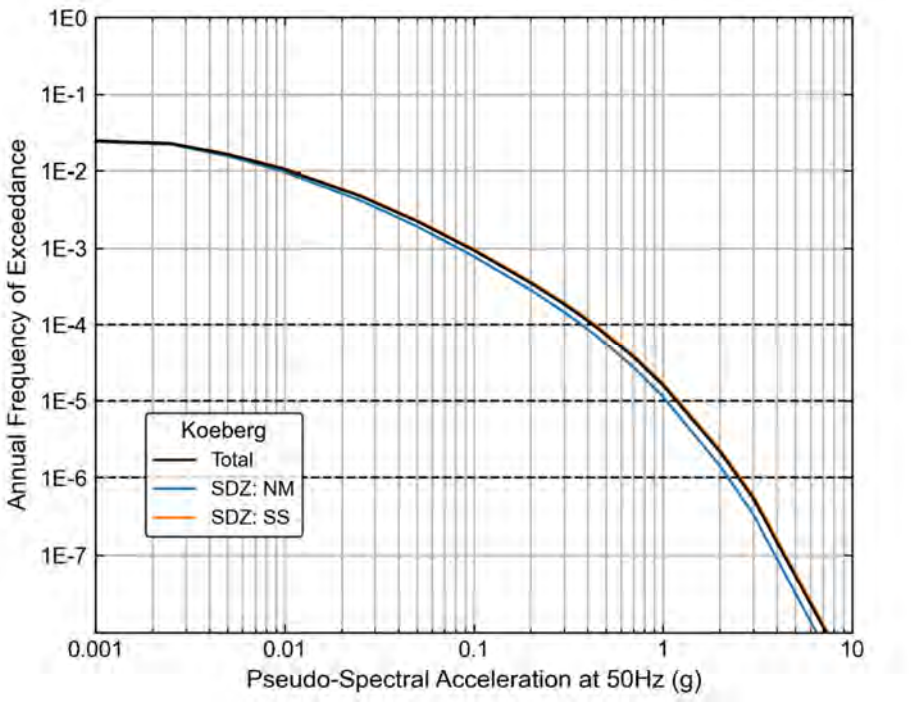

Figure H-50. Hazard sensitivity for 50 Hz to fault mechanism in the host zone for the Koeberg Nuclear Power Station

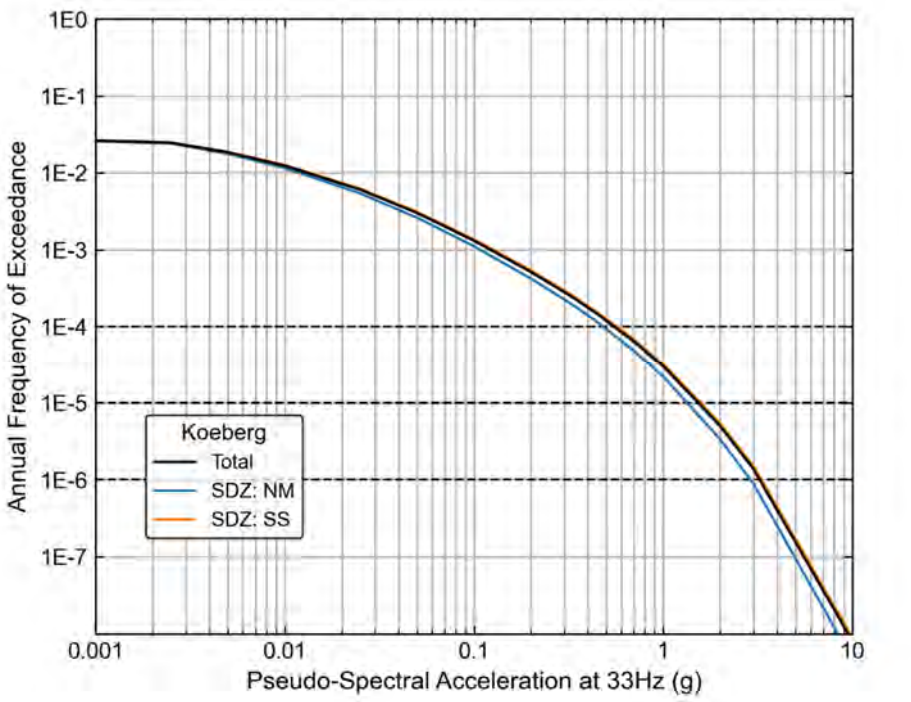

Figure H-51. Hazard sensitivity for 33 Hz to fault mechanism in the host zone for the Koeberg Nuclear Power Station

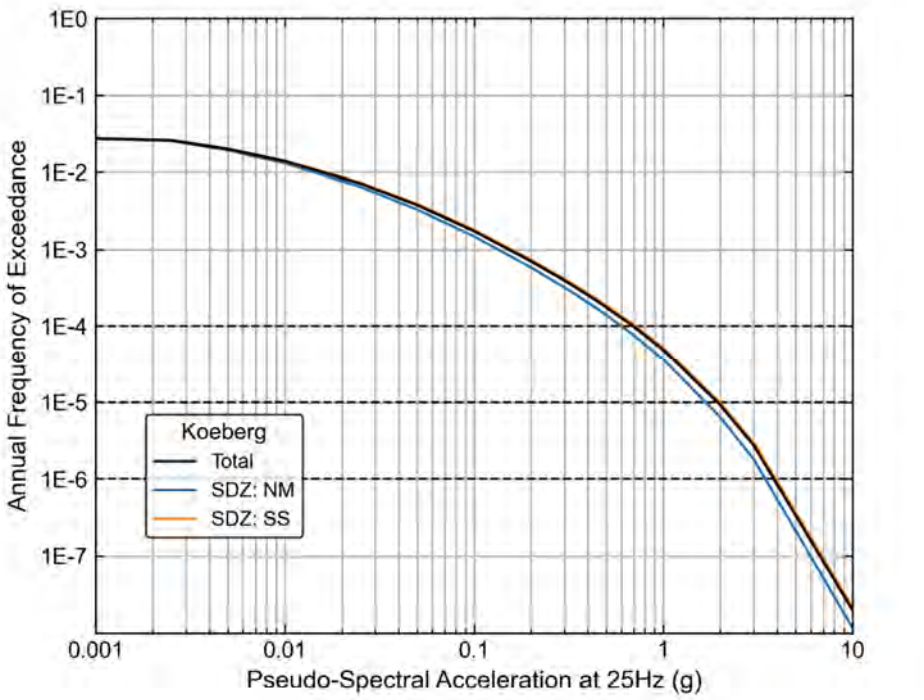

Figure H-52. Hazard sensitivity for 25 Hz to fault mechanism in the host zone for the Koeberg Nuclear Power Station

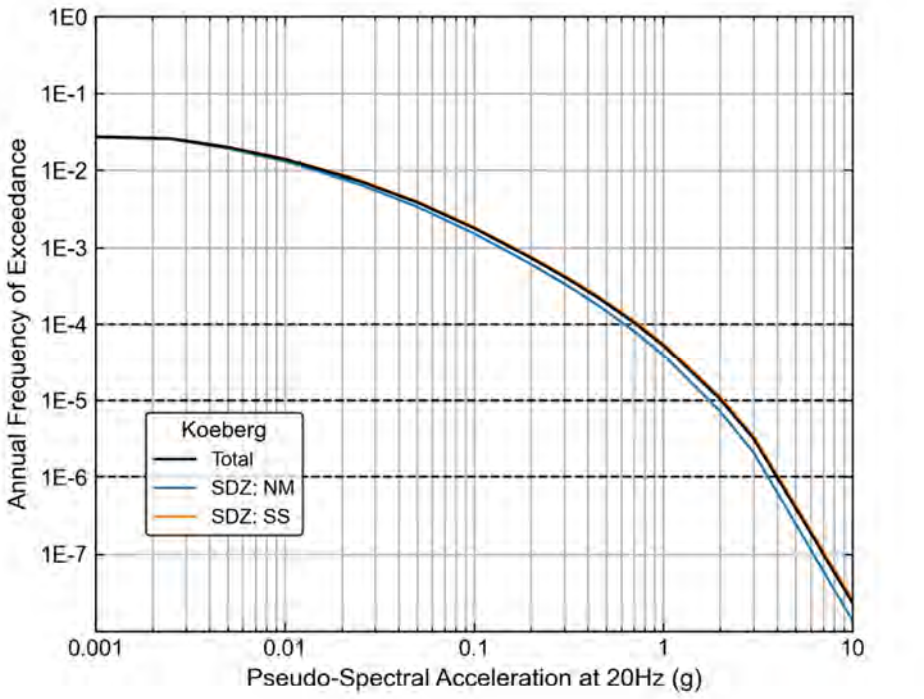

Figure H-53. Hazard sensitivity for 20 Hz to fault mechanism in the host zone for the Koeberg Nuclear Power Station

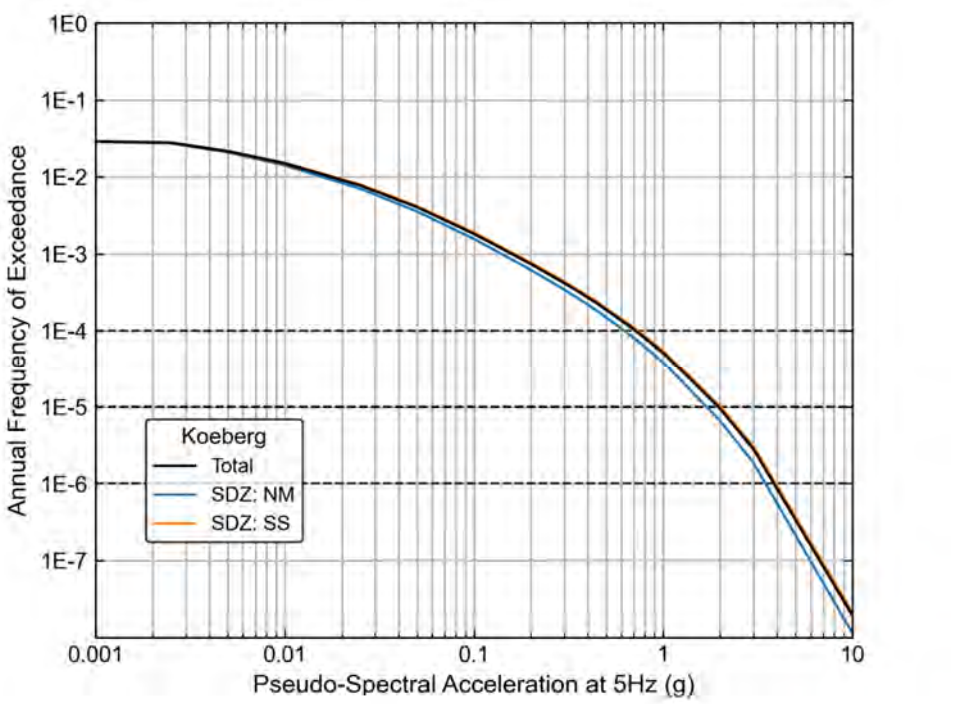

Figure H-54. Hazard sensitivity for 5 Hz to fault mechanism in the host zone for the Koeberg Nuclear Power Station

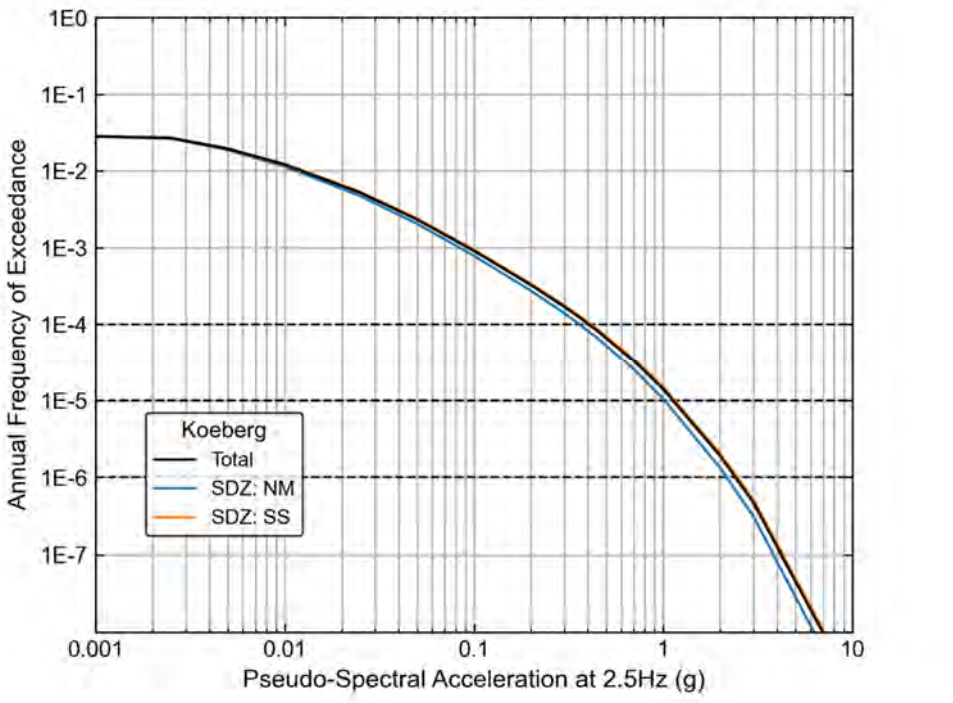

Figure H-55. Hazard sensitivity for 2.5 Hz to fault mechanism in the host zone for the Koeberg Nuclear Power Station

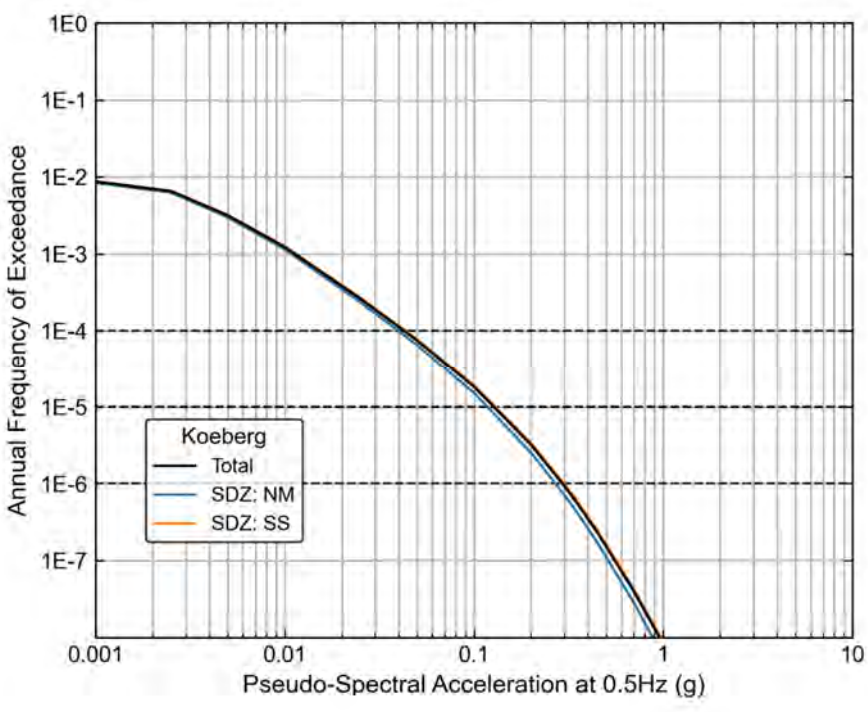

Figure H-56. Hazard sensitivity for 0.5 Hz to fault mechanism in the host zone for the Koeberg Nuclear Power Station

Sensitivity to Regional *b*-Value Calculation Method

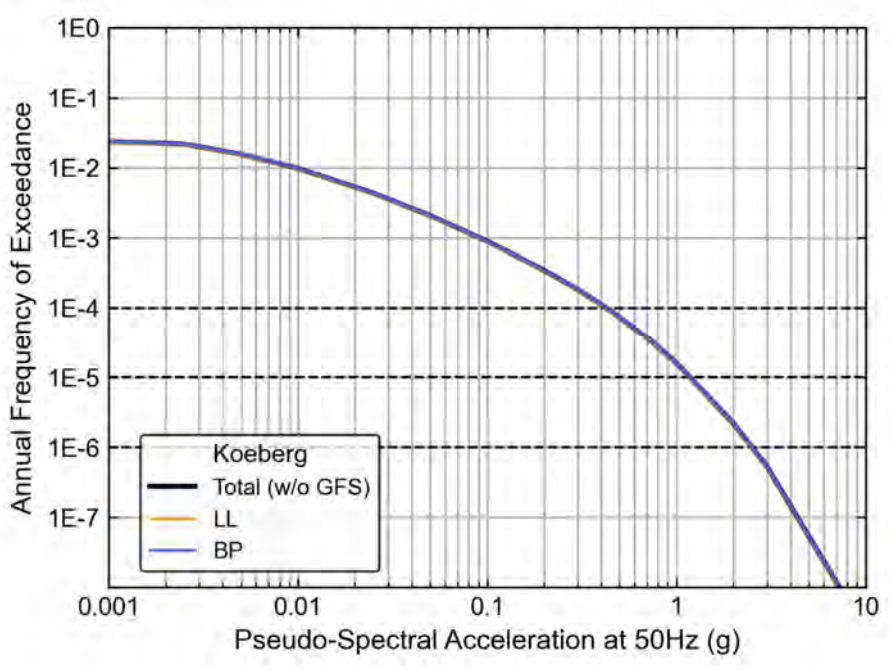

Figure H-57. Hazard sensitivity to regional *b*-value calculation method for 50 Hz at the Koeberg Nuclear Power Station.

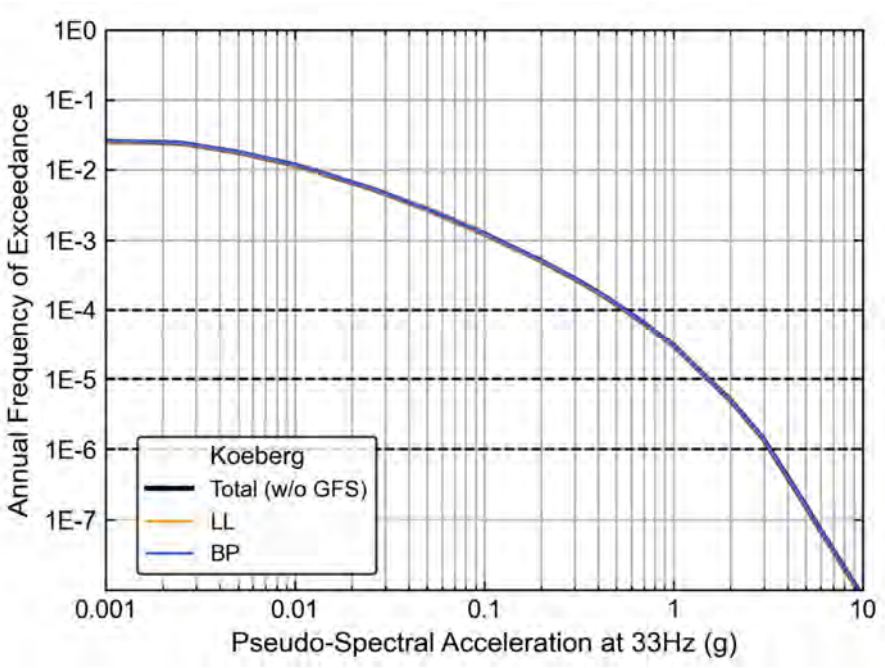

Figure H-58. Hazard sensitivity to regional *b*-value calculation method for 33 Hz at the Koeberg Nuclear Power Station.

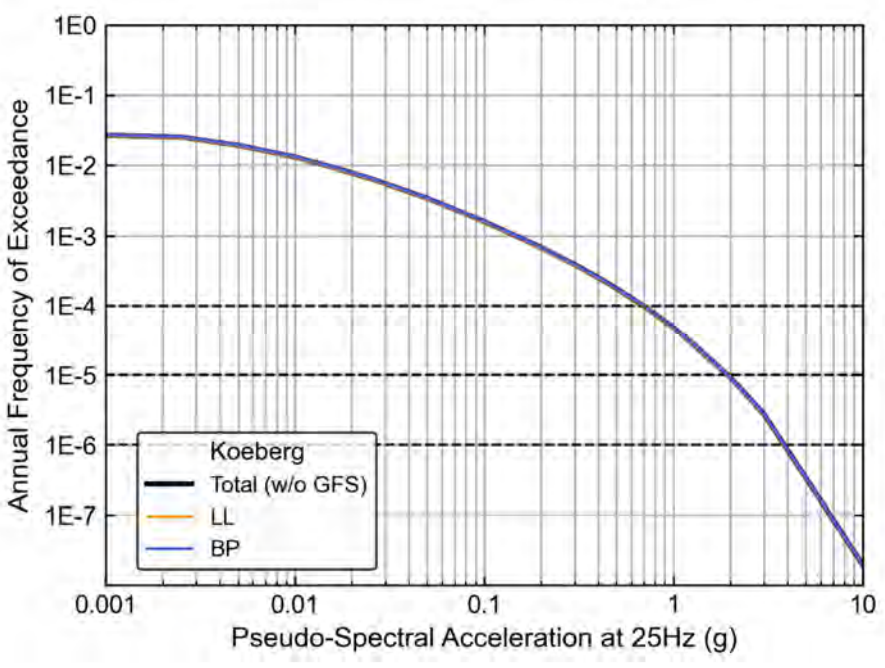

Figure H-59. Hazard sensitivity to regional *b*-value calculation method for 25 Hz at the Koeberg Nuclear Power Station.

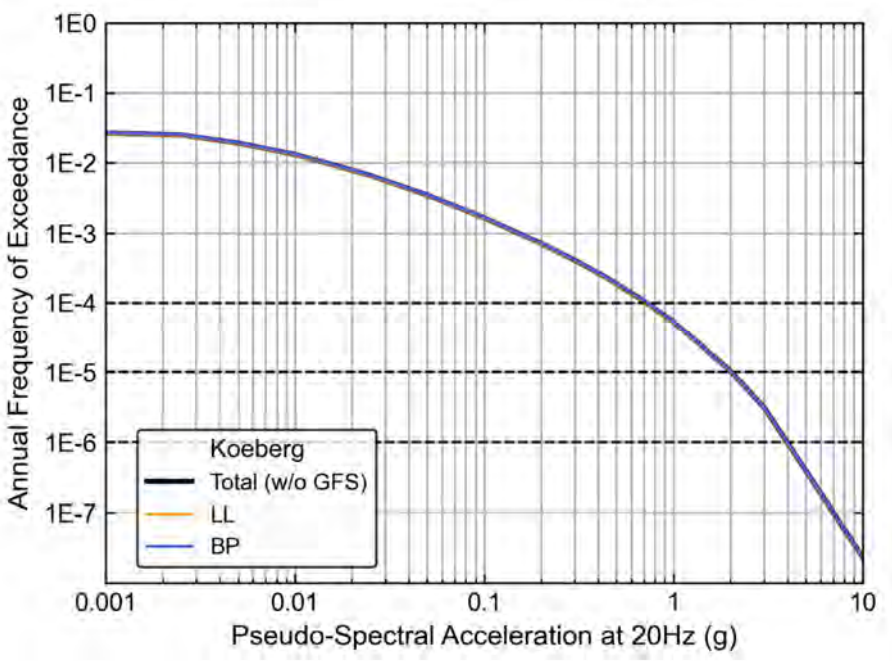

Figure H-60. Hazard sensitivity to regional *b*-value calculation method for 20 Hz at the Koeberg Nuclear Power Station.

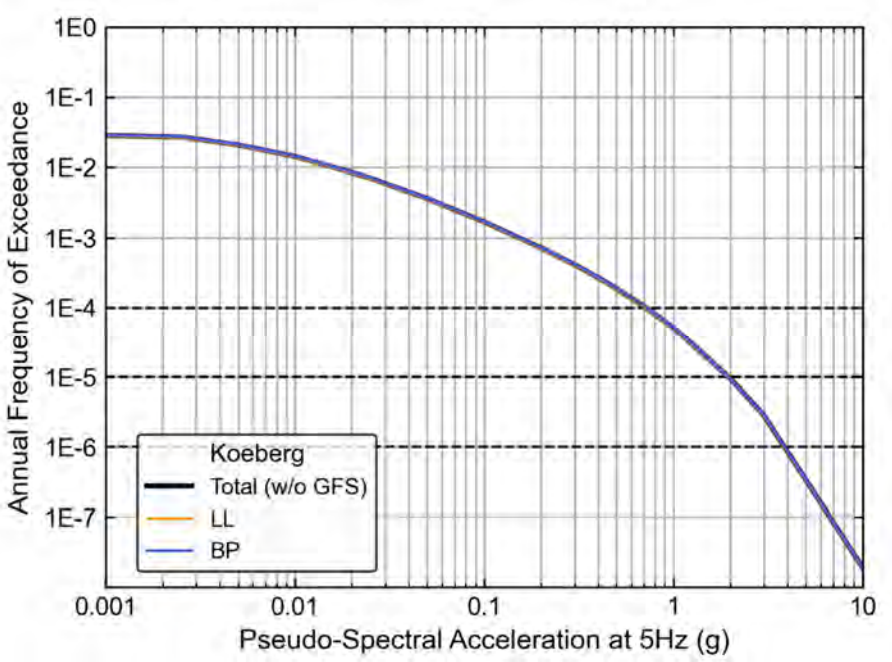

Figure H-61. Hazard sensitivity to regional *b*-value calculation method for 5 Hz at the Koeberg Nuclear Power Station.

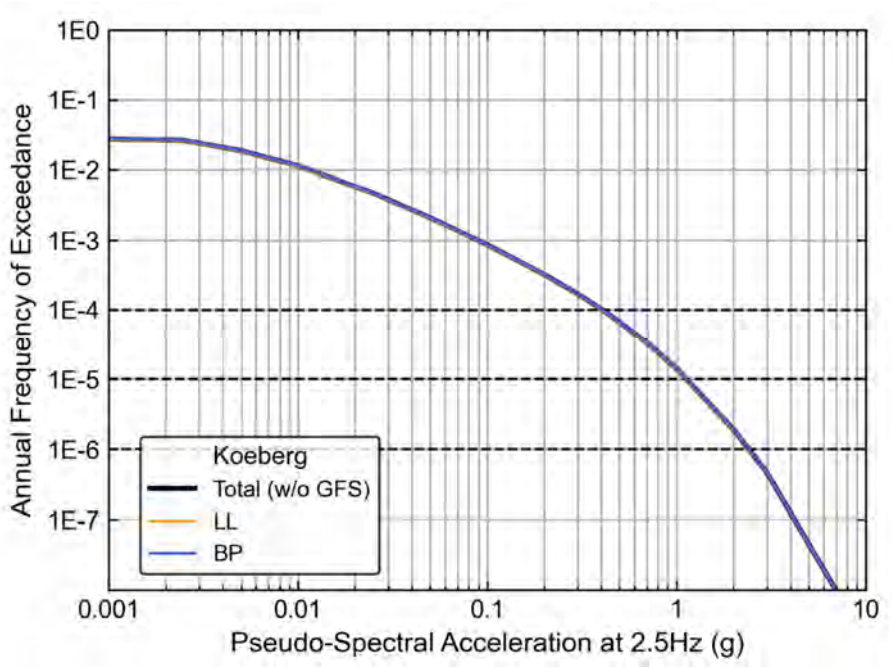

Figure H-62. Hazard sensitivity to regional *b*-value calculation method for 2.5 Hz at the Koeberg Nuclear Power Station.

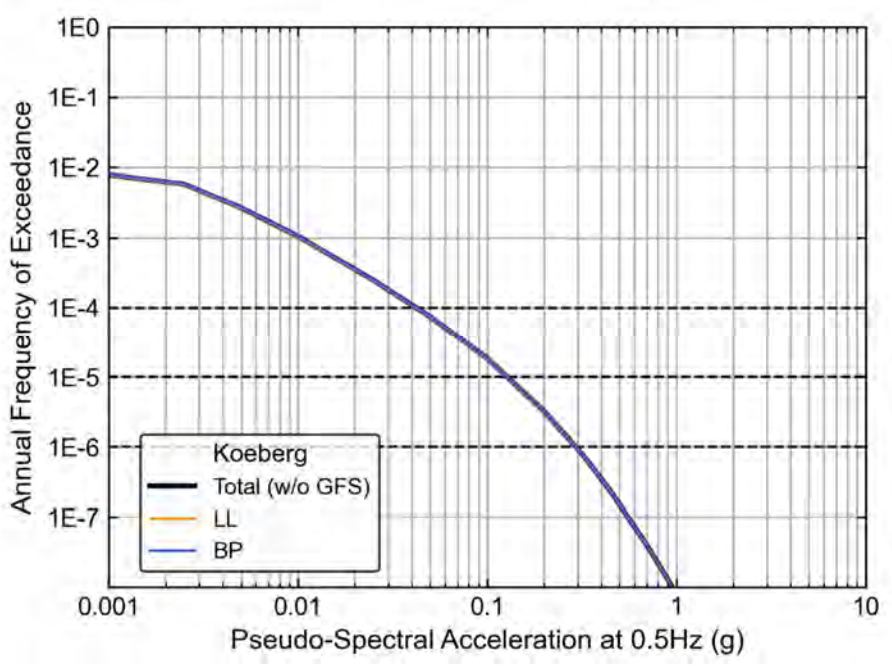

Figure H-63. Hazard sensitivity to regional *b*-value calculation method for 0.5 Hz at the Koeberg Nuclear Power Station.